

**Architecture and origin of fluvial cross-bedding
based on flume experiments and geological
examples field case studies:
Rillo de Gallo, Spain and Northumberland, UK**

María J. Martínez de Álvaro

A thesis submitted to the School of Environmental Sciences of the
University of East Anglia for the degree of Doctor of Philosophy

May 2015

© This copy of the thesis has been supplied on condition that anyone who consults it is understood to recognise that its copyright rests with the author and that use of any information derived there from must be in accordance with current UK Copyright Law. In addition, any quotation or extract must include full attribution.

Acknowledgements

I would like first and foremost to thank my primary supervisor Prof. Jan Alexander for giving me the opportunity to learn and be captivated by rivers and the fascinating world that is hidden behind those ancient rocks. We all enjoy them outdoors on a surface level but only some are fortunate enough to be able to investigate and learn from them. I am very grateful to her for her encouragement, enthusiasm, and interesting and constructive discussions on sediments throughout my Ph.D. I also would like to thank my secondary supervisors, Dr. Jenni Turner and Dr. Trevor Tolhurst for their positive advice, support, and their contribution towards this project. Thanks to my examiners Prof. Adrian Hartley and Prof. Jenni Barclay for taking the time to review this work.

I acknowledge NERC for providing funding for this research and UEA that provided extra funding for conference attendance and fieldwork.

A very special thank you goes to the two first geologists I ever met, who are now very good friends, Yolanda Sánchez Moya and Alfonso Sopeña. Thank you for making me love Geology as I do, for being there all this time, when I ever needed an advice, a compass, a geological hammer, a cup of tea; thank you for introducing me to the beautiful Spanish Sedimentary Triassic Rocks and making me want to be a sedimentologist.

I would like to thank to all those who helped me too with the experimental part of this project and its equipment: Jennie Stevenson, John Brindle, Gareth Flowerdew, Nick Griffin, and Bertrand Lézé. Thanks to Emma and Lynda for being always so helpful when I needed extra laptops and maps from teaching. Thanks so much to Gary Royal and Richard Humphries, thank you for your never-ending patience every time I had issues with my computer. I would like to thank Dr. James Hodson, for spending a fair amount of time training me in how to use the flume. Thanks also to Dr. Rob Macdonald for his help via email any time I needed a quick question to be solved. Thanks to Josh Smith, my field assistant in beautiful North England. Thanks to Christopher Herbert for being a thorough assistant when doing my flume experiments.

I am very grateful to Sue Jickells and Roland von Glasow, thank you for your constructive advices, and your encouragement that kept me motivated during the final stages of my Ph.D. I would like to send a very special thank you to Heather, who has brought the pleasure of playing piano back to my life during my Ph.D. Thanks to my colleagues in our office “The Rock”.

Thanks to the very special friends I have met at UEA, little Mel, Katie, Johanna, Alba, Alessia, Ana, Mi Tian, Maira, Elena; thank you for making this intellectual and challenging process much easier, thanks for all those dinner parties, birthday surprises, days out by the coast and all those fun times together. Elena, thank you for all the statistic tutorials; Mel, thanks for the GIS ones. Alessina, thanks for your sincere friendship. To my lovely Mi, thanks for being always such a supportive and thoughtful friend. My dear Maira, thank you for teaching me so much about myself and the secret of enjoying life; Katie and Jo my best partners in crime, thank you for all the good times and for those when you had to listen to my worries.

Thanks to my very good friends Alice and Rob; thank you for being willing to proof read part of my thesis. Thanks Rob, for those delicious homemade dinners when I did not have the time to cook my own. Thanks to my friend Steph, always there, responding to any of my SOS emails sending his cheering and positive thoughts.

Another very special thank you goes to three very important friends in my life who regardless of anything helped not only during my field work in Molina de Aragón, but always. Patricia, thanks “mi letoncita” for all those interesting discussions in the field and even more for the interesting ones afterwards in the local pub. Charo, the best find in these four years! I’m glad we are still friends after all those dips and strikes I made you annotate in my field notebook, thanks for bringing happiness to the field work. Rocío, my soul mate, thank you so much for all the help, the company, the advice, thank you for being such a good listener. To you three, thanks for being amazing friends.

A sincere thank you to my family, for their support and unconditional love, without it I could have never achieved this Ph.D.

My last thank you goes to Andrew, thank you for being there literally all the time for me, for listening, understanding, supporting, and reminding me every second that I could actually do it. Thank you for being the best Scottish husband!



“La naturaleza está repleta de razonamientos que no tuvo nunca la experiencia”

Leonardo da Vinci

Abstract

Cross-stratified sandstones formed by dunes and unit bars is common in the rock record. Cross-bed architecture is controlled by the size and shape of, and processes on, the original formative bedforms, and processes that truncate, deform or bury the cross-strata.

This thesis reports an investigation of cross-bedded sandstones and their internal sedimentary structures formed in fluvial environments within different depositional settings at Rillo de Gallo, (Spain) and Seaton Sluice, (Northumberland). In addition, flume experiments using well-sorted fine sand were used to investigate some of the factors controlling cross-bed architecture produced by unit bars migrating downstream in a unidirectional flow under controlled conditions over pre-existing topography. New ways of classifying cross-bedding were developed to allow analyses of patterns and relationships between set geometry, flow behaviour and stratigraphic position within sedimentary sequences. The amount and variation in divergence between scour trend and scour-fill laminae dip direction is found to be potentially diagnostic of flow pattern, and should improve palaeoenvironment interpretation. A relationship between the amount of variation in bar lee-face angle with bar height was found in the flume and may be useful for inferring bedform size in the rock record. Integration of laboratory and field observations on lee-face angle, bedform superimposition, reactivation surfaces, topography development and bottomset formation helped to mitigate the issue of preservation level when interpreting rock analogue examples and led to improved interpretations of the ancient fluvial deposits. This is an approach that should help the interpretation of other ancient fluvial sequences.

The mechanisms and patterns of trough scour formation and scour filling have been to a certain extent ignored to date. Herein it is highlighted the need for further research on the understanding of scour formation and fill in association with bedform development and migration leading to improved knowledge of cross-bedded sandstones.

Contents

Acknowledgements	i
Abstract	v
Symbols	xiii
List of Figures	xv
List of Tables	xxi
Chapter 1: Introduction	1
1.1 Definition, classification and origin of cross-stratification (dune and unit bar migration) and classification.....	7
1.2 Introduction to trough cross-bedding and single trough cross bed set term.....	12
1.3 Cross-stratification thickness as an interpretational tool.....	15
1.4 Flume experimental work relevance and its linkage with field studies.....	17
1.5 Terminology.....	19
1.6 Aims.....	23
1.6.1 Rationale and primary aims.....	23
1.6.2 Main Aims.....	25
1.7 Objectives.....	27
1.7.1 Preliminary objectives.....	27
1.7.2 Objectives for the detailed case studies of cross-bedded sandstones (aim 1)	27
1.7.3 Objectives of the integration of a review of previous published studies on scour and scour associated to bedform development, with field observations from the two study sites (aim 2)	29
1.7.4 The objectives of the flume experiments (aim 3)	29
1.7.5 Objectives of the comparison of the field and flume results (aim 4)...	30
1.8 Outlook and thesis organisation.....	31

Chapter 2: Case study I, The Prados Formation	35
2.1 Introduction to the study area at Rillo de Gallo, Guadalajara, Spain.....	37
2.2 Stratigraphic and geological context at Rillo de Gallo.....	39
2.3 Palaeogeography.....	42
2.4 Lithostratigraphy of the Prados Formation.....	47
2.5 Sedimentary Facies analysis.....	50
2.5.1 Facies.....	50
2.5.2 Identification of storeys and facies associations.....	52
2.6 Descriptive analysis of the Prados Formation Sandstones.....	55
2.6.1 Description of Prados sandstones.....	55
2.6.2 Analysis of selected individual exposures of the Prados Formation....	56
2.7 Scours associated with trough cross-bedding (scour structures) and classifications.....	65
2.7.1 Classification of scour structures on the basis of their size, shape and internal architecture.....	65
2.7.2 Classification of Prados Formation cross-bed sets.....	70
2.7.3 Classification of scour structures on basis of their mean laminae dip.....	73
2.8 Analysis of scours associated with trough cross-bedding (scour structures).....	75
2.8.1 Relationship between trough shape and size.....	75
2.8.2 Relationship of trough shape and size to scour structure's stratigraphic position within the sequence.....	77
2.8.3 Relationship of laminae dip direction to scour trend and comparison with trough shape and size.....	78
2.8.4 Relationship of laminae dip direction to scour trend and preservation level of exposure and measurement accuracy.....	84
2.8.5 Relationship of laminae dip to trough shape and size.....	86
2.9 Discussion.....	88
2.9.1 Discussion on class boundaries classification criteria and relationship between classes.....	88
2.9.2 Discussion on the relationship of dip direction modes to trough shape and size; and the stratigraphic location of the structures as an flow pattern	

indicator.....	90
2.9.3 Discussion on the lack of relationship between width:length ratio and laminae dip.....	93
2.9.4 Discussion on the relationship scour trend and mean laminae dip direction.....	95
2.9.5 Discussion of controls on scour structure geometry.....	96
2.10 Re-interpretation of the nature of the original channel.....	100
2.10.1 Discussion of channel depth and flow depth.....	100
2.10.2 Discussion of channel width.....	103
2.10.3 Discussion of channel plan form.....	106
2.11 Conclusions.....	108
Chapter 3: Case study II: The Seaton Sluice Sandstone	113
3.1 Introduction to the study area at Seaton Sluice, North England.....	115
3.2 Stratigraphic and geological context at Seaton Sluice Sandstone.....	117
3.3 Palaeogeography.....	119
3.4 Lithostratigraphy of the Seaton Sluice Sandstone.....	125
3.5 Sedimentary Facies analysis.....	128
3.5.1 Facies.....	128
3.5.2 Facies in the three component parts (storeys) of the Seaton Sluice Sandstone.....	130
3.6 Descriptive analysis of the Seaton Sluice Sandstone.....	131
3.6.1 Analysis of selected sections of the Seaton Sluice exposure.....	131
3.7 Classifications of scours associated with trough cross-bedding.....	138
3.7.1 Classification of Seaton Sluice Sandstone cross-bed sets.....	138
3.7.2 Classification of scour structures on basis of their mean laminae dip.....	140
3.8 Analysis of scours associated with trough cross-bedding (scour structures) in Storey 1.....	141
3.8.1 Relationship between trough shape and size.....	141
3.8.2 Relationship of laminae dip direction to scour trend and comparison with the trough size and shape.....	143
3.8.3 Relationship of lamina dip to trough shape and size.....	147

3.9 Discussion.....	149
3.9.1 Discussion on relationship between classes and mean laminae dip direction.....	149
3.9.2 Discussion on the relationship between scour trend and mean laminae dip direction.....	150
3.9.3 Discussion on relationship between width:length ratio and laminae dip and variation in laminae dip.....	152
3.10 Re-interpretation of the nature of original channel.....	153
3.10.1 Estimates of channel dimensions.....	155
3.11 Conclusions.....	159

Chapter 4: Scour associated with bedforms and basal boundaries of cross-bed sets 163

4.1 Introduction	165
4.1.1 Review of research on bedform origin	166
4.2 Troughs and scours associated with bedforms.....	169
4.3 Mechanisms of scour initiation.....	170
4.4 Controls of scour geometry and scour occurrence.....	174
4.5 Scour and erosive surfaces in the field sites: Rillo de Gallo and Seaton Sluice.....	180
4.6 Other scour features.....	189
4.6.1 Pre-existing erosive surfaces on the channel bed.....	189
4.6.2 Scouring due to obstacle on the river bed.....	192
4.7 Conclusions.....	194
4.8 Suggested further work.....	195

Chapter 5: Flume Experiments 197

5.1 Introduction.....	199
5.1.1 Terminology.....	203
5.1.2 Introduction to the flume experiment with a solitary flume-scale unit bar.....	203
5.2 Experimental procedure.....	208
5.3 General observations on runs.....	211

5.3.1 Bed heights in Run 4.....	220
5.3.2 Water surface elevation in Run 4.....	224
5.3.3 Unit-bar geometry and crest shape evolution.....	226
5.3.4 General observations on the effect of bedform superimposition.....	229
5.3.5 Observations on counter-flow ripples.....	230
5.3.6 Unit-bar migration and the formation of cross-stratification.....	230
5.3.7 The deposits and cross-bed characteristics.....	232
5.3.8 Bar lee-face angle.....	234
5.3.9 Reactivation surfaces and bar lee-face angle variations.....	237
5.3.10 Evolution of bed topography and sediment feedback.....	238
5.4 Discussion.....	239
5.4.1 Classification of cross-stratification.....	239
5.4.2 Bar height variation and bar lee-face angle.....	241
5.4.3 Reactivation surfaces and bar lee-face angle.....	243
5.4.4 Topography variation and bar lee-face angle.....	247
5.5 Conclusions.....	250
Chapter 6: Field and laboratory research synthesis	253
6.1 Introduction.....	255
6.2 Different bedforms, similar processes?.....	257
6.3 What can and cannot be usefully compared?.....	261
6.4 Comparison of specific features.....	264
6.4.1 Lee-face angle.....	264
6.4.2 Superimposed bedforms.....	265
6.4.3 Reactivation surfaces.....	267
6.4.4 Bed topography and bottomset.....	269
6.4.5 Formative bedform crestline shape.....	272
6.4.6 Resulting cross-bedding types.....	273
6.5 What else needs to be considered in the comparison of flume and field research?.....	276
6.5.1 Grain size.....	276
6.5.2 Water discharge and sediment flux variability.....	277
6.5.3 River plan-form and size.....	280

Chapter 7: Conclusions	283
7.1 Addressing the original aims and objectives of this research.....	284
7.2 The main findings of this research that have significance beyond the individual case studies.....	294
7.3 Further work.....	296
References	299
Appendix A	325
Appendix B	373
Appendix C	391

Symbols

A	Cross sectional area of the flow perpendicular to the mean flow direction
d	Bankfull depth (Chapter 2 and 3)
d	Mean flow depth above solid channel base (Chapter 5)
d_b	Mean water depth above the brink point (m)
$d_{x=n}$	Flow depth at streamwise location $x = n$ m
D_m	Mean grain size
D_{50}	Median grain size
h	Bedform height
h_L	Lee-face height
h_m	Mean dune height
h_s	Slip-face height
H	Host bedform height
H_s	Superimposed bedform height
L	Scour structure maximum visible length
L_m	Meander wavelength
L_L	Lee-face length
L_s	Slip-face length
Re	Reynold Number
ST	Scour structure
t	Time (hh:mm:ss)
t_L	Height of lee-face toe
t_s	Height of slip-face toe
T_D	Trough depth at $t = 0$ s

T_L	Trough length at $t = 0s$
U	Mean streamwise velocity
\bar{U}	Mean velocity above the crest of the unit bar calculated from the discharge measured in the return pipes divided by A above the bed.
Q	Mean discharge (measured within the recirculating pipes)
W	Scour structure maximum visible width
W_m	Meander-belt amplitude
W/L	Scour structure width:length ratio
w	Bankfull width
x	Direction parallel to the channel axis with distance measured from the upstream end of the test channel
y	Direction across flow from right to left- looking downstream
z	Direction perpendicular to the solid bed of the test channel
α	Lee-face angle
β	Point-bar dip angle
θ	Angle between the mean laminae dip direction and the scour trend
λ	Bedform length
μ	Viscosity
ρ	Density
σ	Standard Deviation
UC	Unclear observations
N/A	No available data

List of Figures

Figure 1.1 Block diagrams illustrating terms applicable to cross-stratified units (Allen, 1963a).....	8
Figure 1.2 Block diagrams illustrating cross-stratification types and field examples from Seaton Sluice, Northumberland, UK.....	12
Figure 1.3 Block diagram illustrating 3-dimensional filled trough cross-bed scours.....	12
Figure 1.4 Schematic diagram illustrating the evolution from a straight to a sinuous-crested bed wave (Modification of Venditti <i>et al.</i> , 2005).....	13
Figure 1.5 Photographs of trough cross-bedding field examples (Rillo de Gallo, Guadalajara, Spain).....	14
Figure 2.1 Field study site location. (A) Aerial photograph of the region covering the study area; (B) Geological map.....	38
Figure 2.2 Aerial image of the study area illustrating the locations of: (A) exposures; (B) scour structures; (C) palaeocurrent measurements; (D) rock sample sites.....	39
Figure 2.3 Illustration of Lower Triassic (Buntsandstein) stratigraphy of the study region after Ramos, 1979).....	41
Figure 2.4 Model of the evolution of the Buntsandstein Facies in the study area, illustrating geometrical characteristics of alluvial facies (using images modified from Allen, 1965b).....	42
Figure 2.5 (a) Percentage frequency azimuthal plot of all of the palaeocurrent data (from scour structures and other sedimentary structures); (b) Percentage frequency azimuthal plot of the palaeocurrent data measured at the study site in field campaigns May 2011- May 2013 using only the mean value for each scour structure.....	43
Figure 2.6 Aerial photograph illustrating the localities revisited where Prados Formation was identified.....	44
Figure 2.7 Lithological log of the Prados Formation at the location of Rillo de Gallo.....	47
Figure 2.8 Characteristics of depositional facies types of the Prados Formation...	52
Figure 2.9 The Prados Formation hypothetical meandering model representing complete storeys (following Allen 1963b, 1970).....	54

Figure 2.10 (A) Photograph and sketch of the fluvial architecture of Exposure 1 at Rillo de Gallo; (B) Enlargement of area outlined by the box in A; (C) Plan view of cross-sets.....	57
Figure 2.11 Overview of Exposure 2 at Rillo de Gallo.....	58
Figure 2.12 Photographs and sketches of the fluvial architecture of Exposure 2 at Rillo de Gallo. (A) Sector 1; (B) Sector 2; (C) Sector 3; (D) Sector 4.....	61
Figure 2.13 Photograph and sketch of the fluvial architecture of Exposure 3 at Rillo de Gallo.....	64
Figure 2.14 Definition of: (a) Scour structure maximum width (W) and maximum length (L) and (b) Angle between the longer axis of the scour (scour trend) and the mean laminae dip direction. (c) Scour structures shaped in relation with their width:length ratio.....	67
Figure 2.15 Classification of scour structures on the basis of (a) size; (b) shape; (c) relationship between trend of scour and mean laminae dip direction and (d) type of bottomset contact with foreset toe.....	68
Figure 2.16 Classification of scour structures based on the initial scour shape and the angle between laminae dip direction and scour trend.....	69
Figure 2.17 Scour structure maximum measured width compared to maximum length of structures (case study I). (a) Scour structure size classification; (b) Scour structure shape classification.....	76
Figure 2.18 Polar representation of trough width:length ratio versus laminae dip direction (case study I): (a) Graph illustrating all scour structures with visible dimensions; (b) Graph illustrating the same data set in two differentiated modes.....	78
Figure 2.19 Dendrogram resulting from a hierarchical clustering statistical t-student test (square Euclidean distance method). Illustrating the identification of Modes I and II interpreted in Figure 2.18.....	79
Figure 2.20 (a) Polar representation of trough width:length ratio (W/L) versus trend of scour illustrating all scour structures with visible dimensions; (b) Rose diagram illustrating scour trends of the same data (case study I).....	80
Figure 2.21 (a) Relationship between trend of scour and mean laminae dip direction of all scour structures with visible dimensions; (b) Graph showing scour structures that have less than 40° difference between lamina dip direction and scour trend; and (c) Structures with a difference larger than 40° (case study I).....	82
Figure 2.22 Preservation level and field interpretation accuracy on the analysis of scour structure geometry.....	84

Figure 2.23 Relationship of trough dimensions to mean laminae dip angle (case study I).....	86
Figure 3.1 Satellite image covering the study area, Northumberland, UK.....	117
Figure 3.2 (A) Illustration of Upper Carboniferous (Westphalian B) stratigraphic succession; (B) Map of the study area and Westphalian B sequences.....	119
Figure 3.3 Structural framework of the United Kingdom relevant to the Carboniferous sedimentation (modified from Dean <i>et al.</i> , 2011 and Holzweber, 2012).....	121
Figure 3.4 Fluvial system model illustrating a low-sinuosity river with foreset macroforms and isolated linguoid and transverse bars (modified from Miall, 1985).....	122
Figure 3.5 Satellite image with overlapped geological map of the study area (A) Scour structure locations; (B) Bedding plan measurement locations.....	124
Figure 3.6 (a) Percentage frequency azimuthal plot of the palaeocurrent data measured from individual and grouped trough cross-bedding at the study site in field campaign June 2012; (b) Percentage frequency azimuthal plot of the bedding plane measured at the study site in field campaign June 2012.....	124
Figure 3.7 Lithological logs of outcrops: (a) section 1; (b) section 2 and (c) section 3. Satellite image illustrating the locations of lithological logs 1-10 and locations of lithological logs of Sections 1-3.....	126
Figure 3.8 Lithological logs and stratigraphic correlation at the Seaton Sluice study area.....	127
Figure 3.9 Characteristics of depositional facies types of Seaton Sluice Sandstone.....	130
Figure 3.10 Photograph and sketch of the fluvial architecture of Outcrop-Section 1 at Seaton Sluice.....	133
Figure 3.11 Photograph and sketch of the fluvial architecture of Outcrop-Section 2 at Seaton Sluice.....	135
Figure 3.12 Photograph and sketch of the fluvial architecture of Outcrop-Section 3 at Seaton Sluice.....	137
Figure 3.13 Scour structure maximum measured width compared to maximum length of structures (case study II). (a) Scour structure size classification; (b) Scour structure shape classification.....	142
Figure 3.14 Polar representation illustrating (case study II): (a) trough width:length versus trend of scour for all scour structures with visible dimensions; (b) trough width:length ratio versus laminae dip direction.....	143

Figure 3.15 (a) Relationship between scour trend and mean laminae dip direction of scour structures with visible dimensions; (b) Polar representation of trough width:length ration versus the laminae dip direction and scour trend comparison of scour structures less than 40° difference between lamina dip direction and scour trend; and (c) structures with a difference larger than 40° (case study II).....	145
Figure 3.16 Relationship of trough dimensions to mean laminae dip angle (case study II).....	148
Figure 4.1 (A) Illustration of trough between bedforms migrating in a unidirectional flow; (B) Illustration of scour within the trough between two migrating bedforms incising into the underlying sediments.....	170
Figure 4.2 Hypothetical mechanisms of scour initiation	173
Figure 4.3 Illustration of scour development into curved planform scours due to (1) variation of the flow pattern across the channel causing a variation of the bedform migration pattern; and (2) variation of the dominant flow direction downstream, also resulting in variations of bedform migration pattern.....	186
Figure 4.4 Cross-bedding styles and basal erosive surfaces types observed in field case studies.....	188
Figure 4.5 Model of mid-channel bar growth downstream of a confluence scour (modified from Ashworth, 1996).....	191
Figure 5.1 (A) Descriptive diagram of a unit bar and variables measured during the experiment; (B) Definition diagram for unit bars and cross stratification based initially on Allen’s (1963a) classification.....	200
Figure 5.2 (a) Descriptive diagram of flume tank not drawn to scale. (b) Grain size distributions of sediment used in the flume.....	204
Figure 5.3 Initial experimental set up (Runs 1-4).....	206
Figure 5.4 Photographs of Runs 1 and 2 with line drawing of deposit structure observed through side wall at end of each run.....	209
Figure 5.5 Photographs of Runs 3 and 4 with line drawing of deposit structure observed through side wall at end of each run.....	210
Figure 5.6 Location of samples collected at the end of Runs 3 and 4.....	211
Figure 5.7 Representation of lee-face height versus downstream distance in Runs 1-4.....	214
Figure 5.8 Representation of lee-face height versus time in Runs 1-4.....	214

Figure 5.9 Representation of unit-bar lee-face length versus downstream distance in Runs 1-4.....	215
Figure 5.10 Representation of unit-bar lee-face length versus time in Runs 1-4...	215
Figure 5.11 (A) Brink point moving upstream due to bedform superimposition and negative values of migration rate; (B) Increase of slip-face length as bar advances in Run 4.....	218
Figure 5.12 Variation of bed thickness slope with time throughout Run 4.....	222
Figure 5.13 (a) Profile of initial bed topography in Run 4; and mean bed thickness measured at 5 locations along the downstream distance from the flume side walls; (b) Variation of bed thickness at 5 fixed locations.....	223
Figure 5.14 (a) Variation of the static water surface elevation with time in Run 4; (b) Variation of the non-static water surface elevation with time in Run 4.....	225
Figure 5.15 (a) Static water elevation slope variation with time in Run 4; (b) Non-static water surface elevation variation with time in Run 4.....	226
Figure 5.16 Initial stage of the unit-bar stoss face in Runs 1-3.....	227
Figure 5.17 Development of unit-bar crest shape as bar advanced downstream: (A) Run 1; (B) Run 2; (C) Run 3 and (D) Run 4.....	228
Figure 5.18 Photograph illustrating trough deepening due to superimposed bedform reaching the host bedform brink point (Run 1, $t = 08:00$).....	229
Figure 5.19 Superimposed ripples climbing over the unit-bar and consequently the truncation of cross beds.....	232
Figure 5.20 Representation of unit-bar lee-face angle variation with downstream distance in Runs 1-4.....	235
Figure 5.21 Representation of unit-bar lee-face angle variation with time in Runs 1-4.....	235
Figure 5.22 Representation of unit-bar lee-face angle variation with unit-bar height in Runs 1-4.....	236
Figure 5.23 (A) Illustration of reactivation surfaces formation due to tall superimposed bedforms overtaking host bedform; (B) Preservation of reactivation surfaces (Run 1).....	238
Figure 5.24 Variation of the unit-bar migration rate with unit-bar height in Runs 1-4.....	243
Figure 5.25 Preservation of reactivation surfaces	245

Figure 5.26 Evolution of unit-bar morphology as bar advances downstream, showing the development of initial channel bed topography throughout Runs 1-4 and sediment feedback occurred.....	249
Figure A1 Boundary Surfaces classification.....	350
Figure A2 Key for lithological logs (valid for Chapters 2 and 3).....	350
Figure A3 Illustration of field methodology used in this study for the identification of storeys.....	351

List of Tables

Table 2.1 Characteristics of the individual scour structures identified in the Prados Formation.....	70
Table 2.2 Classification of individual scour structures at Rillo de Gallo using class definitions.....	71
Table 2.3 Classification in percentages of individual scour structures at Rillo de Gallo.....	73
Table 2.4 Maximum, minimum and mean laminae dip per scour structure and location of troughs within the sedimentary sequence at Rillo de Gallo.....	74
Table 2.5 Relationship of trough size to shape in percentages (case study I).....	76
Table 2.6 Descriptive statistics values obtained from analysis of the lamina dip direction variable (case study I)	79
Table 2.7 Descriptive statistics obtained from analysis of the scour trend variable (case study I).....	81
Table 2.8 Relationship of trough shape to the angle between the scour trend and lamina dip direction (case study I).....	83
Table 2.9 Relationship between trough size and the angle between scour trend and lamina dip direction (case study I).....	83
Table 2.10 Relationship of trough size to the lamina dip (case study I).....	87
Table 2.11 Relationship of trough shape to the lamina dip (case study I).....	87
Table 2.12 Coefficient of determination and significance of the relationship between scour structure classification classes and other variables (case study I)...	90
Table 2.13 Relationship of mean laminae dip direction modes and scour structure shape (case study I).....	91
Table 2.14 Relationship of mean laminae dip direction modes and scour structure size (case study I).....	91
Table 2.15 Relationship of scour structures size and stratigraphic position within the sequence (case study I).....	92
Table 2.16 Mean laminae dip in Exposures 1-3 at Rillo de Gallo.....	93

Table 2.17 Coefficient of determination and significance of the relationship between trough dimensions and mean lamina dip (case study I).....	94
Table 2.18 Estimates of mean and maximum values of dune height at Rillo de Gallo.....	103
Table 2.19 Estimates of channel depth/flow depth at Rillo de Gallo.....	103
Table 2.20 Estimates of channel width at Rillo de Gallo.....	104
Table 2.21 Previous studies' bankfull estimates empirical methods.....	104
Table 3.1 Characteristics of individual scour structures measured in Storey 1 of the Seaton Sluice Sandstone.....	138
Table 3.2 Classification of individual scour structures at Seaton Sluice using class definitions.....	139
Table 3.3 Classification of scour structures in the Storey 1 of the Seaton Sluice Sandstone.....	140
Table 3.4 Maximum, minimum and mean laminae dip per scour structure and location of troughs within the sedimentary sequence (case study II).....	141
Table 3.5 Relationship of trough size to shape (case study II).....	142
Table 3.6 Descriptive statistics values obtained from a descriptive analysis of the lamina dip direction variable (case study II).....	143
Table 3.7 Descriptive statistics values obtained from a descriptive analysis of the scour trend variable (case study II).....	144
Table 3.8 Mean lamina dip direction and scour trend paired sample t-test results (case study II).....	144
Table 3.9 Relationship of trough shape to the angle between the scour trend and lamina dip direction (case study II).....	146
Table 3.10 Relationship between trough size and the angle between scour trend and lamina dip direction (case study II).....	146
Table 3.11 Relationship of trough size to the lamina dip (case study II).....	147
Table 3.12 Relationship of trough shape to the lamina dip (case study II).....	147
Table 3.13 Coefficient of determination and significance of the relationship between scour structures classification classes and other variables (case study II).....	149

Table 3.14 Coefficient of determination and significance of the relationship between trough dimensions and mean lamina dip (case study II).....	152
Table 3.15 Estimates of mean and maximum values of dune height from Storey 1 and 2 at Seaton Sluice.....	156
Table 3.16 Estimates of channel depth/flow depth at Seaton Sluice.....	156
Table 3.17 Estimates of channel width (based on Storey 1 estimates) at Seaton Sluice.....	157
Table 3.18 Estimates of channel width (based on Storey 2 estimates) at Seaton Sluice.....	157
Table 5.1 Classification of cross-bedding following Allen (1963a) with additions inspired by the experiments described in Chapter 5.....	201
Table 5.2 Experimental conditions in Runs 1 – 4.....	205
Table 5.3 Velocity probe locations in Runs 1-4.....	207
Table 5.4 Water pump start and end times throughout Run 4.....	207
Table 5.5 The bed, superimposed bedforms and deposits.....	219
Table 5.6 Migration rates and distance reached by unit-bar brink point in Runs 1-4.....	232
Table 6.1 Characteristics of planar cross-sets observed at Seaton Sluice and flume experiments (modified of Haszeldine, 1983a).....	275

Chapter 1

Introduction



Photo: Prados Formation, Rillo de Gallo, Spain.

The processes of sediment transport and deposition in rivers and the resulting sedimentary structures are of high interest to sedimentologists, geomorphologists and civil engineers. The study and interpretation of fluvial systems allows palaeoenvironmental reconstruction of the system, understanding the rivers as agents of floodplain construction and modification; and generates reliable information about the engineering issues for navigation and commerce (Allen, 1983a). Fluvial sandstone bodies are oil and gas reservoirs; and a large quantity of the world's potable water is stored in aquifers of fluvial origin (Bridge and Tye, 2000). The study of sediment in fluvial systems has a long history dating back to Sorby (1859) and Gilbert (1914). Their investigations focused on the understanding of sediment transport and bedform behaviour. This thesis, based on the investigation of two field case studies and a series of flume experiments, aims to improve the understanding of fluvial cross-bedded sandstones and the understanding of the physical processes responsible for specific characteristics of sedimentary deposits generated by fluvial systems.

One the most important characteristics of sediment transport over a bed of loose sediment is the development of bedforms. Bedforms are primary sedimentary structures. They form at the time of deposition of the sediment in which they occur and they reflect some characteristic(s) of the depositional environment. The interaction between sediment and water flow generates bedforms; the behaviour of which forms sedimentary structures that may be preserved in the rocks and become part of the sedimentary record preserving snapshots of fluvial systems. Sedimentologists, geomorphologists and civil engineers agree that it is of great importance to better understand the bedform dynamics in river systems. To fully understand bedform development, investigations of scour formation and mechanisms of scour development are necessary. Some of the main reasons why the understanding of bedforms and scour are important are:

1. Bedforms are the most important source of flow resistance in river channels. Scouring influences bedform development and bedform dimensions (e.g., dune height increases with trough-scouring). Evaluating bedform superimposition, bedform dimensions and depth of scouring and the association of formative bedforms and scour are important for the maintenance and safety of any buried infrastructure (i.e., pipelines or cable routes), which must remain underneath the

channel bed (Ampster and García, 1997; van der Mark *et al.*, 2008). The effects of fluid flow on mobile sediment beds is an important subject as it covers the practical problems associated with transporting water. The transport of sediments in excavated canals in unconsolidated sediments results in the formation of bedforms. These can alter the character of the flow and affect fundamental flow properties. The presence of bedforms retard fluid flow and so, it is important in engineering to be able to predict the formation of bedforms and bedform types in order to design canals on unconsolidated sediments.

2. The understanding of the linkage between bedform evolution (often dominated by erosion due to trough-scouring) and sediment transport is of great use for civil engineers for the ultimate control and prediction of the dynamics of the system. Bedform migration constitutes the main process of bedload transport in river channels. Sediment transport within river channels are controlled by bedform initiation, growth, decay and the associated processes of scouring. Sediment transport processes, erosion and scouring will affect the flow dynamics within the channel and within particular places of the channel (Kostaschuck *et al.*, 2009). This will modify the dynamics of bedform development and therefore the resulting sedimentary structures.
3. The understanding of bedform forming processes is crucial in sedimentary geology. Bedform formation and migration may result in sedimentary structures preserved in the rock record and these may be used as evidences of the past fluvial environments (Bridge, 2003). Since bedforms and their behaviour are partially governed by fluid processes, bedform type and the resulting cross-stratification as bedforms migrate provide useful information for making paleohydraulic interpretations of ancient depositional environments. Palaeoenvironmental reconstructions of depositional systems styles from ancient fluvial deposits are heavily dependent on the interpretation of the preserved sedimentary structures. Thus, the investigation on the relationships between the preserved rocks and bedforms dynamics are crucial for accurate interpretations of the original fluvial systems.

Cross-stratification consists of the arrangement of sediment strata deposited at one or more angles to the main stratification. Cross-stratification produced by dunes and unit bars is the most common sedimentary structure in sandy river-channel deposits (Bridge, 1997; Reesink and Bridge, 2007). Cross-bedding analysis is important as it helps the understanding of sedimentary deposits and may be used to understand flow direction, flow velocity, flow character and water depth during the deposition of sediments. Although most published research on cross-bedding focuses on the interpretation and understanding of ancient fluvial systems, the study of these internal structures provides information about how modern bedforms behave and interact with other bedforms. This is very important in fluid dynamics and modelling, because to produce accurate bedform-flow interaction models, it is necessary to fully comprehend bedforms and flow behaviours (Rubin, 1987). Flow dynamics plays an important role in the reconstruction of fluvial systems. Understanding the nature of sedimentary structures from the context of physical processes helps to generate a reliable interpretation of river behaviour from the study of the cross-strata. There are several basic properties of the fluid (water) that should be investigated and understood, such as: water depth, velocity, viscosity, density, discharge and shear bed stress (Bridge, 2003). Two main factors are critical in the study of fluvial systems from cross-bedded deposits, these are: geometry and fluid dynamics.

There is an extensive body of published work on flume experiments, with the main objective of testing and developing theoretical models for interpreting cross-strata thickness, preserved and formed due to the migration of bedforms (e.g., Bridge, 1997; Leclair and Bridge, 2001; Storms *et al.*, 1999). Physical and empirical relationships based on flow and sediment properties from field and flume data were calculated to predict bedform dimensions under steady flow conditions. These relationships present certain limitations such as that bedforms are considered as periodic features. Bedforms that occur in natural fluvial systems are irregular in size, shape and spacing. Therefore applying mean values is not sufficient in all case studies and bedform type and dimensions variability should be taken into account (van der Mark *et al.*, 2006).

This Ph.D focuses on the investigation of cross-bedded sandstones formed by the migration of large-scale bedforms in fluvial environments. In addition, this study aims

to improve the understanding of the geometries resulting from sedimentary structures formed due to large-scale bedform migration. In particular, the investigation of sedimentary structures with concave-up base or scour structures (single trough cross-bed sets) and their association with formative 3-dimensional bedforms and the basal bounding surfaces (scours). The importance of their investigation is highlighted here. A better understanding of scour structures geometries and the processes that formed them will improve our knowledge of:

- Understanding bedform type associated with scour structures.
- Understanding flow conditions characteristic of forming bedform types that will migrate and generate scour structures.
- Understanding formative bedform migration patterns associated with scour. This may provide useful information on channel plan-form type and depositional system type.
- Differentiation from scour structures associated with migrating bedform type and pre-generated scours or due to erosion surfaces.
- Understanding bedform development processes as they migrate downstream forming scour structures.

This will ultimately improve palaeoenvironmental reconstructions of ancient fluvial deposits.

Low-sinuosity, sandy braided rivers and the lower part of point bars in meandering rivers are the most likely geological context for the cross-bedded sandstones formed by fluvial subaqueous dunes and unit bars that were selected for this research. The types of flow systems can be studied at a variety of scales, the sedimentary deposit of a single bar (small scale), or the deposits accumulated by the different processes in a whole river system (large scale). Three different approaches for the study of dunes, unit bars and cross-bedding are: laboratory experimental work, field work on modern rivers and field work on ancient fluvial deposits. This project involved both laboratory experiments and field work on ancient deposits. It also draws on published studies of modern rivers, flume experiments and other research.

1.1 Definition, origin of cross-stratification (dune and unit bar migration) and classification

Cross-bedding has been defined as a structure confined to a single sedimentation unit (Otto, 1938) consisting of internal bedding, called foreset bedding, inclined to the principal surface of accumulation. Other names have been used for cross-bedding such as: cross-lamination, cross-stratification, current bedding, diagonal bedding, false stratification, lee-side concentration, oblique bedding, oblique stratification and some other terms with self-evident modifiers (Potter and Pettijohn, 1963). Most of these terms are no longer widely used. Cross-lamination is broadly used and is generally applied to refer to thin sets that are most likely formed by ripples. The terms cross-bedding and cross-stratification are used interchangeably; cross-stratification has been described in several ways by numerous authors and there is still not an agreed definition (cf. Allen, 1984). Cross-stratification consists of layers arranged at one or more non-zero angles to the primary bedding orientation (McKee and Weir, 1953). Allen (1962) defined this term as layers that are texturally and compositionally distinct and also more or less steeply inclined to the main surfaces of accumulation of the formations in which they occur. These layers are generally, but not always, bounded by erosional bedding surfaces that are often sub-parallel to the main planes, resulting in different types of cross-stratification units and patterns.

Cross-stratification types have been classified based on criteria such as dynamics by kinematics, geometry, lithology, and evidence exclusively observed in two dimensions (e.g., Zhemchuzhnikov, 1926; McKee and Weir, 1953; Jopling and Walker, 1968 and others) (Allen, 1963a and 1984). Put simply, cross-stratification consists of layers within sediment or a sedimentary rock that are orientated at an angle to the depositional horizontal.

The migration of bedforms results in the formation of cross-strata, a common sedimentary structure in sandstones of fluvial origin (Blom and Kleinhans, 2008; Leclair, 2002). According to McKee and Weir (1953) cross-stratum consists of “*a single layer of homogeneous or gradational lithology deposited at an angle to the original dip of the formation and separated by surfaces of erosion, non-deposition, or abrupt change in character*”. Strata thickness will define if the cross-strata are either a

cross-bed (greater than 10 mm) or a cross-lamina (10 mm or less). The migration of ripples forms cross-lamination whilst the migration of larger bedforms, for example dunes, will result in cross-bedding.

Allen (1963a), building on previous work, suggested a classification based on six criteria (Fig. 1.1): (1) type of grouping of cross-stratified set; (2) physical size measured by set thickness; (3) character of lower boundary surface of cross-stratified set; (4) shape of the lower boundary surface of the set or coset of cross-strata; (5) the angular relation of the cross-strata to the lower bounding surface of the set or coset of cross-strata and (6) the degree of lithological uniformity of the cross-strata in the set or coset of the cross-strata.

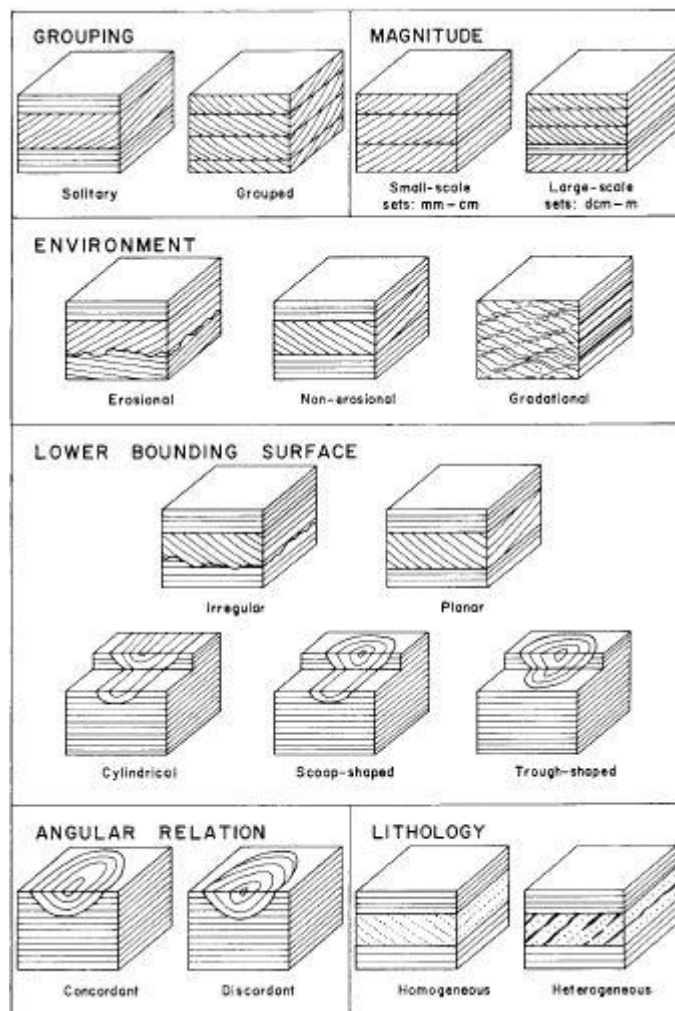


Figure 1.1 Block diagrams illustrating terms applicable to cross-stratified units (Allen, 1963a).

The types of cross-bedding formed by migration of subaqueous dunes and unit bars are central to this project. Bars are large-scale bedforms with width and height dimensions of the same order of magnitude as the channel within which they are formed. Bridge (1997) considers that unit bars are ubiquitous in fluvial systems and are generally under studied. They can be made up of sandy sediment, gravelly material or mixtures of coarse grain sizes. In a sandy channel the surfaces of bar forms are covered with subaqueous dunes, which migrate over the bar surface and result in the formation of units of cross-bedded sands. The term unit bar has been used widely since first defined by Smith (1974) as relatively unmodified bars whose morphologies are mainly determined by depositional processes (e.g., longitudinal, transverse, point and diagonal bars. They are large bedforms and these “mesoforms” (cf. Jackson 1975) are “*quasi-periodic or solitary storage bodies that occur in the channel (scaled to depth)*” (Smith 1974). Ashley (1990) stated that they “*have simple depositional histories controlled by “local” hydraulic conditions such as changes in water depth and flow competence*”. Geoff and Ashmore (1994) defined them as “*any simple, largely depositional form, on the scale of the width of an individual anabranch*” (e.g., diffused gravel sheets and lobes). Sambrook Smith *et al.* (2006) defined them as “*having a shape that remains relatively unmodified during migration, and being simple forms that are not amalgamated/superimposed upon other bar forms*”. They have been also interpreted as active gravel bars with simple histories and depositional morphologies (Hassan, 2009). Ashworth *et al.* (2011) defined them as “*solitary bar forms that have simple depositional histories and a lobate plan-form, with their highest point being at the downstream end of the bar that terminates in an avalanche face that may be at the angle-of-repose*”. Reesink and Bridge (2011) describe unit bars as “*lobate bedforms with lengths that are proportional to the flow width and heights that can approach bankfull depth*”. Unit bars have been also subdivided into different types such as: longitudinal, transverse, point and diagonal bars (Smith, 1974) and crescentic bars (Church and Jones, 1982). The term sand flat also interpreted as unit bar, was subdivided based on bar morphology into symmetric, asymmetric and side-flats (Cant, 1976). Unit bars were also classified based on where they arise within the channel (e.g., confluences, curvatures) and therefore they are described as forced bars if the bar formation was induced by features within the channel (Seminara and Turbino, 1989; Turbino and Seminara, 1990; Whiting and Dietrich, 1993, Tubino *et al.*, 1999). In

contrast, free bars can spontaneously develop and migrate downstream. Rice *et al.* (2009) described the terms flank bar and bar-head unit bar to indicate that unit bars can interact with and be modified by sedimentary structures (e.g., compound bars and islands) within the channel. They subdivided unit bars into primary and secondary origin.

Unit bars have greater lateral extent than smaller bedforms (e.g., dunes) within a single system; which may help to classify migrating bedforms as bars or dunes based on their dimensions. Unit bar lateral extent is related to the bankfull width whereas dune height is related to the bankfull depth. Thus dunes might be distinguished from unit bars within a single system. Larger rivers can have larger dunes, and these could be classified as bars if occurring in a smaller river. The cross-stratification produced by the migration of the bar and dunes or megaripples (cf. Allen, 1963a; Bridge 1997) are very similar in settings where the lee face of unit bars is steep. Therefore accurate interpretations of ancient fluvial deposits identifying if the cross-stratified sets were formed by migrations of steep unit bars or large dunes are still debatable. In this thesis, the interpretation of the formative migrating bedforms is mainly based on the preserved cross-stratified deposits following previous published work in the field sites and by comparison with similar deposits in other areas previously interpreted. On the scale of the bedform, similar processes and resulting deposits occur (cf. Section 6.2); therefore for a better integration of field observations and cross-stratified deposits generated in the flume, dunes and unit bars are herein treated and described as large-scale bedforms.

Following the work of Allen (1963a) based on the shape of the lower bounding surface of the set or coset of cross-strata (criteria 4) cross-bedding is classified as planar, trough-shaped, irregular, cylindrical and scoop-shaped. By taking into account the upper and lower bounding set surfaces there is another type of cross-bedding known as tabular. This thesis includes the study of ancient and experimental examples of planar, trough-shaped and tabular cross-bedding (Fig. 1.2).

Planar cross-bedding results from the migration of straight-crested dunes or unit bars and a flow separation with a weakly developed roller vortex and minor scouring at the reattachment point. The foresets form at the angle in which the sands are resting on the

lee face of the dune. The basal contact becomes angular because of avalanching on to the erosion surface in the trough and the base at the bottom of the cross-bed is flat. Straight-crested bedforms have more or less straight flow-reattachment lines, which generally generate planar surfaces of erosion as the bedforms advance downstream, producing cross-bed sets separated by planar bounding surfaces. This is referred to as planar cross-bedding (Bridge, 2003).

Trough cross-bedding forms from migration of sinuous or isolated (linguoid or lunate) crested dunes or possibly unit bars. This is often associated with flow separation with a strongly developed roller vortex and marked scouring at the reattachment point. The lower contact of the cross beds may form a sharp angle at the base of the avalanching slope or be tangential to the basal boundary. The lower set boundary is not flat. Harms and Fahnestock (1965) defined trough-shaped sets as elongate erosional scours parallel to the local stream flow direction infilled with curved laminae. Curved-crested bedforms present curved flow-reattachment lines and concave-up erosional surfaces bounded laterally by flow-parallel spurs. The migration of curved-crested bedforms forms cross-bed sets whose lower boundary surface is trough-shaped. This is referred to as trough cross-bedding (Bridge, 2003).

Tabular cross-bedding forms due to the migration of bedforms with straight crestlines (e.g., transverse bars) (Jones, 1979). This term is used to define the shape of the sets. Tabular implies that the set erosive bounding surfaces are flat and horizontal or nearly horizontal and parallel (Harms and Fahnestock, 1965). According to Collinson and Thompson (1982) sandwaves generate tabular sets of wide lateral extent with internal foresets either asymptotic (tangential based) or planar (angular-based). Leeder (1999) suggested that tabular cross-laminae result from the migration of straight-crested ripples as well as from the migration of 2D dunes that develop cross-stratification bounded by prominent horizontal to near horizontal scoured surfaces.

Blatt *et al.*, (1980) classified cross-bedding according to the upper and lower bounding surfaces of sets in three main types: (1) Tabular: bounded by essentially plane, parallel surfaces; (2) Wedge-shaped (planar): bounded by plane, non-parallel surfaces and (3) Trough: lower bounding surface is trough or concave-up.

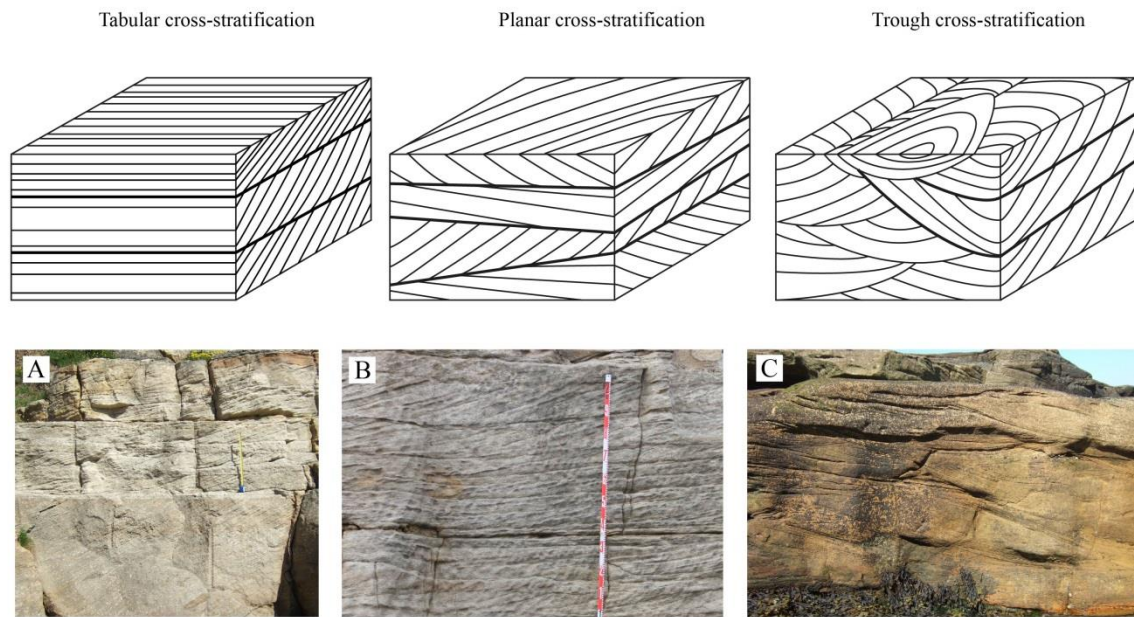


Figure 1.2 Block diagrams illustrating cross-stratification types and field examples from Seaton Sluice, Northumberland, UK. (A) Tabular cross-stratification; (B) Planar cross-stratification and (C) Trough cross-stratification.

1.2 Introduction to trough cross-bedding and single trough-cross bed set term

Trough cross-bed sets consist of erosional scours filled with dipping and concave-upwards laminae. These scours are elongate and generally parallel to the stream flow direction and the internal laminae that fill the scour dip in the downstream direction (Harms and Fahnestock, 1965) (Fig. 1.3).

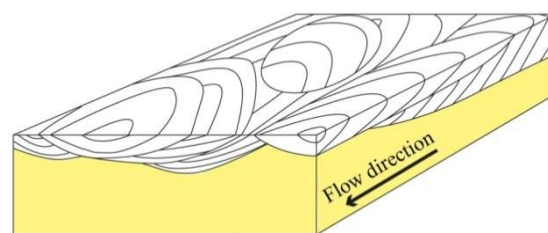


Figure 1.3 Block diagram illustrating 3-dimensional filled trough cross-bed scours.

Allen's (1963a) classification of cross-stratified units includes several types that are characterised by scoop-shaped erosive scours filled with inclined laminae (e.g., types θ , ι , μ , and π ; cf. Allen's classification of cross units, 1963a). Harms and Fahnestock (1965)

also defined them as troughs or scours infilled with scoop-shaped laminae plunging in the downstream direction. Sorby (1852) was the pioneer of palaeocurrent analysis as a tool to carry out palaeoenvironment reconstructions, and used plan-form trough scours as excellent palaeocurrent indicators. Palaeocurrent data analysis provides information on: (1) Local and regional palaeoslope directions; (2) Depositional environment; (3) Origin of sediment supply and (4) Geometries and trends of the lithological facies (Miall, 1984). The initiation of scours occurs due to vortex erosion downstream from the migrating bedform (Miall, 1984). According to Blatt *et al.* (1980) the mechanism that generates scour downstream of 3-dimensional ripple lee face (applicable to 3-dimensional dunes) consists of events of flow separation with formation of a static eddy that rotates around a horizontal axis. This mechanism is also described by Allen (1968a) to explain the formation of sole marks such as flutes. In contrast, Harms and Fahnestock (1965) suggested that if localised scours erode deep and long depressions that are immediately filled with inclined forests as dunes migrate downstream, then that scour formation is not closely related to either bedform lee-face advance or eddies downstream of an advancing dune. They believed that scouring may occur in areas susceptible to erosion and at a relatively high flow velocity near the bed. Scouring is most likely to occur in between dunes and when either there is no avalanche face or if it is very low. Venditti *et al.* (2005a) studied the transition from 2D dunes and 3D dunes (Fig. 1.4).

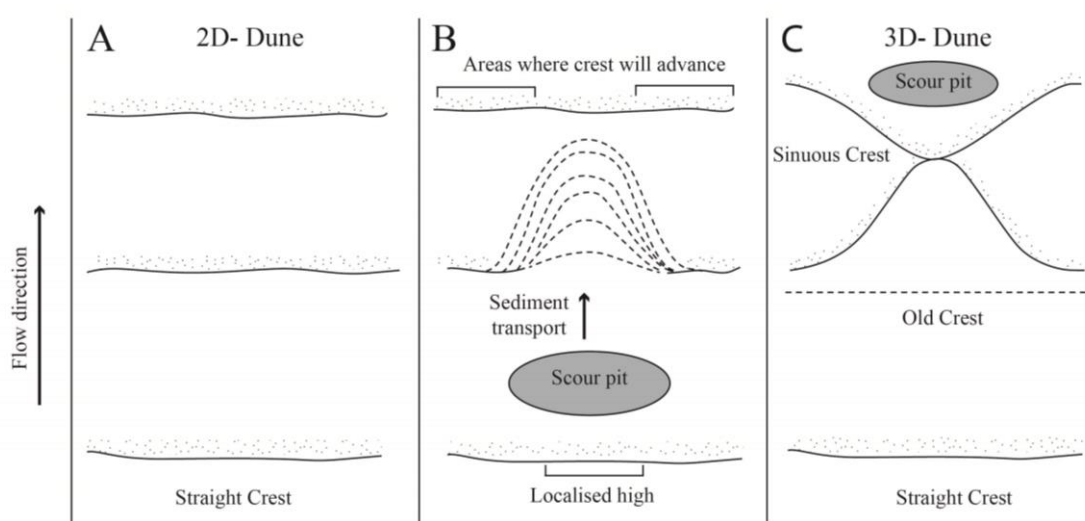


Figure 1.4 Schematic diagram illustrating the evolution from a straight to a sinuous-crested bed wave (modified from Venditti *et al.*, 2005a).

He suggested that 3D dunes form due to the development of scours downstream of the bedforms lee (Fig. 1.4). The lobe extension from a high localised area downstream starves straight crests downstream, generating sinuous crests. The development of the dune-crest shape appears to be associated with the formation of concave-upwards scour-pits and this agrees with the Harms and Fahnstock (1965) theory of “scouring” between bedforms.

Single trough-cross bed sets are formed by the migration of trains of 3-dimensional dunes. Due the long wording of the term, single trough cross-bed set is referred throughout the thesis as ‘scour structure’. These structures have been described and given nomenclatures by numerous authors. In plan-view they are present as a large version of the “rib and furrow” described for cross-lamination (Stokes, 1953) formed by the migration of sinuous ripples.

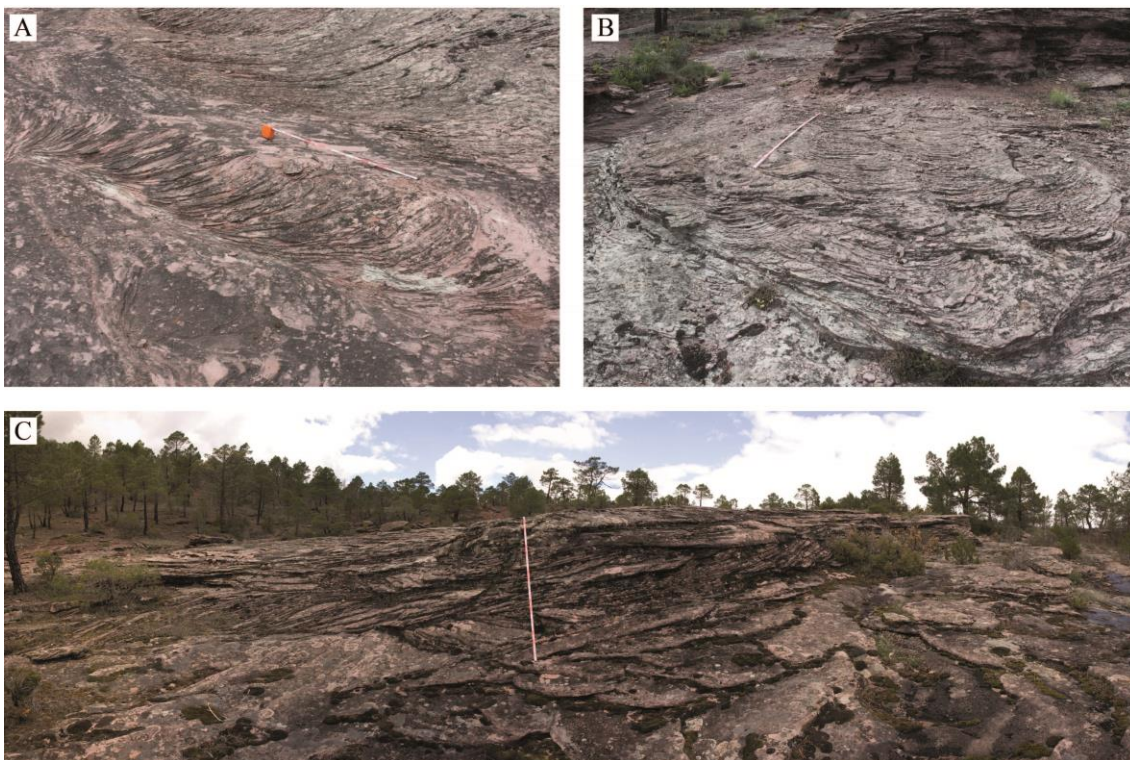


Figure 1.5 Photographs of trough cross-bedding field examples (Rillo de Gallo, Guadalajara, Spain). (A) Plan-view of an isolated trough cross-bed set; (B) Plan-view of grouped trough cross-bed sets; (C) Vertical-3D profile of grouped trough cross-bed sets.

Frazier and Osanik (1961) described similar features observed as distinctive cross-bedded units that rest over a concave-upwards erosive surface and are typified by

concave-upwards bedding planes. Collinson and Thompson (1982) defined them as form sets filled with cross-laminae. These trough cross-bed sets are usually concave-upwards with tangential lower contacts and commonly are concave-up-shaped (Fig. 1.5). Haszeldine (1983a) described them as groups or isolated sets of trough cross-strata generated by dune migration eroding the underlying sediments with concave-up set bases. He suggested that the occurrence of isolated trough sets indicates that the forming dunes were lunate rather than linguoid.

1.3 Cross-stratification thickness as an interpretational tool

Estimating the original heights of bedforms and river channel dimensions is critical to improve the quantitative reconstruction of ancient fluvial systems. In addition, determining the thickness and width of sandstone bodies is one of the main objectives in exploration and development of fluvial reservoirs. Understanding relationships between set size and sandstone body size has important implications. Most ancient systems are not fully preserved due to cross-bed truncation and erosion which generates inaccurate interpretations. Understanding the relation between bedform height and preserved cross-strata thickness should improve techniques of channel dimension estimation and potentially aid sandstone body size estimates.

Paola and Borgman (1991) formulated a theory for the probability density function (PDF) of set thickness produced by topography of random height and considering a state of no net deposition. They assumed that the heights of bed-wave crests and the depth of troughs are equally distributed above the mean bed level. Bridge (1997) stated, that the thickness of cross sets, identified in cross section parallel to mean flow direction at a given point, depends on the following factors: mean deposition rate in relation to the bed-wave migration rate, variability of the height of the bed-waves of a given scour depth passing at the given location and the variation in geometry and migration rate as the bedforms migrate. This last control has still not been proved. Leclair *et al.* (1997) considered that cross-set thickness was underestimated due to the assumption that the height of bedforms spread evenly above and below the mean bed level. Bridge and Best (1997) adapted Paola and Borgman's (1991) theoretical model for aggrading conditions and these results proved that from the distribution of planar laminae; distribution of bedform height, aggradation rate, mean bed wave length or celerity could be estimated.

This new model could be used to estimate the height distribution of bedforms (ripples, dunes and low-relief bed waves). Leclair and Bridge (2001) used data collected from flume experiments and the Mississippi and Calamus rivers to test a new version of Paola and Borgman's (1991) theory, and develop a successful new model that allows the prediction of dune height distribution from the distribution of cross-set thickness and vice versa. Leclair's (2006) model focuses on morphodynamic analysis of subaqueous dunes in order to reconstruct the palaeoenvironmental conditions of fluvial systems. She proposed a new method for the interpretation of fluvial deposits from the cross-strata preserved, taking into account net aggrading rates by combining two theories that relate (1) the geometry of preserved cross-sets to the river bed topography and (2) the active dune topography to the sediment transport. This method improved the interpretation of sedimentary structures and palaeoenvironments and probably can be developed further.

Several authors have attempted to estimate channel dimensions by using empirical equations that depend on channel-pattern parameters derived from modern rivers (Collinson, 1978; Lorenz *et al.*, 1985; Fielding and Crane, 1987 and others discussed by Bridge and MacKey, 1993), but there is a very large scatter in the data. By using larger data sets, interpretations can be more accurate (e.g., Bridge and MacKey, 1993). Bridge and Tye (2000) presented a revised approach, building on previous research for the calculation of ancient fluvial channel dimensions, which includes the interpretation of maximum palaeochannel depth from the thickness of channel bars and the set thickness of cross-strata formed by dunes. Channel-belt width and thickness can vary spatially within one channel belt and between different channel belts making the estimation of channel-belt width particularly difficult. Bridge and Tye's (2000) qualitative approach is supposed to minimise the inaccuracies of the established techniques for the estimation of the widths of the channel belts or connected channel belts that constitute the sandstone bodies. These techniques are: correlation of log signatures between wells; the use of outcrop analogues; empirical equations derived from studies of modern rivers relating channel-bar thickness to maximum palaeochannel depth, channel width, and channel belt width and direct estimation from amplitude analysis of 3D seismic time slices. They proposed a combination of approaches. These are: (1) new models for the 3D variation of lithofacies and petrophysical-log response of river-channel deposits with

explicit recognition of the different superimposed scales of strata, (2) distinction between single and superimposed channel bars, channels, and channel belts, (3) interpretation of maximum palaeochannel depth from the thickness of channel bars and from the thickness of cross-strata formed by dunes and (4) evaluation of methods for estimating widths of sandstone-conglomerate bodies that represent either single or connected channel belts.

The methods used in this research to estimate channel dimensions were (1) the geometry and lithofacies of channel and channel-belt sandstone bodies and (2) using cross-bed set size following the approach of Leclair and Bridge (2001). Reliable interpretations depend on the quality of the exposure and the depositional models used during interpretation. The understanding of modern depositional environments is still not complete due to the lack of quantitative analysis and 3D interpretations (Bridge and Tye, 2000).

1.4 Flume experimental work relevance and its linkage with field studies.

Flume experiments have been carried out to understand the origin of cross-strata based on grain sorting mechanisms. Jopling (1966) undertook several flume tests to study different possible sorting mechanisms responsible for cross-bedded sediments. He showed that internal sedimentary structures are primarily formed by hydrodynamic and rheologic sorting processes under uniform conditions of sediment transport. Mechanisms such as selective transport, dispersive pressure and pulsatory particle movement contribute to the bedded structure formation (Jopling, 1964). The internal structures in cross-bedded sandstones result from the sediment sorting in the avalanche at the lee side of the dune, the selective transport and deposition in the dune troughs. Kleinhans (2004) summarised the factors controlling vertical sorting in dunes and aimed to define a model to predict sediment sorting in dunes. These factors are: sorting of the sediment mixture that reaches the dune brink point; dune or bar height relative to the average grain size of the mixture; flow velocity above the brink point relative to the settling velocity for all grain size fractions and frequency of the grain flows determined by dune celerity and the celerity of the grain flows on the foreset slope. Blom and Kleinhans (2008) presented an evidence of principle for using a new model to estimate

bedform height from the sorting preserved in cross-bed sets formed by dune migration. Their model gives reliable estimates of bedform height under specific restricted conditions but has a few experimental limitations. It systematically underestimates bedform height, which indicates that the obtained values are slightly lower than the original height. This method has only been applied to partially preserved deposits generated in flumes and not to the rock record.

The morphodynamics of bedforms, changes in geometry and the transition between bedform types have been studied by several authors (e.g., Southard, 1971, 1991; Carling *et al.*, 2000; Robert and Uhlman, 2001; Venditti, 2005a; Fernández *et al.*, 2006; Leclair, 2006; Raudkivi, 2006; Van der Mark *et al.*, 2008). A number of experiments carried out in flume laboratories aimed to investigate and develop relationships between the geometry of bedforms, the quantity of transported sediment and the formative bedforms and their evolution (e.g., Alexander *et al.*, 2001; Leclair and Bridge, 2001; Leclair, 2002; Tuijnder, 2009; Warmink *et al.*, 2014). Other types of flume experiments aimed to reproduce realistic models of fluvial systems (e.g., Ashworth, 1996; Peakall *et al.*, 2007) aiming to understand the systems' behaviour; other studies apply flume experiments to investigate particular river characteristics under controlled conditions and then apply the results to ancient and modern systems (Van de Lageweg *et al.*, 2013) and others aimed to improve the understanding of flow conditions, sediment transport and bed morphology (Smith, 1998). Although the outcome of this research is extremely valuable, these studies have an ongoing issue of scaling that has implications in the comparison of field and flume models.

In this thesis, the experimental work was a series of flume experiments using specific setups for each run, enabling focus on specific controls on deposit characteristics and using these observations to improve interpretations of preserved deposits from ancient fluvial systems. Chapter 6 shows some of the features that are found to be comparable in field studies and flume experiments and that add valuable information for the reconstruction of the fluvial systems that formed the sandstones observed in the study sites, as well as improving the understanding of the bedform type that generated specific cross-bedding styles. These features are: (1) the investigation of lee-face angle variation of individual laminae within cross-bedded sandstone and trough sets; (2) the

investigation of the bar lee-face modifications and preserved cross-bedding due to bedform superimposition; and the formation and preservation of reactivation surfaces and the implications that these have on the lee slope variation; (3) the analysis of the relationship between pre-existing bed topography and the resulting cross-bedding type; (4) the formation of bottomsets and their association with formative bedform type (e.g., dunes or/and bars). This will help to understand the flow conditions forming the deposits; and (5) the importance of bedform crestline variation and its effect on bedform geometry as bedforms advance downstream; and the effect of variations of flow direction on bedform migrating patterns and the subsequent changes in bedform crestline morphology.

Although flume experimental work has significant limitations when compared with field observations, the data obtained from flume experiments provide useful information on bedform scales and the associated flow conditions, variation of bedform geometries, migration pattern, reactivation surfaces (formation and preservation), bottomset formation and associated bedform type. This information improves the understanding of bedform development and the resulting deposits and so it will improve palaeoenvironmental reconstructions based on ancient fluvial deposits.

Reconstructions of depositional fluvial environments can be very limited due to the quality of exposure and level of preservation and the limitations involved in using comparisons with artificial fixed systems recreated in flume laboratories (cf. Chapter 6). More investigation using flume experiments, modern systems studies and further interpretations of rock record analogues are necessary to improve our understanding of modern and ancient depositional environments.

1.5 Terminology

An explanation of the terminology used in this thesis is presented below. Because of the confusion in the literature resulting from the diverse nomenclature used by different authors to define the same concepts, here I define how I use terms, to prevent any ambiguity.

Bed: Sedimentary layer thicker than 10 mm bounded by distinctive surfaces (i.e., “*bedding planes*”).

Bedform: Morphological feature formed by the interaction between flow and cohesionless sediment on a bed.

Bed-wave: Term used by several authors equivalent to “*bedform*”.

Bottomset: Basal set formed by deposition of suspended sediment, reworked sediment within the bedform trough and reverse flow small-scale bedform formation (i.e., counter-flow ripples).

Boundary surfaces: Upper and lower surfaces that subdivide sedimentary sequences in different sections. They are classified in a hierarchical order to allow for differentiation of the sedimentary sections that are bounded.

Brink point: Point where sediment particles begin to avalanche down the bedform lee face. This point marks the limit between the stoss and the lee face of the bedform. It is the location at which the flow separates from the bed surface, causing a turbulent counter-flow in the lee of the bedform (Kleinhans, 2004).

Channel-belt: Area of land a channel occupies between successive avulsions. As individual river channels migrate, the channel position within the channel-belt changes, such that channel deposits are found over a greater area than occupied by the channel at any one time.

Coset: A group of sets vertically stacked.

Counter-flow ripple: Ripple formed within the lee-face of a larger bedform that migrates in the opposite direction to that of the host bedform.

Crest: Cross-sectional axis separating lee and stoss face of a bedform.

Cross-bedding: Term interchangeable with cross-stratification.

Cross-lamination: Layers less than 10 mm thick of sediment or sedimentary rock, oriented at an angle to the depositional horizontal (e.g., the migration of ripples form cross-bedding).

Cross-stratification: Layers greater than 10 mm thick of sediment or sedimentary rock that is oriented at an angle to the depositional horizontal (e.g., the migration of larger bedforms form cross-stratification).

Dune: Bedform generated by the interaction of flow and sediment. As sediment transport rate increases in a rippled bed, larger bedform (dunes) form. In Chapter 5 bedforms with $\lambda > 0.180$ m are considered dunes.

Exposure: Visible ancient superficial deposits on the surface of the Earth.

Facies: Body of rock with specified characteristics that reflect the conditions under which it was formed.

Foreset: Cross-laminae formed by deposition onto and grain avalanching flows down the bedform lee face.

Formation: Lithostratigraphic body of material that can be identified by its lithological characteristics and its stratigraphic position. It can also be traced laterally and can be mappable at the surface or in the subsurface.

Height of the lee-face toe: Vertical distance from the lee-face toe to the base of the channel.

Height of the slip-face toe: Vertical distance from the slip-face toe to the base of the channel.

Laminae dip: Dip angle of individual laminae forming cross-bedding.

Laminae dip direction: Direction towards individual laminae forming cross-bedding dip.

Lee face: Bedform front face over which grains avalanche downstream.

Lee-face height: Vertical distance from the brink point to the lee-face toe.

Lee-face length: Length along the bedform slope from the brink point to the lee-face toe.

Package: Rocks grouped in sets or cosets within one storey that refer to the stratigraphic position within the storey (lower, middle or upper part within the storey).

Rib and furrow: Distinctive pattern exposed on the bed surface of curved laminae dipping into the bed in parallel zones. It is the plan-view of trough cross-lamination produced by the migration of current ripples.

Ripple: Bedform generated by the interaction of flow and sediment. As sediment transport rate increases in a rippled bed, larger bedform (dunes) form. In Chapter 5 bedforms with $\lambda < 0.180$ m are considered ripples.

Sand-sheet: Term used in this thesis as other authors in previous studies have used it - large-scale dunes.

Sand-wave: Term used in this thesis as other authors in previous studies have used it - large-scale bedforms (e.g., dunes, bars).

Scour: In this thesis the term scour is used to mean localised erosion from erosional-based troughs.

Scour trend: The mean orientation of the central longer axis of the individual plan-view trough cross-bed sets.

Set: A single unit of cross-laminated, cross-bedded or cross-stratified sediment.

Single trough cross-bed set (scour structure): Individual trough cross-bedded set with a concave-up base formed due to the migration of 3-dimensional dunes.

Slip-face height: Vertical distance from the brink point to the slip-face toe.

Slip-face length: Length along the bedform slope from the brink point to the slip-face toe.

Sole marks (e.g., flutes): Distinctive erosional scours on the bed surface formed by turbulent eddies.

Storey: Preserved sedimentary deposits generated by the activity of one channel, occasionally including floodplain deposits in the upper part.

Stoss face: The upstream side of a bedform that ends at the bedform crest.

Topsets: Upper set that bounds the foresets and is formed by superimposed bedforms migrating over the host bedform, truncating younger foresets.

Trough: Scour generated by erosion near the flow attachment point where the stress increases and ahead of the bedform lee face.

Unit: Group of sediment layers vertically stacked with well-defined upper and lower bounding surfaces.

Unit bar: Large-scale bedform with greater lateral extent that forms cross-beds as it migrates downstream. However, this is a quite controversial term since numerous definitions have been attributed to it (Section 5.1). Different types of bars have been defined based on channel characteristics and position within the channel (e.g. transverse forming where there is a sudden widening of the channel; longitudinal being favoured in wide shallow channels).

2D dunes: Straight-crested dunes.

3D dunes: Sinuous-crested dunes.

1.6 Aims

1.6.1 Rationale and primary aims

Cross-bedding produced by dunes and unit bars is often observed in fluvial channel deposits (e.g., McKee, 1938, 1939; Allen 1965a, Smith, 1972; Puigdefábregas, 1973; Harms *et al.*, 1975; McCabe, 1977; Nijman and Puigdefábregas, 1978; Nami and Leeder, 1978; Cant and Walker, 1978; Collinson, 1978; Bridge and Diemer, 1983; Haszeldine, 1983a; Ramos *et al.*, 1986; Fielding, 1986; Friend *et al.*, 1986; Miall, 1988a; Alexander, 1992 and others). The architecture of fluvial sedimentary structures is important for a wide range of practical applications and research. Cross-stratification is common in sandstones and is used for the interpretation of the depositional environments. A greater understanding of cross-bedding and its analysis will help the understanding of sedimentary deposits and may be used to infer palaeo-flow character during the deposition of sediments. Because of the inherent heterogeneity, it controls the flow of fluid through the rocks and consequently is of importance to hydrocarbon and water production.

The preservation of cross-bedding is most often controlled by channel depth pattern and scour development and the timing of scour relative to dune or unit-bar growth and migration. Detailed investigation of sedimentary structures resulting from bedform migration may lead to a much more detailed understanding of the depositional environments in which fluvial sandstones were deposited. This project aims to improve

the understanding of fluvial cross-bedded sandstones and their internal sedimentary structures as well as to understand the physical processes responsible for particular characteristics of sedimentary deposits generated by unidirectional flow systems.

Although bedforms forming in unidirectional flows have been extensively studied, the understanding of their migration patterns and the resulting sedimentary deposits in relation to the associated bed topography (e.g., a pre-existing erosive surface or a scour associated with the bedform type and bedform evolution as it migrates downstream) need further investigation; in particular, the study of scour initiation mechanisms and bedform development. In addition, further work using experimental data and field observations are needed to discriminate if it is possible to establish that scours have an effect on the resulting geometries of the cross-bedding, and that these scours are associated with 3D formative bedforms.

This study included both laboratory experiments and field work on ancient deposits. The selected field sites are: (1) The Lower Triassic Prados Sandstone, Rillo de Gallo, Spain with very well-preserved plan-view exposures of through cross beds and (2) the Upper Carboniferous Seaton Sluice Sandstones, North England with exceptionally well exposed tabular cross-bedded sandstones in sea cliffs and wave-cut platforms. These sites were selected because: (1) Both sites were thought to be ideal study areas due to the excellent preservation of 3D exposures of cross-bedded sandstones in vertical faces and also plan-view; particularly at Rillo de Gallo where numerous single trough cross-bed sets were identified, and where often the internal individual laminae were visible and well-preserved for obtaining palaeocurrent data. (2) Although cross-bedding types are geometrically the same when they form in different fluvial system types; herein similar cross-bedding types embedded within different depositional systems were compared to identify possible relationships between channel plan-form and resulting cross-bedding types. Hence, these field sites were also selected because they had been previously visited and published work based on these two sites had interpreted their deposits as the sediments transported and deposited by low-sinuosity, sandy braided rivers (Seaton Sluice, Northumberland) and high-sinuosity meandering rivers (Rillo de Gallo, Molina de Aragón, Spain) (e.g., Haszeldine, 1983a and 1983b; Ramos, 1979; Ramos *et al.*, 1986).

1.6.2 Main Aims

The main aims of this project were:

1. **To find out if more detailed investigation of the cross-bedding architecture of the fluvial sandstones would give greater understanding of the flow conditions in which the sediments were deposited.** Could new data be used to investigate palaeo-flow? Would improved understanding of cross-bedding geometries give valuable information for the investigation of the mechanics of fluid flow through the rocks?

As part of this aim (the detailed investigation of cross-bedding architecture) another aim related to the understanding of bedform development and the improvement of knowledge of bedform migration and resulting deposits geometries is herein included; and it relates to the detailed study of specific single trough cross-bed sets (scour structures) observed in sandstones embedded in two different depositional systems.

Related to these aims were secondary aims to improve the understanding of:

- Bedform development related to the resulting cross-stratified deposits.
- Scour trough initiation related to the formative bedform type.
- Bedform migration pattern in relation to the geometry of the resulting cross-stratified sands, via selected field studies.

2. **To improve the understanding of scour associated with formative bedforms and the resulting cross-bedding styles, aiming to improve the understanding of cross-bedded sandstones embedded in different depositional environments by gathering and analysing relevant information on scour and scour associated with bedform development from published work (based on flume experiments and modern rivers); and its link with field observations from both my field sites to: (a) establish that these scours are associated with specifically 3-dimensional bedforms and the resulting preserved cross-bedding; and (b) attempt to distinguish scours associated with formative 3D bedforms from those that correspond to pre-existing erosive surfaces.**

To address this aim two study sites were chosen, presenting excellent exposures of fluvial cross-bedding.

3. **To investigate the factors controlling the formation of cross-bedding styles seen in sandstones.** This aim lead to the objective **to produce cross-bedding in controlled conditions in a flume investigating the formation of cross beds while large-scale bedforms advance downstream, with the ultimate aim that when the structures are seen in the rock record the internal architecture, geometry and flow pattern can be interpreted more precisely.** Related to this, were aims to:

- 3.1. Use flume experiments to investigate if it is possible to clarify the mechanisms controlling the transition from 2D to 3D dunes and then relate the morphology of the crest of bedforms to the geometry of resulting sedimentary structures.

- 3.2. Obtain a better understanding of the mechanisms of trough cross-bed formation and the resulting trough cross-bed sets (defined in Section 1.2). This aim was thus to improve understanding and add new information on the origin of scours downstream of host bedforms that form set boundaries of trough cross-bedding and the basal surfaces of trough cross-bed sets that can be observed in the rock record. This includes improving understanding of the controls on the initiation of scours, their initial shape and size; and the controls on the accumulative scour length/shape. In addition, this project aims to investigate scours as a controlling factor on the type and shape of cross-bed sets and the variations of the angle of large-scale bedform lee face as they migrate into scours.

4. **To integrate flume experimental and field work data on the analysis of bedform geometries and resulting internal architecture formed by bedforms developed downstream, to improve the methodology for the interpretation of ancient cross-bedded sandstones and their origin; and to define some of the factors controlling the geometries of the resulting sedimentary structures investigated in the field.** Some of these factors are: the

variations in the original topography of the river bed, the development of counter-flow ripples in the toe of the lee face of large bedforms, the rate of sediment transport, dimensions and migrating pattern behaviour of superimposed bedforms, recurring erosion of the brink point area of the host bedform, shape of the initial crest of the host bedform and its shape development as the large-scale host bedform migrates downstream.

1.7 Objectives

The objectives explained below were developed to address the project aims listed above. These objectives were slightly modified as the research advanced and the project progressed, due in part to the results of the laboratory and field work.

1.7.1 Preliminary objectives

1. Review literature on bedforms and sedimentary structures.
2. Investigate possible field sites.
3. Plan flume experiments.

1.7.2 Objectives for the detailed case studies of cross-bedded sandstones (aim 1)

The objectives at each selected study site were to document the characteristics of the cross-bedding within the sedimentary deposits of the respective ancient fluvial system.

The objectives were to:

1. Review the literature on each of the study areas to establish the consensus view on the depositional environment of the fluvial system that generated the sedimentary structures; palaeogeography, channel type, palaeoclimate, subsequent geological history.
2. Undertake detailed descriptive analysis of the exposures, identifying features representing scour and cross-bedding within the context of individual sandstone bodies and establish palaeohorizontal.
3. Undertake a new interpretation of the sedimentary sequences and estimate the nature of the channel or channels and their dimensions, and compare these interpretations with published reports.
4. Identify individual and grouped scours associated with cross-bed sets, notably trough cross-bedding. To achieve this objective it was necessary to:

4.1. Investigate their characteristics such as maximum visible length, maximum visible width, length to maximum width ratio, scour trend, lamination dip, lamination thickness of individual cross beds and grain size variation. These measurements were collected to reconstruct the architecture of the trough cross-bed sets and document the variation of structures within particular sandstone bodies.

4.2. Estimate the degree of preservation and if this was only partial then to identify which section of the filling cross beds within the trough was observed and assess whether the exposure allowed measurement of the apparent and true mean trend.

5. Interpret (for each trough cross-bed set) the pattern of palaeocurrents and the stratigraphic position within the sandstone body.
6. Analyse rock samples for mineralogical composition and sandstone type classification.
7. Analyse the data associated with scour structures to identify significant patterns that could clarify scour origin and development.
8. Analyse palaeocurrent data to estimate the variability of flow conditions of the ancient fluvial system that generated the structures; and also for re-assessment of previous interpretations of the channel nature.
9. Propose characteristics controlling the geometry of single trough cross-bed sets:
(a) shape, size and orientation of the initial host bedform, type of crest and its development (transition 2D-3D); (b) shape, size, orientation and development of the initial scour formed as the host bedform advances; (c) characteristics of flow such as: velocity and its variations, water depth, discharge pattern (continuous or varying); (d) channel characteristics such as: width and depth, plan-form; migrating mechanisms of host bedforms advancing and consequently the lee-face angle fluctuations.

1.7.3 Objectives of the integration of a review of previous published studies on scour and scour associated to bedform development, with field observations from the two study sites (aim 2)

To understand, discriminate and narrow down the factors that can explain the scour occurrence and control scour geometry (e.g., scour depth) in relation to the formative bedform and resulting cross-bedding styles. The objectives were to:

1. Review previous published work on bedform initiation and development to firstly introduce the concept of scour in relation to the initiation of the formative bedform.
2. Clarify the concept of trough and scour downstream of the leeside of a migrating bedform to avoid ambiguities often reflected in published studies.
3. Identify and define possible mechanisms of scour initiation.
4. Review published work on scour (e.g., based on flume experiments and modern rivers) and to interpret and identify controls on scour geometry (e.g., scour depth) based on the analysis of the published literature in combination with field observations from the two study sites.
5. Analyse and discuss relevant field observations from the two study sites that can support the main hypothesis presented in this thesis, which states that: the basal erosive surfaces (scours) of the identified scour structures are associated with their formative 3-dimensional bedforms and also with the resulting cross-bedding.
6. Review published work on scours developed due to obstacle presence on the river bed; due to other type flow regimes (e.g., chute-and-pool configurations) and due to streams confluences and chute channels to highlight differences between different types of scours occurring on river beds.

1.7.4 The objectives of the flume experiments (aim 3) were to:

1. Undertake a feasibility study to see whether it is possible to obtain a better understanding of the transition between 2D and 3D dunes in a flume channel, given the theory that 3D forms might be the equilibrium shape and size (Venditti *et al.*, 2005a).

2. Test whether it is possible to obtain the equilibrium pattern for dunes and what defines it.
3. Given that scour pattern is identified as critically important to the shape of preserved cross-bed sets, attempt to replicate Leclair's (2002) experiments on cross-bed preservation that led her to suggest relationships between bedform size and cross-sets thickness. Leclair's flume experiments examined the variability in bedform height and the ratio of the standard deviation of dune height and the deviation of trough scour depth below mean bed level as the main controls on the geometry of cross-sets generated by dunes. To replicate Leclair's experiments aimed at understanding these controls and then relate them to the geometries of cross-bed sets observed in the study areas.
4. Test whether it is possible to identify unit-bar lee face change with advancement downstream over pre-existing topography and quantify the variations.
5. Investigate if bed topography has any implications on the architecture of cross-stratification formed by the migration of steep lee-face unit bars.
6. Observe the evolution of superimposed bedforms and the feedback with the bed that leads to modification of the original topography over which the unit bar migrated.
7. Observe the influence of both down-channel migrating superimposed bedforms on the host bedform and counter-flow ripples in the bedform lee on cross-stratification.
8. Identify and analyse variables controlling the fluctuations of the lee-face angles as unit bars migrate downstream (to be submitted: Martínez de Álvaro *et al.*, 2013).

1.7.5 Objectives of the comparison of the field and flume results (aim 4)

This project aimed to integrate flume analysis with field results to find out whether it is possible to reliably improve interpretations of ancient fluvial systems by studying them in combination with deposits generated in flume experiments. The objectives that address this aim were to:

1. Compare the morphology and the appearance of the cross-bed sets observed in the exposed sandstones and the ones generated by the flume tests.

2. Identify evidence of bedform superimposition and reactivation surfaces that may cause erosion of the brink area of host bedforms in the field exposures and compare these with flume observations and see if this can explain patterns of lee-face angle variation.
3. Compare the pattern of variability of the dunes and unit-bars lee-face angle identified in the field with those generated in the flume experiments.
4. Compare the morphology of the initial bounding surface remains over which large-scale bedforms migrated forming the trough cross-bedding observed in the field and the original topography over which the unit bar advanced in the flume. This is observed to find similarities or differences in how feedback with topography occurs in the flume and in a real case scenario.
5. Compare the cross-stratification (lamination) type from the flume experiments with the ones observed in the field following Allen's (1963a) classification.

1.8 Outlook and thesis organisation

Although there is a large amount of published literature on the analysis of fluvial cross-bedded sandstones; and the two selected case studies, Rillo de Gallo and Seaton Sluice, are well-studied, this thesis aims to improve the methods for the reconstruction of ancient sedimentary environments by investigating in detail the geometries of trough cross-bed sets; and the relationships between flow regime and cross-bed sets dimensions. It is of great importance to understand trough-scour initiation, development and trough filling process as host bedforms migrate downwards in unidirectional flows. This will have significant implications on the final architecture of the trough cross-bedding and sandstone body multi-storey pattern.

Ramos' (1979) Ph.D. Thesis was based on the study of the stratigraphy and palaeogeography of the Permian and Triassic in the western of Molina de Aragón (Guadalajara province, Spain) including the identification and analysis of Prados Formation. Ramos (1979) defined the Prados Formation, as a unit of alternating sandstones and siltstones and mudstones deposited by fluvial system(s) under a continental arid to semi-humid climate forming a fining-upward sequence in a subsiding basin. The Prados Formation is part of the most complete succession of the Buntsandstein described in the Iberian Peninsula, which is located within the Castilian

Section in the Iberian Ranges. The Prados Formation is included in a Triassic strata-typo group refer as the “*Guadalajara Group*” (Sopeña *et al.*, 1983). Like other ancient fluvial deposits (e.g., the Missourian of Oklahoma: Visher, 1960) the Prados Sandstone exposures described here present a vertical variation in sedimentary structures, facies, grain size, cross-bedding type, geometry and morphology of sedimentary structures and units. Ramos (1979) research covered an area of 750 km²; within this area the Prados Formation was identified in Rillo de Gallo and four other localities (Fig. 2.6). Prados Formation thickness varied from 25 m to 50 m within these locations (the exposure at Rillo de Gallo is the best preserved and with better access).

The Seaton Sluice Sandstone (Northumberland, England) is stratigraphically located in the middle formation of the Pennine Coal Measures Group (PCM), which comprises cyclothems alternating sandstone, siltstone, mudstone, coal seams and palaeosol horizons (Waters *et al.*, 2009). It is included in the lower part of the Westphalian B succession; and is up to 15 m thick and can be traced over an area of about 100 km² (O’Mara, 1999). The base of the Seaton Sluice Sandstone is a laterally extensive erosion surface that incises into the underlying coal-bearing coastal alluvial plain sediments (O’Mara, 1999). It was previously interpreted as the deposits of a low-sinuosity river-channel (Land, 1974; Haszeldine, 1983a) at the northern margin of a solitary fluvial sandstone body. Recent studies (Holweber, 2012) suggest that these rocks could have been the result of activity in a higher-sinuosity system. This thesis presents additional data and discusses the possible origin of these deposits.

This thesis is presented in the following order:

- **Chapter 2** presents the investigation of field case study I: The Prados Formation, Rillo de Gallo, Spain. It provides an overview of the site, general description of the identified exposures, and detailed analysis of individual trough cross-bed sets (i.e., scour structures). It also presents a classification of scour structures, analysis of the relationships between trough geometries, flow regime data (e.g., laminae dip direction, laminae dip and bedding plane orientations), and stratigraphic distribution within the sequence. It includes a re-interpretation of the nature of the original channel and channel dimensions estimates.

- **Chapter 3** presents the investigation of field case study II, The Seaton Sluice Sandstone. It follows the same structure layout as Chapter 2.
- **Chapter 4** presents the analysis of published work on scour and scour associated with bedform initiation and development, combined with the most relevant field observations from the two field sites suggesting that the scours observed in the field sites are associated with formative 3-dimensional bedforms. It includes suggested mechanisms of scour initiation and controls on scour geometry.
- **Chapter 5** investigates the formation of cross-stratification generated by the downstream movement of steep-lee-face flume-scale unit bars and the implications of: (1) bar height variation, (2) reactivation surfaces formation and (3) bed topography evolution on bar lee-face angle.
- **Chapter 6** is a synthesis and discussion of all the data presented in this thesis. It aims to link the analysis and results from the field and the laboratory research and to show how the integration of these two types of data set can contribute to science.
- **Chapter 7** presents the main findings and final conclusions.

Chapter 2

Case study I The Prados Formation



Photo: Cross-bedded sandstone, Rillo de Gallo (Spain)

2.1 Introduction to the study area at Rillo de Gallo, Guadalajara, Spain

The site at Rillo de Gallo, in Central Spain (Fig. 2.1), was selected as an ideal study area to quantify and investigate cross-bedded sandstones. Detailed description and study of the geometry and disposition of sedimentary structures and their relationship to other units are critical for the development of facies models, the understanding of fluvial system behaviour and reconstruction of the nature and evolution of these systems. It is also important for understanding analogous hydrocarbon reservoirs and aquifers.

Ramos *et al.* (1986) described the sedimentation of the Alpine cycle in central Spain. This commenced with the Buntsandstein Facies that unconformably overlies the Hercynian metamorphic or Early Permian sedimentary rocks (Ramos and Sopena, 1983). The Buntsandstein Facies correspond to the base of a sedimentary sequence evolving from fluvial siliciclastic to carbonate tidal Muschelkalk sediments (Ramos and Sopena, 1983; Ramos *et al.*, 1986; Sánchez-Moya *et al.*, 1989). This chapter is based on a detailed study of a group of Lower Triassic sandstones referred to as the Prados Formation. These sandstones were selected for the high quality of their exposure, the predominance of plan-view and cross-section surfaces which greatly helped the reconstruction of 3D geometries of trough cross-bedding, and published interpretations of their depositional environment (Ramos *et al.*, 1986; Sánchez-Moya *et al.*, 1989 and Muñoz *et al.*, 1992). The good preservation of these rocks allowed detailed observation of cross-bedding style and geometry from which palaeoflow direction and fluvial conditions could be interpreted.

Field observations and data were collected during field campaigns in 2011-2013. The Rillo de Gallo study area is situated near Molina de Aragón (province of Guadalajara), northern Castilian Cordillera Ibérica (WGS84 / N40°52'59.9110", W001°55'35.9249"). The stratigraphic sequence that includes the studied rocks has a geological extent of approximately 750 km², and is oriented northwest-southeast. The studied sandstones were tracked over an area of 20 x 5 km, passing through the small towns of Teroleja, Cobeta, Riba de Saélices, Santa María del Espino y Luzón. The study area and the localities named above appear on National Topographic Map 1:50,000 scale sheets: 462 (Maranchón), 488 (Ablanque), 489 (Molina), 490 (Odón) and 514 (Taravilla) and

National Geological Map (Magna) 1:50,000 scale sheets: 515 (El Pobo de Dueñas) and 489 (Molina). Figure 2.2 illustrates the geographical locations of data collection including: (1) Described and interpreted key exposures; (2) Scour structure data sites; (3) Palaeocurrent data sites; and (4) Rock sample sites.

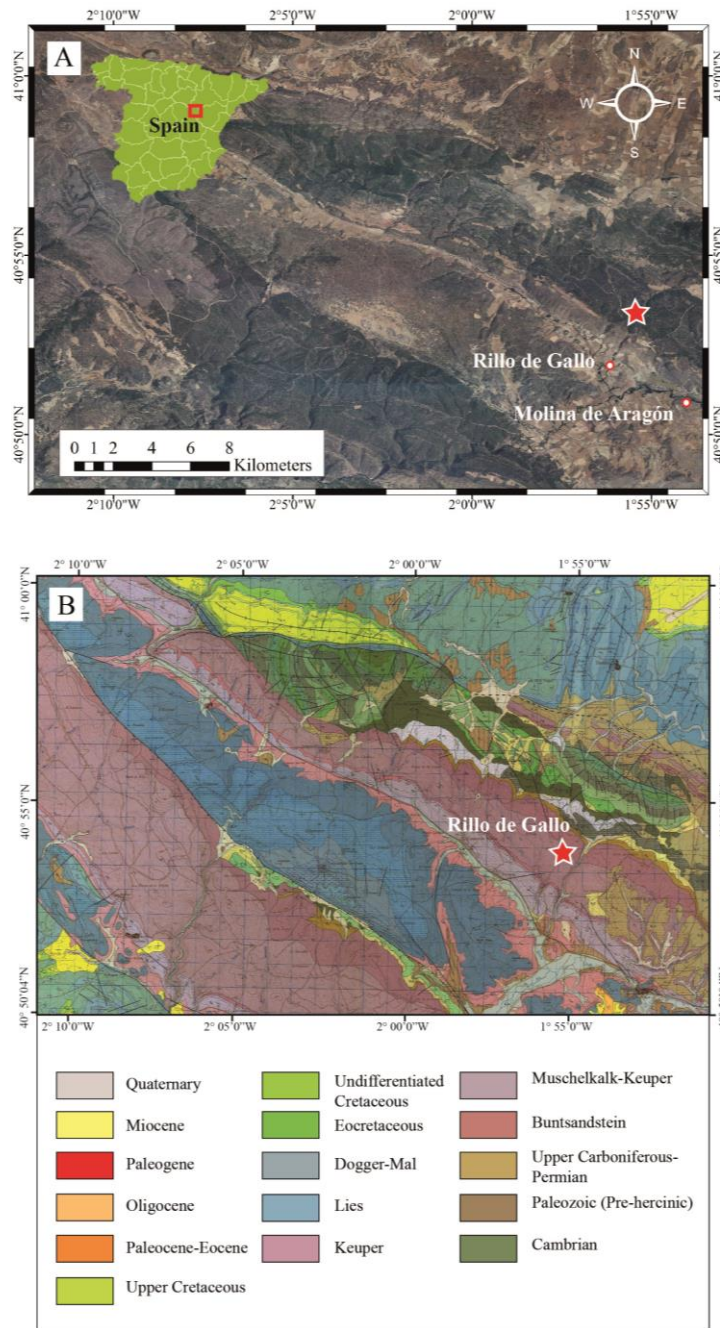


Figure 2.1 Field study site location. (A) Aerial photograph of the region covering the study area (red star shows Rillo de Gallo site) including the nearest localities of Molina de Aragón and Rillo de Gallo (Spain), (photograph supplied by Instituto Geográfico Nacional de España); (B) Geological map of similar area as shown in A National Geological Map – Magna sheet 489 (Molina de Aragón) (Available from the Instituto Geológico y Minero de España, IGME. Authorised: C.S.G. 1972 Depósito Legal: M-6.791-1978).

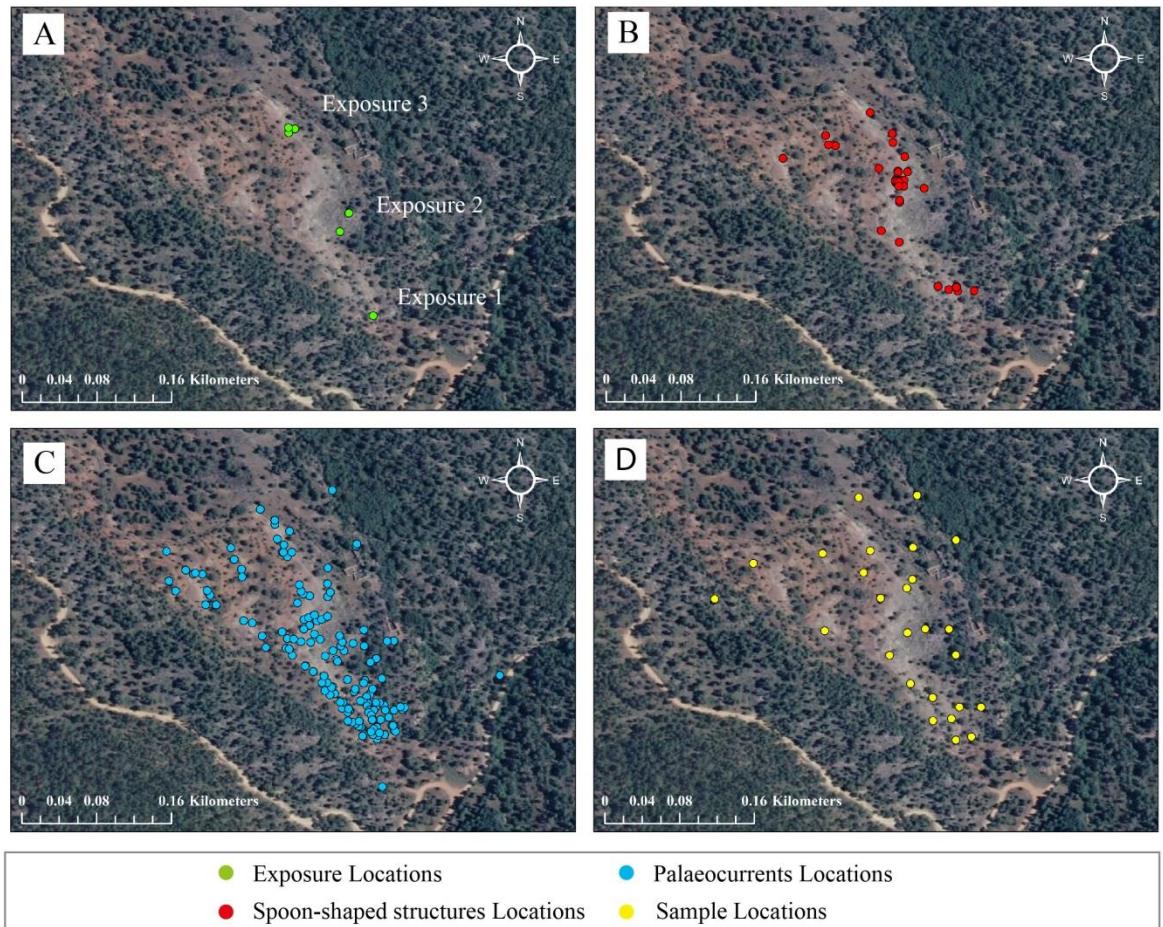


Figure 2.2 Aerial image of the study area illustrating the locations of: (A) exposures described in Section 2.6.2; (B) scour structures described in Appendix A; (C) palaeocurrent measurements collected within Prados Formation; (D) rock sample sites, (photograph supplied by Instituto Geográfico Nacional de España).

2.2 Stratigraphic and geological context at Rillo de Gallo

The Prados Formation is within the Buntsandstein sedimentary sequence, and in this particular site referred as the Guadalajara Sequence that is comprised of the following units in ascending order (Ramos, 1979) (Fig. 2.3):

- (1) *The Hoz del Gallo Conglomerate Formation*. This formation is composed of conglomerates with high quartz content and little sandy matrix with occasional interbedded sandy layers towards the upper part of the formation.
- (2) *The Rillo de Gallo Sandstone Formation*. This formation is composed of fine to coarse sand grade sandstones. These sandstones are intercalated with conglomerate beds and include large-scale trough cross-bedding.

(3) *The Prados Formation*. This formation is composed of bedded sandstones with high content of micas and red mudstones. The sandstones are fine to medium sand grade and contain large-scale trough cross-bedding. Fine-grade sandstones and mudstones occasionally exhibit small-scale trough cross-bedding.

(4) *The Río Arandilla Sandstone Formation*. These sandstones are medium sand grade with fine and coarse grain size and contain large-scale trough cross-bedding. This unit consists mainly of red sandstones however in the upper part of the unit there are intercalated layers of sandy mudstones with occasional small-scale trough cross-bedding.

(5) *Rillo Mudstone and Sandstone Formation*. This formation is an intercalation of sandstones with mudstones. The sandstones are mainly medium sand grade with small-scale trough cross-bedding; grain size occasionally varies to fine and coarse grade. This formation includes carbonate sediments consisting of thin interbedded mudstone and fine grain sandstone with thin carbonate beds.

(6) *Torete Siltstone and Sandstone Formation*. This formation consists of an intercalation of siltstones and sandstones with abundant salt-crystal pseudomorphs. These sandstones are fine sand grade with a clayey matrix and small-scale stratification due to ripples. Layers of dolomitic sands are present higher up in the unit.

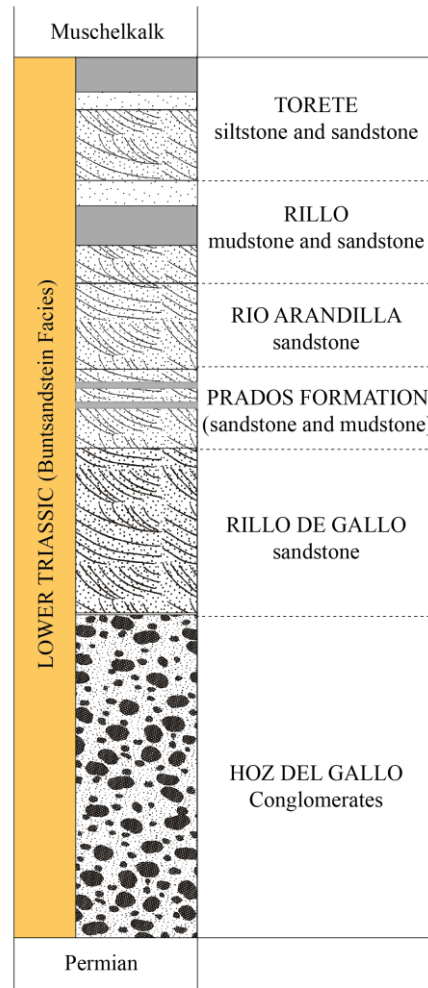


Figure 2.3 Illustration of Lower Triassic (Buntsandstein) stratigraphy of the study region after Ramos, 1979).

Sopeña *et al.* (1989) interpreted the palaeoenvironment as follows: The Hoz del Gallo Conglomerate Formation was deposited by a fan lobe prograding across the alluvial plain within an alluvial fan system. The Rillo de Gallo Sandstone Formation was deposited by a braided fluvial system overlying the conglomerates across most of central Spain. A distal sandy braidplain with ephemeral runoff evolved into a meandering stream system that deposited a series of interbedded sandstones and mudstones that now form the Prados Formation. The Río Arandilla Sandstones that overlie the Prados Formation were interpreted as deposits from low-sinuosity streams that were reactivated tectonic movements (Ramos *et al.*, 1986). The upper units of the siliciclastic non-marine sequence are interpreted as deposits of a more stable fluvial system and of higher sinuosity than the lower Buntsandstein. The Muschelkalk sediments were interpreted as upper-intertidal to supra-tidal flat deposits in marginal

marine environments where the climate was semi-arid. These marine sediments decrease in thickness towards the west of the basin, whereas the siliciclastic non-marine sediments increase in thickness. This is considered as evidence of the western margin of the Tethys Sea (Ramos *et al.*, 1986). The Triassic rocks in the Iberian ranges, consist of architectural elements associated with well-constrained fluvial systems exposed within a sequence that records a transition from non-marine facies, mid and proximal alluvial fan facies, fluvial braided and meandering facies to marine sediments.

The research presented in this chapter is based on the detailed study of the Prados Formation, and was designed to obtain a better understanding of the internal architecture and formation processes of trough cross-bedding, considered as a critical architectural element for understanding sandstones and generating palaeoenvironment reconstructions, palaeochannel and palaeoflow reconstructions and studies of sedimentary architecture for reservoir exploration.

2.3 Palaeogeography

The Buntsandstein Facies were deposited by a complex fluvial system(s) (Ramos *et al.*, 1986) that evolved from alluvial fan(s) into braided rivers and subsequently higher sinuosity systems into a coastal environment (Fig. 2.4).

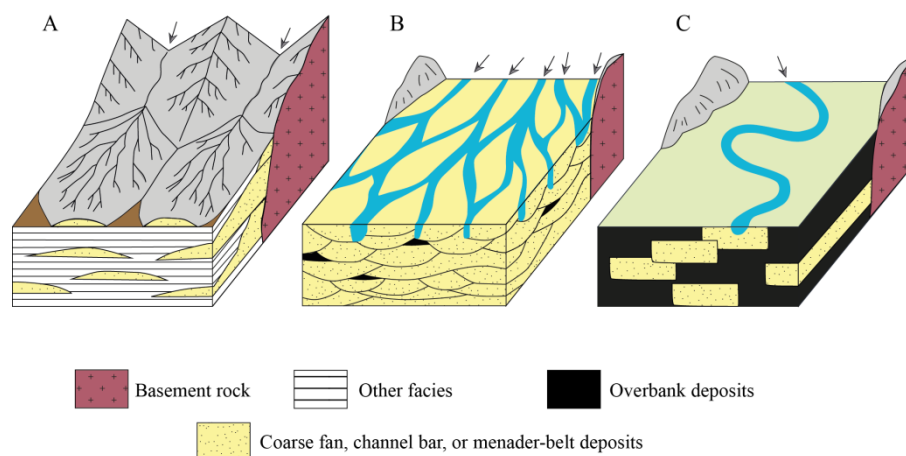


Figure 2.4 Model of the evolution of the Buntsandstein Facies in the study area, illustrating geometrical characteristics of alluvial facies (using images modified from Allen, 1965b). (A) Piedmont formed of alluvial fans; (B) Braided system; (C) Meander stream.

The interpreted regional palaeoslope changed from NNE during deposition of the Rillo de Gallo Conglomerate Formation to SSE during deposition of the Rillo de Gallo Sandstone Formation and subsequently to the southeast during deposition of the Prados Formation. The intercalation of sandstones and mudstones in the Prados Formation has been interpreted as the deposits of high-sinuosity stream systems (Ramos, 1979). Previous studies covered an area of approximately 40×10 km, and record palaeocurrent data with trends generally towards the southeast (Ramos, 1979). The data presented herein is from a smaller area (0.5×0.5 km) in the surroundings of Rillo de Gallo; and it has a polymodal pattern with modes to the south, southwest and west (Fig. 2.5). This pattern is discussed below.

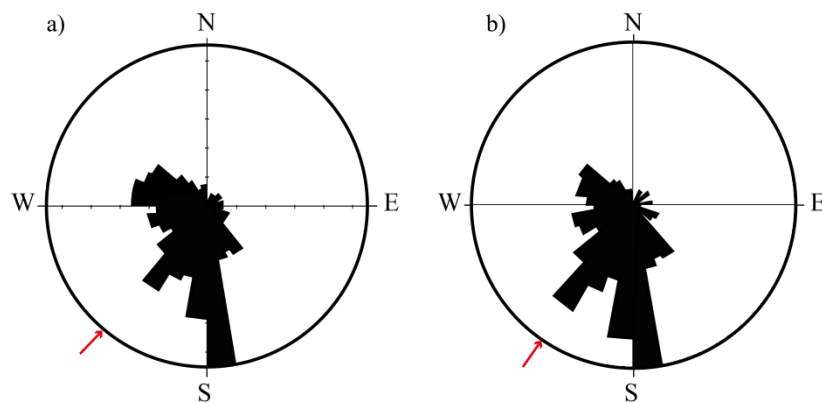


Figure 2.5 (a) Percentage frequency azimuthal plot of all of the palaeocurrent data (from scour structures and other sedimentary structures) measured at the study site in field campaigns May 2011- May 2013 ($n = 498$, scale tick 2%, sector angle 10° , mean resultant direction 223° and $\sigma = 67^\circ$) illustrating three main primary modes, south, southwest and west; (b) Percentage frequency azimuthal plot of the palaeocurrent data measured at the study site in field campaigns May 2011- May 2013 using only the mean value for each scour structure ($n = 392$, scale tick 2%, sector angle 10° , mean resultant direction 213° and $\sigma = 65^\circ$) illustrating two primary modes, one south and the other southwest.

The environmental evolution of this complex system was modified by extensional tectonic activity, which resulted in different fluvial styles in different areas (Ramos *et al.*, 1986). The initial transgression of Tethys affected only the north-eastern part of Spain and the Cordillera Cantábrica. Central Iberia including the study area was also affected by this event, which was recorded by slow sedimentation rates and the retreat of the fluvial system into a more distal environment (Ramos *et al.*, 1986).

Due to the nature of the exposures and the size of the sandstone bodies, the dimensions of preserved sandstone bodies in the Prados Formation could not be measured directly.

Methods to estimate the size of bodies and the channels that formed them were investigated as part of this research and are discussed in Section 2.10. Ramos (1979) recorded a few large-scale lithological logs and some of these sites were revisited (Fig. 2.6).



Figure 2.6 Aerial photograph illustrating the localities revisited where Prados Formation was identified (photograph supplied by Instituto Geográfico Nacional de España).

The contacts between the Prados and the Arandilla Sandstone Formations; and with the underlying Rillo de Gallo Sandstone Formation are concordant. A sharp erosive surface overlain by sandstone with quartz pebbles and mudstone intraformational clasts was observed at the base of Prados Formation above the Rillo de Gallo Sandstone Formation. Strike and dip of surfaces within, over and underlying the Prados Formation were measured in an attempt to constrain the regional tectonic structure.

In an attempt to recognise significant changes in bedform trends, indications of temporal stages and development for clear differentiation of fluvial events, major and minor bounding surfaces were identified. These were ranked by order (cf. McKee and Weir, 1953; Allen, 1983b; Miall, 1988b, c). Herein *first-order surfaces* are planes between cross-bed sets of similar lithology formed by trains of similar bedforms. *Second-order surfaces* are planes between cosets of similar facies interpreted as indicating variations of flow conditions and direction. *Third-order surfaces* have been

interpreted as erosive surfaces truncating underlying cross-bedding generated by large-scale bedforms. Allen (1963b) described these types of surfaces as being equivalent to epsilon surfaces (lateral accretion) or other bar or channel scale surfaces; however lateral accretion was not identified in these exposures. *Fourth-order surfaces* are bounding surfaces between cosets of different facies interpreted as generated by large-scale bedforms. Finally *fifth-order surfaces* are slightly concave-up bounding surfaces representing the base of channel scour (cf. Appendix A, Fig. A1). Other authors have reversed the *order* when defining strata-set bounding surfaces following different criteria in which first order represents major surfaces and surface importance decreases as the order increases (Brookfield, 1977). Bridge and Mackey (1993) defined a different classification based on relative scale and superimposition.

At Luzón, Riba de Saélices, Río Arandilla, and Hoz de Gallo y Teroleja data was recorded from *first* to *fourth-order* surfaces (Fig. 2.6). At Rillo de Gallo strike and dip values were measured on bounding surfaces corresponding to first, second and fifth-orders at different units within sequence (Fig 2.7; Section 2.4 for definition of units in these exposures). Major bounding surfaces (*fifth-order*) were identified representing channel bases eroding into earlier floodplain deposits (mid-lower section and upper section of Unit 2). Trough cross-bedded sandstones overlie these surfaces. Minor bounding surfaces (*first-order*) were identified within Unit 5 between trough cross-bed sets of similar type formed by relatively smaller dunes. *Second-order* surfaces were identified within Unit 7 as bounding surfaces between sets of trough cross-bedded and ripple cross-laminated sandstone deposited by small-scale bedforms. The understanding of facies association and their depositional architecture is critical in palaeoenvironment reconstruction.

There is significant palaeocurrent dispersion (Fig. 2.5). The vector mean of all palaeoflow directions based only on data acquired for this study is towards the southwest. Although this agrees with the mean dip direction of the bounding surfaces (Appendix A, Table A1), the palaeocurrent pattern is polymodal and therefore should be treated with some caution. This may imply that these deposits were formed by a fluvial system(s) with a dominant flow towards the southwest. The data re-plotted using one point to represent mean data from individual sets (Fig. 2.5b) (so as not to risk over stressing directions from sets or co-sets that are particularly well exposed) increases the

strength of the southward and southwestward modes and diminishes the westward mode (Fig. 2.5a) perhaps confirming the palaeoslope (at least locally) to the southwest. This interpreted palaeoslope toward the southwest differs from that stated by Ramos (1979). This difference could be a local deviation (the field study site was a subset that of Ramos, or it could result from a more comprehensive approach to data collection and discrimination of the importance of different subsets of data.

2.4 Lithostratigraphy of the Prados Formation

Approximately 40 m of intercalated sandstones and thin mudstones are well exposed at Rillo de Gallo (Fig. 2.7).

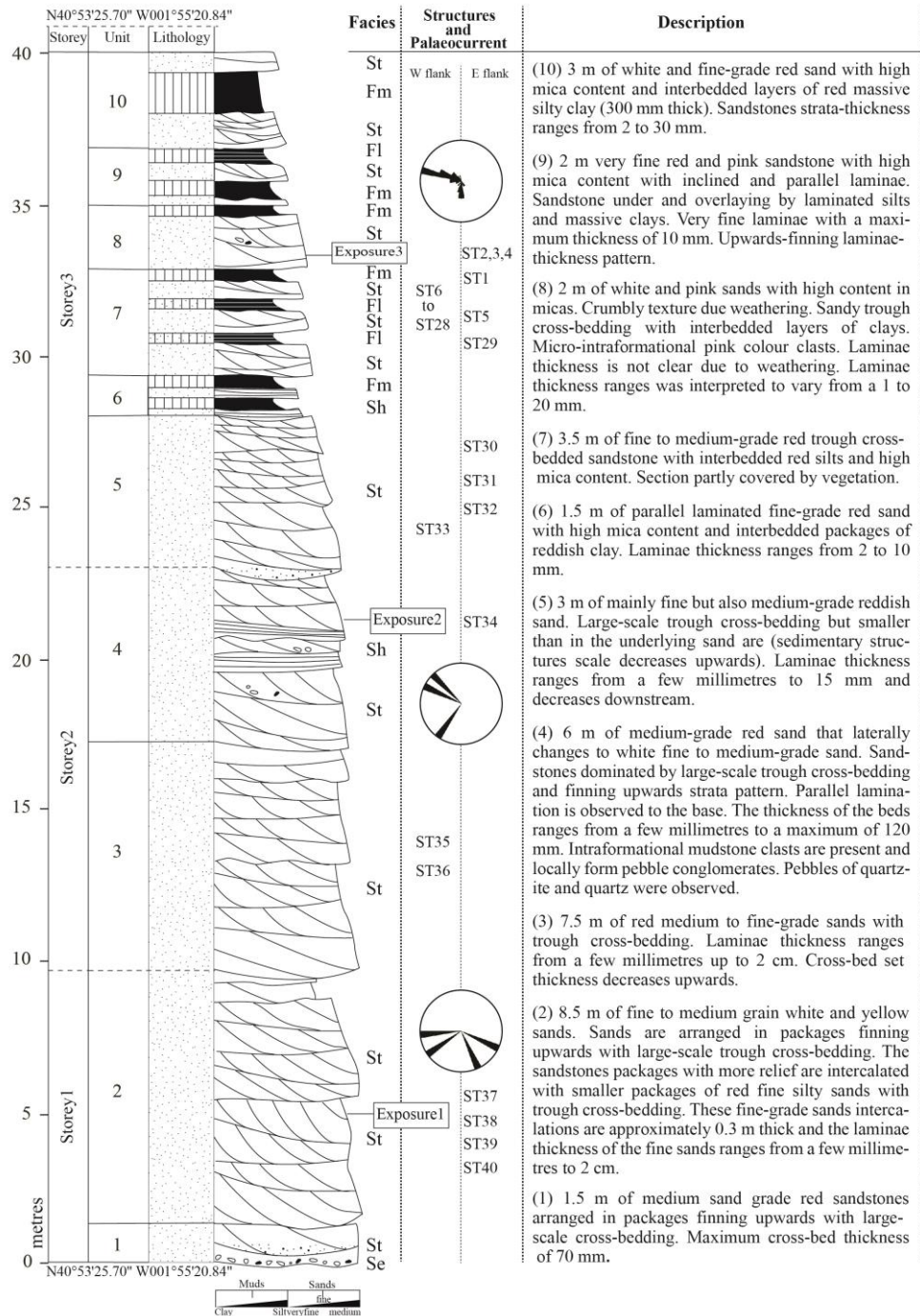


Figure 2.7 Lithological log of the Prados Formation at the location of Rillo de Gallo. The base corresponds to the top of the Rillo de Gallo Sandstone Formation (for key to logs see Appendix A, Fig. A2). This log includes facies distribution, scour structure locations and palaeocurrent data within storeys, and interpretation of storey boundaries. N.B., the structures labelled ST1.1-40 are illustrated and described in Appendix A.

Though cross-bedded scours observed in Rillo de Gallo appear frequently as solitary sets and also as grouped sets stacked vertically in cosets. Several authors described similar dispositions (e.g., Allen, 1965b; Moody-Stuart, 1966; Mossop and Flach, 1983 – solitary sets and Cherven, 1978 – vertically stacked). There is a predominance of large-scale trough-cross-bedded fine to medium-grained sandstone (Facies St) arranged in thinning-upwards and fining-upwards cosets and occasional thin layers of laminated sandstones (Facies Sh). Towards the top of the sequence, fine sediments are more abundant, mica content increases and set thickness decreases. The upper sedimentary packages are formed by smaller scale trough-cross-bedded sandstone, interbedded with thin layers of red laminated silty sandstone that grade towards sandy siltstone and silty claystone (Facies Fl), and packages of massive silty claystone and clayey siltstone (Facies Fm) at the top of the sequences.

The first 23 m (Units 1-4; Fig. 2.7) of the sequence consist of large-scale trough-cross-bedded sandstone (Facies St) representing a period of relatively deep strong flow with sediment transport in migrating 3D-dunes and occasionally horizontal bedding (Facies Sh) with sand sheet migration within upper flow regime flatbed conditions. Facies St are observed in sets of 0.7 m maximum thickness and individual laminae up to 0.05 m thick. Interbedded layers of fine grained red sandstone with parallel stratification (Sh) are observed within packages of Facies St in beds up to 0.3 m thick and topped by layers (< 0.3 m thick) of structureless mudstone with very high mica content (Facies Fm). Erosive surfaces are mostly boundaries between different associated facies and between sets. The erosive surfaces between sets within Facies St represent the basal scour of trough cross-bed sets. Individual trough cross-bed sets observed within the lower 9 m correspond to large-scale scour structures (Section 2.7.1) in which laminae thickness reaches a maximum of ~ 0.12 m and unclear maximum dimensions due to scours overlapping. Laminae dip direction varies considerably (southeast to northwest) and is discussed in Section 2.8.3.

The overlying 6 m (Units 5 and 6; Fig. 2.7) are formed of smaller scale trough-cross-bedded fine to medium grained sandstones, also arranged in fining-upwards packages with intercalation of finer-grained laminated red sandstone and laminated red siltstone (Facies St and Fl). These deposits were generated by the migration of 3D-dunes and bedform superimposition possibly during periods of reduced flow depth than the ones at

the base of the sequence. Laminae maximum thickness is approximately 1.5 cm and the laminae dip main tendency is towards the southeast. This may suggest that these units were deposited by a channel or sub-channel with a different orientation or that these deposits were formed in a section of the river channel susceptible of flow direction variations. Towards the western extent of this package (Units 5 and 6) the sandstone becomes reddish and finer grained, however the troughs become larger.

The following 4 m (Unit 7; Fig. 2.7) consist of trough-cross-bedded sandstone deposited by migrating 3D-dunes (Facies St). These sandstones contain interbedded layers of laminated silty sandstone and sandy siltstone that resulted from the deposition of suspended sediments and weak traction currents associated with the migration of smaller-scale bedforms (Facies Fl). The mica concentration increases towards the top of the entire sequence. These deposits could have been formed due to discharge events of varying magnitude with or without variations in sediment supply. Laminae thickness ranges from a few millimetres to 30 mm and the lamina dip direction is predominately towards the southwest. Laminae thickness varies downstream (15 mm maximum). Palaeocurrent data from Unit 7 varies from southwest to northwest.

The following 4 m of sediments (Units 8 and 9; Fig. 2.7) were the result of similar depth flows and sediment transport as Unit 7 deposits. These are interpreted as trough-cross-bedded sandstone (Facies St) of smaller scale to the ones below in the stratigraphic sequence and intercalated layers of laminated silty claystone and massive claystone (Facies Fl, Fm). Laminae thickness tends to decrease downstream with a maximum of 20 mm and a prominent tendency for laminae dip direction towards the southwest. The upper exposed section of the Prados Formation (Unit 10) consists of small-scale trough-cross-bedded sandstone (Facies St) with interbedded layers of massive sandy siltstone (Facies Fm). These deposits are interpreted as formed by the combination of sediment transport due to the migration of 3D-dunes during periods of relatively shallow flow with intermittent periods of slower flow when fine sediment settled from suspension.

2.5 Sedimentary Facies analysis

2.5.1 Facies

The facies identified in the study are described below, following on from Miall's (1996) nomenclature (Fig. 2.8).

Trough-cross-bedded sandstone (St): This occurs as individual scour structures and grouped forms (i.e., trough cross-bedding cosets). This facies consists of red and white sandstone with grain size varying from very fine to medium sand, with occasionally, gravel-grade clasts of quartz and quartzite. Occasionally, this facies is associated with erosive surfaces that present the geometry of a channel base or possible large-scale scour, with lag deposits (Facies Se). The large-scale sets interpreted as asymmetrical filling of channels. Similar facies in other research areas have been interpreted as the result of linguoid bars or sinuous-crested bars in high-velocity flow regime (Singh and Kumar, 1974; Tyler and Ethridge, 1983), but they could also be formed by the migration of large sinuous-crested dunes. Medium and small-scale sets have been interpreted as the result of sinuous-crested dune migration (Allen, 1968b). This type of facies has also been interpreted as the result of modification of fluvial-bars by bedform superimposition (Cant and Walker, 1978; Crowley, 1983). Here these facies are interpreted as being formed by 3-dimensional dune migration. The dimensions of the resulting sets are related to the channel or flow depth (Section 2.10).

Horizontally bedded sandstone (Sh): Medium to fine sandstone with parallel lamination and parting lineation representing upper bed conditions (Allen, 1965a, Allen & Friend 1968). This facies was observed in beds < 0.10 m thick and frequently occurs overlying Facies St. This facies is often related to fast shallow flow (Allen, 1963b) and may be particularly common in the deposits of flashy flows where flow conditions remain in a critical stage for long time periods (Miall, 1996) or more frequently than in more perennial flow settings. Upper phase plane beds also occur on bar or large dune tops at lower stage flow conditions, which would be consistent with the position of Sh above St in these rocks.

Erosional scours with lag deposit (Se): Erosive surfaces mainly associated with accumulation of pebbles of quartzite and intraformational mudstone clasts. Erosive surfaces were observed between the Prados and the underlying Rillo de Gallo Formation. Erosive surfaces due to scouring were also observed in between sets within sandy

packages. The erosion surfaces with gravel lags could represent the base of channel storeys but could also be within channel scours associated with, for example, a change in bar or bend shape upstream leading to local erosion and deposition of gravel from the channel base.

Laminated sandstone and mudstone (Fl): Layers, patches and lenses of red fine-grained sandstone interlaminated with mudstone with high micas content. The lamination is well preserved although occasionally unclear in some exposures. These deposits represent time periods of flow variation with high sediment concentration and were generated during periods or at sites of low flow velocity allowing fine sediment to settle over the bed.

Massive mudstone (Fm): layers of mud with a massive internal structure have been related to floodplain deposits or deposits from standing water during low-stage flow or channel abandonment (cf. Miall, 1996). These were not studied in detail in this research and therefore any evidence of palaeosols or bioturbation was not recorded.

Ramos (1979) identified other lithofacies (Sr and P; described below) in addition to the ones described above, but these were not observed at the study site presented in this chapter. These facies are characteristic of upper channel or floodplain deposits:

Ripple cross-laminated sandstone (Sr): Medium to fine sand grade. This facies is the result of small-scale ripple migration and it was observed towards the top of the sequence forming packages less than 0.20 m thick. They are occasionally associated with erosive surfaces with intraformational mudstone clasts (Facies Se). This facies was associated to lithofacies (F).

Pedogenic carbonates (P): Structures and textures developed after the floodplain deposits are exposed to soil processes. Ramos (1979) observed thin layers of carbonates within the mudstones (Facies F).

Ramos (1979) identified frequent evidence of bioturbation within the massive mudstones (Fm) and occasionally in Facies (Fl) and (Sr).

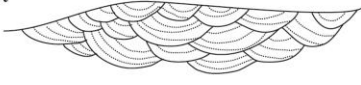
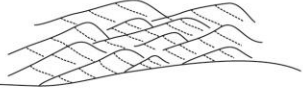
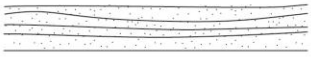




	Facies	Grain size	Bedding and Sedimentary structures	Geometry
Channel - Filling	St 	Medium to very fine sand	Cross-stratification Large-scale trough cross-bedding Group or isolated cross-beds	Lenticular with concave-up base
	Sr 	Medium to fine sand	Small-scale cross-lamination due to ripples	Lenticular with flat or erosive base
Laminated sand sheet	Sh 	Medium	Parallel lamination	Tabular
	Se 	Coarse to fine	Lag deposits associated to erosive surfaces	Undulated and Irregular
Floodplain deposits	Ff 	Fine	Fine lamination due to ripple migration	Irregular or flat
	Fm 	Fine	Massive and structureless siltstone and mudstone	Irregular to associated facies
Processes post-overbank deposition	P 	Fine	Pedogenetic carbonated nodules	Irregular or flat

Figure 2.8 Characteristics of depositional facies types of the Prados Formation.

2.5.2 Identification of storeys and facies associations

To reconstruct the channel style of a river system it is important to understand the architecture of the sedimentary basin and hence the evolution of the channels and channel behaviour. Therefore, the identification of sedimentary storeys is crucial to understand the architecture of the system and for estimates of the dimensions of the channel. Friend (1983) developed a useful classification of channel behaviour. He differentiated three major classes: (1) *sheetflood* in which the flow was not channelized; (2) *fixed channel*, where the channel remained stable between periods of abrupt switching and (3) *mobile channel belt*, where the channel or channels moved within the belt so that most sites within the belt were occupied at some point in time.

The channel or channels behaviour can fit into the three following types: (1) channel stable between switches (when the channel is fixed); and (2) steady lateral channel migration and (3) steady channel migration and switching (when the channel is mobile).

The combination of migration and switching is typical of many belts, whether braided or meandering. Understanding the behaviour of the channel will help in the identification of storeys based on the preserved deposits. Depending on whether the channel was fixed or mobile, the resulting deposits representing the sandstone bodies can be described as ribbon bodies in a fixed channel and sheet bodies in a mobile channel (Appendix A, Fig. A3). The deposits preserved in the study field sites presented in this thesis are interpreted to correspond to mobile channel belts (Fig. A3, a3), where a channel or channels occupied most sites within the belt over a period of time. Channel lateral migration was not identified in either of the field sites.

The criteria herein used for the definition of sedimentary storeys follows traditional field methodologies of identification and tracking of major surfaces of erosion for long lateral distances between layers of stratified sediments. These surfaces indicate the boundaries between the sediments (sandstone bodies and upper channel facies or floodplain deposits) left by the channels at different periods of time. Erosive surfaces can be identified since they may exhibit subtle erosional reliefs, and other features such as distinctive truncation of the underlying deposits overlain by lag gravels or coarser sediments, indicating a boundary separating the resulting deposits from channel/s activity at two different periods of time. In addition, erosion surfaces may be recognisable if a difference in palaeocurrent direction is evident above and below the surface. In the two field sites, where erosive surfaces appeared to dissipate or were difficult to be laterally tracked due to poor preservation, major variations of grain size and palaeocurrent measurements helped to interpret the continuation of the boundaries between storeys, and also lithological correlations of the underlying and overlying sediments (Fig. 3.8). A schematic sketch in Appendix A (Fig. A3) illustrates the basic principles of how to apply this technique to the exposures visited including: (a) identification of type of channel and understanding of architecture of the sandstone bodies observed; (b) selection of well-preserved 3D exposures or 2D exposures (if well-preserved 3D exposures are not available), that allow the identification and tracking of distinctive erosive surfaces indicating the boundary between the preserved channel and flood plain deposits (part of these might have been eroded) due to channel activity at different periods of time; and (c) field interpretation and sketching of 2D and 3D exposures and logging of the maximum thickness between erosive surfaces, which will determine the storey thickness estimates. The methodology and consistency when

describing fluvial sedimentary deposits and the identification of individual storeys are critical for further interpretations of the deposits, and reconstruction and calculation of channel dimensions estimates (cf. Section 2.10).

The total thickness of the Prados Formation varies slightly in the sites visited: Teroleja – 30 m; Hoz del Gallo – covered; Río Arandilla – 50 m; Riba de Saélices – 40 m and Luzón – 25 m (Fig. 2.6). In Rillo de Gallo, the Prados Formation consists of three fining-upwards storeys of an approximate total maximum thickness of 40 m. The facies identified in the Prados Formation can be grouped in facies associations. From the base to the top of the sequence these three storeys have been subdivided as follows (Fig. 2.7):

- Storey 1: 9.7 m thick, consisting of sandstones dominated by large-scale trough cross-bed sets (Association of Facies St, Se).
- Storey 2: 13.3 m thick, consisting of large trough-cross-bedded sandstones and interbedded laminated sandstone (Association of Facies St, Sh).
- Storey 3: 17 m thick, consisting of small and large-scale trough-cross-bedded, laminated silty sandstone and siltstone and massive layers of fine sediment (Association of Facies St, Sh and Fl, Fm).

Storey 3 recalls the sequence strata-type of meandering river deposits that corresponds to the meandering model of Allen (1963b, 1970) (Fig. 2.9).

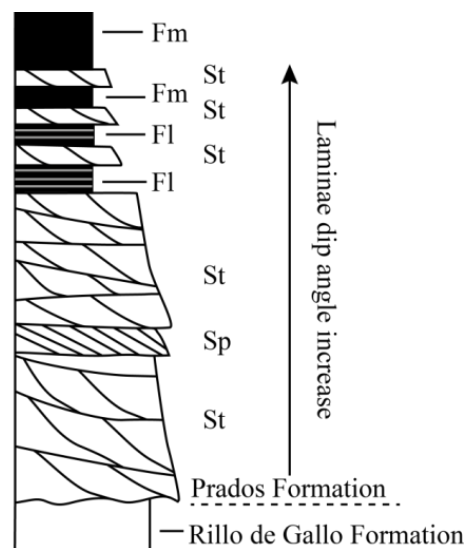


Figure 2.9 The Prados Formation hypothetical meandering model representing complete storeys (following Allen 1963b, 1970).

Assuming that this is the case, the lower storeys of the sequence could represent incomplete association of facies in which, facies characteristics of floodplain deposits are missing. This is interpreted as being caused by erosion and deposition of later cycles.

Although only three storeys were identified with two boundary surfaces delimitating them, the sequence could be formed by more than three storeys but the level of preservation of the exposures allowed confident identification of only two boundary surfaces. If the Prados Formation consists of three fining-upwards and thinning-upwards sedimentary storey, then the Prados Formation can reasonably be interpreted as the product of a river or rivers re-occupying the site at least three times over the period in which the formation was deposited (Fig. 2.7).

2.6 Descriptive analysis of the Prados Formation Sandstones

2.6.1 Description of Prados sandstones

The Prados Formation sandstones consist of 40-74% quartz, 16-40% feldspar, and 2-30% fine lithic fragments (Ramos, 1979). Intraformational mudstone clasts are present and locally form pebble conglomerates. Prados Formation sandstones vary in grain size, composition and thickness. Occasionally these sandstones are coarse grained. The individual sandstone bodies are intercalated with layers of finer sediment arranged in fining-upwards sequences within or between sandstones. The term *fining-upwards cyclothem* was first attributed and described by Dixon (1921) consisting of an erosive-based sandstone overlain by a finer member with intercalations of siltstone and sandstone (Leeder, 1973). Individual units within the Prados Formation vary in composition. The sand within individual storeys tends to fine upwards and successive packages tend to get thinner and finer upwards. There is a variation in cross-bedding style with sandstone composition and position within the Formation. Variations in sedimentary structure plan-form, geometry and dimensions were observed. Concave-upward trough bases were commonly observed over the outcrop in vertical faces and plan view exposures; planar bases were occasionally observed.

Three exposures are described in detail to illustrate the nature of the sandstones and the exposure. These particularly well-exposed sets and cosets of cross-bedded sandstone were selected for detailed study, and are described here to set the scene for the data

analysis on trough cross-bedding architecture that follows (Sections 2.8; 4.2; 4.3 and 4.4). Exposure 1 and 2 are located in the lower units of storey 1 and 2 respectively and Exposure 3 forms part of the upper storey (thinner Facies St).

2.6.2 Analysis of selected individual exposures of the Prados Formation

Exposure 1 in Storey 1

This exposure is 4.60×0.50 m and it is part of Unit 2 of the Prados Formation and Storey 1 (Fig. 2.7). This exposure consists of white micaceous (grey on weathered surface), fine to medium grade sandstone (Fig. 2.9). Due to modern vegetation the boundaries of this sandstone body were not clear, but it appears to have a generally lenticular shape. This lenticular-shaped sandstone body is formed by stacked sets arranged in fining-upwards packages with concave-up boundary surfaces between sets with a dominance of trough cross-bedding (Facies, St and Sr) arranged in cosets. The set thickness varies from 0.05 m to 0.23 m and the cross-bed lamination thickness varies from 2 to 6 mm thinning upwards within the coset. Foreset tangential lower contacts are observed (Fig. 2.10B). Occasionally the slightly eroded brink point of a bedform is preserved (Fig. 2.10B). This sandstone body overlies another sandstone package within the Prados Formation which overlies a layer of fine sediment. Silty fine sandstones overlie and underlie the sandstone body of Exposure 1. The concave-up surface seen in Figure 2.10A is erosional and irregular and interpreted as *first-order* bounding surface.

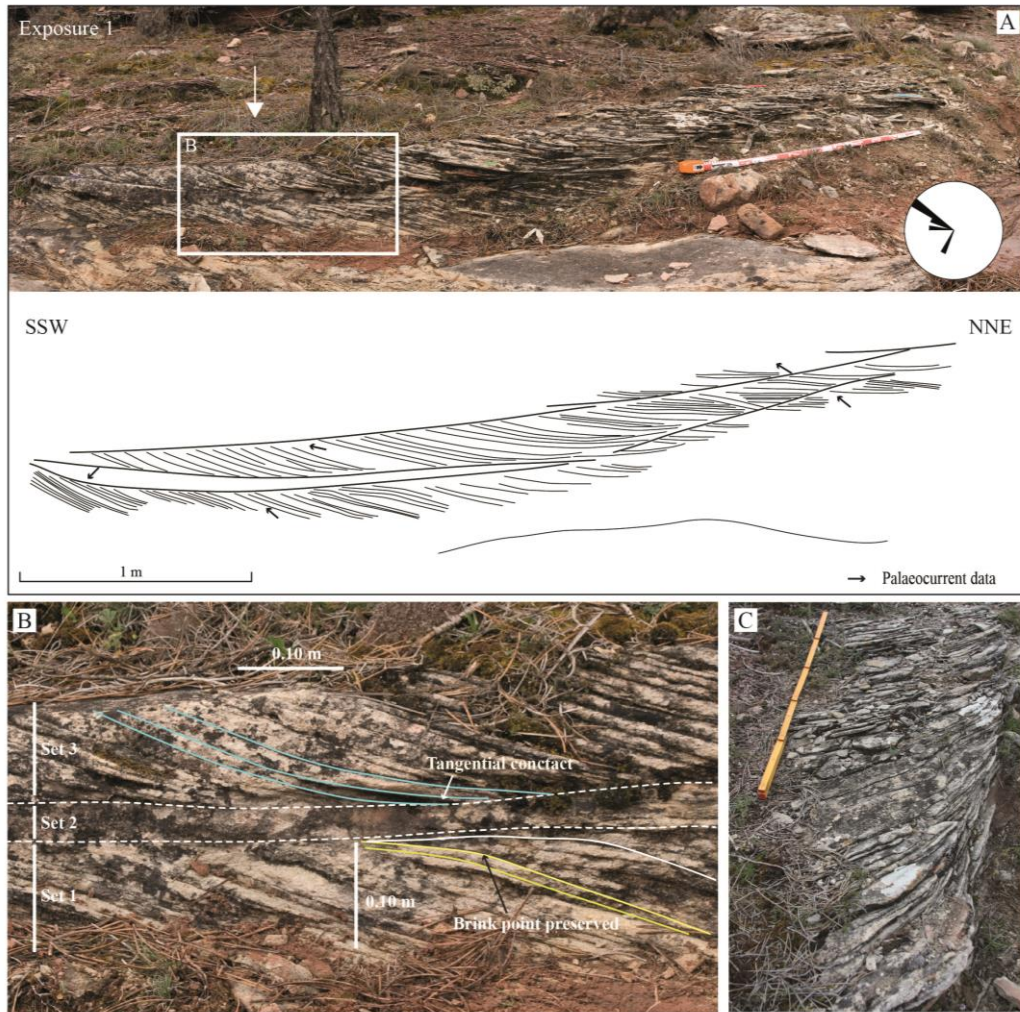


Figure 2.10 (A) Photograph and sketch of the fluvial architecture of Exposure 1 illustrating boundary surfaces between trough cross-bed sets; and internal laminae (foresets). Exposure coordinates: $N40^{\circ}53'26.0''W001^{\circ}55'25.4''$. The exposure trends 005° . Percentage frequency azimuthal plot of the palaeocurrent data ($n = 5$; mean dip direction = 282°). The white arrow indicates the location from where the photograph in C was taken; (B) Enlargement of area outlined by the box in A, illustrating cross-bedding with tangential contacts and preserved foreset brink points of advancing dunes; (C) Plan view of cross-sets. Arrows indicate palaeoflow directions with reference to North at the top of the page (same for the rose diagrams).

There is a predominance of unimodal orientation of trough cross-strata. There is a variation of the laminae dip of the sets, varying from 8° to 30° (mean dip 18°) (Fig. 2.10). These cross-bed sets record bedforms of similar sizes migrating downstream under a near steady flow. This is recorded by the uniform geometry of the elongate trough cross-bed sets with little variation in width (Fig. 2.10C).

Exposure 2 in Storey 2

The sandstone exposed corresponds to Unit 4 and Storey 2 (Fig. 2.7). This package contains reddish to white medium and some fine grained sandstone with moderate concentration of mica. The sandstone is dominated by large-scale trough cross-bed sets and presents a fining-upwards pattern. This exposure is large and easily accessible. Approximately 52 m length of the exposure is described. The dimensions and boundaries delimitating the total geometry of this exposure were not defined. The exposure was divided into four sectors for ease of data collection and description (Fig. 2.11). Due to weathering and vegetation cover detailed observation of lamination was difficult.



Figure 2.11 Overview of Exposure 2 consisting of trough cross-bedded sandstones illustrating the exposure subdivision into four sectors. Two reference points delimitate the ends of this exposure: $N40^{\circ}53'28.38''$ $W001^{\circ}55'25.96''$ and $N40^{\circ}53'29.02''$ $W001^{\circ}55'25.65''$.

Exposure 2: Sector 1

Sector 1 is orientated southwest-northeast and two vertical faces were observed within it. This sector is 9 m long and 1.5 m high and is dominated by medium and large-scale trough cross-bed sets (Facies St) which are arranged in cosets. Parallel lamination (Facies Sh) is only observed underneath the set with higher dip angle. Concave-up boundary surfaces between sets truncate the top of the underlying set. The concave-up surfaces represent the base of scours filled by sediment deposited along the slip faces of migrating dunes. The set thickness varies from 0.3 m to 0.63 m. The larger sets occur within the lower 0.80 m of the vertical section. Laminae thickness varies from a few millimetres to 50 mm. Most of the sets have laminae of very similar thickness, each

thinning downstream similarly. Laminae and sets decrease in thickness downstream giving a wedging effect resulting in tangential contacts. Grain size varies from very fine to medium sand. A gradual and subtle variation in the grain size is observed; increasing slightly upwards in the sequence. Cross-bed sets within this exposure are characterised by their lenticular geometry that records the migration of bedforms of different sizes and also their overlap and superimposition. The laminae dip varies from 8° to 29° . The dip directions of laminae within the same coset vary from 148° to 260° (Fig. 2.12A). Dip direction at the western end of the sector is towards the south and southeast whereas at the eastern end of the sector the main dip direction is towards the south-southwest.

Exposure 2: Sector 2

This sector is the lateral continuation of Sector 1. It measures 6 m long and is 1.2 m high; and it is orientated north-south. Three main trough cross-bed sets (Facies St) are observed (Fig. 2.12B). The basal set corresponds to set 2 in Sector 1. Two well-defined erosive boundary surfaces truncate the underlying sets. A thinning-upwards pattern characterises these sets. The set thickness varies from 0.3 m to 1.0 m and the laminae thickness within each set appears to thin subtly upwards from 0.07 m to 0.01 m. Post-deposition fractures slightly displaced the top and bottom sets. The laminae inclination varies from 16° to 35° and dip direction of foresets is predominantly towards the southwest.

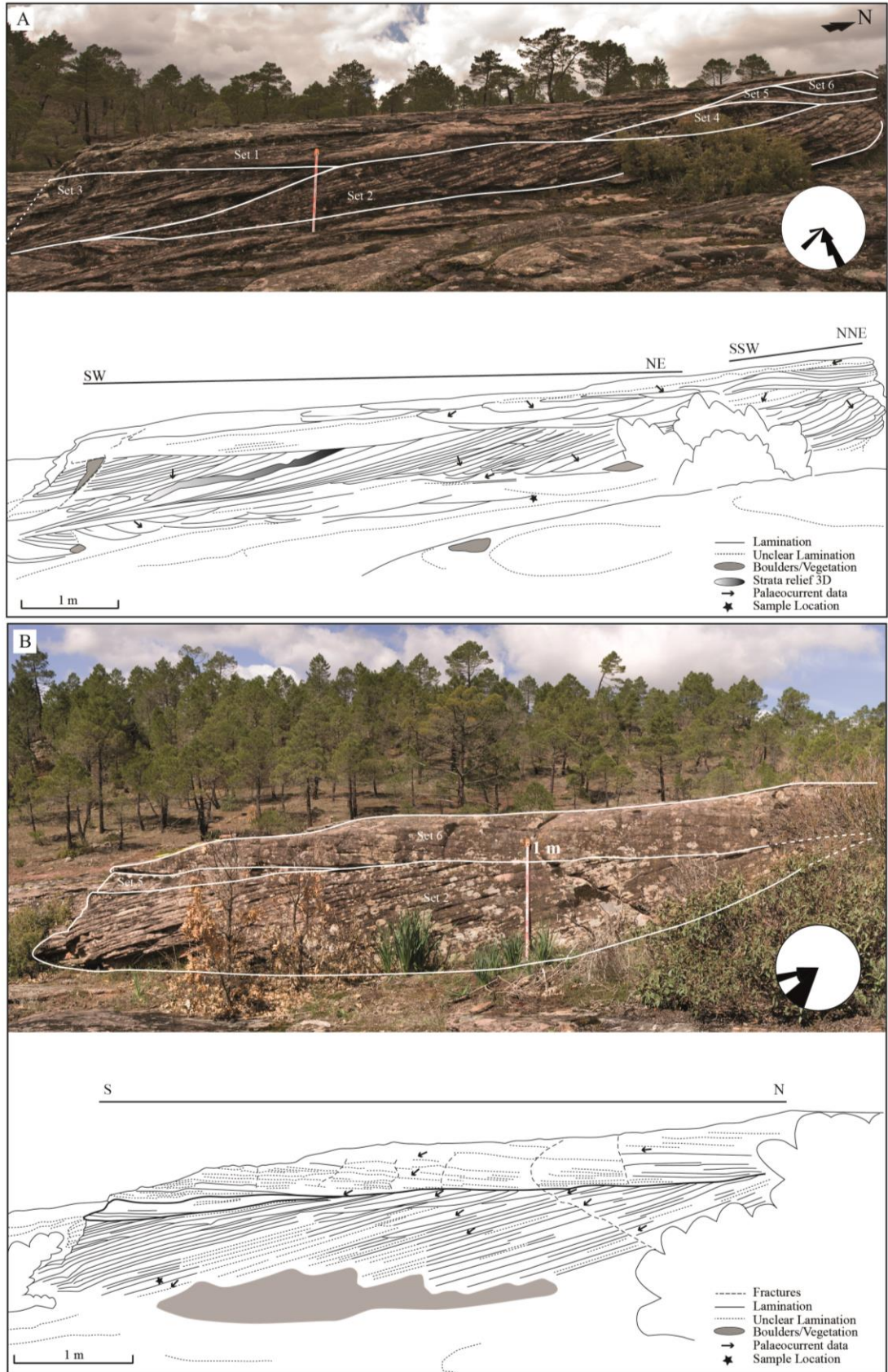
Exposure 2: Sector 3

This 6.2 m long sector is orientated southwest-northeast (Fig. 2.12C). This fine-grained sandstone is dominated by large-scale trough cross-bedding (Facies St) and contains some quartz clasts ($< c. 35 \times 15$ mm) and some mica particularly in the laminae forming in the bottom sets. The 3-dimensional architecture of the cross-stratification in this sector made identification of boundary surfaces between sets difficult. Two well-defined boundary surfaces truncate the underlying sets. The sand within individual sets tends to fine upwards and successive sets tend to get thinner and finer upwards. The set thickness varies from 0.1 m to 1.3 m and the laminae thickness ranges from less than 0.01 m to 0.09 m thickening towards the top where laminae become beds. Lamination within the sets appears to thin upwards but it is a little unclear. Palaeocurrent directions vary from southeast to southwest (Fig. 2.12C).

Exposure 2: Sector 4

Sector 4 consists of two vertical faces; one 4 m long orientated northwest-southeast and one 5.3 m orientated northeast-southwest (Fig. 2.12D). This is a lateral continuation of Sector 3 and exposes fine-grained sandstone with large-scale trough cross-bedding (Facies St) that contains occasional quartz pebbles ($< c. 0.02 \times 0.02$ m). Sets towards the east of this Sector are arranged in a coset. Migration and superimposition of large-scale bedforms were recorded by the preservation of erosive boundaries that truncated the underlying sets. The packages of sandstone present the same thinning-upwards pattern as Sector 3. The set thickness varies from 0.1 m to 1.0 m and the foreset laminae thickness thin upwards from 0.060 m to 0.002 m. Two samples were collected in this exposure; one from the top set and the other the bottom set. The laminae inclination varies from 7° to 25° ; dip directions vary as seen in the rose diagram in Figure 2.12D and the mean dip direction is towards the south (179°).

Summarising, the sandstone seen in Exposure 2 consists of lens-shaped sand bodies composed of stacked sets and mainly arranged in fining-upwards packages characterised by trough cross-bedding (Facies St) with foreset tangential contacts at the bottom of lee faces. Set thickness varies from 0.10 m to 1.00 m and cross-bed lamination thickness varies from 0.002 to 0.090 m generally thinning upwards within the coset. Variation of the laminae dip direction towards the southeast and southwest occurs; and the laminae dip angle ranges from 4° to 35° (mean dip 16°). Although the migration of fields of sinuous-crested dunes probably generated these structures; the larger cross-bed sets may have been formed by unit bars.



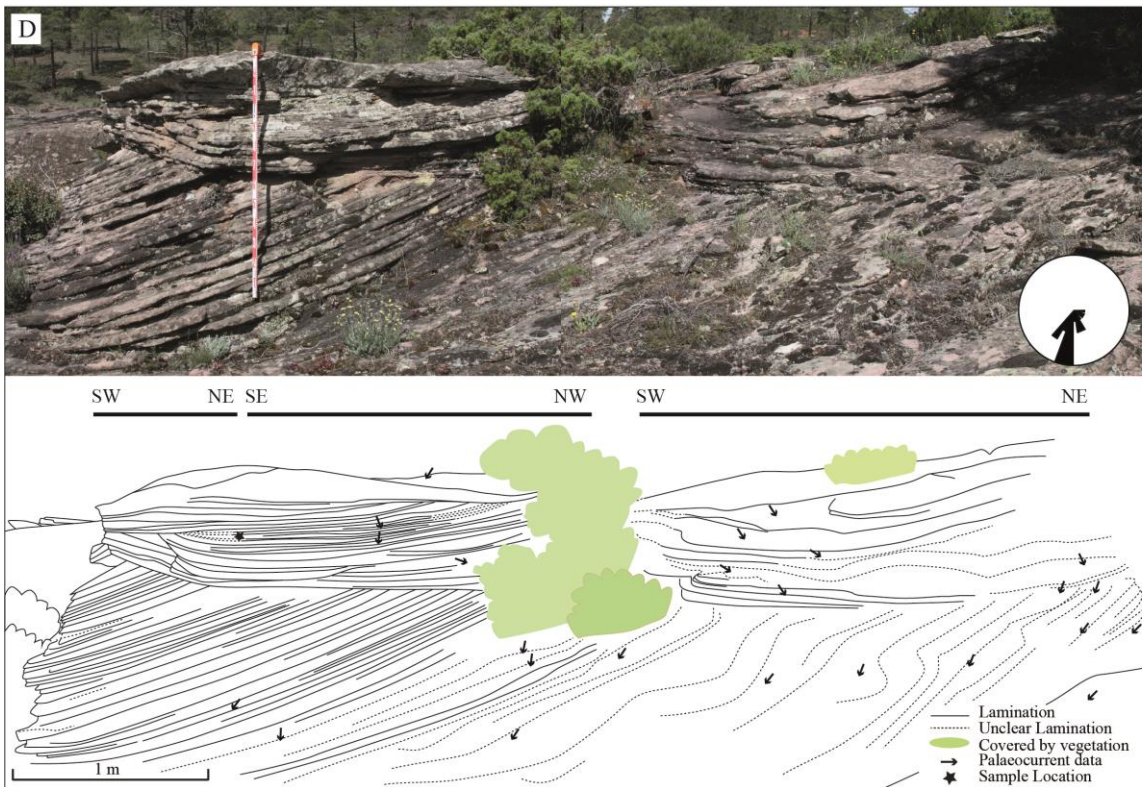
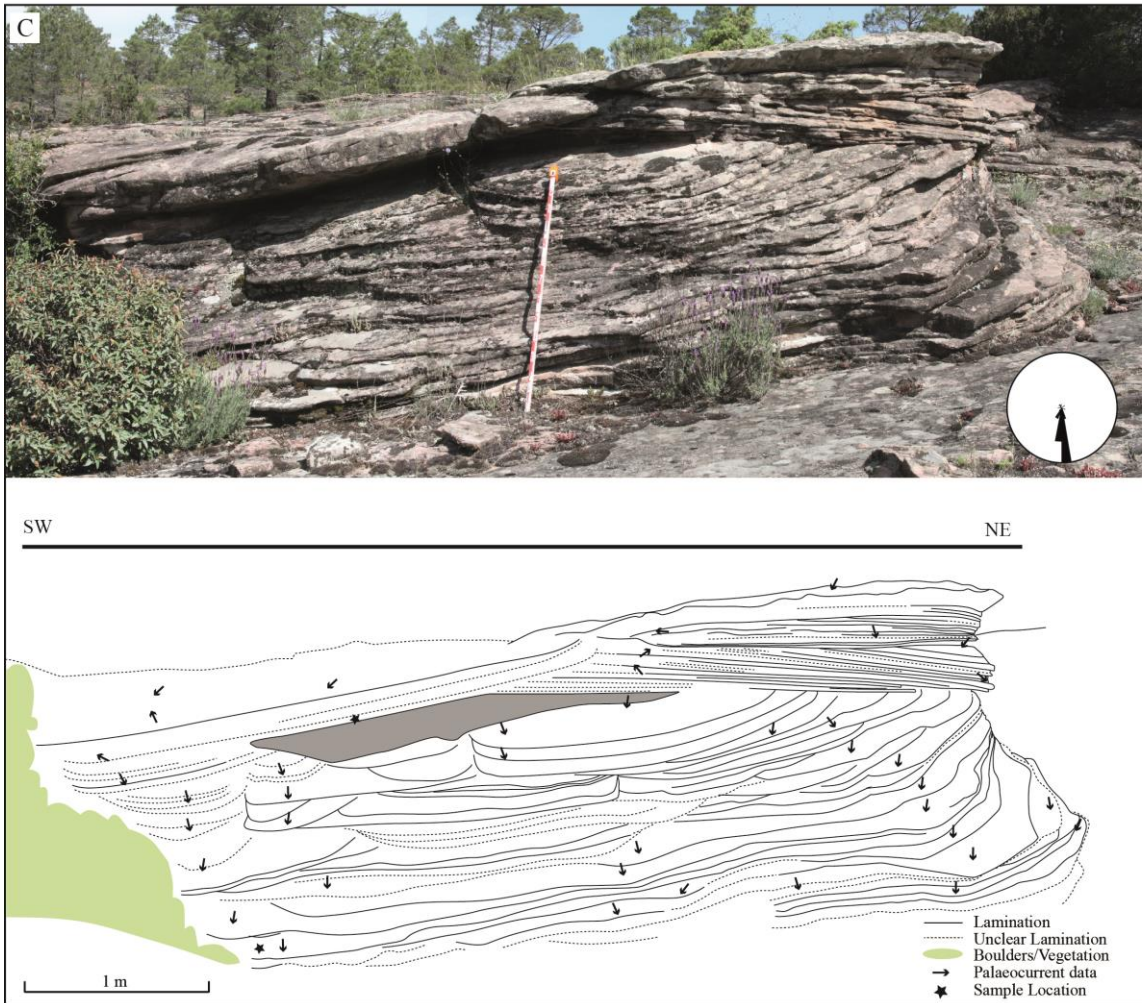


Figure 2.12 Photographs and sketches illustrating the fluvial architecture of Exposure 2; internal lamination and palaeocurrent data. (A) Sector 1; (B) Sector 2; (C) Sector 3 and (D) Sector 4 with relative position as illustrated in Fig. 2.11. Arrows indicate palaeoflow directions with reference to North at the top of the page (same for the rose diagrams). Percentage frequency azimuthal plots of the palaeocurrent data: in A (n = 11; mean dip direction = 184°); in B (n = 11; mean dip direction = 234°); in C (n = 39; mean dip direction = 183°); in D (n = 24; mean dip direction = 181°); Scale from the four sectors varies slightly due to the perspective and size of the photographs.

Exposure 3 in Storey 3

The exposure is 15 × 3 m and it is part of Unit 7 and Storey 3 of the Prados Formation (Fig. 2.7). This exposure consists of red, highly micaceous, fine to medium grade sandstone (Fig. 2.13).

This exposure is formed by stacked sets arranged in fining-upwards packages with concave-up boundary surfaces between sets showing the dominance of trough cross-bedding (Facies St) arranged into a coset. The basal surface is erosional truncating the underlying deposits that consist of a set of fine red trough-cross-bedded sandstones (Facies St). The set thickness varies from 0.05 m to 0.15 m; and the cross-bed lamination thickness varies from 1 to 10 mm. Laminae thickness tends to decrease downstream within the lower sets and tends to increase downstream in the sets identified towards the top of this exposure. Lamina dip direction varies significantly from northeast to southwest (Fig. 2.13). The inclination of the foresets is gentle and ranges from 1° to 18°. The sets within this package are lenticular; the laminae thickness varies from 0.05 to 0.35 m and foreset dip angle varies from 4° to 13° (mean laminae dip 7°). Intercalation of fine-grain red laminated and trough-cross-bedded sandstones (Facies Fl and St) are observed towards the top of this exposure arranged in sets less than 0.10 m thick.

The trough cross-stratified sets (towards the lower and middle parts of Exposure 3) recorded ripple and sinuous-crested dunes that migrated downstream and generated trough scours. The uppermost sediments are interpreted as overbank deposits that are interbedded with bed formed by sandy bedforms possibly filling an abandoned channel or on a bar top.

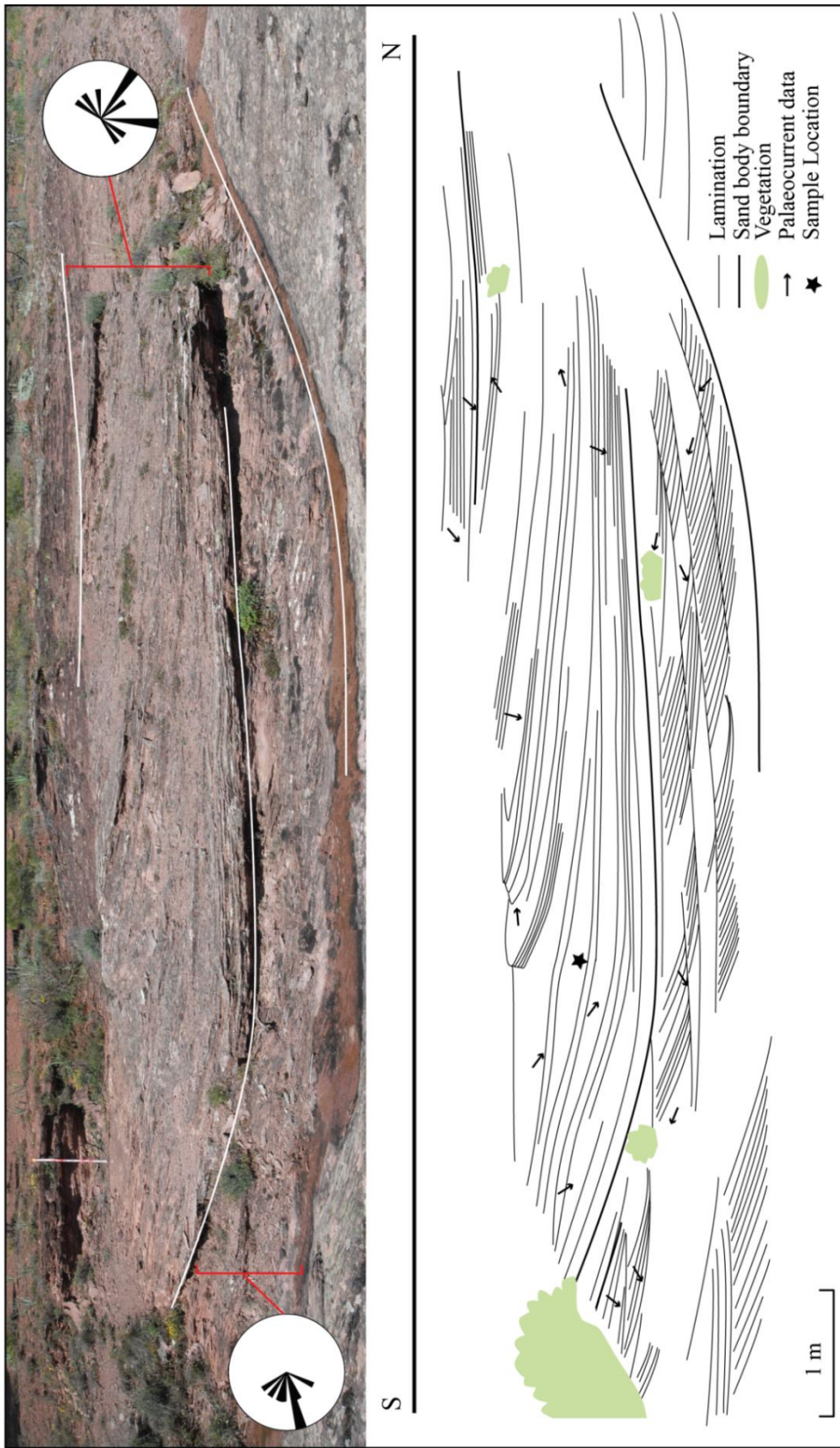


Figure 2.13 Photograph and sketch of the fluvial architecture of Exposure 3 illustrating boundary surfaces between sandstone bodies, internal lamination and palaeocurrent data. Arrows and rose diagrams indicate palaeoflow directions relative to North at the top. Two reference points delimitate the ends of this exposure: N40°53'31.95" W001°55'27.52" and N40°53'31.98" W001°55'27.74". Percentage frequency azimuthal plot of the palaeocurrent data: in A (n = 10; mean dip direction = 142°).

2.7 Scours associated with trough cross-bedding (scour structures) and classifications

During the field campaigns in 2011-2013, individual cross-bed sets were identified and preliminarily classified based on shape and dimensions. These consist of spoon-shaped cross-bed sets also referred to as “scour structures” (Section 1.2). These were identified in most parts of the site. Figure 2.2B presents the geographical distribution of the individual scour structures identified. They were mainly observed in plan-view and occasionally in vertical section. Each scour structure represents a trough-scour of a dune system and contains numerous inclined laminae formed by the toe of a dune prograding into the scour. The scour structures identified in the Prados Formation vary significantly in size. According to Harms and Fahnestock (1965) dimensions of the scours ideally should be measured when the surfaces are parallel or normal to the trend of the scour (trough long axes). For each scour structure the length of the longest axis (maximum length) and the length of the shortest axis (maximum width) were measured. Maximum width ranges from 0.43 m to 5.2 m and maximum visible length varies from 0.53 m to 12.5 m. Lamina thickness varies from 2 to 120 mm. The dip of the laminae varies from a minimum of 5° to a maximum of 30° and generally increases downstream. Trough cross-bed sets are frequently truncated by the scour at the base of a younger set. Some of the younger sets are fully preserved where they are overlain by fine grade facies or are located upper in the sequence. This section presents the data collected with, a new classification of scour structures which is based on geometry and the relationship of scour trend and mean laminae dip direction (in Section 2.9.4, the mismatch between trend of scour and internal laminae dip direction is discussed); and a brief classification of the different scour geometries and the existence of circular plan-form scours.

2.7.1 Classification of scour structures on the basis of their size, shape and internal architecture

Scoured troughs can be classified according to their size, shape and internal architecture. The classifications use terms defined in Figure 2.14. The corresponding boundaries for each class are defined as follows:

- a. Size class. Scour structures were classified from small to very large according to the long axis length:
- (1) Small: if long axis less than 1.50 m
 - (2) Medium: if long axis between 1.50 and 3 m
 - (3) Large: if long axis between 3 and 4.5 m
 - (4) Very large: if long axis greater than 4.5 m
- b. Shape class. Scour structures were classified according to the aspect ratio (width, W to length, L) as:
- (I) Elongate 1 (wider than long): if $W/L > 1.5$
 - (II) Oval 1 (wider than long): if $1.25 < W/L \leq 1.5$
 - (III) Circular or near circular: if $0.75 \leq W/L \leq 1.25$
 - (IV) Oval 2 (longer than wide): if $0.5 \leq W/L < 0.75$
 - (V) Elongate 2 (longer than wider): if $W/L < 0.5$

Elongate 2 troughs appear to have more or less constant width and are elongate in the palaeocurrent direction.

- c. Class based on the relationship of scour to internal lamination. Scour structures can be classified according to the angle, Θ , between the mean laminae dip direction and the scour longer axes trend (Fig. 2.14 and 2.15):
- (a) Scour trend parallel to laminae dip direction: if $\Theta < 5^\circ$
 - (b) Scour trend slightly oblique to laminae dip direction: if $5^\circ \leq \Theta \leq 20^\circ$
 - (c) Scour trend oblique to laminae dip direction: if $20^\circ < \Theta \leq 40^\circ$
 - (d) Scour trend significantly different to laminae dip direction: if $\Theta > 40^\circ$

N.B., the level of preservation of the scour structures has implications for the accuracy of dip laminae angle measurements. Therefore it is important to take into consideration the possibility of inaccuracies in the measurements related to scour trend, mean laminae dip direction and laminae inclination. Herein it is assumed that measurements were taken near the central axis of each trough.

- d. Class based on the type of basal contact between the foreset toe and the scour base.
- (i) Angular: if the toe of the foresets is planar at the contact with the the scour surface or bottom set lamination if present.
 - (ii) Asymptotic: if the toe of the foresets becomes tangential to the scour surface or bottom set lamination if present.

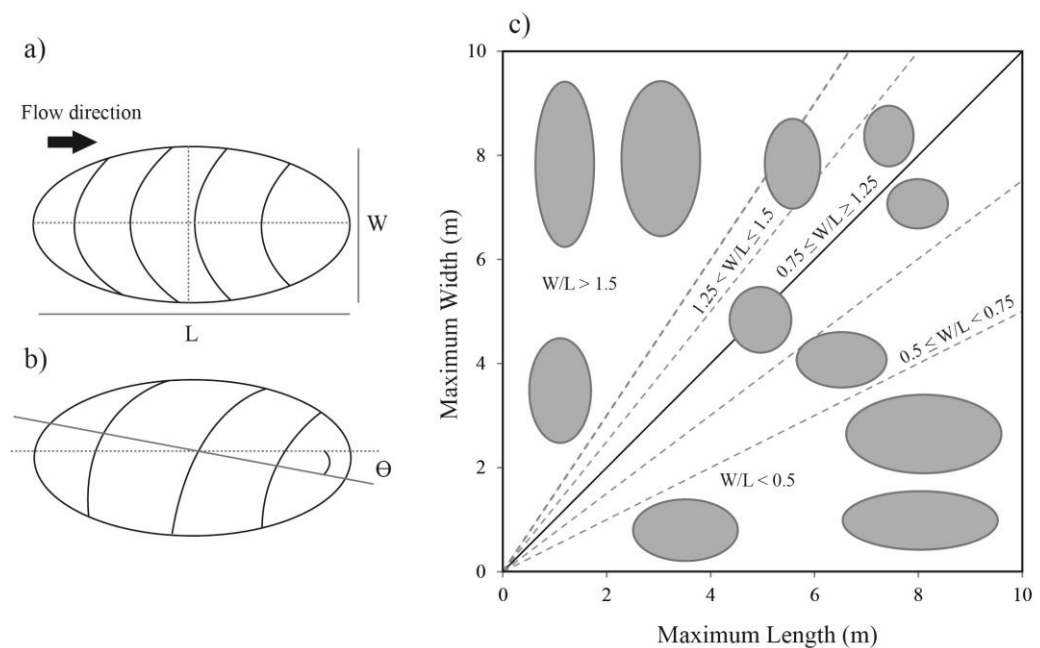


Figure 2.14 Definition of terms used in the classifications explained above. (a) Scour structure maximum width (W) and maximum length (L); (b) Angle between the longer axis of the scour (scour trend) and the mean laminae dip direction; (c) Scour structures shape in relation with their width:length ratio. N.B., The shaded shapes in (c) are not drawn to any scale.

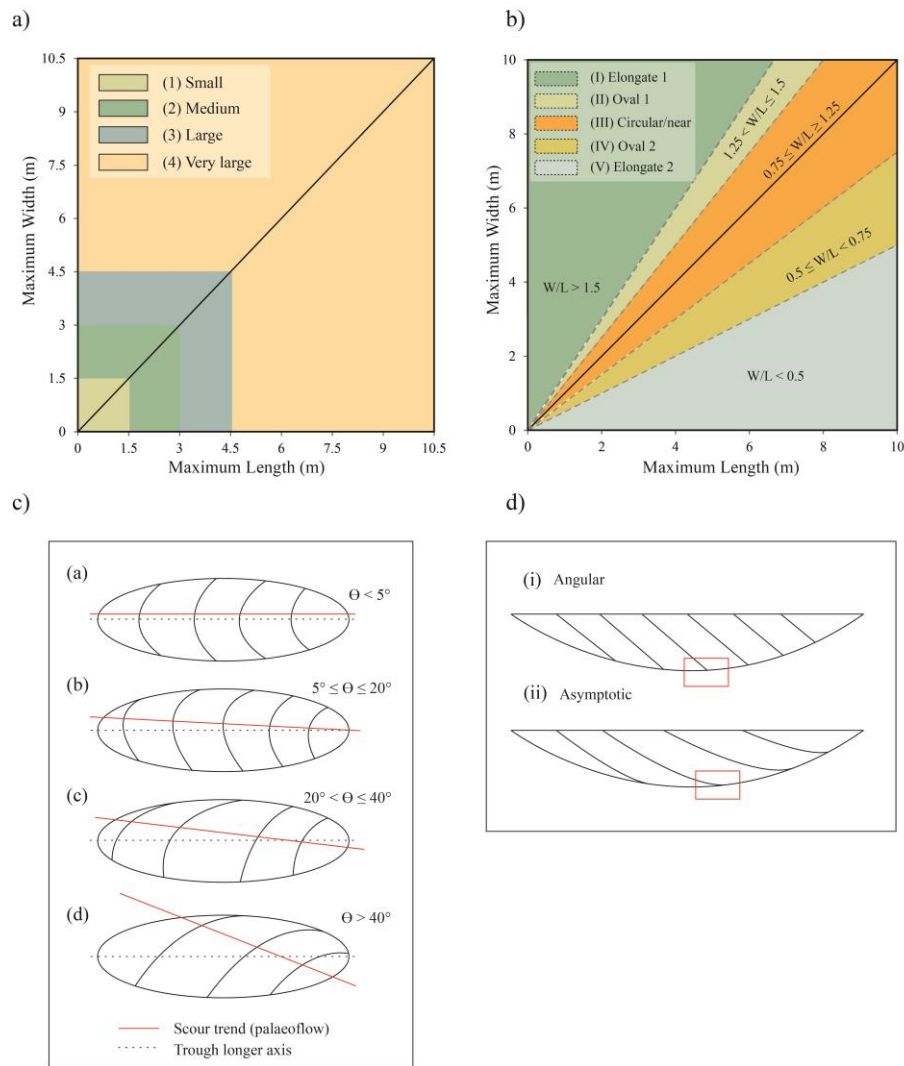


Figure 2.15 Classification of scour structures on the basis of four characteristics: (a) size (category “very large” includes all trough scours with lengths greater than 4.5 m which in some other settings might be a large class); (b) shape; (c) relationship between trend of scour and mean laminae dip direction and (d) type of bottomset contact with foreset toe.

If the mechanism of formation of the scour is taken into account then additional classification methods can be considered although this requires some assumptions about the mechanisms to be made (where as the above classification system is purely geometric and requires no interpretation of the depositional environment). In this study, three possible initial geometries of scour are suggested. These have consequences for the shapes of the resulting scour structures and the development of their geometries. These are: (1) Initial scour with $W/L \sim 1$; (2) Initial scour with $W/L > 1$ and (3) Initial scour with $W/L < 1$. These three types may develop forming circular, oval and elongate shapes. This, combined with classification the relationship between scour trend and

lamina dip direction (a. scour trend and laminae dip direction parallel and b. non parallel) results in six additional types of trough cross-bed scour (Fig. 2.16).

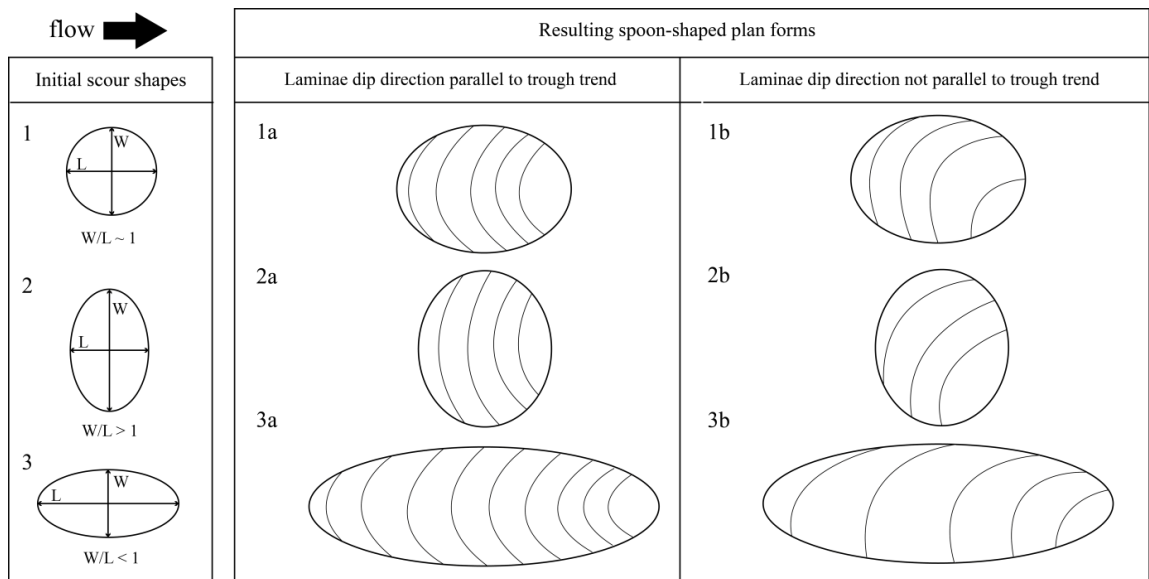


Figure 2.16 Classification of scour structures based on the initial scour shape: (1) $W/L \sim 1$; (2) $W/L < 1$ and (3) $W/L > 1$; and the angle between laminae dip direction and scour trend.

For each type of starting scour shape (1-3) the development of circular and elongate plan-forms is very similar. However if the initial scour shape is type 2 ($W/L > 1$) the host bedform needs to migrate for enough time in order to produce plan-forms at least with $W/L \sim 1$. If the initial scour is type 3 ($W/L < 1$), a wider sediment deposition distribution and flow direction scatter are needed in order to generate round/oval plan-forms.

Scour structures type (a) have laminae dip direction parallel to trend of the scour. In type (b) laminae dip direction and trend of scour are not parallel.

Sometimes scour structures in the Prados Formation were observed not to have a constant width (in these cases an increase in width downstream was observed). This is a complication that has not been incorporated in the above classification system. More examples need to be documented before the foundation of a classification based on these unusual forms can be established.

2.7.2 Classification of Prados Formation cross-bed sets

This section presents data measured for each scour structure (Table 2.1) and their classification based on the classifications defined in Section 2.7.1. Due to the level of preservation and erosion some of the shape and dimensions of some cross-bed sets were unclear. This classification is presented in Table 2.2 and the percentages of each class are shown in Table 2.3.

Table 2.1 Individual scour structure characteristics measured in the Prados Formation including: trough dimensions, width:length ratio, laminae thickness, mean laminae dip, scour trend, mean laminae dip direction and the relationship of trend and dip direction.

Scour structure ID	Max width (m)	Max length (m)	Ratio W/L	Length to max width (m)	Mean Laminae Dip (degrees)	Max laminae thickness (mm)	Trend of scour (degrees)	Mean dip direction (degrees)	Trend & dip direction variation (degrees)
ST1.1	1.13	1.30	0.87	0.55	26	35	182	188	6
ST1.2	0.88	1.51	0.58	0.47	25	20	182	181	1
ST1.3	0.96	1.35	0.71	0.87	24	20	182	178	4
ST02	1.20	1.60	0.75	0.60	22	n/a	180	198	18
ST03	0.97	1.00	0.97	0.50	19	10	182	188	6
ST04	1.70	2.00	0.85	0.84	21	n/a	145	175	30
ST05	3.70	4.10	0.90	2.40	22	10	185	180	5
ST06	1.77	> 2.60	n/a	1.33	11	15	194	142	52
ST07	0.70	2.90	0.24	2.25	21	30	141	285	36
ST08	2.80	3.80	0.74	2.50	14	20	038	302	96
ST09	1.23	> 1.39	n/a	0.84	23	10	024	281	77
ST10	0.98	1.43	0.69	0.63	25	20	165	268	77
ST11	1.10	1.20	0.92	0.64	21	n/a	155	314	21
ST12	1.23	1.50	0.82	0.72	16	n/a	180	299	60
ST13	1.43	1.50	0.95	0.70	18	n/a	044	285	61
ST14	4.05	7.40	0.55	2.73	18	5	035	285	70
ST15	1.10	4.10	0.27	2.25	17	10	165	273	71
ST16	1.57	3.10	0.51	1.35	12	20	180	286	73
ST17	0.77	1.33	0.58	0.67	18	15	036	287	72
ST18	2.10	2.80	0.75	1.70	15	10	040	294	75
ST19	0.93	2.10	0.44	0.50	18	10	036	269	53
ST20	1.21	2.46	0.49	0.93	19	10	026	277	72
ST21	0.84	1.20	0.70	0.62	22	10	010	258	68
ST22	1.95	2.10	0.93	1.05	9	n/a	018	318	60
ST23	1.20	2.00	0.60	0.96	12	10	170	299	51

ST24	0.43	0.53	0.81	0.30	21	10	018	282	84
ST25	1.22	1.70	0.72	1.10	12	5	027	297	90
ST26	0.52	1.40	0.37	0.32	13	15	022	301	81
ST27	0.85	1.21	0.70	1.10	14	10	30	345	45
ST28	0.95	1.50	0.63	0.92	18	5	45	286	61
ST29	4.20	9.80	0.43	5.80	13	5	35	200	15
ST30	0.53	2.00	0.27	0.72	3	15	20	217	17
ST31	0.90	2.00	0.45	0.75	4	10	15	330	45
ST32	1.20	1.50	0.80	0.90	6	1	160	n/a	n/a
ST33	1.55	4.30	0.36	2.60	12	5	12	150	42
ST34	4.30	3.2	1.34	1.50	4	25	70	217	32
ST35	3.50	6.00	0.58	3.90	13	25	35	297	83
ST36	2.00	5.40	0.37	2.80	13	12	165	314	31
ST37	1.28	> 12.5	n/a	n/a	7	40	176	261	85
ST38	1.50	2.10	0.71	1.45	12	20	170	156	14
ST39	> 2	n/a	n/a	n/a	22	15	125	238	67
ST40	5.20	> 4.2	n/a	2.50	9	120	36	114	78

N.B., n/a: data unavailable because the parameters related to those classes could not be observed in the field.

Table 2.2 Individual scour structure classification at Rillo de Gallo using class definitions from Section 2.7.1.

Structure ID	Size	Shape	Scour trend & laminae dip direction relationship	Basal contact (where it could be observed)
ST1.1	Small	Circular	$\Theta < 5^\circ$	Asymptotic
ST1.2	Medium	Oval 2	$\Theta < 5^\circ$	Asymptotic
ST1.3	Small	Oval 2	$\Theta < 5^\circ$	Asymptotic
ST02	Medium	Circular	$5^\circ \leq \Theta \leq 20^\circ$	n/a
ST03	Small	Circular	$5^\circ \leq \Theta \leq 20^\circ$	n/a
ST04	Medium	Circular	$20^\circ < \Theta \leq 40^\circ$	n/a
ST05	Large	Circular	$5^\circ \leq \Theta \leq 20^\circ$	Asymptotic
ST06	Medium*	n/a	$\Theta > 40^\circ$	n/a
ST07	Medium	Elongate 2	$20^\circ < \Theta \leq 40^\circ$	Asymptotic
ST08	Large	Oval 2	$\Theta > 40^\circ$	n/a
ST09	Small*	n/a	$\Theta > 40^\circ$	n/a
ST10	Small	Oval 2	$\Theta > 40^\circ$	n/a
ST11	Small	Circular	$20^\circ < \Theta \leq 40^\circ$	n/a
ST12	Medium	Circular	$\Theta > 40^\circ$	n/a

ST13	Medium	Circular	$\Theta > 40^\circ$	n/a
ST14	Very large	Oval 2	$\Theta > 40^\circ$	Asymptotic
ST15	Large	Elongate 2	$\Theta > 40^\circ$	n/a
ST16	Large	Oval 2	$\Theta > 40^\circ$	n/a
ST17	Small	Oval 2	$\Theta > 40^\circ$	n/a
ST18	Medium	Circular	$\Theta > 40^\circ$	n/a
ST19	Medium	Elongate 2	$\Theta > 40^\circ$	n/a
ST20	Medium	Elongate 2	$\Theta > 40^\circ$	n/a
ST21	Small	Oval 2	$\Theta > 40^\circ$	n/a
ST22	Medium	Circular	$\Theta > 40^\circ$	n/a
ST23	Medium	Oval 2	$\Theta > 40^\circ$	n/a
ST24	Small	Circular	$\Theta > 40^\circ$	n/a
ST25	Medium	Oval 2	$\Theta > 40^\circ$	n/a
ST26	Small	Elongate 2	$\Theta > 40^\circ$	n/a
ST27	Small	Oval 2	$\Theta > 40^\circ$	n/a
ST28	Medium	Oval 2	$\Theta > 40^\circ$	n/a
ST29	Very large	Elongate 2	$5^\circ \leq \Theta \leq 20^\circ$	n/a
ST30	Medium	Elongate 2	$5^\circ \leq \Theta \leq 20^\circ$	n/a
ST31	Medium	Elongate 2	$\Theta > 40^\circ$	n/a
ST32	Medium	Circular	UC	n/a
ST33	Large	Elongate 2	$\Theta > 40^\circ$	n/a
ST34	UC (Large)	Oval 1	$5^\circ \leq \Theta \leq 20^\circ$	n/a
ST35	Very large	Oval 2	$\Theta > 40^\circ$	Asymptotic
ST36	Very large	Elongate 2	$5^\circ \leq \Theta \leq 20^\circ$	Asymptotic
ST37	Very large	n/a-Elongate 2	$\Theta > 40^\circ$	Asymptotic
ST38	Medium	Oval	$5^\circ \leq \Theta \leq 20^\circ$	n/a
ST39	Medium-Large	n/a	$\Theta > 40^\circ$	n/a
ST40	Very large	n/a	$\Theta > 40^\circ$	n/a

* These structures were at this size or greater (due to the level of preservation of the exposure it was not clearly observed). n/a: Data unclear to be assessed.

Table 2.3 Classification in percentages of individual scour structures at Rillo de Gallo.

Classes	Categories					Unclear
a) Size	1. Small	2. Medium	3. Large	4. Very Large		
	23.8 %	42.9 %	19 %	14.3 %		0 %
b) Shape	I. Elongate 1	II. Oval 1	III. Circular	IV. Oval 2	V. Elongate 2	
	0 %	2.4 %	31 %	31 %	26.3 %	9.6 %
c) Θ	a. $\Theta < 5^\circ$	b. $5^\circ \leq \Theta \leq 20^\circ$	c. $20^\circ < \Theta \leq 40^\circ$	d. $\Theta > 40^\circ$		
	7.1 %	19 %	7.1 %	64.3 %		2.4 %
d) Basal contact	i. Angular		ii. Asymptotic			
	-		21.4 (100% of the contacts that could be observed)			78.6 %

2.7.3 Classification of scour structures on basis of their mean laminae dip

Between one and nine laminae dips were measured per scour structure depending on the preservation level. Values of laminae dip range from 5° to 30° (Table 2.4). According to the research reviewed by Thomas *et al.* (1987) the highest value of internal laminae dip measured in similar deposits was 29° . Mean laminae dip for individual trough sets ranges from 3° to 26° .

The scour structures can be classified based on their mean laminae dip as follows:

- (1) If laminae dip $< 5^\circ$
- (2) If laminae dip 5° to 10°
- (3) If laminae dip 11° to 20°
- (4) If laminae dip 21° to 30°

Table 2.4 Maximum, minimum and mean laminae dip per scour structure and location of troughs within the sedimentary sequence. The unit is labelled in Figure 2.7 and the description of the structures is in Appendix A.

Scour structure ID	Number of data (n)	Min & Max Laminae dip (degrees)	Mean laminae dip (degrees)	Laminae dip class (degrees)	Unit in sequence (Fig. 2.7)
ST1.1	5	20-30	26	21-30	7
ST1.2	4	24-25	25	21-30	7
ST1.3	5	21-29	24	21-30	7
ST02	1	22	22	21-30	8
ST03	1	19	19	11-20	8
ST04	1	21	21	21-30	8
ST05	7	18-26	22	21-30	7
ST06	5	6-16	11	11-20	7
ST07	2	19-23	21	21-30	7
ST08	6	8-19	14	11-20	7
ST09	3	21-26	23	21-30	7
ST10	3	23-26	25	21-30	7
ST11	1	21	21	21-30	7
ST12	4	11-19	16	11-20	7
ST13	1	18	18	11-20	7
ST14	9	15-21	18	11-20	7
ST15	6	13-20	17	11-20	7
ST16	5	8-16	12	11-20	7
ST17	5	14-21	18	11-20	7
ST18	5	12-17	15	11-20	7
ST19	8	10-25	18	11-20	7
ST20	5	16-22	19	11-20	7
ST21	4	20-23	22	21-30	7
ST22	3	7-14	9	5-10	7
ST23	4	10-14	12	11-20	7
ST24	1	21	21	21-30	7
ST25	4	5-16	12	11-20	7
ST26	2	11-14	13	11-20	7
ST27	1	14	14	11-20	7
ST28	1	18	18	11-20	7
ST29	3	12-14	13	11-20	7
ST30	3	1-6	3	< 5	5
ST31	1	4	4	< 5	5
ST32	1	6	6	5-10	5
ST33	2	11-13	12	11-20	5
ST34	3	1-6	4	< 5	4
ST35	4	11-16	13	11-20	2
ST36	3	11-16	13	11-20	2

ST37	5	3-11	7	5-10	2
ST38	1	12	12	11-20	2
ST39	1	22	22	21-30	2
ST40	2	13-5	9	5-10	2

2.8 Analysis of scours associated with trough cross-bedding (scour structures)

Prados trough cross-bed sets vary in size, shape and trend of the scour as described above. They all contain inclined laminae, although these vary in dip angle, dip direction, laminae thickness, grain size and composition. These variations might reveal some of the fluvial system controls and conditions of channel behaviour. This section analyses the relationships between these characteristics of: shape, dimensions, internal lamina dip current directions and the general trends of the spoon-shaped scours.

2.8.1 Relationship between trough shape and size

Structures laying on or just above or below of any of the dotted boundary lines in Figure 2.17 can be also considered as structures transitional between two shape categories.

Individual trough cross-bed sets in the Prados Formation are classified according to their shape (Section 2.7.1). Most of the structures (97.3 %) are $W/L < 1$ and the percentages in different shape classes are presented in Table 2.3 and are represented on Figure 2.17. Only one scour structure (e.g., structure 34; Appendix A) has a width:length ratio > 1 . This structure was partially covered or eroded by other individual trough cross-bed sets, which may have resulted in an incorrect assessment of its dimensions.

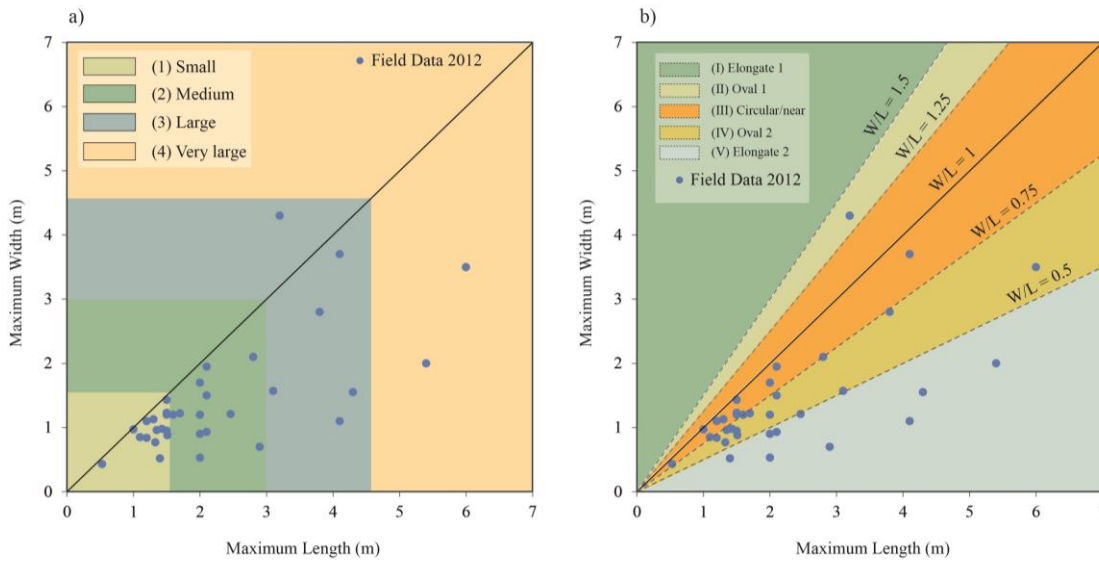


Figure 2.17 (a) Scour structure maximum measured width compared to maximum length of structures whose locations are indicated on Figure 2.2B. The shaded areas correspond to the different size categories defined in Section 2.7.1, and percentages in each category are listed in Table 2.3. (b) Illustration of maximum measured width and maximum visible length of scour structures and their classification into shape categories as defined in Section 2.7.1.

Table 2.5 Relationship of trough size to shape in percentages.

n	Size		Small	Medium	Large	Very Large
	Shape					
13	Circular		7.7	38.5	38.5	15.3
1	Oval 1		0	0	0	100
13	Oval 2		0	38.4	30.8	30.8
0	Elongate 1		0	0	0	0
11	Elongate 2		0	9.1	27.3	63.6

No measurable relationship between the variation of trough shape and size was found (cf. discussion on Section 2.9.1).

2.8.2 Relationship of trough shape and size to scour structure's stratigraphic position within the sequence

The stratigraphic distribution of individual troughs in the Prados Formation at Rillo de allo is shown in Figure 2.7. This distribution, comparing types of classes and facies for each individual trough scour, can be useful indicators to correlate river behaviour and fluvial events (see discussion in Section 2.9.2).

From the base of the sequence upwards; Storey 1 is dominated by large to very large troughs with ratios width:length less than 0.75, and oval 2 and elongate 2 shapes. The larger troughs have more than 40° difference between the scour trend and the mean laminae dip direction; and medium size troughs have an angle variation between 5° and 20°. Towards the base of Storey 2, two very large troughs were described with oval 2 and elongate 2 shapes and a divergence between the scour trend and the mean laminae dip direction greater than 40°, and 5° to 20° respectively. Towards the top of this storey a very large trough was described with an oval 1 shape, and 5° to 20° angle variation between trend scour and laminae dip direction. The full length of this structure was unclear. Numerous scour structures were identified within Storey 3. Towards the base, individual troughs became larger laterally from east to west. Mainly elongate 2 shape and a few near circular shape (the circular ones appear slightly unclear in shape) were described. The angle between trend of scour and mean laminae dip direction varies from category 5°-20° to category > 40°. Upwards in this storey scour structures became smaller. Towards the eastern end of this storey (East flank, Fig. 2.7), medium and small structures with oval 2 and near circular shapes are dominant. The angle between scour trend and lamina dip direction also decreases being for most of the troughs less than 5° or 5° - 20° and occasionally between 20° and 40°. Towards the western end (West flank, Fig. 2.7) individual trough scours are predominantly small and medium size with near circular and oval 2 shapes and occasionally elongate 2-shaped; and the difference between the trend of the scour and the mean laminae dip direction increases significantly, being larger than 40°.

2.8.3 Relationship of laminae dip direction to scour trend and comparison with trough shape and size

Laminae dip direction was measured from well preserved individual laminae within individual scour structures. Some of the trough cross-bed sets, mainly of elongate and oval or transitional shape (from a circular shape to an elongate shape), are curved (they have a curved centre line); and their internal laminae trend and dip angle vary down the length of the set (e.g., see scour structures, Appendix A). Figure 2.18 shows the relationship between trough width:length ratio and mean laminae dip direction of the structures where it was possible to obtain several measurements. Out of the 42 structures identified, only 35 are plotted due to unclear interpretation of the dimensions and dip planes of the reminder. The polar graphs show two different modes; mode I has a mean laminae dip direction towards 185° and mode II towards 294° (Appendix A, Table A2).

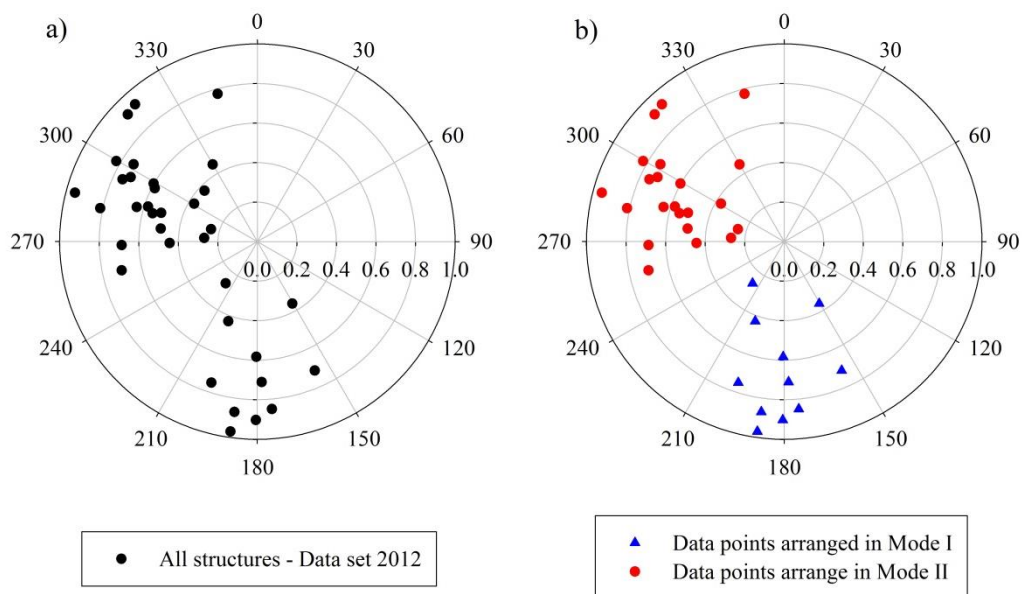


Figure 2.18 Polar representation of trough width:length ratio versus laminae dip direction: (a) Graph illustrating all scour structures with visible dimensions; (b) Graph illustrating the same data set in two differentiated modes. The radial axis represents the W/L.

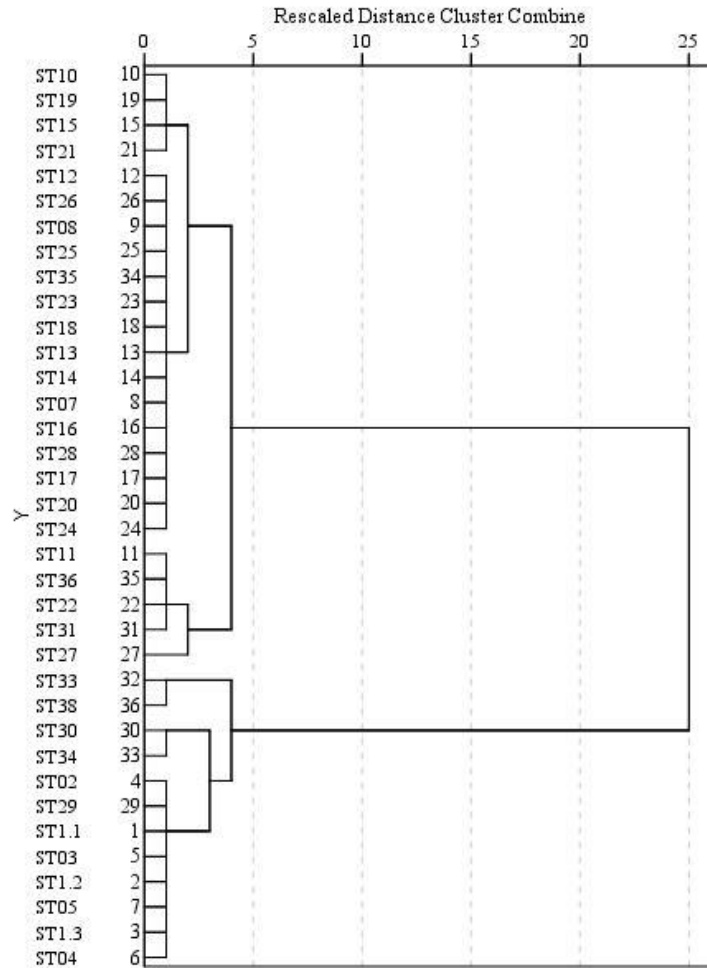


Figure 2.19 Dendrogram using average linkage (between groups) resulting from a hierarchical clustering statistical t-student test (square Euclidean distance method). Illustrating the identification of Modes I and II interpreted in Figure 2.18.

Table 2.6 Descriptive statistics values obtained from analysis of the lamina dip direction variable. The mean value of laminae dip direction was also calculated using mean of series of angles method (circular mean) and this value agrees with the arithmetic mean value presented above.

Descriptive Statistics	N	Minimum	Maximum	Mean	Std. Deviation
Lamine dip direction	36	151°	345°	258°	55

Based on the data of the 35 structures used in this section, the geometry of the trough scours varies. Of the structures within Mode I, 45.4 % are circular, 27.3 % are elongate 2 and 27.3 % are oval 2; 27.3 % are small, 45.5 % are medium, 18.2 % are large and 9 % are very large. Within Mode II, 29.2 % are circular, 29.2 % are elongate 2 and 41.6 % are oval 2; 29.2 % are small, 45.8 % are medium, 12.5 % are large and 12.5 % are very

large (Appendix A, Table A3 and Table A4). Thus, within either direction mode a full range of structure W/L occur, which indicates no relation between trough scour geometry and laminae dip direction. There may be a relationship however, between laminae dip direction and the stratigraphic location of trough cross-bed sets (as discussed in Section 2.9.2). This may be useful for the interpretation and better understanding of the fluvial system that generated these deposits.

The variation of flow direction downstream is moderately preserved as the trend of scours varies in the downstream direction. Figure 2.20 represents the relationship of trough width:length ratio and the scour trend. Although the laminae dip direction has two different modes (Fig. 2.18) the scour trend does not (Fig. 2.20). The trend was measured by holding the compass horizontally over each structure. The lower azimuth number or its complementary number ($+180^\circ$) is valid but as shown in Figure 2.20 all structures are all plotted in half of the circle to recognise clusters. The variation of the trend across the entire exposure is random and does not show a clear variation pattern. Towards the base of the sedimentary sequence, trough scours are mainly orientated NNW. Higher in the sequence, structures within the eastern flank tend to be orientated NNE and towards the western area, scour structures are predominantly orientated NNW.

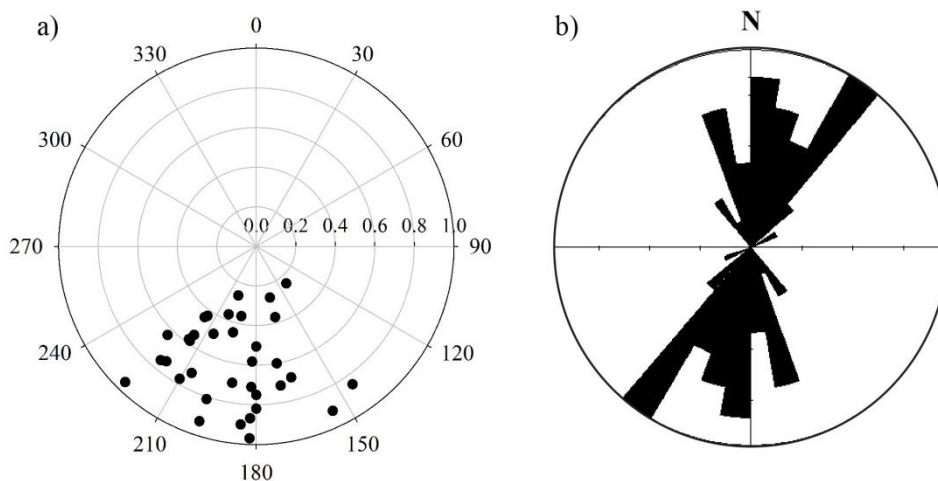


Figure 2.20 (a) Polar representation of trough width:length ratio (W/L) versus trend of scour illustrating all scour structures with visible dimensions ($n = 36$, radial axis represents W/L between 0 and 1, scale tick 0.2); (b) Rose diagram illustrating scour trends of the same data ($n = 36$, scale tick 5 %, sector angle 10° , mean resultant direction 013° - 193°). The radial axis represents the W/L.

Scour trend values between 090° and 270° were used to generate Figure 2.20a in order to avoid splitting modes of natural data. The descriptive statistics are as follows:

Table 2.7 Descriptive statistics obtained from analysis of the scour trend variable. The mean value of scour trend was also calculated using mean of series of angles method (circular mean) and this value agrees with the arithmetic mean value presented above.

Descriptive Statistics	N	Minimum	Maximum	Mean	Std. Deviation
Scour trend (180-360)	36	141°	250°	193°	24°

The angle between the trend of the structure long axis and the lamination dip direction may be zero or up to 90° (Θ). Within a single structure the angle may be constant or variable. This has implications for interpretation of channel palaeocurrent direction (Section 2.9.4). For each scour structure this angle, Θ , has been measured and was used for the classification in Section 2.7.2 and Table 2.3. The mean value of the divergence between laminae dip direction and the scour trend is 65°.

Herein, values of laminae dip direction grouped in two modes and values of scour trend grouped in a single mode were compared to find possible measurable relationships between both parameters (Fig. 2.21). Although there is variation between laminae dip direction and trend of scour for individual trough cross-bed sets, statistical analysis of paired sample t-test shows a non-significant variation between these two variables (Section 2.9.4).

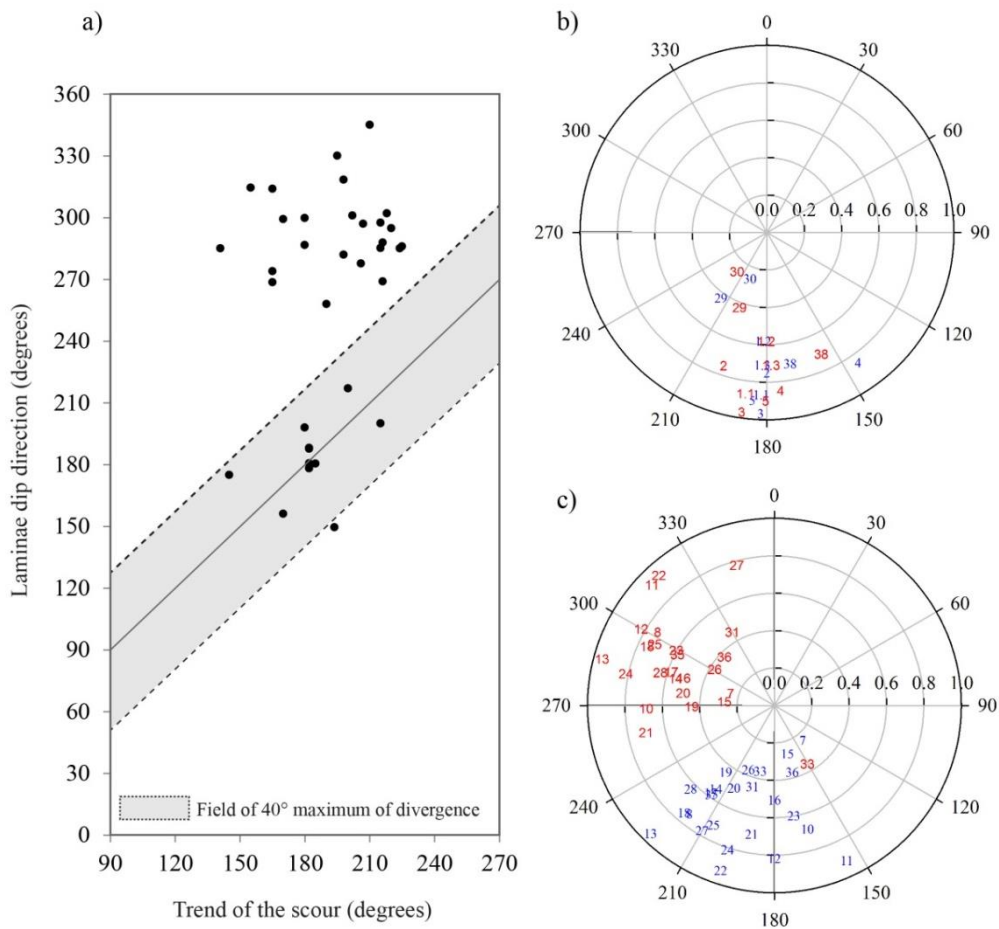


Figure 2.21 (a) Relationship between trend of scour and mean laminae dip direction of all scour structures with visible dimensions. Shaded grey band illustrates scour structures with less than 40° divergence between laminae dip direction and scour trend; (b) Graph showing scour structures that have less than 40° difference between lamina dip direction and scour trend; and (c) Structures with a difference larger than 40° (the radial axis represents the W/L). Note that in order to make an accurate comparison between dip direction and scour trend, the values of trend used for this comparison correspond to the natural data mode presented in Figure 2.19. N.B., the values of angle Θ for structures 7, 11 and 36 appear in this plot to be greater than 40° . However if the values of trend for these three structures were to be the closer azimuth value to the dip direction value for each structure in this case structure 7, 11 and 36 would present an angle Θ less than 40° .

The shape and size of the trough structures is also compared to the divergence between scour trend and lamina dip direction (Tables 2.8 and 2.9). Circular, oval 2 and elongate 2 shapes; and small to medium size predominate with a divergence between laminae dip direction and scour trend greater than 40° . This indicates flow local variations, or variations on bedform migration patterns as it appears to be a clear mismatch between trough orientations and laminae dip direction. Level of preservation can also explain these variations.

Table 2.8 Relationship of trough shape to the angle between the scour trend and lamina dip direction in percentages.

n	Shape	Θ			
		$\Theta < 5^\circ$	$5^\circ \leq \Theta \leq 20^\circ$	$20^\circ < \Theta \leq 40^\circ$	$\Theta > 40^\circ$
13	Circular	7.7	23.1	15.4	46.2
1	Oval 1	0	100	0	0
13	Oval 2	15.4	7.7	0	76.9
0	Elongate 1	0	0	0	0
11	Elongate 2	0	27.3	9.1	63.6
4	Unclear	-	-	-	-

Table 2.9 Relationship between trough size and the angle between scour trend and lamina dip direction, in percentages.

n	Size	Θ			
		$\Theta < 5^\circ$	$5^\circ \leq \Theta \leq 20^\circ$	$20^\circ < \Theta \leq 40^\circ$	$\Theta > 40^\circ$
10	Small	20	10	10	60
18	Medium	5.6	16.7	11.1	61.1
8	Large	0	25	0	75
6	Very Large	0	33.3	0	66.7

Section 2.9.1 shows statistical analysis results demonstrating no measureable relationships between the variations of trough dimensions and the relationship of scour trend to laminae dip direction.

2.8.4 Relationship of laminae dip direction to scour trend and preservation level of exposure and measurement accuracy

Significant variations between laminae dip direction and scour trend can lead to further understanding on river flow behaviour and depositional processes occurring on the lee-face of the host bedform. Similar variations have been observed in previous studies (e.g., Gradzinski, 1970; Mossop and Flach, 1983; and Wood, 1985).

Only 35 % of the scour structures described have similar values or minor mismatches between scour trend and mean laminae dip direction. The geometry of the structures, flow direction variation, and formative bedform crestline have implications on the calculation of the angle between scour trend and laminae dip. In addition, the preservation level of the exposures and field data acquisition accuracy levels have an effect of the divergence between laminae dip direction and scour trend (Fig. 2.22).

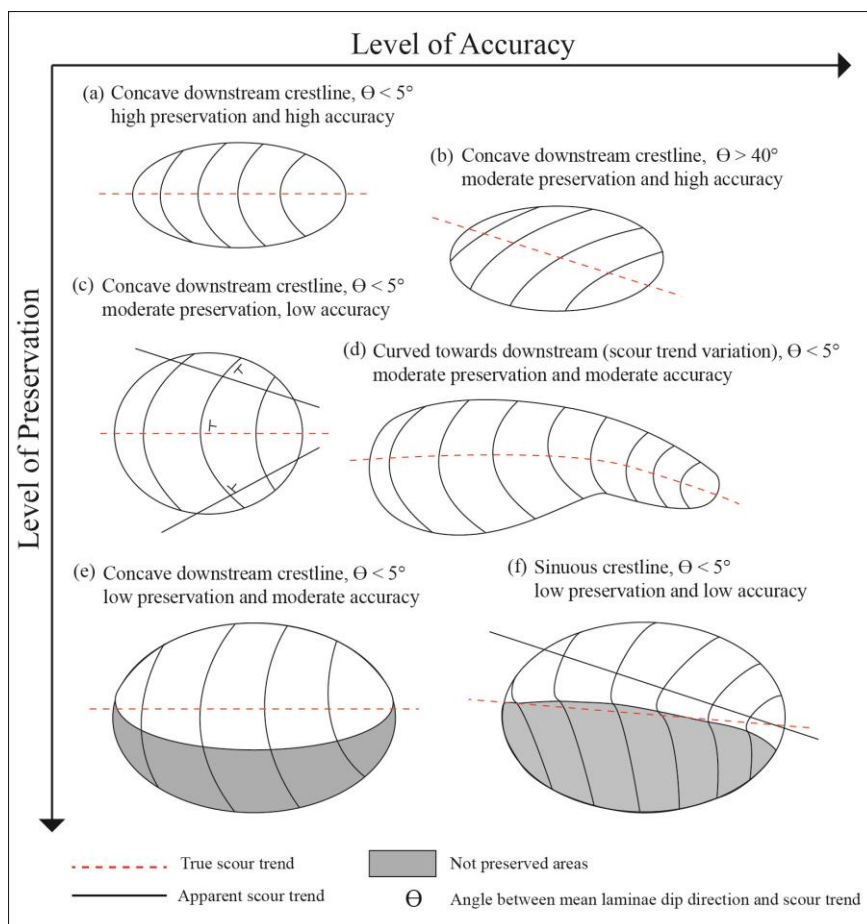


Figure 2.22 Relationship of preservation level and field interpretation accuracy on the analysis of scour structure geometry and estimation of the angle between mean laminae dip direction and scour trend.

In Section 2.7.1 a classification of scour structures based on their shape and dimensions was presented, but consideration of the level of preservation and irregularities in the structure shapes were omitted. These should be taken into account, when considering the classification and implications of structure type. Within this data, some structures exhibit near symmetrical shapes, whereas others tend to be more irregular and curved in the direction of the flow. Some of the structures appear to be fully preserved and some partially preserved (Fig. 2.22).

For the structures that are well preserved, the risk of making a wrong or an accurate interpretation is small (Fig. 2.22a, b). In contrast, less accurate interpretation occurs in cases such as when structures may have had a slightly sinuous lee-face toe, which may have been masked due to the level of preservation (Fig. 2.22f). Also, some structures are preserved with a curved centre line (Fig. 2.22d). In this case, it is possible that (1) the angle between scour long axis and dip direction (Θ) varies with the centreline curve or it may not (i.e., The dune face may have migrated in a constant direction into a curved scour or scour that became curved as the dune advanced) or (2) the lee face may have changed direction with the change of direction of the scour centre line. A third explanation (3) is that the curvature could be a function of partial preservation rather than record the original shape of the scour. If the scour is partially preserved, then, this may have implications for the interpretation and classification of the scour structures; since it will not be possible to assure which one of the possible situations explained above is the correct one and therefore the values of divergence between lamina dip direction and scour trend may or may not be accurate and the level of confidence in the interpretation will be low. There are other cases in which the scours may be full or nearly full preserved and the position where the measurements of dip directions are taken is crucial for an accurate interpretation (Fig. 2.22c). Therefore, assessing the level of preservation of the exposures is critical to accomplish a good interpretation from ancient deposits.

2.8.5 Relationship of laminae dip to trough shape and size

The laminae dip of individual trough cross-bed sets varies. Figure 2.23 relates the width:length ratio of scour structures to the mean laminae dip. Out of 42 structures only 36 were used due to unclear interpretation of their dimensions and dip planes. There is no measureable pattern of variation of width:length ratio with mean laminae dip. Thomas *et al.* (1987) observed that internal laminae dip angles vary down-dip. In 68 % of the structures, the laminae dip angle increases downstream; decreases in 14 % of the structures and fluctuates without any pattern in the last 18 % of the structures. Laminae mean dip angle values for individual trough sets and range from 3° and a maximum of 26° (Tables 2.10 and 2.11).

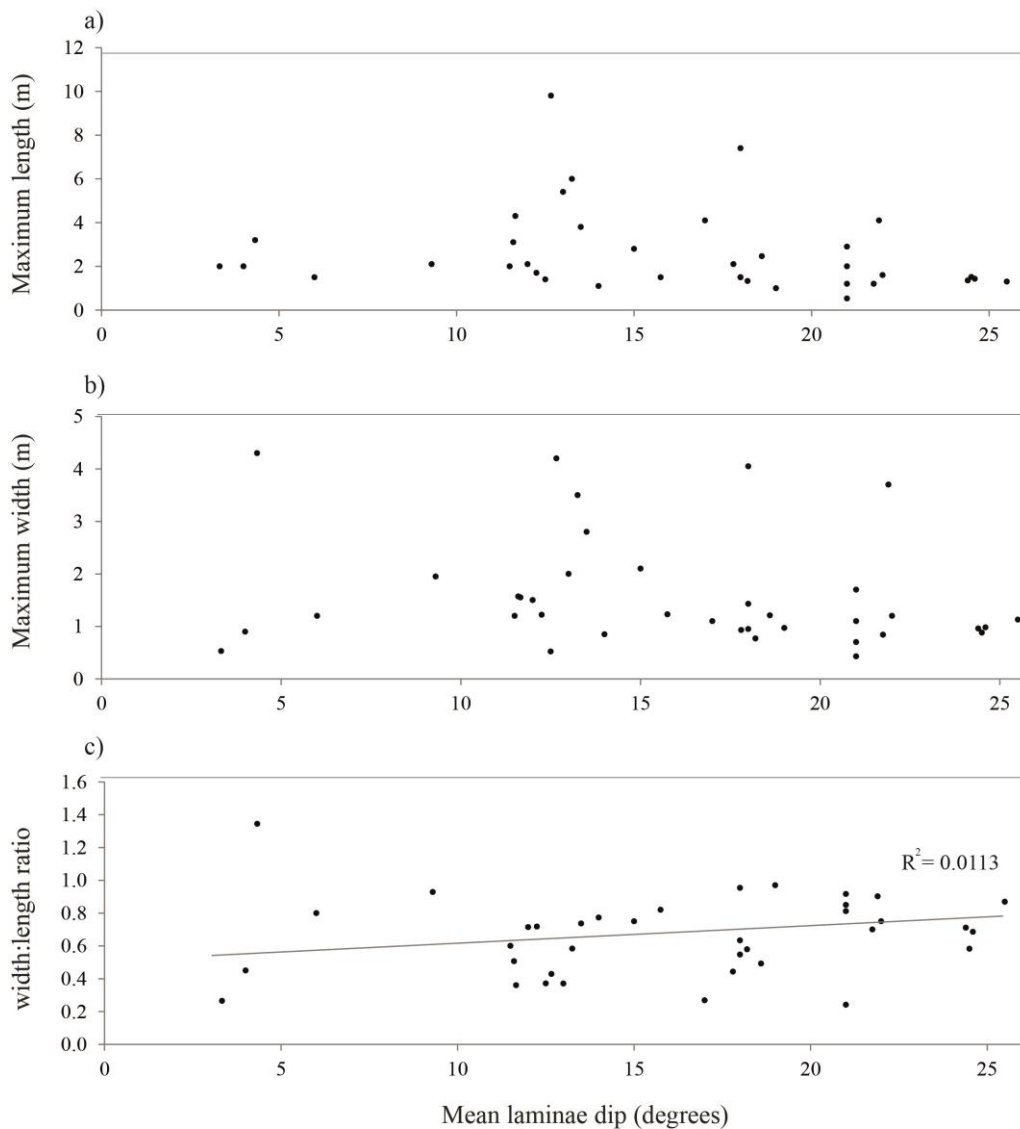


Figure 2.23 Relationship of trough dimensions to mean laminae dip angle. (a) Laminae dip to length; (b) laminae dip to width and (c) lamina dip to width:length ratio.

Table 2.10 Relationship of trough size to the lamina dip in percentages.

n	Size		Small	Medium	Large	Very Large
	Dip					
3	< 5°		0	66.7	33.3	0
4	5° - 10°		0	50	0	50
23	11° - 20°		21.7	39.1	21.7	17.5
12	21° - 30°		41.7	41.7	16.6	0

Table 2.11 Relationship of trough shape to the lamina dip in percentages.

n	Shape		Circular	Oval 1	Oval 2	Elongate 1	Elongate 2	n/a
	Dip							
3	< 5°		0	33.3	0	0	66.7	-
4	5° - 10°		50	0	0	0	25	25
23	11° - 20°		21.7	0	43.5	0	30.4	4.4
12	21° - 30°		50	0	25	0	8.3	16.7

Linear regression tests were performed aiming to find possible relationships between trough dimensions and mean laminae dip. These demonstrate that neither of the plots in Figure 2.23 have any relationship between the trough and the mean lamina dip. There is no measureable pattern of variation of W/L ratio with mean lamina dip angle (Section 2.9.3).

2.9 Discussion

2.9.1 Discussion on class boundaries classification criteria and relationship between classes

In order to differentiate different types of scour structures within the Rillo de Gallo study area, four characteristics were used for construction of classifications (Section 2.7.1). The criteria used to define these classes were based partly on natural clusters of data and were partly arbitrary.

Size is subdivided into four classes (small, medium, large and very large). The small and medium categories were defined following clusters of natural data that lay within fields (1: small) and (2: medium) (Fig. 2.17a). The large category was defined arbitrarily by equal spacing from the small and medium categories (at 4.5 m length). The very large category was also defined arbitrarily. Larger bedforms could have occurred in this system and generated larger scour structures that either were not fully preserved or identified within the study area; in this classification, scour structures with maximum lengths greater than 4.5 m are considered very large.

In the Prados Formation almost all the structures have lengths greater than widths. Only structure ST34 has a ratio width: length > 1 ; in this case field observations were unclear, and therefore there is some uncertainty about the accuracy of these recorded dimensions. In this study, structures with $W/L > 1$ are considered to be related to the preservation level, limited field area access, abundant vegetation coverage and inaccurate field interpretation. Consequently, this classification may be valid only if length \geq width and based on this data, observations that a structure has width $>$ length may suggest incomplete preservation or poor exposure and inaccurate measurement.

The structure shape was initially subdivided into 5 categories (elongate 1, oval 1, circular, oval 2 and elongate 2) (Fig. 2.17b). These were arbitrarily defined by using field observations of the geometries and observations from photographs. The data from the Prados Formation suggests that elongate 1 class does not occur in this field site; scour structure 34 with oval 1 shape is debatable due to preservation and circular and oval 2 are more common (Table 2.3). Since the shape of the structure results from a combination of original scour shape, scour growth and preservation, it is thought to be

adequate to maintain the shape classification subdivided into 5 categories (Section 2.7.1). If the suggested initial scour shape (type 2) (Fig. 2.16) is correct, then scour structures with resulting oval 1 and elongate 1 shapes may form under specific flow conditions with channel bed topography influencing the bedform migration pattern and scour development. Although based on the data presented in this chapter the majority of scour structures show width:length ratios smaller than 1, this data does not preclude shape categories with width:length ratios larger than 1 occurring in other deposits. Further analysis on similar trough-cross-bedded sets will allow subdividing more concisely and accurately the “Shape” classification into only 3 categories (circular, oval and elongate).

The classification based on the relationship of scour trend and mean laminae dip direction has four categories ($< 5^\circ$, 5° - 10° , 11° - 20° , 21° - 40° and $> 40^\circ$). These were defined partly on the basis of natural data clusters. Figure 2.21 shows a group of scour structures with a scour trend and mean laminae dip direction divergence of less than 40° . This boundary is used as the threshold to differentiate structures with a significant angle (Θ) between scour trend and mean laminae dip direction from structures with a moderate angle Θ . The other three categories were arbitrarily, equally spaced to differentiate different levels of Θ divergence within the structures with a moderate angle between the scour trend and the mean lamina dip direction.

The classification of scour structures and the comparisons between the individual categories corresponding to the size, shape and Θ classes indicate that most of the structures are $W/L < 1$ and for all the shape and size types occurring in this study area medium to very large structures predominate and generally the divergence between trend of scour and mean laminae dip direction tend to be greater than 40° (Tables 2.10 and 2.11). Linear regression was used to determine possible relationships between these classes (size, shape and Θ , in Table 2.12).

The width:length ratio was compared to the maximum length, mean laminae dip, angle between trend and mean laminae dip direction, and laminae dip direction modes. The maximum length was also compared to the relationship of mean laminae dip direction to scour trend and the laminae dip direction. None of the statistical tests show any relationship correlating these variables except from the W/L and maximum length

(length represents the class size) (Table 2.12). This relationship suggests that longer scours (elongate 2) are narrower and the wider scours appear to be oval 2 shape. Most of the scours with circular or near circular plan forms are of medium and small size. Whilst, it may be a statistically significant relationship, it only explains 0.1087 of the variability, so the relationship is extremely weak. This suggests that the scour length is controlled by original scour shape and growth, so the longer the scour is active in a migrating system the longer the resulting trough and more likely it is to have an elongate 2 shape. The lack of any correlation between the scour geometry and the other parameters (e.g., laminae dip direction, laminae dip, Θ) may indicate that the preserved maximum length of the scour does not relate to the way in which the dune front migrated into the scour, nor the chance of the direction of that advance differing over time. Other factors such as the life duration of the bedform, space availability (channel dimensions), flow regime and duration of flow in equilibrium, water depth may relate to the variations of the initial scour shape and their growth.

Table 2.12 Coefficient of determination and significance of the relationship between scour structure classification classes and other variables.

	W/L vs size class (length)	W/L vs Laminae Dip	W/L vs Θ class	W/L vs Mean Laminae dip direction	Size class (length) vs Θ class	Size class (length) vs laminae dip direction
R^2	0.1087	0.009	0.031	0.006	0.0022	0.004
Coefficient of Significance	0.0047	0.577	0.311	0.648	0.786	0.731

2.9.2 Discussion on the relationship of dip direction modes to trough shape and size; and the stratigraphic location of the structures as an flow pattern indicator

A hierarchical clustering statistical t-student test groups mean laminae dip direction in two modes (Section 2.8.3) towards the northwest and SSW with 109° divergence. To examine the relationship between width:length ratio (shape) and mean laminae dip direction a linear regression statistical test was run that showed no relationship between these two variables ($R^2 = 0.006$, $S = 0.648$).

Table 2.13 Relationship of mean laminae dip direction modes and scour structure shape (in percentages).

N	Shape	Circular	Oval 1	Oval 2	Elongate 1	Elongate 2	n/a
	Mode						
11	Mode I	45.5	0	27.3	0	27.3	0
24	Mode II	29.2	0	41.7	0	29.2	0
7	n/a	14.3	0	0	0	14.3	56.6

In the Prados Formation the laminae dip direction of individual scour structures varies vertically and laterally in the sequence. Mode I predominantly occurs in Units 7 and 8 (Storey 3) within the western flank of the exposure (Fig. 2.7). Mode II occurs in structures 36, 35, 34 and 31 and these correspond to thicker sets. Structures 7 to 28 are located within Unit 7 in the eastern flank and correspond to thinner sets of Facies St with interbedded and laminated sandy silts (Facies Fl). Scour structures (within Mode I and Mode II) located in Units 7 and 8, show a mean laminae dip direction variation. This infers that the flow direction of the streams that generated the Prados Formation varied at the same stratigraphic surface. This may support previous studies (Ramos, 1979) in which these deposits were interpreted as deposits of high-sinuosity streams, but could also result from different channels occupying the same level either at the same time (anabranching or tributary) or with a short time interval (too small to resolve in the stratigraphic section).

To examine the relationship between the scour structure size and mean laminae dip direction a linear regression statistical test was run that showed no relationship between these two variables ($R^2 = 0.004$, $S = 0.731$) (Table 2.14).

Table 2.14 Relationship of mean laminae dip direction modes and scour structure size (in percentages).

N	Size	Small	Medium	Large	Very large
	Mode				
11	Mode I	27.3	45.6	18.2	8.9
24	Mode II	29.2	45.8	12.5	12.5
7	n/a	0	28.6	42.9	28.5

From the base towards the top of the sequence the size categories vary from the lower to the upper storey (Table 2.15). The lower storeys appear to be dominated by larger structures; medium and smaller structures tend to dominate towards the top of the sequence. Towards the base of Storey 3 individual troughs became larger laterally from east to west. Although there is no measureable relationship between lamina dip direction and trough size, evident variations of the scour developed sizes laterally and upwards in the sequence indicate that the variations of scour size are controlled by variations in the flow, duration of flow and the life time of the beforms that generated these structures. In addition, the level of preservation once again has an important role; poor assessment of preservation level will lead to inaccurate and unrealistic interpretations.

Table 2.15 Relationship of scour structure size and stratigraphic position within the sequence (in percentages).

N	Size				
	Storey	Small	Medium	Large	Very large
6	1	0	16.7	16.7	66.6
5	2	0	60	40	0
31	3	32.3	45.2	16.1	6.4

Beside the limitations in field interpretation related to the preservation level; the detailed analysis of trough cross-bed sets in plan-view and the attempts to interpret where these scour structures are located within the whole sequences corresponding stratigraphic locations help to trace flow variations across individual surfaces (units) adding useful information to the main analysis of palaeocurrent distribution across the study areas.

Herein, from the base of the sequence upwards; in Storey 1 the mean laminae dip of scour structures is 12° ($n = 3$), 10° in Storey 2 ($n = 3$) and 17° in Storey 3 ($n = 35$). Comparison of these mean dip values assumes that they are representative of the storeys but given the small number of data from Storey 1 and 2 here the differences may be a statistical sample selection problem. The laminae dip increases upwards in the sequence (Fig. 2.7) where Facies St become slightly finer and also interbedded layers of mudstone are more frequent.

Exposures 1, 2 and 3 are located within Storeys 1, 2 3 respectively (Fig. 2.7). Palaeocurrent data from Exposures 1-3 (Fig. 2.2A; Section 2.6.2) and palaeocurrent data measured all over the study site (Fig. 2.2C) can also be used to assess the variation of the site dominating trough cross-bed sets laminae dip. Mean laminae dip measured in Exposures 1-3 ranges from 7° to 18° and appears to decrease towards the top of the sequence (Table 2.16). This does not agree with the variation of mean laminae dip observed in Storeys 1-3. This can be explained by the small amount of data points measured in Storeys 1 and 2. The mean laminae dip of all the data covering Rillo de Gallo site is 15° (n = 146).

Table 2.16 Mean laminae dip in Exposures 1-3 (Section 2.6.2).

N. exposure	n	Mean Lamina Dip (degrees)
Exposure 1	21	18
Exposure 2	37	16
Exposure 3	18	7

To summarise, towards the bottom of the sequence scour structures tend to be larger with variable shapes; and towards the top, the number of smaller and near circular to oval shape trough cross-bed sets increase. The laminae dip tends to decrease towards the top of the sequence but it also changes laterally within the top storey. Within individual storeys, individual trough cross-bed sets decrease in size upwards.

2.9.3 Discussion on the lack of relationship between width:length ratio and laminae dip

To examine the relationship between trough dimensions and mean laminae dip a linear regression analysis was performed (Table 2.17). The results demonstrate that there are no measureable relationships between trough visible maximum dimensions and the laminae dip.

Table 2.17 Coefficient of determination and significance of the relationship between trough dimensions and mean lamina dip.

	Length vs Laminae dip	Width vs Laminae dip	W/L vs Laminae dip
R ²	0.041	0.046	0.0113
Coefficient of Significance	0.204	0.232	0.577

In addition, an analysis of paired sample t-test between width:length ratio and mean laminae dip was run indicating no measurable relationship between these two variables ($S = 0.577$).

This indicates that the size of the scour and the dimensions of the host bedform that advances downstream are not closely related to the dune lee-face angle. The lee-face angle is being controlled probably by the grain flow mechanisms on the lee face of the dune, the superimposed bedform dimensions, and the variations of the channel topography (cf. discussion on Chapter 5 and Section 6.4.1). At the same time, these controls are related to sediment supply rate, sediment transport rate and flow conditions, which then will be also related to the variations of host-bedform lee-face angle.

The shape of the scour may be controlled by the water flow in the lee of the dune assuming that they formed in the same flow and not in different times in a changing flow. It may be also controlled by the dimensions of the host dune, which partly define the distance between the lee-face toe and the beginning of the following downstream bedform stoss face and therefore, the size of the scours between migrating host bedforms. Therefore, the controls on grain behaviour on the lee face are not the same as the controls on the scour of the bed in the lee, or that the controls that are the same are not strong enough in respect to other controls to give a correlation in the rock record.

There is no correlation between the relationship scour trend to laminae dip direction and lamina dip. The lamina dip ranges from 5° to 30° and the mean laminae dip ranges from 3° to 26°. In 68 % of the structures the laminae dip tends to increase downstream. The lamina dip variation within a single structure is related to the fluctuations of the host bedform height but not systematically (cf. Section 5.3.8, Fig. 5.22).

2.9.4 Discussion on the relationship scour trend and mean laminae dip direction

The variation in angle between the trend of the long axis of the scours and the mean dip direction of the internal laminae is documented in Sections 2.7.2 and 2.8.3, Tables 2.1 and 2.2). In the Rillo de Gallo data set 64.3 % of the scour structures have a divergence between mean laminae dip direction and trend of the scour greater than 40° (Fig. 2.21). The variation in the mean laminae dip direction records differences in bedform progradation either due to temporal or spatial single or multiple fluvial events. The variation of scour trend indicates variations of flow direction within the same or preceding event, which may or may not have a significant effect on the flow direction. The analysis of the mean dip direction across the study site is necessary to study the occurrence of significant variations of main flow direction and the interpretation of these variations and their implications for the interpretation of channel type.

To examine the relationship between scour trend and mean laminae dip direction a statistical analysis of paired sample t-test was run indicating no relationship between these two variables ($S = 0.268$). This variation may be partly a function of channel regime causing a variation in shape and bedform development, and partly a function of preservation. Some factors that can explain this are: (1) the nature of the exposure, (2) the level of preservation and section observed in the field, (3) the change in flow direction, (4) host bedform crest development, and (5) field interpretation.

Some exposure characteristics such as the type of preserved exposure (i.e., exposure preserved in vertical faces or plan-view forms), regional and local tectonics can generate variations in laminae dip direction and scour trend values. The level of exposure preservation can have major implications on the variation of these two variables. In order to obtain accurate data, it is important to assess the level of preservation of the exposure and to determine which areas are favourable to obtain measurements from (Fig. 2.22). Therefore, it is important to record where the measurements have been taken (e.g., within an individual trough, measurements should be taken at the point nearest to the central axis of the scour). In this study, field assessments on preservation level were carried out to record reliable data. Knowing this, a degree of inaccuracy needs to be taken into account. Unreliable data (e.g., due to preservation) recorded in this study was not used in any statistical test.

The variations between laminae dip direction and scour trend can also be explained as local flow changes within the channel and may indicate that the location where these structures formed was more susceptible to change in the flow regime. The host bedform crest type is another factor that controls the variations of the laminae dip direction and scour trend measured in the field. Most of the trough cross-bed sets in the Prados Formation have been interpreted as Facies St generated by 3-dimensional dunes with sinuous crests. Large and very large structures could also have been formed by large bedforms such as bars. Not entirely preserved plan-forms generated by the migration of large-scale bars can be mistaken for smaller scour structures generated by dunes. Consequently, measurements of laminae dip direction and especially measurements of the scour longer central axis can be poorly estimated if scour structures generated by bars are interpreted as generated by dunes.

The variation (greater than 40°) between the lamina dip direction and the scour trend in 64 % of the observed scour structures may infer that (1) irrespective to the orientation of the main channel or sub-channel, in which these sediments were transported, this divergence may occur. This is probably related to the inherent variation in orientation of the bedforms, their nature (bedform sinuosity) and the inherent variation in the long axis of the scours relative to the mean flow direction as bedforms advance downstream. Divergence of 45° between the axis of the scour and the main flow direction are commonly observed in other systems (e.g., Ripples observed on the Rio Grande bed (Harms and Fahnstock, 1965) in structures formed by small-scale bedforms defined as linguoid ripples by Allen (1963b); (2) and also this variation may be related to the channel type and they interaction between bedforms within the main channel or sub-channel and their exact positions within it.

2.9.5 Discussion of controls on scour structure geometry

Based on previous studies mentioned in preceding sections and the data gathered in this study, some of the factors associated with the development of scour downstream of large migrating bedforms are discussed. Although it is possible that bedforms may prograde into scours formed by previous flow conditions; it is probably more common for the initial scours that result in scour structures to be initiated in response to flow patterns downstream of bedforms formed due to the interaction between flow and sediments. Variations in flow, the nature of the river channel, variations in sediment

supply and type of sediment will have some impact on the initiation of scours (timing, size and shape). Also, specific areas within the channel are more susceptible to scouring. This depends on the morphology and dimensions of the channel and the dominating flow regime and its variations. Together these can generate areas with more turbulence or more coherent flow structures (cf. Best, 2005) that may generate localised increase in sediment entrainment (erosion) and thus scours.

Bed irregularities, such as growing bedforms may produce cross-stream variations in flow pattern and thus localised areas of high bed shear stress that may trigger scour growth. Conversely, the development of a scour may trigger initiation of bed topography downstream of the scour (as the displaced sediment is re-deposited). Thus there is a chicken and egg problem and once bedforms with scours are initiated they will evolve due to changes in flow and migration of bedforms. Harms and Fanhestock (1965) suggested that a train of 3-dimensional bedforms is needed for the development of scoop-shape structures. Controlling factors on the type of bedforms that form will directly relate to the initiation of spoon-shape scours such as: (1) the flow regime that determines the bedform configuration (Simons *et al.*, 1965), the development of trains of 3-dimensional bedforms and the subsequent concave-upward deeps (i.e., scours) in between bedforms; (2) the mode of bedload transport and transport rate associated with bedform dimensions and bedform migration rate that will affect the scour rate, depth and propagation length and (3) the geometry of the primary channel that also relates to bedform type and configuration.

The size and shape of the scours are controlled by the flow, channel dimensions, flow duration and topography of the channel floor (including initial geometry of bedform). The migration of bedforms and the transition between 2-dimensional to 3-dimensional bedforms control the development of local scours between bedforms. In the case of scours that form in repose to coherent flow structures formed downstream of a bedform, the depth of scour may increase when bedforms crestlines become strongly concave downstream (Venditti *et al.*, 2005). If the depth of a scour is increased the bedform that migrates into it may decelerate (unless local sediment flux increases) as the volume of sediment needed for the bedform migration increases. Thus, the host bedform crestline morphology and its development are significantly related to the evolution of the initial scours. Bedform crestlines develop by the lobe extension mechanism and the growth of

the scours between bedforms. A continuous increase in bedform height and length will maintain the lobe extension mechanism and consequently scour growth (Venditti *et al.*, 2005a) (cf. Fig. 1.4 on Chapter 1).

In Section 2.7.1 a classification of scour structures based on the initial shape of the scours was suggested, that due to the lack of literature on scour formation in association with bedforms was based on three hypothetical cases of scour initiation (Fig. 2.16). In the Prados Formation, troughs of large dimensions and elongate shape present more or less a constant width and are elongate in the palaeocurrent direction. Assuming steady flow; if the initial scour had a width:length ratio close to 1, and develop in length downstream as the bedform migrates, it will have taken longer for the laminae set to prograde down and into a longer and wider trough. If the initial scour had a width:length ratio considerably less than 1 (elongate 2 shape with central long axis parallel to the flow), then the scour will take longer to generate cross-bedded trough with a W/L close to 1. If the initial scour was slightly wider than long, then the duration of the flow will mainly determine the final shape and dimensions of the trough.

Sediment transport rate, flow velocity, channel depth and width and water depth are factors that affect the development of the trough scour from its initial stage to its final fill. Distribution of flow pattern transporting sediments downstream across the bedform crest may also have implications in the geometry of the resulting scour structures. In addition to these factors, the period of scour growth determines the final morphology of individual trough cross-bed sets. If dunes migrate at a constant rate (a big assumption) then to prograde down a longer trough will take longer. Variable flow conditions and palaeocurrent data dispersion help scour structures to grow in different directions and develop from circular, oval to elongate shape, preserving evidence of flow direction, channel physical geometries and information on the deposits in relation to the location of deposition within the main channel or distributary channels. In a straight braided system or the straight section of any other type of channel system, elongate troughs can be interpreted as the result of rapid events where sediment deposition was fast and flow direction was steady or in longer periods of time in which the flow was steady and reached an equilibrium stage which allowed the scour to develop evenly recording longer periods of growth. Thus, the scour might be fast formed and not necessarily related to steadiness or uniformity or it might form over a longer time because of a

longer lived pattern of flow over the bedform. Circular troughs can be interpreted as the result of shorter lived pattern of flow over a bedform and fast sediment deposition, single predominant flow direction, constrained channel dimensions and flow steadiness and uniformity.

From the data presented in this thesis it is not possible to resolve confidently the causes of scour initiation and the factors that are related to their growth and development. Further investigations on modern systems and flume work will be needed to study accurately the three hypothetical initial scour shapes here suggested. Flume work will be useful to investigate the scour initiation and development on the basis of three variables, sediment rate, flow velocity and morphology of the channel. Studies on modern systems will be useful for the comparison with flume results and assess the level of accuracy obtained by using flume laboratories.

The detailed analysis of scour structure dimensions, laminae dip direction, laminae dip, scour trend amongst other variables allows understanding of the nature of the river and the bedforms that were generated, as well as local variations of the flow within the main channel and in local sections of the channel. In addition, the analysis of scour structures geometries allows larger-scale information on set thickness (this is better observed in vertical faces), bedform height and estimation of bedform dimension, flow depth, and estimation of channel width to be obtained.

The scour structures observed in the Prados Formation (Rillo de Gallo) include a full range of sizes from small to very large with a predominance of medium and small structures indicating bedforms of various scales forming trough cross-bedding. The Prados Formation sequence that is subdivided in three upward-fining cycles presents a predominance of smaller structures towards the top of the sequence (the number of smaller sized bedforms increases upwards in the sequence). This indicates variations in the flow regime towards the top of each storey and also variations of the flow dynamics as the channel migrated. This can be explained by a decrease in flow velocity and grain size. Based on the defined shape class (Section 2.7.1) these structures appear to be circular, oval 2 and elongate 2 types indicating a width:length ratio less than 1 in all cases. The occurrence of scour structures of different shapes and dimensions indicates flow regimes of different velocity and duration and possibly variations in sediment rate;

the occurrence of different type of structures within a close area of the same stratigraphic surface indicates rapid variations in flow. Single and multiple flow periods can generate these structures. The structures vary in size and shape vertically in the sequence and across units. This indicates variations of flow in space and time. The level of preservation and quality of field interpretation are critical points that will direct final interpretations to an accurate outcome (Fig. 2.22).

2.10 Re-interpretation of the nature of the original channel

Channel geometry is defined by depth, width/depth ratio and plan form shape (including sinuosity and braiding index). In this section the channel dimensions have been estimated based on the preserved cross-set thickness following previous studies (e.g., Leeder, 1973; Ethridge and Schumm, 1978; Leclair and Bridge, 2001).

2.10.1 Discussion of channel depth and flow depth

The depth of the channel(s) that deposited the sandstones in the Prados Formation has been estimated initially by following the methods of Leeder (1973) and Ethridge and Schumm (1978). They suggested useful relationships relating bankfull depths and widths that can be used for palaeochannels that deposited fining-upwards sequences. According to Allen (1970) fining-upwards cycles are formed by a (1) coarse member consisting of large-scale cross-stratified units, upper phase plane beds and small-scale cross-stratified units; and (2) fine sediment due to vertical accretion representing periods of abandonment or channel avulsion. The bankfull channel depth is commonly estimated from the decompacted thickness of untruncated channel bar/fill deposits (Bridge, 2003). The thickness of the coarse member (1) equals the bankfull depth of the river (Leeder, 1973).

The most complete and thickest fining-upwards cycle identified in the Prados Formation is c. 17 m thick (Section 2.5.2), however the thickest coarse member appears to be the one corresponding to Storey 2, 13.3 m thick (Fig. 2.7). If Leeder (1973) was correct, then the bankfull depth estimate is 13.3 m. However most likely Leeder's (1973) estimates can be underestimated because (a) channels often do not fill to bank full level and upper parts full of overbank deposits are difficult to identify in the rock record, (b)

the storey thicknesses may be underestimated because of truncation and (c) the channels may not have been meandering.

There are a number of reasons why this estimate might not be reliable. Most importantly it assumes that there is full preservation of the thickness of the channel fill, and that the top of the channel fill has been reliably identified. It also assumes that there has been no reduction in thickness resulting from consolidation or compaction after deposition and during burial. In addition, the bankfull depth of the channel is most likely larger than the channel fill sandstone (Bridge and Mackey, 1993). In this study, it is assumed that the Prados formation consists only of three storeys. It is common for channels to enlarge due to extreme, rapid events, with a long time span for recovery in which high discharge, high flow velocity and large-scale bedforms truncate and erode masking previous deposits (Yu and Wolman 1987). Therefore, the estimation of channel dimensions based on cross-bed set thickness may reflect an extreme size of the channel in discharge conditions or partially the full channel dimensions, and so this methodology should be used with caution.

In addition, large-scale bedform deposits thickness can vary laterally in space in different locations within a meander (e.g., bar deposits, Bridge *et al.*, 1995) and consequently the storey varies in thickness, and therefore these estimations will not be fully representative of the channel dimensions. Indeed studies of modern point bars illustrate that the bar top does not often equate to the bank full level, and that it changes around the bend of a meander, and in different meanders within one meander belt (Gawthorpe *et al.*, 1993; Bridge *et al.*, 1995).

Leclair and Bridge (2001) suggested that mean dune height can be calculated directly from cross-bed set thickness and vice versa, independently of aggradation rate. They suggest a method which allows to quantitative interpretation of sedimentary structures formed by dunes:

$$h_m = 2.9 \times \text{mean cross-set thickness} \quad (\text{Leclair and Bridge 2001}) \quad (2.1)$$

Herein, the mean dune height in the Prados Formation was estimated as 1.23 m using Leclair and Bridge's (2001) relationship with set thickness. Mean dune height generally

increases with flow depth (Yalin 1964; Allen 1982; Bridge and Tye 2000). The flow depth:mean dune height ratio tends to vary significantly (e.g., $3 < h_m/d < 20$); this variation can be explained because dunes were most likely not in equilibrium and also dune height is relative to their wavelengths and flow depth, which increases drastically in the transition between bedform stability fields. For dunes that reach equilibrium the window h_m/d is smaller (6-10) (Bridge and Tye, 2000). Leclair and Bridge's (2001) theoretical model for the dune height estimation from the thickness of sets of cross strata was based on experimental data from a range of flumes and rivers, which most likely has an inherent degree of error due to unrealistic experimental settings in comparison to natural rivers (e.g., channel width, morphology and topography of the channel). Although prediction of flow depth from cross-set thickness and dune height is imprecise, it provides useful information for other methods for estimating flow depth from sedimentary information.

The mean flow depth of the channel was estimated following Yalin's, (1964) and Allen's (1970) empirical relationships between mean dune height and depth:

$$\frac{d}{h_m} = 6 \quad (\text{Yalin, 1964}) (2.2)$$

$$d = 11.6 h_m^{0.84} \quad (\text{Allen, 1970}) (2.3)$$

Hence, by using Yalin's (1964) and Allen's (1970) relationships, the estimations for the channel flow depth are 7 m and 14 m respectively (Table 2.19).

This method also introduces inaccuracy to the dune height estimates and consequently to the estimates of the bankfull depth. It assumes that the cosets of cross-strata within the fluvial system are homogeneous, indicating that there is not a clear spatial variation in thickness of the cross-bed sets, and so that the dunes did not vary significantly in geometry; and this is unlikely to happen. In the Prados Formation set thickness varies (Section 2.6.2); therefore the size of the bedforms that generated these deposits also varied and so did the water depth. In addition, cross-stratification generated by larger bedforms tends to be preserved whereas the cross-stratification generated by smaller scale bedforms is often eroded and truncated by the migration of larger bedforms. This

infers that the observed deposits may represent stages where the channel had enlarged due to extreme and rapid events. Values of mean dune height (Table 2.18) were used to estimate the channel dimensions (Tables 2.19 and 2.20).

Table 2.18 Estimates of mean values of dune height.

Equation	Reference	Mean dune height (m)
$h_m = 2.9 \times$ mean cross-set thickness	(Leclair and Bridge, 2001)	1.23

Table 2.19 Estimates of channel depth/flow depth

Basis of estimate	Equation	Reference	Resulting depth estimate (m)
Depth = storey thickness	$d =$ coarse member of preserved fining-upwards cycle	Leeder 1973	13.3
Depth from dune height	$\frac{d}{h_m} = 6$	Yalin (1964)	7
Depth from dune height	$d = 11.6 h_m^{0.84}$	Allen (1970)	14

2.10.2 Discussion of channel width

The width of the channels is more difficult to estimate from the preserved deposits. Leeder (1973) suggested that the width of a point bar is approximately two thirds of the total channel bankfull width. Leeder (1973) demonstrated that using the 95 % confidence limits and data from Endrick, Mississippi and Klaralven amongst others (e.g., Fisk, 1944; Sundborg, 1956; Leopold and Wolman, 1960; Rozovski, 1963; Schumm, 1963; Chitale, 1970 and Bluck, 1971); upper values of channel width can be estimated from storey thickness. He compared data from low to high sinuosity rivers and no direct relationship between bankfull depth and width was observed; in contrast he found that width and depth were related by using data corresponding only to high-sinuosity rivers.

The close empirical relationship between width and depth of the channel is:

$$\log w = 1.54 \log h + 0.83 \quad (\text{Leeder, 1973}) \quad (2.4)$$

$$w = 6.8 h^{1.54} \quad (\text{Leeder, 1973}) \quad (2.5)$$

where w = bankfull width and h = bankfull depth.

Table 2.20 Estimates of channel width

Equation used to calculate channel depth	Channel assumed (m)	Equation used to calculate channel width	Estimated channel width (m)
Leeder (1973)	13.3	$w = 6.8 h^{1.54}$	366
Yalin (1964) (2.2)	7	$w = 6.8 h^{1.54}$	148
Allen (1970) (2.3)	14	$w = 6.8 h^{1.54}$	387

N.B., Two channel depths and widths are calculated per method by using the mean dune height estimates.

The bankfull width cannot be measured straight forwardly. Other previous studies present empirical equations to estimate the channel width, and these are related to parameters such as the point-bar dip angle, the meander wavelength and, meander-belt amplitude (Leeder, 1973; Collinson, 1978 and Lorenz, 1985) (Table 2.21).

Table 2.21 Other previous studies' bankfull estimates empirical methods.

Reference	Equation	Legend
Leeder (1973)	$w = 1.5h/\tan\beta$	w = bankfull width h = bankfull depth β = point-bar dip angle
Leopold <i>et al.</i> (1964)	$L_m = 10.9 \times w^{1.01}$	L_m = meander wavelength w = bankfull width
Lorenz (1960)	$W_m = 7.44 \times w^{1.01}$	W_m = meander-belt amplitude w = bankfull width
Collinson (1978)	$W_m = 64.6 \times h^{1.54}$	W_m = meander-belt amplitude w = bankfull width

None of the architectural elements revealing the dimensions needed to calculate bankfull width estimates shown in Table 2.20 were identified in the study site.

Ramos *et al.* (1986) described the overall deposits of the Guadalajara Sequence described in Section 2.2 as the main infilling of channel system/s, which is comparable to the South Saskatchewan type of Miall (1977 and 1978). Cant and Walker (1978) described the major channel dimensions of the braided South Saskatchewan River as up to 5 m deep and 200 m wide. The lower units of the Buntsandstein sequence (Fig. 2.3), which includes the Prados Formation, record a variation in fluvial styles due to the tectonic activity that occurred during the Triassic sedimentation. These fluvial systems were first dominated by broad braided channels with high width/length ratios that evolved into higher-sinuosity channel/s. The Prados Formation is dominated by cross-stratified deposits that record major bedform migration within a higher sinuosity channel or a bend within a reach of a braided river. These channels are expected to be comparable in size to previous dominating systems with high width/length ratios (Ramos, 1986). Thus, the channel estimates resulting from dune mean height appear to be realistic and agree with previous published work. Based on these estimates, the Iberian River compares to medium meandering river examples considering the wide range of channel dimensions estimates obtained herein (Table 2.20). Yalin's (1964) channel estimates appear to be close to what was expected, whereas the estimates according to Leeder (1973) and Allen (1970) suggest a deeper channel. Although the comparison of channel dimensions with the following examples is not a perfect fit, it gives an idea of the scale of this river. Estimates within a section of the Rhine River, Germany suggest channel widths up to 500 m and channel depth of 7 m (Carling *et al.*, 2000). Shadid and Mountney's (2009) channel bankfull depth estimates from fining-upwards cycles of the Permian Warchha Sandstone (Pakistan) varied from 3 to 5 m. Considering the large channel estimates compared to the size of the exposure, the river at Rillo de Gallo could also be compared to a braided river reach; and considering the lack of evidence that the Prados Formation was formed by a high-sinuosity river, braided fluvial-style should still be considered as the possible formative river.

Channel dimension estimates based on maximum dune height values (3.77 m maximum dune height at Rillo de Gallo) indicate the hypothetical dimensions of the channel in the maximum stage of enlargement possibly due to an extreme and rapid flooding event,

which will give a suggestion of channel dimensions under extreme flow and sediment transport rate conditions. This would indicate that the Iberian Triassic River was moderately large, which appears to be reasonable in the case of a channel at its largest stage due to extreme fluvial conditions. Channel width estimates using the maximum dune height (839 m by Yalin, 1964 and 1623 m by Allen, 1970) are similar to other low and high-sinuosity river systems and hence, the river that generated the Prados Formation could compare to moderately large meandering rivers, although the channel depth estimates from The Prados Formation appear to be deeper than the following examples. Moody-Stuart (1966) suggested meander belts to be up to at least 1.5 km in width from Devonian deposits of Spitsbergen, Norway. Smith (1987) described an exhumed example of Permian point bar deposits in the southwest Karoo, South Africa, and estimated the channel width to be 3 km. Estimates from a multi-meandering channel, multi-storey fluvial meander –belt sandstone bodies in the Palaeogene Boyabat Basin (North-Central Turkey) suggested a channel width up to 900 m and channel depth of 5 m (Guinassi *et al.*, 2014).

2.10.3 Discussion of channel plan form

Reconstructions of channel plan-form from ancient fluvial deposits; sinuosity and braid index, are very difficult to estimate unless there is access to well-preserved wide range of scale deposits and large plan-view exposures of preserved palaeochannels or bars. Traditional methods of interpreting plan-form facies patterns (e.g., interpretation of fluvial deposits in the rock record) can be unreliable. Methodologies using well-logs and cores rather than only interpretations from outcrop analogues will give more accurate results (e.g., Bridge and Tye, 2000). Other methodologies such as quantitative seismic geomorphology and 3D-seismic interpretations of channel patterns have improved interpretations for the rock record but are still ambiguous. Rivers may change plan-form over short distances and at any one place over relatively short time periods (Ethridge, 2011). Accurate understanding of sandstone bodies dimensions in the fluvial rock record is necessary for the improvement of fluvial system reconstructions. Holzweber *et al.*, (2014) suggested remote sensing imagery as a method that allows estimation of large-scale bedforms dimensions and therefore to reconstruct their plan forms. This will provide useful information in the reconstruction of the 3D-architecture of fluvial deposits. In this study, only traditional methods have been used due to the specifications and possibilities available; and this data and the compiled interpretations

aimed to add useful information on the type of the fluvial system forming the Prados Formation.

Following Friend *et al.* (1979), Friend (1983) and Blakey and Gubitosa (1984) this channel would be classified as a “*mobile-channel*” characterised by being filled by a process of channel migration or switching within a single major scour. According to Ramos (1979), sandstones within the Prados Formation were deposited by high-sinuosity rivers. The Prados Formation exposed in Rillo de Gallo consists of three fining-upwards sedimentary storeys with a total maximum thickness of c. 40 m, and dominated by large-scale trough cross-bedding. These represent three channels occurring within the study site. The fining-up and thinning-up sets of cross-bedding are characteristic of a *point-bar cycle*, but similar patterns can form in different plan-form systems (Ethridge, 2011). The absence of overbank fines in the two lower storeys may result from erosional truncation by the channel that formed the upper storeys. It could have also occurred that fine sediments were never deposited towards the top of Storeys 1 and 2, being the channel fill elements the main element characterising these two channels, which is more characteristic of braided systems. No evidences of sigmoidal cross-strata (cf. Allen 1963b) were found. This is evidence of the lateral-accretion off lap sequence type and is one type of inclined heterolithic stratification (Thomas *et al.*, 1987). Often, when a lateral accretion surface dips at a low angle it can be masked by the scour surfaces and constructional bedding surfaces (Fielding *et al.*, 1999).

The data presented herein correspond to smaller area than the area surveyed by Ramos (1979); the palaeocurrent data recorded over the site show variations of the flow direction showing a polymodal pattern with modes to the south, southwest and to the west (Fig. 2.5). Previous studies in this site (Ramos, 1979) do not clarify if the interpretation based on the palaeocurrent data took into account a subdivision of the Prados Formation in fining-upwards sequences. The use of that data as one full set may have led to the conclusion that a high-sinuosity system generated these deposits, rather than concluding that three channels occurred leaving these deposits behind. Then, the variation of the flow may be explained by the variation of orientations of each individual channel.

The palaeocurrent data also show flow variations within individual storeys. Storey 1 has two modes towards the southeast and the southwest; Storey 2 has two modes towards the southwest and northwest and Storey 3 has two modes towards the south and the northwest. The flow variations in the Storeys 1-3 could be interpreted as local variations of the flow within similar time intervals and also as variations in the flow due to a higher-sinuosity system plan form. However this cannot be assured confidently in Storeys 1 and 2 due to the small number of data.

Assuming that scour structures are well preserved, then, the 64.3 % of the scour structures with significant divergence between trend scour and laminae dip direction and the variation of laminae dip direction larger than 40° (Section 2.7.1, Table 2.3) indicate local flow direction variations. This may either support previous interpretations of Prados deposits as being the result of a high-sinuosity system or simply indicate that independently of the channel plan-form this variation may occur and the deposits were formed in areas within the channel more susceptible to flow variations. It may also give indications about the geometry of the bedforms and bedform crest line and how they interacted together possibly causing variations in their orientations as they migrated downstream.

Although there is not enough evidence to assure that this is the case, during the re-visit to this field case study and its analysis, two characteristics of high-sinuosity rivers were observed in the Prados Formation: (1) scoured basal contacts and concave-up bounding surfaces and (2) three fining-up sequences with an upwards-decrease in grain size and set thickness and an increase in fine sand, silt and clay sediment towards the top of the sequence. Based on the data available and considering the size of the exposure, the Prados Formation could have been the result of a moderately high-sinuosity system, and the Prados deposits could correspond to one bend within a meander. Given this, and considering the lack of diagnostic elements of high-sinuosity rivers, it can be said that although field observations can support the hypothesis that Prados Formation was accumulated in a high-sinuosity fluvial system, these deposits could have also been formed within a higher sinuosity reach of a straighter river. Then, these deposits are interpreted as the result of the activity of the low to moderately-high sinuosity system.

2.11 Conclusions

The Prados Formation was studied in detail at Rillo de Gallo. The main findings of this descriptive analysis are:

1. Based on the descriptive analysis of the entire exposure:

- Five lithofacies are recognised and they are generally arranged in fining-upwards sequences. These lithofacies are: St (trough cross-bedded sandstone), Sh (horizontally-bedded sandstone), Se (erosional scours with lag deposit), Fl (laminated sandstone and mudstone), Fm (massive mudstone). In addition to these, Ramos (1979) working over a wider geographic area recorded lithofacies Sr (rippled cross-laminated sandstone), P (pedogenic carbonates), and observed evidence of bioturbation. These lithofacies are arranged in facies associations interpreted as architectural elements: sandy bedforms; overbank fines and possibly macroforms foresets.
- The associated facies are organised into fining-upwards cycles (storeys), that when complete include facies St > Sh > Fl > Fm > P, the fine-grained facies corresponding to late channel abandonment fill and floodplain deposits are absent in the two lower cycles due to erosion and deposition of the later cycles.
- In the locality of Rillo de Gallo, the Prados Formation is 40 m thick and individual fining-upward cycles (lower to upper storey) are 9.7; 13.3 and 17 m. Each successive cycle becomes thinner and finer than the one underneath it. Large amounts of fine facies (silt and clay) accumulate towards the top of the sequence.

2. Based on the detailed analysis of individual trough cross-bed sets (scour structures):

- The initial scour shape and growth is related to the initial interaction between flow and sediments and bedform development. Three hypothetical initial geometries for scours are suggested: (1) Initial scour with $W/L \sim 1$; (2) Initial scour with $W/L > 1$ and (3) Initial scour with $W/L < 1$. *N.B., Further investigations on modern systems and flume work will be needed to study accurately the three hypothetical initial scour shapes here suggested.*

- The geometry of scour structures varies. They have been classified on the basis of (a) size, (b) shape, (c) the relationship of mean laminae dip direction and scour trend and (d) basal contact.
- Scour structure laminae dip direction can either be parallel or have an angle to the longer axis of the trough. Based on this, six different types of trough cross-bed scours have been defined (Fig. 2.16).
- Shape: All the structures except for structure 34 have a width:length ratio < 1 . Thirty-one percentage of the structures are circular ($0.75 \leq W/L \leq 1.25$), 31 % are oval 2 ($0.5 \leq W/L < 0.75$), 26.3 % are elongate 2 ($W/L < 0.5$) and 2.4 % is elongate 1 ($W/L > 1.5$) correspond to structure 34 (due to poor preservation level).
- Size: 23.8 % are small structures, 42.9 % medium, 19 % large and 14.3 % very large structures. Medium to very large structures are frequent in the lower storeys. Towards the upper storey the number of small scour structures increases. Within each storey individual trough cross-bed sets decrease in size.

3. Based on the palaeocurrent data:

- Palaeocurrent analysis reveals a polymodal pattern with mean dip directions towards the south, southwest and northwest.
- Palaeocurrent data within each individual storey also show flow direction variations. These are interpreted as local variations of the flow within individual channels or as a function of channel-sinuosity.
- Palaeocurrent data within individual trough cross-bed sets vary laterally within the same sedimentary surface and upwards in the whole sequence. This can be explained by local variations of the flow, the type of channel plan form (sinuosity index) or due to variations in the main orientation of the three channel that deposited each individual storey.
- In 64.3 % of the individual cross-bed sets there is a divergence between the mean laminae dip direction and the scour trend larger than 40° . This is a function of channel system regime causing variation in shape and bedform development and occasionally it is also a function of preservation and field interpretation accuracy.

- The dip angle of the internal laminae of scour structures varies from 5° to 30°; and within individual structures tends to increase downstream.

4. Based of statistical analysis of relationships between the characteristic of scour structures:

- Contrary to previous expectations, there are no measurable relationships between W/L and: maximum length, mean laminae dip, angle between trend and mean laminae dip direction, and laminae dip direction modes.
- There are no relationships between maximum length and: and the relationship of mean laminae dip direction to scour trend and the laminae dip direction.
- There is no measurable relationship between scour trend and mean laminae dip direction for individual trough cross-bed sets.

5. Based on fluvial system reconstruction:

- Various methods of estimating channel dimensions (e.g., Yalin, 1964; Allen, 1970; Leeder, 1973 and Ethridge and Schumm, 1978) suggest that the channel was greater than 7 m deep and could be as much as 14 m also estimated that the width could be 148 m or as much as 387 m.
- The Prados Formation is dominated by trough cross-bed sets are arranged in cosets and occasionally separated by finer grain size laminated sands. The upper finer units correspond to floodplain fine deposits possibly due to vertical accretion of the fine sediments following meander abandonment or channel avulsion.
- Large-scale dipping surfaces (epsilon cross-stratification of Allen, 1963b) indicating successive increment of lateral growth (lateral accretion) of point bars were not identified in the locality of Rillo de Gallo.
- Although the Prados Formation architecture is defined within a multi-storey pattern and some of the sedimentary characteristics observed are characteristic of sand-dominated high-sinuosity systems and therefore, this study would agree with previous work interpretations, there is not enough definite evidence to confirm that these deposits were generated by a meandering system. In addition, these deposits cannot be framed within any of the already-made fluvial system models that are summarised in Miall (1985). Considering the descriptive

interpretation of the sediments, channel estimates and size of the exposure available, herein, the Prados Formation could be interpreted as the result of fluvial activity within a meandering system or a bend within a braiding reach. Therefore, these deposits fluvial in origin were deposited by either a high sinuosity system or low to moderately high-sinuosity system.

Chapter 3

Case study II Seaton Sluice Sandstone



Photo: Tabular cross-bedded sandstones at Seaton Sluice, Northumberland.

3.1 Introduction to the study area at Seaton Sluice, North England

The fluvial sandstones exposed at Seaton Sluice, Northumberland, England (WGS84 / N55°4' 57.36", W1°28'40.08") (Fig. 3.1) were selected as a case study because they are exceptionally well exposed and have been previously documented (Haszeldine, 1983a, b and Holzweber, 2012). Haszeldine (1981) studied the Upper Carboniferous Seaton Sluice Sandstone and reconstructed the deposits generated by a large bar in an ancient river. He used this information to develop further interpretations about the depositional environment and the processes that formed the sandstones internal structure (Haszeldine, 1983a, 1983b). The Seaton Sluice Sandstone is a good comparison for the Prados Formation described in Chapter 2 and flume experiments described in Chapter 5 and these comparisons are discussed in Chapters 4 and 6 respectively. The analysis of the geometry and disposition of the sedimentary structures identified (below) helped to obtain a better understanding of bedform initiation, and sedimentary structure generation and evolution.

Jones (1967) studied the geology of the coast section from Tynemouth to Seaton Sluice and referred to it as "*one of the few surface exposures of Coal Measure strata in the country and finest exposures of Coal Measure in Britain*".

The Seaton Sluice Sandstone, in the lower part of the Westphalian B succession (Fig. 3.2A), has been interpreted as the deposits of a low-sinuosity river-channel (Land, 1974; Haszeldine, 1983a) at the northern margin of a solitary fluvial sandstone body. This sandstone body is up to 15 m thick and can be traced over an area of about 100 km² (O'Mara, 1999). Haszeldine (1983a) interpreted a section of the Seaton Sluice Sandstone exposed in the Cut at Seaton Sluice as the deposits of medial bars which accreted onto the northern bank of a westward-flowing river to form a large compound lateral bar (Outcrop-Section 3 on Fig. 3.12, and also the photograph shown on the first page of this chapter). The base of the Seaton Sluice Sandstone is a laterally extensive erosion surface that incises into the underlying coal-bearing coastal alluvial plain sediments (O'Mara, 1999). The rocks exposed at the coast around Seaton Sluice present a dominant sandy sequence similar to the lower Crag Point Sandstone (Jones, 1967) (Fig. 3.2). Two large faults affect the area in which the study site is located (Fig. 3.2B); this makes stratigraphic correlations difficult. Absalom and Hopkins (1926) and Jones

(1967) considered that despite the difference in dip due to the faulting affecting the site, the Seaton Sluice Sandstone (dipping towards the north) that overlies the Charley's Garden Sandstone (dipping towards the southeast) (Fig. 3.2) are part of the same sandy sequence overlying coal seam S5 (High Main Seam) (Fig. 3.2B). O'Mara and Turner (1999) described the Seaton Sluice Sandstone as coarse grained, poorly sorted, arkosic to subarkosic sheet sandbodies; however in this study it is observed that they vary in grain size, geometry, and lithofacies architecture over the exposure.

The Seaton Sluice exposure predominately consists of white and yellowish, fine to coarse grain sandstones, arranged in sets and cosets. Layers of laminated mudstones and discontinuous layers of coal are interbedded with the sandstones. Haszeldine (1983a) described a 0.01-0.05 m thick conglomeratic layer near the sandstone base which includes well-rounded extraformational quartz granules and pebbles (< 0.01 m diameter) and rounded calcite pebbles (< 0.05 m diameter). The sandstones vary in grain size, thickness and composition. They contain lithic clasts, feldspar, sub-angular quartz and muscovite (Holzweber and Hartley, 2011). The mica content is higher in some of the sandstone packages than in others. Finer grained sandstone layers are intercalated with thicker and coarser grained sandstone sets. Set thickness decreases upwards. There is a variation in cross-bedding style with sandstone composition and position within the sandstone body.

Field observations and data presented herein were collected during field campaigns in 2011-2012. The studied sandstones were tracked over an area of 1 x 0.5 km, from the sumps end at Seaton Sluice around Seaton Sluice Point across and up the Cut, Charley's Garden, Collywell Bay to Grag Point (Fig. 3.2B). The study area is on Geological Map 1:50000 (Sheet 15, Tynemouth).

The primary aim of the work presented in this chapter was to improve understanding of cross-bedded sandstone by analysing cross-bedding in a well-documented site, to supply data for comparison with the Prados Formation and flume experiment results. The second aim was to assess whether cross-bed analysis could lead to improvement on the published interpretations of the depositional processes and environments.



Figure 3.1 Satellite image covering the study area, Northumberland, UK (image supplied by Google, Bluesky, 2014).

3.2 Stratigraphic and geological context at Seaton Sluice Sandstone

The Seaton Sluice Sandstone is within the lower Westphalian B sequence. This sequence was traced as described by Jones (1967) from Crag Point to Seaton Sluice Point and the Sumps as follows (Fig. 3.2A):

(1) *Crag Point Sandstone*. This consists of two types of sandstone separated by a conglomeratic layer of pebbles of quartz and feldspar and a coarse matrix. The lower sandstone is dominantly fine-grained with trough cross-bedding and layers of black siltstone containing fragments of plant debris. The upper sandstone is mainly coarse-grained and is dominated by planar cross-bedding.

(2) *Collywell Bay Sequence*. These sediments are mainly siltstones and claystones. They include shale with abundant marine fossils interbedded with sandy layers. Five coal seams were mapped within these sediments (S1-Bottom Yard Seam; S2-Top Yard Seam;

S3-Bottom leaf of Grey Seam, S4-Top leaf of Grey Seam and S5-High main Seam). Shale with iron bands and mussels; and sandstones with bands of shale are predominantly observed between coal seam S3 and S4 (c. 9 m thick); a thin layer of clay underlies coal seam S4. Coal seam S4 is overlain by shale with iron bands and mussel, then a layer of clay just underlying coal seam S5. These rocks are cut by an igneous intrusion (the Collywell Dyke – part of the Mull Dyke Swarm) associated with faulting.

(3) *Charleys' Garden Sandstone and the Seaton Sluice Sandstone (From Seaton Sluice Point to the Sumps, Fig. 3.2B)*. The shale conglomerate overlying seam coal S5 represents the base of Charley's Garden Sandstone (c. 7 m thick). Overlying this sandstone there is series of siltstones (haematite stained) with micaceous sandy bands and then a sequence of mainly sandstone and siltstone. Charley's Garden Sandstone can be traced further into the sandy packages observed in Seaton Sluice Point. They appear to be similar to the sandstone observed in the lower part of Crag Point. South of the Seaton Sluice Cut, sandstones are coarse-grained and have a conglomeratic base. On the other side of the Cut, which constitutes the area survey in this research, the Seaton Sluice Sandstone becomes medium grained. Robson (1980) suggested that coarse grained sand was interpreted as main channel fill however medium grained size has been noted in this study to be the predominant grain size of channel-fill elements.

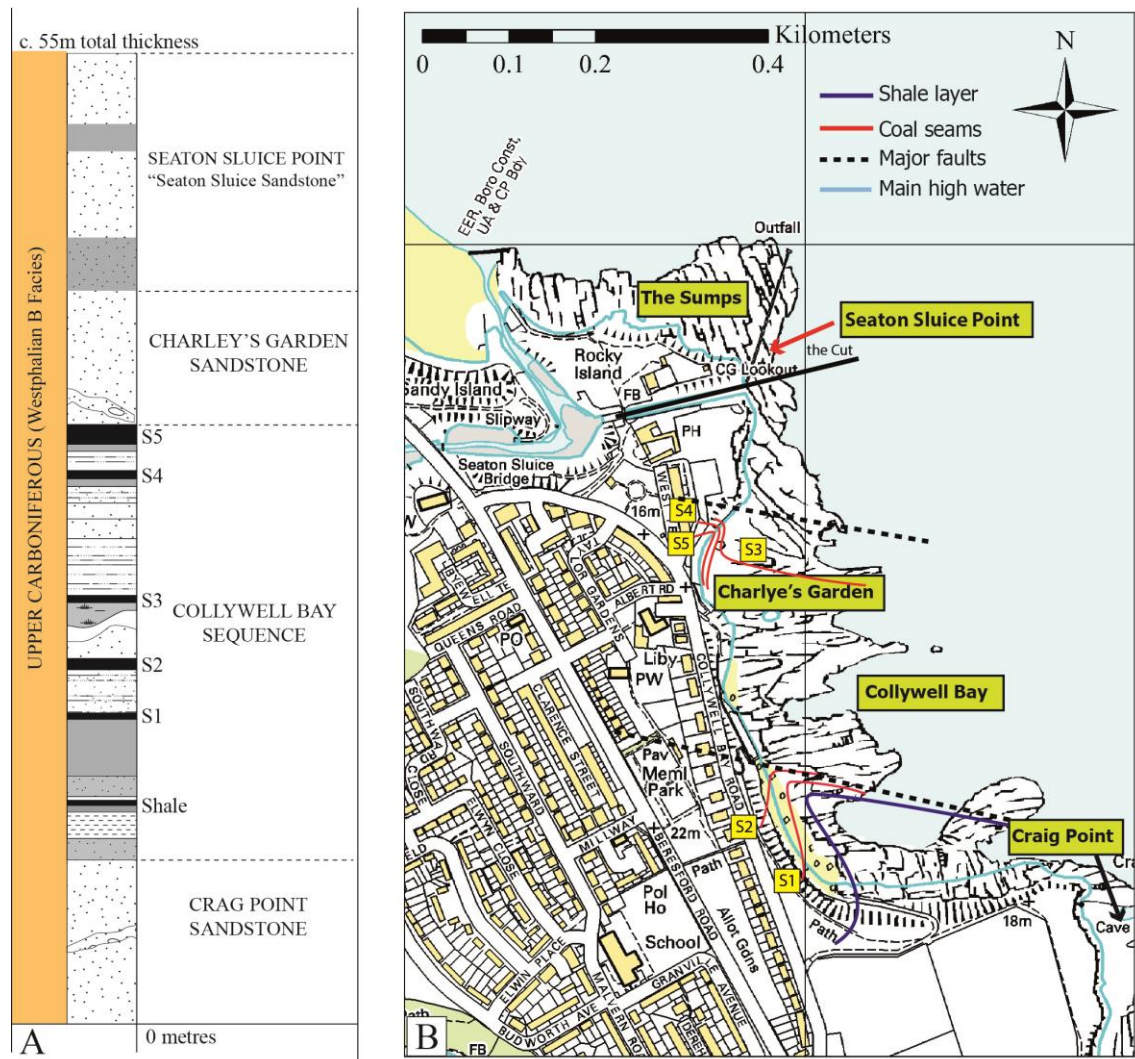


Figure 3.2 (A) Illustration of Upper Carboniferous (Westphalian B) stratigraphic succession showing coal seams (black) sandstone (stippled) and mudstone (grey) (Modified from Jones, 1967); (B) Map showing the study area and Westphalian B sequences (Modified from MasterMap 1:10 000 Raster [TIFF geospatial data], Scale 1:10000, Tiles: nz37nw, Updated: 22 March 2013, Ordnance Survey (GB), Using: EDINA Digimap Ordnance Survey Service, <<http://digimap.edina.ac.uk>>, Downloaded: Mon Jul 28 10:24:01 BST 2014). N.B., Coal seams on the map as red lines are: S1-Bottom yard; S2-Top yard; S3-Bottom leaf of grey; S4-Top leaf of grey and S5-high main seam. Shale layer on the map is represented with a dark blue line and corresponds to the shale layer on the stratigraphic log.

3.3 Palaeogeography

Northumberland is bounded to the north by the Southern Uplands High and to the south by the Wales-London-Brabant High. The sedimentation in Northumberland during the Carboniferous was mainly controlled by the Lower Palaeozoic basement consisting of sedimentary and volcanic extrusive rocks intruded by granites (Robson, 1980). The reactivation of late Caledonian basement structures due to north-south extension episodes dominated the sedimentation continued through the Carboniferous into the

Namurian (Davies *et al.*, 2012). The Alston Block was uplifted relative to the Northumberland Trough located on the margin of that block (Fig. 3.3). Displacement across a series of faults generated a deep sedimentary basin (the Northumberland Trough), where the deposits formed, which are now seen exposed at Seaton Sluice. During the Westphalian the influence of blocks and basins was more subtle and rifting activity was less significant (Davies, 2008).

During the Westphalian, Northeast England formed part of a subdued coastal plain crossed by rivers that probably fed lake and coast deltas (Haszeldine, 1983a). These Westphalian depositional environments formed interbedded claystones, siltstones, sandstones, intraformational conglomerates and coal seams (Fielding, 1986). During the Westphalian the climate was humid with short dry intervals. This is recorded in the study area, where organic material accumulated into thick beds on low-gradient depositional plains leading to coal formation. The widespread marine bands within the Westphalian strata record high-magnitude sea level oscillations, and have been used as stratigraphic markers. Large fluvial systems incised into these non-fluvial deposits during periods of low-eustatic sea level (Davies, 2008).

The Seaton Sluice Sandstone is stratigraphically located within the Pennine Coal Measures Group, which comprises cyclothem alternating sandstone, siltstone, mudstone, coal seams and palaeosol horizons. This group is subdivided in formations: lower, middle and upper. The Seaton Sluice Sandstone is within the Middle Coal; Measures Formations (Stubblefield and Trotter, 1957) which is also named the Pennine Middle Coal Measures (Waters *et al.*, 2009).

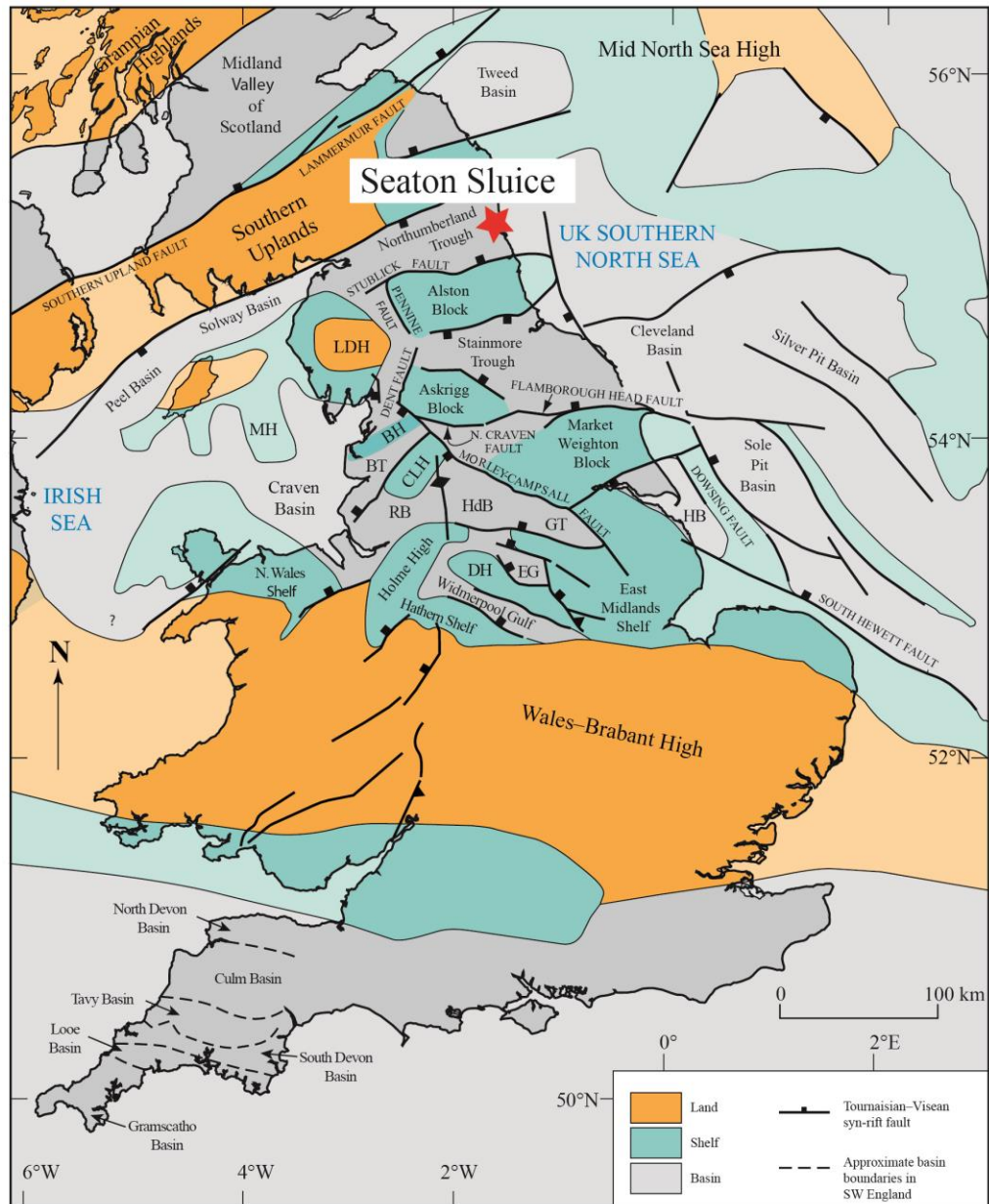


Figure 3.3 Structural framework of the United Kingdom relevant to the Carboniferous sedimentation. Seaton Sluice (star) is in the Northumberland Trough. Legend: AB- Askrigg Block; BH- Bowland High; BT- Bowland Trough; CLH- Central Lancashire High; DF- Dent Fault; DH- Derbyshire High; EG- Edale Gulf; FHF- Flamborough Head Fault; GT- Gainsborough Trough; HdB- Huddersfield Basin; HB- Humber Basin; HH- Holme High and Heywood High; HS- Hathern Shelf; LDH- Lake District High; MCF- Morley-Campsall Fault; MH- Manx High; NCF- North Craven Fault; NT- Northumberland Trough; PF- Pennine Fault; RB- Rossendale Basin; SF- Stubbleck Fault; WG- Widmerpool Gulf (modified from Dean *et al.*, 2011 and Holzweber, 2012).

The deposits forming the Pennine Coal Measures Group including the Seaton Sluice Sandstone, are interpreted as having accumulated in delta-top environments with large distributary rivers filled by sand leaving thick sets of sandstones (Guión *et al.*, 1995)

and sediment deposition in lakes and lagoons with emergent surfaces susceptible of organic matter accumulations (Waters *et al.*, 2009).

Following Haszeldine's (1983a) interpretation of the Seaton Sluice Sandstone (Section 3.1) and Miall's (1985) classification of fluvial systems types, this fluvial system may approximate to Miall's model 10, which represents a sandy low-sinuosity river with sand flats, and large-scale bedforms such as linguoid and transverse bars (Fig. 3.4).

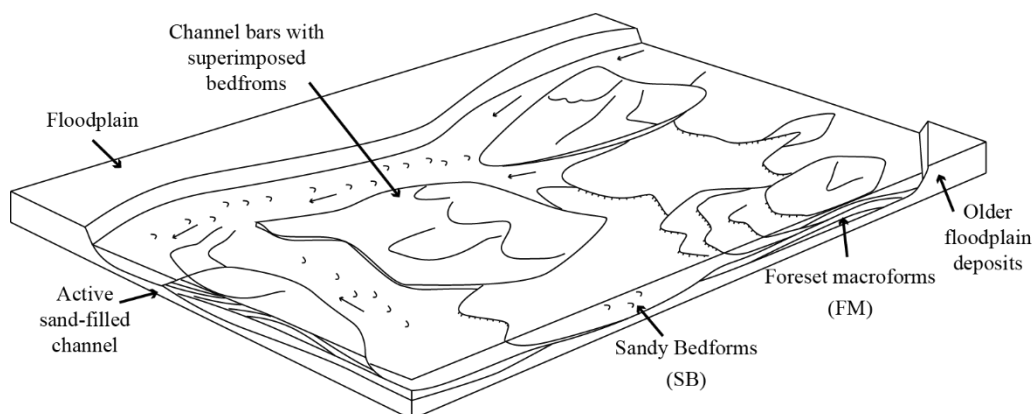


Figure 3.4 Fluvial system model illustrating a low-sinuosity river with foreset macroforms (“sand flats” or “shoals”) and isolated linguoid and transverse bars (modified from Miall, 1985).

Haszeldine (1983b) identified several facies inferring that there was a hierarchy of bedforms: (1) superimposed bedforms descending and truncating sand sheets; (2) sand sheets advancing over sand-waves' lee sides and (3) lobate-crested sand waves migrating downstream superimposed on slow-moving bars. There is considerable controversy about the names of bedforms (Smith, 1974; Cant, 1976; Church and Jones, 1982; Ashley, 1990; Cadle and Cairncross, 1993; Goff and Ashmore, 1994; Lunt *et al.*, 2004; Bernini *et al.*, 2006) and sand waves here are probably equivalent to what are called dunes in this thesis, while Miall's (1985) linguoid and transverse bars are types of unit bars (Section 3.5.1; Large-scale Facies Sp). It is unclear whether Haszeldine's “lobate-crested sand waves” are the same as sinuous-crested dunes or unit bars in this context.

In this study, data were collected from the scour structures, long axes of troughs and bedding planes (boundary surfaces of *first* and *second-order*) (Fig. 3.5). Trough cross-bedding lamination dip directions show a dominant palaeoflow direction towards the west; and bedding plane dip directions are predominantly orientated towards the northwest (Fig. 3.6). The deposits exposed in the area of Charley's Garden (Fig. 3.2B) south of the fault near Seaton Sluice Point have a tectonic tilt of up to 40° towards the southeast. This was estimated from the dip on the coal seams in Collywell Bay. In the north part of the study site, north of the fault, the Seaton Sluice Sandstone is gently inclined towards the north; however there is little evidence on which to accurately estimate palaeohorizontal because individual bedding surfaces within the sandstone body are unlikely to have been horizontal when formed. Thus, the tectonic tilt could not be accounted for in either the palaeocurrent direction but probably contributes towards the predominant bedding plane mean dip direction of 303° . Trough-scour trends are mainly orientated west-northwest (Section 3.8.2). These measurements suggest that all sets measured are descending sets; and reflect that these deposits were formed by a fluvial system(s) with a dominant flow towards the west-northwest (WNW). Palaeocurrent data collected by previous workers show that these Westphalian sands were transported towards the WNW; this is confirmed by new data (Fig. 3.6a).

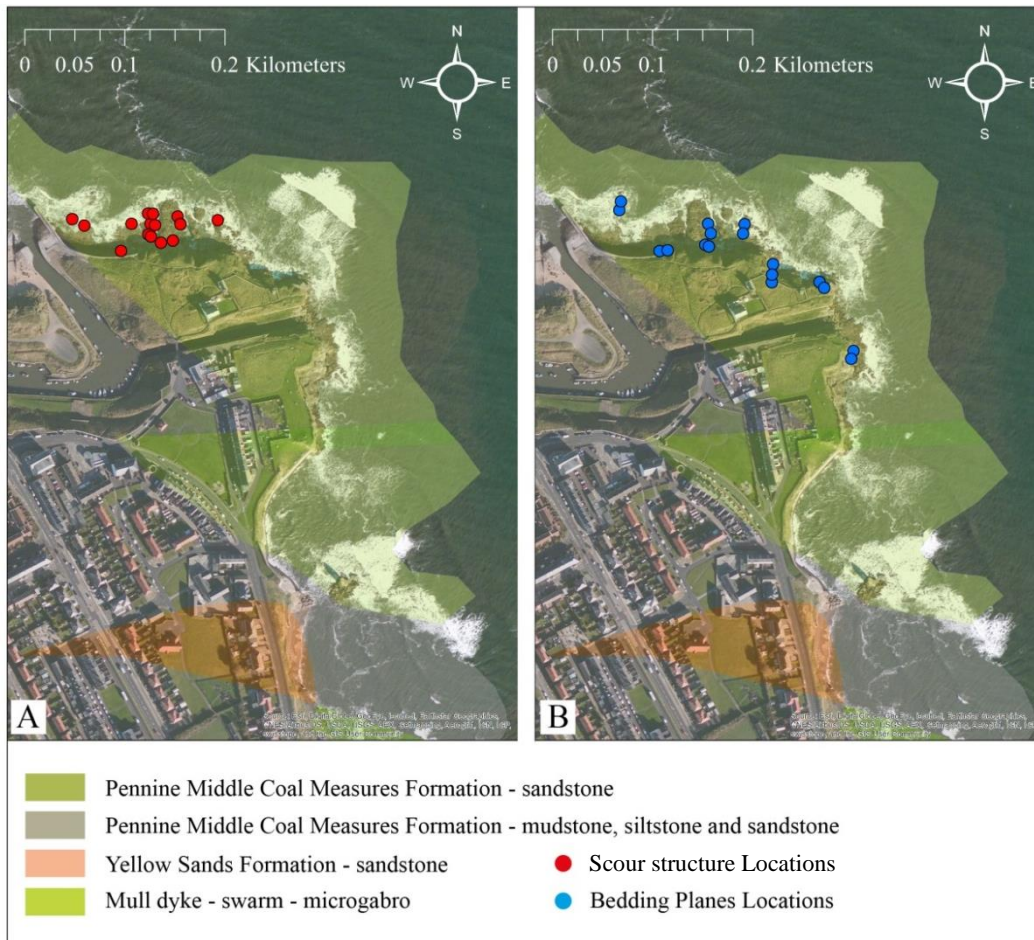


Figure 3.5 Satellite image with overlapped geological map of the study area (satellite image supplied by ArcGIS world imagery and geological map supplied by BGS onshore Digital Maps, 1:50000). (A) Scour structure locations and (B) Bedding plan measurement locations.

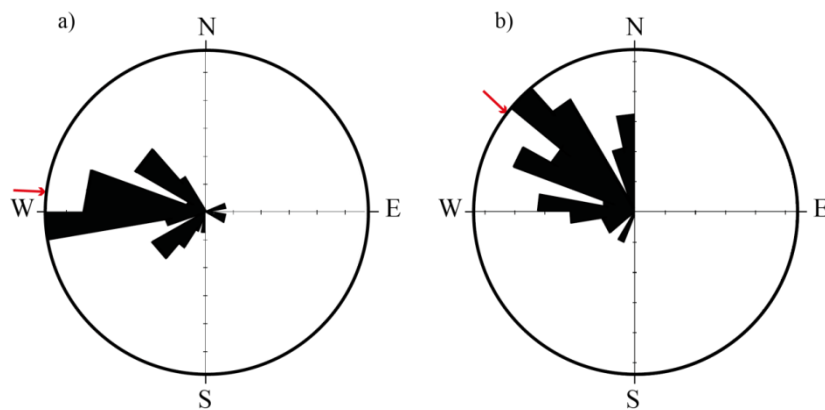


Figure 3.6 (a) Percentage frequency azimuthal plot of the palaeocurrent data measured from individual and grouped trough cross-bedding at the study site in field campaign June 2012 ($n = 46$, scale tick 3%, sector angle 10° , mean resultant direction 274° and $\sigma = 56^\circ$) illustrating a primary mode towards the west; (b) Percentage frequency azimuthal plot of the bedding plane data (boundary surfaces 1st and 2nd order) measured at the study site in field campaign June 2012 ($n = 31$, scale tick 3%, sector angle 10° , mean resultant direction 303° and $\sigma = 36^\circ$) illustrating 3 modes; primary mode towards the northwest.

3.4 Lithostratigraphy of the Seaton Sluice Sandstone

Two short field campaigns were carried out in July 2011 and June 2012 covering the Seaton Sluice Sandstone exposure revealing signatures of fluvial bars of a relatively deep and straight channel. There is limited access to some areas of the exposure, and because it is a coastal location, the exposed rocks are high weathered and locally encrusted with marine biota, which limited interpretations to some extent. The whole length of the Seaton Sluice exposure (c. 300 m) was examined. The lithostratigraphy was logged at 10 stations (Figs. 3.7 and 3.8). Three outcrop sections with good preservation and good-quality exposure were selected for detailed descriptions and to show lithostratigraphic variations at these three locations within several sandstone storeys (Fig. 3.7). The outcrop section that Haszeldine (1983a) described corresponds to Outcrop Section 3 in this thesis (Fig. 3.7c and Fig. 3.12).

Although this study mainly consisted of the detailed study of individual trough cross-beddings and where these were located within the exposure, an attempt at a general interpretation of the stratigraphy of the whole sequence was carried out to understand the chronological location of the individual trough cross-beds (i.e., scour structures; Section 3.7). Two main erosive surfaces were identified dividing the Seaton Sluice Sandstone into three main sandstone packages or storeys (Storeys 1-3, Section 3.6.1). Holzweber (2012) identified five erosive surfaces along at least 250 m of length of the Seaton Sluice exposure; overlain by coarser sandstones, dividing the exposure into six sandstone packages. In this thesis, Storey 1 corresponds to the two lower sandstone packages described by Holzweber (2012); Storey 2 corresponds to Holzweber's middle packages and Storey 3 corresponds to the upper package defined in Holzweber's (2012) work.

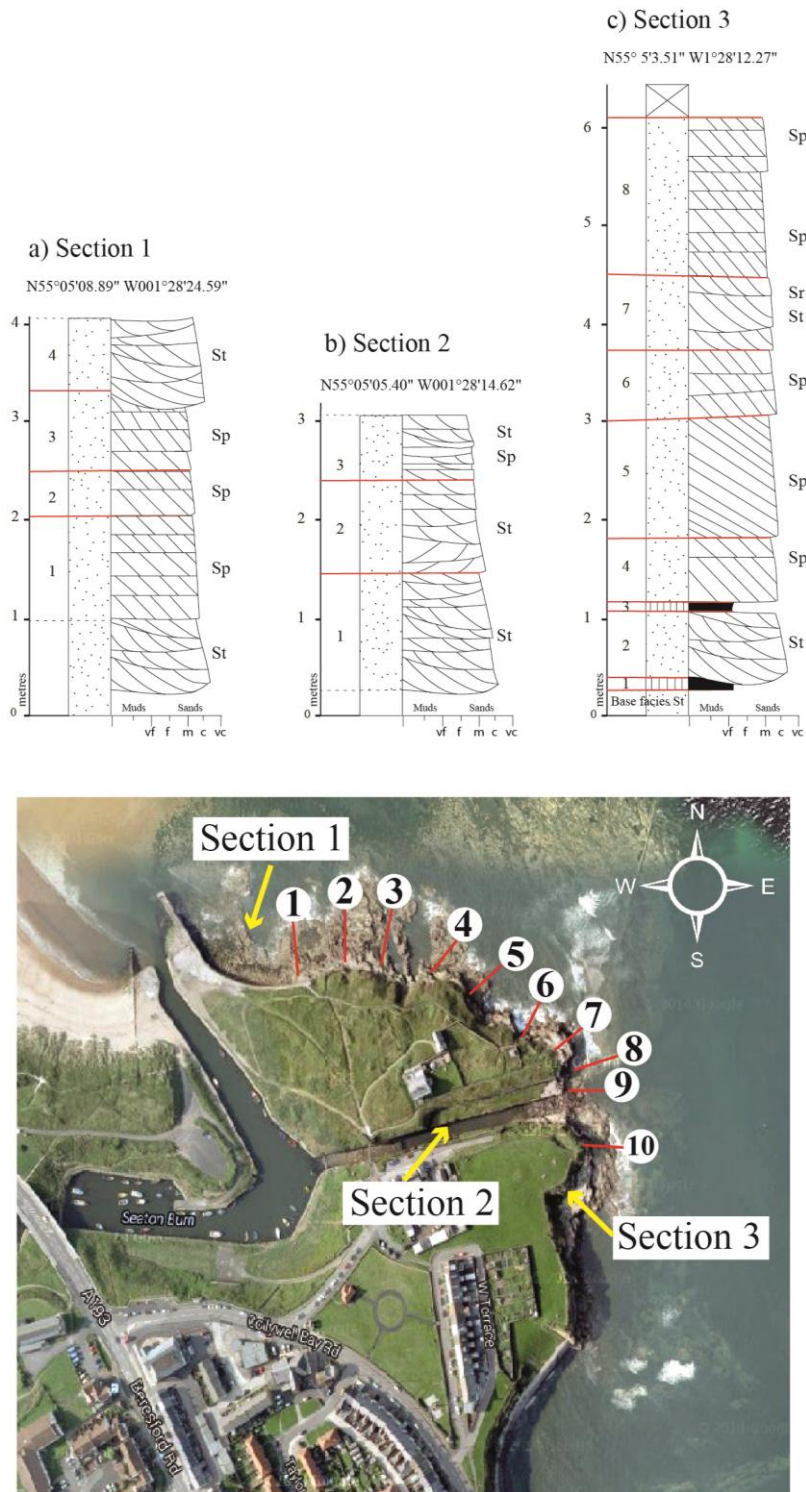


Figure 3.7 Lithological logs of outcrops: (a) Section 1; (b) Section 2 and (c) Section 3 (Section 3 was described previously by Haszeldine, 1983a); distinctive internal surfaces separating well defined sets and cosets are marked in red (for key to logs see Appendix A, Fig. A1). Satellite image illustrating the locations of lithological logs 1-10 (Fig. 3.8) and locations of lithological logs of Sections 1-3 (image supplied by Google, Bluesky, 2014).

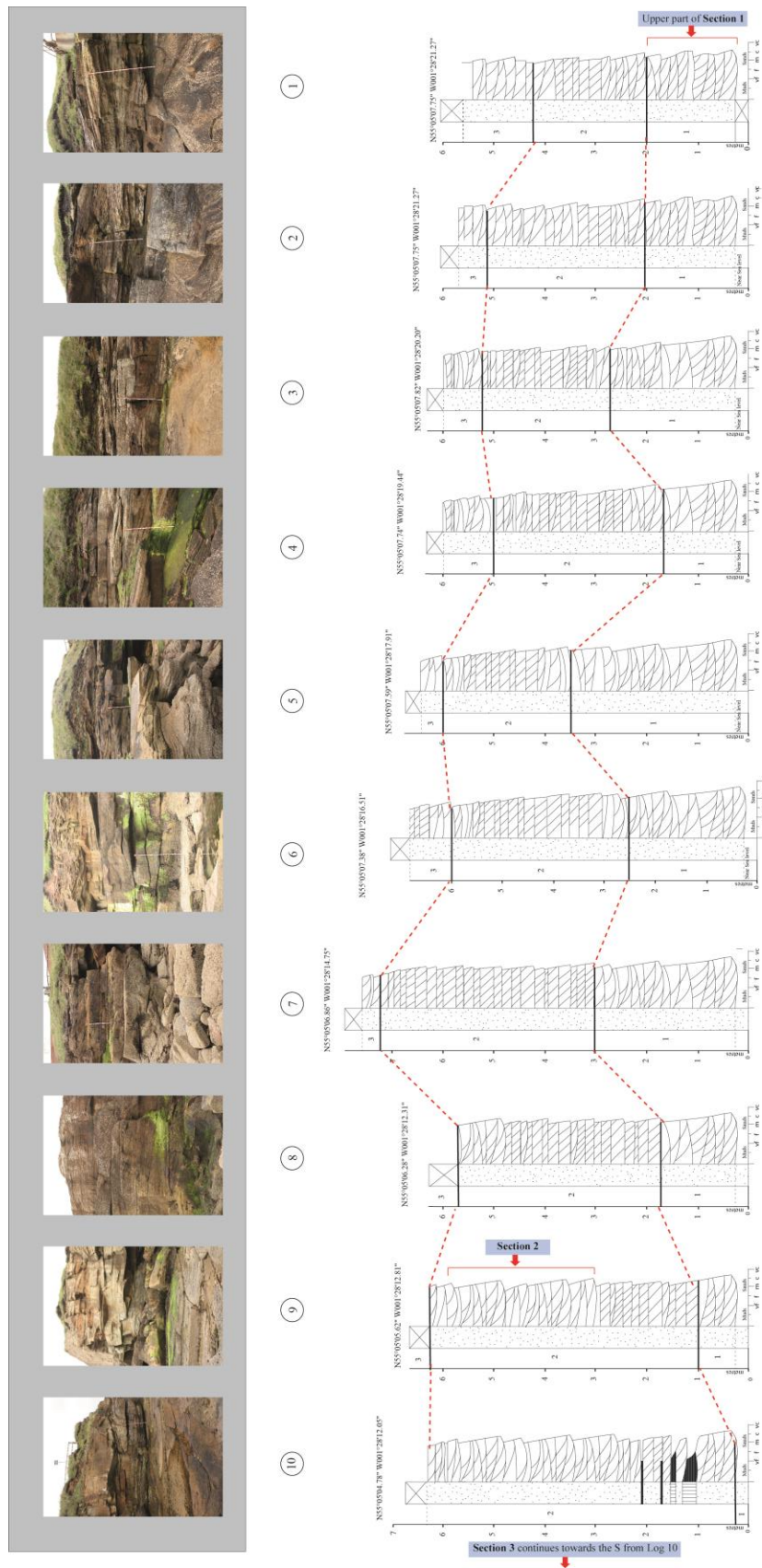


Figure 3.8 Lithological logs and stratigraphic correlation at the Seaton Sluice study area.

3.5 Sedimentary Facies analysis

3.5.1 Facies

The facies identified in the study area are described below following Miall's (1996) nomenclature (Fig. 3.9), in the same way as for the Prados Formation (Chapter 2) to maintain consistency of the facies system terminology in both case studies.

Trough-cross-bedded sandstone (St): These are observed as individual and grouped scour structures in plan view and vertical faces. This facies grain size varies from medium to coarse sand. Large-scale trough cross-bedding is formed by migrating linguoid bars and sinuous-crested dunes; and medium and small-scale sets have been interpreted as the result of migration sinuous-crested dune and ripple (Allen, 1983; Miall, 1985).

Planar-cross-bedded sandstone (Sp): Fine to coarse grained sand. According to Collinson (1970), Harms *et al.*, (1975), Cant and Walker (1978) and Allen (1983) this type of facies is the result of straight-crested dune migration, or longitudinal and transverse bars. Haszeldine (1983b) interpreted this facies as the result of the combination of large and small-scale sand-sheets and sand-wave migration on the channel bed. Set boundary surfaces are generally flat (tabular) with indications of scouring indicating either a new incisive channel base or minor incisive erosive surfaces within the same channel due to variations on flow conditions and so the character of advancing bedforms.

Ripple cross-laminated sandstone (Sr): Ripple-laminated fine to medium grade sandstones. Occasionally ripples are fully preserved and crests are visible, indicating rapid deposition of younger sediments on the lee face of the preserved ripples. This facies is interpreted as the result of asymmetric ripple migration.

Erosional surfaces with lag deposit (Se): Erosive scour bounding surfaces commonly associated to accumulation of intraclasts of mudstone and siltstone and lag deposits representing channel-bed deposits. These were frequently observed as boundaries between sets of Facies St and Sp representing the geometry of a channel base or possible large-scale scour bases and lag deposits. These are channel bar erosion surfaces or erosion surfaces within channel deposits where a local change occurred accompanied with supply of gravel grade interclasts.

Laminated claystone (Fsm): Laminated layers of clay that were deposited under low flow-regime conditions representing overbank (floodplain) deposits or channel abandonment, lake deposition or low flow (dry season) conditions. These appear intercalated with Facies St.

Haszeldine (1983a) identified five main facies and used a different nomenclature. His facies are:

- Facies S1: Large planar cross-bedded sandstones
- Facies S2: Large trough cross-bedded sandstones
- Facies S3: Small trough cross-bedded sandstones
- Facies S4: Small planar cross-bedded sandstones
- Facies S5: Complex coset consisting of associations of sets of trough and planar cross-beds of facies S3 and S4 and ripples cross-lamination.

In addition to the facies described by Haszeldine (1983a) Holzweber (2012) identified Facies Sh consisting of horizontally bedded sandstones formed under upper phase plane bed condition.

Holzweber (2012) estimated the percentages of different facies in the Seaton Sluice Sandstone and considered it was made up of 25% planar bedded and low angle laminated sandstone; 30% trough cross-bedded sandstone and 45% planar cross-bedded sandstone. This chapter focuses on the trough cross-bedded sandstones, which are a major component facies of Seaton Sluice.






Facies		Interpretation	Grain size	Bedding and Sedimentary structures	Geometry
Channel - Fill Sandstones	St	 Linguoid bars and sinuous-crested dunes (low-flow regime to upper low-flow)	Coarse to fine sand	Cross-stratification Large-scale trough cross-bedding Group or isolated cross-beds	Lenticular with concave-up base
	Sp	 2D bars and straight-crested dunes (lower-flow regime)	Coarse to fine sand	Cross-stratification Large-scale planar cross-bedding	Tabular with planar base
	Sr	 Asymmetric ripples (low-flow regime)	Medium to fine sand	Small-scale cross-lamination due to ripples	Lenticular with flat or erosive base
	Se	 Boundary surface	Coarse to fine	Lag deposits associated to erosive surfaces	Undulated and Irregular
Floodplain deposits	Fsm	 High concentration of sediment in suspension and deposition in low-flow regime areas	Very fine	Fine lamination due to ripple migration	Irregular or flat

Figure 3.9 Characteristics of depositional facies types of Seaton Sluice Sandstone.

3.5.2 Facies in the three component parts (storeys) of the Seaton Sluice Sandstone

The facies are arranged in thinning-upwards cosets (Fig 3.11 and Fig. 3.12). Towards the base of the sequence layers of 0.20 m maximum thickness of mudstones are intercalated with the sandy facies. These fine sediments appear to be topping Facies St towards the lower part of Outcrop-Section 3 (Fig. 3.12).

The three storeys have similar association of facies. Storey 1 consists of mainly Facies St and Sp. Storey 2 consists mainly of Facies St and Sp and their proportion of occurrence varies laterally. It includes occasional Facies Sr (Fig. 3.12). Facies Fms and intermittent layers of coal are also observed near the base of Storey 2 (Fig. 3.8). The upper part of Storey 3 appears truncated or absent in most of the stations where it was described (Fig. 3.8); only interbedded Facies Sp and St are observed. Based on the proportions of the two main Facies identified (St and Sp) at each log station, the estimate percentages of these Facies at the Seaton Sluice site are: 66 % St and 34 % Sp. These numbers differ from Holzweber's (2012) estimates. This difference is because (a) she included planar bedded and low-angle laminated Facies and a lot of such beds when examined in 3D perspective rather than on vertical faces are trough cross-bedded (this was only observed when 3D exposures were available) and (b) by a sampling difference depending on how in detailed different sections of the exposure were described. Because this study was particularly interested in comparing data with the predominately

trough cross-bedded sandstones exposed at Rillo de Gallo there may have been a bias in the log station and outcrop section selection thus overlooking part of the exposure dominated by planar cross-bedding at Seaton Sluice.

Haszledine (1983a) describes the Seaton Sluice Sandstone (Outcrop-Section 3 within Storey 2) as being dominated by cosets of planar and tabular geometry of facies S1 and S4 (large and small planar trough cross-bedded sandstones) and these were interpreted as the deposits generated by the migration of sand-sheet bedforms over a large sand-wave bedform. He interbedded these with facies S2 and S3 forming S1-S2 and S3-S4 facies associations (Section 3.5.1). Facies Association S3-S4 he interpreted as the record of lunate megaripples and sand sheets migrating over a bar and representing the bar tail; and the Facies Association S1-S2 he suggested recorded the migration of larger bedforms in deeper water which he interpreted as the deposits of the fore-bar pool area (Haszeldine, 1983a). Facies S5 were identified towards the top of the sequence representing the deposits at the bar head due to sand sheets and megaripples migration downstream.

3.6 Descriptive analysis of the Seaton Sluice Sandstone

3.6.1 Analysis of selected sections of the Seaton Sluice exposure

Three sections within the complete exposure the Seaton Sluice Sandstone were selected for detailed descriptions due to their good quality of preservations and their easy access. These three sections almost cover the 10 m thickness of the entire sequence. No sections corresponding to the top of storey 3 were selected for detailed analysis because of the low level of preservation and difficult access.

Outcrop-Section 1 in Storey 1

This 60 × 2 m section is within the upper part of Storey 1, above more sets of the same sandstone (Figs 3.7a and 3.10). Storey 1 corresponds to the two lower sandstone packages described by Holzweber (2012). Its minimum thickness varies from 0.5 to 3.5 m, and tends to decrease towards the south until it is totally covered by sea or it is absent. Although this section is affected by several fracture systems the exposure is good, but due to the dense barnacle encrustation, the set boundaries and the cross-bed lamination is not clear. The section exposes reddish medium grade sandstones arranged

in tabular sets (Facies Sp) towards the middle part of the section with nearly parallel boundary surfaces in between sets emphasizing the tabular pattern. Numerous concave-up boundary surfaces present evidence for the dominance of trough cross-bedding (Facies St) towards the top and the base of the section (Fig. 3.10). These trough cross-bed sets record bedforms that migrated downstream and generated the trough scours. Towards the top of the section, trough cross-bed sets truncate the nearly horizontal boundary surfaces of the tabular sets. Most of the scour structures described later in this chapter occur at this level within the Seaton Sluice Sandstone (cf. red arrows in Fig. 3.10), which indicates that these scour structures were generated not only by the same river but also within the same channel, unless over this plan-view exposure there are significant erosive surfaces that have not been identified; in that case these structures could be located within the same stratigraphic level but at different depositional times, and therefore the scour structures could have been formed by the same river. The set thickness varies from 0.1 m to 0.95 m; and each set decreases in thickness downstream. There is little variation in the laminae dip direction of the sets measured in the northern end of the section (Fig. 3.10; mean dip direction 291° and $\sigma = 27^\circ$).

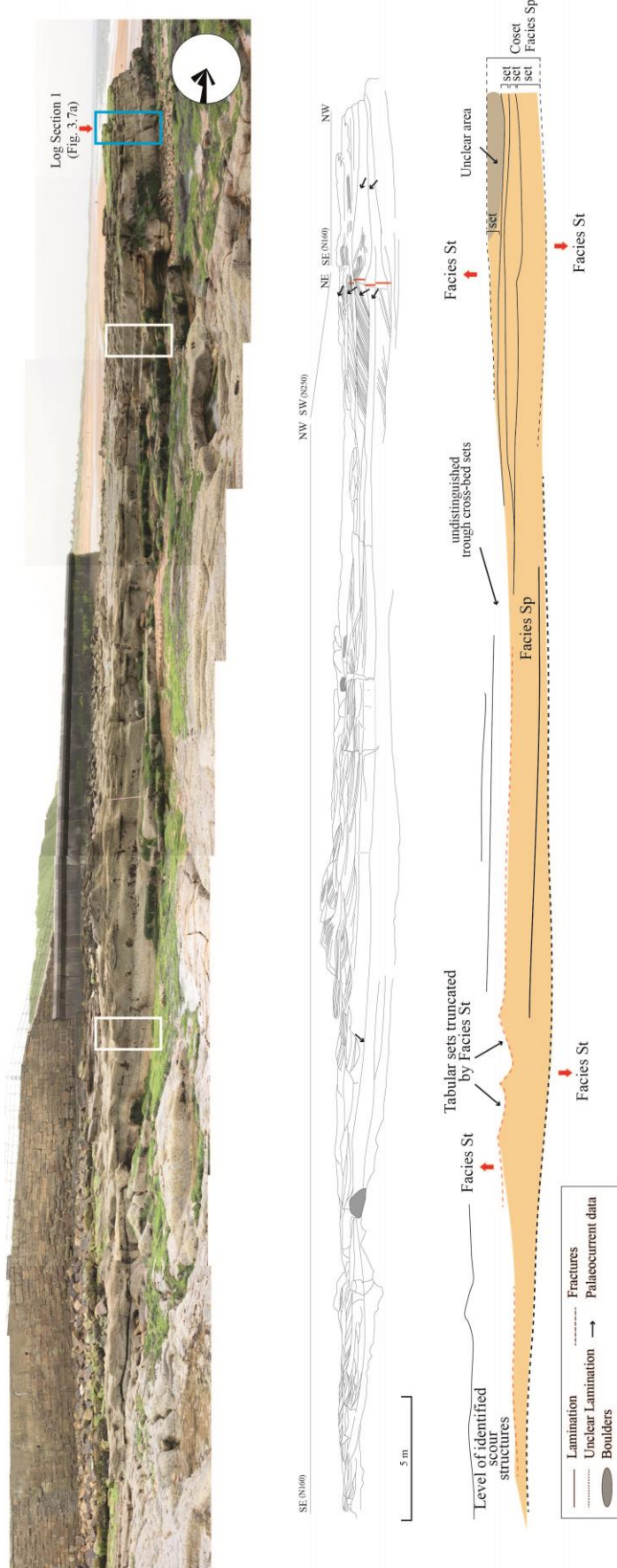


Figure 3.10 Photograph and sketches illustrating the fluvial architecture of Section 1; internal lamination and palaeocurrent data ($n = 7$; mean resultant dip direction = 291°). Location coordinates: $N55^\circ05'09.35'' W001^\circ28'24.54''$ southeast end and $N55^\circ05'07.89'' W001^\circ28'23.97''$ northwest end. Arrows indicate palaeoflow directions with reference to North at the top of the page (same for the rose diagram). Orange shaded areas indicate tabular and planar trough cross-bedding. Red solid lines indicate sets. Above red dotted line trough cross-bedding dominate and this is the level where most of the spoon-shaped structures were identified (Appendix C). Blue box indicates location of log Section 1 (Fig. 3.7a) and white boxes indicate two more logs that correlate well with the previous one.

Outcrop-Section 2 in Storey 2

Section 2 is a vertical face, approximately 58 m long and 3 m high that cut east-west through part of Storey 2 about 2 m above its base (Figs. 3.7b and 3.11). Its thickness fluctuates (2.2 to 5.8 m) and tends to increase towards the south. This section was logged at a regular lateral spacing of 5 metres and sedimentary structures and sets traced along the face (Fig. 3.11). The facies identified in this section are trough cross-bedding (St), cross-lamination due to ripple migration (Sr) and thin interbedded muddy laminated layers (Fl).

This section is dominated by trough cross-bedding with concave-up set boundaries. Some sets have obvious tangential contacts and others have slightly sharper contacts. Towards the east end, the exposure has a 3D character and therefore it was easier to identify concave-up surfaces here. The cross-bedding is arranged in sets grouped in cosets. These are separated by nearly horizontal boundary surfaces giving a tabular aspect. Layers of mudstone were locally observed between cosets. The set thickness ranges from 0.05 to 0.5 m and tends to decrease upwards in the sequence and also thins towards the east (Fig. 3.11). The cross-bed-lamination thickness was difficult to assess due to the exposure quality.

Within the same section and underlying the sands described above, there is a layer of very fine mudstone approximately 1 m thick. Towards the east a large concave-up surface truncates the underlying sets. This surface could be interpreted as a third-order surface, possibly indicating lateral accretion (Allen, 1963a) however there is not enough evidence to confidently confirm this. Trough cross-bed sets in the western end filled this bottom channel base. No reliable palaeocurrent data were recorded due to the 2 dimensionality of the exposure.

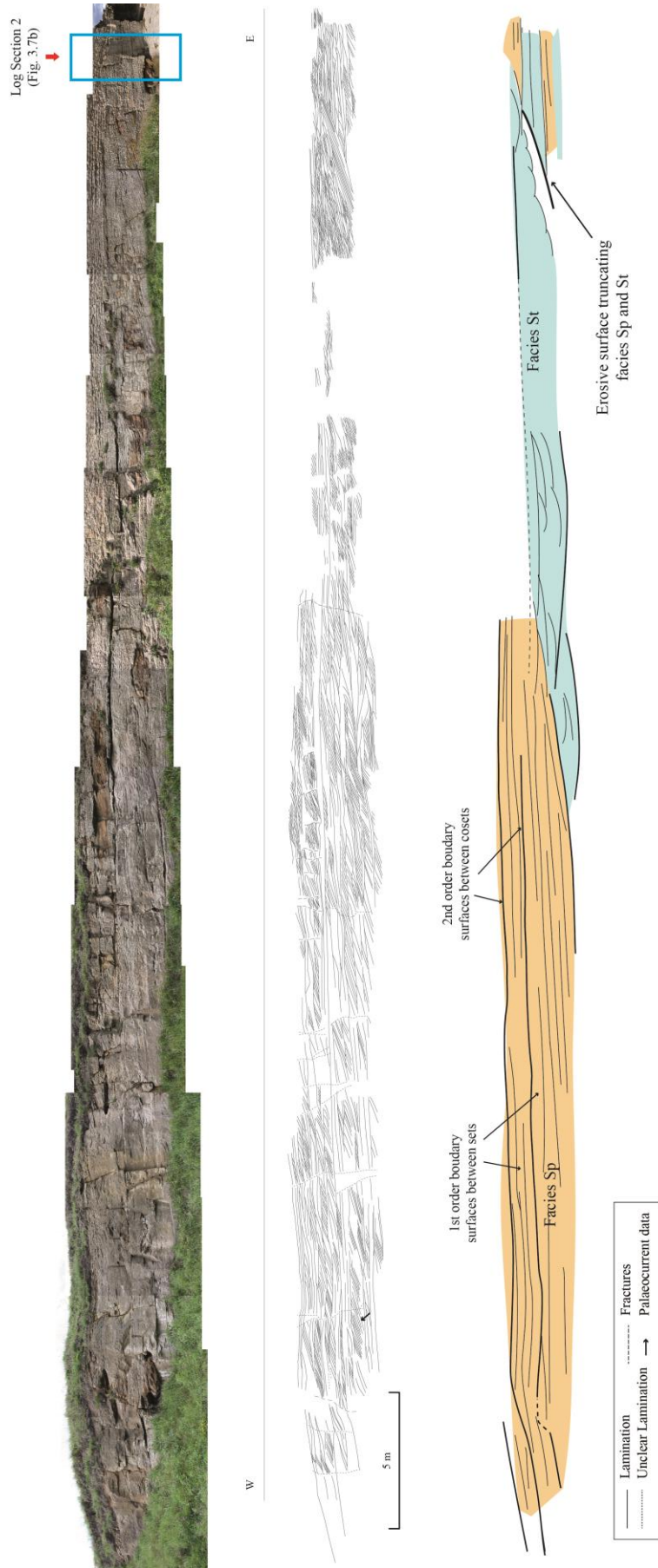


Figure 3.11 Photograph and sketches illustrating the fluvial architecture of Outcrop-Section 2. Location coordinates: N55°05'05.55" W001°28'12.98" west end and N55°05'05.61" W001°28'13.14" east end. Arrows indicate palaeoflow directions with reference to North at the top of the page. Orange shaded areas indicate tabular and planar cross-bedding and blue shaded areas indicate trough cross-bedding. This section corresponds to the upper sandy packages defined by Holzweber (2012). Although 13 logs were recorded at regular spacing of 4 m, only one log corresponds to a well exposed 3-dimensional area at the east end of the section. Blue box indicates location of log Section 2 (Fig. 3.7b).

Outcrop- Section 3 in Storey 2

This section is orientated WSW-ENE; is approximately 12 m long and 4 m high and cuts through part of Storey 2 (Figs. 3.7c and 3.12). This storey 3 is mainly truncated or absent and it has a maximum visible thickness of approximately 1.5 m. This section exposes of pale grey medium to coarse grade sandstone with locally observed fine grade beds. The facies exposed include trough and planar cross-bedded sandstone (St and Sp), ripple cross-laminated sandstone (Sr) and laminated fine sediments (Fsm). The sandstone is dominated by tabular cross-bed sets arranged into tabular cosets. The set thickness ranges from 0.06 to 1.4 m and decreases upwards towards the west (Fig. 3.12). The sets within the cosets are formed by tangential foresets (upper cosets) and straight foresets (lower cosets). Towards the middle of the section cosets consist of the intercalation of Facies St and Sr sets. Below the larger planar cross-bed set (Fig. 3.12) the exposure continues and it is formed by planar and trough cross-bed sets arranged in 3 cosets. Two distinctive mudstone layers are interbedded with these lower cosets. The laminae dip direction varies slightly with a mean resultant direction towards the 268° ($\sigma = 16^\circ$). Laminae dip ranges from 13° to 30°. Foreset angle tends to decrease in higher sets.

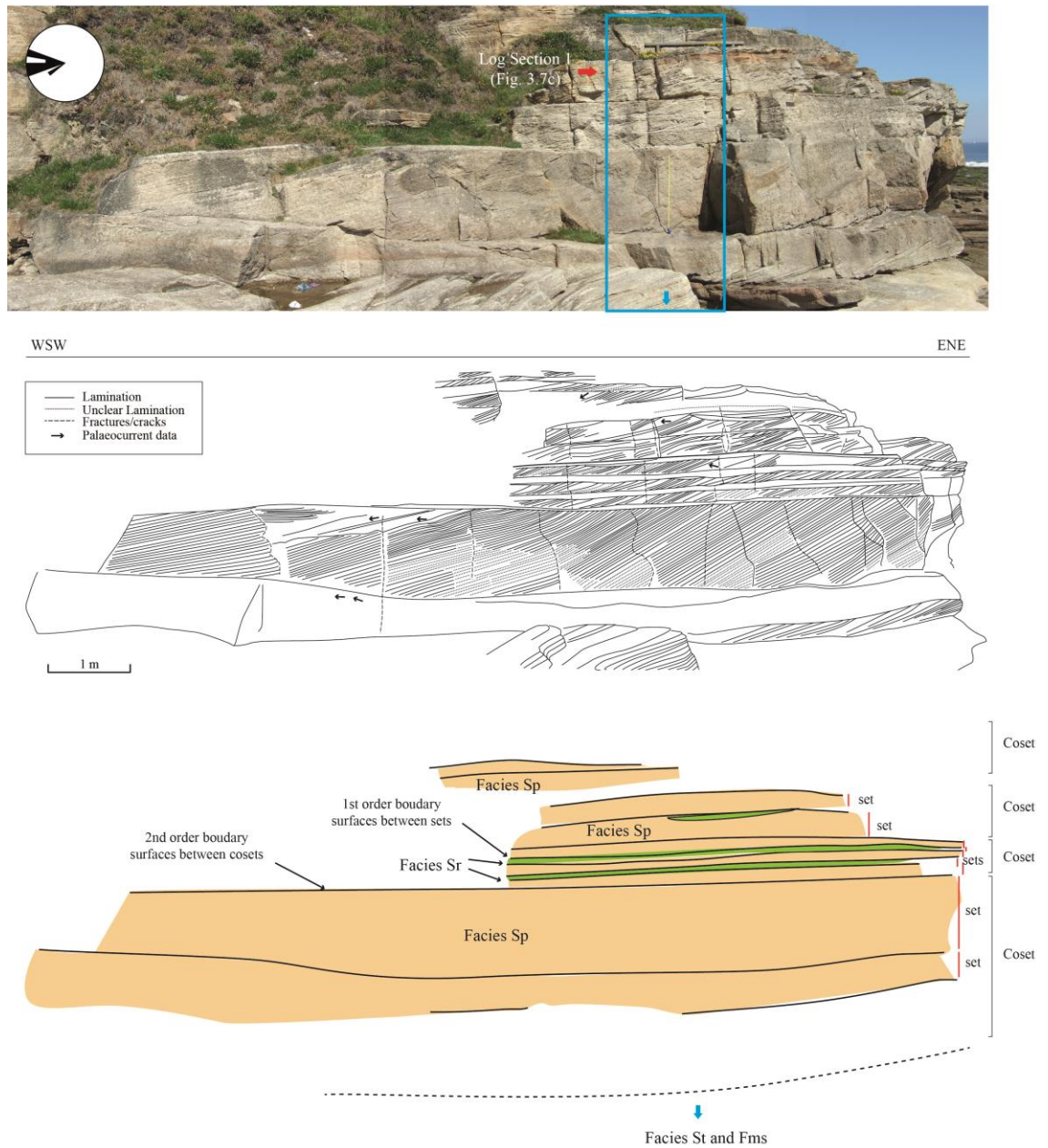


Figure 3.12 Photograph and sketches illustrating the fluvial architecture of Outcrop-Section 3; internal lamination and palaeocurrent data ($n = 8$; mean resultant dip direction = 268°). Location coordinates: $N55^\circ05'03.46''$ $W001^\circ28'12.46''$. Arrows indicate palaeoflow directions with reference to North at the top of the page. Orange shaded areas indicate tabular and planar cross-bedding and green shaded areas indicate ripple cross-lamination. This section corresponds to the sandy packages 3-6 defined by Holzweber (2012), packages 1 and 2 correspond to the lower Facies St and Fms. Blue box indicates location of log Section 3 (Fig. 3.7c). Blue arrow indicates Facies St and Fms, not seen in the photograph but included in log Section 3.

3.7 Classifications of scours associated with trough cross-bedding

During the field campaign (June 2012), individual sets of spoon-shaped cross-bedding were observed in plan-view and in vertical section. Nineteen individual cross-bed sets were described and preliminarily classified based on shape and dimensions. All the structures were identified in the upper part of Outcrop-Section 1, within Storey 1 (Fig. 3.10). Each scour structure represents a trough-scour and contains numerous inclined laminae formed by the toe of a dune prograding into the scour. Frequently, trough cross-bed sets are observed to be truncated by the concave-up base of a younger set. The maximum visible length and width of these structures range from 0.55 to 4 m and 0.58 to 6.6 m respectively. Lamina thickness varies up to 15 mm. Dip of the laminae varies from 11° to 26°; and within each individual set the laminae dip tends to increase downstream (Table 3.1). This section introduces the data and the classification of the scour structures identified at Seaton Sluice on the basis of their geometry, laminae dip and the relationship of scour trend to mean laminae dip direction. In Section 3.8.2, the trend of scour and mean laminae dip direction divergence is discussed.

3.7.1 Classification of Seaton Sluice Sandstone cross-bed sets

In order to make a comparison of these deposits with the Prados Formation, the structures identified at Seaton Sluice were classified following the criteria defined in Section 2.7.1 (Fig. 2.14). Due to the level of preservation and erosion some of the shape and dimensions of some cross-bed sets were unclear (Table 3.1). The scour structures' classification is presented in Table 3.2; the percentages of each class are shown in Table 3.3.

Table 3.1 Individual scour structure characteristics measured in Storey 1 of Seaton Sluice Sandstone including: trough dimensions, width:length ratio, laminae thickness, mean laminae dip, scour trend, mean laminae dip direction and the relationship of trend and dip direction.

Scour structure ID	Max width (m)	Max length (m)	Ratio W/L	Length to max width (m)	Mean Laminae Dip (degrees)	Max laminae thickness (mm)	Trend of scour (degrees)	Mean dip direction (degrees)	Trend & dip direction variation (degrees)
ST01	2.7	4.5	0.60	1.6	19	10	275	207	68
ST02	2	n/a	n/a	1.6	25	n/a	300	310	10
ST03	n/a	3.7	n/a	n/a	24	n/a	275	301	26
ST04	3.4	n/a	n/a	1.6	23	10	310	325	15
ST05	3.2	4.4	0.73	2	18	n/a	290	253	37

ST06	4	6.6	0.61	5.1	21	n/a	305	286	19
ST07	1.5	n/a	n/a	0.72	25	n/a	n/a	n/a	n/a
ST08	0.55	0.58	0.95	0.29	18	n/a	275	270	5
ST09	1.3	1.5	0.87	0.8	11	n/a	280	265	15
ST10	1.2	1.6	0.75	0.82	18	n/a	310	270	40
ST11	1.3	1.6	0.81	0.92	25	n/a	290	298	8
ST12	1	2.2	0.46	1.43	26	n/a	290	290	0
ST13	1	1.5	0.67	0.8	20	n/a	300	315	15
ST14	1.2	1.6	0.75	0.9	19	n/a	248 to 290	320	50
ST15	2.7	n/a	n/a	1.2	26	n/a	275	219	56
ST16	1.9	3	0.63	1.9	20	15	290	279	11
ST17	0.83	1.3	0.64	0.7	25	10	270	288	18
ST18	0.55	1.2	0.46	0.5	20	15	300	258	42
ST19	> 115	3	n/a	1.55	19	10	280	300	20

N.B., n/a: data unavailable because the parameters related to those classes could not be observed in the field.

Table 3.2 Individual scour structure classification at Seaton Sluice using class definitions from Section 2.7.1.

Structure ID	Size	Shape	Scour trend & laminae dip direction relationship	Basal contact (where it could be observed)
ST01	Large	Oval 2	$\Theta > 40^\circ$	Asymptotic
ST02	Medium onwards	n/a	$5^\circ \leq \Theta \leq 20^\circ$	n/a
ST03	Large	n/a	$20^\circ < \Theta \leq 40^\circ$	Asymptotic
ST04	Large onwards	n/a	$5^\circ \leq \Theta \leq 20^\circ$	Asymptotic
ST05	Large	Oval 2	$20^\circ < \Theta \leq 40^\circ$	n/a
ST06	Very large	Oval 2	$5^\circ \leq \Theta \leq 20^\circ$	Asymptotic
ST07	Medium onwards	n/a	n/a	n/a
ST08	Small	Circular	$5^\circ \leq \Theta \leq 20^\circ$	n/a
ST09	Medium	Circular	$5^\circ \leq \Theta \leq 20^\circ$	n/a
ST10	Medium	Circular	$20^\circ < \Theta \leq 40^\circ$	n/a
ST11	Medium	Circular	$5^\circ \leq \Theta \leq 20^\circ$	n/a
ST12	Medium	Elongate 2	$< 5^\circ$	n/a
ST13	Medium	Oval 2	$5^\circ \leq \Theta \leq 20^\circ$	n/a
ST14	Medium	Circular	$\Theta > 40^\circ$	n/a
ST15	Medium onwards	n/a	$\Theta > 40^\circ$	n/a
ST16	Large	Oval 2	$5^\circ \leq \Theta \leq 20^\circ$	Asymptotic
ST17	Small	Oval 2	$5^\circ \leq \Theta \leq 20^\circ$	n/a

ST18	Small	Elongate 2	$\Theta > 40^\circ$	n/a
ST19	Large	n/a	$5^\circ \leq \Theta \leq 20^\circ$	n/a

N.B., n/a: data unavailable because the parameters related to those classes could not be observed in the field.

Table 3.3 Classification of scour structures in the Storey 1 of the Seaton Sluice Sandstone.

Classes	Categories					Unclear
a) Size	1. Small	2. Medium	3. Large	4. Very Large		0 %
	15.8 %	47.4 %	31.6 %	5.3 %		
b) Shape	I. Elongate 1	II. Oval 1	III. Circular	IV. Oval 2	V. Elongate 2	9.6 %
	0 %	0 %	26.3 %	31.6 %	10.5 %	
c) Θ	a. $\Theta < 5^\circ$	b. $5^\circ \leq \Theta \leq 20^\circ$	c. $20^\circ < \Theta \leq 40^\circ$		d. $\Theta > 40^\circ$	5.3 %
	5.3 %	15.8 %	52.6 %		21.1 %	
d) Basal contact	i. Angular		ii. Asymptotic			73.7 %
	0		23.3 %			

3.7.2 Classification of scour structures on basis of their mean laminae dip

Between 1 and 3 laminae dips were measured per scour structure depending on the preservation level. Dip ranges from 9° to 35° (Table 3.4). Mean laminae dip for individual trough sets ranges from 11° to 26° . The scour structures are classified following the laminae dip criteria defined in Section 2.7.3 as follows:

Table 3.4 Maximum, minimum and mean laminae dip per scour structure and location of troughs within the sedimentary sequence. All of these were measured within Storey 1 labelled in Figures 3.7a and 3.10 and the description of the structures is in Appendix C.

Scour structure ID	Number of data (n)	Min & Max Laminae dip (degrees)	Mean laminae dip (degrees)	Laminae dip class (degrees)
ST01	3	18-21	19	11-20
ST02	1	25	25	21-30
ST03	3	21-31	24	21-30
ST04	1	23	23	21-30
ST05	2	17-19	18	11-20
ST06	3	15-26	21	21-30
ST07	1	25	25	21-30
ST08	1	18	18	11-20
ST09	2	9-13	11	11-20
ST10	1	18	18	11-20
ST11	2	23-27	25	21-30
ST12	2	25-26	25	21-30
ST13	2	19-21	20	11-20
ST14	1	19	19	11-20
ST15	3	20-35	26	21-30
ST16	1	20	20	11-20
ST17	1	25	25	21-30
ST18	1	20	20	11-20
ST19	1	19	19	11-20

3.8 Analysis of scours associated with trough cross-bedding (scour structures) in Storey 1

3.8.1 Relationship between trough shape and size

The maximum observed width of troughs ranges from 0.55 m to 4.00 m and maximum measurable length varies from 0.58 m to 6.60 m. Because of the level of preservation only 13 structures out of the 19 identified, have been fully measured and are plotted in Figure 3.13. All the measured structures are longer than they are wide ($W/L < 1$) and are mainly within the near circular and oval 2 shape fields; and small-medium size (Fig. 3.13). The bigger troughs tend to be more elongate (Table 3.5 and Fig. 3.13b).

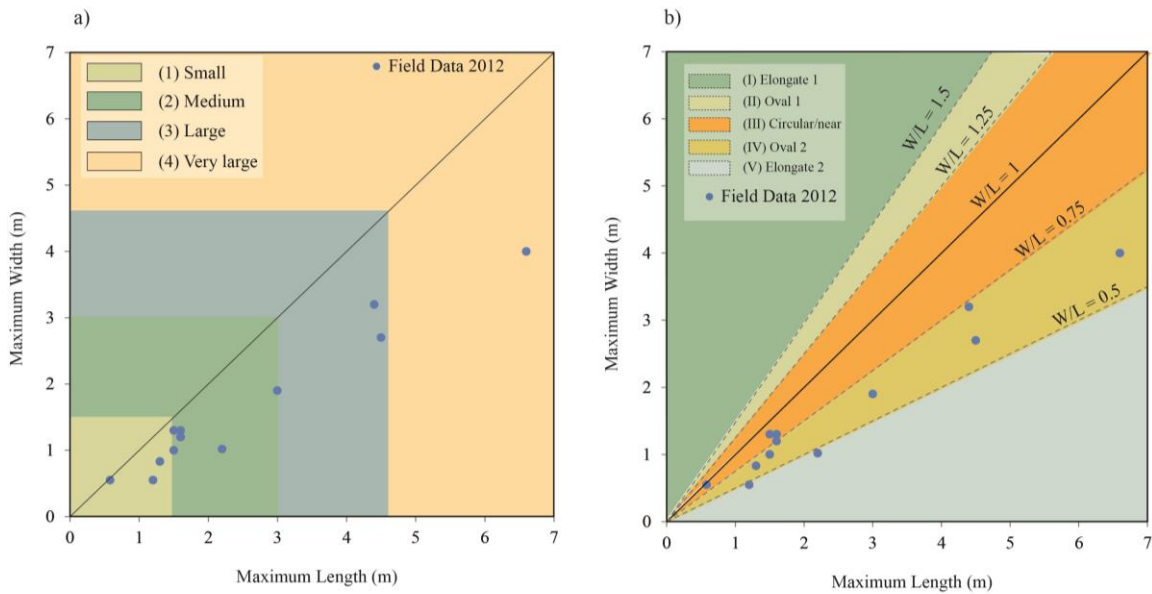


Figure 3.13 (a) Scour structure maximum measured width compared to maximum length of 13 structures whose locations are indicated on Figure 3.5. The shaded areas correspond to the different size categories defined in Section 2.7.1, and percentages in each class are listed in Table 3.3. (b) Illustration of maximum measured width and maximum measured length of scour structures and their classification into shape categories as defined in Section 2.7.1.

Table 3.5 Relationship of trough size to shape in percentages

n	Shape	Size			
		Small	Medium	Large	Very Large
5	Circular	20	80	0	0
0	Oval 1	0	0	0	0
6	Oval 2	16.7	16.7	50	16.7
0	Elongate 1	0	0	0	0
2	Elongate 2	50	50	0	0
6	n/a & unclear	0	50	50	0

There is no measurable relationship between trough shape and size and this is discussed in Section 3.9.1.

3.8.2 Relationship of laminae dip direction to scour trend and comparison with the trough size and shape

Out of the 19 structures identified only 13 were analysed because the others' dimensions or dip planes were unclear. The scour trends have one primary mode with a mean resultant direction 288° (Fig. 3.14a). The mean laminae dip direction within individual structures has one main mode towards the northwest with a mean dip direction of 280° (Fig. 3.14b). Thus in these structures the troughs' trend and the cross-bed lamination dip imply almost identical palaeocurrent direction. Comparison of these directions with trough shape (Fig. 3.14) demonstrate no relationship between direction and width:length ratio (Section 3.9.2).

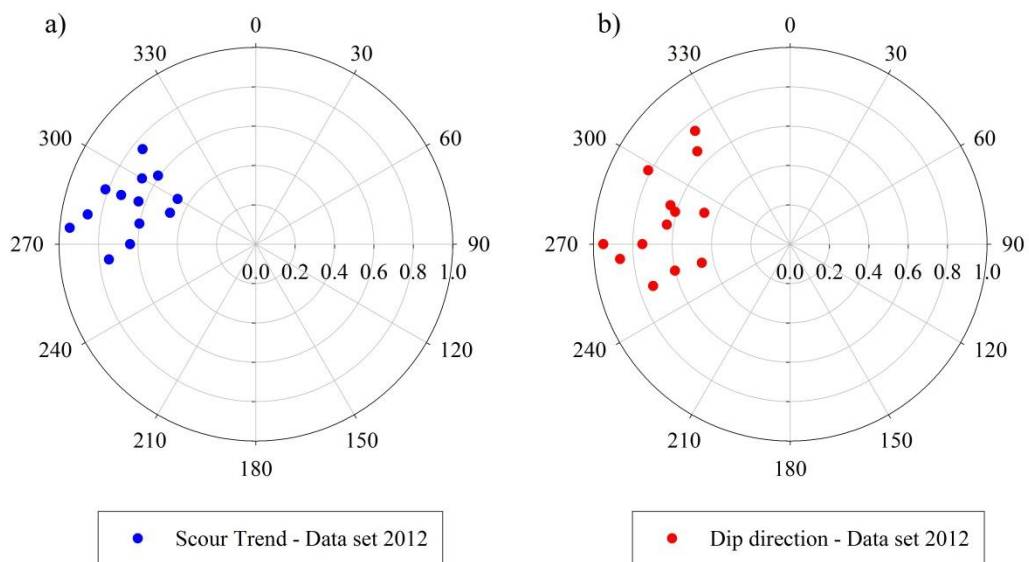


Figure 3.14 Polar representation illustrating: (a) trough width:length versus trend of scour for all scour structures with visible dimensions ($n = 13$) and (b) trough width:length ratio versus laminae dip direction. The radial axis represents the W/L.

Table 3.6 Descriptive statistics values obtained from a descriptive analysis of the lamina dip direction variable.

Descriptive Statistics					
	N	Minimum	Maximum	Mean	Std.
Laminae Dip Direction	13	253	320	280	21

Table 3.7 Descriptive statistics values obtained from a descriptive analysis of the scour trend variable.

Descriptive Statistics					
	N	Minimum	Maximum	Mean	Std. Deviation
Scour trend	13	264	310	288	13

Comparison of the trend of the scour long axes and the internal laminae dip direction demonstrates a variation from 0° to 56° and an average of 22°. Twenty-three percent of the scours have a mean laminae dip direction and scour trend divergence larger than 40° (Fig. 3.15). Paired sample t-test shows a non-significant variation between the trend of the scour long axes and the internal laminae dip direction (Table 3.8).

Table 3.8 Mean lamina dip direction and scour trend paired sample t-test results.

Paired Samples Statistics					
		Mean	N	Std. Deviation	Std. Error Mean
Pair 1	Trend	288	13	13	3.8
	Dip direction	280	13	21	5.9

N.B., A few trough cross-bed sets have long central axis that curve towards downstream direction; consequently internal laminae dip and trend varied. For these ones, mean values of scour trend and laminae dip direction have been used to calculate the divergence between trend and dip direction. This can be a function of the flow character and preservation levels and therefore a degree of inaccuracy might add to these results.

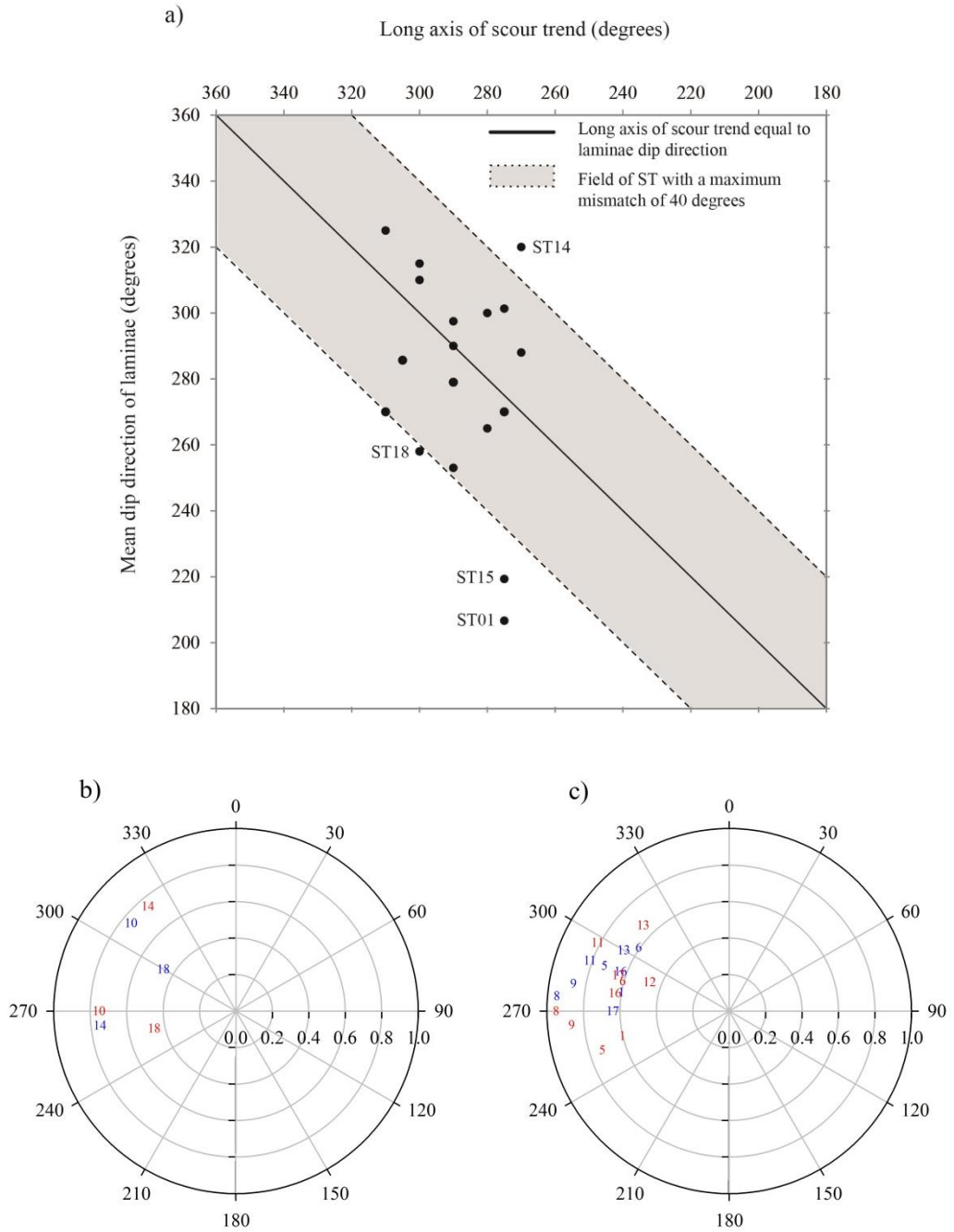


Figure 3.15 (a) Relationship between scour trend and mean laminae dip direction of all 13 scour structures with visible dimensions. Shaded grey band illustrates scour structures with less than 40° divergence between laminae dip direction and scour trend. (b) and (c) Polar representation of trough width:length ratio versus the laminae dip direction and scour trend comparison. Numbering in blue illustrates scour trend data and red numbering illustrates laminae dip direction data: (b) showing scour structures that have less than 40° difference between laminae dip direction and scour trend; and (c) structures with a difference larger than 40° (The radial axis represents the W/L). Note that in order to make an accurate comparison between dip direction and scour trend, the values of trend used for this comparison correspond to the natural data mode presented in Figure 3.14a.

According to the scour structure classification (Section 2.7.1, Fig. 2.16) 77 % of these structures corresponds to type (a) (structures with no significant divergence between scour trend and laminae dip direction). This non-significant variation between scour trend and laminae dip direction can explain local flow variations within a single event preserved in one sandy package (Outcrop-Section 1 of exposure at Seaton Sluice, Fig. 3.10) and maintaining the main downstream flow current indicating flow-regime change susceptible areas within the channel.

The shape and size of the trough structures is also compared to the divergence between scour trend and lamina dip direction (Tables 3.9 and 3.10). Circular and oval 2 shapes and medium size structures predominate with a divergence between 5° to 20° , which indicates that the majority of the structures grow downstream with a more or less constant flow direction. Section 3.9.1 presents results on statistical analysis that does not find relationships between the trough dimensions and the relationship of scour trend to laminae dip direction.

Table 3.9 Relationship of trough shape to the angle between the scour trend and lamina dip direction in percentages.

n	Shape \ Θ	Unclear	$\Theta < 5^\circ$	$5^\circ \leq \Theta \leq 20^\circ$	$20^\circ < \Theta \leq 40^\circ$	$\Theta > 40^\circ$
5	Circular	0	0	60	20	20
0	Oval 1	0	0	0	0	0
6	Oval 2	0	0	66.7	16.7	16.7
0	Elongate 1	0	0	0	0	0
2	Elongate 2	0	50	0	0	50
6	n/a & unclear	16.7	0	50	16.7	16.7

Table 3.10 Relationship between trough size and the angle between scour trend and lamina dip direction, in percentages.

n	Size \ Θ	Unclear	$\Theta < 5^\circ$	$5^\circ \leq \Theta \leq 20^\circ$	$20^\circ < \Theta \leq 40^\circ$	$\Theta > 40^\circ$
3	Small	0	0	66.7	0	33.3
9	Medium	11.1	11.1	44.4	11.1	22.2
6	Large	0	0	50	33.3	16.7
1	Very Large	0	0	100	0	0

3.8.3 Relationship of lamina dip to trough shape and size

According to the level of preservation between 1 and 3 measurements of laminae dip were collected per scour structure (Table 3.4). Laminae dip angle ranges from a minimum of 9° to a maximum of 35°. Laminae mean dip angle values for individual trough sets and range from 11° and a maximum of 26° (Tables 3.11 and 3.12).

Table 3.11 Relationship of trough size to the lamina dip in percentages.

N	Dip	Size			
		Small	Medium	Large	Very Large
0	< 5°	0	0	0	0
0	5° - 10°	0	0	0	0
10	11° - 20°	20	40	40	0
9	21° - 30°	11.1	55.6	22.2	11.1

Table 3.12 Relationship of trough shape to the lamina dip in percentages.

N	Dip	Shape						n/a
			Circular	Oval 1	Oval 2	Elongate 1	Elongate 2	
0	< 5°		0	0	0	0	0	0
0	5° - 10°		0	0	0	0	0	0
10	11° - 20°		40	0	40	0	10	10
9	21° - 30°		11.1	0	22.2	0	11.1	55.6

Comparative analysis of size and shape trough and laminae dip does not indicate a variation pattern (Section 3.9.3).

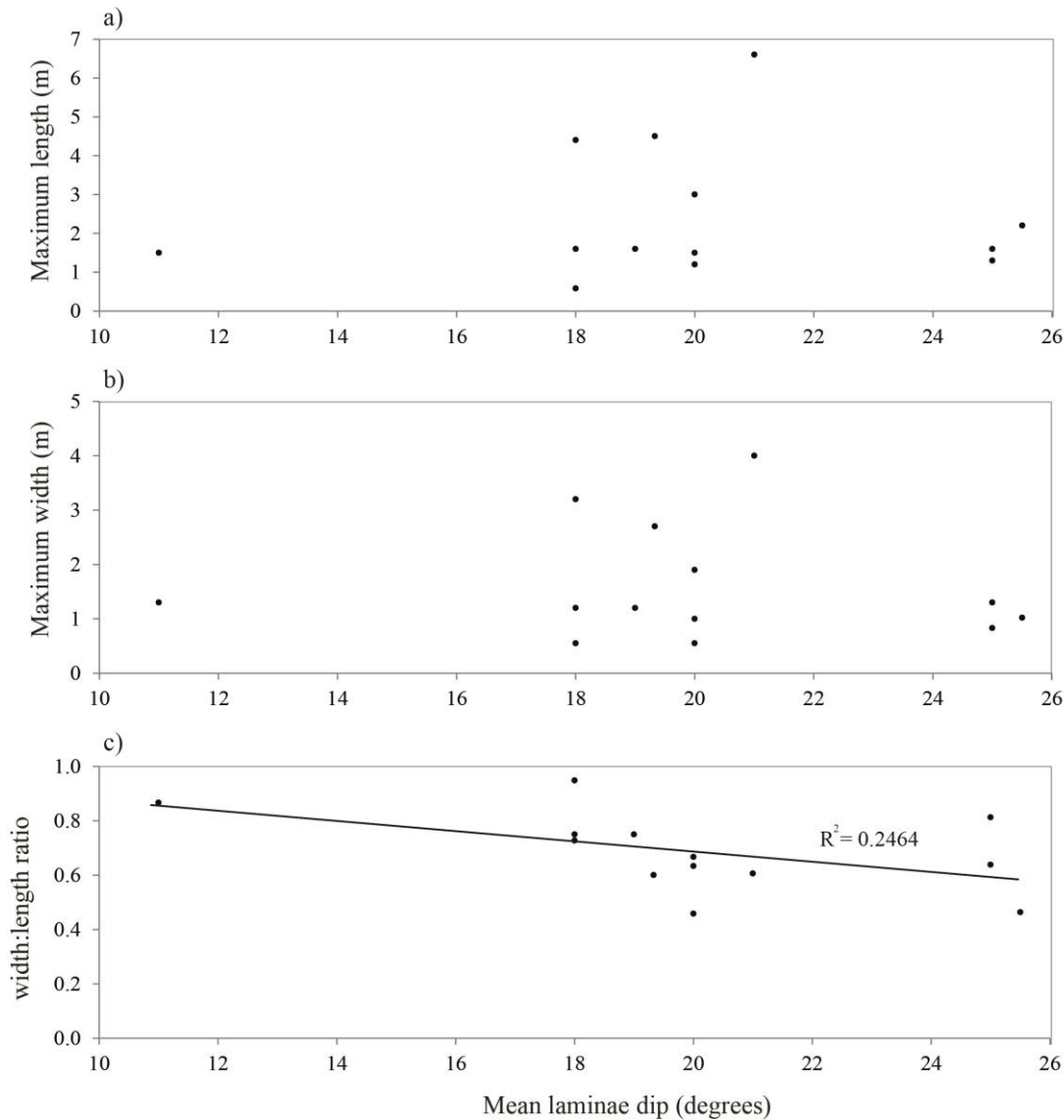


Figure 3.16 Relationship of trough dimensions to mean laminae dip angle: (a) Mean laminae dip to length; (b) Mean lamina dip to width and (c) Mean lamina dip to width:length ratio.

Linear regression tests were performed aiming to find possible relationships between trough dimensions and mean laminae dip. These demonstrate that neither of the plots in Figure 3.16 show any relationship between the trough and the mean laminae dip. There is no measureable pattern of variation of width:length ratio with mean laminae dip angle (Section 3.9.3).

3.9 Discussion

3.9.1 Discussion on relationship between classes and mean laminae dip direction

The scour structures at Seaton Sluice have been classified following the classifications defined in Section 2.7.1 used to classify the Prados Formation. This aimed to find relationships between the geometry of troughs and river flow conditions; also to discriminate geometrical characteristics that can be used to distinguish types of depositional systems based on the architecture of their final deposits.

All of the structures identified at Seaton Sluice are $W/L < 1$ and have the same dip direction. There is a predominance of medium to large structures with $0.5 \leq W/L < 0.75$ (oval 2 shape), scour trend and mean lamina dip direction divergence between 5° and 20° (Table 3.3, Fig. 3.13). Regression linear statistical test has been performed aiming to find possible relationships between these classes (size, shape and Θ). These demonstrate that there is no measurable relationship between classes (a) size, (b) shape and (c) angle between scour trend and mean lamina dip direction.

In addition, the width:length ratio have been compared to the maximum length, angle between trend and mean laminae dip direction, and lamina dip direction single mode. The maximum length has also been also compared to the relationship of mean laminae dip direction to scour trend and the lamina dip direction. None of these statistic tests show any relationship correlating these variables (Table 3.13).

Table 3.13 Coefficient of determination and significance of the relationship between scour structures classification classes and other variables.

	W/L vs size class (length)	W/L vs Θ class	W/L vs mean laminae dip direction	Size class (length) vs Θ class	Size class (length) vs laminae dip direction
R^2	0.095	0.006	0.001	0.001	0.052
Coefficient of Significance	0.305	0.808	0.931	0.920	0.452

These results suggest that the dimensions of resulting sedimentary structures are not closely related to each other, neither with the variation of lamina dip direction or the divergence between scour trend and mean laminae dip.

There must be other variables to be studied that relate to the variations in scour structure dimensions. Flow-regime, type of sediment and channel dimensions will determine the type of bedforms that will develop. Although these can be the most obvious factors controlling the dimensions of sedimentary structures dimensions, any variable controlling the morphology of migrating bedforms, such as variations in flow velocity, water depth, sediment supply and duration of the bedform forming mechanisms, can directly affect the dimensions of the resulting scour structures. The type of depositional system, its nature and its developing mechanisms can also explain the variations in the geometry of scour structures, their predominance within individual exposures and their distribution across the channel. Flume experiments have demonstrated that specific sedimentary structures are directly related to sediment transport and the dynamics of the channel flow (Visher, 1960). In addition, variation in grain size has some influence on the variation in type of sedimentary structures which can be also related to a variation in the dimensions of structure preserved. In ancient fluvial systems, the internal preserved structures of the sand bodies are the traces that allow the reconstruction of the depositional systems.

3.9.2 Discussion on the relationship between scour trend and mean laminae dip direction

There is a small variation between the scour trend and the mean lamina dip direction of the scour structures. In 77 % of the structures that divergence is less than 40° (Fig. 3.15). To examine the relationship between scour trend and mean laminae dip direction a statistical analysis of paired sample t-test was performed ($S = 0.352$) and a linear regression statistical test were also performed ($R^2 = 0.033$; $S = 0.554$). These demonstrated that there is no measureable relationship the variations of scour trend and laminae dip direction.

Any variation in the mean laminae dip direction records differences in bedform progradation. Also this divergence may be an indication of the degree of sinuosity of bedform crests. Herein, palaeocurrent data from individual trough cross-bedded sets reflects one single mode that agrees with the main flow direction; then if all the scour structures (troughs) are aligned with the flow direction and crests are sinuous, as the bedforms advance downstream it is likely that a proportion of the trough will fill at an angle to the trough long axis. In addition, this variation may be partly a function of

channel regime causing a variation in shape and bedform development, and partly a function of preservation. Haszeldine (1983a) described a section of these deposits (within Storey 2, Fig. 3.12) as the deposits formed by a low-sinuosity river with alternate bars. This interpretation is consistent with the little variation found between the laminae dip direction and the scour trend. Although the statistical analysis indicates no significant variation between scour trend and lamina dip direction, this might be because of the small number of structures used in this analysis (13 structures) and some possible bias in preservation patterns.

Also, based on this study and the erosive surfaces that have been observed, the river (or rivers) occupied this site for at least three different periods, recorded by the three storeys preserved (Fig. 3.8) and possibly 6 if Holzweber's (2012) interpretation is correct. The scour structures studied at Seaton Sluice are all in the lower storey (Storey 1) of the sequence (Fig. 3.8 and Fig. 3.10). The arrangement of lithofacies within Storeys 1 and 2 is slightly different, with Facies St more predominant in Storey 1, suggesting that the nature of the river channel that deposited these storeys was slightly different to the following river channel (Fig. 3.12). Therefore it should not be assumed that Haszeldine's (1983a) interpretation for the conditions that deposited Storey 2 were the same as the ones that deposited Storey 1.

The way bedforms migrate downstream and change their migration direction and what causes these variations can also explain variations in the laminae dip direction. The channel width, flow regime and sediment transport can be related to the quantity and style of subchannels (or anabranches) within a braided system (or system that becomes braided at low flow stages), such component channels cause multiple flow directions within a main river channel. This can explain variations in bedform migration and geometry and consequently the divergence between the scour trend and the main direction of the laminae. The level of sinuosity of the component channels or whole channel and the specific area where the bedform migrate forming cross beds also explains the variations in bedform progradation and as a result the variation between laminae dip direction and scour trend. The flow regime within different parts of the meander will determine bedform migration pattern and the lee-face developing direction; also within smaller areas higher flow variations are susceptible to occur and therefore it is likely that the main orientation of the longer axis of the bedform scour differs from

the migrating direction. Therefore, a good level of preservation and plan-view exposure and larger amount of data could lead to an improvement in the interpretation of some characteristics related to flow-regime and nature of fluvial depositional systems.

3.9.3 Discussion on relationship between width:length ratio and laminae dip and variation in laminae dip

The lamina dip has been investigated within each individual scour structure. Level of preservation was critical in this exposure and only in 9 scour structures was it possible to collect multiple measurements of laminae dip. Figure 3.16 shows the relationship between lamina dip and maximum trough length, maximum width and width:length ratio. To examine the relationship between trough dimensions and mean laminae dip a linear regression analysis was performed. This demonstrates that there are not close relationships between the trough visible maximum dimensions and the laminae dip.

Table 3.14 Coefficient of determination and significance of the relationship between trough dimensions and mean lamina dip.

	Length vs Laminae dip	Width vs Laminae dip	W/L vs Laminae dip
R ²	0.0009	0.009	0.250
Coefficient of Significance	0.951	0.757	0.082

Although the relationship of width:length ratio to laminae dip appears to be closer ($R^2 = 0.25$; $S = 0.082$) than the relationships between the other variables (Table 3.14); it is not considered as a significant correlation due to the small amount of data used in the statistical test (13 scour structures). Hence, based on the data presented it is not possible to resolve which factor or factors affect the variation in the internal laminae dip within individual cross-bed sets. The level of preservation and the ability to measure features in the field (Fig. 2.22) could have affected the results and may have led to misleading results.

Other factors, not directly related to the dimensions of trough cross-bed sets that may explain the variations in lamina dip can be: (1) the specific areas within the channel where bedforms were formed; and how far downstream they reached before they dissipated. This relates to the geometry of the depositional system that generated the

migrating bedforms. (2) The initial topography of the channel bed and how this topography evolved as bedforms developed; (3) the development of counter-flow ripples on the toe and lower part of the host bedform lee face that can modify the cross-bed deposition as sediments reach the toe of the bedform lee face; (4) bedform superimposition and bedform amalgamation and (5) flow regime, sediment supply and grain size influence depositional process on the lee face and also the distance sediments reach forming grain flows down the avalanche; this also explains changes in the laminae dip.

3.10 Re-interpretation of the nature of original channel

The detailed analysis of scour structures and cross-bedding characteristics and the overall study of the Seaton Sluice Sandstone aimed to add useful information to previous published interpretations of these deposits. Haszeldine (1981, 1983a) based mainly on the deposits corresponding to Storey 2 herein described, interpreted the Seaton Sluice Sandstone as the result of medial bars that accreted onto the north bank of a westward flowing low-sinuosity river channel that formed one large compound lateral bar. He identified trough and planar cross-bedding and classified them into five types of lithofacies (S1-S5). He also identified bounding surfaces that he interpreted as being formed by large-scale bedforms. Holzweber (2012) disagreed with Haszeldine (1983a) interpretation and stated that it is not possible to establish the initial deposition as a mid-channel bar from the available data. She identified large-scale inclined erosion surfaces interpreted as possible lateral accretion features and she suggested that a lateral bar or a point bar could be the origin of Seaton Sluice Sandstones deposition.

This study, identified two main erosive boundaries in the Seaton Sluice Sandstone subdividing it into three main storeys (that could be subdivided locally cf. Holzweber, 2012). Five lithofacies are identified in the Seaton Sluice Sandstone: St, Sp, Sr, Se and Fms. Trough and planar cross-bedding are arranged in thinning-upward cosets. These facies change laterally (e.g., from tabular to lens-shaped) forming complex coset architecture, especially towards the southern part of the site (Fig. 3.8; Logs 9 and 10; and log representing Outcrop-Section 3 in Fig. 3.7c). Facies St, and Sp are interpreted as major channel deposits. Beds of mudstone (Facies Fms) cover large areas of Facies St, which are interpreted as abandoned bedforms (cf. Guión *et al.*, 1995). Most of the

bedding surfaces are inclined-down in the same direction as the interpreted palaeocurrent direction (Fig. 3.6) and are interpreted as downstream accreting bar forms (even allowing for the uncertainty of the local tectonic tilt). There is some variation in bedding plane inclination that is consistent with the sort of variation that might be found within lateral or medial bars, but not a lot of variation that might be expected within higher sinuosity systems. Facies Sr (rippled cross-stratification) is rarely identified and appears on top of the upper planar cross-bed sets. The erosive surfaces and sandstone packages can be traced for long distances over more or less horizontal surfaces.

Palaeocurrent data from all three storeys in the Seaton Sluice Sandstone shows a dominant single mode of lamina dip direction towards 274° (Fig. 3.6a); palaeocurrent data which is believed to have been measured within the same stratigraphic and chronological horizon (upper part of Outcrop-Section 1, Figs. 3.10 and 3.14b) shows a dominant lamina dip direction towards 280° and bedding plane orientations were also measured throughout the vertical sequence showing a mean orientation towards 303° (Fig. 3.6b). Little variation in palaeocurrent data is observed; this can be explained by: (a) irregularities in the flow; (b) the level of preservation and field measurement accuracy; (c) morphology of the river channel (the existence of islands or bars in a braided morphology and the index of sinuosity within a low-sinuosity system); (5) the morphology of bar crests and their evolution; (6) variations in sediment supply that can be related to variations in flow behaviour. This strong consistency in the principal flow direction suggests that these deposits were formed by a river with low-sinuosity.

Hence, based on the data available in this study, the Seaton Sluice Sandstone is interpreted as the fluvial deposits generated by a multiple channel low-sinuosity river by the migration of large-scale bedforms. Contrary to Haszeldine interpretations (1983a, b), the sandstone represents more than one active channel reoccupying the site, recorded in several storeys. The exposure contains channel deposits and deposits corresponding to periods of channel abandonment (following avulsion or lateral movement of the channel from the site). The abandonment and over bank sediments are often absent, due to erosion by a channel reoccupying the site and depositing the overlying sediments. The strong single palaeo-flow direction, downstream inclined bedding surfaces, and the decrease in set thicknesses in the palaeo-flow direction suggests that descending cross-sets were mainly preserved. This agrees with Hazeldine's (1983a) first interpretation.

The predominance of trough and planar cross-bedding filling the channel is typical of low-sinuosity rivers. Although previous interpretations (Holzweber, 2012) suggest that these deposits could have been formed in sinuous systems based on palaeocurrent variability and third-order bounding surfaces, in this study lateral accretion surfaces characterising high-sinuosity plan form channels were not identified. Although within storeys sets are arranged in cosets with a thinning-upwards tendency, there is no clear pattern of fining-upwards, which is a characteristic of many high-sinuosity systems. In highly seasonal semi-arid and semi humid tropical settings point bar deposits may also lack identifiable lateral accretion surfaces and have only poorly developed fining-up patterns but have thinning-up set architectures (cf. Fielding *et al.*, 2009). Herein, the palaeoclimate has been described as humid with drier short periods and thus this is a possible interpretation.

According to Miall's (1985) compilation of fluvial system models and based on the interpretation above, the Seaton Sluice Sandstone could be classified as a fluvial system with similar characteristics to model 10 (Fig. 3.4). This model is also characterised by having distinctive facies and channel deposits mainly formed by compound bars. This agrees with this interpretation and Haszeldine (1983a) initial interpretation. However it could also be a strongly seasonal meandering system similar to those described by Fielding *et al.* (2009).

Further investigations of critical architectural elements such as the lateral accretion surfaces identified by Holzweber (2012) are need in order to improve the interpretation of the origin of the Seaton Sluice Sandstone.

3.10.1 Estimates of channel dimensions

Herein the channel dimensions have been estimated based on the methodologies followed in Section 2.10. Channel estimations have been calculated from set thickness measurements from Storeys 1 and 2. The full thickness of Storey 1 was not observed because the exposure at the base of Storey 1 was below sea level and so only one erosive surface bounding the top of this Storey was defined (Fig. 3.8). Therefore, the calculations based on Storey 1 observations give a minimum estimate of the channel dimensions. Two bounding surfaces delimitate Storey 2; and although these estimates may also infer minimum dimensions of the channel if part of this Storey has not been

preserved, these estimations are likely to be more accurate than the calculations for Storey 1. Storey 3 appears mostly truncated, eroded or absent, therefore no channel dimensions were calculated based on observations of Storey 3.

Following Leclair and Bridge's (2001) method (cf. Section 2.10.1; Equation 2.1) dune height estimates are:

Table 3.15 Estimates of mean values of dune height from Storeys 1 and 2.

Storey	Equation	Reference	Mean dune height (m)
1	$h_m = 2.9 \times \text{mean}$	(Leclair and	1.52
2	cross-set thickness	Bridge, 2001)	1.88

Herein, the flow depths were estimated following Yalin's (1964) and Allen's (1970) empirical relationships between mean dune height and depth (cf. Section 2.10.1; Equations 2.2 and 2.3) (Table 3.16).

Table 3.16 Estimates of channel depth/flow depth.

Reference	Leeder (1973)	Yalin (1964) (Equation 2.2)	Allen (1970) (Equation 2.3)
	$d = \text{coarse member}$		
Storey	of preserved fining-upwards cycle	using h_m	using h_m
1	n/a	9 m	16 m
2	5.8 m	11 m	20 m

N.B., where h_m is the mean dune height.

As in the Iberian channel, herein the bankfull depth estimates according to Yalin (1974) using the mean dune height, appear to be reasonable as they compare to other rivers (e.g., Fielding, 1986). The values of depth estimated following Leeder's (1973) method appears to be significantly shallower than the depths estimated following other methods. This indicates that Leeder's (1973) channel depths are underestimated due to

preservation level, erosion, bedload:channel size ratio. Therefore, Leeder's (1973) bankfull depth estimates should be treated with caution.

Although the preferred interpretation of the depositional environment is in a low-sinuosity river system, there is not enough evidence to confidently preclude high-sinuosity (as discussed above) and based on this, and following Leeder's (1973) channel width estimation that applies for rivers with a certain sinuosity, the channel width was calculated to present a possible hypothetical estimation (cf. Section 2.10.2; Equation 2.5) (Tables 3.17 and 3.18).

Table 3.17 Estimates of channel width (based on Storey 1 estimates).

Equation used to calculate channel depth	Channel depth assumed (m)	Equation used to calculate channel width	Estimated channel width (m)
Leeder (1973)	n/a	n/a	n/a
Yalin (1964) (2.2)	9	$w = 6.8 h^{1.54}$	205
Allen (1970) (2.3)	16	$w = 6.8 h^{1.54}$	509

N.B., In Table 3.16 and 3.17 two channel depths and widths values are calculated per method by using the mean dune height estimates.

Table 3.18 Estimates of channel width (based on Storey 2 estimates).

Equation used to calculate channel depth	Channel depth assumed (m)	Equation used to calculate channel width	Estimated channel width (m)
Leeder (1973)	5.8	$w = 6.8 h^{1.54}$	102
Yalin (1964) (2.2)	11	$w = 6.8 h^{1.54}$	284
Allen (1970) (2.3)	20	$w = 6.8 h^{1.54}$	670

N.B., Two channel depths and widths are calculated per method by using the mean dune height estimates.

Based on the estimations resulting from using values of dune mean height, the Northumberland River can be interpreted as medium to large size. The bankfull depth estimates calculated following Yalin's (1964) model are reasonable (Table 3.16) and

compare to channel estimates published on rivers of the Carboniferous of North England (e.g., Haszeldine 1983a, b; Fielding 1986) whereas the estimates based on Allen's (1970) model are significantly larger, hence they should be carefully considered. As previously mentioned, the calculations of the bankfull widths should be taken with certain reservations since both the Yalin (1974) and Allen (1970) models are preferably used for systems of a certain sinuosity.

Channel depth and width estimates using the maximum dune height (2.75 m maximum dune height in Storey 1 and 4.06 m in Storey 2 at Seaton Sluice) are up to 24 m and 929 m by using Yalin's (1964) model and 38 m and 1815 m by using Allen's (1970) model. These estimates indicate that the Northumberland River was larger than expected; and significantly deeper than other rivers that transported sediments in the Upper Carboniferous of North England. These values correspond to the hypothetical dimensions of the channel in the maximum stage of enlargement possibly due to an extreme and rapid flooding event but they would not be representative of the true mean dimensions of a channel in a non-extreme stage.

The comparison of channel dimensions with the following examples is not a perfect fit, but it gives an idea of the scale of this river. Thus, the Northumberland River is comparable to other shallower examples. For example the Sagavanirkitok River (braided and anastomosing) with main channels between 50 and 250 m wide and depths at bankfull stage of 2.7 m to 3.9 m (Lunt *et al.*, 2013); the Saskatchewan River (Ashworth *et al.*, 2011) with anabranching channels presenting main channels at low flow up to 3 m deep and up to 150 m wide, are considered to be medium size rivers. Rodrigues *et al.*, 2011 described alternating migrating bars in an anabranch of the Loire River; these reach 1.5 m in height and 300 m width, which give a suggestion of the channel dimensions.

Rivers in the Carboniferous were expected to be very large with estimated dimensions between 10 to 12 m depth and up to 5 km width. Fielding (1986) studied the fluvial channel deposits from the Westphalian of the Durham coalfield in North England and according to his proposed model, major distributary channels formed the main avenues of sediment transport across the plain. He described that these channel deposits occurred in elongate belts up to tens of kilometres long and generally up to 5 km wide. He

estimated from sandstone internal architecture that the channels have bankfull depths of the order of 10 to 12 m, and widths of 1 to 2 km. These large sequences corresponding to the major distributary channels compare well to the channel facies in the Westphalian B of North England (Seaton Sluice) described by Haszeldine (1983a, b). In addition, Bristow (1993) described part of the deposits of the Rough Rock Sandstone, Carboniferous of North England as sandstone sheets formed in a braided river at least 6.5 m deep and approximately 1 km wide. Given all this, realistic channel estimates for the Northumberland River would be in the order of 10 to 12 m deep and up to 2 km wide.

3.11 Conclusions

The main findings of the study of the Seaton Sluice Sandstone and the descriptive analysis of the internal sedimentary structures are:

1. Based on the descriptive analysis of the entire exposure:

- Five lithofacies are recognised and they are arranged in thinning-upwards sequences. These are: St (trough cross-bedded sandstone), Sp (planar cross-bedded sandstone), Sr (rippled cross-laminated sandstone), Se (erosional surfaces), and Fms (laminated claystone). These lithofacies are arranged in facies associations interpreted as architectural elements: sandy bedforms; overbank fines and possibly macroforms foresets. Haszeldine (1983a) only described Facies St and Sp. Holzweber (2012) also includes Facies Sl (planar-bedded and low-angle laminated sandstones).
- These lithofacies are generally arranged in facies associations that when complete include facies St > Sp > Sr > St/Sp > Fms. The Seaton Sluice exposure mainly preserved channel filling deposits (Facies St and Sp). The fine grained facies corresponding to late channel abandonment fill and floodplain deposits are mostly absent. Some are observed towards the contact between Storey 1 and Storey 2.
- The Seaton Sluice Sandstone is c. 7 m thick (Haszeldine (1983a) estimated 10 m thickness; this difference is possible due to where and at what time measurements were taken since part of the exposure is below the sea level). It is subdivided in three storeys. Storey thickness varies throughout the exposure.

Storey 1 minimum thickness varies from 0.5 to 3.5 m, and tends to decrease towards south until it is totally covered by sea or it is absent. Storey 2 thickness fluctuates (2.2 to 5.8 m) and tends to increase towards the south. Storey 3 is mainly truncated or absent; its maximum visible thickness is c. 1.5 m.

- Set thickness tends to decrease upwards in each storey.

2. Based on the analysis of individual trough cross-bed sets (scour structures):

- The geometry of scour structures varies. These have been classified on the basics of class (a) size, class (b) shape (c) the relationship of mean laminae dip direction and scour trend and (d) basal contact.
- Shape: All the structures have a width:length ratio < 1 . Of the 19 structures, 26.3 % are circular ($0.75 \leq W/L \leq 1.25$), 31.6 % are oval 2 ($0.5 \leq W/L < 0.75$) and 10.5 % are elongate 2 ($W/L < 0.5$).
- Size: 15.8 % are small structures, 47.4 % medium, 31.6 % large and 5.3 % very large structures.
- All the structures analysed are located within the same stratigraphic unit and therefore no pattern between of variation in the dimensions and stratigraphic position was found.

3. Based on the palaeocurrent data:

- Palaeocurrent analysis from all three storeys reveals a single flow direction mode with a resultant mean direction towards 274° with relatively low variance ($\sigma = 56^\circ$). This suggests that each time a channel occupied the site it had similar (or the same) orientation.
- Palaeocurrent data from within each individual storey shows small flow direction variations. This can be explained by irregularities in the flow due to discharge variability. It can also be a function of the level of preservation and field measurement accuracy. In addition the morphology of the river channel and bedform crestline shape influence variations in the migrating pattern of bedforms within the main channel resulting in slight palaeocurrent scatter.
- Palaeocurrent data from individual trough cross-bed sets (scour structures) shows a single mode towards 280° .

- Mean bedding plane orientation data measured in the entire exposure shows a resultant direction of 303° and variation of 36° . Although interpretation of the local tectonic tilt is not possible, this suggests that there is a preferred direction of preserved inclination in addition to any tectonic tilt.
- All palaeocurrent data and bedding plane orientations suggest one string single palaeo-flow direction towards the WNW and that most of the sets preserved are descending sets, possible preserved on the downstream side of bars (of large-scale dunes).
- In 23 % of the individual cross-bed sets a divergence between the mean laminae dip direction and the scour trend occurs is greater than 40° . This is a function of channel system regime causing variation in bedform shape (e.g., as sinuous-crested bedforms migrate, the degree of sinuosity of their crests will also influence the angle variation between scour trend and laminae dip direction). It can also be a function of preservation.
- The dip of the internal laminae of the scour structures varies from 9° to 35° . Within individual structures the lamina dip tends to increase downstream however there is not enough data in this case study to assure this confidently. If this is a real pattern then it is suggesting that sediments were transported and deposited under unsteady flow conditions causing laminae dip variations.

4. Based of statistical analysis of relationships between the characteristic of scour structures:

- There are no measurable relationships between W/L and: maximum length, mean laminae dip, angle between trend and mean laminae dip direction, and laminae dip direction mode in the data collected.
- There are no relationships between maximum length and: the relationship of mean laminae dip direction to scour trend and the laminae dip direction.
- There is no measurable relationship between scour trend and mean laminae dip direction for individual trough cross-bed sets.

5. Based on fluvial system reconstruction:

- Various methods of estimating channel dimensions (e.g., Yalin, 1964; Allen, 1970; Leeder, 1973 and Ethridge and Schumm, 1978) suggest that the channel

was greater than 5.8 m deep and could be locally as much as 20 m also estimated that the width could be 102 m or as much as 670 m. This then represents a moderately large channel system and the exposure is relatively small.

- The Seaton Sluice Sandstone is fluvial in origin. Based on this study, the Seaton Sluice Sandstone is interpreted as deposits accumulated by multiple low-sinuosity river channel/s by the migration of large-scale bedforms with bedform superimposition. One strong single flow direction mode suggests the low-sinuosity character of the system and that when rivers re-occupied the site they had a similar orientation.
- Inclined bedding surfaces and the decrease in set thickness in the palaeo-flow direction suggests that descending cross-sets were mainly preserved.
- Following Miall's fluvial system model compilation (1985), the Seaton Sluice Sandstone can be interpreted as a low-sinuosity river, relatively deep with foreset macroforms and isolated linguoid and transverse bars, which partly agrees with Haszeldine's (1983a) interpretation. On the contrary, Holzweber (2012) suggested that these deposits could be interpreted as the result of a high-sinuosity river, which could be a possible interpretation as lateral accretion can be absent on certain seasonal meandering system as those described by Fielding *et al.* (2009). Based on this study, there is not enough evidence to consider a high-sinuosity river as the main system that generated the Seaton Sluice Sandstone.
- Therefore, further investigations will be the great use aiming a more complete interpretation of the depositional system and clarify the diverse hypothetical interpretations.

Chapter 4

Scour associated with bedforms and basal boundaries of cross-bed sets

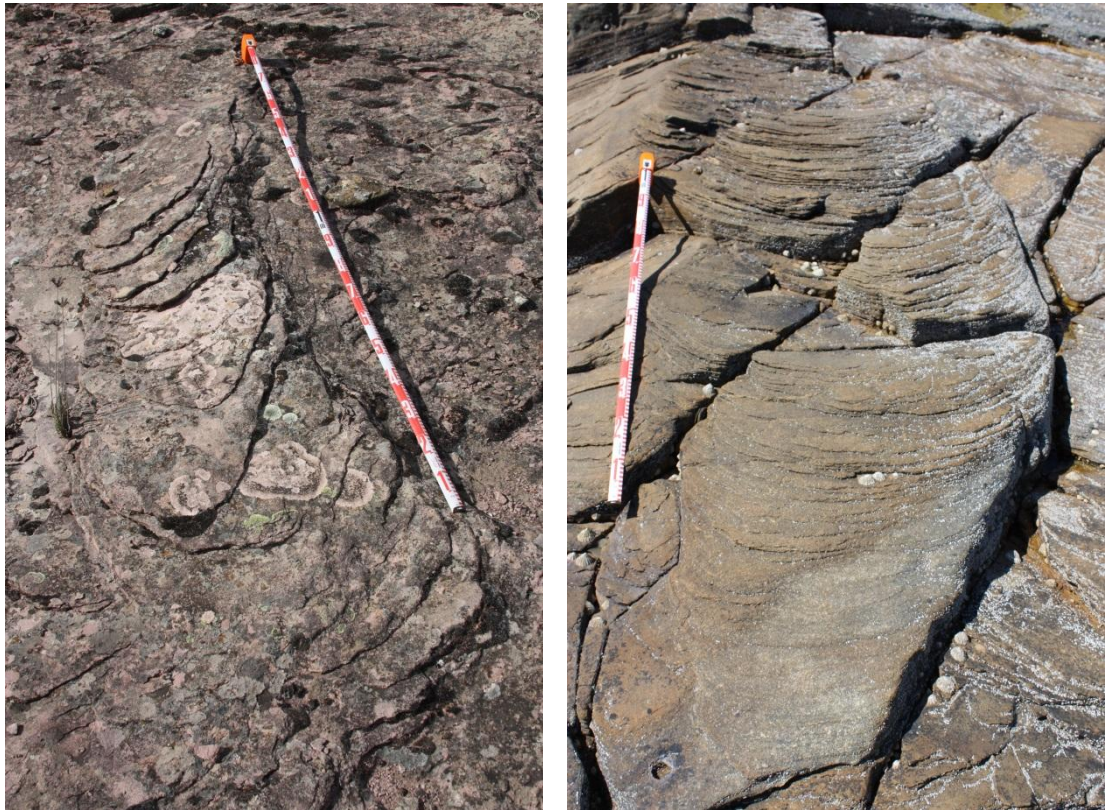


Photo: Scour structures at The Prados Formation (left) and the Seaton Sluice Sandstone (right)

4.1 Introduction

Bedforms arise from the interaction between flow and mobile sediment. They develop due to flow over a sediment bed and the flow pattern will be modified by the morphology of the migrating bedforms. Up to the present date sedimentologists have primarily focused on the study of what forms on the channel bed (i.e., bedforms), largely ignoring erosion of the bed. Thus, although there is an extensive body of published work on bedforms and bedform development (e.g., Sorby, 1852; Raudkivi, 1966; Coleman and Melville, 1996; McLean, 1990; Best 2005; Coleman and Nikora, 2009) there is a large gap in the literature on associated bed scours and the mechanisms of scouring as bedforms form and migrate in unidirectional flows. Very little is published relating scour type to cross-bedding style. Investigation of scour mechanisms associated with bedforms would improve the understanding of: the development of bedforms, corresponding flow resistance, sediment transport processes, preservation of sedimentary structures in relation to bedforms, and the resulting sedimentary structures. Greater understanding of scour in association with unit bar and dune development is essential to improve understanding of the architecture of cross-bedded sandstone.

Understanding scour type in relation to sedimentary structures and cross-bedding styles is key to obtaining realistic interpretations of the formative bedform types, flow dynamics and river dimensions. Therefore, to find links between sedimentary structures, their basal bounding surfaces (formed by the development of a scour or scours over time) and the migrating bedform type that formed the cross-bedding styles observed at Rillo de Gallo (Chapter 2) and Seaton Sluice (Chapter 3), this chapter reviews published work on scour formation and bedform development in experimental unidirectional flows and also bedform evolution tracking in modern rivers. To better understand scour in relation to the formative bedform, and the processes that can trigger the initiation of scour, this chapter begins with a brief review of bedform initiation and bedform development. Data from Chapters 2 and 3 are discussed in the light of this review in an attempt to improve the understanding of basal bounding surfaces of cross-bed sets associated with bedform type and cross-bedding thickness; and to find links between published experimental work and field work observations to improve methodologies for interpreting bedform dynamics and making palaeoenvironmental reconstructions of the forming river systems.

4.1.1 Review of research on bedform origin to better understand relationship to scour

Bedform Initiation

In most rivers, bedform initiation occurs on the river bed due to bed irregularities (including antecedent bedforms). In natural settings flow is rarely over homogeneous smooth surfaces. In contrast, most flume studies initially have flat beds prior to bedform initiation. Flat sand beds under a unidirectional subcritical water flow become unstable and disturbed when the bed shear-stress exceeds the threshold for sediment movement, generating irregularities on the flat bed observed as regular pattern of small sand wavelets (Coleman and Melville, 1996). Then, small ripples will develop from these wavelets by processes of reorganization.

The principal types of bedform initiation are (1) initiation from a pre-existing bed defect and (2) instantaneous initiation (Raudkivi 1963 and 1966). Bedform initiation due to a defect occurs when there is an initial disturbance in the flat bed and the applied bed shear stress is high enough to produce sediment transport, otherwise the bed defect will not evolve and eventually decay (Raudkivi, 1966). In this situation it is envisaged that it is possible to generate bedforms without significant scour if sediment supplied from upstream satisfies or exceeds the local transport capacity. Instantaneous bedform initiation occurs at higher shear stress, and a uniform field of small bedforms appears spontaneously covering the previously flat surface (Gyr and Schmid, 1989; Venditti *et al.*, 2005b). Venditti (2013) described the evolution of this spontaneously formed field of bedforms. First, a regular pattern of “*chevron-shaped scallops*” develops; second, these forms start migrating and incipient crestlines develop; third, these small bed features become well-defined 2D forms with straight crestlines; and fourth, bedforms develop and grow. As this initiation of bedforms requires no supply of sediment from upstream, to build positive areas on the bed (crests) requires erosion of negative areas (scours). Although his description of the morphology of the initial bed features as *chevron-shaped scallops* may imply scour, Venditti did not describe the scours.

When bedforms arise from an initially flat bed, this indicates that there is a basic bed instability that will prompt the initiation of bed disturbances (McLean, 1990). Coleman and Nikora (2009) reviewing published work summarised two mechanisms that can

explain “sediment-wave” initiation: (1) motion of turbulent fluid (i.e., instantaneous initiation; bedforms generated due to large-scale turbulent structures such as fluid bursts: cf. Jackson, 1976); (2) flow instability (i.e., instability of the fluid-sediment flow system due to initial disturbances); and added a third: (3) granular transport mechanics (bed instability occurs due to the nature of granular motions such as saltation with jump length related to particle size causing periodic bed irregularities). None of the published descriptions of these mechanisms mention the formation of scours even though the formation of positive features on a bed requires sediment supply from somewhere. When water flows over erodible surfaces, scouring is expected and sediment mobilised from the original bed as scours develop may be re-deposited forming bedforms. In contrast, when bedforms form due to sediment flux over a non-erodible bed (e.g., a consolidated sediment bed or bedrock) trough-scouring is less likely to occur.

Perillo *et al.* (2014b) investigated bedform initiation from artificially generated negative defects on a flat bed under unidirectional flow. Defects must be larger than those generated by coherent turbulent flow structures (e.g., Best, 1992), so that the defect propagation threshold decreases and the defect will develop into a field of bedforms. The difference in height between the edge of the defect, which was observed to be slightly higher than the flat bed, and the surrounding flat bed causes a small flow separation zone that generates localised areas of higher bed shear stress to produce sediment transport, which will result in “*two-lobe horn*” geometries. Although the geometrical pattern developed was not any of the known bedforms types (i.e., ripples, dunes, bar), it is likely that a field of bedforms could be formed in this way. Negative bed features that may generate a bedform field in this way could occur on natural beds by, for example, animal activity, or the presence of natural objects such as dead wood and plants. Thus, scour is potentially very important to bedform development. More focused research is needed to fully understand the importance of scour development and geometries for bedform type and the architecture of final deposits.

Bedform development

Bedform growth varies with the location of the maximum shear stress relative to the bed topography (Smith, 1970). Bedforms increase and decrease in size due to the local flow field. Venditti (2013) identified three main types of bedform growth and dampening within a channel: “(1) *bedform growth from a flat bed or bed with incipient wavelets at*

steady flow; (2) changes in individual bedform geometry at a constant flow after the features have grown to equilibrium dimensions; and (3) changes in the bedform field due to changes in flow conditions". The full process of bedform growth can be divided into four stages independently of flow type (Perillo *et al.*, 2014a): (1) incipient bedforms: this stage covers the time interval in which sediment transport starts to occur and until the very first incipient forms appear; (2) growing bedforms: in this stage the bed is already covered by bedforms and these increase in size mainly by bedform amalgamation but also due to sediment deposition (agreeing with Raudkivi and Witte's, 1990 theory of bedform growth primarily by bedform amalgamation); (3) stabilizing bedforms: described as the time interval between the end of bedform growth and time when the bed reaches equilibrium with the flow; and (4) fully developed bedforms: this stage is reached once the bedforms are fully in equilibrium with the flow. In a series of flume experiments, Perillo *et al.* (2014a) observed that the bedform growth path has the same trend regardless of flow type (unidirectional, oscillatory and combined), bedform size, bedform shape, bedform planform geometry and sediment grain size.

Leclair's (2002) flume experiments suggested that trough-scouring influences bedform height variations. Schindler and Robert (2005) suggested that variations of bedform size depend on downstream sediment transport rate and erosion rate at reattachment resulting in sediment deposition at the crest of a downstream bedform causing an increase of height. Raudkivi (2006) also observed that an increase in bedform height was associated with higher erosion rates in the reattachment region and the height increased partly due to deeper scouring in the bedform lee side (thus increased height tends to produce more scour and more scour tends to produce increase in height). Jerolmack and Mogrig's (2005) flume studies show that variations of bedform size and shape are sensitive to local bed topography, which influences the initiation and decay of bedforms and the interaction between bedforms.

Although published work suggests relationships between bedform size and scour (Leclair, 2002; Schindler and Robert, 2005; Raudviki, 2006), and that subaqueous bedform growth, irrespective of whether they are silt ripples (Bass *et al.*, 2011), sand dunes (Leclair, 2002) or larger bedforms (Schindler and Robert, 2005), is mainly controlled by the scour development in the reattachment region of the migrating bedform, a lot more research on this subject is needed. Not least because external

factors must control scour and bedform development, but more importantly for this thesis because the shape, character, planform and development of scours in relation bedforms, is not known and thus the relationship between basal erosion surfaces and cross-bed architecture is poorly understood.

4.2 Troughs and scours associated with bedforms

How scours occur in association with bedforms is poorly recorded in the literature. A better understanding of the relationship between bedforms and scour geometry and how this is recorded in the rock record will improve field interpretations. There are ongoing issues of terminology ambiguities where the terms scour and trough are often used interchangeably although they do not mean the same thing. “Trough” means a low area, whereas although scour is also a low area the word implies erosion formed the low. Consequently any depression (e.g., between two bedforms) can be called a trough, not all of them are scours.

A bedform trough can be defined as a “deep” area downstream of the bedform crestline, and limited by the stoss face of the next bedform downstream (i.e., deep between the crests of two bedforms) (Fig. 4.1). The area of the trough may be defined by the limits of the area below the mean bed elevation (Fig 4.1). Bedform troughs become more distinguishable as bedforms develop and increase in height, and consequently deeps are more noticeable. In very rare cases, where sediment flux is very high, the bed aggrades and bedforms climb, no erosion will occur on active bedforms. In all other situations there will be some erosion associated with bedforms. In situations with sediment flux over a non-eroding bed, the bottom of the trough will not be a scour although erosion will generally occur on the bedform stoss slopes with deposition on the lee sides allowing the bedforms to migrate downstream. This local erosion on the stoss of bedforms that leads to bedform migration is not termed scour in this thesis as it does not form new or deeper lows.

The term scour implies sediment erosion and this may lead to incision below the mean bed level. In this thesis the term scour is used to mean localised erosion from erosional-based troughs (Fig. 4.1B). Scours can form on river beds due to disturbance on the flow by irregularities on the bed or the presence of natural obstacles, such as plants, dead

wood, pebbles, cobbles and boulders that cause localised high bed shear stress and remobilization of sediments (Section 4.5.2). Scour can also occur at the flow reattachment point in the lee of bedforms and this will cause remobilization of sediment in the trough (in the deepest part or on the stoss of the next-downstream bedform).

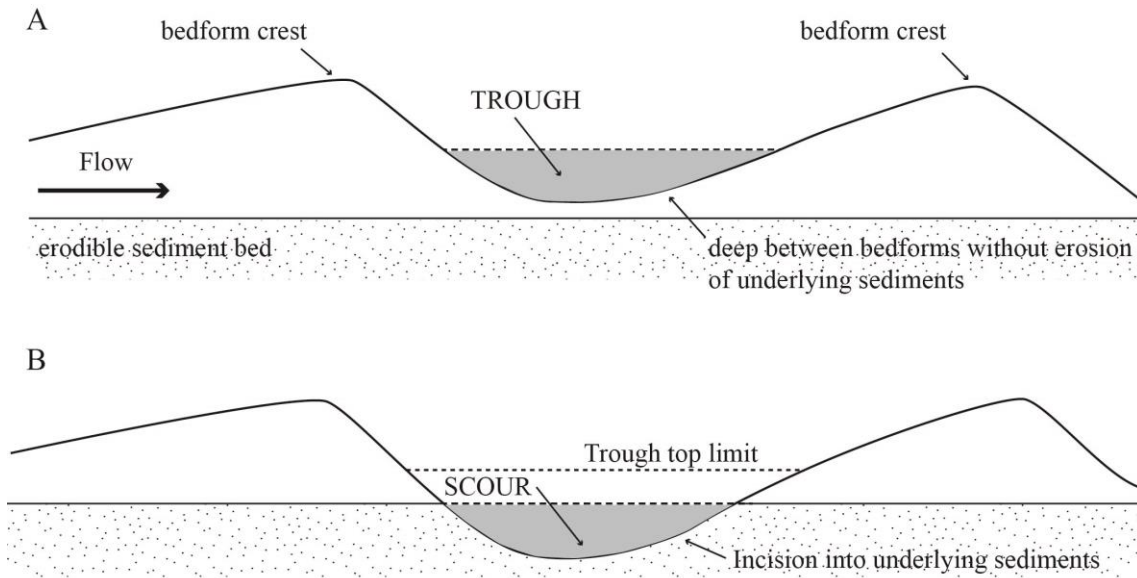


Figure 4.1 (A) Illustration of trough between bedforms migrating in a unidirectional flow; (B) Illustration of scour within the trough between two migrating bedforms incising into the underlying sediments.

The sedimentary structures resulting from dune or unit-bar migration over a trough-shaped topography, be that a scour or not, are known as trough-cross bedding. Although the resulting cross-bedding styles are referred to with the same name, the mechanisms that formed them may be slightly different. If it is possible to identify the difference between scour and no scour trough-cross bedding in preserved deposits, this may improve palaeoflow reconstructions. Whether or not it is possible to distinguish between pre-existing troughs or pre-existing scours and scours that develop in association with migrating is discussed in Section 4.6.

4.3 Mechanisms of scour initiation

Scour occurs when bed shear stress locally exceeds the threshold shear stress for entrainment of particles from the bed. This can result from coherent flow structures generated within the flow or resulting from external controls. The theories on bedform initiation due to channel bed defects (Section 4.1.1), can work with either negative or

positive relief creating initial disturbances over the channel bed, and is not dependent on how these develop. However, any bedform field with scours may inspire the questions; what came first, the scour (generating the sediment) or the positive relief of the initial wavelet (generating the flow structure that causes local scour)? Can scour and bedform be initiated simultaneously? Are scour and bedform mutually dependent? To better understand the cross-bedding styles formed by bedform migration and their architecture in association with the formative bedforms, several theories of scour initiation are suggested herein. These consider (a) that scour is directly associated with the formative bedform, or (b) that scour is not dependent on the migrating bedform and therefore the scour may have developed prior to bedform migration, or be caused by some external control (e.g., animal activity, natural obstacles). To aid palaeoenvironmental reconstruction of fluvial deposits, the relationship between scours and formative bedforms and the architectural implications for the deposits; and how these can be identified in the rock record must be considered. Four theories on trough and scour genesis in relation to bedform migration are presented here:

- 1. A bedform migrating over an unrelated pre-existing trough:** Due to the undulating morphology of the bed topography a trough exists before arrival of a migrating bedform. A bedform unrelated to the bed topography advances over the trough, which does not scour in response to the migrating bedform. This will result in a trough-shaped basal surface overlain by cross-bedding, and it will be interpreted in the rock record as trough cross-bedding. (This is like the experiments presented in Chapter 5).
- 2. A bedform migrating over an unrelated pre-existing defect resulting in local scour that subsequently becomes associated with the migrating bedform:** Due to bed irregularities or defects a scour forms on the channel bed. Then a bedform, unrelated to the scour, advances over the scour and the scour develops more in response to the flow pattern associated with the migrating bedform. This will result in a concave-up bounding surface cutting into the underlying sediments and filled with cross-bedding. This will also be interpreted in the rock record as trough cross-bedding.
- 3. A pre-existing defect on the channel bed triggers downstream bedform initiation:** A defect on the channel bed develops into a scour pit. The difference in height between the edge of the scour and the flat bed can cause flow

separation that might generate localized zones of high bed shear stress that allow bedload sediment transport downstream the scour (cf. Perillo *et al.*, 2014b). This will result in downstream bedforms that may erode the bed in their lee causing concave-up bounding surfaces. In addition, under sediment flux and flow conditions that develop irregularities on the flat bed and therefore can trigger bedform initiation, the scours due to pre-existing defects can be filled by the upstream sediments transported by the migration of these new bedforms. Then these scours will develop in response to the migration of the new unrelated upstream bedforms (Theory 2) forming concave-up bounding surfaces between cross-bedded sets.

- 4. Bedform initiation due to irregularities on flat bed and subsequent scour development:** Instantaneous disturbances on the bed can modify flat-bed topographies (as described above in Section 4.1.1). Intense turbulence may initiate local area of erosion and deposition. The development from 2D bedforms to curved crests will change the maximum magnitude and pattern of bed shear stress and may initiate scour. In this case, bedforms develop first and they evolve towards more 3D geometry. The geometry varies due to flow dynamics, channel planform and morphology of the river reach. Thus, bedform and scour will develop simultaneously as the bedform migrates downstream. This will result in a concave-up bounding surfaces overlain by cross-beds resulting in trough cross-bed sets, in which scour is filled by the foresets deposited due to the migration of curved-crested bedforms associated with the scour.

In natural rivers, flat-bed configurations are rare, and although it is possible to envisage theories 1-3 occurring, theory 4 is more likely to explain the relationship between scour and bedform observed in most field sites. Despite this, theories 1-3 should not be ignored and deserve more research.

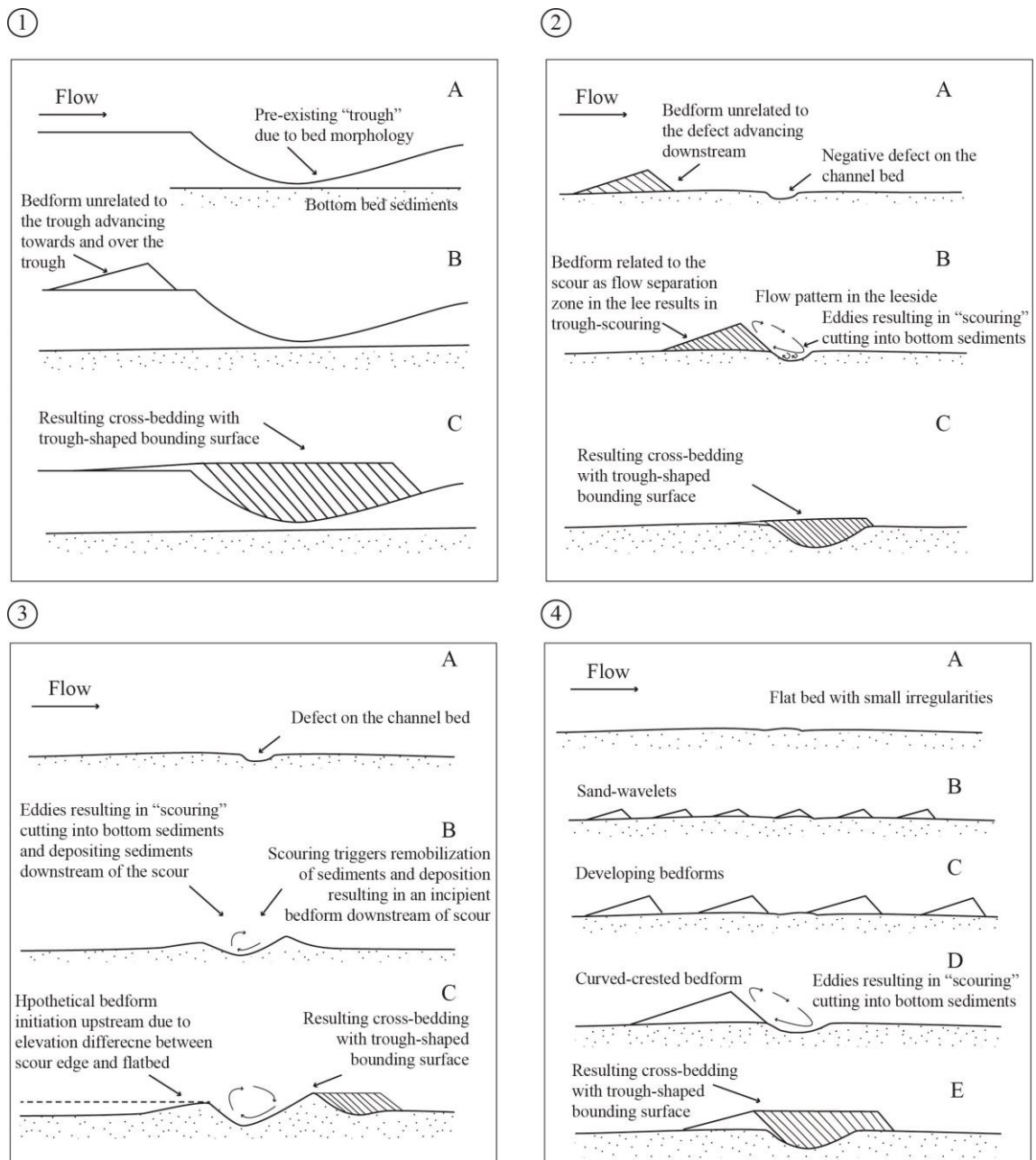


Figure 4.2 Hypothetical mechanisms of scour initiation: (1) Unrelated bedform migrating over a pre-existing trough; (2) Unrelated bedform migrating over a pre-existing defect that results in a local scour and subsequently becomes associated to the migrating bedform; (3) Pre-existing defect on the channel bed triggers downstream bedform initiation; and (4) Bedform initiation due to irregularities on flat bed and subsequent scour development.

The basal bounding surfaces of the scour structures observed in Rillo de Gallo (Chapter 2) and Seaton Sluice (Chapter 3) are concave-up, and individual cross beds fill the scours with tangential contacts onto the basal scour surface (e.g., Fig 2.10). These basal bounding surfaces are herein interpreted as erosion surfaces formed by the scours associated with the geometry of the formative bedforms and associated with their 3D

character, and therefore, to the resulting cross-bedded architecture. The evidence for this is discussed in Section 4.5. This interpretation is based on field observations in combination with the scour controls (Section 4.4), and the mechanisms of scouring presented in this section.

The shape of individual basal bounding surfaces of trough cross-bed sets is unlikely to be the shape of the scour at any one time because the scour will evolve as the bedform migrates and parts of it may be filling while other parts are still eroding. The following section discusses links between scours and migrating bedforms for better interpretations of ancient fluvial deposits. It focuses on the evidence that can establish that scours are spoon-shaped erosive surfaces associated with the formative bedform rather than pre-existing erosive surfaces. Other types of scour common on river beds are also reviewed highlighting the significance of scale in order to distinguish the formation of scours associated with bedforms from pre-existing scours such as chute channels and obstacle marks.

4.4 Controls of scour geometry and scour occurrence

Numerous studies monitoring the formation and evolution of bedforms in modern rivers and flumes have been published. Very few of these mention the presence of scours, their geometries, and whether the scour initiation was on a flat surface and within a bedform trough or the controls on scour geometry. Of those that do, of particular interest are: Gabel (1993), Ten Brinke *et al.* (1999), Carling *et al.* (2000), Leclair (2002), Parsons *et al.* (2005), Reesink and Bridge, (2007) and Reesink *et al.* (2014).

Scour geometry may be described by a combination of components including depth, planform shape and size. Most published research on bedforms and their associated scour has only described scour depth. Preliminary controls on scour formation and scour geometry suggested in published studies and research presented in this thesis are: (1) discharge (controlled by water depth and mean flow velocity); (2) bedform height (partly controlled by water depth); (3) bedform crest morphology (partly controlled by mean flow velocity and time); (4) bedform migration pattern (related to control 3 and to sediment properties); (5) bed load and suspended load flux; bed and suspended load grain size distributions; (6) sediment types (for example quartz sand, organic particles);

(7) bed consolidation (this influences ease of erosion). Many of these factors are mutually dependent and only some of the relationships between them have been investigated.

Scour depth in relation to bedform height

Leclair (2002) investigated the controls on the geometry of cross-bed sets formed by sinuous-crested dunes in rivers and flumes. She did little work on scour initiation, geometry or 3D scour fill architecture. She investigated the relationship between dune height and scour depth (trough-scouring). She observed erosion in dune troughs, measured trough-scour depth relative to the mean bed level, and considered this the main control on dune height variation. On this basis, bedforms with deeper troughs are expected to have greater heights. Due to trough-scouring in dunes, temporal variations in bedload and suspended load transport within the separation zone occur; sediment eroded in the trough is transported up the stoss of the next downstream bedform, causing variations in the dune height. Higher dunes produce stronger flow separation and greater bed-shear stress in the reattachment area leading to faster scour. Leclair's flume experiments were set up initially with flat beds of homogeneous well-sorted mono-modal sand. In natural rivers, these conditions are rare, so although Leclair's conclusions on dune height and scour depth are useful to establish preliminary relationships between bedform size and scour depth; experiments using initial setups and sediments more likely to be expected in natural rivers need to be undertaken.

Although Leclair (2002) considered trough-scouring as the main and most common control on dune height increase, this is often the result of bedform superimposition (Fernández *et al.*, 2006; Reesink and Bridge, 2007; 2009). This affects the flow field in the trough downstream of the host bedform, which may cause sediment erosion within the trough (trough-scouring). Some implications of bedform superimposition are presented in Section 6.4.2. Leclair (2002) recorded some rapid dune height variations due to bedform decay and bedform amalgamation; causing a rapid decrease in scour depth.

Leclair (2002) suggested that the geometry of dunes does not vary systematically with aggradation rate and that the mean dune height does not change systematically with flow velocity. Leclair's observations indicated that although the magnitude of variations

in dune height does not depend on flow velocity, changes in dune height and scour depth occur more rapidly with increasing velocity. If dune scour depth is dependent on dune height; the implication of Leclair's theory is that scour depth does not depend on aggradation rate or flow velocity. There are problems with the application of this however, particularly to any system where flow conditions change, because it assumes a bed in (or near) equilibrium with the flow and this will often not be the case. In situations where flow conditions change rapidly and often, because scour is more rapid at faster flow velocities, the relationships between preserved scour dimensions and related dune height may differ considerably to that suggested by Leclair, and this is yet to be investigated.

It is not known how well Leclair's relationships can be applied outside the range of conditions of her experiments. The interpreted height of the bedforms responsible for the cross-bedded sandstone at the case study sites described in Chapters 2 and 3 were much greater than those in Leclair's (2002) flume experiments and the sediment more variable. The Triassic river that deposited the Prados Formation (Chapter 2) was active under more arid climate than Iberia experiences today. It is likely to have had very variable flow conditions (seasonal and flashy) and higher sediment supply (mountainous source area and low vegetation cover). Sediment supply and rapid discharge variations may have big impacts on dune heights and scour depths (see next section), and thus Leclair's suggested relationships between dune height and scour depth should be applied with considerable caution in the Prados case. In the Seaton Sluice Sandstone sediment is interpreted to have been deposited in deeper water with larger bedforms (Section 3.10), but accumulated in thinner storeys (Section 3.6). The most likely explanation for this is that the more humid climate and less flashy discharge pattern combined with lower sand flux relative to discharge. In this case, sediment flux and rapid discharge variation may have had less impact on dune height and scour depth variations than in the Prados river.

Scour depth associated with sediment character, flux and bed aggradation

Grain size, size sorting, and the quantity of bedload and suspended sediment influence bedform stability and consequently variations in bedform morphology (Schindler and Robert, 2005). These may also cause variations of scouring in troughs, and hence variations in scour geometry, but have yet to be researched in any depth. Leclair and

Blom's (2005) analysis of experimental dune forming conditions suggested bed shear stress and vertical grain size sorting as the major controls on the probability distribution of dune-surface elevation (and the structure of the associated deposits). They suggested that under certain sediment transport and grain size conditions, the variability in dune height and trough-scour depth can depend on grain-size sorting. Although they did not investigate direct relationships between scour depth, sediment flux and grain size; given Leclair (2002) association between dune height and trough scour depth, it is inferred that the factors controlling dune-surface elevation will relate to scour depth as scour depth and dune height appear to be mutually dependent. The apparent contradiction with Leclair's (2002) results may relate to the differing time taken to reach bedform equilibrium in flow conditions with differing sediments, rather than differences at steady state relationships.

The relationships between dune elevation, sediment transport and cross-strata suggested in most previous studies were based on experiments with no aggradation (constant mean bed level). In natural rivers, aggradation may occur, as may bed degradation and fluctuations of the mean bed level. Based on a small number of experiments with aggrading sand beds, Leclair (2002) suggested that dune geometry does not vary systematically with aggradation rate. Leclair (2006) however, suggested that the variation of dune trough-scour depth as dunes migrate depends on the dune shapes, flow conditions and sediment transport rate. Although there is not a direct relationship between transport rate and bed aggradation, this suggests that a lot more research is needed to investigate the impact of both on dune and scour geometries.

In Chapters 2 and 3, river character and flow depth estimates are presented based on the architecture of the preserved cross-bedding and published models that enable calculation of dune height and bankfull depth from the preserved cross-strata (Section 2.10.1 and 3.10.1). These models (Leclair and Bridge, 2001; Yalin, 1964; Allen, 1970 and Leeder, 1973) assumed no bed aggradation. Modification of these models may be needed to consider sediment aggradation to improve the accuracy of bedform height and flow depth estimates.

Scour depth in relation to discharge and flow depth

It is widely accepted that mean dune height increases with flow depth (Yalin 1964; Allen 1982; Bridge and Tye 2000, Lunt *et al.*, 2004). This suggests that dunes with greater heights will develop in rivers with greater flow depths. Since scour depth relates to dune height, and dune height relates to flow depth, this infers that variations in dune scour depth also depend on flow depth. This, however, is a rather generalised view and will only be true in steady flow conditions when bedforms and related scour patterns are in equilibrium with the flow.

Gabel's (1993) seminal work (building on Gabel, 1991 and Bridge and Gabel, 1992) on the geometry and kinematics of dunes in the Calamus River, Nebraska, tested models for dune geometry in steady and unsteady flow; and focused on the creation and destruction of dunes describing stages of bedform development. Monitoring the variation in dune height in response to discharge over long periods, indicated that the mean dune height increased significantly more with discharge during high flows compared to low flow stages; and that dunes are smaller during rising discharges and bigger with falling discharges at comparable water depths (bedform hysteresis). This hysteresis is likely to be a result of the bedforms not reaching full equilibrium with the flow and the shorter time scales when discharge is rising (discharge tends to rise faster than it falls). However, Gabel ignored the importance of scouring for bedform development and she did not analyse the deposits. Although Gabel (1993) did not describe scours in dune troughs, Bridge *et al.*'s (1998) ground-penetrating radar data acquired at some of the same Calamus River sites identified erosion surfaces overlain by medium-scale trough-cross-beds. Thus, it is likely that some if not all of the dunes monitored by Gabel (1993) had scours in their troughs. If, as stated by Leclair (2002) scour depth is related to dune height, then it follows that it will also be related to discharge variations. If dune height varies with discharge and scour depth varies with dune height, then scour depth also depends on discharge variations and higher dunes with deeper scours are expected to occur in falling flow stages. Differences in bed scour and bedform height between rising and falling flow stages might be important from an engineering point of view for the management of modern rivers and navigational commerce as well as for palaeoenvironmental reconstructions (interpretation of cross-bed coset patterns).

Given the climatic settings in the study sites (Chapters 2 and 3), the discharge varied and may have varied very rapidly in the arid conditions of the Spanish Triassic. Thus, scour and dune height and hence set size and shape is likely to have varied and this might allow better understanding of the architecture, although adding possible error to estimates of flow depth.

Scour depth, planform and occurrence in relation to morphology of bedform crestline and bedform type

Scour occurrence, location between bedform crests and depth are related to bedform crestline morphology and formative bedform type (Venditti *et al.*, 2005a; Carling *et al.*, 2005). Scours have been reported in troughs of sinuous-crested dunes as “sand-waves”, but not with straight crested bedforms in fluvial and tidal environments (e.g., Parsons *et al.*, 2005; Dalrymple *et al.*, 1978; Elliot and Gardiner, 1981). Curved-crested bedforms influence the lee-side fluid dynamics and may result in the formation of scour in the troughs downstream the dunes lee side (Best, 2005). The changes of crestline morphology as a bedform migrates downstream, influences the dynamics in the flow separation zone beyond the lee side and the morphology of the trough (Venditti *et al.*, 2005a; Best, 2005 and references therein). Carling *et al.* (2005) showed that straight-crested dunes form from initial 3D defects, presenting distinctive lee slopes with no visible bed scour on the lee sides. They observed that as bed shear stress increased, 2D-dunes developed into sinuous long-crested transverse bedforms and then were replaced by lunate dunes or transitional wavy-crested bedforms with scours in their lee. Parsons *et al.* (2005) tracking bedforms in the Paraná River, Argentina, also showed that curved-crested dunes form scour in the troughs. They observed that lee side troughs varied in scour depth parallel to the dune crestlines and this variation correlated to the planform crestline curvature; for instance bedforms with saddle-shaped crestlines appeared to have greater scour depth variability than straighter-crested bedforms. This variation in scour depth with sinuosity of crestline explains some of the scatter around Leclair’s (2002) relationship between dune height and scour depth, and confirms the importance of considering time take to reach equilibrium.

Contrary to the inferences above, that scour occurs in relation to bedform crest curvature, Reesink *et al.* (2014) produced scour within the trough of experimental 2D bar forms with fixed and non-fixed troughs. The depth and length of the scours were

observed to vary with the flow velocity. The scour in the trough of these bars increased in depth and decreased in downstream length with increasing velocity over the crest. This suggests that flow dynamics and variation in the lee of different types of bedform may influence scour occurrence and scour planform variations. Scour patterns in association with bars may be different to those in association with dunes. Flume experiments presented in Chapter 5, on the development of initial 2D single bars in unidirectional flows did not produce scour in the bar lee trough but did form a bottomset within the trough, which agrees with Reesink and Bridge's (2009) flume experiments. This difference between the observations in Chapter 5 and Reesink *et al.* (2014) and others' work on dunes may be because bars are likely to persist for longer in conditions where the bedform is not in equilibrium with the flow, whereas dunes become modified more quickly, approaching equilibrium (cf. Section 4.5, Implications of 2D and 3D bedforms and crestline bedform development on scour occurrence).

Thus scour and bedform type may be related, so that troughs between bedforms are associated with a straight-crested bedform field and deeper scours (with a more 3D shape because of variation across the flow) within troughs are associated with 3D sinuous-crested bedforms. Further investigations of bedform shape and scour occurrence are needed and also investigation in to any difference between bars and dunes to determine if bedform type determines scour occurrence and geometry.

4.5 Scour and erosive surfaces in the field sites: Rillo de Gallo and Seaton Sluice

The geometries of individual scours in relation to the filling cross-bedding and thus the final architecture of the single trough cross-bed sets suggest that scours developed simultaneously as large-scale bedforms migrated downstream. The erosion surface forming the bounding surface of cross bed sets may be the instantaneous shape of one scour, but is more likely to be the result of the scour shape evolution over a period of time when the bedform was migrating. The significant field observations, drawn from the literature, which suggest that scours in the study sites developed simultaneously with bedform migration are: (1) the contact between concave-up erosive surfaces and the over and underlying sediments; (2) cross-bed set thickness; (3) formative bedform

scale estimates; (4) flow pattern; and (5) formative bedform shape and crestline bedform development (2D and 3D bedforms).

Relationships between scours, bedforms and the underlying sediments

Harms and Fahnestock (1965) investigated trough cross-stratification generated by the migration of large-scale bedforms observed via shallow trenches in the bed of the modern Río Grande, Texas, and defined spoon-shaped scours. They suggested that these scours may have been formed before bedform migration and, if so, they were not related to the flow-separation eddy in the lee of dunes. They justified this by suggesting that the variable symmetry of the cross beds filling the troughs indicated that there was no relationship between the location of the scours and the infilling cross beds. However, they did not describe the cross bed symmetry variation that led them to this conclusion. Factors such as discharge and water depth can change the flow dynamics in the lee of a migrating bedform, as can the changing planform shape of migrating dunes, causing variation in the scour and the geometry (e.g., lamina dip magnitude and direction) of the infilling cross beds. Thus, contrary to Harms and Fahnestock's (1965) theory, cross-bed architecture may vary considerably while maintaining an association between the formative bedform, scour and infilling cross-bedding. Surprisingly, little research has been undertaken correlating the three dimensional and time evolution of dunes and bars as they advance over scours that were either formed by the flow structure in the lee of the bedform or preceded it. Computer simulations by Rubin (1987) made a start at visualising this, but because of the lack of knowledge of real behaviours these computer simulations are not very helpful currently. Until very recently research on three dimensional and time evolution of dunes and bars as they advance over scours was difficult or impossible because of the lack of adequate technology, but now it is becoming possible. Further investigation on variation of the internal geometry and symmetry of infilling cross beds is needed and a little of this is reported in the flume experiments in Chapter 5.

Interpretation of features in the sandstones of the two field studies (Chapter 2 and 3) suggest that in these cases scours that formed the bottom bounding surfaces of trough-cross-bed sets were not formed prior to bedform development. In the Seaton Sluice Sandstone (Chapter 3), scour structures include individual and grouped cross-bed sets of fine to coarse sand. Scours crosscut underlying cross-bed sets. Laminae dip magnitude

varies up to 10° within individual scours, and the laminae dip direction does not vary significantly. This is consistent with the sets and scours being of related origin. The cross-bedding geometry and location within each scour structure indicate that each scour is filled by cross-bedding corresponding to a single bedform suggesting the relationship between formative bedform and scour. Thus, as a bedform migrated, scouring occurred downstream of it, and the scour developed in response to bedform evolution and migration. In the Prados Sandstone (Chapter 2), individual scours are frequently filled by individual fine to medium (occasionally coarse) sand grain size cross-bed sets. The scours are also observed in grouped sets stacked vertically in cosets. The infilling cross beds are geometrically similar and the laminae dip magnitude within each scour varies up to 10° . However the laminae dip direction varies considerably in some scour structures. This laminae dip direction variation within individual scours is another indication of the association between scour and formative bedform, and is interpreted as the result of changing flow structure through time as the scour and fill develop and not as a result of antecedent scour formation. These patterns are discussed in Sections 2.9.4 and 3.9.2.

Relationships between scour, cross-bed set thickness and formative bedform magnitude

Allen (1982) described the relationship between dune geometry and associated cross-bedding and Paola-Borgman (1991) presented an empirical quantitative model relating dune geometry to the preserved cross-bedding. Bridge (1997), Bridge and Best (1997) and Leclair and Bridge (2001) improved this model that allowed estimates of the distribution and mean of dune height to be inferred from cross-set thickness independently of aggradation rate (assuming Leclair's, 2002 relationships to apply over the full range of natural conditions). Given Leclair's (2002) relation between dune height and scour depth, and the relationship between cross-bedding thickness and dune height, scour depth can be related to cross-bed set thickness. If these theories that were established on empirical relationships can be widely applied (and this has not yet been proven as very little suitable data are available) then the thickness of preserved cross-bed sets, and scour surface amplitude should scale with the size of the formative bedform.

The maximum and mean dune heights in the rivers that formed the Seaton Sluice and Prados cross-bedded sandstones were estimated (Sections 2.10.1 and 3.10.1) following Leclair and Bridge's (2001) model. From these the mean scour depth associated with the cross-bedding can be estimated. In the Prados Sandstone mean dune height is estimated as 1.23 m; the estimated mean scour depth corresponding to the deepest part of the dune trough is > 0.62 m. In the Seaton Sluice Sandstone, the mean dune height is estimated as 1.88 m and the mean scour depth is > 0.94 m.

The mean dune size of 1.23 m in Prados and 1.88 m in Seaton although large, are comparable to some of the large dunes observed in modern natural rivers (e.g., Rhine River, Germany; Paraná River, Argentina). The estimated mean dune heights and scour depths imply that water depth in Northumberland was greater than in Rillo de Gallo, and the channels in Northumberland consequently much deeper although the preserved thickness of the sandstone bodies is not greatly different. The Northumberland River was deeper, with higher bedforms and some large-scale straight-crested bedforms also occurred. In contrast, only 3-dimensional bedforms of various scales are recorded in the Prados Sandstones. However, given that the Prados river was probably more flashy and had greater variation in sediment load, the interpretation of dune size and scour depth from the cross bedding may be less reliable (see discussion above). The differences in storey thickness in comparison with interpreted water depth may be unreliable and other factors such as preservation of storey thickness (better preservation at Rillo de Gallo) need to be considered. However less bedload in the Northumberland river in comparison to the channel depth can explain the difference in storey thickness in relation to cross-bed set thickness, and the sand-component of any complex bar would not reach the bank top (thus sandstone storeys less thick than channel depth).

Leclair and Bridge (2001) assumed that the distribution of cross-set thickness is due primarily to variations in dune height (and associated trough depth), and that cosets are homogeneous in strata type and grain size, inferring that dunes did not vary significantly in size during formation of a co-set. In most natural rivers, there is likely to be considerable variation in discharge and possibly also grain size at a site over the time it take to build a complex bar (e.g., a point bar) and consequently cosets may be far more variable than suggested by Leclair and Bridge. Thus, although their model is a useful empirical relationship that allows estimates of bedform size and thus water depth

a degree of error must be considered in the final estimate calculations of dune height distribution and scour depths. This is largely because of the limited range of conditions (steady or near steady, mono-modal fine-medium sand in straight reaches of channel) used to establish the relationships.

Scour associated with formative bedform and relation to flow pattern

In most natural rivers, the flow is not steady over long periods. Variations of the flow pattern influence sediment transport, turbulence and therefore the morphology of the migrating bedforms and their dynamics within the channel. Scour geometry, particularly depth and planform also depend on the flow pattern and flow depth as bedforms migrate downstream. This can be illustrated by some of the well-exposed and preserved sedimentary structures in Prados (Appendix A, Plates of scour structures 10 and 19).

The palaeocurrent data from the Prados Formation (all data including individual scour structures data; Chapter 2) has three main primary modes (south, southwest and west) a resulting direction 223° (Fig. 2.5). Data from single trough cross-bed sets have two main modes of laminae dip direction; towards 185° and 294° . In contrast, the Seaton Sluice Sandstone palaeocurrent data has one primary mode towards the west with a resultant direction 274° ; and the palaeocurrent data from individual trough cross-bed sets has one primary mode towards 288° . These record the difference in flow pattern between the two fluvial systems which may have influenced the differences in planform of the scour structures observed in the field sites.

The lamina dip direction from individual scour structures at Seaton Sluice is mono-modal recording one main flow direction, which can be explained by the channel being relatively straight. This explains the straighter planform of the scour structures suggesting less local variations of the flow as bedforms migrated. In contrast, some of the scour structures in the Prados Formation have curved planforms, suggesting that scours developed with the migration bedforms as local flow pattern changed. These curved scour structures may occur in particular locations within the channel that may be more susceptible of flow changes (e.g., river bend). Variations of flow can cause the irregular advance of bedform lee faces resulting in variations of the crestline planforms (Section 4.4) and thus, bedforms may advance at an angle to the main flow direction (Fig. 4.3). Then, the curvature of the scour structures can be explained by the response

of bedforms to channel geometry and flow conditions, which can be oblique to the river trend causing variations between the scour trend and the laminae dip direction (Section 2.9.4). Thus, as flow conditions changed, bedform migration direction changed and so did the scour development pattern (Fig. 4.3). The laminae dip direction varies with the curvature of scours suggesting that scour developed as bedforms, influenced by variations of the flow migrated. Thus, these scours and their corresponding associated curved scour structures are interpreted as signatures of simultaneous development of scour and bedform. This fits within Theory 3 and 4 suggested in Section 4.3.

Although the lamina dip direction of the scour structures in Prados Formation has two modes (towards 185° and 294°), the scour direction single mode trend of 193° , suggests one main flow direction consistent with Mode I (185°) (Section 2.8.3). The divergence of 109° between the two modes of the laminae dip direction in the Prados Formation may be explained by local flow variations in time or space and the simplest explanation is the local geometry of the channel (e.g., an evolving meander, or a bend within a straighter channel) when bedform migration pattern changed as the bend grew (Fig. 2.18). This emphasises the importance of considering both scour geometry and cross bed architecture when interpreting the palaeoenvironment.

The Prados Formation may have been formed by a channel of higher sinuosity than the one that formed the Seaton Sluice Sandstone (or at least near or at a bend in the channel). Alternatively the Prados channel may have been a sand-load-dominated system with large bedforms formed at high stage when there was little variation in flow direction and when the scours formed. Subsequently, as the stage fell there would have been more variation in flow direction (divergence around large bedforms) and this was when some of the scours developed as they were filled resulting in curved-shape scour structures with curved basal surfaces (scours).

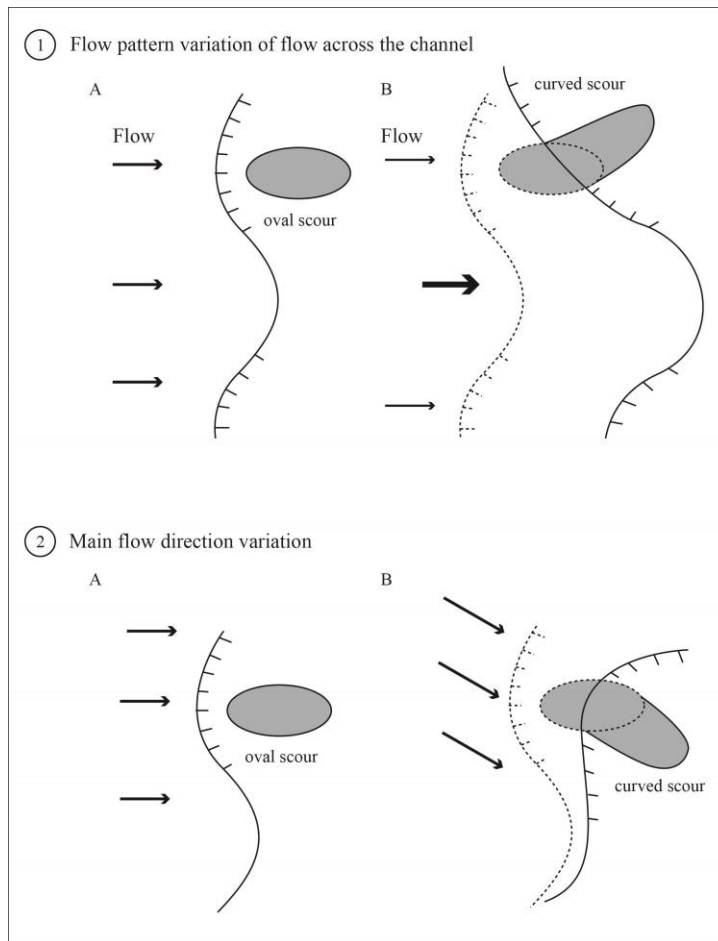


Figure 4.3 Illustration of scour development into curved planform scours due to (1) variation of the flow pattern across the channel causing a variation of the bedform migration pattern; and (2) variation of the dominant flow direction downstream, also resulting in variations of bedform migration pattern.

In the classification of scour structures on the basis of their width:length ratio in Sections 2.7.1, 2.7.2, and 3.7.1 (Table 2.2 and 3.2) there are two main shape types; circular and elongate. In the Prados Formation both elongate and near circular-shaped scours filled with cross-bedding were observed in close proximity at the same stratigraphic level. This might infer local variations of flow pattern (possibly discharge variation), which resulted in variation in bedform longevity and bedform equilibrium during migration. In the Seaton Sluice Formation all the scour structures were observed within the same stratigraphic unit. The majority of these scours vary from near circular to oval shapes (although there are a few scours with elongate shape). This suggests less variation in flow pattern within the same stratigraphic unit compared to the Prados Sandstone and limiting factors for individual scour longevity. This may suggest that individual scours ceased forming quicker at Seaton Sluice than at Rillo de Gallo. This

might be explained by a faster decrease in bedform height at Seaton Sluice (Section 4.4, scour depth in relation to bedform height). This demonstrates the need for more research on the evolution of scours over time in relation to migrating bedforms in varying fluvial conditions.

Implications of 2D and 3D bedforms and crestline bedform development on scour occurrence

Venditti *et al.* (2005a) suggested that incipient scour pits form when straight-crested bedforms are modified and evolve into more sinuous-crested bedforms. They described the growth of crestline lobes, as a mechanism that triggers the transition between 2D and 3D bedforms and the initiation of trough-scouring in bedform lee due to the irregularities of the crestline morphology localising eddies within the lee (cf. Section 1.2, Fig. 1.4). The basal erosive surface of individual trough-cross-bed sets described in Chapters 2 and 3 (Appendix A and B – scour structures plates), are interpreted as caused by scours evolving in associated with the formative bedform.

One big difference between the two field studies (Chapter 2 and 3) is that planar cross-bedding occurs in the sandstone at Seaton Sluice but not in the sandstone at Rillo de Gallo (Fig. 4.4). The majority of the bedforms that generated the deposits seen in the Prados Formation were sinuous-crested or isolated (linguoid or lunate) crested dunes or possibly unit bars with curved crests, which formed cross-bed sets with trough-shaped lower boundaries. Some of the bedforms that generated the Seaton Sluice Sandstone were straight-crested dunes or unit bars with nearly straight flow-reattachment lines, which generated planar surfaces of erosion as they advanced downstream forming cross-bed sets separated by planar bounding surfaces (Section 3.6.1, Fig. 3.12). The tabular character of cross-bed sets at Seaton Sluice is interpreted as formed by the migration of straight-crested large-scale bedforms (e.g., bars, dunes) resulting in steep and planar configuration of the cross-strata. Similar bedforms did not occur in Rillo de Gallo or aggradation, truncation and burial patterns did not preserve them (i.e., similar bedforms occurred but their resulting deposits were not preserved).

In both field sites, the scour structures identified (Appendix A and B, Plates) are the result of sinuous-crested dunes. Following previous published work on scour associated with crestline morphology (e.g., Venditti *et al.*, 2005a; Carling *et al.*, 2005; Parsons *et*

al., 2005 and others), herein it is interpreted that the erosive basal surfaces of the scour structures observed in both field sites are associated to their corresponding formative bedforms during migration and so to the resulting cross-bedding styles. Although there are numerous published studies that support this interpretation, further work is required to clarify if bedform type also controls the development of scour within the erodible trough downstream the bedforms.

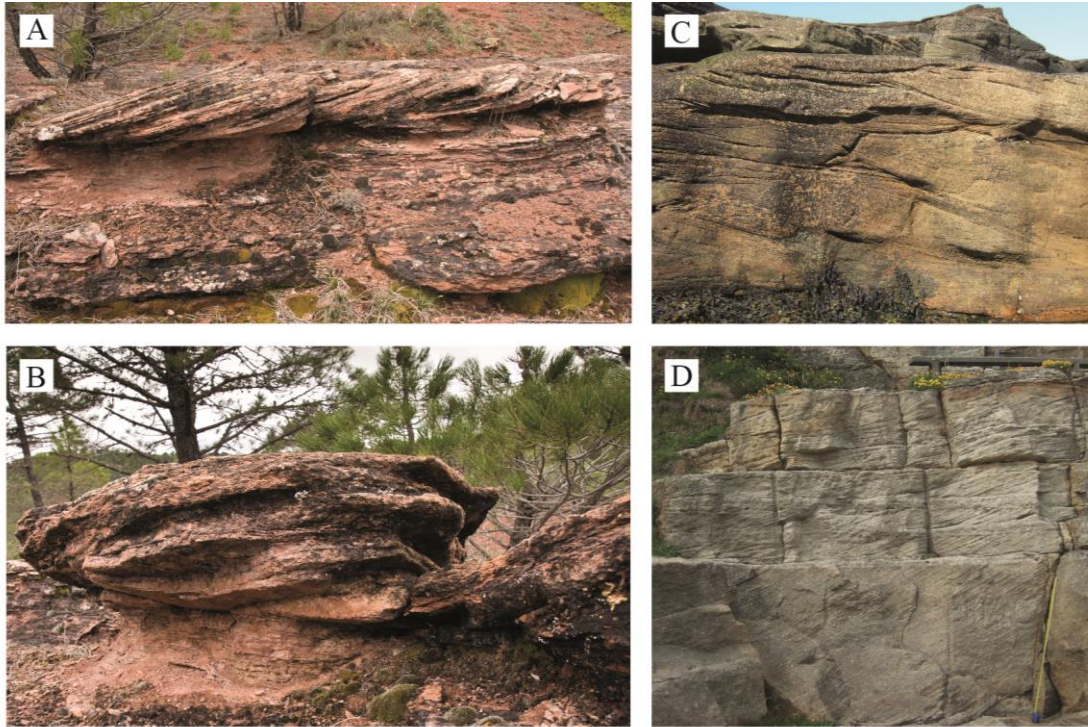


Figure 4.4 Cross-bedding styles and basal erosive surfaces types observed in field case studies. In Prados, (A) single trough cross-bed set associated to spoon-shaped basal surface observed in flow parallel section; (B) detail of the basal erosive surface with spoon shaped of scour structure shown in A. At Seaton Sluice, (C) Trough-shaped scours filled with cross-bedding formed by migration of curved-crested bedforms; (D) Planar cross-bedding and basal bounding surfaces formed by the migration of straight-crested bedforms.

Reesink *et al.* (2014) observed the evolution of straight-crested bars over mobile and fixed topographies in a flume. They observed scour in the lower part of the trough downstream of a 2D bar. Section 4.4 and references cited therein and above suggested that scour occurs in the trough downstream of 3D dunes. Chapter 5 reports on a series of flumes experiments investigating the development of single bars as they migrated downstream. In each flume run, the bar was straight-crested and crestline morphologies changed with time, becoming more sinuous. In these experiments scouring within the bar trough did not occur, whereas sediment deposition and sediment feedback within the

bar trough were clearly identified in all the runs forming bottomsets up to 0.08 m thick (Section 5.4.4, Fig. 5.26). This may have been due to the initial flume configuration. Thus, there is not enough evidence to clarify if scouring in bar troughs is a function of the bar crest shape or the longevity of the bars before their shape is modified. These experiments do not contradict those of Reesink *et al.*, (2014) because the flume conditions were different, but do suggest that further thoughts and comparison with other experiments are needed to determine if bedform crestline morphology controls scour formation for a particular type of bedforms (dunes) under certain flow conditions or for all types of bedforms in all conditions.

4.6 Other scour features

Other types of scour observed in rivers are described below to differentiate them from those associated with bedforms. These features are associated with factors such as bed topography, flow regime, channel behaviour and the presence of natural or artificial obstacles on the river bed.

4.6.1 Pre-existing erosive surfaces on the channel bed

The scour structures associated with single trough cross-bed sets described in Chapter 2 and 3 are interpreted to have resulted from scour and related bedform migration. To understand the genesis of the erosion surfaces observed as basal surfaces of single trough cross-bed sets (i.e., scour structures), it is important to establish if these scours could be interpreted as pre-existing erosive surfaces formed due to prior incision for example relating to chute channels, stream confluences; hydraulic jumps, obstacles on the bed. This section discusses situations where bedforms migrate over pre-generated spoon-shaped scours; and highlight some of the characteristics that may allow such antecedent scours to be differentiated from scours associated with bedforms.

Chute channels

A chute channel is a relatively small channel (compared to the main channel) that forms a short cut, for example cutting into the top of a meander. It can result in an erosion surface into complex bar deposits that will be overlain by other channel deposits and may appear as a bounding surface within a sandstone body. Chute channels typically form in favour of low areas adjacent to inner convex banks or between older bar forms

within point and braided bars (Bridge, 2003). They connect the two closest parts of a river bend causing the abandonment of that curved bend (i.e., chute cut-off) and continue straight downstream. The development of a chute channel at a meander bend requires mechanisms with an increase in stream power or shear stress to force flow over a developing point bar, or over-bank across a meander bend, with subsequent scour and incision (Johnson and Paynter, 1967; Peakall *et al.*, 2007; Grenfell *et al.*, 2012). These erosion surfaces may be recognisable if their lateral extent can be identified (greater extent than expected from bedform associated scour) and if a difference in palaeocurrent direction is evident above and below the surface.

Scours associated with stream confluences

Bed morphology at stream confluences is characterised by avalanching faces at the mouth of the confluent channels, a confluence scour into which avalanche faces dip, and a bar downstream of the scour. The main controls on this bed configuration are the junction angle and the discharge ratio between the two channels (Best, 1986, 1987, 1988). Best's (1988) flume experiments suggested that scour depth increased systematically with junction angle, and that scour is absent at angles of $<15^\circ$. In addition, scour longer axis becomes more parallel to the confluence stream as the channel discharge ratio increases. Best (1988) suggested that tributary and main channel bedload transport in relation to their flow patterns and the channel discharge ratio significantly influence the bed morphology in the confluence area.

The sediment segregation from two channels and transport through and around the confluence scours favour the formation of bars downstream of the scour. Ashworth (1996) observed that bars form immediately downstream of confluence-scour zone (Fig. 4.5), but he did not describe sediment transport and deposition within the confluence scour. Upstream of these scours avalanche faces have been observed dipping into the scours. These have been referred to informally as chute bars in some settings but have not been fully described or formally defined. Best (1988) suggested that when junction angles and channel discharge ratios are higher and large confluence scours form, large avalanche slopes can migrate into the scour to fill it, forming very large single cross-bed set with a basal scour surface that may be of a scale with the channel depth and oversized compared to other cross bed sets in the channel deposits (Fig. 4.5D).

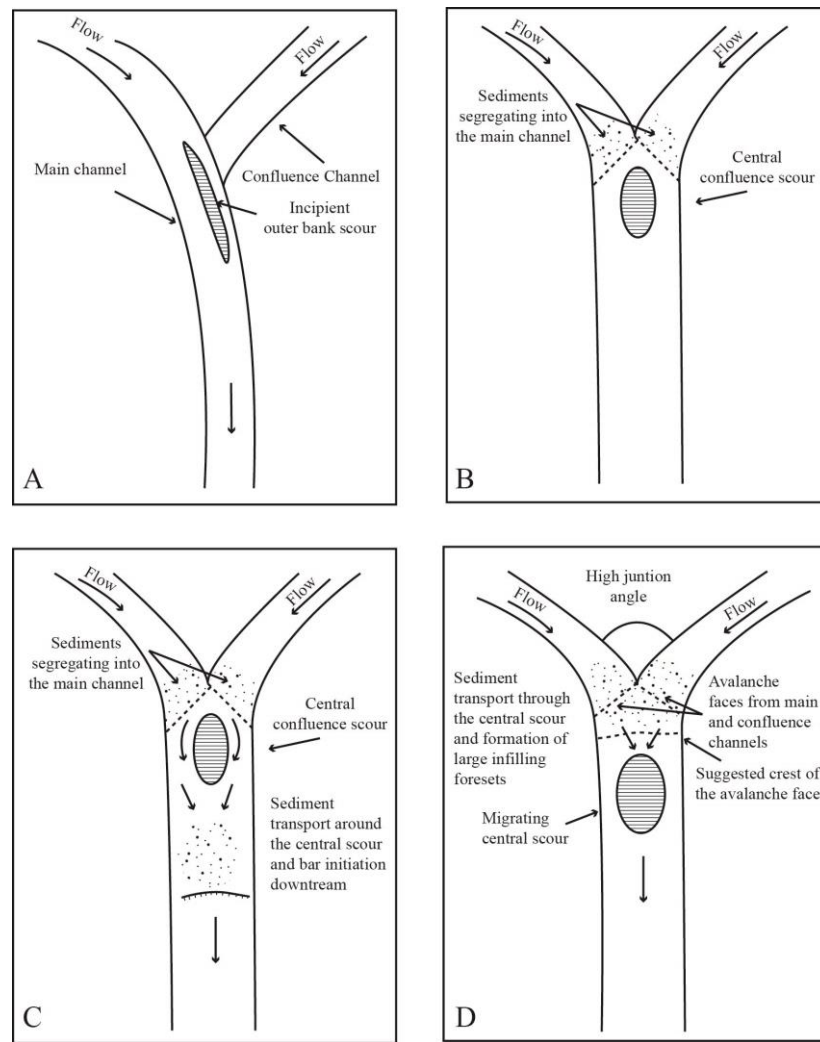


Figure 4.5 Model of mid-channel bar growth downstream of a confluence scour (modified from Ashworth, 1996). (A) Initiation of the junction of main and confluence channels with the development of an incipient outer bank scour; (B) Development of a central confluence scour in the mouth of the stream junction; (C) Segregation of sediment bedload from main and confluence channels, and sediment transport around the confluence scour resulting in deposition of coarse sediments and initiation of a bar migrating downstream the confluence scour; and (D) Higher values of junction angle and channel discharge ratio resulting in the development of large central confluence scour and sediment avalanching into the migration scour forming large-scale steep foresets.

The concave-up erosive surfaces formed by confluence scour are expected to be much larger features than the concave-up basal surfaces of the individual trough cross-bed sets (i.e., scour structures) related to dune or unit bar immigration as observed in the two field case studies. Scaling plays an important role for the bedform and scour geometry relationship (Leclair, 2002), and so it can be used as an indicator to differentiate between scours related to dunes and unit bars (Section 4.3) and those related to confluence .

Scoured surfaces associated with supercritical flow

Scours formed prior to bedform migration can be generated by other processes due to flow pattern variations. The development of a hydraulic jump within a channel can generate concave-up scour bases. Jopling and Richardson (1966), Alexander *et al.* (2001), Fielding (2006) and Duller *et al.* (2008) identified elongate, spoon-shaped scours filled by massive, diffusely banded or laminated sediment resulting from this. Occasionally, these trough-shaped bases can be filled by dip downstream laminae and laminae nearly parallel to the basal erosional surface (Alexander *et al.*, 2001 and reference therein) however their character and distribution is likely to make them easily distinguishable from scour structures associated with dunes or unit bars because of the difference in sediment characteristics. Internal sedimentary structures typical of supercritical flows (e.g., undulated lamination, upstream dipping laminae and massive sand) are expected overlying and possibly underlying these surfaces.

In some settings it is possible to envisage that concave-up erosive surfaces formed by supercritical flow could be overlain by downstream-dipping cross-bedding, which could be misinterpreted as cross-bedding resulted from the migration of subcritical bedforms (e.g., dunes). Cartigny *et al.* (2014) observed in flume experiments that chute-and-pool deposits under low aggradation rates may appear like trough cross-bedding. However chute-and-pool structures are unlikely to be preserved in many natural settings where aggradation rate is low as any change in flow conditions is likely to re-work the structures just formed. However it is worth bearing in mind this possibility when examining cross-bedded sandstone. Further investigation is needed to clarify the conditions under which different scour patterns can be preserved and characteristics that may differentiate of scour genesis and its relationship with the formative bedform.

4.6.2 Scouring due to obstacle on the river bed

Obstacles (e.g., cobbles, pebbles, plants, dead wood, pipelines, and bridge piers) on the bed of a river cause flow deflection and flow separation which cause areas of scour due to local areas high-bed shear stress. The remobilized sediment is often deposited in the vicinity of the obstacle. The resulting sedimentary configurations formed by the interaction between sediment particles and flow and the deformation of flow induced by obstacles are known as obstacle marks (Dzulynski and Walton, 1965; Karcz, 1968). Allen (1982) described and classified obstacle marks under unidirectional and

oscillatory flows. He described obstacle marks typical of unidirectional flows previously named as “*current crescents*” to “*U-shape furrows*” by Peabody (1947). These consist of a scour hole upstream of the obstacle with scoured “arms” that develop downstream to the sides of the obstacle and with one or more flow-aligned sediment ridges directly downstream of the obstacle. This pattern is related to the turbulent horseshoe vortex system formed around the obstacle.

Karcz (1968) showed that the obstruction size and shape, flow depth, flow velocity, grain size and the spacing between obstacles (i.e., when there are several boulders located on the channel bed more or less aligned downstream) control the scour development and scour geometry. There is a large body of published work on obstacle marks and scouring near obstacles; however there is not a lot on the cross-bedding development within these pre-existing scours. What little there is (e.g., Fielding *et al.*, 1999; Nakayama *et al.*, 2002 and Jan Alexander, personal communication), indicates that changes in flow or sediment flux result in a change in scour geometry (e.g., during the falling stage of a flood in the Burdekin River, Queensland, scours formed around trees growing on the river bed, became filled by sediment as an advancing avalanche face into the horse-shoe shaped scour).

Bedforms upstream of the scour migrating downstream may subsequently fill or partly fill the scour forming an erosional based cross-bed set. The suggested scour genesis theories (1, 2 and 3) suggested in Section 4.3 could also occur due to the presence of this type of scours, which may or may not become related to the migrating bedforms. Further work for clarification of the development of these pre-existing scours in relation with the development of bedforms upstream the scours are needed. It may be possible to distinguish obstacle marks (and resulting scour-based cross bedding) from dune and bar associated scour structures by the lamination pattern, identification of the associated obstacle. Literature review on flow around obstacles and subsequent bedform development highlights two main points: (1) the importance of the presence of natural or man-made obstacles in a river system for the mechanism of scouring, initiation and development of bedforms; and (2) the significant gap in the literature on investigation of mechanisms of scour development, scour filling and fill architecture.

4.7 Conclusions

- Although there has been a lot of research on bedforms and cross bedding, there is little published on the character of erosion surfaces bounding cross bed sets and scour associated with dunes and unit bars.
- The erosional basal bounding surface of an individual set of trough cross bedding may have formed (1) before, and be unrelated to, the bedform migrated into it to fill it, (2) before the bedform but becoming modified by the flow in the lee of the bedform as it migrated to fill the scour and becoming associated with the migrating bedform, or (3) formed because of the flow pattern generated in the lee of the bedform, evolving and filling as the bedform migrated (i.e., scour development in association with the bedform). In this later case, the geometries of the scours (or the erosion surface resulting from the evolution of the scour over time) in relation to the filling cross-bedding and thus the final architecture of the single trough cross-bed set may be used to suggest that scour and bedform developed simultaneously during bedform migration.
- Scour development in association with bedforms can be related to: (1) bedform height; (2) water depth in relation to the bedform height (controlling flow separation patterns and thus bed shear stresses); (3) bedform crestline morphology (both curvature and height variation along the crest; (4) grain size distribution and sediment type; (5) bedload and suspended sediment flux; and (6) bedform migration pattern.
- Very few of the relationships between scour geometry and the controlling factors have been investigated in much detail, and very little research on the relationship between scour geometry, bedform character and cross-bed architecture has been investigated. Those few that have been studied (e.g., the relationship between scour depth and bedform height) are not known for a wider range of natural conditions and should be applied with care.
- Basal bounding surface of trough cross-bed units that were formed from concave-up scours in association with bedforms may be differentiated from similar structures resulting from cross bed filling pre-existing or contemporary but unrelated scours by the scale in relation to cross bedding and interpreted channel size, and the geometry and characteristics of the scour fill, evidence of obstacles (e.g., boulders or logs).

- Concave-up basal bounding surfaces of single trough cross-bed sets (i.e., scour structures) described in the Prados Formation (Chapter 2) and the Seaton Sluice Sandstone (Chapter 3) are interpreted as scours associated with the bedforms that formed the cross-bed set that fills them. This conclusion is drawn from: (1) architecture of infilling cross-bedding and basal contact with the underlying sediments; (2) the cross-bed set thickness and scour amplitude compared to the scale of the bedforms likely to occur in the interpreted depositional environment; (3) dimensions of formative bedforms and infilling cross-bedding overlying the concave-up scours agree; and (3) scour planform shape and curvature in agreement with anticipated flow and bedform migration patterns.
- In the Prados Sandstone, curved scour structures were recorded with planform curvature consistent with the variations of the dip direction of the infilling lamina, suggesting that scour and bedform developed simultaneously as the flow pattern and bedform migration direction changed.
- Scour planform shape is related to scour longevity. In the Prados Sandstone, elongate and near circular-shaped scours were observed in close proximity within same stratigraphic levels. Elongate scour structures were rarely observed in the Northumberland case study. This suggests a different pattern of scour longevity in relation to bedform migration at the two sites. It is not known what controls the longevity of individual scours during bedform migration.
- Estimates of mean and maximum scour depths at Prados based on established relationships (Leclair and Bridge, 2001) > 0.62 and 0.94 m respectively. In the Seaton Sluice Sandstone the estimated mean and maximum scour depths are > 1.89 and 2.03 m respectively.

4.8 Suggested further work

It is very evident that more research is needed to understand on scour associated with bedforms and the formation of basal boundaries of cross-bed sets. Monitoring the development of bedforms and associated scours on modern river bed and with analysis of resulting sedimentary structures would be most useful, but this is still technically challenging and likely to be both time consuming and expensive. Large flume experiments with configurations appropriate to different natural river settings would also help. There is a need to better understand the development of bedforms in relation

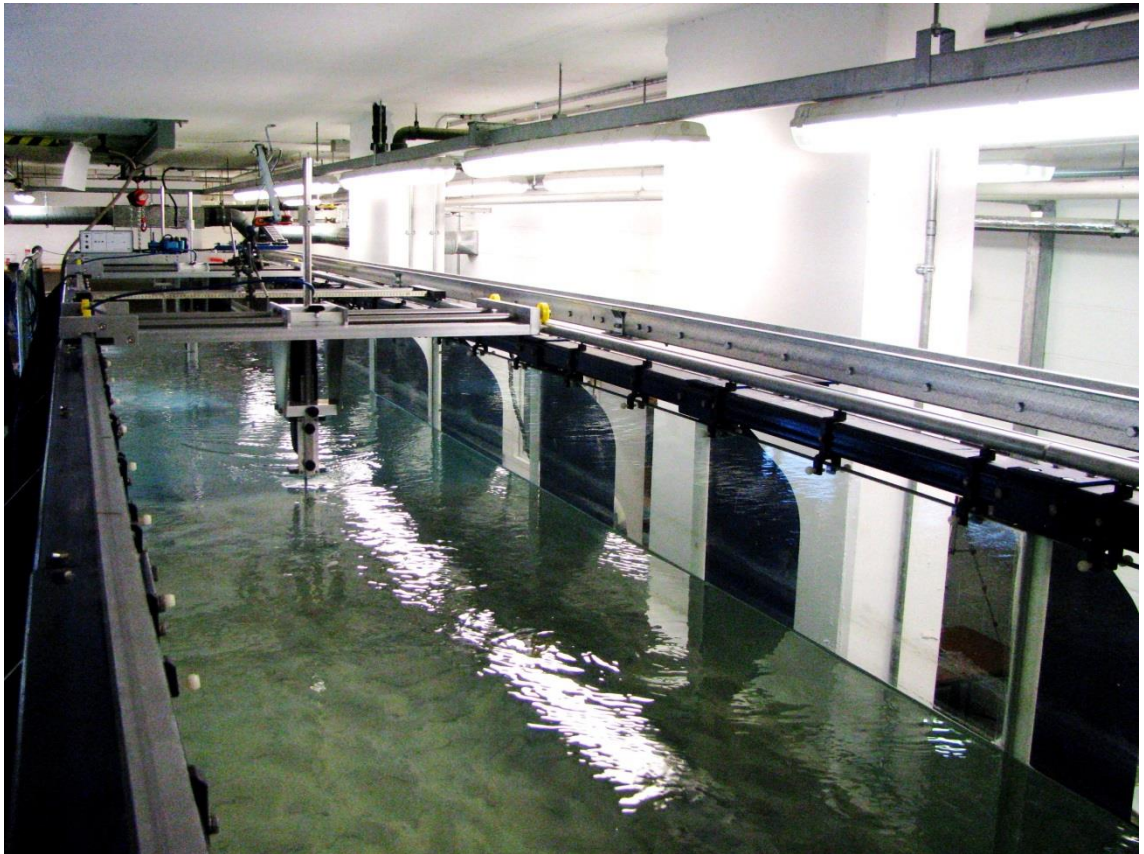
to scour initiation, with the ultimate aim of improving the understanding of bedforms dynamics in river systems. It would be good if research could focus on the following:

- Tracking scour initiation and development in relation with bedform character and migration on modern river beds, investigating the implications of flow pattern variations and bedform development in a range of different locations (e.g., in straight reaches, at bends, at confluences, near lateral bars) within channels would improve the understanding on scour influence on bedform development and resulting fluvial architecture.
- Although an association between dune height and scour depth has been suggested (Leclair and Bridge, 2001; Leclair, 2002), this is based on a very limited range of bedform conditions and should be investigated over a much wider range if they are to be reliably applied to interpret cross-bedding in the rock record..
- The influence of discharge variation on scour depth (cf. Gabel, 1993) needs further investigation in different settings to understand the implication for interpretation of individual cross-bed sets and also cosets that be used to interpret discharge variability.
- Bedform superimposition influences bedform height (cf. Sections 5.3.4), hence it is likely to influence scour depth, but this has not been investigated yet. Flume experiments are needed to test how bedform superimposition affects scour development and if it is a determining control on scour geometry.
- There is some suggestion that the scour associated with dunes and unit bars may, although resulting from similar mechanisms, form different patterns of scours structures and fill architecture (e.g., Reesink *et al.*, 2014 suggesting scour may occur downstream of straight crested unit bars, but this has not been observed with straight crested dunes); and because unit bars can persist longer out of equilibrium with the flow conditions, this needs research to establish if the relationships are real and to see if they can be usefully used to differentiate dunes and unit bars in the rock record; and to determine if type of formative bedform (dune or bar) is a determining control for the formation of scours.

Chapter 5

Flume Experiments

“Cross-stratification formed by downstream movement of steep-lee-face unit bars”



5.1 Introduction

Cross-stratification is common in sandstones and used for the interpretation of depositional environments. Analysis of cross-stratification may be used to infer palaeo-flow direction, velocity and its character during the deposition of sediments. Because of its inherent heterogeneity, cross-stratification also controls the flow of fluid through the rocks and consequently is of some importance to hydrocarbon and water production.

There is considerable confusion in the literature on bedform nomenclature and classification and on the definition of resulting cross-stratification. Unit bars are large bedforms and these “mesoforms” (cf. Jackson 1975) are “*quasi-periodic or solitary storage bodies that occur in the channel (scaled to depth)*” (Smith 1974). Ashley (1990) stated that they “*have simple depositional histories controlled by "local" hydraulic conditions such as changes in water depth and flow competence*”. They include forms that have variously been called: longitudinal bars, tributary bars, scroll bars, chute bars, lobes, and sediment bores (Smith 1974; Hein and Walker 1977; Cant and Walker 1978; Needham and Hey 1991). Bridge (1997) considers that unit bars are ubiquitous in fluvial systems and are generally under studied. The morphology and variability of large-scale bedforms of this type are related to flow strength; mean flow velocity and shear stress (Yalin 1964; Raudkivi 1966; Southard 1971). Needham and Hey (1991), using a flume experiment, developed a general shallow water theory to describe the propagation of sediment bores (their term for a type of unit bar) down a straight channel. They postulated that in natural environments these sediment bores are generated by achieving an initial equilibrium water flow and sediment flux (with a steady sediment supply for the system to reach equilibrium) then, more than doubling the sediment supply rate to initiate the sediment bore. Once formed, the sediment bore slowly advances downstream. These bedforms generally have a gentle stoss side and a steep lee side and smaller bedforms may be superimposed on them (Fig. 5.1A).

In settings where the lee face of unit bars is steep, the cross-stratification that is produced by the migration of the bar has many similarities to that produced by dunes or megaripples (cf. Allen, 1963a; Bridge 1997) and it is likely that this type of cross-bedding is often misinterpreted as originating from dune migration. Cross-stratification

produced by the growth and migration of steep lee-face unit bars was first described by Allen (1963a) and is likely to be common in ancient fluvial deposits.

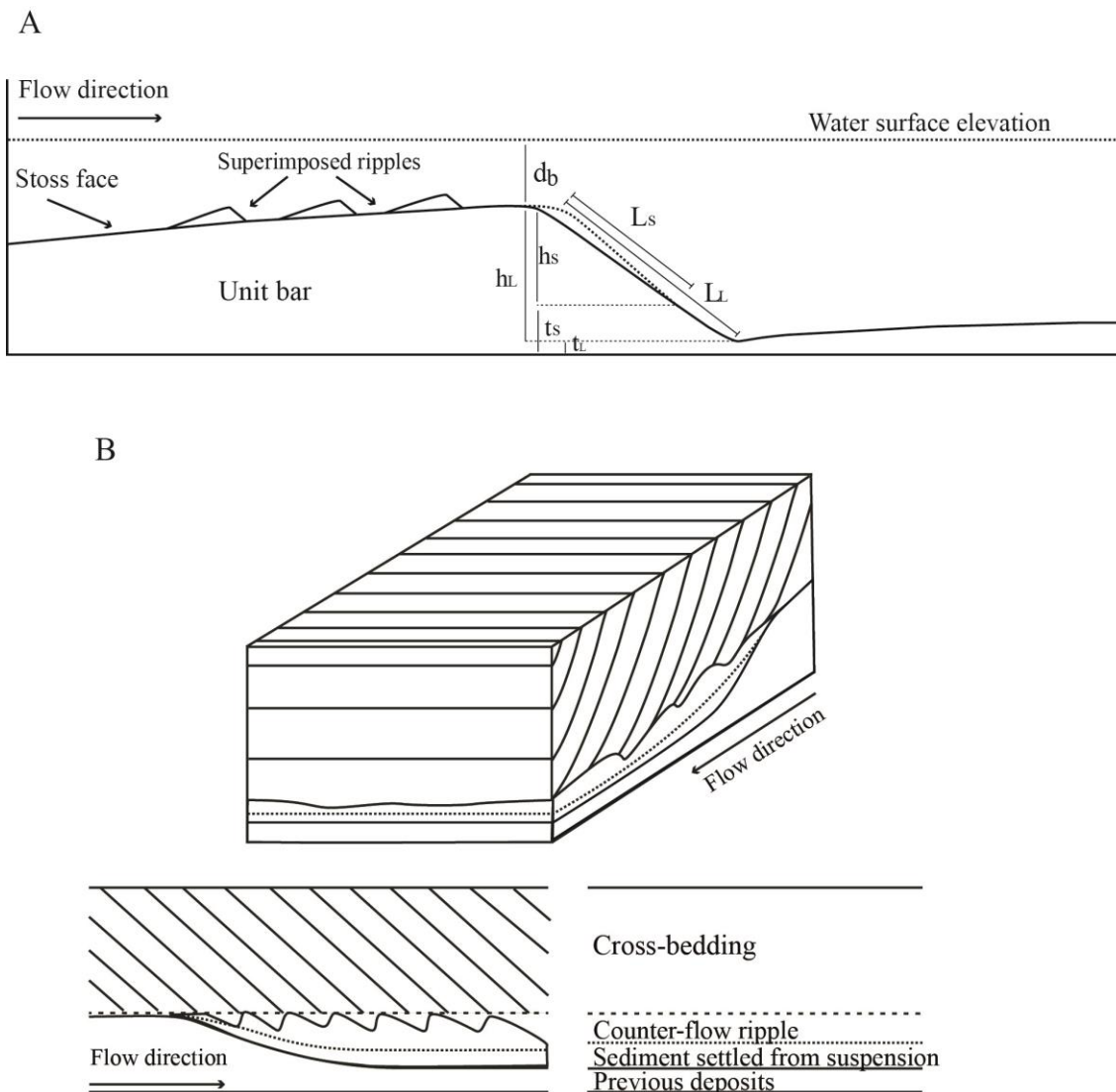


Figure 5.1 (A) Descriptive diagram of a unit bar and variables measured during the experiment; where L_S is the slip-face length; L_L is the lee-face length; d_b is the water depth above the unit-bar brink point; h_S is the slip-face height (vertical distance from brink to slip-face toe); h_L is the lee-face height (vertical distance from brink to toe of the lee face); t_s is the height of the slip-face toe and t_L is the height of the lee-face toe; (B) Definition diagram for unit bars and cross stratification based initially on Allen's (1963a) classification.

The cross-stratification created by dune and unit-bar formation and migration and by other mechanisms were systematically described and classified by Allen (1963a) partly following the classification of McKee and Weir (1953). Herein, Allen's (1963a) nomenclature is followed with some modifications resulting from the observations of the flume experiments described (Table 5.1).

Allen's (1963a) Cross-stratified Unit Classification																	
											Martinez de Alvaro additional types						
Types	Alpha	Beta	Gamma	Epsilon	Zeta	Eta	Theta	Iota	Kappa	Lambda	Mu	Nu	Xi	Omikron	Pi	Rho	Sigma
Allen's Criteria																	
Grouping																	
Solitary	x	x	x	x	x	x	x	x									x
Grouped									x	x	x	x	x	x	x		x
Physical size																	
Small									x	x	x	x					
Large	x	x	x	x	x	x	x	x					x	x	x		x
Erosional	x	x	x	x	x	x	x	x						x	x		x
Non-erosional	x																x
boundary surface																	
Gradational									x	x							
Irregular																	x
Planar	x	x		x							x	x	x	x	x		x
Cylindrical																	
Scoop-shaped																	x
Trough-shaped																	x
Other																	x
Angular contact between cross-strata and lower surface																	
Concordant																	x
Discordant	x	x	x	x	x	x	x	x	x	x	x	x	x	x	x		x
Homogeneous	x	x	x														x
Heterogeneous																	-

Table 5.1 Classification of cross-bedding following Allen (1963a) with additions inspired by the experiments described in this chapter.

Allen (1963a) classified cross-stratification units based on six objective criteria: (1) type of grouping of the set of cross-strata, (2) the thickness of sets within a coset, (3) the character of the lower bounding surface of the set of cross-strata or the lower bounding surfaces in a coset, (4) the shape of the lower bounding surface of the set or the lower bounding surfaces in a coset, (5) the angular contact of the cross-strata to the lower bounding surface of the set or coset and (6) the level of lithological uniformity of the cross-strata in the set or coset. Allen (1963a) distinguished fifteen types of cross-stratification named alpha to pi in the Greek alphabet. The cross-stratified sets produced in the flume experiments described herein do not fit perfectly into any of Allen's fifteen classes and two new classes are proposed; *rho* and *sigma* (Table 5.1).

There are numerous variables that control internal architecture and geometry of unit bars including: mean flow velocity, steadiness, duration, water depth relative to bar height, bed topography, sediment supply and supply variability, grain size and sorting, grain composition and sorting, grain shape and sorting, superimposed bedforms and interactions between successive unit bars. In addition, the preserved cross-stratification depends on processes that subsequently truncate, deform and bury the cross-strata. Reesink and Bridge (2007) considered that the major controls on the architecture of unit-bar cross-stratification are superimposed bedforms, flow unsteadiness and grain sorting mechanisms in addition to the size and shape of the unit bar, and the processes occurring on it during the bar migration. Reesink & Bridge (2007, 2009) used flume experiments to suggest that flow unsteadiness causes changes in the grain size sorting of transported sediment and the migration trends of the superimposed bedforms. Together, these control variations in the sorting patterns and geometries of the resulting cross strata. They considered that superimposed bedforms are a major control on cross-bed architecture when their height exceeds 25% of the host bedform height; at this size the inclination of the unit-bar lee face is slightly reduced. They observed that superimposed bedforms travel faster than the host unit bar and therefore overtake it.

This study aimed to investigate the control of bed topography on the architecture of cross-stratification formed by the migration of steep lee-face unit bars. This chapter concerns the importance of the geometry of scours (troughs) downstream of bars, into which those bars prograde and how the bed topography changes and interacts with the bar. This chapter is based on four long experimental runs (a total of 142 hours and 56

minutes) in which unit bars migrated down a test channel. In these experiments, the topography onto which the bar advanced was flat in the deepest part of the trough with an upstream-sloping distal end rising to a flat bed. Observations are also presented on the evolution of superimposed bedforms and the feedback with the bed, including formation and migration of counter-flow ripples that led to modification of the original topography over which the unit bar migrated.

5.1.1 Terminology

Previous literature highlights as main elements in the morphology of a bedform: stoss face, lee-face bedform height and bedform length. Throughout numerous studies based on flume experiments there are subtle differences between the terminology used for bedform morphology, which appears to be omitted or simply overlooked. Herein, an improved terminology is suggested to distinguish different parts of the unit bar and different stages in its growth as it advances downstream (Fig. 5.1).

In this chapter, the evolution of an artificial unit bar as it advances downstream has been observed and described; and therefore, the terminology used varies slightly throughout the chapter to make a clear distinction between the terms “*slip*” and “*lee*” and all the terminology that derives from these two terms (cf. Section 5.3 and Figs. 5.7-5.10).

5.1.2 Introduction to the flume experiment with a solitary flume-scale unit bar

The methodology used in the four flume runs was similar in many respects to that of Reesink & Bridge (2007; 2009), however, the UEA flume is larger, the sand grain size different and the duration of the experiments considerably longer. The UEA flume has a glass-sided test channel that is 10 m long, 1 m wide and 1 m deep. It recirculates water and sediment continuously around a closed loop of pipes and pumps with no settling tank (Fig. 5.2). The sediment used has a median diameter of 0.24 mm, is well-sorted and quartz-rich. Run 1 lasted 15 hours, Run 2 and 3 were both 24 hours long and Run 4 lasted a total of 79 hours and 56 minutes (Table 5.2). Because of the long duration of these runs, time after the start of the run, t , is given herein as hours:minutes:seconds. Runs 1-3 used the same initial experiment set-up and similar flow conditions, Run 4 differed in both initial conditions and run conditions. In all runs the flume channel was horizontal. The starting topography for all the runs consisted of a unit bar upstream of a flat-floored depression extending across the full flume width. This trough consists of a

downstream dipping slope, a flatter deeper part and an upstream dipping slope rising to the shallower flatter sand bed with a thickness average of 0.15 m in Runs 1-3 and 0.12 m in Run 4 (Fig. 5.3; Table 5.2). In Runs 1-3 the sediment bed was prepared by mounding a large amount of sand at the upstream end of the channel, upstream of the observation window. The sand mound was manually sculptured into a shape close to a natural unit bar and was quickly modified by the initial water flow to form a large-scale bedform with characteristic gentle stoss and steep lee face. This setup is similar to that of Reesink and Bridge (2007, 2009) and was used initially in an attempt to reproduce their results, so that the differences caused by bed topography could be assessed.

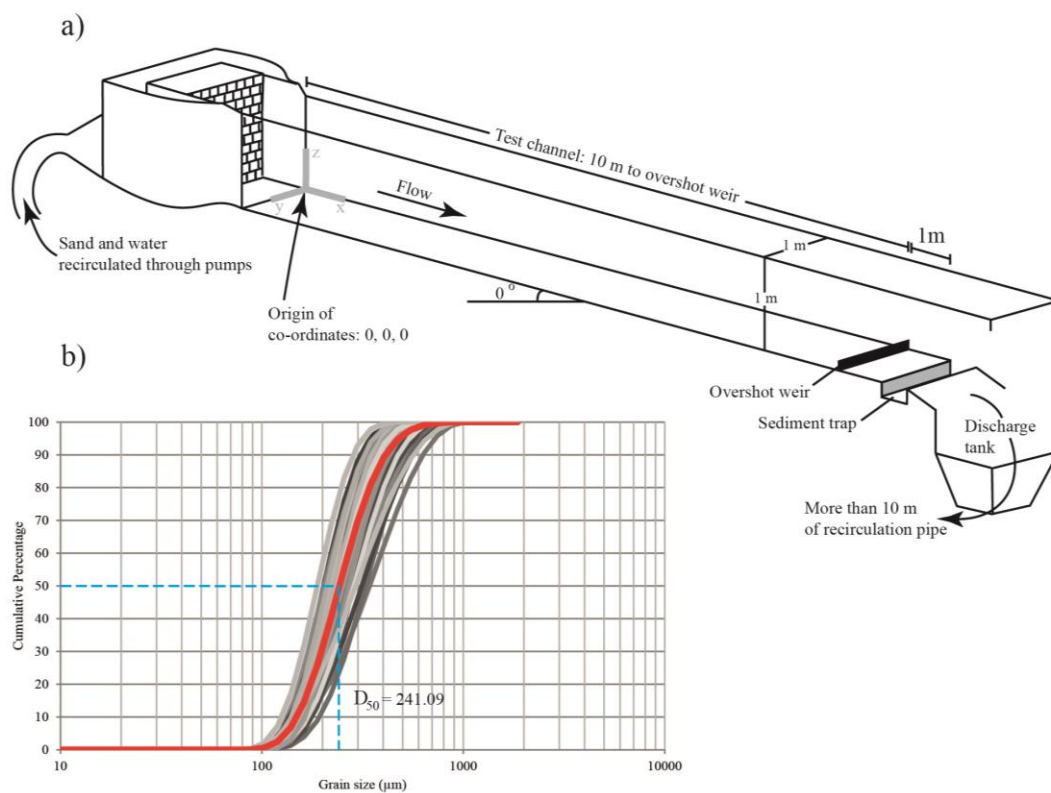


Figure 5.2 (a) Descriptive diagram of flume tank not drawn to scale. (b) Grain size distributions of sediment used in the flume.

In Run 4, the procedure was modified; a unit bar was formed in the middle section of the channel, to allow the flow in the channel to develop a more natural velocity pattern approaching the crest of the bar (nearer to a hyperbolic velocity profile) and so that the development and migration of small bedforms superimposed on the stoss side of the unit bar could be observed directly (Fig. 5.3D).

High-resolution acoustic Doppler velocimeters (Vectrino) were used to measure 3D flow velocity, recording 10 samples per second. The echo sounder measured the distance to the bed with sub millimetre accuracy. Three velocimeter probes were used in Runs 1, 2 and 3, initially at fixed positions (Fig. 5.3).

Table 5.2 Experimental conditions in Runs 1 – 4.

Run Number	1	2	3	4
Total duration each run (hours:minutes)	15:00	24:00	24:00	79:56
Mean discharge measured within the recirculating pipes Q ($\text{m}^3 \text{s}^{-1}$)	92.2×10^{-3}	90.0×10^{-3}	87.9×10^{-3}	122×10^{-3}
Mean water depth above the brink point d_b (m)	0.201	0.265	0.266	0.379
Mean velocity at the bar crest* (m s^{-1})	0.459	0.340	0.330	0.322
Static water depth above solid channel base at $t = 00:00:00$ (m)	n/a	n/a	n/a	n/a
Mean flow depth above solid channel base, d (m)	0.50	0.49	0.49	0.69
Reynolds Number	92200	90000	87900	122000
Mean bed thickness at $t = 00:00$	n/a	n/a	n/a	0.22
Mean sand bed thickness down stream of depression before run at $t = 00:00$ (m)	0.18	0.16	0.17	0.15
Median grain size, D_{50} (mm)	n/a	n/a	0.26	0.24
Bar brink point position at $t = 00:00:00$ (m)	0.41	0.14	0	4.55
Trough length at $t = 00:00:00$, T_L (m)	0.71	1.60	1.37	1.20
Trough depth at $t = 00:00:00$, T_D (m)	0.082	0.25	0.12	0.13
Vertical distance from brink point to toe of the lee face at $t = 00:00:00$, h_L (m)	0.28	0.48	0.49	0.30
Trough volume (m^3)	0.0365	0.2912	0.1207	0.0943
Lee-face toe height at $t = 00:00:00$, t_L (m)	0.06	0	0	0

N.B., The trough and bar were the full channel width (1 m). *Mean velocity at the bar crest, $\bar{U} = \frac{Q}{A}$ where A is the cross sectional area of the portion of the channel occupied by the flow. The Reynolds number, Re , is the ratio of inertial to viscous forces ($Re = \frac{\rho U d}{\mu}$) where ρ is density and μ is viscosity.

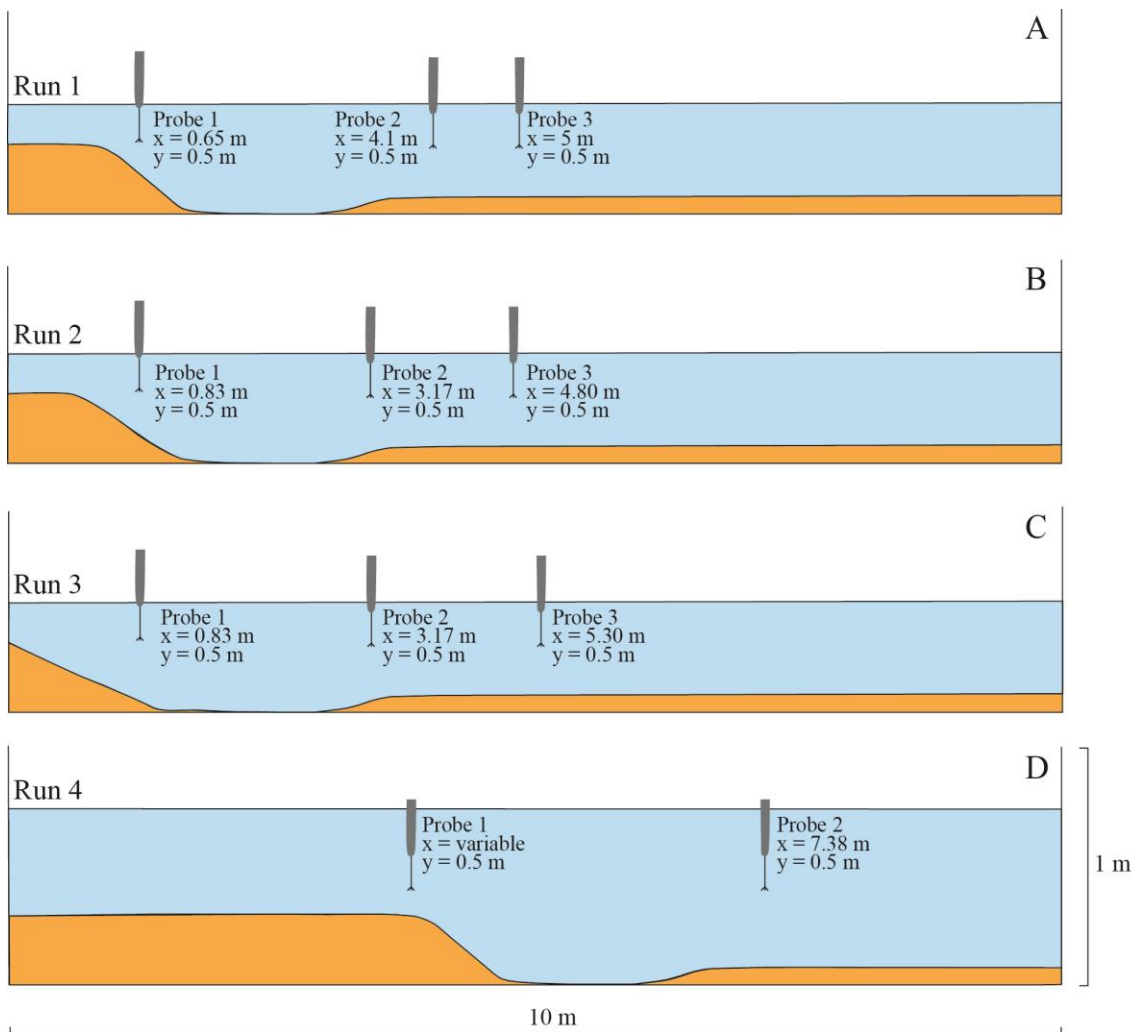


Figure 5.3 Illustration of initial setup of the four runs (A) Run 1; (B) Run 2; (C) Run 3 and (D) Run 4, indicating probes (velocimeters) positions within the tank.

Output from the velocimeters was recorded for the first 600 s of each hour. In each run, as the unit bar migrated downstream the probe located upstream (near bar crest) was relocated to keep its position constant relative to advancing bar (Table 5.3). In Run 4 two velocimeters were used; one in a fixed position on the stoss side of the bar and the other mobile through the experiment (Fig. 5.3D).

In Runs 1-3, in addition to direct observations, both side walls were systematically photographed hourly to record bed topography, water depth, and developing internal sedimentary structures. Run 4 was intensively monitored for the first 3 hours at 600 s intervals and subsequently at longer intervals. In this run, the flume was run steadily for 7 hours 50 minutes; then it was stopped (overnight) and restarted with the same pumping rate and run for similar durations the following days (Table 5.4). This run was

continued in this way until the cross strata completely filled the trough that was initially downstream of the unit bar. The total cumulative run time was 79 hours and 56 minutes. Each time the pumps were turned off or on the flow and sediments were observed carefully.

Table 5.3 Velocity probe locations in Runs 1-4.

Run Number	Probe location in x coordinate along the flume (m)							
	1		2		3		4	
	Start	End	Start	End	Start	End	Start	End
Probe 1	0.65	3.70	0.83	1.70	0.83	1.3	4.36	5.48
Probe 2	3.10	3.10	3.17	3.17	3.17	3.17	5.96	5.96
Probe 3	5.00	5.00	4.80	4.80	5.30	5.30	N/A	N/A

N.B., Vectrino probes were positioned in the flume centre line ($x = 0.5$ m), with fixed vertical position. Their distance above the bed varied as the bed topography changed through each run.

Table 5.4 Times when the flume pumps were started and stopped throughout Run 4.

Date	Start Time (hh:mm)	End Time (hh:mm)	Total Time (hh:mm)
24/04/2013	10:10	18:00	07:50
25/04/2013	10:10	18:00	07:50
26/04/2013	09:10	18:00	08:50
27/04/2013	09:05	13:03	03:58
29/04/2013	07:48	20:00	12:12
30/04/2013	08:00	19:10	11:10
01/05/2013	07:39	18:40	11:01
02/05/2013	08:00	18:30	10:30
03/05/2013	07:58	15:03	07:05

In these runs, small bedforms superimposed the flume-scale unit bar. It was not always possible to discriminate between dunes and ripples, on the basis of the fluid dynamical characteristics and it is likely that they were in a transitional state in these runs (e.g., Southard, 1991; Robert and Uhlman, 2001). Several authors studied some of the factors that are indicative of the ripple-dune transition (e.g., the formation of a greater than average height or “rogue” ripple; different height and celerity of ripples; amalgamation; sedimentation transport rate fluctuations; the increase of flow intensity and variations on the mean and turbulent flow field due to bedform superimposition (Robert & Uhlman,

2001; Raudkivi, 2006; Fernández *et al.*, 2006; Schindler and Robert, 2005). Herein, for simplicity, a bedform wavelength of 0.18 m is used arbitrarily to define the boundary between ripples and dunes. This arbitrary value was chosen for convenience and unlikely to be a reliable discriminating value, not least because the size ranges of ripples and dunes overlap.

5.2 Experimental procedure

The pumping rate was increased rapidly at the start of each run and then maintained at a constant rate throughout Runs 1-3 and for each separate run period of Run 4 (Table 5.2). In each run, the position and shape of the unit bar; brink point; lee-face height; slip-face height; lee-face length; slip-face length (Fig. 5.1), sediment thickness, water depth and water surface elevation relative to the channel were measured at intervals. Photographs were taken frequently from a number of different positions to record the size, shape and movement of superimposed bedforms throughout each run. After each run, the flume was drained slowly to minimise reworking of the bed. The lamination patterns within the deposit were traced on both channel side walls and photographed (Fig. 5.4 and Fig. 5.5). Three sediment samples were collected from the deposits after Run 3; from the proximal, middle and distal areas of the top part of the cross-bed set. Fifty samples were collected from the Run 4 deposit; from proximal (17), middle (23) and distal (10) areas within the cross-bed set. Samples were collected from the top, middle and bottom part of the cross-bed set. Some samples were taken from the counter-flow ripple layer (3) and resulting bottom set (3) (Fig. 5.6).

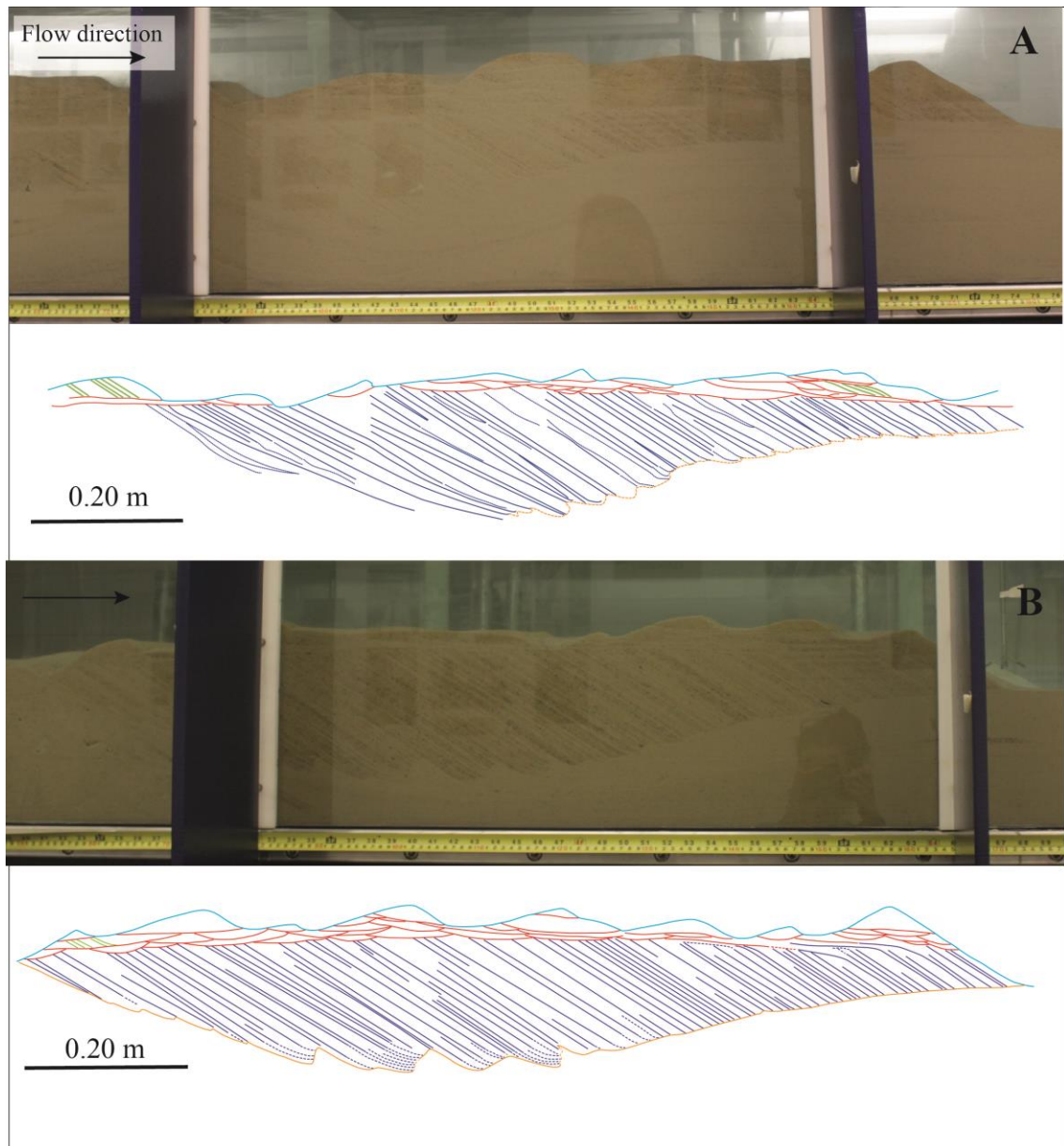


Figure 5.4 Photographs of Runs 1 and 2 with line drawing of deposit structure observed through side wall at end of each run. (A) Run 1 and (B) Run 2. (Orange indicates the bottomset showing counter-flow ripple top profiles; dark blue indicates unit-bar cross-bedding; red indicates surfaces truncating the underlying cross beds due to superimposed bedforms; green indicates ripple-lamination and light blue indicates top surfaces).

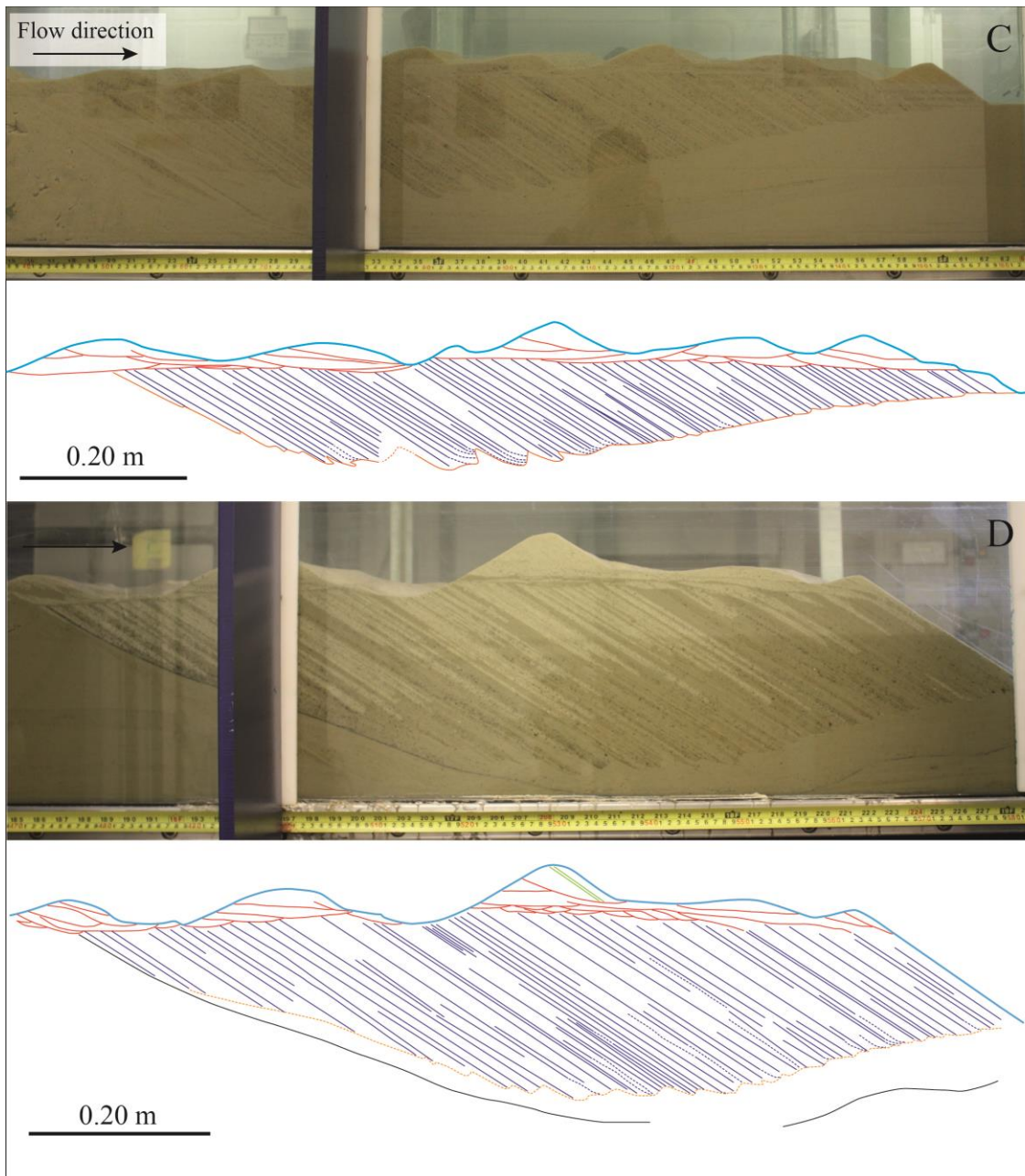


Figure 5.5 Photographs of Runs 3 and 4 with line drawing of deposit structure observed through side wall at end of each run. (C) Run 3 and (D) Run 4. N.B., Photographs were taken just before switching off the flume pumps. This explains the mismatch between top surfaces in photo and line drawing. Photographs of the end of Runs 1-3 runs (static water) were not taken.

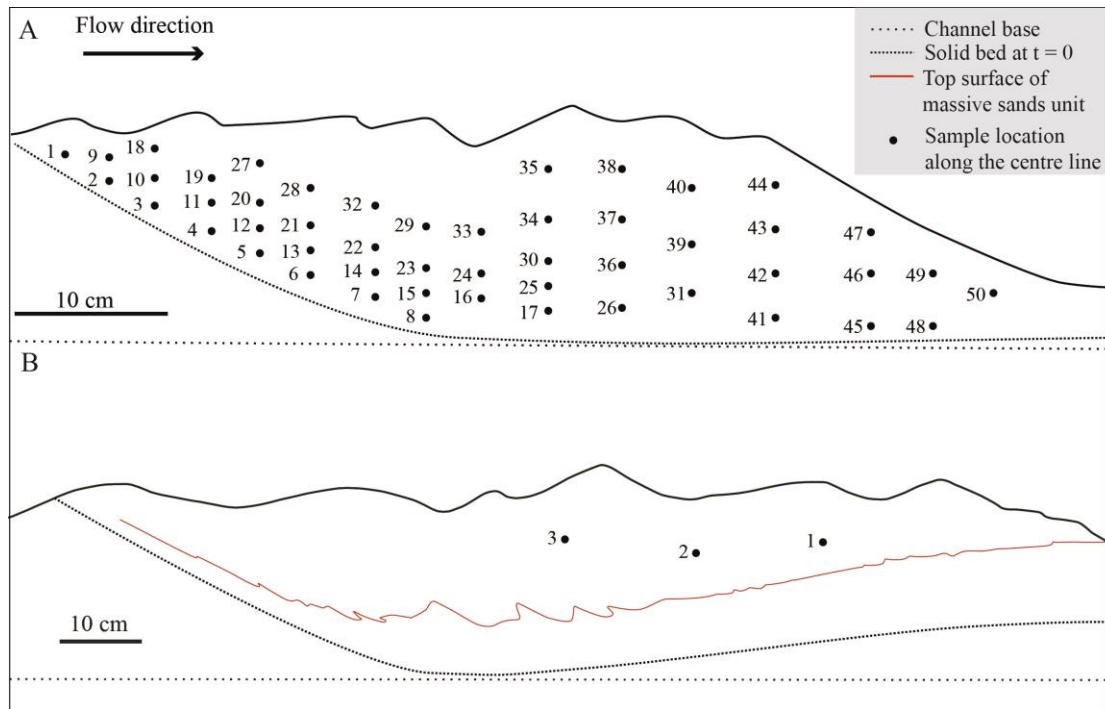


Figure 5.6 Location of samples collected at the end of (A) Run 4 and (B) Run 3.

5.3 General observations on runs

Run 1

When pumping started, the water level increased rapidly above the sand mound and the crest was rapidly modified, creating a gentler stoss side and steep (avalanche) lee slope (Fig. 5.1). In the few seconds after the pumps were started, the flow above the bar accelerated from 0 to 0.658 m s^{-1} and intense turbulence occurred above the bar crest and the upper part of the bar lee. Fast eddies induced sediment avalanching down the bar's steep lee face and rapidly modified the bar crest. As the water depth over the bar crest increased, bar height decreased and velocity and turbulent intensity decreased.

Throughout the run, bedforms with a range of sizes and geometries continuously formed, migrated and interacted with each other and with the bar (Table 5.5). Ripples and small dunes formed on the stoss face of the solitary flume-scale unit bar. Only ripples were observed at the toe of the lee face and in the trough. Superimposed ripples formed on the stoss face of the bar had wavelengths of 0.060 to 0.179 m, heights of 0.002 to 0.032 m and h/λ ratios of 0.09 to 0.25. They varied in shape: asymmetrical with a concave-up stoss face and straight lee face; asymmetrical with straight stoss and lee faces and sharp crest axis slightly asymmetrical with a round crest axis. The dunes on the stoss side of

the bar had wavelengths of 0.180 to 0.540 m, heights from 0.015 to 0.05 m and h/λ from 0.06 to 0.18. Dune shape included: asymmetrical with a straight stoss and lee face; asymmetrical with a slightly concave-up stoss face and straight lee face and the larger dunes had similar geometries to the unit bar with a nearly horizontal stoss face and steep lee face. Occasionally, rapid erosion occurred locally in the troughs of these superimposed bedforms, modifying their morphologies. Small counter-flow ripples ($\lambda < 0.060$ m, $h \leq 0.008$ m) were formed on the lowest part of the unit-bar lee face and in the trough.

The bar advanced at a mean rate of 7.94×10^{-5} m s⁻¹ over the full length of the depression and continued beyond it. As it advanced, the bar height (considered to be the vertical distance from the brink to the lee-face toe, h_L) decreased and with time the mean bed level reached approximately the initial value of bar height. It took less than 5 hours for the unit bar to advance over the trough (filling the depression). Then, the toe of the unit bar extended beyond the area of the original depression, the unit bar decreased in height as it moved downstream, until it could no longer be easily distinguished from the ripples and small dunes (Fig. 5.7). When the pumps stopped, the sand bed morphology changed only slightly, until the water became still and this change did not significantly alter the morphology of the final bed. The trough fill was made up of cross-stratified sand, ripple cross-laminated sand and massive sand.

Run 2

The initial setup and start of the run was very similar to Run 1 (Table 5.2). At the start of the run the stoss side of the bar could not be observed because the crest of the bar was at the upstream end of the test channel. The higher point of the mound of sand manually built up at the upstream end was at the same level as the water surface. As the pumps were activated high concentrations of sediment were transported downstream and intense turbulence occurred. By $t = 01:00:00$ the water depth at the bar crest was 0.23 m and the sediment transport and turbulence above the brink and lee face of the bar had decreased.

During the first hour, the bar moved downstream so that 0.60 m of the stoss face could be observed. Ripples formed on the stoss with wavelengths of 0.050 to 0.179 m and heights from 0.01 to 0.05 m ($0.07 \leq h/\lambda \leq 0.29$). Ripple shapes included the same types

observed in Run 1 and also slightly asymmetrical with straight stoss. Dunes formed with wavelengths of 0.180 to 0.270 m and heights from a 0.002 to 0.037 m ($0.04 \leq h/\lambda \leq 0.19$). Dune shape types were as in Run 1 and also asymmetrical with slightly concave-up stoss face and concave-up lee face.

Counter-flow ripples started to form in the lee of the unit bar very soon after the start of the run. These ripples moved towards the toe of the bar lee face and a little way up it. Grain flows down the unit-bar lee face formed laminae that progressively buried these ripples. Counter-flow ripples reached a maximum wave length of 0.11 m and heights just less than 0.02 m. The largest counter-flow ripples formed in the flatter and deeper section of the trough just after $t = 02:00:00$, when the unit bar was 0.20 m high with a lee face 0.39 m long. After $t = 03:30:00$ the deepest part of trough had been filled with sediment, the unit-bar height (h_L) had decreased to 0.19 m and counter-flow ripples had become smaller. By $t = 06:00:00$ the bar lee face (L_L) had decreased to 0.29 m and counter-flow ripples had stopped forming (Fig. 5.10). The initial shape of the crest was nearly straight, but throughout the experiment the crest varied and became curved and diagonal to the cross section of the flume. Because of the variation in unit-bar shape across the flume, the counter-flow ripples persisted longer on the right side of the channel than the other. Through the 24 hour duration of Run 2, the bar moved downstream with a mean rate of $1.93 \times 10^{-5} \text{ m s}^{-1}$ until the crest was at $x = 1.71 \text{ m}$. The height of the unit bar above the trough decreased with time (Fig. 5.8). The downstream end of the depression was at 2.10 m, and therefore the bar did not advance over the full length of the depression. By the end of the run, the trough was completely filled with sediment.

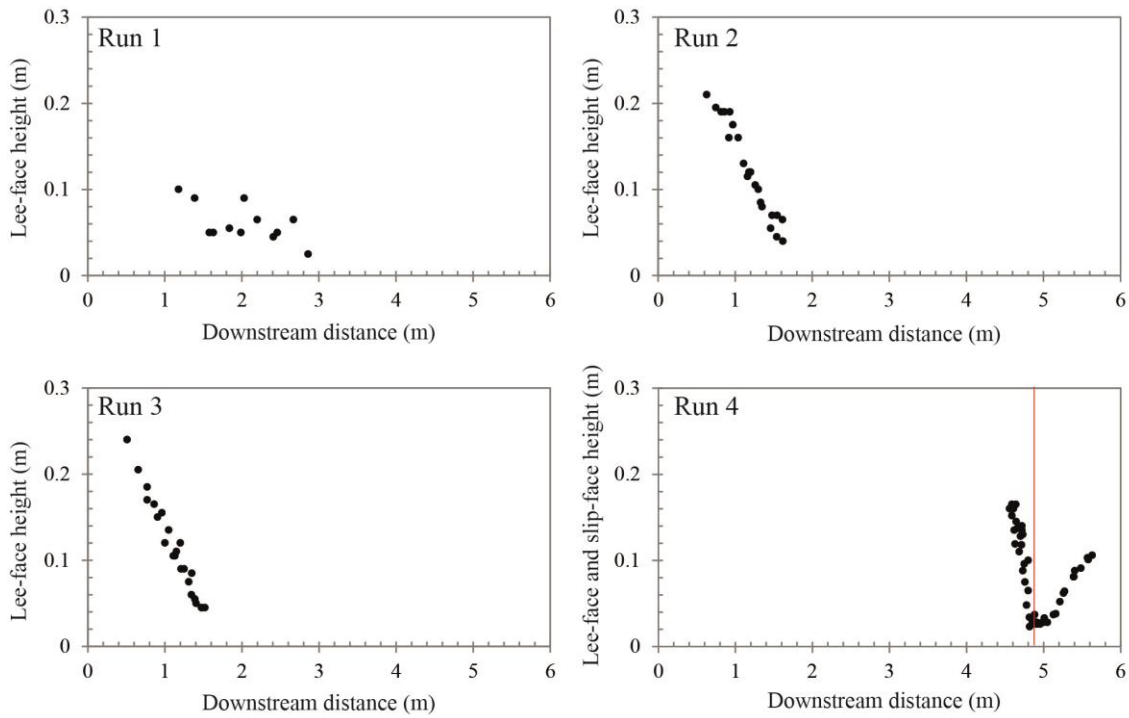


Figure 5.7 Representation of lee-face height versus downstream distance (Runs 1-4). In Run 4, towards the left of the red line shows the slip-face height variation and to the right of the red line indicates when the slip-face height equals the lee-face height.

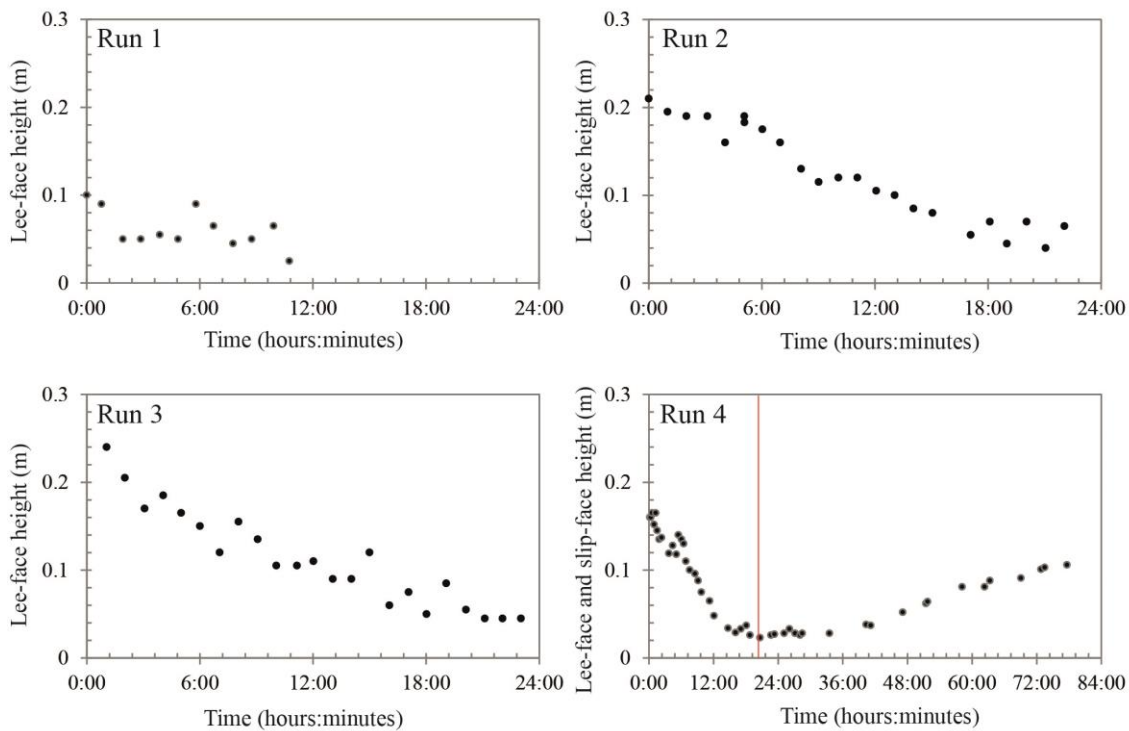


Figure 5.8 Representation of lee-face height versus time (Runs 1-4). In Run 4, towards the left of the red line shows the slip-face height variation and to the right indicates when the slip-face height equals the lee-face height.

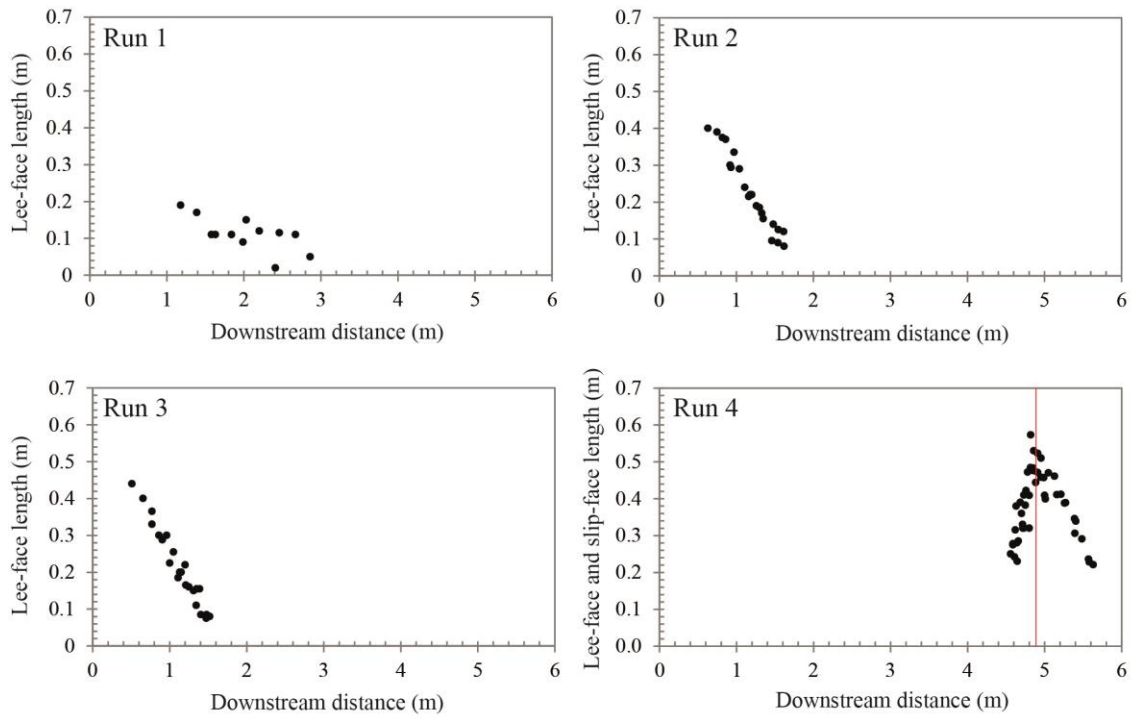


Figure 5.9 Representation of unit-bar lee-face length versus downstream distance (Runs 1-4). In Run 4, towards the left the red line shows the slip-face length variation and to the right indicates when the slip-face height equals the lee-face height.

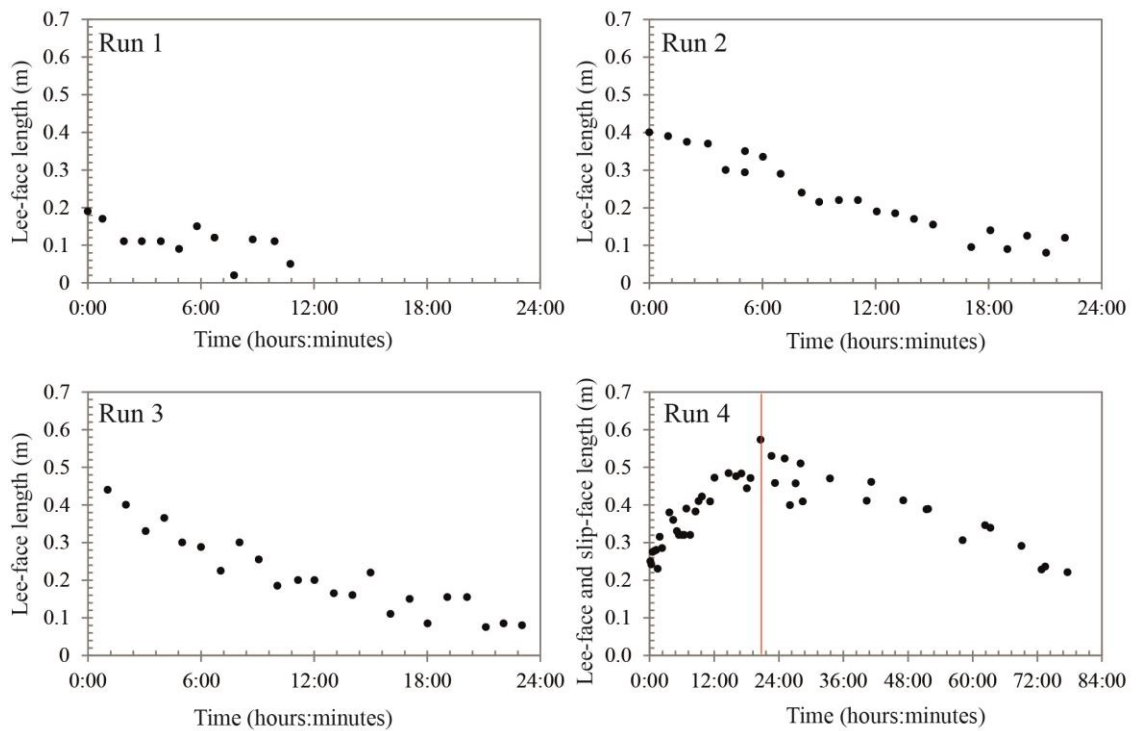


Figure 5.10 Representation of unit-bar lee-face length versus time (Runs 1-4). In Run 4, towards the left of the red line shows the slip-face length variation and to the right indicates when the slip-face height equals the lee-face height.

Run 3

The initial conditions were as in Run 1 and 2, although the exact shape of the depression was a little different (Table 5.2). By $t = 01:00:00$ the bar had advanced downstream so that 0.53 m of the stoss face was visible through the test channel glass wall.

Throughout the run, ripples and dunes formed on the stoss face of the bar. These ripples had wavelengths of 0.060 to 0.179 m; heights from 0.002 to 0.042 m and h/λ ratios of 0.08 to 0.35. The dunes had wavelengths from 0.180 to 0.230 m and heights from 0.012 m to 0.050 m ($0.05 \leq h/\lambda \leq 0.23$). Ripple shape types varied as in Run 2.

Counter-flow ripples formed in the lee of the unit bar on the floor of the trough and on the lower part of the unit-bar lee face. They started to form soon after the start of the run, had maximum wavelength of 0.08 m and heights just below 0.02 m. As in Run 2, counter-flow ripples were largest in the deeper section of the trough when there was an area of near-flat bed downstream of the unit-bar lee face (a little after $t = 02:00:00$). At this point the unit bar was 0.24 m high with a lee face 0.44 m long. As the unit bar advanced up the trough slope, and the height of the bar (defined as the vertical distance from the brink to the lee-face toe, h_L) declined, counter-flow ripples stopped forming (at about $t = 09:00:00$). Because of the variation in unit-bar shape across the flume, they persisted longer on the left side of the channel than the right side.

The bar advanced at a mean rate of $1.84 \times 10^{-5} \text{ m s}^{-1}$ and decreased in size downstream. By $t = 24:00:00$ the bar crest reached $x = 1.59 \text{ m}$ (depression at downstream end was at 1.86 m) and the trough was completely full of sediment even though the bar had not advanced over its downstream end. The height of the bar above the trough decreased with time (Fig. 5.8).

Run 4

The initial position of the bar crest at $x = 4.5 \text{ m}$ allowed superimposed bedforms to be observed on the stoss side. The position of the unit bar and the depth of water above the bar crest have significant implications for the initial stage of bar evolution. The initial interaction between the flow and the sediments in Run 4 is significantly different to Runs 1-3. Just before the start of the run black sand was scattered over the manually sculptured topography of the unit bar and the trough to make the original surface

visually more prominent in the deposits. After the pumps were started, a small turbulent sediment-laden plume was observed above the crest of the unit bar moving a lot of sediment into the trough. Within a few minutes this plume had dissipated.

In this run, it was observed that the avalanching face or slip face tends to grow from the beginning of the run until it reaches the same length as the unit-bar lee face (Figs. 5.7-5.10). This implies that: (1) A distinction should be made between slip-face length (L_S), defined as the sloping distance from the brink to the toe of the slip face and lee-face length (L_L) defined as the sloping distance from the brink to the toe of the lee face (2) In addition, the height of the slip-face toe (t_S) and height of the lee-face toe (t_L) should be differentiated; (3) It is necessary to differentiate between the slip-face height (h_S) (vertical distance from the brink point to the toe of the slip face) and the lee-face height (h_L) (vertical distance from the brink point to the toe of the lee face).

Initially sediment gravity flow on the lee of the unit bar did not descend to the deepest part of the trough; rather, as the steep lee face of the unit bar advanced, the slip-face length increased from 0.25 m at $t = 00:11:00$ to 0.57 m at $t = 20:37:00$ (Fig. 5.10 and Fig. 5.11B). The lee-face length then decreased to 0.22 m at $t = 77:37:00$.

Superimposed bedforms (ripples and dunes) formed within the first 600 seconds and climbed up and over the host bedform continuously (Table 5.5). Although there was a lot of variation in their shape and dimensions, the range of bedform sizes remained fairly constant until $t = 72:56:00$, when bedforms became significantly smaller with minimum lengths of 0.05 m and heights of a few millimetres.

Over short time intervals the crest sometimes moved upstream as the result of the arrival of a superimposed bedform, which modified the bar brink (Fig. 5.11A).

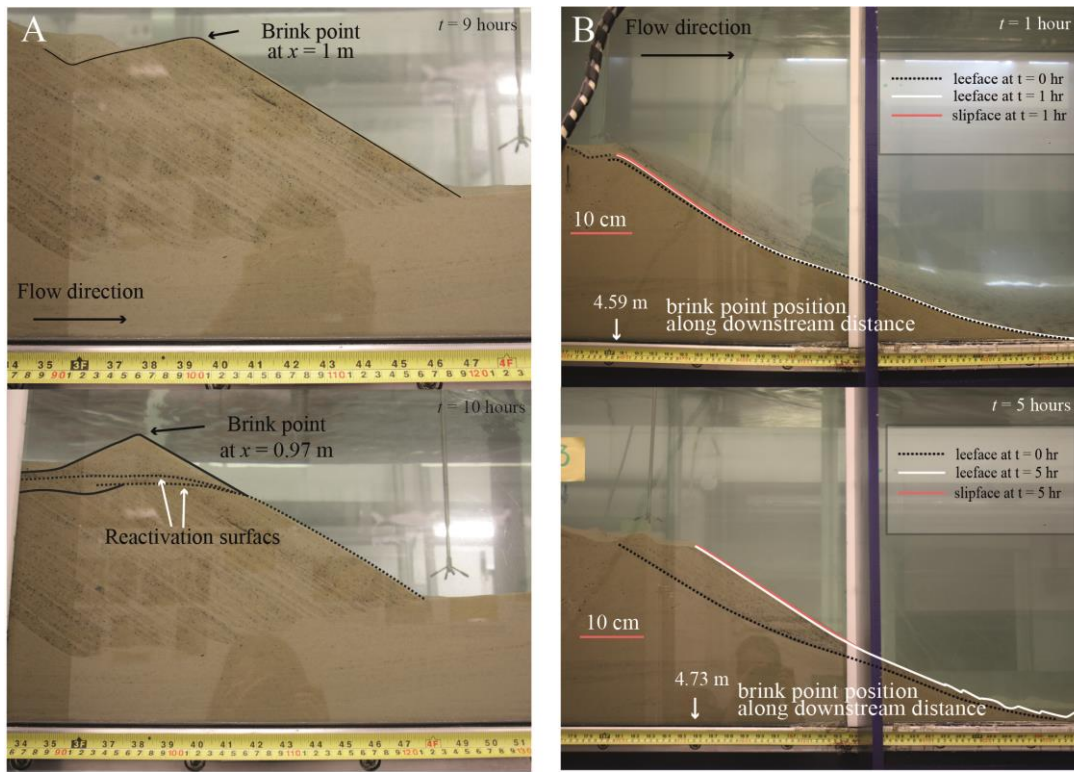


Figure 5.11 (A) Brink point moving upstream due to bedform superimposition and negative values of migration rate; (B) Increase of slip-face length as bar advances in Run 4.

Counter-flow ripples formed soon after the pumps were started; observed in the central part of the trough, but not near the tank walls at $t = 00:16:00$. Small counter-flow ripples started forming near the walls at $t = 01:32:00$. Counter-flow ripples climbed up the bottom of the unit-bar lee face by $t = 03:49:00$. The pattern of ripples on the lower part of the unit-bar lee face and in the trough across the full width of the channel was similar to ripple fans described by Allen (1982) with honeycomb-like crest pattern in the deepest part of the trough. As the run progressed, the depth of the trough varied across the width of the channel and where it was deeper and the floor relatively flat, counter-flow ripples persisted through the entire run. In the area of the trough that became shallower, counter-flow ripples persisted until about $t = 41:00:00$. The ripples in the deepest part of the trough were largest after $t = 05:00:00$, when the bar's slip face was 0.33 m long. The vertical distance from the brink to the toe of the slip face was 0.18 m and the lee-face length was 0.58 m.

Counter-flow ripples observed near the right side wall tended to have a more regular spacing (e.g., at $t = 12:21:00$) than those observed near the left side. Up to $t = 27:25:00$ counter-flow ripples were large near the channel sides and were present in the trough. These ripples moved towards the toe of the unit-bar lee face but did not climb up the face before being buried by grain flows down that face. They became smaller after $t = 39:23:00$. As the bar advanced across the trough, the field of counter-flow ripples was displaced downstream and as it advanced onto the upstream-facing slope of the depression the size of the counter-flow ripples declined and eventually they stopped forming. At this point, the brink point of the bar was at 5.20 m; the unit-bar height (h_L) was 0.21 m and the lee face was 0.40 m long.

The bar crest advanced to $x = 5.84$ m (the downstream end of the depression was at $x = 6.00$ m). The bar advanced at a mean rate of $1.95 \times 10^{-6} \text{ m s}^{-1}$ and decreased in height downstream (Fig. 5.7; Table 5.5). By $t = 76:00:00$, even though the bar had not advanced over the downstream end of the depression ($x = 6.00$ m) the trough was completely full of sediments.

Table 5.5 The bed, superimposed bedforms and deposits.

	Run 1	Run 2	Run 3	Run 4
The flume-scale unit bar and its resulting cross-strata set				
Distance brink point moved (m)	1.84	1.6	1.52	1.09
Brink progradation rate (m s^{-1})	7.94×10^{-5}	1.93×10^{-5}	1.84×10^{-5}	1.95×10^{-6}
Preserved cross-bed set length (m)	1.2	1.3	1.6	1.2
Preserved cross-bed set thickness after truncation by migrating superimposed bedforms (m)	0.22	0.27	0.25	0.28
Ripples on unit-bar stoss				
Wavelength λ (m)	0.060 - 0.179	0.050 - 0.179	0.060 - 0.179	0.050 - 0.179
Height h (m)	0.002 - 0.032	0.01 - 0.05	0.002 - 0.042	< 0.05
Aspect ratio h/λ	0.09 - 0.25	0.07 - 0.29	0.08 - 0.35	0.09 - 0.33
Ripple types *	a, c, d	a, c, d, e	a, b, c, d, e	a, b, c, d, e, f
Dune on unit-bar stoss				
Wavelength λ (m)	0.18 - 0.54	0.180 - 0.270	0.180 - 0.230	0.2 - 0.32
Height h (m)	0.015- 0.05	0.002 - 0.037	0.012 m - 0.050	0.03-0.05
Aspect ratio h/λ	0.06 - 0.18	0.04 - 0.19	0.05 - 0.23	0.14 - 0.20
Dune types**	b, e, f	a, b, e, f, g	a, c, e	a, b, c, d

Counter-flow ripple in the lee of the unit bar				
Wavelength λ (m)	<0.06	< 0.11	< 0.08	< 0.08
Height h (m)	< 0.008	< 0.02	< 0.02	0.04

N.B., Although Run 1 lasted 15 hours, after $t = 05:00:00$ the unit bar had migrated over and a little beyond the trough and by $t = 05:00:00$ the unit bar was unidentifiable and ripples and small dunes advanced over a flat topography.

*Ripple shapes (a) asymmetrical with a concave-up stoss face and straight lee face; (b) asymmetrical with concave-up stoss and concave-down lee faces; (c) asymmetrical with straight stoss and lee faces; (d) slightly asymmetrical with a round crest axis (e) slightly asymmetrical with straight stoss and (f) asymmetrical with slightly concave-down stoss face and straight lee face.

**Dune shape (a) asymmetrical with concave-up stoss and concave-down lee faces; (b) asymmetrical with straight stoss and lee faces; (c) slightly asymmetrical with a round crest axis and (d) asymmetrical with a rounded crest, (e) asymmetrical with a slightly concave-up stoss face and straight lee face; (f) large dunes had similar geometries to the unit bar with a nearly horizontal stoss face and steep lee face, (g) asymmetrical with slightly concave-up stoss face and concave-up lee face.

5.3.1 Bed heights in Run 4

Bed height changed continuously through Run 4 with topography of the unit bar slowly varying as it advanced downstream. Throughout Run 4 sediment thickness was measured on both channel side walls simultaneously at 5 locations (Fig. 5.13). Superimposed bedforms caused scatter in the bed thickness data. The mean bed thickness over the length of the run and the length of the channel was 0.21 m. Sand moved along the channel and recirculated through the pipes. No sediment was added or removed from the flume during the run, but the mean bed thickness within the channel declined from 0.22 to 0.17 m (Fig. 5.12). Although the change in bed thickness may be partly explained by changing amounts of sediment in the recirculating pipes, it is better explained by a change in sediment packing in the bed and a consequent decrease in porosity.

At the most upstream location 1 ($x = 0.48$ m) the sediment thickness initially increased, reaching a maximum of 0.258 m on the right side at $t = 11:30:00$ and 0.252 m at $t = 07:48:00$ on the left side. It then decreased gradually to 0.083 m on the right side and

0.008 m on the left side at $t = 79:56:00$. At location 2 ($x = 2.54$ m) the sediment thickness at the right side fluctuated until $t = 46:31:00$ between 0.188 m and 0.232 m. Then, the thickness increased to a maximum of 0.296 m at $t = 51:32:00$, and it decreased gradually until $t = 79:56:00$. Near the left wall from $t = 00:00:00$ to $t = 40:38:00$ thickness changed between 0.255 m and 0.194 m; then increasing to 0.270 m at $t = 76:50:00$.

At location 3 ($x = 4.50$ m), near the initial unit-bar brink point, sediment thickness generally decreased. Near the right side wall it varied between 0.280 m and 0.339 m from $t = 00:00:00$ to $t = 28:36:00$ and then decreased to 0.218 m at $t = 76:50:00$ and finally increased to 0.257 m. Near the left wall, thickness varied between 0.280 m and 0.370 m from $t = 00:00:00$ to $t = 21:34:00$, then decreased to 0.235 m at $t = 79:56:00$.

At location 4 ($x = 7.19$ m) there was no clear tendency of sediment thickness change. The right side varied between 0.134 m at $t = 04:12:00$ and 0.172 m at $t = 57:43:00$; $72:35:00$ and $79:56:00$. The left side varied between 0.137 m at $t = 79:56:00$ and 0.197 m at $t = 00:16:00$; $01:05:00$; $01:17:00$ and $03:37:00$.

At location 5 ($x = 9.49$ m) the sand bed thickness varied similarly as in location 4, staying nearly constant (around 0.166 m) with a slight increase to 0.209 m at $t = 72:07:00$.

The bed slope was calculated for individual time intervals (Fig. 5.12). The bed data also confirm that although there were local short term variations, the sediments behaved homogeneously across the width of the channel and downstream, preserving a more or less constant topography of the sand bed as the bar migrated.

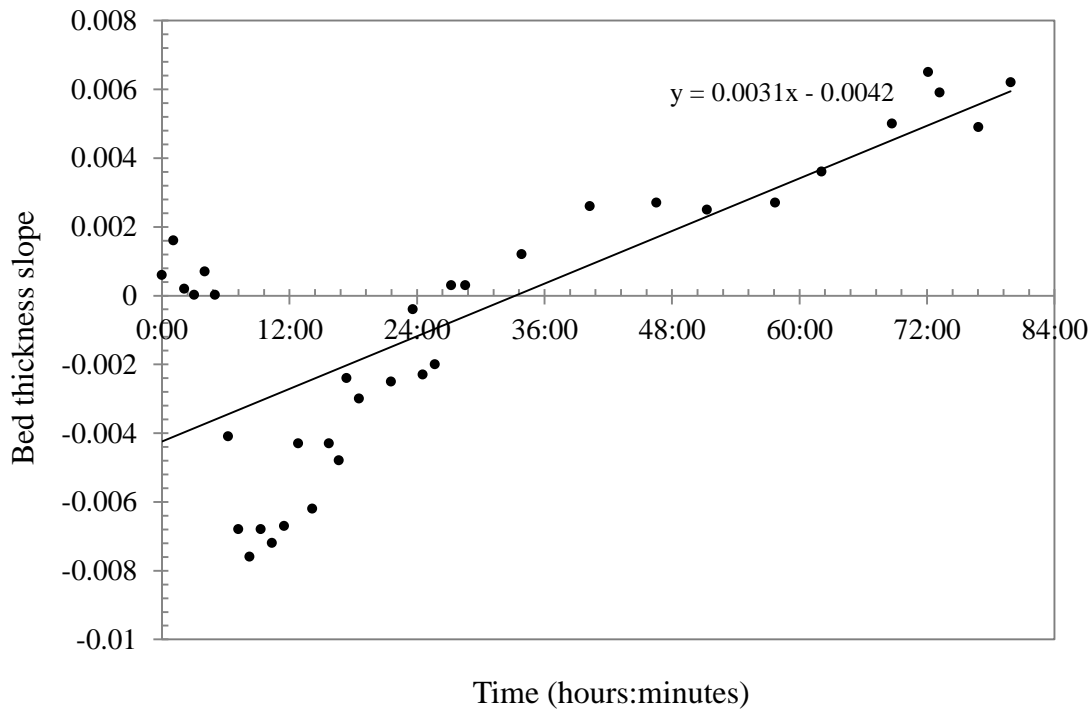


Figure 5.12 variation of bed thickness slope with time throughout Run 4.

Figure 5.12 represents the variation of the bed thickness slope with time between the downstream distance $x = 0.48$ m (location 1) and $x = 9.49$ m (location 5). The bed thickness slope throughout Run 4 is 0.0031 indicating a slight upslope downstream. However, the bed slope is not calculated over a long enough distance to allow highlighting the influence of the local topography of the bar.

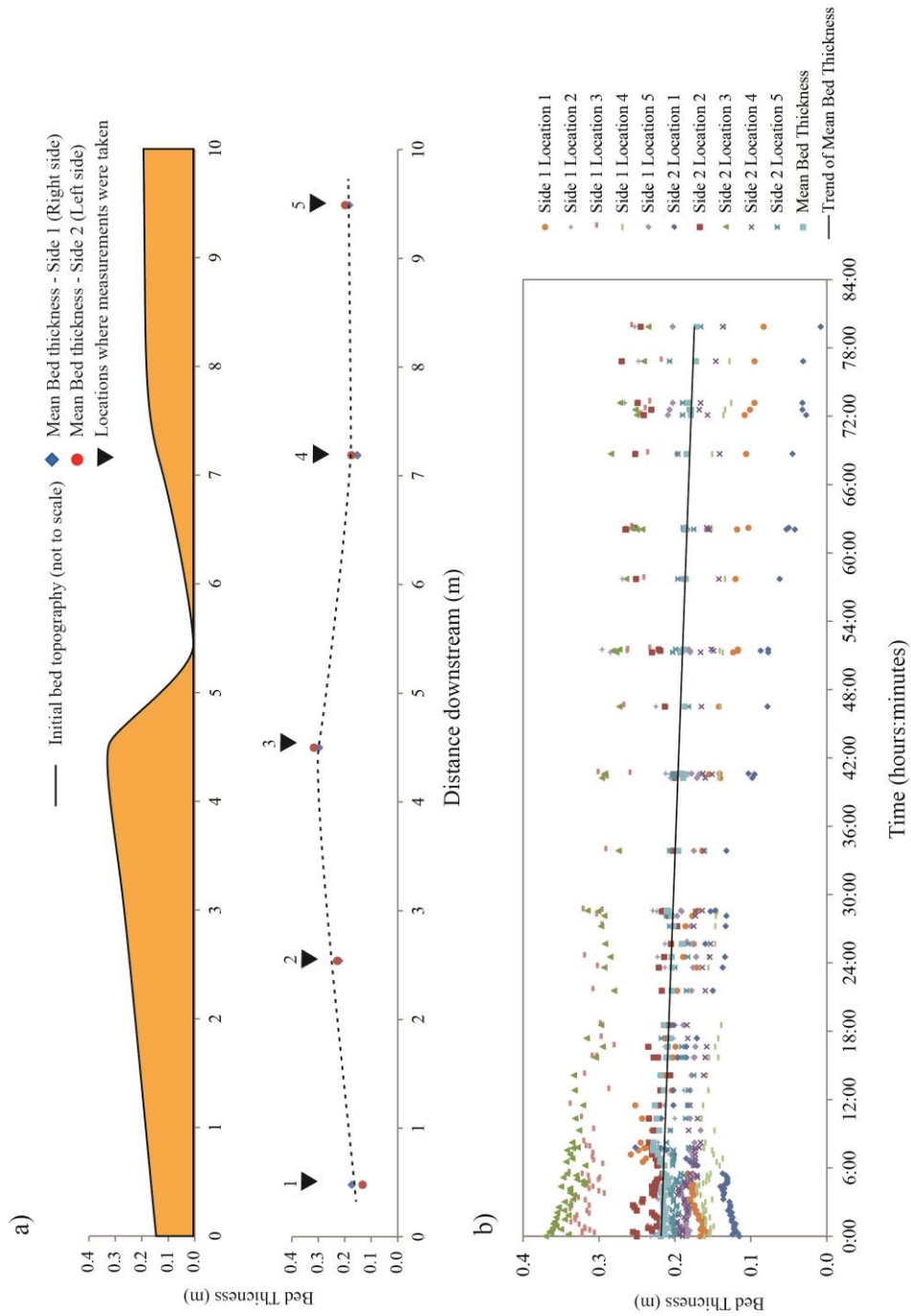


Figure 5.13 (a) Profile of initial bed topography in Run 4; and mean bed thickness measured at 5 locations along the downstream distance from the flume side walls; (b) Variation of bed thickness at 5 fixed locations throughout Run 4.

5.3.2 Water surface elevation in Run 4

Throughout Run 4 static and non-static water surface elevation were measured on both channel side walls simultaneously at 5 locations (Fig. 5.14).

Static water surface elevation was measured at each no-pumping interval in Run 4. It ranged between 0.713 and 0.647; and it decreased by 66.5 mm through the run due to leakage from the flume that was initially not identified. The mean static water elevation was 0.678 m. The non-static water surface elevation ranged between a maximum of 0.721 and 0.647 m and decreased at intervals by a maximum of 0.017 m throughout Run 4. The mean non-static water surface elevation is 0.687 m (Fig. 5.14).

The static water slope was calculated at intervals during Run 4 and shows positive gradients (Fig.5.14). This highlights measuring errors. Non-static slope were calculated for individual times. The positive gradients indicate an upslope towards downstream. This could be explained by inaccuracy of the flume tilt calibration and inaccuracy of measurement (e.g., the floor of the flume must have been slightly sloping when measurements were taken and the slope of the channel bed changed over time). The non-static water slope varied significantly but no increasing or decreasing tendency was observed (Fig. 5.15).

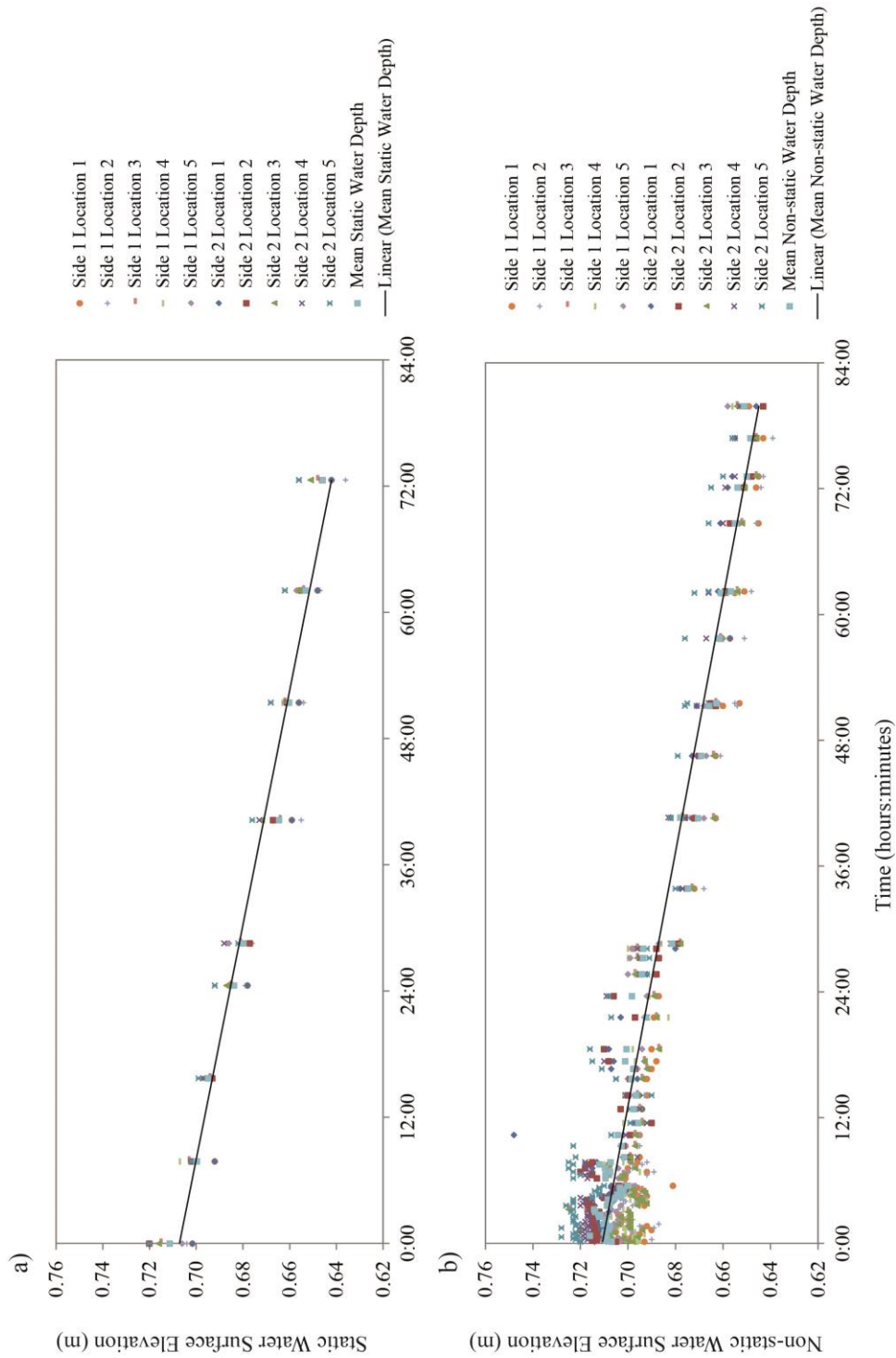


Figure 5.14 (a) Variation of the static water surface elevation with time (Run 4); (b) Variation of the non-static water surface elevation with time (Run 4).

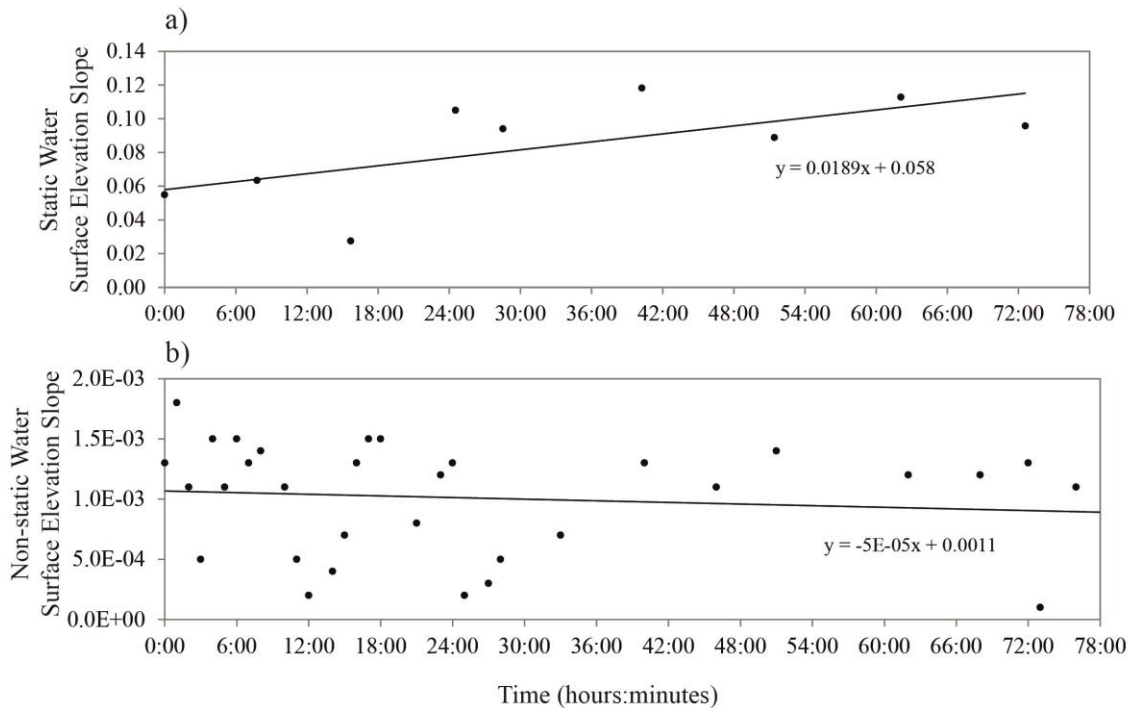


Figure 5.15 (a) Static water elevation slope variation with time in Run 4; (b) Non-static water surface elevation variation with time in Run 4.

5.3.3 Unit-bar geometry and crest shape evolution

In Runs 1, 2 and 3 the bar stoss face was initially short or absent (Fig. 5.16). In Run 4 the stoss face was initially longer and at a lower angle. In all cases, the shape changed through the run, with the stoss side increasing in length by 1.31; 1.61; 1.53 and 1.01 m in Runs 1-4 respectively. This raises the question: where does the stoss face end and when does the unit bar stop being a unit bar?

In all four runs, the unit-bar crest plan shape was initially straight and at 90° to the channel and it changed slightly as the bar moved. During Run 1 the crest became asymmetrically lunate (Fig. 5.17A). In Run 2 the crest became sinuous with two lobes (Fig. 5.17B); in Run 3 it became sinuous with one lobe (Fig. 5.17C). In Run 4 the unit-bar crest was straight and slightly curved at the very beginning of the run, became straight and later became very subtly curved when the centre part of the crest advanced a little bit faster than the edges (Fig. 5.17D). The variation of the host bedform crestline may have implications on lee-face angle variation (Section 6.4.5).

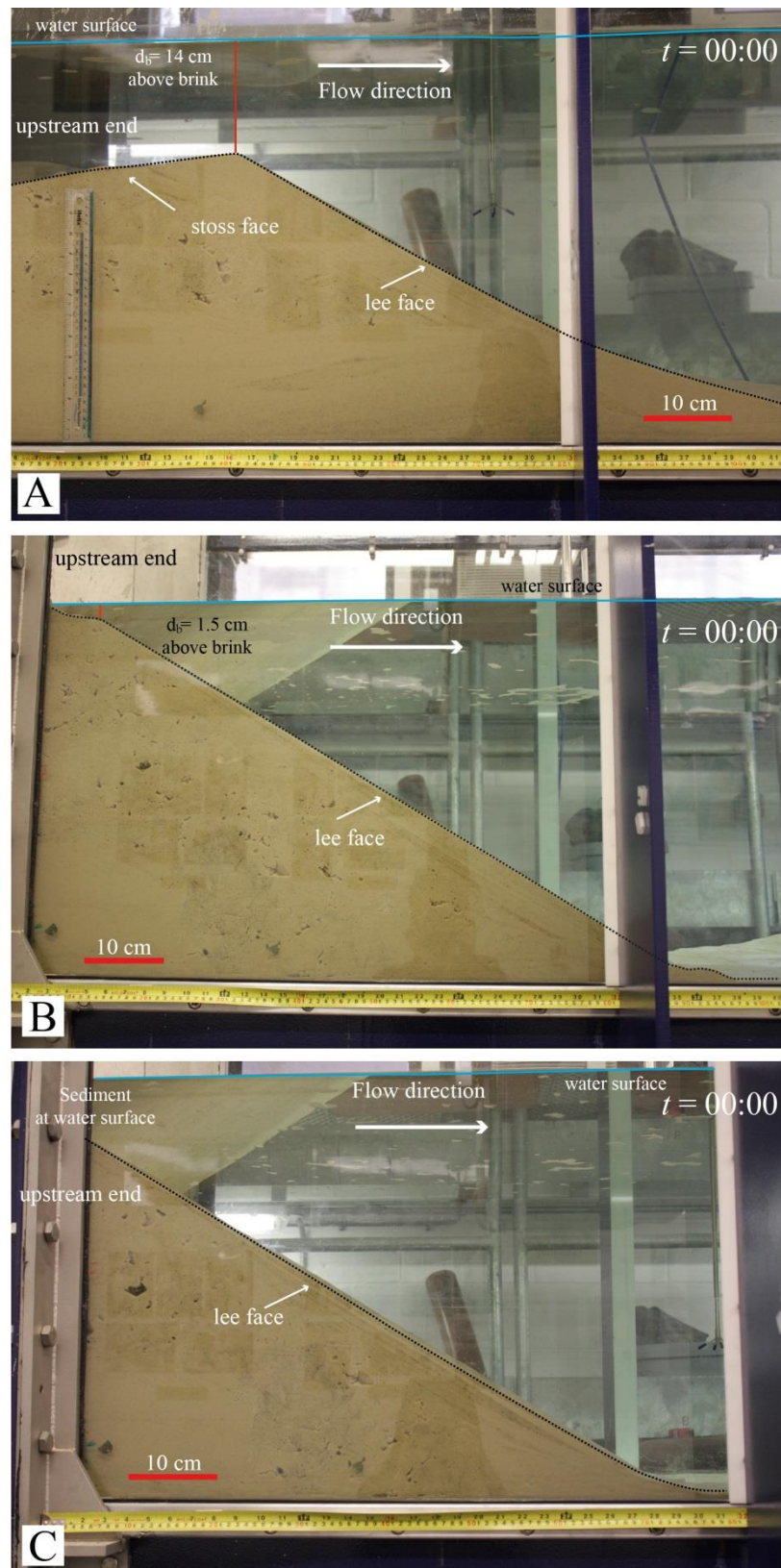


Figure 5.16 Upstream-end in Runs 1-3 indicating the initial stage of unit-bar stoss face. (A) Run 1; (B) Run 2 and (C) Run 3.

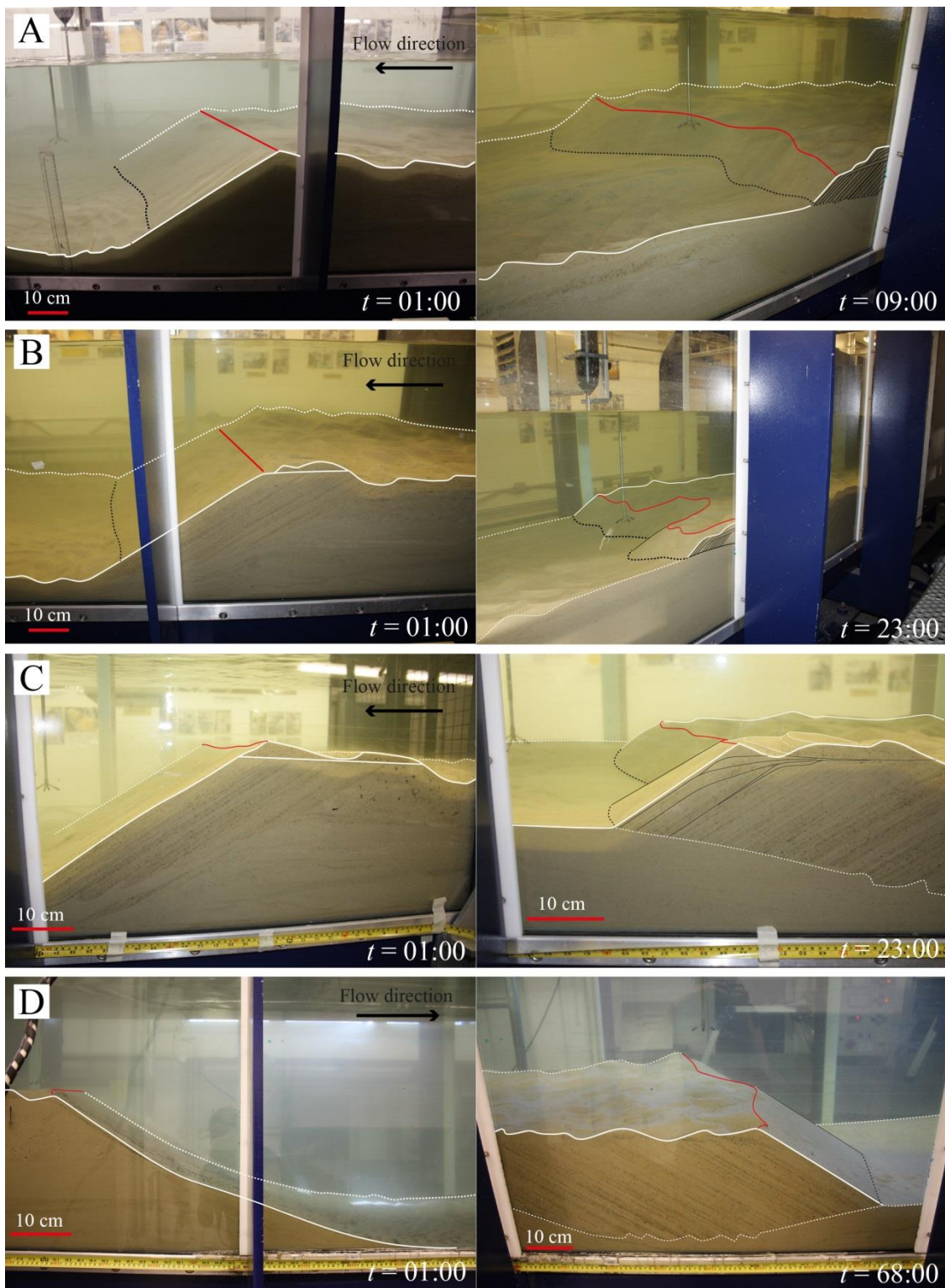


Figure 5.17 Development of unit-bar crest shape as bar advanced downstream. (A) Run 1; (B) Run 2; (C) Run 3 and (D) Run 4. N.B., Time = hours:minutes.

5.3.4 General observations on the effect of bedform superimposition

Superimposed bedforms climbed the stoss face and approached the crest of the unit bar causing variations in the shape and height of the bar crest. As they approached the unit-bar crest they caused changes in the behaviour of sediment avalanching down the unit-bar lee face. Sediment transport, turbulence and reworked sediments within the superimposed bedform troughs generate scouring. Superimposed bedforms moving towards or growing near the unit-bar brink add to the height of unit bar, increasing the length of the bar's lee face. As the next upstream bedform approached the brink there was a tendency for the trough between the two superimposed bedforms to deepen and the downstream bedform to grow (Fig. 5.18).

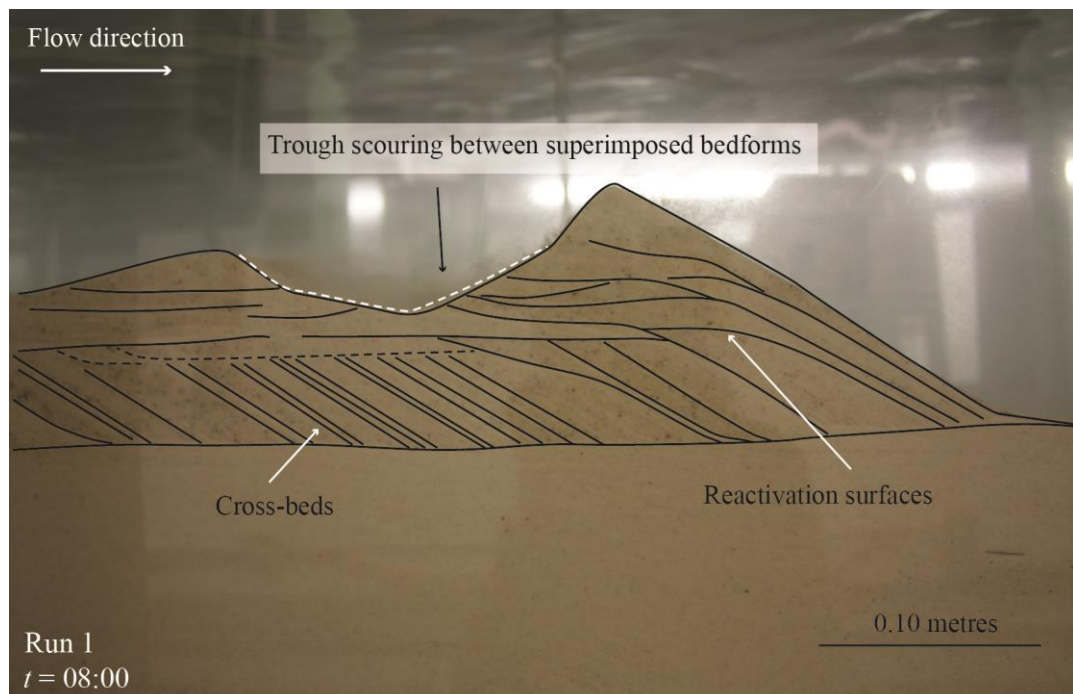


Figure 5.18 Photograph showing superimposed bedforms migrating over a host bedform and trough deepening occurring due to superimposed bedform reaching the host bedform brink point (Run 1, $t = 08:00$ hours).

When this occurred near to the unit-bar crest, the height of the unit-bar lee face increased and the position of the bar's lee-face brink point moved rapidly upstream. The unit-bar brink point moved a little way upstream while the slip face as a whole continued to migrate downstream (giving a negative brink-point migration rate, Fig. 5.11A). In contrast, when the trough of a superimposed bedform approached the unit-bar crest and spans a lot of the width of the test channel, the velocity variation (direction and speed) of flow in the trough could be very erratic and caused rapid scour and

energetic sweeps and bursts of moved pulses of sediment onto the unit-bar lee face generating small quick grain flows. These in turn triggered energetic eddies in the water on the lee face, which in turn can trigger other grain flows. The scouring lowered the height of the bar's lee face brink and truncated the top of foreset lamination.

5.3.5 Observations on counter-flow ripples

The formation of counter-flow ripples depends on the strength of the return flow in the separation eddy in the lee of the bar. They will only form if the bar crest is sufficiently high and the trough big enough for the return flow velocity to generate ripples. Thus, counter-flow ripples did not form throughout the trough, or for the full duration of all the runs. In Runs 1-3, counter-flow ripples preferentially formed towards the sides of the channel, with only incipient ripples seen in the central part of the channel. In Run 4, counter-flow ripples formed over the full width of the channel. The upstream progression of the small counter-flow ripples from the trough and climbing up the lower part of the unit-bar lee face reduced the lee-face dip and produced tangential contacts between the foreset laminae and the underlying lamination. Grain flows reach the counter-flow ripples crest and continue forming over the ripple stoss face. Once a ripple is buried by grain flows, new grain flows lay over the ripple, giving the bar lee face a tangential contact with the floor in the trough of the ripples. As more laminae form the contact angle increases into the trough of the next ripple until the grain flows reach the next ripple crest and the process repeats. The formation of tangential foreset toes by counter-flow ripples is similar to that described by MacDonald *et al.* (2013). Counter-flow ripple growth and migration generated small packages of ripple cross-lamination near the toe of the unit-bar lee face as a bottomset bed that merges with the bottom of the unit-bar cross-bed set. Cross beds formed as the unit bar advanced and locally they became tangential to the deepest area of the trough where counter-flow ripples reworked the sediment in the trough and interacted with grain flows on the lee of the bar.

5.3.6 Unit-bar migration and the formation of cross-stratification

Given that the discharges were similar in Runs 1-3 and because sediment and water are recirculated in a closed loop, the initial assumption was that the sediment flux to the bar brink would be similar, however, the bars migrated at different rates (Table 5.6). In the earliest stages of Runs 1-3 there were no obvious superimposed bedforms; and grain flows were the main mechanism generating cross-bed laminae.

Initially grain-flows did not reach the toe of the unit-bar lee face. The slip-face length increased until the grain flows reached the bottom of the trough. This caused a variation of the slip-face length and a variation of the laminae thickness. During this early interval the brink of the bars migrated at 1.92×10^{-4} ; 1.71×10^{-4} and 1.44×10^{-4} m s⁻¹.

Within the first hour of each run superimposed bedforms developed and continued to form throughout each run. The mechanisms generating cross-bed lamination became more complex, and the bar migration rates changed. During the first few minutes of Runs 1-3 a large amount of sediment was rapidly transported and deposited within the unit-bar trough, forming part of the resultant basal unit (i.e., bottomset) formed mainly due to sediment aggradation. During the first 60 minutes of each run, the initial unit-bar lee faces (artificially made) decreased in length: from 0.70 to 0.19 m in Run 1; 0.91 to 0.40 m in Run 2 and 0.89 to 0.44 m in Run 3. Then, the profile of the host bedform in Runs 1-3 became closer to one corresponding to a flume-scale unit bar.

In Runs 1-3 the length of the slip face very quickly became equal to the length of the bar lee face; and, as the bar advanced further into the depression, the length of the slip face (lee face) tended to decrease (Fig. 5.10). In Run 4, the initial shape of the artificial host bedform was closer in shape to a flume-scale unit bar; so the sediment transport in the first minutes of this run was slower, therefore there was enough time to observe the growth of the slip face until it reached the full length of the lee face. Figure 5.10 shows how the slip face increased in length until $t = 20:37:00$ and then, decreased until the end of the run.

The average bar migration speeds in the early stages were 1.92×10^{-4} m s⁻¹ in Run 1; 1.71×10^{-4} m s⁻¹ in Run 2, 1.44×10^{-4} m s⁻¹ in Run 3, and 8.33×10^{-5} m s⁻¹ in Run 4. The average bar migration rates from $t = 03:00:00$ onwards were 4.37×10^{-5} m s⁻¹ in Run 1; 1.28×10^{-5} m s⁻¹ in Run 2 and 1.27×10^{-5} m s⁻¹ in Run 3 (cf. discussion in Section 5.4.4).

In Run 4, superimposed bedforms developed much sooner in the run and the bar migration rate was fairly constant (mean 1.95×10^{-6} m s⁻¹) until $t = 72:56:00$ when the bedform size decreased and the bar migration rate was 4.01×10^{-6} m s⁻¹.

As the bar advanced downstream superimposed bedform scour associated with varying size of bedforms truncated the cross-bed laminae of the bar (Fig. 5.19).

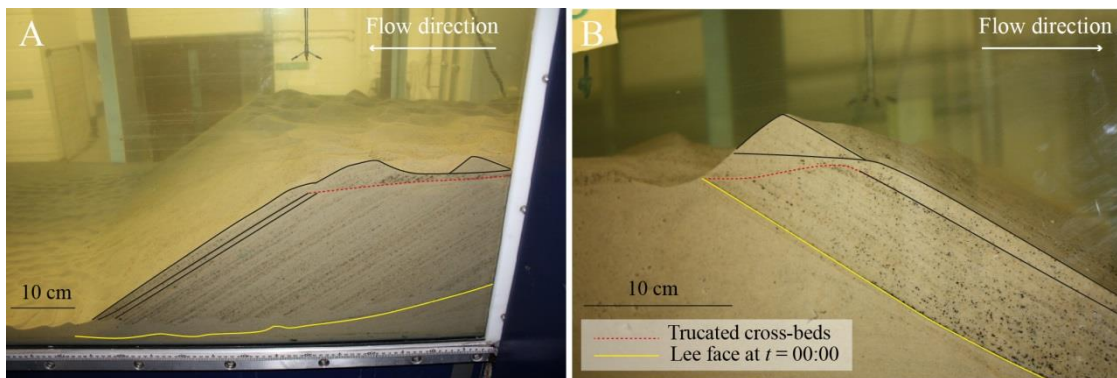


Figure 5.19 Superimposed ripples climbing over the unit-bar and consequently the truncation of cross beds. (A) Flume left side and (B) Flume right side.

Table 5.6 Migration rates and distance reached by unit-bar brink point in Runs 1-4.

Run	Cumulative time (sec)	Distance advanced by brink point (m)	Migration Rate (m s^{-1})
1	18000	1.84	7.94×10^{-5}
2	82800	1.6	1.93×10^{-5}
3	82800	1.52	1.84×10^{-5}
4	560340	1.09	1.95×10^{-6}

N.B., Run 1 lasted 15 hours. However once the 5th hour was completed the unit bar had already migrated over the trough and a little bit further over the shallowest flat sand bed. Beyond this point (From hour 6 to hour 15) the unit bar disappeared and observations showed the formation of ripples and small dunes advancing over a flat topography.

5.3.7 The deposits and cross-bed characteristics

In these flume runs the original bed depressions were filled by: (1) sediments avalanching on the unit-bar lee face forming foreset lamination, (2) sediments deposited from suspension (or temporary suspension) on the lee face and on the floor of the depression, and (3) sediments reworked by return flow in the separation eddy in the bar-lee separation zone. The resulting deposits had two main components: the unit-bar foreset (above) and at the base (or bottomset), an apparently massive unit overlain or not by a ripple cross-laminated layer (maximum thickness 0.06-0.08 m). This bottomset is mainly formed by processes 2, 3 and also rapid sediment transport settling the excess of sediment in the upstream end.

In these runs, the top surface of the basal unit preserved counter-flow ripples, but in some settings these might not form and the basal unit would have a nearly flat top boundary delimitating the cross-bed set formed by the migration of the unit bar. Due to the slight variations of the depression dimensions and the water depth, the unit-bar migration rate and the resulting cross-set dimensions differed (Appendix C, Table C.9).

The Run 1 unit-bar cross-bed set was 1.49 m long and maximum thickness of 0.25 m (Fig. 5.4A). The thickness of individual laminae within this set was < 0.003 m, and their calculated dip varied from 26° to 37° . The preserved length of the individual laminae ranged from 0.05 to 0.45 m. The top of the set was truncated due to erosion in the troughs of superimposed bedforms. Below unit-bar foresets and above the surface representing the original depression topography, there was a bottomset (max. thickness 0.08 m, length 0.92 m) that formed from suspension fallout and by reworking in counter-flow ripples. This bed was lens-shaped and its lower boundary was the initial bottom topography. The top surface of this unit preserved the buried counter-flow ripples. The repeated process of counter-flow ripples climbing and being partly buried by lee-face avalanches generated an unusual type of climbing-ripple cross-lamination. Cross-bed sets formed by the superimposed bedforms on the stoss of the unit bar had preserved lengths between 0.19 m and 0.25 m and thickness of 0.02 m to 0.03 m.

The Run 2 unit-bar cross-bed set was 1.3 m long with a maximum thickness of 0.27 m (Fig. 5.4B). The preserved individual laminae lengths varied from 0.08 to 0.33 m and these were truncated by the erosion associated with superimposed bedforms. The individual laminae thickness was < 0.003 m. The calculated cross-bed angle varied between 30° and 35° . Between the foreset and the pre-run bed surface there was a bed (up to 0.06 m thick and 0.82 m long) with preserved buried counter-flow ripples ($\lambda < 0.08$ m, height < 0.02 m) on the top boundary. Above the unit-bar cross-bed set smaller sets were preserved (thickness < 0.08 m, length < 0.15 m) formed by ripples and small dunes.

In Run 3 the unit-bar cross-bed set was 1.6 m long and 0.25 m thick (Fig. 5.5C). The preserved laminae length varied from 0.05 and 0.27 m and they were truncated by erosion associated with the migration of the superimposed bedforms. Within the unit-bar foreset, laminae thickness was < 0.003 m. The calculated dip angle of the laminae

ranged between 21° and 37° . The preserved bottomset was < 0.08 m thick and 0.95 m long. It included counter-flow ripples cross-lamination and an underlying massive part. The lower surface of this unit was similar to the original channel topography having been formed by some sediment reworking in the trough. The upper boundary preserved the signature of counter-flow ripples ($\lambda < 0.08$ m, height < 0.007 m) that formed within the deepest part of the trough and at the bottom of the lee-face toe. Above the unit-bar foreset, thin cross-bed sets (lengths < 0.22 m, thicknesses < 0.01 m) were preserved that formed by migration of superimposed bedforms.

In Run 4 the unit-bar cross-bed set was 1.2 m long with a maximum thickness of 0.28 m (Fig. 5.5D). Individual laminae within the set had preserved lengths from 0.08 to 0.35 m and were truncated due to superimposed bedforms. Laminae thickness was < 0.003 m. The calculated foreset dip varied between 28° and 37° within 1.07 m horizontal distance along the tank. There was a basal unit (thickness < 0.06 m, length < 0.73 m) and shape in phase with the original topography. The top surface of this unit preserved counter-flow ripples ($\lambda < 0.08$ m, height < 0.01 m). Cross-bed sets formed by superimposed bedforms were preserved with lengths up to 0.19 m and thickness < 0.02 m.

5.3.8 Bar lee-face angle

As the bar moved downstream over the depression, the angle of its lee face varied. Variation occurred rapidly on small sections of the lee face (e.g., the upper 3rd) and cumulatively over the whole face. The unit-bar lee-face angle, was estimated by $\theta = \sin^{-1}(h_L/L_s)$, where h_L is the vertical distance from the unit-bar brink to the toe of the lee face and L_s is the length of the slip face (Fig. 5.1). Once the slip-face length is equal to the lee-face length then the lee-face angle was estimated by $\theta = \sin^{-1}(h_L/L_L)$ where L_L is the length of the lee face. No systematic pattern of lee-face angle variation with time (or distance down the flume channel) was observed in any of these runs (Fig. 5.20 and Fig. 5.21).

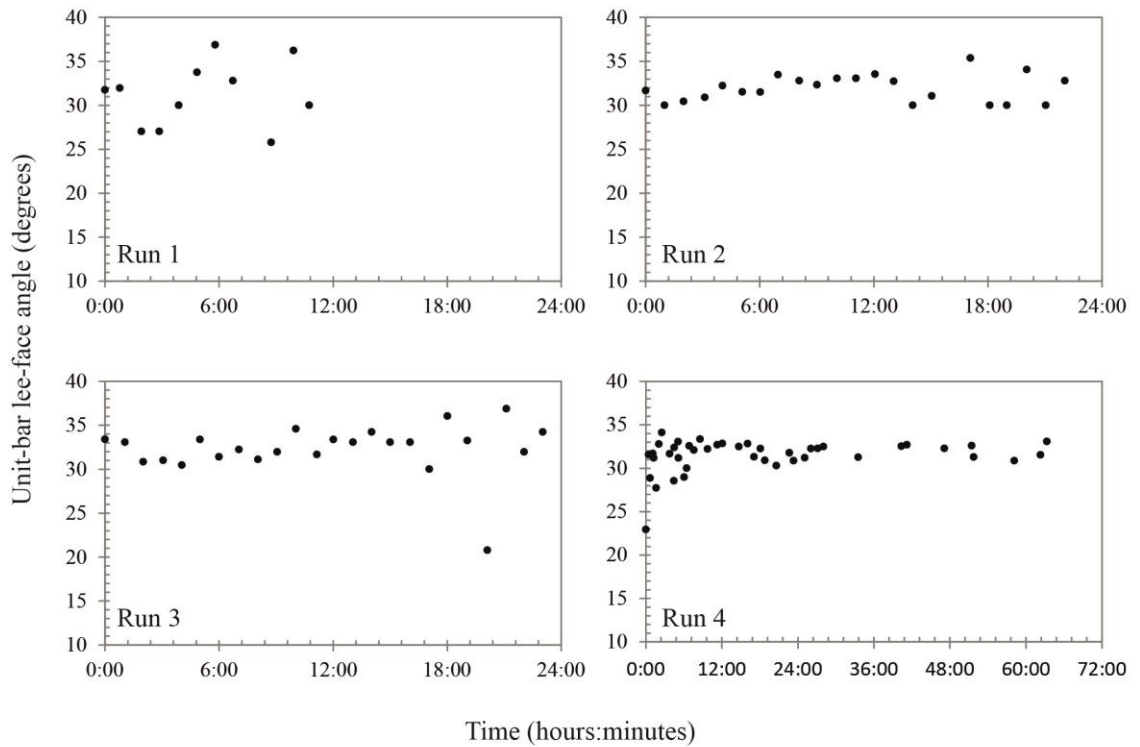


Figure 5.20 Representation of unit-bar lee-face angle variation with downstream distance (Runs 1-4). N.B., In Runs 1-3 *h* and *l* were measured at 1 hour interval. In Run 4 they were measured at short time intervals (600s) for the first 3 hours, and at longer time intervals later in the run. Values of unit-bar lee-face angle larger than 35° are considered unrealistic in real systems (values over 40° have not been represented. These high values may be the cause of non-systematic measurement errors).

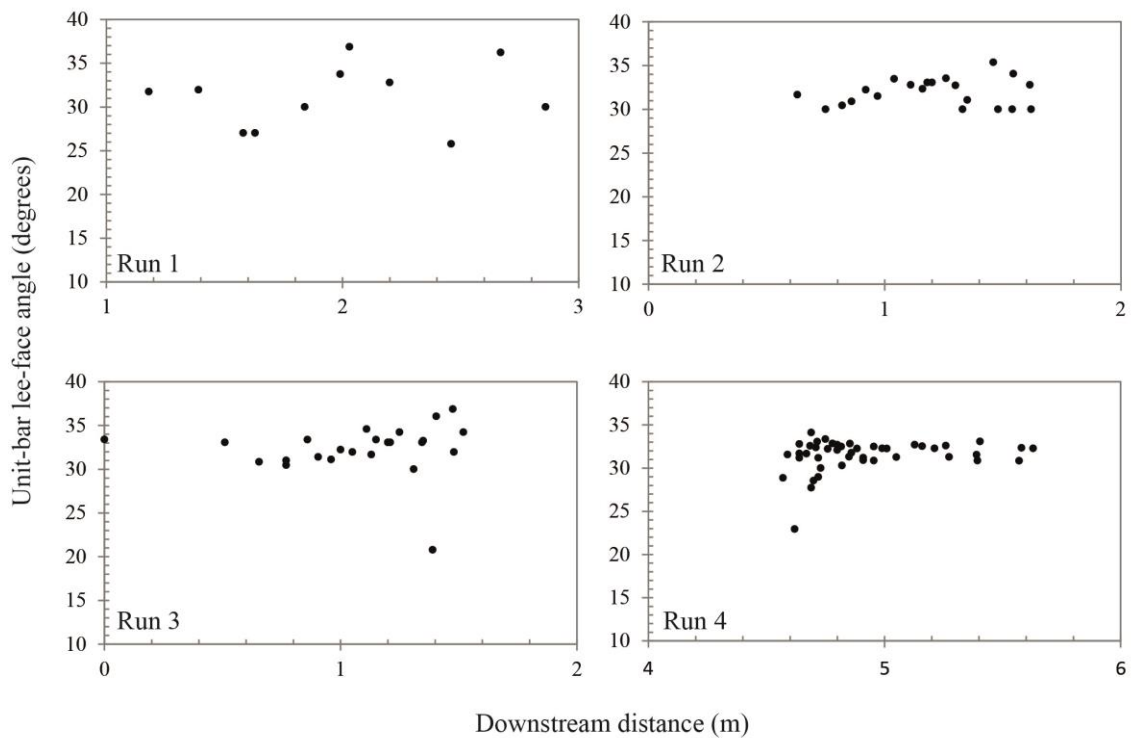


Figure 5.21 Representation of unit-bar lee-face angle variation with time (Runs 1-4).

Aiming to find what factors may control the variation of unit-bar cross-bed inclination and following the theory that the different contributions of avalanching sediment and suspension fallout could change the slope with different sized slip faces; the lee-face angle was compared to the unit-bar height (Fig. 5.22) (cf. discussion Section 6.4.1).

Although, no apparent resolvable relationship between bar height and bar lee-face angle was found in this set of experiments, Figure 5.22 shows the lee-face angle fluctuations become smaller as the bar height increases. This indicates that bar height variations as the unit bar moves over the topography may only have a small laminae-scale impact on the variation of the lee-face angle. Although the bar height (referred as the lee-face height; cf. Fig. 5.8) decreases gradually with time and the bar advances downstream in Runs 1-4, the mean elevation of the brink point with respect to the bottom of the channel did not vary significantly. Herein, it remains unclear, if this could explain if the no measureable relationship between bar lee-face angle and bar height variations.

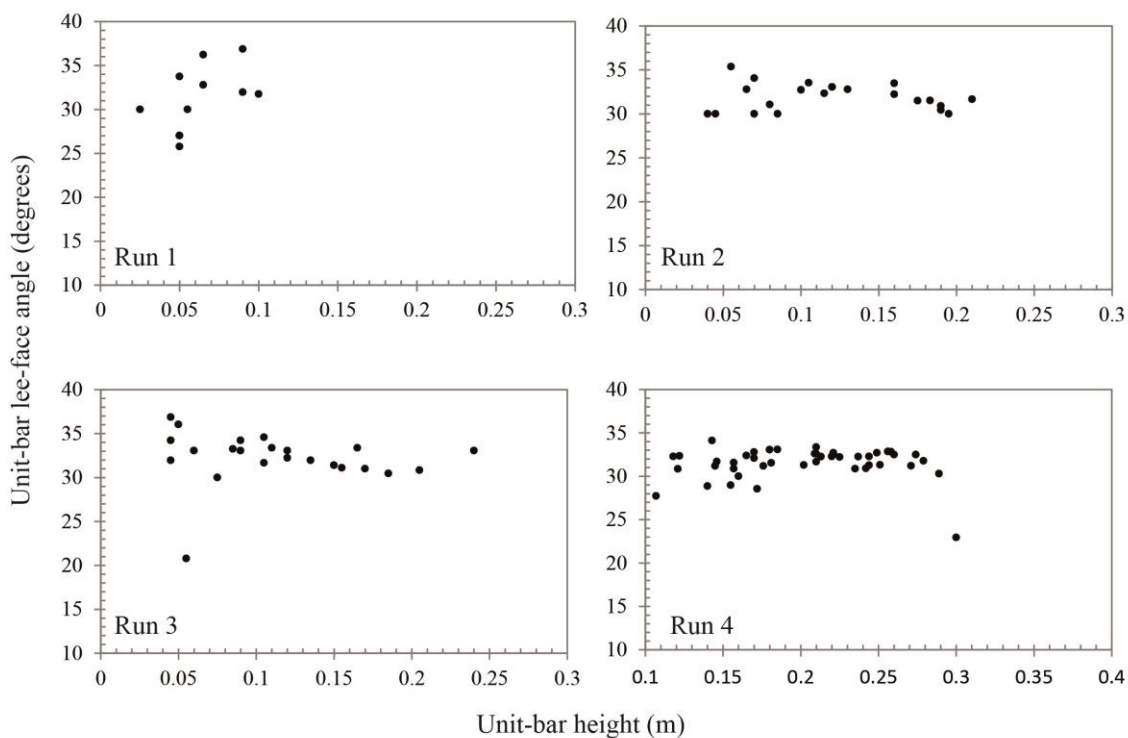


Figure 5.22 Representation of unit-bar lee-face angle variation with unit-bar height (Runs 1-4).

5.3.9 Reactivation surfaces and bar lee-face angle variations

Reesink & Bridge (2007) described examples in their flume experiments where locally the inclination of the foresets of unit bars decreased and the brink points were eroded, and referred to these as reactivation surfaces. In these experiments, reactivation surface formation was observed in all four runs, but due to subsequent bedform superimposition most of these surfaces were truncated and only the final deposits of Runs 2 and 4 preserved recognisable reactivation surfaces (Figs. 5.4 and 5.5). Inherent in the formation of these surfaces is a temporal change in the bar lee-face angle, at least in its upper part. These surfaces may be misnamed as, in this case, they do not relate to changes in mean flow conditions, as for example occurs in tidal settings where reactivation surfaces are often observed (McCabe and Jones, 1977), but rather being due to the passage of larger superimposed bedforms over the crest of the bar. However, because of the established usages of “reactivation surface” for this geometry of lamination its use is continued herein (cf. Section 6.4.3).

As these tall superimposed bedforms get near the brink of the bar, a smaller separation zone forms in the upper part of the unit-bar lee and the flow erodes the unit-bar brink point, reducing the dip of the bar’s lee face, forming what appears to be a “reactivation surface”. The tall superimposed bedform amalgamates with the unit-bar brink point and reduces in height due to erosive eddies in the top of the unit-bar lee face and sediment avalanching down the lee face over a softer lee-face angle preserving the “reactivation surface”. A new superimposed bedform of smaller scale approaches the unit-bar brink point and re-establishes the longer and steeper slip face as the superimposed bedform slip face merges with the unit bar’s lee face (Fig. 5.23). Reesink & Bridge (2009) considered reactivation surfaces of this type as evidence for superimposed bedforms exceeding 25 % of the host bedform height, generating a decrease in the lee slope angle.

In Runs 1, 2 and 4 reactivation surfaces were preserved beyond the topographic depression after the unit bar had moved downstream and filled the depression.

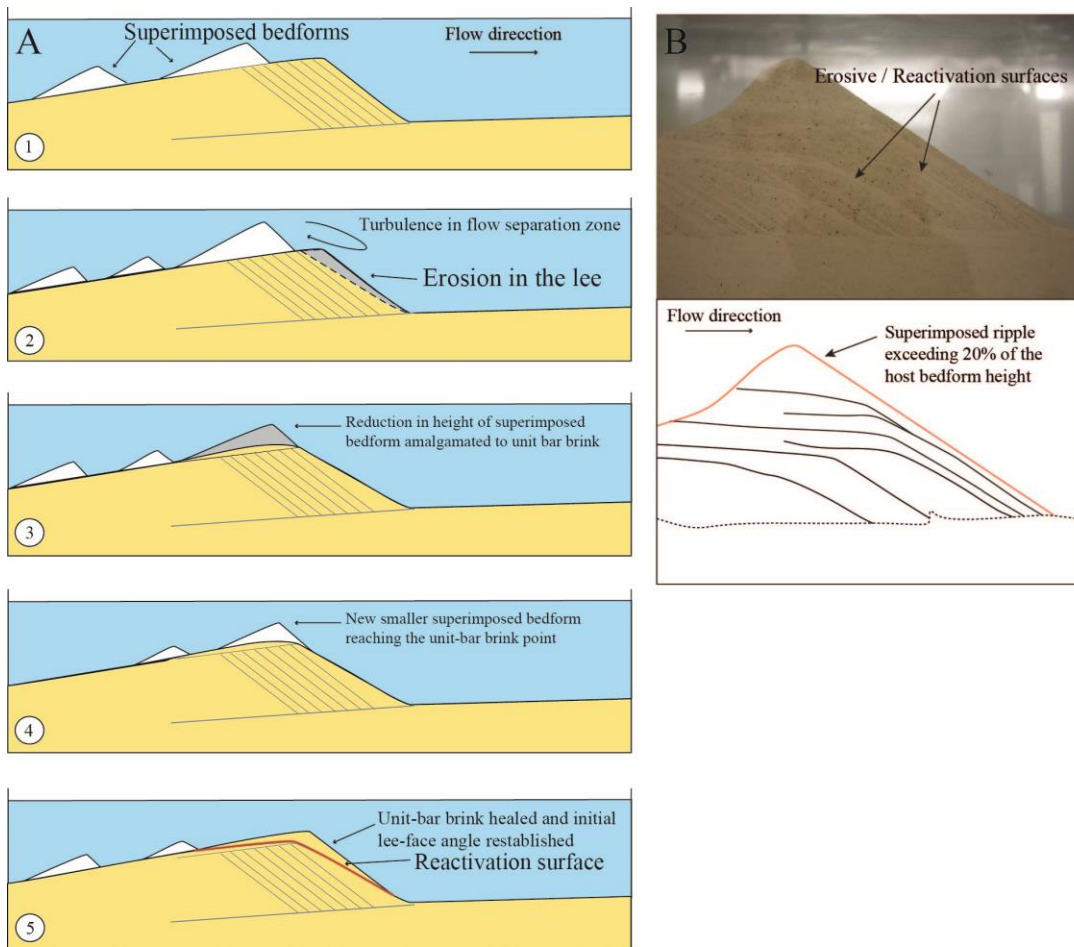


Figure 5.23 (A) Illustration of reactivation surfaces formation due to tall superimposed bedforms overtaking host bedform: (1) Bedforms migrating over a unit bar; (2) Tall superimposed bedform approaches unit-bar brink point causing erosion of the unit-bar lee face temporarily reducing the lee-face angle; (3) Tall superimposed bedform amalgamates with unit-bar brink point and reduces in height due to turbulent eddies in the flow separation zone above the lee and sediment avalanching down the lee face forming a reactivation surface; (4) Smaller-scale superimposed bedform approaches the unit-bar brink point; (5) Small-scale superimposed bedform reaches the brink point and re-establishes the longer steeper slip face, as the superimposed bedform slip face merges with the unit bar's lee face; (B) Preservation of reactivation surfaces (Run 1).

5.3.10 Evolution of bed topography and sediment feedback

As a unit bar advances downstream, its dimensions change and the topography over which it moves evolves, because of feedback between the flow, sediment transport and the sand bed. The main factors involved in this feedback are: sediment flux from upstream, entrainment of sediment from the bar stoss, deposition from saltation and suspension, sediment avalanching down the unit-bar lee face, reworking of sediment within the separation eddy in the lee of the bar, and the pattern of water flow.

Sand bed load moving downstream towards the unit-bar lee-face brink avalanches down the slip face incrementally advancing the bar face downstream. Sediment carried in suspension from upstream, may deposit on the unit-bar lee face adding to its advance; or it may travel some distance beyond the toe of the unit bar depositing in the trough or further downstream. Suspension fallout in the trough is encouraged by the flow separation and contributes to the basal unit thickness and reduces the depth of the trough (cf. bottomset formation on Sections 5.3.7 and 6.4.4). The sediment on the unit-bar lee-face toe and the floor of the trough may be reworked by the return flow in the separation zone. At the start of each run the channel bed within the trough was smooth and mainly flat, but soon after starting the runs, counter-flow ripples formed by reworking the sand that initially formed the pre-run bed of the trough (cf. counter-flow ripple formation on Section 5.3.5). Towards the downstream end of the trough (rising to the flat bed), sedimentation occurs by suspension fallout and downstream traction (growth of ripples).

5.4 Discussion

5.4.1 Classification of cross-stratification

The cross-stratified units formed in Runs 1-4 do not fit easily into Allen's (1963a) classification. Following Allen's (1963a) six objective criteria (*op sit*) Runs 1-4 sets are *large-scale solitary* cross-stratification sets, underlain by *non-erosional and erosional essentially planar-shaped surfaces but also trough-shaped surfaces* (assuming some 3 dimensionality if the flume were wider). The sets are *discordant* with respect to the lower boundary and *lithologically homogeneous*. Thus, these sets have some aspects of Allen's alpha, beta, gamma, theta and omikron types. Types *Alpha*, *Beta*, *Gamma* and *Theta* are large-scale solitary cross-stratified sets. The cross beds are discordant with the lower boundary surface of the set and are lithologically homogeneous. The surfaces beneath alpha, beta and gamma set types are planar non-erosional, planar erosional and irregular erosional respectively. Theta cross-stratification is dominated by erosional trough-shaped lower set boundaries. *Omikron* type cross-stratification is lithologically homogeneous grouped large-scale sets, where sets are separated by planar and erosional surfaces. Cross beds are discordant only in one direction and in the front section layers are evenly parallel. These classes were most likely formed due to the construction of

solitary banks with straight or curved edges in shallow water. They could have also been formed due to migration of trains of large-scale ripples mainly with straight crests. The cross-stratification in Runs 1-4 had erosional/non-erosional, planar/irregular lower boundary surfaces (trough-shaped boundary surface could be also considered: however, herein due to the experiment set up the basal surface is most likely to represent a planar shape, which can be compared to Facies Sp observed at Seaton Sluice, cf. Section 6.4.6). Within the trough, between the initial topographic surface and the bottom of the cross beds, was a layer of massive sand (or bottomset) passing up into ripple cross-lamination with counter-flow ripples causing irregularities at the base of the cross set. Occasionally, irregularities over the sand bed were observed due to the formation of small ripples and/or undulations caused by flow behaviour. Due to the dimensions of the flume and the conditions applied in this set of experiments, the resulting deposits formed only one set of bar-scale cross beds, however, this set was truncated and overlain by structures formed by superimposed bedforms. If Runs 1-4 had lasted longer, erosional surfaces would have separated this set from any that formed subsequently.

The cross-strata sets produced in the flume experiments do not fit perfectly into any of these classes. In addition, Allen's (1963a) classification did not take into account the evolution of the initial topography over which the cross beds formed and so, the possibility of a general planar or trough-shaped base as the boundary surface between (1) the main cross set from (2) the underlying bottomset generated by sediment feedback with topography, which may also have an irregular surface caused by counter-flow ripples (cf. Section 5.3.7). Thus, two new classes are proposed herein; *rho* and *sigma*. Both classes are dominated by the same characteristics. *Rho* type cross-stratification is a solitary set and *Sigma* are grouped sets. Both classes include a section of planar underlying surface and also concave-up surface (Table 5.1).

These two new types of cross-stratified unit involve several sedimentation mechanisms including: deposition at the bar crest and grain flow down the lee face, deposition from suspension on the lee face and in the trough, and sediments reworking in traction within the flow separation zone (including counter-flow ripple formation in the trough and on the lower parts of the bar lee face). In these experiments the deposit is relatively homogeneous because of the restricted sediments used (Fig. 5.2b).

5.4.2 Bar height variation and bar lee-face angle

Sediment supply and flow velocity affect the distance reached by grain flows down the unit-bar avalanche face, which influences slip-face angle and may be also related to the fluctuations in unit-bar height. Although a continuous pattern of variation between the height and lee-face angle was not observed, a scatter of the bar height was observed in relation to the advance of the bar downstream as it migrated over a non-fixed topography. In addition, the lee-face angle variations appear to decrease as the bar height increased. Given this, it is likely that variations in bedform height may relate to certain extent to the variations in the lee-face angle. If this is true, this could lead to new understanding of large-scale bedform dynamics and their variations.

Then, in addition to the variations of sediment flux and water depth that control variations of bedform height; in these experiments the variation of the unit-bar height above the trough was also affected by (1) the progradation of the unit-bar over the non-fixed topography; (2) superimposition of bedforms on the stoss with the associated trough scouring and lee-face amalgamations; (3) formation and behaviour variation of counter-flow ripples in the lee and the bar trough; and (4) changing topography of the depression as the unit bar migrated.

The factors controlling the height variations of host or superimposed bedforms as they advance downstream in unidirectional steady and unsteady flow conditions have become easier to study with improving technology. Gabel (1993) observing dunes in the Calamus River, Nebraska, USA, found that the size of individual dunes changed as they migrated under unsteady or steady flow. The constant creation and destruction of dunes observed in Runs 1-4 was also seen in the Calamus River and Gabel (1993) attributed this to variations in sediment transport rate and bed shear stress and not to discharge variations. Higher sediment transport rates can produce an increase in bedform height and scour depth. This agrees with Bennett and Bridge's (1995) experimental work that showed that the increase of bedform height and length could be a response to an increase of bedform period at higher shear stresses. Under longer unsteady flow conditions, bedforms have more time to grow and therefore, they tend to have a higher mean height. Hence, under equivalent shear stress in steady equilibrium flow conditions, dunes will reach higher heights than dunes under unsteady flows. Furthermore, dunes

forming under unsteady flow conditions will increase in height as the water depth and duration of flow increase (Lunt *et al.*, 2004).

The shape and dimensions of the flow separation zone on dune lee sides has an effect on sediment transport (Bennett & Bridge, 1995); which can also contribute to variations of the topography within the trough and then to the host bedform height. In Runs 1-4, the topography downstream of the unit bar changed during each run, affecting the development of the unit bar. Then, by comparison, variations of the dimensions of the initial depression downstream of the unit bar in the experiments described in this chapter control the variation of the unit-bar height.

Bedform superimposition can contribute to an increase in the height of the host bedform. Superimposed bedforms moving at different migrating rates tend to amalgamate each other and frequently they generate a higher bedform that will significantly increase the host bedform height as it reaches its brink point. In these experiments it is observed how trough-scouring in between superimposed bedforms climbing over the unit-bar stoss face tends to increase the height of the downstream superimposed bedform closer to the host bedform brink point and then, this will most likely contribute to an increase in the height of the unit bar (Section 5.3.4). This agrees with Leclair's (2002) experimental observations suggesting non-systematic variation in dune heights with dune height increasing due to trough-scouring, superimposition of ripples and by amalgamation with adjacent dunes. Interaction between the host and superimposed bedforms explains many aspects of the three-dimensional geometries of the resulting cross-bedding. Flow unsteadiness causes variations in the type and direction of migration of ripples and dunes superimposed on bars (Reesink & Bridge, 2011). Smaller ripple-scale bedforms superimposing on unit bars can generate a decrease of lee-faces length and steeper cross-bedding angles.

Lunt *et al.* (2004) states that “*generally as the height increases then the migration rate decreases*”. In Run 3, the migration rates at 1 hour intervals (over the total 24 hours run) appear mainly to decrease as the bar height increased and vice versa (Appendix C, Table C9), supporting this contention; but in Runs 1, 2 and 4, there is no obvious relationship between height of the unit-bar and migration rates. This data does not show a systematic pattern that relates migration rate and bedform height (Fig. 5.24). In

contrast, Leclair's (2000) observations suggest that no correlation between migration rate and dune height is measurable.

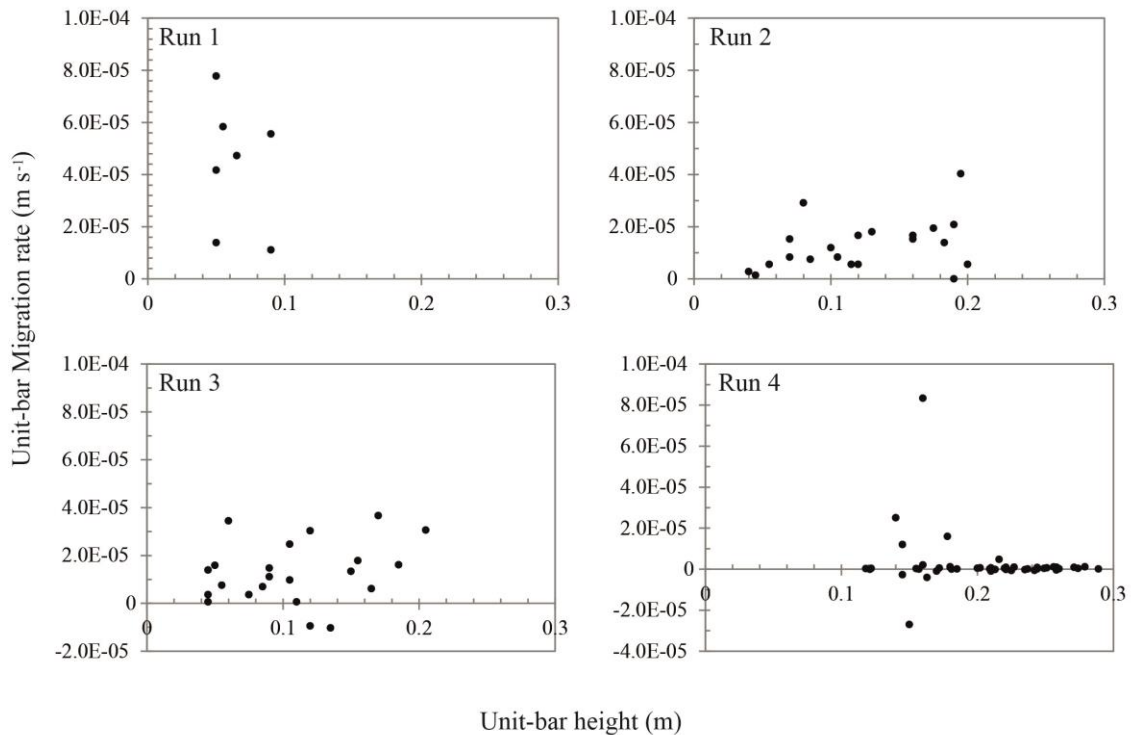


Figure 5.24 Unit-bar migration rate variation with the unit-bar height (Runs 1-4).

5.4.3 Reactivation surfaces and bar lee-face angle

Reactivation surfaces have been observed in several different environments and attributed to different mechanisms. Jopling (1965) described a type of surface equivalent to a reactivation surface as being formed in a flume at certain depth by the action of waves generating round bedform crests. Collinson (1970) observed reactivation surfaces on bars in the Tana River, Norway, formed during low-modification stages of large-scale bedforms. Klein (1970) attributed similar structures in tidal dunes to changes in tide direction. Allen (1973) identified reactivation surfaces that formed under a constant discharge due to the interaction between smaller-scale bedforms superimposition on a larger bedform. Jackson (1976) added that vigorous eddies in the bedform lee were favourable for the formation of these surfaces. McCabe & Jones (1977) defined reactivation surfaces as “*inclined surfaces within a cross-bed set which separates adjacent foresets, with similar orientations, and truncates the lower foreset laminae*”. They used a superimposed flume delta and they set steady flow conditions; the reactivation surfaces were generated as individual ripples were washed out (they

also form under unsteady flow conditions). They applied these observations to a range of environments including in-channel deltas and large-scale bedforms with superimposed bedforms. Jones (1979) identified two types “*internal erosive surfaces*” that truncate the foresets within Upper Carboniferous fluvial deposits, in the southern Pennines, England: convex upwards and concave upwards. Reesink and Bridge (2009) suggested that superimposed ripples that exceed 25% of a host dune height form reactivation surfaces and reduce the lee slope of the host bedform.

In Runs 1-4 multiple reactivation surfaces formed under steady flow conditions in a recirculating straight flume (as suggested by Allen, 1973) and some of them were preserved in the deposits. These reactivation surfaces formed due to the interaction of superimposed bedforms and the unit bar by modification of the crest of the bar (cf. Jones, 1977). In Runs 1-4 reactivation surfaces formed when the superimposed bedforms exceeded at least 30% of the unit-bar height. This agrees with Reesink and Bridge’s suggestion that superimposed bedforms must exceed 25 % of the unit-bar height. Reesink and Bridge’s suggested threshold of ($H_s/H > 0.25$) was not verified since no reactivation surfaces formed by superimposed bedforms with heights exceeding between 25 % and 30 % were observed in these experiments.

When a superimposed bedform approached the brink of the unit bar; often there was another superimposed bedform near the brink (Fig. 5.25A, B). This was washed out once the larger superimposed bedform reached the brink and amalgamated with the remaining part of that smaller ripple. Due to the flow pattern, the size of the small ripple closer to the brink decreases; and the erosion rate increases in the scour up-channel of this ripple as a new tall superimposed bedform approaches. Then, as the new amalgamated tall superimposed bedform approaches to the unit-bar brink point, the unit-bar lee-face angle decreases due to erosion of the brink point and upper part of the slip face. The tall superimposed bedform finally overtakes the unit-bar as it reduces its height due to eddies in the upper lee face and sediment avalanching down the lee face forming a reactivation surface. This surface will be preserved by a new smaller-scale superimposed bedform reaching the unit-bar brink point. As this new superimposed bedform overtakes the unit bar, the brink will be healed and the initial inclination of the unit-bar foresets will be re-established. This indicates that the decrease in lee-face angle is only temporary (Fig. 5.25C).

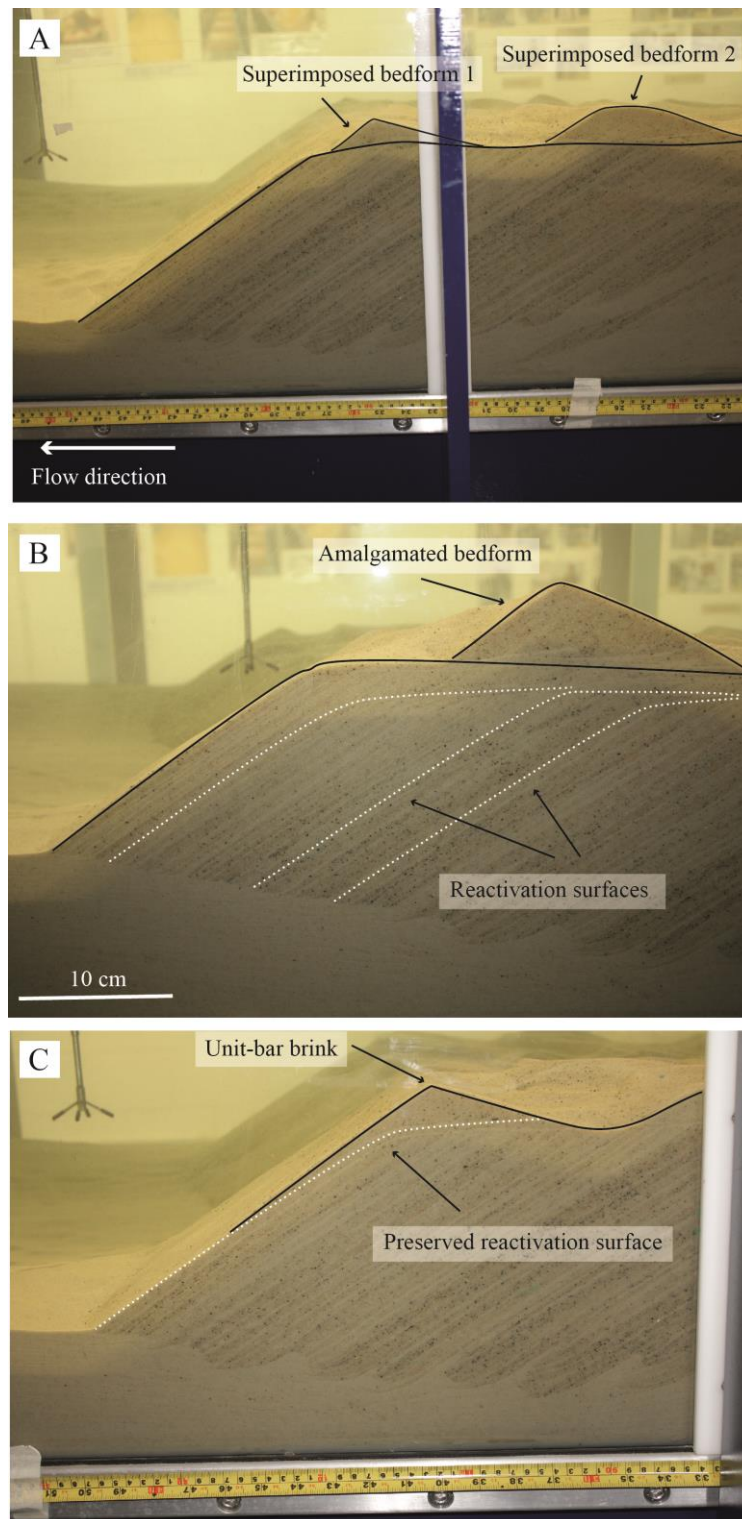


Figure 5.25 Preservation of reactivation surfaces. (A) Superimposed bedforms advancing over the unit-bar stoss face; (B) Superimposed bedforms amalgamated forming a taller bedform reaching the unit-bar brink and (C) Superimposed bedform already amalgamated with the unit-bar brink (slightly eroded) and preserved reactivation surface. N.B., These photographs were not taken chronologically; they correspond to Runs 1 and 2 and they were selected to illustrate the referred text.

A reactivation surface can be formed from the relic of the profile of a single large bedform, or by amalgamation of surfaces formed by several superimposed bedforms eroding the stoss face of the unit bar creating this continuous lower-angle surface separating the unit-bar cross-bed sets from the superimposed bedform set. The depth of erosion of the reactivation surfaces is important and varies depending on the intensity of the erosion generated within the scour just up-channel of the crest of the unit bar (McCabe & Jones, 1977). When scour is intense, reactivation surfaces cut deeper into the bar and are more likely to be preserved (Jones, 1977). The grade of preservation also depends on the level of truncation events due to later superimposed bedforms.

In the flume, when a superimposed bedform reached the brink of the bar, the height of bar was increased by the height of the superimposed bedform, however, this increase only lasted for a short time before sediment at the brink collapsed and avalanched down the unit-bar lee face. As the trough in the lee of the successive bedform approached the bar crest, scour cut down the bar brink, forming a reactivation surface that is then buried as the superimposed bedform prograded over it. If the superimposed bedforms were of a uniform size and shape, the passage of each one would destroy the evidence for the earlier ones. The size of superimposed bedforms varies however, and some sequences of size variation produce a deep incision into the bar lee face deposits and subsequent rebuilding of the bar face, forming pronounced reactivation surfaces.

Well preserved unit-bar crests or brink point areas form part of cross beds with lower angle, which in previous studies has been interpreted as reactivation surfaces and also as stages in which the lee-face angle of the unit bar decreases. According to Reesink & Bridge (2007) superimposed bedforms that are 25% the height of the host bedform, will overtake the host and generate a slight decrease in the inclination of the foresets. However, this is not what was observed in the runs presented herein. On the basis of the various definitions of a “reactivation surface”, which summarising consists of the modification of a steep angle cross bed already formed, the formation of reactivation surfaces does not produce a decrease in the unit-bar lee-face angle but a modification of the shape of the deposited cross beds and this modified surface has a lower angle than the cross bed deposited previously or subsequently. These surfaces become bounding surfaces distinguishing intra-sets within a set. According to Klein (1970), when a

reactivation surface forms due to a change in flow direction, the flow can re-establish the current direction; then new foresets with the initial steep inclination will form over the erosive surface. In these experiments the flow conditions were constant, therefore after the formation of the reactivation surface, cross beds formed at the initial steep angle. Stating that reactivation surfaces decrease the angle of foresets can mislead us to think that a reactivation surface corresponds to an original unit-bar stoss face while a large superimposed bedform overtook a large-scale bedform. The decrease in lee-face angle did not occur while the cross beds were forming but by erosion and preservation of the erosion surface by new cross-beds formation. The reactivation surfaces dip at less than the angle-of-repose and indicate erosion of the unit-bar brink due to bedform superimposition by bedforms exceeding at least 30% of the host-bedform height in these experiments and 25% according to Reesink and Bridge (2009) (cf. Section 6.4.3).

5.4.4 Topography variation and bar lee-face angle

Although there have been numerous studies on the morphology of river beds and their evolution focusing on bedform development and the impact of this for fluvial system responses and interaction between the dynamics of the flow, sediment transport and grain flow development (e.g., Alexander, 1992; Miall and Jones 2003; Best *et al.*, 2003; Kleinhans, 2004; Reesink and Bridge, 2011; Rodrigues *et al.*, 2012; Parsons and Best, 2013 and Guinassi *et al.*, 2014) there is a lack of literature on the specific effect of scour topography on the evolution of bedforms, and little published on scour dimensions and longevity. Variation of scour geometry has an effect on the evolution of the bed morphology. In Runs 1-4, although the initial topography was imposed, it changed through the runs (Fig. 5.26). Sediment transported from upstream avalanched down the bar's lee face into the trough, entered the flow separation zone and fell to the bed, and sediment on the bed in the trough was reworked by the return current in the flow separation eddy. Together these three mechanisms caused the depression to change, resulting in a feedback with the advancing bar and flow (Fig. 5.26). In Run 1, the depression (initial volume $3.65 \times 10^{-2} \text{ m}^3$) filled in approximately 5 hours and the mean water surface elevation was 0.496 m. Under these conditions, the sediment volume due to feedback was approximately $9.5 \times 10^{-2} \text{ m}^3$. In Run 2, the initial depression volume and the water surface elevation were 0.2 m^3 and 0.488 m respectively. In the time interval of 24 hours, the sediment volume due to feedback was approximately of $13.05 \times 10^{-2} \text{ m}^3$. In Runs 1 and 2, the sediment volume due to feedback included sediment deposited over

the flat bed beyond the depression. In Run 3, the depression was filled within 24 hours; the bar depression volume was approximately of $9.25 \times 10^{-2} \text{ m}^3$ and mean water surface elevation was 0.491 m. The resulting sediment due to feedback that occurred during the run was $9.12 \times 10^{-2} \text{ m}^3$. Finally, Run 4 with duration of 79 hours and 56 minutes; the volume of the initial depression of $9.43 \times 10^{-2} \text{ m}^3$ and mean water elevation of 0.695 m resulted in $7.07 \times 10^{-2} \text{ m}^3$ of sediment volume due to feedback. In Runs 1-3, where the bar was built at the upstream end, flow velocities were higher and water levels were shallower, sediment deposited due to feedback were also higher than in Run 4 in which the set-up was built in the middle of the channel, flow velocity was lower and water level was higher.

In Runs 2-4 the sediment volume due to feedback (sediment that formed the basal unit) was smaller than the initial volume of the trough. In contrast, in Run 1 this sediment was larger than the initial volume of the trough by 5.85 m^3 . This can be explained by the ratio between the amount of sand dumped in the upstream end and the initial size of the trough and the higher migration rate just after starting the pumps. This highlights the importance of an appropriate and accurate experiment set-up. In Run 4, the shape of the artificially built unit bar was more realistic, and hence so are the resulting deposits. Observations throughout Runs 1-3 showed that sediment feedback occurs mainly during the first minutes of each run until the excess of sediment in the upstream end settled. This explains the rapid decrease of migration rates (Runs 1-3) from $t = 02:00$ and $t = 03:00$ onwards (in Run 1: from $1.92 \times 10^{-4} \text{ m s}^{-1}$ to $4.37 \times 10^{-5} \text{ m s}^{-1}$; in Run 2: from $1.71 \times 10^{-4} \text{ m s}^{-1}$ to $1.28 \times 10^{-5} \text{ m s}^{-1}$; in Run 3: from $1.44 \times 10^{-4} \text{ m s}^{-1}$ to 1.27×10^{-5}). In Run 4, the sediment feedback occurs mainly during the migration of the unit bar downstream. The location of bedforms within the channel, flow velocity and water depth control the sediment deposited because of feedback. Sediment deposition and reworked sediment, causing an aggradational massive sandy base, control the preservation of the unit-bar dimensions and the life time of these large bedforms. The lee-face angle at lower set boundaries varies progressively due to the dynamics of counter-flow ripples. The topography variation by the increase of bottomset depths and influences the variations on bar height; and as mentioned previously, lee-face angle scatter in these experiments related to height variations. In addition, formation of counter-flow ripples in trough of the unit bar modified the topography.

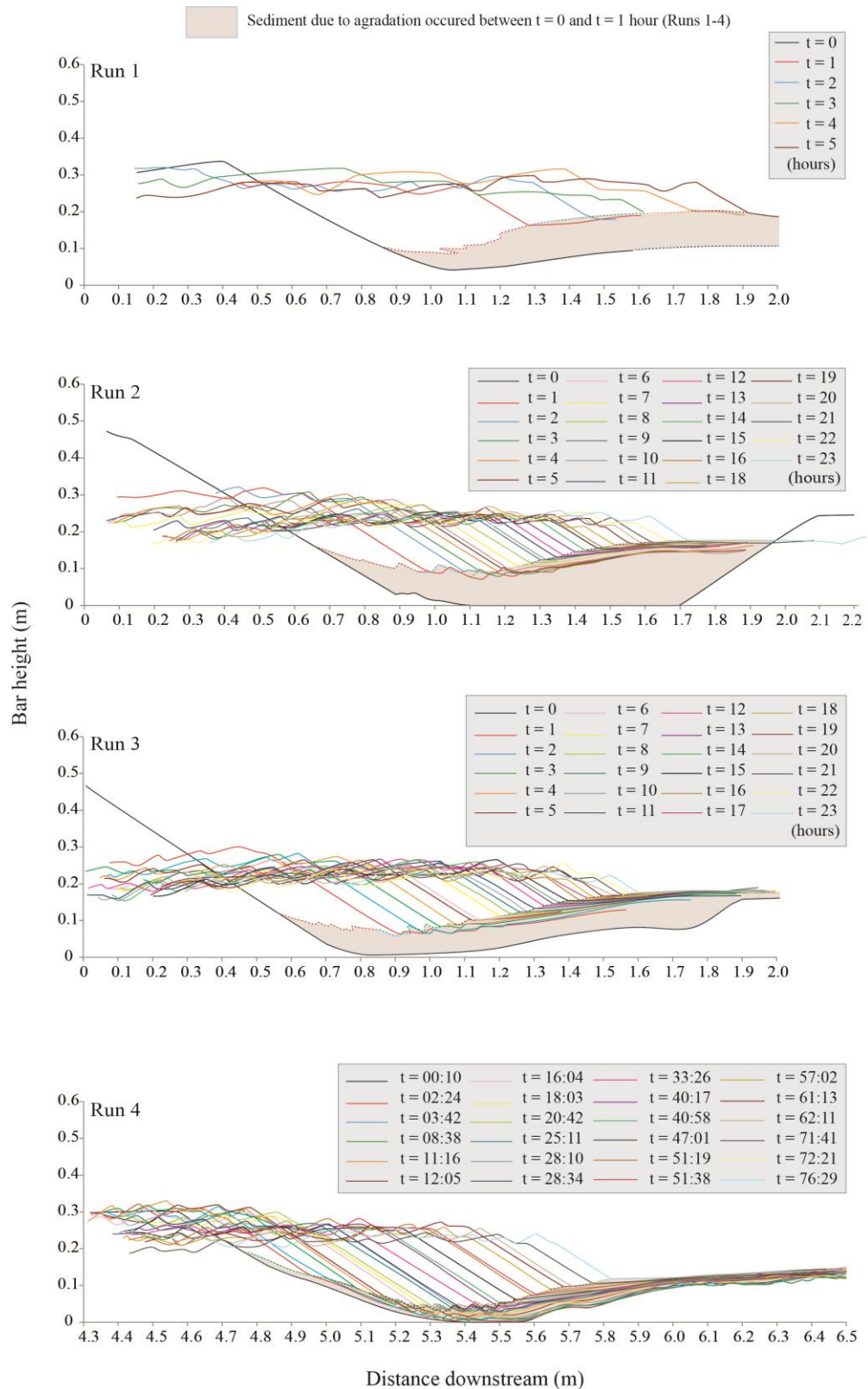


Figure 5.26 Evolution of unit-bar morphology as bar advances downstream, showing the development of initial channel bed topography throughout Runs 1-4 and sediment feedback occurred mainly by sediment deposition and aggradation between $t = 0$ and $t = 1$ hours. N.B., in the Run 4 sketch, the sediment due to aggradation appears slightly masked due to the colour lines.

5.5 Conclusions

This chapter is based on four long experimental flume runs and observations of flume-scale unit bars migrating downstream over a non-fixed topography, under steady flow conditions. The main findings following the work in Runs 1-4 are:

- No resolvable relationship between bar height and bar lee-face angle under a constant discharge with the sediment and flume scale used was observed.
- The bar height scatter decreases as the bar progrades downstream over a non-fixed depression and the lee-face angle scatter decreases as the bar height increases.
- No systematic pattern of bar lee-face angle variation was found.
- The mean vertical distance (distance from brink point to the bottom of the channel) does not vary significantly.
- There is a decrease in mean bed thickness of 0.05m and mean static and non-static water surface elevation of 0.06 and 0.07 m respectively throughout the runs. The sediment loss was interpreted as sediment deposited within the close loop of pipes in the flume and possibly due to the sediment packing arrangement and porosity variation. The decrease in water surface elevation occurred due to initially unidentified tank leaks. These variations can also contribute to the bar height scatter.
- Bedform superimposition influences and bedform amalgamation near the unit-bar brink point influences sediment avalanching down the unit-bar lee face and contributes to variations of unit-bar height.
- Reactivation surfaces formed in Runs 1-4, when superimposed bedform heights exceeded at least 30 % of the unit-bar height and eroded the bar brink point as they overtook the unit bar. This partly agrees with Reesink and Bridge's (2009) suggestion of reactivation surfaces indicating superimposed bedforms with heights exceeding 25% of the host bedform height. These surfaces can be wrongly interpreted as cross beds within the same set, dipping at less than the angle of repose, indicating a decrease of the unit-bar lee-face angle. They indicate significant erosion of the unit-bar brink due to bedform superimposition and can cause temporal variation of lee-face angle as the new foresets after the formation of a reactivations surface will have the initial steeper inclination.

- The initial topography over which the bar progrades can be altered by grain falls (settling of suspended sediment), sediment previously deposited in the bar trough remobilised by reverse flows resulting on small counter-flow ripples forming in the trough and lower part of the lee face.
- The continuous formation of counter-flow ripples in the lower part of the unit-bar lee face reduces the lee-face angle producing tangential contacts between the foreset laminae and the trough ahead of the counter-flow ripple. This causes alterations in the initial topography that will affect the variations of the unit-bar height.
- Sediment bottomsets between 0.06 and 0.08 m thick form underlying the cross beds. They consist of a layer of structureless sand with a ripple-cross laminated upper surface; and they form due to sediment deposition mainly by (1) settling of suspended sediment on the lee face and floor of the depression and (2) reworked sediment by the return flow in the lee of the bar.
- Allen's classification (1963a) did not take into account the evolution of the initial topography over which the cross-strata. Therefore cross-stratification (lamination) resulting from Runs 1-4 were used to add to new types to Allen's (1963a) classification and were described as large-scale solitary (*Type Sigma*) and grouped (*Type Rho*) cross-stratified sets underlain by non-erosional and erosional surfaces, with either trough, planar or irregular lower boundary shape, discordant and lithologically homogeneous respect to the lower boundary.
- The position of the host bedform within the channel determines to certain extent the character and relative importance of superimposed bedforms and the factors controlling the final architecture of cross-bedding. Although this could be seen as a serious limitation of flume experimentation it is also suggestive that location within a natural channel will be important and should be investigated.
- The dimensions of the unit-bar initial depression influence the architecture of the preserved cross-stratification.
- Further investigations, based on experimental work using a fix-designed bed using several steady and unsteady flow conditions, will help to determine and discard variables as controls of the internal architecture of cross-stratification and its variations.

Chapter 6

Field and Laboratory Research Synthesis

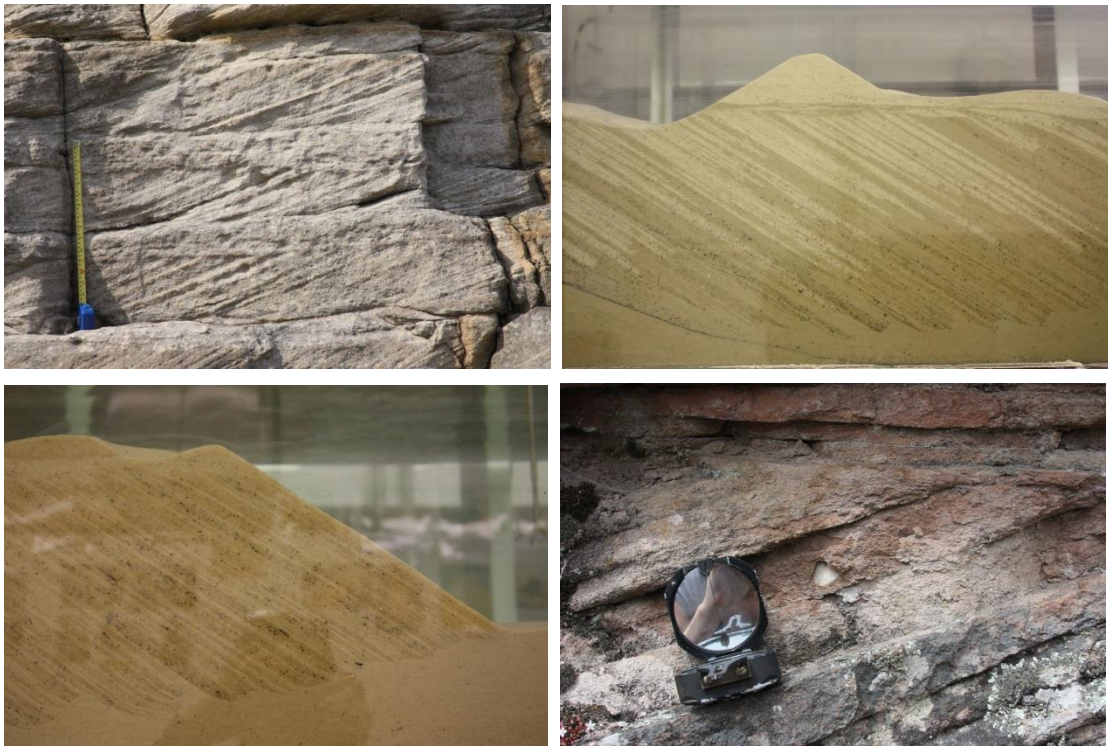


Photo: Flume and rock record examples of cross-stratification

6.1 Introduction

This project aims to improve the understanding of fluvial cross-bedded sandstones and the physical processes responsible for particular characteristics of sedimentary structures generated by unidirectional flow that may form cross-bedded sand. In this chapter, aspects of the field and flume research are compared in an attempt to address this aim.

In the flume, the conditions and factors that modified or affect the architecture of cross-bedding were observed. In the field, the preserved cross-bedding were studied to determine what the flow and river conditions were when the sediment was deposited. Initially, interpretation of cross-bedded sandstones often seems very straight forward, particularly where it is following on from previous work. Generally geologists tend to follow some previous classification system using traditional definitions of architectural elements and facies, and they “*see*” what they have been taught to look for. Small details that might be important clues to interpretation are often overlooked, either being considered as not relevant or not taken into account for some other reason.

In the flume, it is possible to use specific setups for each run, enabling to focus on specific controls on deposit characteristics and use these observations to improve interpretations of preserved deposits from ancient fluvial systems. There are very many different factors to investigate, and what can be investigated depends on the laboratory configuration, particularly scale limitations and the time and equipment available.

Initially, part of this research project aimed to investigate the transition from 2D to 3D dunes with the intention of examining equilibrium dune pattern in different flow conditions (cf. Venditti *et al.*, 2005a). Several trials were undertaken in an attempt to address this aim, using the flume described in Chapter 5, but because of the limitations of channel shape and scale (particularly problems with width and side wall influence) the bedforms had to be very small to allow any consideration of 3-dimensional development. Their scale was near that of the ripples formed in the sand used; consequently it was not practical to proceed with these experiments because of the difficulty distinguishing bedform types and the complex interactions between ripples and dunes at this scale. A considerably deeper and wider flume is needed for these

investigations to allow generation of bigger dunes and avoid the limitation on 3-dimensional shape development by the side wall effects. As part of the trial experiments to investigate 2D to 3D dune transition, the flume was run for 20 hours, with some interruptions, slowly increasing water velocity to observe the evolution of bedforms from an initially flat-bed topography, and bedform migration downstream. Observations of this run suggested that the initiation of scour, its size and shape, are important for better understanding the 2D-3D dune transition and the resulting architecture of preserved cross-bed sets.

Attempts were also made to replicate Leclair's (2002) experiments on cross-bed preservation that suggest relationships between bedform size and cross-bed set thickness. Leclair (2002) investigated variations in the bed topography by using an ultrasonic bed profiler that recorded measurements of bed heights in the centre line within the experimental window of the flume at 0.2 s intervals. She also observed the effects of sediment aggradation on variation of bedform characteristics. She proposed an empirical relationship between the changes in dune-trough scouring and the migration rate for the simulation of dune migration and formation of cross-sets. This flume trial aimed to observe the controls of cross-bed formation and relate them to the geometries of cross-bed sets observed in the study areas. Due to the equipment limitations (e.g., the sonar bed profiler was not able to measure transects along the flume at short enough time intervals to record useful data), it was unable to monitor the evolution of dune-trough scouring reliably, and according to Leclair (2002), that appears to be the main mechanism by which dunes increase in height.

Following these relatively unsuccessful flume studies, new flume experiments were designed that were more suitable for the restrictions of the flume laboratory and the time available to address specific topics to help field interpretations of fluvial cross-bedded sandstones. These were: (1) lee-face angle, (2) influence of pre-event bed topography, (3) development of superimposed bedforms and their influence on the cross-beds formed by the host bedform and (4) the formation and characteristics of reactivation surfaces. The factors that need to be considered when comparing these flume experiments with the field research are discussed below (Section 6.3). These include: (1) dominant grain size and how this relates to the final sedimentary deposits, (2) discharge and sediment flux variability, and (3) river channel plan-form.

6.2 Different bedforms, similar processes?

The flume experiments described in Chapter 5 involved bed features of unit-bar type and the cross-bedding studied in detail in both field sites is mainly interpreted as the result of the migration of dunes. The obvious question therefore is what features and processes can be compared between different bedforms.

In the flume experiments described in Chapter 5, the resulting deposits formed by movement of the unit-bar were planar cross-bedded. Due to the nature of the flume tank the initial topography was nearly flat and the bottom of the initial trough was also nearly flat. In contrast in the field studies, trough cross-bedding dominated the Prados Formation and the Seaton Sluice Sandstone contains both trough and planar cross-bedding. Here as in many publications (e.g., Allen, 1968, 1983; Miall, 1977, 1985) trough cross-bedding is interpreted as the result of 3-dimensional dune migration (Section 2.5.1), although it could also be formed by linguoid bars or sinuous-crested bars in high-velocity flow (e.g., Singh and Kumar, 1974; Tyler and Ethridge, 1983) or result from the modification of fluvial-bars by bedform superimposition (Cant and Walker, 1978; Crowley, 1983). Planar cross-bedding observed in the Seaton Sluice Sandstone (Section 3.5.1) is common in the fluvial rock record and has been interpreted as the result of migration of straight-crested dunes (Alexander and Gawthorpe, 1993), longitudinal or transverse bars (Smith, 1972; Cant and Walker, 1978; Reesink and Bridge, 2011) and sandwaves (Harms *et al.*, 1975). Terminology is an issue since different authors have attributed the term “*sandwave*” to dunes and bars. Ashley (1989) summarised the consensus of a Meeting of SEPM (Society for Sedimentary Geology) in 1987 that attempted to unify several terminologies into one to define large-scale bedforms, without a great deal of success.

The discussion on the differentiation between large-scale dunes and unit bars is ongoing. Previous literature classified bedforms on the basis of their shape and size; and therefore unit bars are described as larger bedforms than dunes. Harm and Fahnestock (1965) differentiated dunes and bars by the continuity, orientation and scale of crest lines; and described bar crest lines as relatively long, even and commonly oriented at large angle to local current direction. Allen (1983b) differentiates dunes from bars based on their smaller size and interlocking nature. Best *et al.* (2003) classified sedimentary structures

observed in the Jamuna River, Bangladesh as formed by dunes or bars and distinguished them by their lateral and vertical extent (i.e., unit bars with larger vertical and lateral extension than dunes).

Bedforms are periodic and their morphology is related to the mean flow velocity and shear strength (e.g., Yalin, 1964; Southard, 1971; Raudviki, 1966). Dunes have been described as bedforms typical of higher-velocity ranges of subcritical flow where bedform height and flow depth are related. Unit bars are thought to be quasi-periodic or solitary storage bodies (Smith, 1974) within a channel. Other authors (e.g., Leopold and Wolman, 1957; Smith, 1971, 1974) suggested that unit bars form by a local hydraulic change (e.g., changes in water depth and flow regime) that reduces transport capacity, depositing the coarsest load and building up a sediment mound. Water surface configuration, flow structure and sediment transport rate are also controls on bedform morphology. Carling *et al.* (2000) suggested that the interaction of water surface with bedform crest characterises dune morphologies (i.e., dunes with gentle lee faces relate to weak flow separation).

In order to clarify and unify bedform descriptions, Ashley (1990) compiled a series of descriptors that should be used to describe and classify bedforms, these are: (1) size and shape; (2) bedform superimposition, grain size and sorting and (3) bedform profile, flow structure (time-velocity characteristics), bedform behaviour, migration; fraction of bedform covered by other bedforms, and relative strength of opposing flows.

All these classifications and various definitions of dunes and bars are acceptable and commonly used but because they may result in the same bedforms being classified in different ways they cause considerable disagreement and debate. Numerous previous studies tend to unify these terms and not to differentiate dunes from unit bars; and as a result the question on what units bar are and how to define them remains unclear. Identifying what characteristics allow the determination of which deposits were generated by dunes and which by unit bars would improve the understanding of the former system or is the formation of cross-bedding by one directly comparable with the other. This leads to other questions such as: Why do unit bars not appear in bedform stability diagrams? Where is the field dimension boundary between dune and bar? Does that depend on the dimensions of the channel?

Very large periodic bedforms in a large channel may be referred as dunes whereas bedforms with the same geometry and size in a smaller channel may be considered bars (as they appear to scale with the channel dimensions). Unit bars and dunes both take time to form and to change dimensions; and the bigger the bedform, in relation to the sediment flux, the longer it will take for it to change. Consequently, there will often be conditions where the bedforms interact in a flow that is different to that in which they formed. It takes less time to build big bedforms under deeper flow, than it takes for bedform size to diminish with reduced stage (Bridge, 2003). Dunes formed in one channel at high stage may act as bars in that same channel at low stage.

Small to medium-scale trough cross-bed sets formed by superimposed ripples and dunes are often observed truncating unit-bar deposits (Reesink and Bridge, 2011) and superimposed bedforms on large dunes are likely to behave similarly. The level of preservation controls the outcome of field interpretations and consideration of this generates questions such as: How much of a unit bar deposit will be preserved? Will cross-bedding formed by superimposed dunes on bars obscure the identification of unit bar deposits? Is the scale of the preserved cross-bed set(s) an indication of bar or dune size and occurrence? Do the relationships proposed by Leclair (2002) for dunes apply also to unit bars?

In this study dunes and unit bars are simply considered as large-scale subaqueous bedforms. This makes comparative analysis of the laboratory and field results easier. This is feasible because on the scale of the bedform similar processes occur, even though the initial formation mechanism and controls on the bedform may be different.

The variation in bedform geometry may be caused by slight variations in the processes occurring on the lee-face of the host bedforms (e.g., dune and unit bar). Sedimentation within the lee of bedforms occurs from three main processes and their interaction with one another: (1) grain flow; (2) grain fall (grain settling) and (3) remobilisation within the trough (e.g., formation of counter-flow ripples by traction). Kleinhans (2004) suggested as another depositional process in the lee of dunes “[individual] *grain rolling down the slope*”. Herein, this process is included in (1) and considered as the stage prior to grain flow down the lee slope. Based on previous literature, these processes are as likely to occur on steep-lee-face unit bars and dunes. Considering the sediment in the

bedload (moving in traction on the bed, saltating or in partly suspended) on the stoss side of a bedform, once it reaches the brink point of the bedform, be that a dune or a bar, some of it will be deposited on the lee face, and some will move well beyond the brink and be deposited lower on the lee face or in the trough or even the stoss face of the next bedform downstream if there is one (cf. Kleinhans, 2004). Added to this, sediment in suspension above the bed may enter the recirculation eddy in the lee of the bedform and settle to the bed. The sediment that is deposited on the lee slope accumulates until this fails and then the grains will avalanche down the lee face (grain flow). The sediment that settles from suspension (or partial suspension) within the trough of the host bedform (grain fall), with some of the distal parts of grain-flow deposits and possibly older sediment from previous deposits below the scour can be captured by reverse flow in the separation zone and be remobilised forming the bottomset of the bedform. In addition, counter-flow ripples may form in the trough of the bedform.

Although these processes occur on dunes and bars, the sediment deposition, size sorting and cross-strata type will depend on the controls on the processes such as: grain size distribution supplied, flow velocity above the brink point and discharge variability. Bedform size in relation to the flow depth and velocity controls the flow separation zone extent and recirculation speed and consequently sediment remobilization. Consequently the relative importance of the three main processes may differ in different settings. According to Reesink and Bridge (2009) higher rates of sediment transport cause frequent grain flows and larger amounts (and grade) of sediment in suspension that can be deposited on the bedform lee slope and trough.

Some characteristics observed in flume experiments may help to distinguish between bars and dunes. As mentioned above, some of the sediment settles within the trough of the bar or dune and form a bottomset. Reesink and Bridge (2009) suggested that thick and fine-grained bottom sets indicated that the formative bedform is a unit bar due to the deceleration within the separation zone in the lee of the bedform. This is consistent with the bedform phase diagram presented by Martinius and Van den Berg (2011), which considers the range of conditions in dunes where bottomsets will form. This concurs with Reesink and Bridge's (2009) flume experiments where counter-flow ripples were poorly developed in dune troughs. In the experiments reported in this thesis

counter-flow ripples were well developed within the unit-bar troughs (this is discussed further in Section 6.4.4).

Bedform superimposition influences the mean and turbulent flow field and causes large changes in sediment transport over bedforms (Fernandez *et al*, 2006). According to Reesink and Bridge (2011) cross-stratification formed by the migration of unit bars reflects variations of the type, geometry, and direction of migration of the superimposed bedforms that occurred. These variations cause changes in the grain size sorting of the sediment in transport. Also, bar sets are frequently intersected by low-angle reactivation surfaces formed by superimposed bedforms (see discussion in Section 5.4.3).

6.3 What can and cannot be usefully compared?

Although it may initially appear simple to do analytical flume tests and compare them with field observations of ancient sandstones, there are inevitably a very large number of assumptions needed to make such comparisons. There are factors that may have been overlooked in selecting flume experiments to compare with ancient deposits (or vice versa) due to the research time available, limited knowledge of controls, or experimental restrictions. To make any comparison between these different systems it is essential to consider, what can and cannot be usefully compared.

Some aspects that can be reasonably compared based on the work achieved in the laboratory and field are:

1. Lee-face angle and angle variation within individual laminae within cross-bedded sandstone and trough sets may be usefully compared with lee-face dip of a flume bedform at a single point in time or as the lee face advances with time. This comparison is sensible because the mechanisms that control the lee-face angle operate on both dunes and steep-lee face unit bars. The lee-face angle variation may be slightly different in a migrating dune compared with a migrating unit bar. Both types of bedform are characterised by different morphologies and also the topography of their troughs may differ. There are some distinctive characteristics that hint at the causes of the variation in lee-face angle, and the difference in lee-face variation pattern between the flume and the two field studies suggest that this is a topic that is deserving of further research.
2. The modifications of the bar lee face and preserved cross-bedding as

- superimposed bedforms grow and migrate, can be compared with set boundaries and laminae architecture caused by superimposed bedforms in the case studies. This includes the formation and preservation of reactivation surfaces and the implications that has on the lee slope variation.
3. Although the relationship between initial bed topography and the resulting architecture of cross-bedding cannot be analysed in ancient rocks; this can be observed by using flume experiments, which facilitates the effects of types of bed topography on the final architecture of sedimentary structures to be described. This could then be used as a tool for field interpretations.
 4. Bottomsets formed in the flume and bottomsets can be preserved in cross-bedded sandstones (although they were not observed in either of the case studies). Given that bedforms in the flume are unit bars and trough cross-bedding preserved in the field case studies is interpreted as formed by dune migration it would be useful to investigate whether similar bottomsets form as dune and bar migrate (this would require a different flume). Martinius and Van den Berg (2011) proposed a bedform stability diagram with fields indicating where bottomsets were likely to form or not form in relation to dunes. In the flume experiments described in Chapter 5, a bottom layer of structureless sand was formed during Runs 1-4. The comparison of this layer with bottomsets identified in cross-bedded sandstone would allow some assessment of how realistic the bottomsets generated in the flume are; and if they are comparable to natural bottomsets this would help to understand flow conditions forming the field deposits.
 5. Variations on the crestline of the unit bar and the implications on the bar lee-face angle observed in the flume, can be compared with the cross-bedding types observed in the field and the palaeocurrent variations within individual laminae of cross-sets. Although this can add useful information, field observations should be taken with care when the formative bedform has curved foresets, in which case, laminae dip variations can be apparent and not true.
 6. The comparison of the resulting cross-beds from the flume experiments, which involves the new two types of cross-stratified units added to Allen's (1963a) classification in this thesis, can be compared to the planar cross-bedding identified at Seaton Sluice. This highlights the importance of encouraging further work on bottomset formation and its implications on field interpretations.

With the available data there was not enough information to address the following questions:

1. Scour initiation and shape of the initial spoon-shape scours (Section 2.7.1) cannot be investigated in the flume and this has implications for the architecture of cross-bedding. In the flume experiments, it is possible to describe and quantify the dimensions and shape of the trough downstream the host bedform, but in the experiments presented here this was an antecedent feature and not formed by the flow that formed the cross-bedding. In the rock record only the final resulting scours filled with cross-bed can be described, the shape and size of the initial scour is not preserved. Therefore, investigations of scour in modern rivers are needed by monitoring bedform migration and trough development.
2. In the flume experiments, the relationship between the variation of the lee-face angle and the dimensions and depth of the host bedform scour can be observed. However, this cannot be investigated in the rock record, where only the preserved truncated sets and the final evolved stage of the scour can be observed. The preserved scour may be diachronous with the more downstream parts evolving as the upstream parts are being buried below the advancing bedform. Thus, relationships between variation of lee-face angle and trough dimensions in flume are not directly comparable to the cross-set and scour dimensions in the rock record.
3. The evolution of bed topography and its implications on final deposit architecture. In the flume experiments, three main processes are observed to modify the channel topography resulting in a feedback with the advancing bar and flow, these are: (1) sediment transport from upstream down the bar lee face into the trough separation zone; (2) reworking of sediment within the trough and (3) counter-flow ripples forming in the trough and on lee-face toe (Section 5.4.4). Although these processes would have occurred over the bedforms that formed the cross-bedded sandstone, the evolution of the topography cannot be assessed as the bedforms are only very partly preserved thus this is another topic that needs to be investigated further in modern rivers to assess the value of the comparisons with ancient rocks.

6.4 Comparison of specific features

6.4.1 Lee-face angle

In the Prados Formation, laminae dip angle was measured from individual internal laminae of scour structures. In the structures that were better preserved and well exposed, the laminae dip angle was measured in more than one point within individual sets. Although in some of the structures the angle fluctuated without any systematic pattern in most of the structures lee-face angle increased downstream (Section 2.8.5). The level of preservation and quality of exposure was not as good in the Seaton Sluice Sandstone, and several measurements of lamina dip angle were recorded from only nine of the better preserved scour structures; five of them had a laminae dip increase downstream. In the flume experiments the lee-face angle varied downstream however there was no systematic change observed (Section 5.3.8; Fig. 5.20). Thus, the lee-face angle of the individual laminae within individual sandstone trough cross-sets varies and tends to increase downstream, but this was not observed in flume experiments. These experiments were run under constant steady-flow conditions with homogeneous grain size. The difference in pattern may be explained by comparing flume and field observations:

- (1) There was a variation in grain size supplied to the dunes' lee face and the composition of the sediment may also have varied. The Prados Formation has intercalation of fine layers of fine sand with high mica content. These are more frequent higher up in the sequence. In the Seaton Sluice Sandstone occasional intercalated layers of finer sediment and higher mica content were observed within individual cross-bed sets. These variations in grain size and sediment type may have caused variations in grain flow behaviour and the formation of avalanching faces on the lee slopes, although no systematic change downstream within individual sets was recorded (it was not looked for).
- (2) Variations in the flow conditions may cause variations in the dimensions and behaviour of the superimposed bedforms (and the ratio of their height to the host bedform height) and therefore may have affected the lee slope. It is not possible to assess this variation at current levels of knowledge from the rock record and the flume experiments were run with steady flow.
- (3) In natural rivers, changes in flow behaviour, flow depth, discharge and sediment flux are likely to occur. These can cause variations in the bedform dynamics and their

geometry. Temporal changes in bedload and suspended load transport added to the recirculation of part of the downstream dune sediment favours trough-scouring (Leclair, 2002). Following the relationship between bar height and bar lee angle found in Section 5.4.2 then, if trough-scouring causes variations in dune height, it may also contribute to lee-face angle variations.

In the flume experiments, lee-face angle varied (Section 5.4.2) and this variation was compared to the duration of each run, the downstream distance and the variations of the unit-bar height. No measureable systematic relationships were found between these variables. However, the amount of scatter in the plot of lee-face angle and unit-bar height appears to decrease with the increase in bar height (Section 5.3.8; Fig. 5.21). Consequently, the control on the unit-bar height may also affect the amount of variation in lee-face angle either directly or indirectly. Insufficient data were available from the rock record examples to be able to assess whether the variation dip of lamination within individual scour structures is related to set thickness (making an assumption that set thickness is related to bedform size this might be expected). Sediment supply, variations of the flow velocity and water depth have an influence on bedform size and then on variations of bedform height, but in the flume experiments these were steady (or near steady). Lunt *et al.* (2007) suggested that variations of unit-bar height are controlled by the variations of the water depth and flow duration increase. The set thickness in both sites, especially in Rillo de Gallo, tends to decrease upwards in the sequence. Although the cross-bed sets only represent a minimum estimate of the true dune heights, the general upwards decrease of set thickness indicates decrease in dune height. The observations from the flume, thus suggest that there will be significantly more variation in lamination dip upwards in the sequences as the bedform height decrease.

Bedform superimposition, bedform amalgamation and the formation of reactivation surfaces have direct influence on the variation of the host bedform height and thus on lee-face angle variations.

6.4.2 Superimposed bedforms

Bedform superimposition is known to influence host bedform lee-face angle (Reesink and Bridge, 2007, 2009) and was observed to do so in a complex way in the flume (Section 5.4.3). Previous studies suggested that bedform superimposition increases the host-bedform height, which influences the mean and turbulent flow field (Fernández *et*

al., 2006). Earlier studies suggested that the superimposition of large-scale transverse bedforms implies large and rapid hydrological changes (Allen and Collinson, 1974), but later work indicates that superimposed bedforms form in steady conditions also (as in the flume experiments described here). Later research focused on bedform superimposition and their effect on cross-strata (Reesink and Bridge, 2009, 2011) supports the idea that variations in shapes and sorting patterns of cross-strata is a function of bedform superimposition type and host bedform height. Bedform superimposition is one of the major factors that controls the architecture of unit-bar cross-stratification (Reesink and Bridge, 2007), influencing temporary decrease in unit-bar lee-face angle as superimposed bedform approach the host bedform crest as long as the heights exceed 25% of the host bedform height.

Superimposed bedforms were observed in flume Runs 1-4 forming over the unit-bar stoss face, amalgamating with each other near the host bedform brink point; and climbing over the unit-bar brink point. In contrast, the rock record only preserves truncation surfaces as evidence of bedform superimposition, although Kleinhans (2004) suggested that in some cases the nature of the layering in cross-bedding can be explained by superimposed bedforms.

Variations of the lee-face angle are rapidly noticeable when relatively tall superimposed bedforms overtake the host bedform and the slip-face length is smaller than the lee-face length. In the rock record case studies, cross-bed sets are mostly top-truncated so that the type and size of superimposed bedforms cannot be assessed directly. However, given the estimated river depths (7-35 m in Rillo de Gallo and 6-38 m in Seaton Sluice) and the sediment grain size (fine to coarse in both sites but predominantly fine to medium in Rillo de Gallo) it is very likely that superimposed bedforms formed over the dunes that formed the cross sets. These would have influenced variations in the dune heights and therefore, would have affected the final cross-set thickness and dip angles.

In the flume experiments, bedform amalgamation over the unit-bar stoss faces was observed. Superimposed bedforms amalgamated at irregular time intervals at the unit-bar brink point causing variations of the unit-bar height and also causing occasional unit-bar brink retreats upstream (cf. Fig. 5.11). In the Prados Formation, sets within the same horizontal surfaces appear interconnected and overlapped, truncating the

underlying sets. This suggests bedform superimposition and therefore, bedform amalgamation is also likely to have occurred. In the Seaton Sluice Sandstone, distinctive horizontal bounding surfaces show a bedform multi-stacking pattern that indicates bedform superimposition and most likely bedform amalgamation. Best *et al.* (2013) described bedform amalgamation in different stages and suggested that the separation zone and shear layer become smaller as the upstream bedform approaches the downstream bedform causing erosion of the stoss face of the host bedform (downstream bedforms) and then, a decrease in its height.

The results from Runs 1-4 do not reveal a pattern that relates lee-face angle and unit-bar height (Section 5.4.2) but do suggest the lee-face angle scatter decreases as host bedform height increases; consequently bedform superimposition and bedform amalgamation should also influence lee-face angle variations. This may also explain the resultant variation in bed thickness.

Due to the level of preservation in the rock record bedform superimposition is not always easy to identify. Hence, some questions arise such as: Is it possible to find relics of superimposed bedforms? How can stacked sets formed by superimposed bedforms be distinguished from cross-sets vertically stacked formed at different times by different host bedforms? Does set truncation mean superimposition or simply the stratigraphic position of chronological events?

6.4.3 Reactivation surfaces

As a consequence of bedform superimposition, when bedforms overtake the brink point of the host bedforms, reactivation surfaces can be formed and these can impact the lee slope. Due to the level of preservation, full preserved top sets were not frequently observed in the two case study areas; and there was no unequivocal evidence of occurrence of reactivation surfaces. In the Seaton Sluice Sandstones, fully preserved top sets were identified but without signs of reactivation surfaces (Section 3.6.1 on Fig. 3.12) and in the Prados Formation, there were patterns of lamination that hint at reactivation surfaces (discussed below).

Reactivation surfaces as defined by Jopling, (1965) Collinson (1970), Jackson (1976) and others, have been studied experimentally and they have been identified in the field

(Jones, 1979) and used to infer information on flow conditions and bedform dimensions. They are also described as surfaces that separate foresets within the same cross-set and truncate the lower foreset (McCabe and Jones, 1977). However, how these surfaces get preserved in the rock record is not well documented. If the form of the superimposed bedforms is not preserved, it can be difficult to recognise these surfaces. Are they simply overlooked and interpreted as foresets with slightly steeper angle in many ancient sequences? Can reactivation surfaces be reliably recognised in the rock record?

In the flume experiments presented in this thesis, reactivation surfaces were observed in Runs 1, 2 and 4 as the bar migrated downstream. They mostly were observed where the bar front moved over in the flat bed beyond the original bed trough and they were only preserved in the deposits in this area. This may indicate that truncation events were more likely to occur as the bar migrated over the trough washing out any evidence of reactivation surfaces. The ratio of superimposed bedform height to unit-bar height was greater beyond the (buried) depression, and reactivation surfaces are more likely to form when that ratio is bigger. In addition, the flow depth above the unit-bar brink point increased as the bar advanced beyond the trough and this favoured less erosion and better preservation of the top sets (Sections 5.3.9 and 5.4.3). The lee-face angle varied temporally by the formation of these surfaces as tall superimposed bedforms overtook the unit-bar, afterwards foresets continued forming at a similar angle to that before the bar advanced. In the resulting cross-bedding from the flume experiments, random foresets appear to have steeper inclinations in between foresets with similar slope angles; these may be the remaining record of reactivation surfaces preserved in the lower part of the cross-bedding. This is the most likely explanation of these patterns and implies the presence of superimposed bedforms. Reesink and Bridge (2007; 2009) suggested that the formation of reactivation surfaces indicates that superimposed bedform heights exceeded at least 25% of the host bedform; and consequently the inclination of the foreset will decrease. The results of the flume experiments presented here, agree with Reesink and Bridge's suggestion that the relative height of superimposed bedforms must exceed some threshold, but in these experiments as reactivation surfaces were observed when superimposed bedform heights were at least 30 % larger than the unit-bar height.

These series of flume trials and the final four long-duration experiments helped to better understand what may have occurred in the rivers that formed the deposits examined in the two case studies; and observations on foreset formation, reactivations surfaces, and consequently foreset truncation, added value to the field observations hinting at what to look for in future field work.

6.4.4 Bed topography and bottomset (massive sand layer and counter-flow ripples)

Variations in bed topography affect the growth, duration and dynamics of bedforms; and hence, the final architecture of the deposits formed by their migration. In addition to the controls that explain unit-bar height variations that may relate to lee-face angle variation, the morphology of the bedform migrating and the shape of the scour over which it advances may also explain lee-face angle variations. The antecedent river (or flume) bed topography controls the height difference between bedform crest and downstream trough. In the flume experiments this was initially controlled but evolved with time; in the field examples it was unknown. In addition, trough scouring was evident in the rock record examples but not in the flume due to the nature of the experimental setup reproducing a flume-scale unit bar with a nearly flat trough downstream, so its influence was not directly investigated.

In these flume experiments, the bottom of the initial unit-bar depression was nearly flat and it was observed that unit-bar dimensions and shape of the bar initial trough and bed topography varied as the bars advanced downstream. In the field, the dunes advanced over concave-up scours that are thought to have formed downstream of the dunes in the flow conditions that controlled the dunes. Variation of the trough topography as the unit-bar advanced downstream was caused by: (1) high rates of sediment transport from the upstream end; (2) suspended sediment within the unit-bar lee that settled in the trough and on the toe of the unit-bar lee face; (3) pattern of water flow and (4) development of counter-flow ripples in the trough and on the toe of the unit-bar lee face. These added to the two main controls on the bedform height variation (sediment flux and water depth) by changing the trough depth. In addition, the formation of counter-flow ripples that is controlled in part by the height of the unit-bar lee face, influences lee-face angle variations at least in the lower part of the set (Herbert *et al.*, 2015) forming gentle tangential contacts of the cross beds with subtle decrease in the angle of the lee face.

In the flume experiments, initially in all runs, a large amount of sediment was rapidly transported and deposited within the unit-bar trough as the bar rapidly adjusted to the imposed flow conditions forming a basal unit of aggraded sediment, subsequently feedback between the flow and the sediment reworked the top of that unit and incorporated additional sediment that reached the trough. In Runs 1-4 the preliminary set-ups were slightly different and these differences were reflected in the resultant geometry of this basal layer of sand. High sediment flux, lower mean flow depth above the brink point of the host bedform and the host bedform being closer to areas susceptible to high flow velocities resulted in a high aggradation rate, and therefore thicker basal layer. This layer becomes the bottomset underlying the unit-bar foresets. When a large amount of sediment is deposited in this way it can extend beyond the trough and the resulting volume of the sediment in the basal unit exceeds the original volume of the unit-bar trough (Section 5.4.4). Consequently, the unit-bar cross beds will overlay a higher channel bed (modified trough) and this may have implications for the evolution of the unit bar and final cross-bed architecture. In contrast, with less sediment flux and higher mean water depth above the bar brink point within parts of the channel where conditions are closer to an equilibrium stage, will result in thinner bottomsets and the trough morphology will persist for longer.

The formation of the bottomsets, their thickness and grain-size distribution may be diagnostic of the formative bedform type: dune or unit bar. These basal layers do not always form and may not be always preserved in the rock record.

Although formed bottomsets are likely to be preserved, neither in the Seaton Sluice Sandstone or the Prados Formation, were bottomsets identified at the base of cross-bedded sets (trough and planar). Therefore, it is unclear if bottomsets were ever formed or not, and if beside flow regime, the formative bedform type is a significant factor dictating their formation. Blom (2008) observed in flume experiments with dunes that bottomsets can be preserved if dunes migrate over them under low flow energy. Reesink and Bridge (2009) observed that the relationship between height and flow depth in bars is larger than in dunes. This generates a greater deceleration of the flow in the lee of the unit bars relative to the dunes. The deceleration in the unit-bar lee enhances settling of fine-grained suspended sediment in the trough, and so the formation of bottomsets are distinctly finer-grained than the cross-bedding. Based on this, they suggested that thick

and fine-grained bottomsets are indicative of unit bars as the bedforms that generated the deposits. However, Martinius and Van den Berg (2011) suggested that finer-grained bottomsets formed in dunes troughs are more commonly preserved since low flow regime is required; in contrast, strong flows parallel to unit-bar front are common and these will prevent fine sediment settling. In the flume experiments reported in this thesis, well-defined bottomsets were formed and preserved as unit bars migrated downstream, and due to the flume lateral restriction any crest-parallel flow was limited. It can be concluded therefore, that fine bottomsets may form in association with either dunes or bars if the conditions are suitable and their presence is not diagnostic of bedform type, but it might be diagnostic of the relative size of the bedform to the flow depth and velocity.

Van den Berg and Van Gelder (1993) suggested a new bedform stability diagram, where bedforms are defined in relation to grain mobility (parameter that relates in a dimensionless form flow depth and grain size (D_{90}), cf. Van den Berg and Van Gelder 1993) and the mean grain size (D_{50}). This diagram includes fields marking favourable conditions for the development of dune-related bottomsets. Assuming the mean grain size (D_{50}) of the Prados and Seaton Sluice Sandstones are $400\mu\text{m}$ and $550\mu\text{m}$ respectively and considering that in neither of the case studies were bottomsets identified; then, from Van den Berg and Van Gelder's (1993) diagram higher values of mobility parameter can be inferred and that the trough cross-bedding identified (formed by 3D dunes) in both sites was formed under relatively high flow energy that did not allow fines settling in bedforms lees. Having calculated estimates of bankfull depth for both rivers, detailed grain size analysis could facilitate more accurate estimates of what bedform type generated the trough cross-bedding in the two case studies, and where exactly within the Van den Berg's stability diagram they fit. Thus, it may be possible to establish whether bottomsets formed or not. Therefore, estimates of grain size (D_{50} and D_{90}) and flow depth can help interpretations of formative bedforms, and also indicate their relationship to bottomset formation associated with flow conditions. In this thesis grain size analysis was unable to be accomplished in the time frame available.

Planar cross-bedding resulting from the flume experiments were compared to the planar cross-bedding identified in the Seaton Sluice Sandstones aiming to compare geometries and basal layer formation. No evidence of bottomsets or counter-flow ripples was found.

This may indicate that the flow conditions occurring were suitable for 2D dunes or bars to form but that the conditions under these bedforms migrated added to the particle size distribution did not allow bottomset formation or preservation (Blom, 2008).

Previous flume experiments and those presented in this thesis, suggest that bottomsets with evidence of counter-flow ripple formation form in a wider window of flow conditions with unit bars than with dunes because of the way in which the host bedforms are controlled by the flow conditions (Martinius and Van den Berg, 2011; Herbert *et al.*, 2015). Although dunes migrating out of equilibrium could also generate counter-flow ripples outside the conditions suggested by Herbert *et al.* (2015). Although the results from these flume experiments agree with Reesink and Bridge's suggestion on basal layer formation, several questions arise from theirs and Martinius and Van den Berg's (2011) theories on the preservation of bottomsets: When and how do they get preserved? Are they always recognised correctly in the rock record? Would their character be diagnostic of the flow conditions? Do bottomsets form more commonly with unit bars or dunes? Does the planar cross-bedding identified in Seaton Sluice with no evidence of bottomset indicate that straight-crested dunes are more likely to have been the forming bedforms than bars?

As an ongoing issue, field analysis can only be based on the final geometries of cross-beds and preserved bounding surfaces (Section 2.3). Monitoring the evolution of the channel base in flume experiments and the effect on the resulting geometries can be very helpful; so that experimental resultant geometries can be compared to ancient deposits. This would add useful information to field interpretations, especially to those still based on traditional methodologies without the support of other techniques. There is a lack of literature on the specific effect of scour topography on the evolution of bedforms. Herein, the need for further work using flume experiments to investigate this issue and then, to find the most reliable way to apply the results in field interpretations aiming to improve the understanding of ancient fluvial systems is highlighted.

6.4.5 Formative bedform crestline shape

The crestline of the bedform forming the cross-bedding may control the variations of the lee-face angle. In the flume, the crest-plan shape of the flume-scale unit bar was initially straight and at 90° to the channel. It changed slightly to a more sinuous shape as

the bar moved. The deposits observed in the Prados Formation are interpreted as being generated by the migration of sinuous-crested dunes; and in the Seaton Sluice Sandstone cross-bedding was formed by sinuous and straight-crested dunes (or bars). In the flume, as the bar crestline changed in shape, the front lee slope of the bar did not advance evenly. This caused variation of the lee-face dip (direction and possibly locally angle) in different areas of individual foresets and therefore, variation of the angle of foresets as the bar advanced downstream. These variations are also observed at Seaton Sluice. Various laminae dip measurements were recorded within individual laminae of plan-view trough cross-bed sets (when preservation allowed it); indicating dip variations across individual foresets of migrating bedforms. In cases where the migrating bedforms have curved lee faces, bedform migration patterns and flow changes cause laminae dip directions variations. These can be mistaken as lee-face angle variations in the field especially when observations are taken from vertical exposures.

6.4.6 Resulting cross-bedding types

In addition to the comparison in the previous subsections, a brief assessment of the external architecture of the resulting planar cross-bedding observed in the flume and at the Seaton Sluice site was attempted. This involved the modified classification presented in Section 5.1 and Table 5.1 which adds two new types of cross-bedding to Allen's (1963a) classification. These types take into account the basal layer (bottomset) formation. The new *Sigma* type (obtained in the flume) is a solitary large-scale cross-stratified unit, non-erosional (it could also be erosional), essentially planar and tabular or lens-shaped and occasionally with irregularities in between the laminae. In natural channels and in larger flumes it may be possible to generate grouped cross beds of this type (*Rho* type). The comparison between the different cross-stratified units classes observed in the flume and field aimed to find relationships between: flow conditions, scour shape and bed topography development with the deposits identified in the rock record.

Although the geometry of the cross-strata formed in Runs 1-4 depends to a certain extent on the flume dimensions and the conditions used, similar structures form in natural river channels. Planar cross-bedding identified in the Seaton Sluice Sandstone were initially interpreted as formed by straight-crested dunes or longitudinal and transverse bars. Haszeldine (1983a) interpreted the planar cross-bedding within the

Seaton Sluice Sandstone as the combination of large and small-scale sand-sheets and sand-wave migration on the channel bed (dunes and bars); and subdivided them into three subgroups according to their size and the way they were grouped with other facies (S1, S4 and S5). Table 6.1 shows a classification of the Facies Sp and Association of Facies Sp and St identified at Seaton Sluice and the cross-bedding type generated in the flume. Similar facies (S4) were also observed in Namurian sandstones in the English Pennines (Jones, 1979), dominated by tabular cross-bedding and interpreted as formed by migration of straight-crested forms (transverse bars). The earlier Triassic fluvial deposits in the Spanish central ranges also have similar characteristics (Ramos *et al.*, 1986; Muñoz *et al.*, 1992) with individual and grouped sets of trough and planar cross-bedding.

Further investigations for evidence of the formation of structureless sandy bottomsets would be useful to compare new and past interpretations of study sites, which will add useful additional information.

Table 6.1 Characteristics of sets in sandstone Facies at Seaton Sluice and flume experiments (modified of Haszeldine, 1983a).

Facies (Martínez de Alvaro)	Facies (Haszeldine, 1983a)	Interpretation	Grain size	Set thickness & width in cosets	Cross-bed shape	Foreset bottom contact	Topset contact	2D Shape of set
Sp (large-scale) (formed by straight-crested dunes or longitudinal, transverse bars)	S1	Deposited by large-scale straight-crested sandsheets within sandwaves in deep water channel pool	Medium coarse	0.2-1.2 m > 10 m	Planar/ Gently concav e-up	Angular & slightly tangential Non-erosional	Planar	Tabular
Sp (small/medium scale) (formed by straight-crested dunes)	S4	Deposited by sandsheets within curved crestline sandwaves of bar platform and tail	Medium / granules	0.15-0.30 m > 5 m	Planar/ Gently concav e-up	Angular, tangential Non-erosional	Occasionally coarser planar	Tabular
Sp and St (formed by straight-crested and sinuous-crested dunes)	S5	Deposited by sandsheets and megaripples within bar lee deposits at bar head	Silt/ granules	0.15-0.40 m > 0.20 m	Planar/ Gently concav e-up/ Strongly concav e-up	Usually tangential Erosional and non-erosional	-	-
Sigma Type (solitary unit)	Runs 1-4	Deposited by a flume-scale unit bar within the bar lee, trough and downstream end	Medium	~ 0.25 m	Planar/ Gently concav e-up	Angular, tangential Erosional and non-erosional	-	Tabular and Erosive wedge/spoon-shaped basal contact

6.5 What else needs to be considered in the comparison of flume and field research?

6.5.1 Grain size

Other variables such as sediment grain size, grain size distribution and grain sorting, and their variation as bedforms advance downstream and their influence on lee-face processes and suspended sediment load (Bass *et al.*, 2011) should be taken into consideration. Unfortunately there was not enough time to evaluate these with sufficient data in this research, but the importance is recognised.

The two field sites were selected because the grain size distribution was generally similar to the one that could be used in the flume. This was an attempt to take any major control by grain size on the sedimentary processes, and certainly was a better attempt than comparing flume results with e.g., gravel or mixed sediment settings. Although the grain size distribution varied within and between both sites, in both case studies the grain size ranges from fine to coarse grade. In the Prados Formation fine to medium grain size predominates (Sections 2.5.1 and 3.5.1). Ramos (1979) presented a first estimation of the Prados Formation grain size and mineral composition: 40-74 % of fine to medium, sub-angular and sub-rounded grains of quartz; 16-40 % of feldspars and 2-30 % of rock fragments (e.g., quartzite, shale and schist). The matrix varies from 5 to 20 % of clay (e.g., micas). The Seaton Sluice Sandstone mineralogy consists of lithic clasts, feldspar, sub-angular quartz and muscovite (Holzweber and Hartley, 2011). In the flume experiments, the bedforms formed in well-sorted sand ($D_{50} \sim 241 \mu\text{m}$, cf. Fig 5.2b on Chapter 5). For the comparison of the flume deposits and the two case studies the similarity in grain size appeared adequate to allow good comparison. However, because of the variation in grain size and composition (and consequently grain shape) of the rock record case studies, the behaviour of the grains as they are transported, the dynamic sorting and depositional patterns vary; and this is likely to be a significant influences on the cross-bedding architecture.

Previous work suggested the importance of grain size distribution and dynamic sorting in mixed bed-loaded rivers forming cross-stratification (Ghoshal *et al.*, 2010; Baas *et al.*, 2011; Frings, 2011). Grain size distribution within individual cross-bed sets and more widely within a channel may be indicators of bedform type and position within the

channel where the deposits were formed (cf. Lunt and Bridge, 2004). Kleinhaus (2004) compiled sorting/grain size patterns that characterised cross-stratification formed by dunes and bars such as: intercalation of layers due to couplets of grain flow and grain fall (in fine grained dunes); layering marked by grain dip direction of asymmetric grains (in dunes and bars of mixed coarse sediment); layering marked by the variation of mixture of composition (in dunes and bars of mixed coarse sediments) and others. In both field case studies, intercalations of very thin layers of very fine sand with high mica content were observed. In the Prados Formation, these layers were frequently identified and always appeared interbedded with coarse sandy laminae within individual cross-sets. Although the sediment used in the flume was homogeneous, small volumes of darker coloured sand grains of blast furnace origin were added to more easily identify the cross-beds forming; and a subtle tendency of layering occurred. The variations of the layering and grain size distribution patterns in both field sites cannot be directly related to the flume experiments where the sediment was much better sorted and of a single dominant mode.

In rivers dominated by mixed bedloads (gravel and sand), different patterns of grain-size sorting occur due to higher bed permeability, the proportion between different types of grain sizes and superimposed bedforms grain-sorting patterns. This can significantly affect the processes occurring in the flow separation zone in the lee and at the crest of the host bedform (Lunt and Bridge, 2007). Although gravel was very rare at both field sites, there was a little in the Seaton Sluice Sandstone.

The influence of sediment grain size, sorting, composition and shape (e.g., mica proportion, and grain size and shape) needs a lot more research to discriminate the scale of their impact on variations in the host and superimposed bedform processes.

6.5.2 Water discharge and sediment flux variability

The variations in water discharge and sediment flux are other factors of significant importance for the architecture of the cross-bedding and understanding of the system that formed it. Sediment and water supply are controlled by regional climate, tectonics and the nature of the drainage basin or catchment area. The density of the catchment area that supplies water and sediment to the river system depends on climate, surface permeability, precipitation rate, erosion, and vegetation coverage. Drainage density

tends to be high in semiarid climates due to temporal concentrated precipitations and run off and the lack of vegetation. In contrast, it tends to be lower in humid regions because of the vegetation cover. Rivers with high drainage density are often flashy with greater flood risk. Hence, the predominant climates when the fluvial systems were active and the history of weather events significantly control the variation in discharge and sediment flux.

Flow variability has a significant impact on the rate of sediment transport (Grenfell *et al.*, 2014). The variation of the water discharge and precipitation rate influences the variations in sediment flux and becomes the main control factor on sediment flux in most settings (Wulf *et al.*, 2010). Previous studies on the relationship between sediment flux and climate change suggested that under constant climate an increase of precipitation leads to an increase in sediment flux. In addition, under constant levels of rainfall and increase in temperature leads to a decrease of sediment flux. Thus, the combination of climate change and rainfall determines the variation in sediment flux (Zhu, *et al.*, 2007). However these patterns are strongly influenced also by seasonality and flashness (e.g., Fielding *et al.*, 2009). Higher sediment flux is expected when there is higher transport capacity and higher sediment availability.

Although in both study areas similar facies were identified, these were deposited under different weather conditions. The Prados Formation that is part of the Buntsandstein sequence, was characterised by a semi-arid climate; whereas the Seaton Sluice Sandstone was deposited under more humid conditions with short dry periods. These differences must have implications for the resulting deposits, but as yet these are poorly known because of insufficient published studies of natural rivers in such settings (Fielding *et al.*, 2011). Intuitively, it might be anticipated that higher sediment supply would be available to the Northumberland River than the Iberian River because the former occurred under a wetter climate and also higher mean annual specific runoff. However this may not have been the case because the wetter conditions may have led to denser vegetation cover and so less sediment availability. Also, although a wetter climate may lead to greater average runoff, stronger seasonality and less dense vegetation cover both lead to more runoff efficiency; then more flashy flow pattern with greater discharge peaks proportionately.

The size of the channels is controlled by the runoff pattern taking into account intra- and inter-annual variability in discharge. Considering the climate characteristics and channel dimensions estimates of the Northumberland River (Section 3.10.1), the distinctive large scale of the bedforms interpreted in the Seaton Sluice can be explained by higher rates of discharge and greater bankfull channel depth. Hence, it is likely that some of the variations in the architecture of the rocks in Seaton Sluice and Rillo de Gallo can be explained by sediment flux and discharge variations, but not enough is yet known about their influence on bedform development and deposit characteristics.

In addition, discharge and flow variability also influence fluvial style (e.g., an increase in flow can result in channel pattern change from meandering to braiding). For example, in straight channels sediment deposited tends not to be reworked quickly and so the channel cannot rearrange its sinuosity following changes in discharge, sediment supply and slope, whereas meanders tend to rework older deposits continuously (Grentell *et al.*, 2014). Based on the data presented the Triassic River (Prados Formation) was interpreted as a low to high sinuosity river (Section 2.10.3). The palaeocurrent variability between different storeys in the Prados Formation may be explained by flow regime variability and therefore a slight change of fluvial style.

Other factors that are not considered here and should probably be taken into account are the catchment size and topography and geology, vegetation (density and type), and variations of river network resulting from the climate change as all of these have influence on the sediment flux and so on cross-bedding architecture.

There was not sufficient time available within this project to consider such variations in the flume experiments which were run under constant conditions, but it is important to consider temporal variability when comparing experimental results with the sedimentary record. Although the experiments in the flume are independent of any influence of sediment flux and discharge variations, the mechanism by which the sediment is supplied into the tank (river) may have an effect on the final deposits. Kleinham (2005) suggested that dune irregularities and feedback are related to the sediment feeding or recirculating method in flumes. He said that dune scour in recirculating flumes is less deep than in feed flumes (where water may be recirculated but sediment is not) and that the vertical sorting and transported sediment composition

are different. He compares the way the sediment is supplied in a recirculating flume (as in Chapter 5) to rivers that generate lag layers; and confirmed that these experiments representing upstream sediment supply can compare with natural rivers. This leads to a further question on the formation of bottom layers: does the bottomset formation, discussed in Section 6.4.4, depend not only on the formative bedform (dune or unit bar) but also on the type of mechanism of sediment supply? Does the formative bedform matter at all? This has not been assessed in this thesis but it is another topic that should be looked at in future studies.

6.5.3 River plan-form and size

Other factors to take into consideration when comparing sedimentary structures generated in the flume and deposits identified in the field are the plan-form of the system and the scale of the channel relative to the scale of the observations.

In the flume, the unit bars advanced downstream within a straight and laterally constrained unidirectional system; and so the space available for bedforms to form and migration direction variability are limited. The Prados Formation is interpreted as formed by a low to high sinuosity system and the Seaton Sluice Sandstone was deposited by a multiple-channel low-sinuosity river system. In these settings there is potential for oblique bedforms to form; and also for cross channel components of flow, which are much stronger (relative to scale of bedform) than observed in the flume.

The flume channel is straight (10 m long and 1 m wide); and the channel depth and width estimates for both sites (Section 4.4.4) range between 5.8 to 20 m and 102 to 670 m respectively. The difference in scale between laboratory and field implies that in the flume, the maximum bedform height is 0.29 m whereas the estimates for the mean dune height in the field sites are approximately 1.23 m and 1.88 m for the Prados Formation and the Seaton Sluice Sandstone respectively. The classification of bedforms means that dunes scale with flow depth and bars with channel dimensions such as width. Then, the bars in the flume are smaller than small dunes in either river. However, as discussed above, it is the relative importance the sedimentation processes and erosion that control the cross-bed architecture rather than the size of the bedform. In addition, it has not been established really that the bedform type is particularly relevant.

Others factors like climate, geology and tectonics also influence the fluvial style that can vary from one type to another. Thus, comparisons between artificial and natural bedforms should be done with certain reservations since the flume experiments do not consider any of those external factors that modify the fluvial style, bedforms and then cross-bedding architecture.

Chapter 7

Conclusions

This thesis comprises a series of two studies on cross-bedding architecture in fluvial sandstones formed by the migration of large-scale bedforms and flume experiments on cross-bedding formation. The analysis of the two study areas included: descriptions of the exposures, identification and interpretation of the facies, analysis of the geometry and orientation of trough cross-bed sets (scour structures), interpretation of palaeocurrent pattern of individual trough sets and their stratigraphic position within sandstone bodies, trough cross-bed set palaeocurrent analysis related to the interpretation of the variability of flow conditions in the fluvial systems that generated the deposits and assessment of sandstone and channel types. A review of published work relevant on scour and scour associated with bedform development and its link with field observations from the two sandstone case studies is herein included to improve the understanding of scour associated with formative bedforms and the resulting cross-bedding styles. To understand some of the factors controlling the formation of cross-bedding styles seen in the rock record, a series of flume experiments were undertaken in which cross-bedding was produced under controlled conditions.

7.1 Addressing the original aims and objectives of this research

In this section the success or otherwise of achieving the original aims and objectives of the research that are stated in Chapter 1 are summarised as follows:

Addressing Aim 1: *To find out if more detailed investigation of the cross-bedding architecture of the fluvial sandstones would give greater understanding of the flow conditions in which the sediments were deposited*

Research presented in this thesis confirms that more detailed investigation of cross-bedding architecture will improve the understanding of the flow conditions but that a large number of factors are still poorly understood. Chapter 2 and Chapter 3 report investigations of the cross-bedding architecture in the Prados Formation and the Seaton Sluice Sandstone. This leads to the following conclusions:

- Scour structures are mainly $W/L < 1$. Structures with $W/L > 1$ were attributed to a poor level of preservation level, or inaccurate measurement caused by limited field access, vegetation cover or misinterpretation. Consequently the classification of structures on the basis of width:length ratio may only be valid if length is greater than or equal to the width.
- There are relationships between scour structure dimensions and stratigraphic position. In the Prados Formation size decreases and circular and “oval 2” shapes (cf. Section 2.7.1) were more frequent upwards in the sequence. Thus, the stratigraphic distribution of the individual cross-bedded sets within a sedimentary sequence is a useful indicator of changing depositional conditions.
- Within individual scour structures, individual laminae dip direction varies slightly. This can be caused by flow irregularities, variations in bedform morphology and the bedform migration pattern. The level of preservation and the accuracy of measuring can also explain these variations.
- Within individual scour structures scour trend and laminae dip direction vary. The divergence between these can be an indicator of flow behaviour and bedform dynamics variations. In addition, it may indicate differences in channel setting and influence of preservation level.
- Within individual scour structures, laminae dip tends to increase downstream. This pattern was evident in 25 structures (out of 36 measured) in the Prados Formation and 5 structures (out of 9 measured) in the Seaton Sluice Sandstone.

- No measurable relationships were found between trough dimensions (size, shape and width:length ratio), laminae dip and divergence between laminae dip direction and scour trend. This result was not expected; problems with sampling methodology and issue with level of preservation may explain these results. Further analysis is required.
- Palaeocurrent data have a polymodal pattern in the Prados Formation and a single mode in the Seaton Sluice Sandstone. In the Prados Formation the resultant palaeocurrent mode is towards the southwest and differs from that reported by Ramos (1979). This difference is either due to local deviation since this site was a subset of Ramos' study area or as a result of the more comprehensive approach to the data collection in the research reported in this thesis. In the Seaton Sluice Sandstone the palaeocurrent data agrees with previous published work (Haszeldine, 1983a).
- Based on previous published studies, the depositional environments of the Prados Formation and the Seaton Sluice Sandstone were thought to be very different. Palaeocurrent data, facies percentages (Sp/St), cross-bedded set architecture, individual cross-bedded set geometry and stratigraphic location within the sandstone indicate that although part of the resulting deposits are similar, the two formative systems were probably different in plan-form. The Prados Formation is interpreted as being generated by the migration of large-scale 3D dunes within a low to moderately high-sinuosity river in the early Triassic. The Seaton Sluice Sandstone was deposited by the migration of large-scale 3D dunes and 2D dunes or longitudinal and transverse bars within multiple-channels of a low-sinuosity river.
- Published empirical relationships were used to estimate channel depth from sandstone storey thickness and channel width from the estimated flow depth. The channel(s) are estimated to have been 7 to 14 m deep and 148 to 387 m wide for the Iberian River (the upper estimates are likely to considerably overestimate mean channel dimensions) and 5.8 to 20 m deep and 102 to 670 m wide for the Northumberland River.
- On the basis of published empirical relationships between cross-bed set thickness with flow depth, bankfull depth was estimated as up to 20 m at Seaton Sluice and up to 14 m in the Prados Formation.

- Depth estimates for the Seaton Sluice Sandstone following Leeder's (1973) method (or other similar methods), that considers the storey thickness equal to the bankfull channel depth, are probably misleading. The sandstone storey thickness is low in the Seaton Sluice Sandstone relative to the water depth estimated from cross set thickness, suggesting that the channel was only partly filled by sand grade sediment, possibly because of low sand flux compared to the channel size and water depth. Alternatively this may be caused by poor storey preservation.
- Due to the various possible interpretations on fluvial-channel styles and given the size of the two channels and the relatively small size of the exposures compared to the channel size; the deposits at Rillo de Gallo could correspond to one bend within a meandering system or straighter river; and the deposits at Seaton Sluice could correspond either to those within a straighter channel system or within a straight reach between two bends.

Aim 1 and the objectives that addressed it were mostly accomplished: the data sets collected in this study have improved the interpretations of palaeo-flow and cross-bedding geometries. The original objectives that were set to address Aim 1 have or have not been achieved as listed below.

Objectives Accomplished:

- Review of the literature.
- Detailed descriptive analysis of the exposures, identifying features representing scour and cross-bedding within the context of individual sandstone bodies. It was not possible however to establish local palaeohorizontal accurately.
- A new interpretation of the sedimentary sequences and estimates of the nature of the channel or channels and their dimensions, and a comparison of these interpretations with published reports.
- Identification and investigation of individual and grouped scour structures associated with cross-bed sets, notably trough cross-bedding.
- Interpretation, for each scour structure, of palaeocurrent pattern and its relationship with their stratigraphic position within the sandstone body.

- Analysis of the data associated with scour structures to identify significant patterns that could clarify scour origin and development. Although this was not finalised, a first attempt was carried out in this thesis.
- Analysis of palaeocurrent data to estimate the variability of flow conditions of the ancient fluvial system that generated the structures; and re-assessment of previous interpretations of the channel nature.
- Identification of some characteristics controlling the geometry of scour structures such as: (a) shape, size and orientation of the initial host bedform, type of crest and its development (transition 2D-3D); (b) shape, size, orientation and development of the initial scour, formed as the host bedform advances; (c) characteristics of flow such as velocity and its variations, water depth and discharge pattern (continuous or varying); (d) channel characteristics such as width, depth and planform; (e) migrating mechanisms of host bedforms advancing and consequently the lee-face angle fluctuations.

Not accomplished:

- The grain size and mineralogical composition analysis of these rocks to estimate relationships between grain size, mineral composition and geometry of the scour structures was not achieved due to limited time.

Addressing Aim 2: *To improve the understanding of scour associated with formative bedforms and the resulting cross-bedding styles, aiming to improve the understanding of cross-bedded sandstones embedded in different depositional environments by gathering and analysing relevant information on scour and scour associated with bedform development from published work; and its link with field observations from both my field sites to: (a) establish that these scours are associated with specifically 3-dimensional bedforms and the resulting preserved cross-bedding; and (b) attempt to distinguish scours associated with formative 3D bedforms from those that correspond to pre-existing erosive surfaces.*

Chapter 4 reviewed published work on scour formation and bedform development in experimental unidirectional flows and also bedform evolution tracking in modern rivers; and discussed published experimental work with field observations on sedimentary structures, their basal bounding surfaces and the migrating bedform type that formed the

cross-bedding styles observed at Rillo de Gallo (Chapter 2) and Seaton Sluice (Chapter 3). This leads to the following conclusions:

- The erosional basal bounding surface of an individual set of trough cross bedding may have formed (1) before, and be unrelated to, the bedform migrated into it to fill it, (2) before the bedform but becoming modified by the flow in the lee of the bedform as it migrated to fill the scour and becoming associated with the migrating bedform, or (3) formed because of the flow pattern generated in the lee of the bedform, evolving and filling as the bedform migrated (i.e., scour development in association with the bedform). In this later case, the geometries of the scours (or the erosion surface resulting from the evolution of the scour over time) in relation to the filling cross-bedding and thus the final architecture of the single trough cross-bed set may be used to suggest that scour and bedform developed simultaneously during bedform migration.
- Scour development in association with bedforms can be related to: (1) bedform height; (2) water depth in relation to the bedform height (controlling flow separation patterns and thus bed shear stresses); (3) bedform crestline morphology (both curvature and height variation along the crest); (4) grain size distribution and sediment type; (5) bedload and suspended sediment flux; and (6) bedform migration pattern.
- The very few relationships previously published between scour geometry and the controlling factors (e.g., the relationship between scour depth and bedform height) are not known for a wider range of natural conditions and should be applied with care.
- Concave-up basal bounding surfaces of single trough cross-bed sets (i.e., scour structures) described in the Prados Formation (Chapter 2) and the Seaton Sluice Sandstone (Chapter 3) are interpreted as scours associated with the bedforms that formed the cross-bed set that fills them. This conclusion is drawn from: (1) architecture of infilling cross-bedding and basal contact with the underlying sediments; (2) the cross-bed set thickness and scour amplitude compared to the scale of the bedforms likely to occur in the interpreted depositional environment; (3) dimensions of formative bedforms and infilling cross-bedding overlying the concave-up scours agree; and (3) scour planform shape and curvature in agreement with anticipated flow and bedform migration patterns.

- In the Prados Sandstone, curved scour structures were recorded with planform curvature consistent with the variations of the dip direction of the infilling lamina, suggesting that scour and bedform developed simultaneously as the flow pattern and bedform migration direction changed.
- Scour planform shape is related to scour longevity. In the Prados Sandstone, elongate and near circular-shaped scours were observed in close proximity within same stratigraphic levels. Elongate scour structures were rarely observed in the Northumberland case study. This suggests a different pattern of scour longevity in relation to bedform migration at the two sites.
- Estimates of mean and maximum scour depths at Prados based on established relationships (Leclair and Bridge, 2001) > 0.62 and 0.94 m respectively. In the Seaton Sluice Sandstone the estimated mean and maximum scour depths are > 1.89 and 2.03 m respectively.

Aim 2 and the objectives that addressed it were accomplished. These are listed in Section 1.7.3.

Addressing Aim 3: *To investigate the factors controlling the formation of cross-bedding styles seen in sandstones.*

Chapter 5 describes a series of flume experiments producing cross-bedding in controlled conditions. These experiments investigate the formation of cross beds whilst large-scale bedforms advance downstream in a flume. They examine more precisely the factors that control the formation of cross-bedding styles observed in the studied sandstones. These experiments lead to the following conclusions:

- No resolvable relationship was found between bar height and bar lee-face angle under the presented conditions and flume set-up.
- The bar height scatter decreases as the bar progrades downstream over a non-fixed depression.
- The bar lee-face angle scatter decreases as the bar height increases.
- Bedform superimposition and bedform amalgamation near the unit-bar brink point influence grain flows down the bar lee face and contribute to variation in the host bedform height variation.

- In these experiments reactivation surfaces formed when superimposed bedforms were at least 30 % of the height of the host-bedform at the time they overtook the unit bar. These surfaces can be wrongly interpreted as cross beds within the same set dipping at less than the angle of repose indicating a decrease of the unit-bar lee-face angle, whereas actually they indicate significant erosion of the unit-bar brink due to bedform superimposition when those bedforms exceed 30% of the host-bedform height. They only contribute to a temporary decrease of the unit-bar lee-face angle.
- The topography of the trough downstream of a unit-bar is modified by grain fall (settling of suspended sediment) and remobilisation of sediment previously deposited in the trough by reverse flows resulting in small counter-flow ripples forming in the trough and on the lower part of the lee face.
- Fine-grained bottomsets (0.06 to 0.08 m thick) form as unit bars migrated under the controlled conditions used in these experiments. They form due to sediment deposition mainly by (1) suspension fallout on the lee face and floor of the depression and (2) reworking of sediment by the return flow in the lee of the bar.
- Continuous formation of counter-flow ripples on the lower part of the unit-bar lee face reduces the lee-face angle, producing tangential contacts between the foreset laminae and the trough floor. This causes alterations of the topography that will affect the variation in unit-bar height.
- The resulting cross-stratification formed in Runs 1-4 helped to add two new types of cross-stratified units to Allen's (1963a) classification, taking into account bottomsets as part of the resulting cross-bedding. These types are large-scale solitary (*Type Sigma*) and grouped (*Type Rho*) cross-stratified sets underlain by non-erosional and erosional surfaces, with either trough, planar or irregular lower boundary shape, discordant and lithologically homogeneous with respect to the lower boundary.
- The position of the host bedform within the channel to some extent determines the character and relative importance of superimposed bedforms and the factors controlling the final architecture of cross-bedding. Although this could be seen as a limitation of flume experimentation it is also suggestive that location within a natural channel will be important and should be investigated.

- The dimensions of the initial depression downstream of the unit bar influence the architecture of the preserved cross-stratification.

Aim 3 and the objectives that addressed it were mostly accomplished. The factors that control the formation of cross-bedding styles seen in sandstones were investigated by producing cross-bedding, under controlled conditions, emplaced by a large-scale bedform migrating downstream in a flume. The objectives that have and have not been achieved for Aim 3 are listed as follows:

Accomplished:

- Investigation about whether it is possible to identify unit-bar lee face change in deposits advancing downstream over pre-existing topography and quantify the variations.
- Investigation of bed topography implications on the architecture of cross-stratification formed by the migration of steep lee-face unit bars.
- Monitoring the evolution of superimposed bedforms and feedback with the bed, which leads to modification of the original topography over which the unit bar migrated.
- Observations on the influence of both down-channel migrating superimposed bedforms on the host bedform and counter-flow ripples in the bedform lee on cross stratification.
- Identification and analysis of the controls on lee-face angle fluctuations as unit bars migrate downstream.

Attempted:

- Investigation on the transition from 2D to 3D dunes, with the intention of examining equilibrium dune pattern and the effect of different flow conditions (cf. Venditti *et al.*, 2005a). Due to limitations of channel shape and scale it was not practical to proceed with these experiments, because of the difficulty in distinguishing bedform types and the complex interactions between ripples and dunes at this scale.
- Reproduction of Leclair's (2002) experiments on cross-bed preservation that led her to suggest relationships between bedform size and cross-sets thickness to understand controls on the variation of dune height and then relate them to the

geometries of cross-bed sets observed in the study areas. Due to equipment limitations, the evolution of dune-trough scouring was unable to be monitored; which, according to Leclair (2002), appears to be the main mechanism by which dunes increase in height.

Addressing Aim 4: *To integrate flume experimental and field work data on the analysis of bedform geometries and resulting internal architecture formed by bedforms developed downstream, to improve the methodology for the interpretation of ancient cross-bedded sandstones and their origin, and to define some of the factors controlling the geometries of the resulting sedimentary structures investigated in the field.*

In Chapter 6 the experimental and field data were compared and contrasted to improve interpretations of ancient fluvial systems. This discussion led to the following conclusions:

- Although numerous assumptions are considered when comparing flume experiment conclusions and rock analogues examples, this study demonstrates that useful information in the interpretation of the cross-bedded sandstones at Seaton Sluice and Rillo de Gallo was added by using the flume data results presented here.
- Based on the relationship between lee-face angle variations and bar height explained in Chapter 5 and the fining-upwards pattern observed in both case studies, greater variations in lee-face angle upwards in the sedimentary sequences are expected. Further experimental work with superimposed bedforms forming stacked cross-bed sets would be useful for further clarification of this pattern.
- It remains unclear what the diagnostic features of dune and bar cross-bedding are. This is because the same processes operate on both bedform types and any differences in the main depositional processes that occur on the lee face of dunes and bars have not been identified. Further studies on bedform dynamics associated to flow depth and channel dimensions may clarify if the depositional processes are the same. The distinction between bedform type by size relationships (dunes relate to flow depth and bars to channel dimensions) is

unhelpful in natural systems where flow depth varies given time taken for bedforms to generate and migrate.

- Scour development and filling processes and the consequent formations of bottomsets associated with certain flow conditions could be indicators of formative bedform type and be useful in defining specific differences between dune and bar development and the resulting cross-bedding architecture, but further research is needed to test whether this is the case.

The objectives that have and have not been achieved for Aim 4 are listed as follows:

Accomplished:

- Comparison of the morphology and the appearance of the cross-bed sets observed in the exposed sandstones and the ones generated by the flume tests (planar cross-bedding was compared between the flume and the Seaton Sluice Sandstone).
- Observations on erosion of the brink area of host bedforms in the field exposures and a comparison of these with flume observations to see if this can explain patterns of lee-face angle variation (identification of reactivation surfaces and bedform superimposition). This could not be observed in the field, however flume observations were useful for the discussion on reactivation surfaces and bedform superimposition.
- Comparison of the pattern of variability of the dunes and unit-bars lee-face angle identified in the field, with those generated in the flume experiments. By comparing the lamina dip angle variations from the field sites with the variations of the lee-face angle of the bar formed in the flume, to find out whether this revealed lee-face angle variation patterns.
- Comparison of the bounding surfaces preserved in the field (representing the topography over which large-scale bedforms migrated to form the trough cross-bedding) with the initial and final topography over which the unit bar advanced in the flume (identification of bottomsets). This was used to determine similarities or differences in how feedback with topography occurs in the flume and in a real case scenario.
- Comparison of the resulting cross-stratification (lamination) type from the flume experiments with the ones observed in the field following Allen's (1963a) classification.

- In addition to this, in Chapter 6, other factors relating to the cross-bedding architecture, such as grain size, sediment flux, discharge variability and channel plan-form, were briefly discussed.

7.2 The main findings of this research that have significance beyond the individual case studies

The research presented in this thesis highlights topics that are important for improving both the understanding of fluvial cross-bedded sandstone and the resultant reconstructions of fluvial depositional systems. These are summarized as follows:

1. *Addition of two new types of cross-stratified units to Allen's (1963a) classification.* These take into account the formation of bottomsets and may be associated with specific formative flow and bedform conditions allowing detailed classification of cross-beds in relation to not only bedform type but flow conditions.
2. *New classifications of individual trough cross-bed sets on the basis of geometry (size and shape), divergence between scour trend and laminae dip direction, laminae dip and basal contact between foreset toe and scour base* to aid analysis of patterns. Classification of set types will allow analysis of relationships between sedimentary structure geometry and palaeocurrent, and variations with the stratigraphic position within units, storeys and sequences with the potential for better interpretation of channel types and changing environments of deposition.
3. *The ongoing issue of interpreting rock analogues based on the preserved deposits.* Herein, new classification of scour structures on the basis of width:length ratio suggests that scours will always present ratios < 1 unless interpretations are based on poorly preserved exposures and or inaccuracy of measurements.
4. *Identification of divergence between lamina dip direction and scour long axis* occurs and differs between study sites. Where systematic patterns are present, this records differences in flow conditions at the time of formation. It is likely to be related to the location within the channel system, style of channel system and bedform migrating pattern within the channel.
5. *The importance of further investigations on the character of erosion surfaces bounding cross bed sets and scour associated with dunes and unit bars.*

Although there has been a lot of research on bedforms and cross bedding, there is little published on this subject and further investigations will improve the understanding of bedform type associated with architecture of cross-bedding styles.

6. *The importance of the differentiation of basal bounding surface types in association with the filling cross beds to better understand origin and architecture of cross-bed sets.* Basal bounding surface of trough cross-bed units that were formed from concave-up scours in association with bedforms may be differentiated from similar structures resulting from cross bed filling pre-existing or contemporary but unrelated scours by the scale in relation to cross bedding and interpreted channel size, and the geometry and characteristics of the scour fill, evidence of obstacles.
7. *Relationship between bar lee-face angle variation and bar height* may be used to infer bedform size variations and therefore flow conditions associated to these changes, and ultimately improve interpretations of fluvial cross-stratified deposits.
8. *The importance of identifying and understanding the mechanism of reactivation surfaces* and their relationship with lee-face angle variations in previous and future interpretations. Their analysis in this thesis highlights that these surfaces are often wrongly interpreted as cross beds within cross-stratified units indicating variations of the laminae dip and subsequently variations on parameters associated to lee-face angle; whereas what they represent are temporary angle variations associated with movement of superimposed bedforms.
9. *The importance of the mechanisms and patterns of scour formation and scour filling with the associated formation of bottomsets* for the clarification of formative flow and bedform type, and the understanding of cross-stratification architecture. This is a subject that has largely been ignored to date and any advance of understanding of scour formation and fill in association with bedform development and migration would greatly advance knowledge of cross-bedded sandstones.

7.3 Further work

Some additional questions that have arisen during this thesis that would be useful for interpreting fluvial cross-stratification and allow a better understanding of their depositional systems are presented below:

- Data sets from the field case studies demonstrated that no measurable relationships are found between scour structures geometry and flow characteristics. This was unexpected; sampling methodologies may have caused these results. Therefore, further investigations are needed for clarification.
- Grain size and mineral composition analysis are needed to determine if these characteristics correlate with the geometries of the sedimentary structures.
- Investigations of the relationship between set thickness and trough dimensions in plan-view are required to determine whether bedform dimensions and scour shape are related. Further work needs to be performed using the set thickness (width:set thickness ratio) as a variable to classify scour structures.
- The scour shape is a function of: (a) the original style and pattern of scour which are in part controlled by the morphology of bedform crests, (b) the longevity of scouring as the bedform advances to fill the scour, and (c) subsequent preservation. None of these three controls has been fully investigated and work on these would advance understanding of cross-bedding.
- It appears that the crestline of the host bedform influences the scour shape. Therefore, further investigations are suggested on this subject to answer questions such as: Is the bedform crest always initially straight before the scour is formed? In that case, unit bars could be still considered as formative bedforms of scour structures. Or does the initial bedform crest need to be already sinuous to generate a scour structure? Additional studies on crestline development would also be useful.
- Further investigations on modern systems and flume work are required to accurately study bedform migration, trough development and the three hypothetical initial scour shapes suggested here (Section 2.7.1).
- Due to the diverse interpretations of bottomset formation, further studies on the formation of bottomsets generated by dunes and unit-bars and the flow conditions suitable for their formation are required.

- Additional flume work using beds of several grain sizes and compositions are required for more realistic comparisons between flume and field deposits.
- Because of the variability in field sampling methodologies, interpretations of the depositional systems of the same deposits vary. Therefore, further work with a more complete interpretation of the depositional system would help to clarify the diverse hypothetical interpretations.
- The depositional processes on the lee of dunes and bars have previously been described as following the same dynamics. However, different bedforms are expected to show variations in behaviour and this may influence sediment depositional processes. Then, what are the differences during sediment deposition? Given the similarity (and differences) in processes that operated in the flume and are likely to have operated in the river when the case-study sandstones were deposited, understanding these differences may be useful to differentiate deposits generated by dunes and unit bars.
- Further investigations based on experimental work using a fix-designed bed, with several steady and unsteady flow conditions will help to determine and discard variables as controls on the internal architecture of cross-stratification and its variations.

Fluvial style, channel dimensions and plan-form influence flow regime, sediment transport and depositional processes; and therefore variations on forming bedforms and cross-bedding type are expected (e.g., different types of bars are more susceptible to form in different parts of the channel). Thus, only a very small number of factors could be investigated in the time available and it was not possible to account for the influence of all the other factors because not enough research has been done by anyone yet. To conclude, the analysis on cross-bedded sandstones, detailed study of the scour structures; the comparison of similar deposits embedded within different fluvial depositional systems and the integrations of flume experiment observations, that is part of the work herein presented, improves the understanding of the depositional environments that generated the Prados Formation and the Seaton Sluice Sandstone by adding more detailed interpretations to previous published studies.

References

- Absalom, R. G. and Hoppkins, W.** (1926) The geological relations of the coast sections between Tynemouth and Seaton Sluice. *Proc. Univ. Durham Phil. Soc.*, **7**, 142-157.
- Alexander, J.** (1992) Nature and origin of a laterally extensive alluvial sandstone body in the Middle Jurassic Scalby Formation. *Journal of the Geological Society*, **149**(3), 431-441.
- Alexander, J., Bridge, J. S., Cheel, R. J. and Leclair, S. F.** (2001) Bedforms and associated sedimentary structures formed under supercritical water flows over aggrading sand beds. *Sedimentology*, **48**(1), 133-152.
- Alexander, J. and Gawthorpe, R. L.** (1993) The complex nature of a Jurassic multistorey, alluvial sandstone body, Whitby, North Yorkshire. In: *Characterization of fluvial and aeolian reservoirs*. Geological Society of London, Special Publication, **73**, 123-142.
- Allen, J. R. L.** (1962) Petrology, origin and deposition of the highest lower Old Red Sandstone of Shropshire, England. *Journal of Sedimentary Research*, **32**(4), 657-697.
- Allen, J. R. L.** (1963a) The classification of cross-stratified units. With notes on their origin. *Sedimentology*, **2**(2), 93-114.
- Allen, J. R. L.** (1963b) Henry Clifton Sorby and the sedimentary structures of sands and sandstones in relation to flow conditions. *Geol Mijnbouw* **42**, 223-228.
- Allen, J. R. L.** (1965a) The sedimentation and palaeogeography of the old red sandstone of Anglesey, North Wales. *Proceedings of the Yorkshire Geological Society*, **35**(2), 139-185.
- Allen, J. R. L.** (1965b) A review of the origin and characteristics of recent alluvial sediments. *Sedimentology*, **5** (2), 89-191.

- Allen, J. R. L.** (1965c) Sedimentation to the lee of small underwater sandwaves: an experimental study. *Journal of Geology*, **73**, 95-116.
- Allen, J. R. L.** (1968a) Flute marks and flute separation. *Nature*, **219**(5154), 602-604.
- Allen, J. R. L.** (1968b) Current ripples. North Holland, Amsterdam.
- Allen, J. R. L.** (1970) Studies in fluvial sedimentation: a comparison of fining-upward cyclothems, with special reference to coarser-member composition and interpretation. *Journal of Sedimentary Petrology*. **40**, 298-323.
- Allen, J. R. L.** (1973) Features of cross-stratified units due to random and other changes in bed forms. *Sedimentology*, **20**(2), 189-202.
- Allen, J. R. L.** (1982) *Sedimentary Structures: Their Character and Physical Basis*, Volume I. Developments in Sedimentology 30. Elsevier Science Publishers, Amsterdam.
- Allen, J. R. L.** (1983a) River bedforms: progress and problems. *International Association of Sedimentologists, Special Publications*, **6**, 19-33.
- Allen, J. R. L.** (1983b) Studies in fluvial sedimentation: bars, bar-complexes and sandstone sheets (low-sinuosity braided streams) in the Brownstones (L. Devonian), Welsh Borders. *Sedimentary Geology*, **33**, 237 – 293.
- Allen, J. R. L.** (1984) Soft-sediment deformation structures. In: *Developments in Sedimentology 30. Sedimentary Structures: Their character and physical basis, Volumen 1*, 2nd Edn, pp. 345-346. Elsevier, Amsterdam.
- Allen, J. R. L.** and **Collinson, J. D.** (1974) The superimposition and classification of dunes formed by unidirectional aqueous flows. *Sedimentary Geology*, **12**, 169-178.
- Allen, J. R. L.** and **Friend, P. F.** (1968) Deposition of the catskill facies, appalachian region: With notes on some other old red sandstone basins. *Special paper of the Geological Society of America* **106**: 21-74.
- Amsler, M. L.** and **García, M. H.** (1997) Discussion: Sand dune geometry of large rivers during floods. *Journal of Hydraulic Engineering*, **123**, 582-585.
- Ashley, G. M.** (1990) Classification of large scale subaqueous bedforms: a new look at

an old problem. *Journal of Sedimentary Research*, **60**, 160-172.

Ashworth, P. J. (1996) Mid-channel bar growth and its relationship to local flow strength and direction. *Earth Surface Processes and Landforms*, **21**, 103-123.

Ashworth, P. J., Sambrook Smith, G. H., Best, J. L., Bridge, J. S., Lane, S. N., Lunt, I. A., Reesink, A. J. H., Simpson, C. J., and Thomas, R. E. (2011) Evolution and sedimentology of a channel fill in the sandy braided South Saskatchewan River and its comparison to the deposits of an adjacent compound bar. *Sedimentology*, **58**(7), 1860-1883.

Bass, J. H., Best, J. L. and Peakall, J. (2011) Depositional processes, bedform development and hybrid bed formation in rapidly decelerated cohesive (mud-sand) sediment flows. *Sedimentology*, **58**, 1953-1987.

Bennette, S. J. and Bridge, J. S. (1995) Mean flow and turbulence structure over fixed, two-dimensional dunes: implications for sediment transport and bedform stability. *Sedimentology*, **42**(3), 491-513.

Bernini, A, Caleffi, V. and Valiani, A. (2006) Numerical modelling of alternate bars in shallow channels. In: *Braided Rivers Process, Deposits, Ecology and Management* (Eds G.H. Sambrook Smith, J.L. Best, C.S. Bristow and G.E. Petts). *International Association of Sedimentologists Special Publication*, **36**, 154-175.

Best, J. L. (1986) The morphology of river channel confluences. *Progress in Physical Geography*, **10**(2), 157-174.

Best, J. L. (1987) Flow dynamics at river channel confluences: implications for sediment transport and bed morphology. *Recent Developments in Fluvial Sedimentology*, SEPM (Society for Sedimentary Geology), **39**, 27-35.

Best, J. L. (1988) Sediment transport and bed morphology at river channel confluences. *Sedimentology*, **35**(3), 481-498.

Best, J. L. (1992) On the entrainment of sediment and initiation of bed defects: insights from recent developments within turbulent boundary layer research. *Sedimentology* **39**(5), 797-811.

- Best, J. L.** (2005) The fluid dynamics of river dunes: A review and some future research directions. *Journal of Geophysical Research*, **110**, F04S02.
- Best, J. L., Asworth, P. J., Bristow, C. S. and Roden, J.** (2003) Three-Dimensional Sedimentary Architecture of a Large, Mid-Channel Sand Braid Bar, Jamuna River, Bangladesh. *Journal of Sedimentary Research*, **73**(4), 516-530.
- Best, J. L., Blois, G., Barros, J. and Christensen, K.** (2013) The dynamics of bedform amalgamation: new insights from very thin flume. In: *Marine and River Dune Dynamics – MARID IV*, Bruges, Belgium.
- Blatt, H., Middleton, G. and Murray R.** (1980) Primary sedimentary structures. In: *Origin of Sedimentary Rocks*, 2nd Edn, pp. 127-205. Prentice-Hall, Inc., Englewood Cliffs, New Jersey.
- Blom, A. and Kleinhans M. G.** (2008) Estimating bed form height from sorting preserved in sedimentary records of river dunes, deltas and bars. In: *River, Coastal and Estuarine Morphodynamics: RCEM 2007, Two Volume Set* (Eds. C. Marjolein Dohmen-
- Bluck, B. J.** (1971) Sedimentation in the meandering River Endrick. *Scottish Journal of Geology*, **7**, 93-138.
- Bridge, J. S.** (1985) Paleochannel patterns inferred from alluvial deposits: a critical evaluation. *Journal of Sedimentary Petrology*, **55**(4), 579-589.
- Bridge, J. S.** (1997) Thickness of sets of cross strata and planar strata as a function of formative bed-wave geometry and migration, and aggradation rate. *Geology*, **25**(11), 971-974.
- Bridge, J. S.** (2003) *Rivers and Floodplains: Forms, Processes, and Sedimentary Record*, Blackwell, Oxford. 17, 78-107, 402-403 pp.
- Bridge, J. S. and Gabel, S. L.** (1992) Flow and sediment dynamics in a low-sinuosity, braided river: Calamus River, Nebraska Sandhills. *Sedimentology*, **39**, 125-142.
- Bridge, J. S. and Diemer, J. A.** (1983) Quantitative interpretation of an evolving ancient river system. *Sedimentology*, **30**(5), 599-623.

- Bridge, J. S. and Mackey S. D.** (1993) A Theoretical Study of Fluvial Sandstone Body Dimensions. In: *The Geological Modelling of Hydrocarbon Reservoirs and Outcrop Analogues* (Eds. S. S. Flint and I. D. Bryant), pp. 213-236. Blackwell Publishing Ltd., Oxford.
- Bridge, J. S., Alexander, J., Collier, R. E. LL., Gawthorpe, R. L. and Jarvis, J.** (1995) Ground-penetrating radar and coring used to study the large-scale structure of point-bar deposits in three dimensions. *Sedimentology*, **42**, 839–852.
- Bridge, J. S. and Best, J.** (1997) Preservation of planar laminae due to migration of low-relief bed waves over aggrading upper-stage plane beds: Comparison of experimental data with theory. *Sedimentology*, **44**(2), 253-262.
- Bridge, J., Collier, R. and Alexander, J.** (1998). Large-scale structure of Calamus River deposits (Nebraska, USA) revealed using ground-penetrating radar. *Sedimentology*, **45**(6), 977-986.
- Bridge, J. S. and Tye, R. S.** (2000) Interpreting the dimensions of ancient fluvial channel bars, channels, and channel belts from wireline-logs and cores. *American Association of Petroleum Geologists Bulletin*, **84**(8), 1205-1228.
- Bristow, C. S.** (1993) Sedimentology of the Rough Rock: a Carboniferous braided river sheet sandstone in northern England. In: *Braided Rivers* (Eds. J. L. Best and C. S. Bristow), Geological Society Special Publication, **75**, 291-304.
- Brookfield, M. E.** (1977) The origin of boudig surfaces in ancient Aeolian sandstones. *Sedimentology*, **24**, 303-332.
- Bryant, M., Falk, P. and Paola, C.** (1995) Experimental study of avulsion frequency and rate of deposition. *Geology*, **23**(4), 365-368.
- Cadle, A. B. & Cairncross, B.** (1993) A sandy, bed-load dominated fluvial system deposited by lateral-accretion: Permian Karoo Sequence, South Africa. *Sedimentary Geology*, **85**, 435-455.
- Cant, D. J.** (1976) Sandy Braided Stream Sedimentation in the South Saskatchewan River. Unpublished PhD thesis, McMaster University, pp 248.
- Cant, D. J. and Walker, R. G.** (1978) Fluvial processes and facies sequences in the

sandy braided South Saskatchewan River, Canada. *Sedimentology*, **25**, 625-648.

Carling, P. A., Götz, E., Orr, H. G. and Radecki-Pawlik, A. (2000) The morphodynamics of fluvial sand dunes in the River Rhine, near Mainz, Germany. I. Sedimentology and morphology. *Sedimentology*, **47**(1), 227-252.

Carling, P. A., Richardson, K. and Ikeda, H. (2005) A flume experiment on the development of subaqueous fine-gravel dunes from a lower-stage plane bed. *Journal of Geophysical Research*, **110**, F04S05.

Cartigny, M. J. B., Ventra, D., Postma, G. and Van der Berg, J. H. (2014) Morphodynamics and sedimentary structures of bedforms under supercritical-flow conditions: New insights from flume experiments. *Sedimentology*, **61**(3), 712-748.

Cherven, V. B. (1978) Fluvial and deltaic facies in the Sentinel Butte Formation, central Williston Basin. *Journal of Sedimentary Research*, **48**(1), 159-170.

Chitale, S. V. (1970) River channel patterns. *Journal of Hydraulics Division, American Society of Civil Engineers*, **96**, 201-21.

Church, M. and Jones, D. (1982) Channel bars in gravel-bed rivers. In: *Gravel-Bed Rivers Fluvial Processes, Engineering and Management* (Eds R.D. Hey, J.C. Bathurst and C.R. Thorne), *John Wiley & Sons*, Chichester, 291-324.

Coleman, S. E. and Melville, B. W. (1996) Initiation of Bed Forms on a Flat Sand Bed. *Journal of Hydraulic Engineering*, **122**(6), 301-310.

Coleman, S. E. and Nikora, V. I. (2009). Bed and flow dynamics leading to sediment-wave initiation. *Water Resources Research*, **45**(4), W04402.

Collinson, J. D. (1970) Bedforms of the Tana river, Norway. *Geogr. Ann., Series A, Physical Geography*, **52**, 31-56.

Collinson, J. D. (1978) Vertical sequence and sand body shape in alluvial sequences. In: *Fluvial Sedimentology* (Ed. A. D. Miall) Canadian Society of Petroleum Geologist, *Memorium*, **5**, 577-586.

- Collinson, J. D. and Thompson, D. B.** (1982) Depositional structures of sands and sandstones. In: *Sedimentary Structures*, 1st edn, pp. 59-104. George Allen and Unwin, London.
- Crowley, K. D.** (1983) Large-scale bed configurations (macroforms), Platte River Basin, Colorado and Nebraska: Primary structures and formative processes. *Geological Society of America Bulletin*, **94** (1), 117-133.
- Dalrymple, R. W. Knight, R. J. and Lambiase, J. J.** (1978) Bedforms and their hydraulic stability relationship in a tidal environment, Bay of Fundy, Canada. *Nature*, **275**, 100-104.
- Davies, S. J.** (2008) The record of Carboniferous sea-level change in low-latitude sedimentary successions from Britain and Ireland during the onset of the late Paleozoic ice age. *Geological Society of America Special Papers*, **441**, 187-204.
- Davies, S. J., Guión, P. D. and Gutteridge, P.** (2012) Carboniferous Sedimentation and Volcanism on the Laurussian Margin. In: *Geological History of Britain and Ireland* (Eds. Woodcock, N. and Strachan, R.), pp. 231-273. John Wiley & Sons, Ltd, Chichester, UK.
- Dean, M. T., Browne, M. A. E., Waters, C. N. and Powell, J. H.** (2011) A lithostratigraphical framework for the Carboniferous successions of northern Great Britain (onshore); *British Geological Survey*, 165pp.
- Dixon, E. E. L.** (1921) Geology of the South Wales Coalfield, Part 13. The country around Pembroke and Tenby. *Geological Survey Great Britain Memoir*, p. 220.
- Duller, R. A., Mountney, N. P., Nigel, P., Russel, A. J., and Cassidy, N. C.** (2008) Architectural analysis of a volcanoclastic jökulhlaup deposit, southern Iceland: sedimentary evidence for supercritical flow. *Sedimentology*, **55**(4), 939-964.
- Dzulynski, S. and Walton, E. K.** (1965) Sedimentary features of Flysch and Graywackes. Elsevier, Amsterdam.
- Elliott, T. and Gardiner, A. R.** (2009) Ripple, Megaripple and Sandwave Bedforms in the Macrotidal Loughor Estuary, South Wales, U.K. In: *Holocene Marine*

Sedimentation in the North Sea Basin, (Eds. Nio, S.-D., Shüttenhelm, R. T. E. and Van Weering, Tj. C. E.), Blackwell Publishing Ltd, Oxford, UK, pp. 51-64.

Ethridge, F. G. (2011) Interpretation of ancient fluvial channel deposits: review and recommendations. In: *From river to rock record*. (Eds. S. K. Davidson, S. Leleu, and C. P. North). Society for Sedimentary Geology (SEMP), Special Publication, **97**, 9-35.

Ethridge, F. G., and **Schumm, S. A.** (1978) Reconstructing palaeochannel morphologic and flow characteristics: methodology, limitations and assesment. In: *Fluvial sedimentology*. (Ed. A. D. Miall), Memoir of Canadian Society of Petroleum Geologists, **5**, 703-722.

Fernandez, R., Best, J. and López, F. (2006) Mean flow, turbulence structure, and bed form superimposition across the ripple-dune transition. *Water Resources Research*, **42**(5), W05406.

Fielding, C. R. (1986) Fluvial channel and overbank deposits from the Westphalian of the Durham coalfield, NE England. *Sedimentology*, **33**, 119-140.

Fielding, C. R. (2006) Upper flow regime sheets, lenses and scour fills: Extending the range of architectural elements for fluvial sediment bodies. *Sedimentary Geology*, **190**, 227-240.

Fielding, C. R., Alexander, J. and McDonald, R. (1999) Sedimentary facies from GPR surveys of the modern, upper Burdekin River of north Queensland, Australia: consequences of extreme discharge fluctuations. In: *Fluvial Sedimentology VI* (Eds N.D. Smith and J. Rogers), IAS Special Publication, **28**, 347–362. Blackwell Publishing, Oxford.

Fielding, C. R. and Crane, R. C. (1987) An application of statistical modelling to the prediction of hydrocarbon recovery factors in fluvial reservoir sequences. In: *Recent Developments in Fluvial Sedimentology* (Eds. F. G. Ethridge, R. M. Flores, and M. D. Harvey), **39**, 321-327. Society of Economic Paleontologists Mineralogists Special Publication.

Fielding, C. R., Allen, J. P., Alexander, J. and Gibling, M. G. (2009) Facies model for fluvial systems in the seasonal tropics and subtropics. *Geology*, **37**(7), 623-626.

- Fielding, C. R., Allen, J. P., Alexander, J., Gibling, M. R., Rygel, M. C. and Calder, J. H.** (2011) Fluvial systems and their deposits in hot, seasonal semiarid and subhumid settings: Modern and ancient examples. In: *From River to Rock Record* (Eds. S. K. Davison, S. Leleu, C. P. North), SEMP Special Publication, **97**, 89-111.
- Fisk, H. N.** (1944) Geological investigation of the alluvial valley of the Lower Mississippi River. *Rep. Mississippi River Commission*, Vicksburg, Miss. 78 pp.
- Frazier, D. E., and Osanik, A.** (1961) Point bar deposits, Old River Locksite, Louisiana. *Gulf Coast Association of Geological Societies Transactions*, **11**, 121-137.
- Friend, P. F.** (1983) Towards the field classification of alluvial architecture or sequence. In: Modern and ancient fluvial systems. *Special publications of the International Association of Sedimentologists*, 345-354.
- Friend, P. F., Slater, M. J. and Williams, R. C.** (1979) Vertical and lateral building of river sandstone bodies, Ebro Basin, Spain. *Journal of the Geological Society*, **136**, 39-46.
- Friend, P. F., Hirst, J. P. P. and Nichols, G. J.** (1986) Sandstone-body structure and river process in the Ebro Basin of Aragón, Spain. *Cuadernos de Geología*, **10**, 9-30.
- Frings, R. M.** (2011) Sedimentary characteristics of the gravel-sand transition in the river rhine. *Journal of Sedimentary Research*, **81**(1), 52-63.
- Gabel, S. L.** (1991) Geometry and kinematics of dunes in the Calamus River, Nebraska. PhD thesis, State University of New York at Binghamton.
- Gabel, S. L.** (1993) Geometry and kinematics of dunes during steady and unsteady flows in the Calamus River, Nebraska, USA. *Sedimentology*, **40**(2), 237-269.
- Gawthorpe, R. L., Collier, R. E. LL., Alexander, J., Bridge, J. S., and Leeder, M. R.** (1993) Ground penetrating radar: application to sandbody geometry and heterogeneity studies. In: *Characterization of fluvial and aeolian reservoirs*. (Eds. C. P. North and D. J. Prosser). Geological Society London, Special Publication, **73**, 421-432.
- Ghinassi, M., Nemeč, W., Aldinucci, M., Nehyba, S., Ozaksoy, V. and Fidolini, F.** (2014) Plan-form evolution of ancient meandering rivers reconstructed from longitudinal outcrop sections. *Sedimentology*, **61**, 952-977.

- Ghoshal, K., Mazumber, B. S. and Purkait, B.** (2010) Grain-size distributions of bed load: Inferences from flume experiments using heterogeneous sediment beds. *Sedimentary Geology*, **223**(1–2), 1-14.
- Gilbert, G. K.** (1914) The transportation of debris by running water. *US Geological Survey professional paper* **86**.
- Goff, J. R. and Ashmore P.** (1994) Gravel transport and morphological change in braided Sunwapta River, Alberta, Canada. *Earth Surface Processes and Landforms*, **19**, 195-212.
- Google Earth** (2014) Seaton Sluice 55°05'03.25"N 1°28'17.03"W, Eye alt 585 m. Infoterra Ltd. & Bluesky, 2012. (Accessed in June 12, 2014).
- Gradzinski, R.** (1970) Sedimentation of dinosaur-bearing Upper Cretaceous deposits of the Nemegt Basin, Gobi dessert. *Palaeontology, Pol*, **21**, 147-229.
- Grenfell, S. E., Aalto, R. and Nicholas, A.** (2014) Fluvial connectivity and climate: A comparison of channel pattern and process in two climatically contrasting fluvial sedimentary systems in South Africa. *Geomorphology* **205**, 142-154.
- Guión, P. D., Fulton, I. M. and Jones, N. S.** (1995) Sedimentary facies of the coal-bearing Westphalian A and B north of the Wales-Brabant High. *Geological Society Special Publication*, **82**, 45-78.
- Gyr, A. and Schmid, A.** (1989) The different ripple formation mechanism. *Journal of Hydraulic Research* **27**, 61-74.
- Hassan, M. A., Marren, P. M. and Schwartz, U.** (2009) Bar structure in an arid ephemeral stream. *Sedimentary Geology*, **221**, 57-70.
- Harms, J. C. and Fahnestock R. K.** (1965) Stratification, bed forms, and flow phenomena (with an example from Río Grande). In: *Primary Sedimentary Structures and Their Hydrodynamic Interpretation* (Ed. G. V. Middleton), *Society for Economic Paleontologists Mineral Special Publication*, **12**, 84-115.
- Harms, J. C., Southard, J. B., Spearing, D. R. and Walker, R. G.** (1975) Depositional environments as interpreted from primary sedimentary structures and stratification sequences. *Society of Economic Paleontologists, Mineral Short Course* **2**.

- Haszeldine, R. S.** (1981) *Westphalian B coalfield sedimentology in NE England and its regional setting*. Unpublished Ph.D. Thesis. University of Strathclyde, UK.
- Haszeldine, R. S.** (1983a) Descending Tabular Cross-Bed Sets and Bounding Surfaces from a Fluvial Channel in the Upper Carboniferous Coalfield of North-East England. In: *Modern and ancient fluvial systems* (Eds. J. D. Collinson and J. Lewin. Blackwell Publishing Ltd.) *Special Publication International Association of Sedimentologists*, **6**, 449-456.
- Haszeldine, R. S.** (1983b) Fluvial bars reconstructed from a deep, straight channel, Upper Carboniferous coalfield of Northeast England. *Journal of Sedimentary Research*, **53**(4), 1233-1247.
- Hein, J. and Walker, R. G.** (1977) Bar evolution and development of stratification in the gravelly, braided, Kicking Horse River, British Columbia. *Canadian Journal of Earth Sciences*, **14**, 562-570.
- Herbert, C. M., Alexander, J., and Martínez de Álvaro, M. J.** (2015) Back-flow ripples in the troughs of bars: formation, preservation and value for interpreting flow conditions. *Sedimentology*.
- Holzweber, B. L. and Hartley, A. J.** (2011) Generation of 3-D Outcrop models: A study from Seaton Sluice. Poster presented at the Annual Meeting of the British Sedimentological Research Group, London.
- Holzweber, B. I.** (2012) *Bar-scale Alluvial Geometry: Controlling Parameters, Identification in the Rock Record and Implications for Reservoir Modelling*. Unpublished Ph.D. Thesis. University of Aberdeen, UK.
- Holzweber, B. I., Hartley, A. J. and Weissmann, G. S.** (2014) Scale invariance barforms: implications for interpretation of fluvial systems in the rock record. *Petroleum Geoscience*, **20**, 211-224.
- Jackson, R. G.** (1975) Hierarchical attributes and a unifying model of bedforms composed of cohesionless sediment and produced by shearing flow. *Geological Society of America Bulletin*, **86**, 1523-33.

- Jackson, R. G.** (1976) Sedimentological and fluid-dynamic implications of the turbulent bursting phenomenon in geophysical flows. *Journal of Fluid Mechanics*, **77**, 531-560.
- Jerolmack, D.** and **Mohrig, D.** (2005) Interactions between bed forms: Topography, turbulence, and transport. *Journal of Geophysical Research: Earth Surface* **110**, F02014.
- Johnson, R. H.** and **Paynter, J.** (1967) Development of a cut off on the River Irk at Chadderton, Lancashire. *Geography*, **52**, 41-49.
- Jones, J. M.** (1967) Geology of the coast section from Tynemouth to Seaton Sluice and Millerite from Boldon Colliery. *Transactions of the Natural History Society of Northumberland, Durham and New Castle Upon Tyne*, **15**, n.3.
- Jones, C. M.** (1977) The sedimentology of Carboniferous fluvial and deltaic sequences. The Roaches Grit Group of the south west Pennines and the Pennant Sandstone of the Rhondda Valleys. Unpublished Ph.D. Thesis, University of Keele, United Kingdom.
- Jones, C. M.** (1979) Tabular cross-bedding in Upper Carboniferous fluvial channel sediments in the southern Pennines, England. *Sedimentary Geology*, **24**(1-2), 85-104.
- Jopling, A. V.** (1964) Laboratory study of sorting processes related to flow separation. *Journal of Geophysical Research*, **69**(16), 3403-3418.
- Jopling, A. V.** (1965) Hydraulic factors controlling the shape of laminae in laboratory deltas. *Journal of Sedimentary Research*, **35**(4), 777-791.
- Jopling, A. V.** (1966) Origin of cross-laminas in a laboratory experiment. *Journal of Geophysical Research*, **71**(4), 1123-1133.
- Jopling, A. V.** and **Richardson, E. V.** (1966) Backset bedding developed in shooting flow in laboratory experiments. *Journal of Sedimentary Research*, **36**(3), 821-825.
- Jopling, A. V.** and **Walker, R. G.** (1968) Morphology and origin of ripple-drift cross-lamination, with examples from the Pleistocene of Massachusetts. *Journal of Sedimentary Research*, **38**(4), 971-984.
- Karcz, I.** (1968) Fluvial obstacle marks from the wadis of the Negev (Southern Israel). *Journal of Sedimentary Petrology*, **38**, 1000-1012.

- Klein, G. D.** (1970) Depositional and dispersal dynamics of intertidal sand bars. *Journal of Sedimentary Research*, **40**(4), 1095-1127.
- Kleinhans, M. G.** (2004) Sorting in grain flows at the lee side of dunes. *Earth-Science Reviews*, **65**(1-2), 75-102.
- Kleinhans, M. G.** (2005) Upstream sediment input effects on experimental dune trough scour in sediment mixtures. *Journal of Geophysical Research*, **110**, F04S06.
- Kostaschuk, R., Shugar, D., Best, J., Parsons, D. Lane, S., Hardy, R. and Orfeo, O.** (2009) Suspended sediment transport and deposition over a dune: Río Paraná, Argentina. *Earth Surface Processes and Landforms* **34**(12), 1605-1611.
- Land, D. H.** (1974) Geology of the Tynemouth District. *Memoirs of the Geological Survey of Great Britain*.
- Leclair, S. F.** (2002) Preservation of cross-strata due to the migration of subaqueous dunes: An experimental investigation. *Sedimentology*, **49**, 1157-1180.
- Leclair, S. F.** (2006) New pieces to the puzzle of reconstructing sediment paleofluxes from river dune deposits. *Geology*, **34**(5), 401-404.
- Leclair, S. F., Bridge, J. S. and Wang, F.** (1997) Preservation of crossstrata due to migration of subaqueous dunes over aggrading and non-aggrading beds: Comparison of experimental data with theory. *Geoscience Canada*, **24**(1), 55-66.
- Leclair, S. F. and Bridge, J. S.** (2001) Quantitative interpretation of sedimentary structures formed by river dunes. *Journal of Sedimentary Research*, **71**(5), 713-716.
- Leclair, S. F. and Blom, A.** (2005) A Qualitative Analysis of the Distribution of Bed-Surface Elevation and the Characteristics of Associated Deposits for Subaqueous Dunes. In: *Fluvial Sedimentology VII* (Eds. M. D. Blum, S. B. Marriott and S. F. Leclair), Blackwell Publishing Ltd., Oxford, UK.
- Leeder, M. R.** (1973) Fluvial fining-upwards cycles and the magnitude of palaeochannels. *Geological Magazine*, **110**(03), 265-276.

- Leeder, M. R.** (1999) Bedforms and structures formed by unidirectional water flows over granular sediment. In: *Sedimentology and Sedimentary Basins. From turbulence to tectonics*. 1st edn, pp. 145-160. Blackwell Science, Oxford.
- Leleu, S. Van Lanen, X. M. T. and Hartley, A. J.** (2010) Controls on the architecture of a Triassic sand fluvial system, Wolville Formation, Fundy Basin, Nova Scotia, Canada: Implications for the interpretation and correlation of ancient fluvial successions. *Journal of Sedimentary Research*, **80**, 867-883.
- Leopold, L. B. and Wolman, M. G.** (1960) River meanders. *Geological Society of America Bulletin*, **71**, 769-94.
- Lorenz, J. C., Heinze, D. M. Clark, J. A. and Searls, C. A.** (1985) Determination of widths of meander-belt sandstone reservoirs from vertical downhole data, Mesaverde Group, Piceance Creek Basin, Colorado. *Bulletin American Association of Petroleum Geologists*, **69**, 710-721.
- Lunt, I. A. Bridge, J. S. and Tye, R. S.** (2004) A quantitative, three-dimensional depositional model of gravelly braided rivers. *Sedimentology*, **51**, 377-414.
- Lunt, I. A. and Bridge, J. S.** (2007) Formation and preservation of open-framework gravel strata in unidirectional flows. *Sedimentology*, **54**(1), 71-87.
- Lunt, I. A., Sambrook Smith, G. H., Best, J. L., Ashworth, P. J., Lane, S. N. and Simpson, C. J.** (2013) Deposits of the sandy braided South Saskatchewan river: Implications for the use of modern analogs in reconstructing channel dimensions in reservoir characterization. *AAPG Bulletin*, **97**(4), 553-576.
- IGME (Instituto Geológico y Minero de España Magna)** (1979). Sheet 489 (1st Series), *Molina, Spain*. 1:50000. Authorised: C.S.G. 1972 Depósito Legal: M-6.791-1978, Madrid.
- IGME (Instituto Geográfico Nacional de España)**. Colour digital orthophotograph of Spain, Molina de Aragón Area, <http://www.ign.es/wms-inspire/pnoa-ma>.
- Martinius, A. W. and Van den Berg, J. H.** (2011) Atlas of sedimentary structures in estuarine and tidally-influenced river deposits of the Rhine-Meuse-Scheldt system. European Association of Geoscientists & Engineers, Houten, pp 85.

- McCabe, P. J.** (1977) Deep distributary channels and giant bedforms in the Upper Carboniferous of the Central Pennines, northern England. *Sedimentology*, **24**, 271-290.
- McCabe, P. J.** and **Jones, C. M.** (1977) Formation of reactivation surfaces within superimposed deltas and bedforms. *Journal of Sedimentary Research*, **47**(2), 707-715.
- MacDonald, R. G., Alexander, J., Bacon, J. C., and Cooker, M. J.** (2013) Variations in the architecture of hydraulic-jump bar complexes on non-eroding beds. *Sedimentology*, **60**, 1291-1312.
- McKee, E. D.** (1938) Original structures in Colorado River flood deposits of Grand Canyon. *Journal of Sedimentary Research*, **8**(3), 77-83.
- McKee, E. D.** (1939) Some types of bedding in the Colorado River delta. *Journal of Geology*, **47**, 64-81.
- McKee, E. D.** and **Weir, G. W.** (1953) Terminology for stratification and cross-stratification in sedimentary rocks. *Geological Society of America Bulletin*, **64**(4), 381-390.
- McLean, S. R.** (1990) The stability of ripples and dunes. *Earth-Science Reviews* **29**(1-4), 131-144.
- Miall, A. D.** (1977) A review of the braided depositional environment. *Earth-Science Reviews*, **13**, 1-62.
- Miall, A. D.** (1978) Lithofacies and vertical profile models in braided rivers: a summary. In: *Fluvial Sedimentology* (Ed. A. D. Miall), *Canadian Society of Petroleum Geologists*, **5**, 597-604.
- Miall, A. D.** (1984) Collecting data and Basin mapping methods. In: *Principles of Sedimentary Basin Analysis*, 1st edn, pp. 7-71; 213-275. Springer-Verlag, New York.
- Miall, A. D.** (1985) Architectural-Element Analysis: a new method of facies analysis applied to fluvial deposits. *Earth-Science Reviews*, **22**, 261-308.
- Miall, A. D.** (1988a) Architectural elements and bounding surfaces in fluvial deposits: anatomy of the Kayenta Formation (Lower Jurassic), Southwest Colorado. *Sedimentary Geology*, **55**, 233-262.

- Miall, A. D.** (1988b) Reservoir heterogeneities in fluvial sandstones; lessons from outcrop studies. *American Association of Petroleum Geologists Bulletin*, **72**(6), 682-697.
- Miall, A. D.** (1988c) Facies architecture in clastic sedimentary basins. In: *New perspectives in basin analysis* (Eds. K. Kleinspehn and C. Paola) pp. 67-81. Springer, Berlin Heidelberg, New York.
- Miall, A. D.** (1996) Lithofacies. In: *The Geology of Fluvial Deposits*, (Ed. Miall, A. D.) Springer-Verlag, New York, 109-122.
- Miall, A. D. and Jones, B. G.** (2003) Fluvial architecture of the Hawkesbury Sandstone (Triassic), near Sydney, Australia. *Journal of Sedimentary Research*, **73**(4), 531-545.
- Moody-Stuart, M.** (1966) High- and low-sinuosity stream deposits, with examples from the Devonian of Spitsbergen. *Journal of Sedimentary Research*, **36**(4), 1102-1117.
- Mossop, G. D. and Flach, P. D.** (1983) Deep channel sedimentation in the Lower Cretaceous McMurray Formation, Athabasca Oil Sands, Alberta. *Sedimentology*, **30**(4), 493-509.
- Muñoz, A., Ramos, A., Sánchez-Moya, Y., and Sopena, A.** (1992) Evolving fluvial architecture during a marine transgression: Upper Buntsandstein, Triassic, central Spain. *Sedimentary Geology*, **75**(3-4), 257-281.
- Nakayama, K., Fielding, C. R. and Alexander, J.** (2002) variations in character and preservation potential of vegetation-induced obstacle marks in the variable discharge Burdekin River of north Queensland, Australia. *Sedimentary Geology*, **149**, 199-218.
- Nami, M. and Leeder, M. R.** (1978) Changing channel morphology and magnitude in the Scalby Formation (M. Jurassic) of Yorkshire, England. In: *Fluvial Sedimentology* (Ed. A. D. Miall) *Canadian Society of Petroleum Geologist, Memorium* **5**, 431-440.
- Needham, D. J. and Hey, R. D.** (1991) On nonlinear simple waves in alluvial river flows - A theory for sediment bores. *Philosophical Transactions of the Royal Society of London, Series A – Mathematical Physical and Engineering Sciences*, **334**, 25-53.
- Nijman, J. and Puigdefábregas, C.** (1978) Coarse-grained point bar structure in a molasse-type fluvial system, Eocene Castisent sandstone Formation, south Pyrenean

Basin. In: *Fluvial Sedimentology* (Ed. A. D. Miall) Canadian Society of Petroleum Geologist, *Memorium*, **5**, 487-510.

Okazaki, H., Nakazato, H. and Kwak, Y. (2013) Application of high-frequency ground penetrating radar to the reconstruction of 3D sedimentary architecture in a flume model of a fluvial system. *Sedimentary Geology*, **293**, 21-29.

O'Mara, P. T. and Turner, B. R. (1999) Sequence stratigraphy of coastal alluvial plain Westphalian B Coal Measures in Northumberland and the southern North Sea. *International Journal of Coal Geology*, **42**(1), 33-62.

Ordnance Survey (2013) MasterMap 1:10000 Raster [TIFF geospatial data], Scale 1:10000, Tiles: nz37nw, Updated: 22 March 2013, Ordnance Survey (GB), Using: EDINA Digimap Ordnance Survey Service, <<http://digimap.edina.ac.uk>>, Downloaded: Mon Jul 28 10:24:01 BST 2014.

Otto, G. H. (1938) The sedimentation unit and its use in field sampling. *Journal of Geology*, **46**, 569-582.

Paola, C. and Borgman, L. (1991) Reconstructing random topography from preserved stratification. *Sedimentology*, **38**(4), 553-565.

Parsons, D. R., Best, J. L., Orfeo, O., Hardy, R. J., Kostaschuck, R. and Lane, S. N. (2005) Morphology and flow fields of three-dimensional dunes, Rio Paraná, Argentina: Results from simultaneous multibeam echo sounding and acoustic Doppler current profiling. *Journal of Geophysical Research: Earth Surface*, **110**, F04S03.

Parsons, D. R. and Best, J. (2013) Bedforms: views and new perspectives from the third international workshop on Marine and River Dune Dynamics (MARID3). *Earth Surface Processes and Landforms*, **38**(3), 319-329.

Peabody, F. E. (1947) Current crescents in the Triassic Moenkopi Formation. *Journal of Sedimentary Petrology*, **17**(2), 73-76.

Peakall, J. Ashworth, P.J. and Best, J. L. (2007) Meander-bend evolution, alluvial architecture, and the role of cohesion in sinuous river channels: A flume study. *Journal of Sedimentary Research*, **77**, 197-212.

- Perillo, M. M., Best, J. L., Yokokawa, M. Sekiguchi, T., Takagawa, T. and García, M. H.** (2014a). A unified model for bedform development and equilibrium under unidirectional, oscillatory and combined-flows. *Sedimentology* **61**(7), 2063-2085.
- Perillo, M. M., Prokocki, E. W., Best, J. L. and García, M. H.** (2014b). Bed form genesis from bed defects under unidirectional, oscillatory, and combined flows. *Journal of Geophysical Research: Earth Surface*, **119**(12): 2014JF003167.
- Potter, P. E. and Pettijohn, F. J.** (1963) Cross-Bedding and Ripple Marks. In: *Paleocurrents and basin analysis* (Eds. P. E. Potter and F. J. Pettijohn), pp. 62-113. Springer-Verlag OHG, Berlin, Göttingen, Heidelberg.
- Puigdefabregas, C.** (1973) Miocene point-bar deposits in the Ebro Basin, Northern Spain. *Sedimentology*, **20**(1), 133-144.
- Ramos, A.** (1979) *Estratigrafía y Paleografía del Pérmico y Triásico al Oeste de Molina de Aragón (provincia de Guadalajara)*. Ph.D. Thesis. Universidad Complutense Madrid: Spain.
- Ramos, A. and Sopena, A.** (1983) Gravel bars in low-sinuosity streams (Permian and Triassic, Central Spain). *Modern and ancient fluvial systems*, 301-312.
- Ramos, A., Sopena, A. and Pérez-Arlucea, M.** (1986) Evolution of Buntsandstein fluvial sedimentation in the Northwest Iberian ranges (Central Spain), *Journal of Sedimentary Petrology*, **56**(6), 862-875.
- Raudkivi, A. J.** (1963) Study of sediment ripple formation. *Journal of the Hydraulics Division, ASCE*, **89**, 15-33.
- Raudkivi, A. J.** (1966) Bedforms in alluvial channels. *Journal of Fluid Mechanics*, **26**(3), 507-514.
- Raudkivi, A.** (2006) Transition from Ripples to Dunes. *Journal of Hydraulic Engineering*, **132**(12), 1316-1320.
- Raudkivi, A. J. and Witte, H. H.** (1990). Development of Bed Features. *Journal of Hydraulic Engineering* **116**(9), 1063-1079.

- Reesink, A. J. H. and Bridge, J. S.** (2007) Influence of superimposed bedforms and flow unsteadiness on formation of cross strata in dunes and unit bars. *Sedimentary geology*, **202**, 281-296.
- Reesink, A. J. H. and Bridge J. S.** (2009) Influence of bedform superimposition and flow unsteadiness on the formation of cross strata in dunes and unit bars - Part 2, further experiments. *Sedimentary Geology*, **222**, 274-300.
- Reesink, A. J. H. and Bridge, J. S.** (2011) Evidence of bedform superimposition and flow unsteadiness in unit bar deposits, South Saskatchewan River, Canada. *Journal of Sedimentary Research*, **81**, 814-840.
- Reesink, A. J. H., Ashworth, P. J., Sambrook Smith, G. H., Best, J. L., Parsons, D. R., Amsler, M. L., Hardy, R. J., Lane, S. N., Simpson, C. J. and Szupiany, R. N.** (2014) Scales and causes of heterogeneity in bars in a large multi-channel river: Río Paraná, Argentina. *Sedimentology*, **61**(4), 1055-1085.
- Rice, S. P., Church, M., Wooldridge, C. L. and Hickin, E. J.** (2009) Morphology and evolution of bars in a wandering gravel-bed river; lower Fraser river, British Columbia, Canada. *Sedimentology*, **56**, 709-736.
- Robert, A. and Uhlman, W.** (2001) An experimental study on the ripple-dune transition. *Earth Surface Processes and Landforms*, **26**(6), 615-629.
- Robinson, J. W. and McCabe, P. J.** (1997) Sandstone-body and shale-body dimensions in a braided fluvial system: Salt Wash Sandstone Member (Morrison Formation), Garfield County, Utah. *The American Association of Petroleum Geologists Bulletin*, **8**, 1267-1291.
- Robson, D. A.** (1966) A guide to the Geology of Northumberland and the borders. *Transactions of the Natural History Society of Northumberland, Durham and New Castle Upon Tyne*, **16**, n.1.
- Robson, D. A.** (1980) The geology of North East England. (Eds. Robson, D. A.), *Special publication The Natural History Society of Northumbria*, pp. 11-35.

- Rodrigues, S., Claude, N., Juge, N. and Breheret, J. G.** (2012) An opportunity to connect the morphodynamics of alternate bars with their sedimentary products. *Earth Surface Processes and Landforms*, **37**(2), 240-248.
- Rozovski, I. L.** (1963) Flow in bends of open channels. *Israel program for Scientific Translations*, Jerusalem, 233 pp.
- Rubin, D. M.** (1987) *Cross-bedding, Bedforms and palaeocurrents*. SEPM (Society for Sedimentary Geology), Tulsa.
- Sambrook Smith G. H., Ashworth, P. J., Best, J. L., Woodward, J. and Simpson, C. J.** (2006) The sedimentology and alluvial architecture of the sandy braided South Saskatchewan River, Canada. *Sedimentology*, **53**, 413-434.
- Sánchez-Moya, Y., Muñoz, A., Ramos, A. and Sopena, A.** (1989) Arquitectura fluvial de las “Areniscas del Río Arandilla”, Triásico de Molina de Aragón (Guadalajara). *Estudio Geológico*, **45**, 195-204.
- Schindler, R. J. and Robert, A.** (2005) Flow and turbulence structure across the ripple–dune transition: an experiment under mobile bed conditions. *Sedimentology*, **52**(3), 627-649.
- Schumm, S. A.** (1963) Sinuosity of alluvial rivers on the Great Plains. *Geological Society of America Bulletin*, **74**, 1089-1100.
- Seminara, G. and Tubino, M.** (1989) Alternate bars and meandering: free, forced and mixed interactions. In: *River Meandering* (Eds S. Ikeda and G. Parker), *AGU Water Resources Monograph Series*, **12**, 267-320.
- Shadid, G. and Mountney, N. P.** (2009) Facies and architectural element analysis of a meandering fluvial succession: the Permian Warchha Sandstone, Salt Range, Pakistan. *Sedimentary Geology*, **221**, 99-126.
- Simons, D. B., Richardson, E. V. and Nordin JR., C. F.** (1965) Sedimentary structures by flow in alluvial channels. In: *Primary sedimentary structures and their hydrodynamic interpretation*, (Ed. G. C. Middleton), Society of Economic Palaeontologists and Mineralogists, Special Publication, **12**, 34-52.

- Singh, I. B. and Kumar, S.** (1974) Mega- and giant ripples in the Ganga, Yamuna, and Son Rivers, Uttar Pradesh, India. *Sedimentary Geology*, **12**(1), 53-66.
- Smith, C. E.** (1998) Modeling high sinuosity meanders in a small flume. *Geomorphology*, **25**, 19-30.
- Smith, N. D.** (1972) Some sedimentological aspects of planar cross-stratification in a sandy braided river. *Journal of Sedimentary Petrology*, **42**, 624-634.
- Smith, J. D.** (1970) Stability of a sand bed subjected to a shear flow of low Froude number. *Journal of Geophysical Research*, **75**, 5928-5939.
- Smith, N. D.** (1974) Sedimentology and bar formation in the upper kicking horse river, a braided outwash stream. *Journal of Geology*, **82**, 205-223.
- Smith, R. M. H.** (1987) Morphology and depositional history of exhumed Permian point bars in the southwest Karoo, Sout Africa. *Journal of Sedimentary Petrology*, **57**, 19-29.
- Sopeña, A., Ramos, A., and Pérez-Arlucea, M.** (1989) Permian and Triassic fluvial systems in Central Spain. In: *Excursion Guidebook, No. 2. Proc. 4th ICFS* (International Conference Fluvial Sedimentology) (Eds. M. Marzo and C. Puigdefábregas), Barcelona, p. 82.
- Sopeña, A., Virgili, C., Arche, A., Ramos, A. and Hernando, S.** (1983) El Triásico. In: *Geología de España*, (Ed. J. M. Ríos, Libro Jubilar). Tomo II, pp.47-62.
- Sorby, H. C.** (1852) On the oscillation of the currents drifting the sandstone beds of the south-east of Northumberland, and on their general direction in the coal field in the neighbourhood of Edinburgh. *Proceedings of the Yorkshire Geological Society*, **3**, 232-240.
- Sorby, H. C.** (1859). On the structures produced by the currents present during the deposition of stratified rocks. *Geologist*, **2**, 137-147.
- Southard, J. B.** (1971) Representation of bed configurations in depth-velocity-size diagrams. *Journal of Sedimentary Research*, **41**(4), 903-915.

- Southard, J. B.** (1991) Experimental determination of bed-form stability. *Annual Review of Earth and Planetary Sciences*, **19**, 423-455.
- Storms, J. E. A., Van Dam, R. L. and Leclair, S. F.** (1999) Preservation of cross-sets due to migration of current ripples over aggrading and non-aggrading beds: comparison of experimental data with theory. *Sedimentology*, **46**, 189-200.
- Stokes, W. L.** (1953) Primary sedimentary trend indicators as applied to ore finding in the Carizo Mountains, Arizona and New Mexico: U. S. Atomic Energy Commission, 3043.
- Stubblefield, C. J. and Trotter, F. M.,** (1957) Divisions of the Coal Measures on Geological Survey Maps of England and Wales. *Bulletin of the Geological Survey of Great Britain*, **13**, 1-5.
- Sundborg, A.** (1956) The River Klaralven: a study of fluvial processes. *Geogr. Amir.* **38**, 127-316.
- Ten Brinke, W. B. M., Wilbers, A. W. E. and Wesseling, C.** (1999). Dune Growth, Decay and Migration Rates during a Large-Magnitude Flood at a Sand and Mixed Sand–Gravel Bed in the Dutch Rhine River System. In: *Fluvial Sedimentology VI*, (Ed.s. Smith, N. D. and Rogers, J.) Blackwell Publishing Ltd, Oxford, UK, pp. 15-32.
- Thomas, R. G., Smith, D. G., Wood, J. M., Visser, J., Calverley-Range, A. E., and Koster, E. H.** (1987) Inclined heterolithic stratification—Terminology, description, interpretation and significance. *Sedimentary Geology*, **53**(1–2), 123-179.
- Tubino, M and Seminara, G.** (1990) Free-forced interactions in developing meanders and suppression of free bars. *Journal of Fluid Mechanics*, **214**, 131-159.
- Tubino, M., Repetto, R. and Zolezzi, G.** (1999) Free bars in rivers. *Journal of Hydraulic Research*, **37**, 759-775.
- Tuijnder, A. P., Ribberink, J. S., and Hulscher, S. J. M. H.** (2009) An experimental study into the geometry of supply-limited dunes. *Sedimentology*, **56**(6), 1713-1727.
- Tyler, N. and Ethridge, F. G.** (1983) Depositional setting of the Salt Wash Member of the Morrison Formation, southwest Colorado. *Journal of Sedimentary Petrology*, **53**(1), 67-82.

- Van Der Mark, C. F., Blom, A., Hulscher, S. J. M. H., Leclair, S. F. and Mohrig, D.** (2006) On modeling the variability of bedform dimensions. *River, Coastal and Estuarine Morphodynamics: RCEM 2005 - Proceedings of the 4th IAHR Symposium on River, Coastal and Estuarine Morphodynamics*, **2**, 831-841.
- Van de Mark, C. F, Blom, A. and Hulscher, S. J. M. H.** (2008) Quantification of variability in bedform geometry. *Journal of Geophysical Research-Earth Surface*, **113**, F03020.
- Van der Mark, C. F., Blom, A. and Hulscher, S. J. M. H.** (2008) Variability in bedform characteristics using flume and river data. In: *River, Coastal and Estuarine Morphodynamics: RCEM 2007*, (eds: Dohmen –Janssen & Hulscher), London, Taylor & Francis Ltd.
- Van Den Berg, J. H. and Van Gelder, A.** (1993) A New Bedform Stability Diagram, with Emphasis on the Transition of Ripples to Plane Bed in Flows over Fine Sand and Silt. In: *Alluvial Sedimentation* (Eds. M. Marzo and C. Puigdefábregas), Blackwell Publishing Ltd., Oxford, UK. Special Publication IAS, **17**, 11-21.
- Venditti, J. G., Church, M. and Bennet, S. J.** (2005a) On the transition between 2D and 3D dunes. *Sedimentology*, **52**(6) 1343-1359.
- Venditti, J. G., Church, M., and Bennett, S. J.** (2005b) Bed form initiation from a flat sand bed. *Journal of Geophysical Research: Earth Surface* **110**(F1), F01009.
- Venditti, J. G.** (2013) Bedforms in sand-bedded rivers. In: *Treatise on Geomorphology*, **9**, 137-162 (Eds., Shroder, J. and Wohl, E.). Academic Press, Sand diego, CA.
- Visher, G. S.** (1960) Fluvial processes as interpreted from ancient and recent fluvial deposits. In: *Primary Structures and their Hydrodynamic Interpretation*, (SP12), (Ed. Middleton, G. V.). *The Society of Economic Paleontologists and Mineralogists (SEMP)*, **12**, 116-132.
- Warmink, J. J., Dohmen-Janssen, C. M., Lansink, J., Naqshband, S., van Duin, O. J. M., Paarlberg, A. J., Termes, P. and Hulscher, S. J. M. H.** (2014) Understanding river dune splitting through flume experiments and analysis of a dune evolution model. *Earth Surface Processes and Landforms*, **39**, 1208–1220.

- Waters, C. N., Waters R. A., Barclay, W. J. and Davies, J. R.** (2009) A lithostratigraphical framework for the Carboniferous successions of southern Great Britain (onshore). *British Geological Survey Research Report*.
- Waters, C. N., Glover, B. W. and Powel, J. H.** (1994) Structural synthesis of S. Staffordshire, UK: implications of the Variscan evolution of the Pennine Basin. *Journal of Geological Society London*, **151**, 697-713. **Wood, J. M.** (1985) Sedimentology of the late Cretaceous Judith River Formation, "Cathedral" area. Dinosaur provincial park, Alberta. Unpublished, MSc. Thesis. University of Calgary.
- Wells, N. A. and Dorr, J. A.** (1987) Shifting of the Kosi River, northern India. *Geology*, **15**, 204-207.
- Whiting, P. J. and Dietrich, W. E.** (1993) Experimental constraints on bar migration through bends: implications for meander wavelength selection. *Water Resources Research*, **29**, 1091-1102.
- Wilson, L.** (1973) Variations in mean annual sediment yield as a function of mean annual precipitation. *American Journal of Science*, **273**(4), 335-349.
- Wulf, H., Bookhagen, B., and Scherler, D.** (2010) Seasonal precipitation gradients and their impact on fluvial sediment flux in the Northwest Himalaya. *Geomorphology*, **118**(1-2), 13-21.
- Yalin, M. S.** (1964) Geometrical properties of sand waves: American Society of Civil Engineers Proceedings, *Journal of the Hydraulics Division*, **90**, 105-119.
- Yu, B. and Wolman, M. G.** (1987) Some dynamic aspects of river geometry. *Water Resources Research*, **23**, 501-509.
- Zhemchuzhnikov, Y. A.** (1926) Type of cross-bedding as criteria of origins of sediments. *Leningrad Institute of Mines*, **7**, 35-69.

Appendices

Appendix A: Case study I, The Prados Formation

Appendix B: Case study II: The Seaton Sluice Sandstone

Appendix C: Flume Experiments

Appendix A

Table A1. Strike and dip measurements of bounding surfaces identified at: Prados Formation; Rillo de Gallo Sandstone Formation and Arandilla Sandstone Formation measured at localities of Luzón, Riba de Saélices, Hoz del Gallo, Teroleja and Rillo de Gallo where these formations crop out.

Locality Formation	Luzón	Riba de Saélices	Arandilla	Hoz del Gallo	Teroleja	Rillo de Gallo
Río Arandilla Sandstone	N/A	144/3SW 132/6SW		N/A	127/29SW 106/33SSW 099/41SSW	N/A
Prados Sandstone	N/A			N/A	N/A	118/12SW 142/18SW 120/12SW 122/17SW
Rillo de Gallo Sandstone	N115/31SSW N121/25SSW N130/20SSW N150/12SW		142/3SW	142/3SW	112/13SW 074/14SSE 116/11SW	

Table A2. Sour structures corresponding to Modes I and II resulting from the relationship trough W/L and laminae dip direction.

Mode I (185°)		Mode II (294°)		
ST1.1	ST30	ST07	ST16	ST24
ST1.2	ST33	ST08	ST17	ST25
ST1.3	ST38	ST10	ST18	ST26
ST02		ST11	ST19	ST27
ST03		ST12	ST20	ST28
ST04		ST13	ST21	ST31
ST05		ST14	ST22	ST35
ST29		ST15	ST23	ST36

Table A3. Relationship between Mean lamina dip direction Modes and scour structures shape class.

n	Shape	Oval 1	Circular	Elongate 2	Oval 2	n/a	Unclear
11	Total in %						
	Mode I	0 %	45.4 %	27.3 %	27.3 %	0 %	0 %
24	Total in %						
	Mode II	0 %	29.2 %	29.2 %	41.6 %	0 %	0 %
7	n/a	14.3 %	14.3 %	14.3 %	0 %	28.6 %	28.6 %

Table A4. Relationship between Mean lamina dip direction Modes and scour structures size class.

n	Size	Small	Medium	Large	Very large
11	Total in %				
	Mode I	27.3 %	45.5 %	18.2 %	9 %
24	Total in %				
	Mode II	29.2 %	45.8 %	12.5 %	12.5 %
7	n/a	0 %	28.6 %	42.9 %	28.5 %

Table A5. Field Observations on scour structures of the Prados Formation.

Seaton Sluice scour structures field observations									
ID	Max width (m)	Max Length (m)	W/L	Length to Max Width (m)	Average Dip Angle (degrees)	Lamina Thickness (m)	Trend of Scour (Respectively to the North)	Average dip direction (degrees)	Difference Trend – Dip (degrees)
ST1.1	1.13	1.30	0.87	55	26	< 0.035	182	188	6
ST1.2	0.88	1.51	0.58	47	25	< 0.02	182	181	2
ST1.3	0.96	1.35	0.71	87	24	< 0.02	182	178	4
ST02	1.20	1.60	0.75	60	22	-	180	198	18
ST03	0.97	1.00	0.97	50	19	< 0.01	182	188	6
ST04	1.70	2.00	0.85	84	21	-	145	175	30
ST05	3.70	4.10	0.90	240	22	< 0.01	185	180	5

ST06	1.77	2.60*	-	133	11	< 0.015	n/a	142	n/a
ST07	0.70	2.90	0.24	225	21	< 0.03	141	248	107
ST08	2.80	3.80	0.74	250	14	< 0.02	218	302	84
ST09	1.23	1.39*	-	84	23	< 0.01	204	255	51
ST10	0.98	1.43	0.69	63	25	< 0.02	165	238	73
ST11	1.10	1.20	0.92	64	21	-	155	269	104
ST12	1.23	1.50	0.82	72	16	-	180	300	120
ST13	1.43	1.50	0.95	70	18	-	224	285	61
ST14	4.05	7.40	0.55	273	18	< 0.005	215	285	70
ST15	1.10	4.10	0.27	225	17	< 0.01	165	274	109
ST16	1.57	3.10	0.51	135	12	< 0.02	180	287	107
ST17	0.77	1.33	0.58	67	18	< 0.015	216	288	72
ST18	2.10	2.80	0.75	170	15	< 0.01	220	295	75
ST19	0.93	2.10	0.44	50	18	0.01	216	269	53
ST20	1.21	2.46	0.49	93	19	0.01	206	278	72
ST21	0.84	1.20	0.70	62	22	0.01	190	258	68
ST22	1.95	2.10	0.93	105	9	-	198	318	120
ST23	1.20	2.00	0.60	96	12	0.01	170	299	129
ST24	0.43	0.53	0.81	30	21	0.01	198	282	84
ST25	1.22	1.70	0.72	110	12	0.005	207	297	90
ST26	0.52	1.40	0.37	32	13	0.015	202	301	99
ST27	0.85	1.10	0.77	70	14	0.01	210	345	135
ST28	0.95	1.50	0.63	92	18	0.005	225	286	61
ST29	4.20	9.80	0.43	580	13	0.005	215	200	15
ST30	0.53	2.00	0.27	72	3	0.015	200	217	17
ST31	0.90	2.00	0.45	75	4	0.01	195	330	135
ST32	1.20	1.50	0.80	90	6	0.01	160	field error	n/a
ST33	1.55	4.30	0.36	260	12	0.005	192	151	42
ST34	4.30	3.20	1.34	150	4	0.025	250	338	88
ST35	3.50	6.00	0.58	390	13	0.025	215	298	83
ST36	2.00	5.40	0.37	280	13	0.12	165	314	149
ST37	2.80	12.50*	-	230	7	0.04	176	261	85
ST38	1.50	2.10	0.71	145	12	0.02	170	156	14
ST39	2.00*	UC	-	150	22	0.015	125	238	113
ST40	5.20*	4.20*	-	250	9	0.12	216	114	102

* Values of maximum length and width onwards the value in the table. N.B., Field Descriptive Notes and Data (data collected from upstream).

Table A6. Values of individual laminae dip and dip direction per scour structure.

Structure 01.1					
Direction	Dip Angle	Orientation	Sign	Palaeocurrent	Corrected Palaeocurrent
N103	25	SW	90	193	193
N85	30	SSE	90	535	175
N102	23	SW	90	192	192
N98	20	SW	90	188	188
N100	28	SW	90	190	190
Structure 01.2					
Direction	Dip Angle	Orientation	Sign	Palaeocurrent	Corrected Palaeocurrent
N87	24	SSE	90	537	177
N94	25	SW	90	184	184
N91	25	SW	90	181	181
N90	24	S	90	180	180
Structure 01.3					
Direction	Dip Angle	Orientation	Sign	Palaeocurrent	Corrected Palaeocurrent
N90	29	S	90	180	180
N83	21	SSE	90	533	173
N89	23	SSE	90	539	179
N86	25	SSE	90	536	176
N93	24	SSW	90	183	183
Structure 02					
Direction	Dip Angle	Orientation	Sign	Palaeocurrent	Corrected Palaeocurrent
N108	22	SW	90	198	198
Structure 03					
Direction	Dip Angle	Orientation	Sign	Palaeocurrent	Corrected Palaeocurrent
N98	19	SW	90	188	188
Structure 04					
Direction	Dip Angle	Orientation	Sign	Palaeocurrent	Corrected Palaeocurrent
N85	21	SSE	90	535	175
Structure 05					
Direction	Dip Angle	Orientation	Sign	Palaeocurrent	Corrected Palaeocurrent
N270	26	S	-90	180	180
N102	25	SW	90	192	192
N82	25	SSE	90	532	172
N90	22	S	90	180	180
N87	19	SSE	90	537	177
N86	18	SSE	90	536	176
N96	18	SSW	90	186	186
Structure 06					
Direction	Dip Angle	Orientation	Sign	Palaeocurrent	Corrected Palaeocurrent
N207	16	SE	-90	117	117
N243	11	SE	-90	153	153
N252	6	SE	-90	162	162

N234	10	SE	-90	144	144
N225	11	SE	-90	135	135
Structure 07					
Direction	Dip Angle	Orientation	Sign	Palaeocurrent	Corrected Palaeocurrent
N139	23	SW	90	229	229
N176	19	WSW	90	266	266
Structure 08					
Direction	Dip Angle	Orientation	Sign	Palaeocurrent	Corrected Palaeocurrent
N148	16	SW	90	238	238
N195	19	WNW	90	285	285
N251	11	NW	90	341	341
N238	8	NW	90	328	328
N223	13	NW	90	313	313
N217	14	NW	90	307	307
Structure 09					
Direction	Dip Angle	Orientation	Sign	Palaeocurrent	Corrected Palaeocurrent
N157	26	SW	90	247	247
N166	21	SW	90	256	256
N172	21	SW	90	262	262
Structure 10					
Direction	Dip Angle	Orientation	Sign	Palaeocurrent	Corrected Palaeocurrent
N142	23	SW	90	232	232
N156	26	SW	90	246	246
N146	25	SW	90	236	236
Structure 11					
Direction	Dip Angle	Orientation	Sign	Palaeocurrent	Corrected Palaeocurrent
N179	21	WSW	90	269	269
Structure 12					
Direction	Dip Angle	Orientation	Sign	Palaeocurrent	Corrected Palaeocurrent
N213	19	NW	90	303	303
N204	11	NW	90	294	294
N212	18	NW	90	302	302
N210	15	NW	90	300	300
Structure 13					
Direction	Dip Angle	Orientation	Sign	Palaeocurrent	Corrected Palaeocurrent
N195	18	NW	90	285	285
Structure 14					
Direction	Dip Angle	Orientation	Sign	Palaeocurrent	Corrected Palaeocurrent
N173	20	SSW	90	263	263
N196	17	WNW	90	286	286
N190	18	WNW	90	280	280
N202	21	NW	90	292	292
N194	19	WNW	90	284	284
N210	16	NW	90	300	300

N203	21	NW	90	293	293
N191	15	WNW	90	281	281
N197	15	WNW	90	287	287
Structure 15					
Direction	Dip Angle	Orientation	Sign	Palaeocurrent	Corrected Palaeocurrent
N175	20	WSW	90	265	273
N182	13	WNW	90	272	272
N185	18	WNW	90	275	275
N187	18	WNW	90	277	277
N189	17	WNW	90	279	279
N178	17	WSW	90	268	268
Structure 16					
Direction	Dip Angle	Orientation	Sign	Palaeocurrent	Corrected Palaeocurrent
N173	9	WSW	90	263	263
N205	16	WNW	90	295	295
N211	12	WNW	90	301	301
N204	13	WNW	90	294	294
N190	8	WNW	90	280	280
Structure 17					
Direction	Dip Angle	Orientation	Sign	Palaeocurrent	Corrected Palaeocurrent
N193	21	WNW	90	283	283
N190	19	WNW	90	280	280
N195	21	WNW	90	285	285
N199	16	WNW	90	289	289
N212	14	WNW	90	302	302
Structure 18					
Direction	Dip Angle	Orientation	Sign	Palaeocurrent	Corrected Palaeocurrent
N208	14	WNW	90	298	298
N215	16	WNW	90	305	305
N193	12	WNW	90	283	283
N208	17	WNW	90	298	298
N200	16	WNW	90	290	290
Structure 19					
Direction	Dip Angle	Orientation	Sign	Palaeocurrent	Corrected Palaeocurrent
N185	25	WNW	90	275	275
N184	19	WNW	90	274	274
N187	20	WNW	90	277	277
N190	21	WNW	90	280	280
N174	18	WSW	90	264	264
N185	16	WNW	90	275	275
N155	14	WSW	90	245	245
N172	10	WSW	90	262	262
Structure 20					
Direction	Dip Angle	Orientation	Sign	Palaeocurrent	Corrected Palaeocurrent

N175	21	WSW	90	265	265
N185	22	WNW	90	275	275
N199	18	WNW	90	289	289
N194	16	WNW	90	284	284
N185	16	WNW	90	275	275
Structure 21					
Direction	Dip Angle	Orientation	Sign	Palaeocurrent	Corrected Palaeocurrent
N162	21	SW	90	252	252
N169	20	SW	90	259	259
N172	23	SW	90	262	262
N169	23	SW	90	259	259
Structure 22					
Direction	Dip Angle	Orientation	Sign	Palaeocurrent	Corrected Palaeocurrent
N222	14	NW	90	312	312
N210	7	NW	90	300	300
N253	7	NW	90	343	343
Structure 23					
Direction	Dip Angle	Orientation	Sign	Palaeocurrent	Corrected Palaeocurrent
N192	14	WNW	90	282	282
N198	12	WNW	90	288	288
N221	10	WNW	90	311	311
N226	10	WNW	90	316	316
Structure 24					
Direction	Dip Angle	Orientation	Sign	Palaeocurrent	Corrected Palaeocurrent
N192	21	WNW	90	282	282
Structure 25					
Direction	Dip Angle	Orientation	Sign	Palaeocurrent	Corrected Palaeocurrent
N204	16	WNW	90	294	294
N220	14	NW	90	310	310
N204	14	NW	90	294	294
N200	5	NW	90	290	290
Structure 26					
Direction	Dip Angle	Orientation	Sign	Palaeocurrent	Corrected Palaeocurrent
N189	14	WNW	90	279	279
N233	11	NW	90	323	323
Structure 27					
Direction	Dip Angle	Orientation	Sign	Palaeocurrent	Corrected Palaeocurrent
N255	14	NW	90	345	345
Structure 28					
Direction	Dip Angle	Orientation	Sign	Palaeocurrent	Corrected Palaeocurrent
N196	18	WNW	90	286	286
Structure 29					
Direction	Dip Angle	Orientation	Sign	Palaeocurrent	Corrected Palaeocurrent
N85	12	SSE	90	535	175

N115	14	SSW	90	205	205
N130	12	SSW	90	220	220
Structure 30					
Direction	Dip Angle	Orientation	Sign	Palaeocurrent	Corrected Palaeocurrent
N195	3	ESE	-90	105	105
N121	1	SW	90	211	211
N65	6	NW	-90	335	335
Structure 31					
Direction	Dip Angle	Orientation	Sign	Palaeocurrent	Corrected Palaeocurrent
N60	4	NW	-90	330	330
Structure 32					
Direction	Dip Angle	Orientation	Sign	Paleocurrent	Corrected Palaeocurrent
N100	6	n/a	n/a	n/a	n/a
Structure 33					
Direction	Dip Angle	Orientation	Sign	Palaeocurrent	Corrected Palaeocurrent
N65	11	SE	90	515	155
N56	13	SE	90	506	146
Structure 34					
Direction	Dip Angle	Orientation	Sign	Palaeocurrent	Corrected Palaeocurrent
N67	6	NW	-90	337	337
N46	6	NW	-90	316	316
N90	1	N	-90	0	0
Structure 35					
Direction	Dip Angle	Orientation	Sign	Palaeocurrent	Corrected Palaeocurrent
N115	12	SW	90	205	205
N44	14	NW	-90	314	314
N45	16	NW	-90	315	315
N86	11	NNW	-90	356	356
Structure 36					
Direction	Dip Angle	Orientation	Sign	Palaeocurrent	Corrected Palaeocurrent
N50	11	NW	-90	320	320
N54	12	NW	-90	324	324
N28	16	NW	-90	298	298
Structure 37					
Direction	Dip Angle	Orientation	Sign	Palaeocurrent	Corrected Palaeocurrent
N125	11	SW	90	215	215
N128	9	SW	90	218	218
N33	4	NW	-90	303	303
N43	7	NW	-90	313	313
N167	3	SW	90	257	257
Structure 38					
Direction	Dip Angle	Orientation	Sign	Palaeocurrent	Corrected Palaeocurrent
N66	12	SE	90	516	156
Structure 39					

Direction	Dip Angle	Orientation	Sign	Palaeocurrent	Corrected Palaeocurrent
N148	22	SW	90	238	238
Structure 40					
Direction	Dip Angle	Orientation	Sign	Palaeocurrent	Corrected Palaeocurrent
N188	13	ESE	-90	98	98
N40	5	SE	90	490	130

N.B., Units: degrees.

Table A7. Values of individual laminae dip and dip direction of Exposures 1-3.

EXPOSURE 1						
ID Number	Strike	Dip Angle	Orientation	Sign	Palaeocurrent	Corrected Palaeocurrent
1	N120	21	SW	90	210	210
2	N185	30	WNW	90	275	275
3	N40	12	NW	-90	310	310
4	N23	21	NW	-90	293	293
5	N35	8	NW	-90	305	305
EXPOSURE 2						
Sector 1						
1	N70	12	SSE	90	520	160
2	N90	29	S	90	180	180
3	N77	8	SSE	90	527	167
4	N135	11	SW	90	225	225
5	N80	19	S	90	530	170
6	N140	25	W	90	230	230
7	N58	16	SE	90	508	148
8	N70	17	SSE	90	520	160
9	N70	20	SSE	90	520	160
10	N170	16	W	90	260	260
11	N100	15	SSW	90	190	190
Sector 2						
1	N130	35	SW	90	220	220
2	N115	19	SW	90	205	205
3	N128	25	SW	90	218	218
4	N135	26	SW	90	225	225
5	N170	22	SW	90	260	260
6	N150	23	SW	90	240	240
7	N166	26	SW	90	256	256
8	N120	16	SW	90	210	210
9	N175	30	WSW	90	265	265
10	N155	6	SW	90	245	245
11	N140	10	SW	90	230	230
Sector 3						
1	N300	11	SW	-90	210	210

2	N265	4	NNW	90	355	355
3	N230	5	NW	90	320	320
4	N260	20	SSE	-90	170	170
5	N264	20	SSE	-90	174	174
6	N262	22	SSE	-90	172	172
7	N273	22	SSW	-90	183	183
8	N273	22	SSW	-90	183	183
9	N270	16	S	-90	180	180
10	N290	21	SW	-90	200	200
11	N261	20	SE	-90	171	171
12	N270	23	S	-90	180	180
13	N271	21	SSW	-90	181	181
14	N270	24	S	-90	180	180
15	N265	26	SSE	-90	175	175
16	N265	26	SSE	-90	175	175
17	N180	9	W	90	270	270
18	N145	11	NE	-90	55	55
19	N70	5	NW	-90	340	340
20	N271	26	SSW	-90	181	181
21	N268	25	SSE	-90	178	178
22	N264	20	SSE	-90	174	174
23	N262	22	SSE	-90	172	172
24	N304	14	SSW	-90	214	214
25	N272	23	SSW	-90	182	182
26	N265	20	SSE	-90	175	175
27	N296	16	SW	-90	206	206
28	N80	13	SE	90	530	170
29	N253	28	SSE	-90	163	163
30	N273	22	SSW	-90	183	183
31	N275	25	SSW	-90	185	185
32	N274	22	SSW	-90	184	184
33	N272	23	SSW	-90	182	182
34	N270	25	S	-90	180	180
35	N270	22	S	-90	180	180
36	N271	19	SSW	-90	181	181
37	N294	7	SW	-90	204	204
38	N210	7	SE	-90	120	120
39	N268	25	SSE	-90	178	178
40	N281	18	SSW	-90	191	191
Sector 4						
1	N304	20	SW	-90	214	214
2	N270	17	S	-90	180	180
3	N255	7	SE	-90	165	165
4	N278	10	SW	-90	188	188

5	N310	10	SW	-90	220	220
6	N185	5	ESE	-90	95	95
7	N275	20	SSW	-90	185	185
8	N271	22	SSW	-90	181	181
9	N290	19	SW	-90	200	200
10	N290	25	SW	-90	200	200
11	N250	9	SE	-90	160	160
12	N249	16	SE	-90	159	159
13	N210	13	SE	-90	120	120
14	N240	8	SE	-90	150	150
15	N292	20	S	-90	202	202
16	N215	11	SE	-90	125	125
17	N280	18	SW	-90	190	190
18	N284	18	SSW	-90	194	194
19	N258	19	SE	-90	168	168
20	N280	23	SSW	-90	190	190
21	N285	25	SW	-90	195	195
22	N295	18	SW	-90	205	205
23	N304	15	SW	-90	214	214
24	N290	21	SW	-90	200	200
EXPOSURE 3						
1	N40	13	NW	-90	310	310
2	N15	10	WNW	-90	285	285
3	N165	6	SW	90	255	255
4	N55	5	NW	-90	325	325
5	N170	12	W	90	260	260
6	N155	125	W	90	245	245
7	N5	4	W	-90	275	275
8	N115	8	SW	90	205	205
9	N55	2	SE	90	505	145
10	N35	3	SE	90	485	125
11	N100	8	S	90	190	190
12	N31	6	SE	90	481	121
13	N172	3	E	90	262	262
14	N96	3	S	90	186	186
15	N150	5	ENE	-90	60	60
16	N145	14	SW	90	235	235
17	N130	1	NE	-90	40	40
18	N125	18	SW	90	215	215

N.B., Units: degrees.

Table A8. Palaeocurrent data of the Prados Formation covering the study site at Rillo de Gallo.

ID	GPS Location	Direction	Dip Angle	Orientation	Sign	Palaeocurrent	Corrected Palaeocurrent
1	096	N152	13	SW	90	242	242
2	096	N166	9	SW	90	256	256
3	097	N154	13	SW	90	244	244
4	098	N120	21	SW	90	210	210
5	099	N132	8	SW	90	222	222
6	100	N85	19	SSE	90	535	175
7	101	N115	2	SSW	90	205	205
8	102	N38	18	SE	90	488	128
9	103	N25	11	SE	90	475	115
10	104	N44	10	SE	90	494	134
11	106	N39	10	SE	90	489	129
12	107	N102	23	SSW	90	192	192
13	108	N96	21	SSW	90	186	186
14	109	N92	29	SSW	90	182	182
15	110	N113	10	SW	90	203	203
16	111	N63	17	SE	90	513	153
17	112	N78	16	SE	90	528	168
18	113	N132	15	SW	90	222	222
19	114	N81	13	SSE	90	531	171
20	115	N111	22	SW	90	201	201
21	116	N30	1	SE	90	480	120
22	117	N180	4	E	-90	90	90
23	118	N100	20	SSW	90	190	190
24	119	N118	23	SW	90	208	208
25	121	N123	14	SW	90	213	213
26	122	N104	16	SW	90	194	194
27	123	N125	12	SW	90	215	215
28	124	N74	14	SSE	90	524	164
29	125	N150	25	SW	90	240	240
30	126	N99	26	SSW	90	189	189
31	127	N138	14	SW	90	228	228
32	128	N125	14	SW	90	215	215
33	129	N150	29	SW	90	240	240
34	130	N123	18	SW	90	213	213

35	131	N125	13	SW	90	215	215
36	132	N122	15	SW	90	212	212
37	133	N144	13	SW	90	234	234
38	134	N124	21	SW	90	214	214
39	135	N104	18	SW	90	194	194
40	136	N140	22	SW	90	230	230
41	137	N122	14	SW	90	212	212
42	138	N65	20	SE	90	515	155
43	139	N55	22	SE	90	505	145
44	140	N59	19	SE	90	509	149
45	141	N51	19	SE	90	501	141
46	142	N82	17	SSE	90	532	172
47	143	N159	19	SW	90	249	249
48	146	N169	14	SW	90	259	259
49	147	N174	20	SW	90	264	264
50	148	N73	5	SSE	90	523	163
51	149	N85	14	SSE	90	535	175
52	150	N38	14	SE	90	488	128
53	151	N50	7	NW	-90	320	320
54	152	N5	25	WNW	-90	275	275
55	153	N163	26	SW	90	253	253
56	154	N130	15	SW	90	220	220
57	155	N130	15	SW	90	220	220
58	156	N35	21	NW	-90	305	305
59	157	N172	15	ENE	-90	82	82
60	158	N94	20	SSW	90	184	184
61	159	N32	7	NW	-90	302	302
62	160	N40	13	NW	-90	310	310
63	161	N125	12	NE	-90	35	35
64	162	N180	6	E	-90	90	90
65	163	N101	12	SW	90	191	191
66	164	N136	14	SW	90	226	226
67	165	N14	9	SE	90	464	104
68	166	N44	14	SSE	90	494	134
69	167	N77	14	SSE	90	527	167
70	168	N30	14	SE	90	480	120
71	169	N100	15	SW	90	190	190

72	170	N82	4	SSE	90	532	172
73	170	N125	11	NE	-90	35	35
74	171	N53	13	SE	90	503	143
75	172	N105	12	SW	90	195	195
76	173	N122	12	SW	90	212	212
77	174	N172	6	ENE	-90	82	82
78	175	N50	7	NW	-90	320	320
79	176	N40	10	NW	-90	310	310
80	177	N125	12	SW	90	215	215
81	178	N36	17	NW	-90	306	306
82	179	N98	11	NE	-90	8	8
83	180	N85	22	SSE	90	535	175
84	181	N60	12	SE	90	510	150
85	182	N90	25	S	90	180	180
86	183	N124	8	SW	90	214	214
87	184	N138	7	SW	90	228	228
88	185	N98	12	SW	90	188	188
89	186	N118	9	SW	90	208	208
90	187	N63	8	SE	90	513	153
91	188	N109	16	SW	90	199	199
92	189	N162	5	NE	-90	72	72
93	190	N10	13	NW	-90	280	280
94	191	N56	8	NW	-90	326	326
95	192	N130	10	NE	-90	40	40
96	193	N40	2	NW	-90	310	310
97	194	N153	19	SW	90	243	243
98	195	N25	14	NW	-90	295	295
99	196	N142	5	NE	-90	52	52
100	197	N66	9	NW	-90	336	336
101	198	N142	19	SW	90	232	232
102	199	N177	18	WSW	90	267	267
103	200	N120	12	SW	90	210	210
104	201	N170	7	WSW	90	260	260
105	202	N165	13	SW	90	255	255
106	203	N144	10	NE	-90	54	54
107	204	N154	23	SW	90	244	244
108	205	N121	14	SW	90	211	211

109	206	N190	17	WNW	90	280	280
110	207	N160	24	SW	90	250	250
111	208	N118	26	SW	90	208	208
112	209	N21	12	SE	90	471	111
113	210	N54	16	NW	-90	324	324
114	211	N135	6	SW	90	225	225
115	212	N128	20	SW	90	218	218
116	213	N55	2	NW	-90	325	325
117	214	N79	12	NW	-90	349	349
118	215	N89	16	SSE	90	539	179
119	216	N142	26	SW	90	232	232
120	217	N36	15	NW	-90	306	306
121	218	N115	10	SW	90	205	205
122	219	N65	7	NW	-90	335	335
123	220	N78	22	SSE	90	528	168
124	221	N125	19	SW	90	215	215
125	222	N126	20	SW	90	216	216
126	223	N60	18	SE	90	510	150
127	224	N115	22	SW	90	205	205
128	225	N135	14	SW	90	225	225
129	226	N115	11	SW	90	205	205
130	227	N136	3	SW	90	226	226
131	228	N65	21	SE	90	515	155
132	229	N115	24	SW	90	205	205
133	230	N50	18	SE	90	500	140
134	231	N85	19	SSE	90	535	175
135	232	N80	29	SSE	90	530	170
136	233	N60	18	SE	90	510	150
137	234	N90	28	S	90	180	180
138	235	N68	24	SE	90	518	158
139	236	N125	11	SW	90	215	215
140	237	N122	16	SW	90	212	212
141	238	N110	12	SW	90	200	200
142	239	N105	12	SW	90	195	195
143	240	N140	9	SW	90	230	230
144	241	N82	21	SSE	90	532	172
145	242	N75	12	SE	90	525	165

146	243	N58	14	SE	90	508	148
-----	-----	-----	----	----	----	-----	-----

N.B., Units: degrees.

Table A9. Palaeocurrent data of the Arandilla Sandstone Fm and the Rillo de Gallo Sandstone Fm (measurements taken in the area of Rillo de Gallo).

Arandilla Sandstone Formation - overlying unit							
ID	GPS Location	Strike	Dip Angle	Orientation	Sign	Palaeocurrent	Corrected Palaeocurrent
147	244	N122	13	SW	90	212	212
148	245	N186	19	ESE	-90	96	96
149	246	N117	23	SW	90	207	207
150	247	N72	17	SSE	90	522	162
151	248	N80	17	SSE	90	530	170
152	249	N50	18	SE	90	500	140
153	250	N62	21	SE	90	512	152
154	251	N60	23	SE	90	510	150
155	252	N81	14	SSE	90	531	171
156	253	N57	19	SE	90	507	147
157	254	N100	24	SW	90	190	190
158	255	N55	22	SE	90	505	145
159	256	N97	15	SSW	90	187	187
Rillo de Gallo Sandstone Formation - underlying unit							
160	257	N110	25	SW	90	200	200
161	258	N27	14	SE	90	477	117
162	259	N150	14	SW	90	240	240
163	260	N65	16	SE	90	515	155
164	261	N145	10	SW	90	235	235
165	262	N123	6	SW	90	213	213

N.B., Units: degrees.

Table A10. GPS Points Data Field Campaign 2011.

GPS Point	Latitude	Longitude	Altitude (m)	Date	Time	Description
001	40.891372	-1.924275	1062.61	28-May-11	13:01:48	Study area main location
002	40.891255	-1.924432	1065.02	28-May-11	13:55:05	Feature, marcas de obstaculos
003	40.890584	-1.923722	1062.61	28-May-11	16:07:06	Exposure 1
004	40.890570	-1.923719	1068.38	28-May-11	18:06:16	Exposure 1
005	40.891769	-1.924142	1085.93	28-May-11	18:32:53	scour structure
006	40.891250	-1.923833	1059.49	29-May-11	09:19:59	Exposure 2
007	40.891223	-1.923861	1058.29	29-May-11	09:21:37	Exposure 2
008	40.891334	-1.923833	1060.93	29-May-11	09:22:27	Exposure 2
009	40.891363	-1.923753	1069.82	29-May-11	12:00:55	unknown
010	40.891339	-1.923740	1069.58	29-May-11	12:01:05	unknown
011	40.891323	-1.923806	1069.82	29-May-11	12:01:17	Exposure 2, sector 3
012	40.643873	-2.530377	828.06	29-May-11	17:43:56	unknown

013	40.892000	-1.924167	1079.20	03-Jun-11	18:11:34	unknown
014	40.892000	-1.924167	1077.52	03-Jun-11	18:12:21	unknown
015	40.891973	-1.924194	1078.48	03-Jun-11	18:13:02	unknown
016	40.892084	-1.924250	1079.20	03-Jun-11	19:56:16	unknown
017	40.891667	-1.924194	1087.61	04-Jun-11	09:32:46	Point view
018	40.891723	-1.924111	1087.13	04-Jun-11	09:42:21	scour structure
019	40.891695	-1.924083	1088.09	04-Jun-11	10:51:34	Scour structure
020	40.891699	-1.924128	1094.58	04-Jun-11	12:10:29	Grouped structures
021	40.891723	-1.924111	1094.58	04-Jun-11	12:41:36	Grouped structures
022	40.891639	-1.924083	1096.02	04-Jun-11	13:21:46	Grouped structures
023	40.891695	-1.924111	1095.30	04-Jun-11	13:22:21	Grouped structures
024	40.891723	-1.924111	1096.02	04-Jun-11	13:23:16	Grouped structures
025	40.891667	-1.924000	1097.46	04-Jun-11	13:29:26	Grouped structures
026	40.891695	-1.924111	1096.98	04-Jun-11	13:30:38	Grouped structures
027	40.891723	-1.924111	1097.70	04-Jun-11	13:32:45	Grouped structures
028	40.891695	-1.924111	1097.94	04-Jun-11	13:48:59	Grouped structures
029	40.891639	-1.924083	1103.47	04-Jun-11	15:55:05	Grouped structures
030	40.891667	-1.924056	1102.99	04-Jun-11	15:56:01	Grouped structures
031	40.891667	-1.924111	1104.19	04-Jun-11	15:56:31	Grouped structures
032	40.891667	-1.924111	1104.19	04-Jun-11	15:57:00	Grouped structures
033	40.891897	-1.924086	1114.05	04-Jun-11	17:33:25	Scour structure
034	40.891868	-1.924019	1114.29	04-Jun-11	17:34:39	Scour structure
035	40.891881	-1.924058	1114.29	04-Jun-11	17:35:24	Scour structure
036	40.89187	-1.924086	1114.29	04-Jun-11	17:36:10	Scour structure
037	40.891877	-1.924094	1114.05	04-Jun-11	17:37:15	Scour structure
038	40.891994	-1.924217	1113.80	04-Jun-11	17:38:32	Scour structure
039	40.891862	-1.924071	1113.80	04-Jun-11	17:40:17	Unknown
040	40.892207	-1.924311	1138.08	05-Jun-11	11:08:28	Exposure 3
041	40.892168	-1.92437	1131.35	05-Jun-11	11:09:04	Exposure 3, log
042	40.892217	-1.924373	1143.85	05-Jun-11	11:09:24	Exposure 3
043	40.892183	-1.924361	1138.32	05-Jun-11	11:15:50	Cancelled
044	40.89222	-1.92438	1139.28	05-Jun-11	11:17:27	Exposure 3
045	40.892173	-1.924341	1138.56	05-Jun-11	11:20:07	Cancelled
046	40.892159	-1.924339	1130.87	05-Jun-11	11:21:49	Cancelled
047	40.892174	-1.924339	1128.71	05-Jun-11	11:24:12	Cancelled
048	40.892189	-1.924331	1122.70	05-Jun-11	11:25:48	Cancelled
049	40.892224	-1.924378	1122.70	05-Jun-11	11:29:59	Exposure 3
050	40.892163	-1.924349	1139.76	05-Jun-11	11:34:57	Exposure 3
051	40.892192	-1.924368	1133.99	05-Jun-11	11:37:07	Exposure 3
052	40.892208	-1.924375	1140.24	05-Jun-11	11:39:07	Cancelled
053	40.892119	-1.924373	1136.64	05-Jun-11	11:40:06	Exposure 3
054	40.892147	-1.924375	1135.91	05-Jun-11	11:42:44	Exposure 3
055	40.892181	-1.924371	1140.72	05-Jun-11	11:43:39	Unknown
056	40.892206	-1.924362	1129.67	05-Jun-11	11:44:49	Exposure 3

057	40.892183	-1.924413	1140.96	05-Jun-11	11:46:19	Cancelled
058	40.892158	-1.924394	1140.72	05-Jun-11	11:48:09	cancelled
059	40.892182	-1.924439	1141.20	05-Jun-11	11:49:59	Exposure 3
060	40.892208	-1.924373	1136.16	05-Jun-11	11:52:05	Unknown
061	40.891571	-1.924115	1083.04	09-Jun-11	13:25:51	Exposure 5
062	40.891587	-1.924117	1083.52	09-Jun-11	13:27:45	Exposure 5
063	40.891580	-1.924122	1079.68	09-Jun-11	13:30:59	Exposure 5
064	40.891536	-1.924158	1082.32	09-Jun-11	13:36:54	Exposure 5
065	40.891591	-1.924092	1084.00	09-Jun-11	13:42:26	Exposure 5
066	40.891566	-1.924104	1084.73	09-Jun-11	13:44:59	Exposure 5
067	40.891548	-1.924084	1083.52	09-Jun-11	13:47:50	Exposure 5
068	40.891550	-1.924123	1083.28	09-Jun-11	13:52:57	Exposure 5
069	40.891565	-1.924115	1084.97	09-Jun-11	13:57:39	Exposure 5
070	40.891565	-1.924083	1084.97	09-Jun-11	14:04:19	Exposure 5
071	40.891588	-1.924061	1085.45	09-Jun-11	14:10:41	Exposure 5
072	40.891561	-1.924093	1084.97	09-Jun-11	14:18:00	Exposure 5
073	40.891552	-1.924097	1085.45	09-Jun-11	14:19:27	Exposure 5
074	40.891566	-1.924102	1084.24	09-Jun-11	14:21:57	Exposure 5
075	40.891536	-1.924157	1083.28	09-Jun-11	14:26:13	Exposure 5
076	40.891565	-1.924124	1084.73	09-Jun-11	14:30:33	Exposure 5
077	40.891529	-1.924141	1084.00	09-Jun-11	14:33:07	Cancelled
078	40.891493	-1.92414	1083.28	09-Jun-11	14:35:35	Exposure 5
079	40.891529	-1.924168	1085.93	09-Jun-11	15:10:10	Exposure 5
080	40.891514	-1.924145	1087.13	09-Jun-11	15:10:28	Cancelled
081	40.891540	-1.924115	1087.13	09-Jun-11	16:22:53	Exposure 5
082	40.891549	-1.924129	1087.37	09-Jun-11	16:30:25	Unknown
083	40.892163	-1.924382	1096.74	09-Jun-11	16:41:28	Exposure 3
084	40.892204	-1.924369	1097.46	09-Jun-11	16:47:26	Exposure 3
085	40.892206	-1.924313	1097.70	09-Jun-11	17:01:00	Exposure 3
086	40.892184	-1.924369	1098.66	09-Jun-11	17:17:03	Exposure 3
087	40.892174	-1.924348	1098.42	09-Jun-11	17:24:25	Exposure 3
088	40.892128	-1.924318	1099.63	09-Jun-11	17:32:39	Exposure 3
089	40.892151	-1.924357	1099.39	09-Jun-11	17:37:51	Exposure 3
090	40.892063	-1.924208	1097.94	09-Jun-11	17:49:20	Exposure 4
091	40.892070	-1.924226	1098.66	09-Jun-11	17:52:20	Exposure 4
092	40.892037	-1.924181	1093.38	09-Jun-11	18:01:43	Exposure 4
093	40.892008	-1.924207	1098.66	09-Jun-11	18:03:42	Exposure 4
094	40.891994	-1.924184	1099.87	09-Jun-11	18:29:02	Exposure 4
095	40.891975	-1.924171	1099.14	09-Jun-11	18:31:03	Exposure 4
096	40.891994	-1.924171	1096.74	09-Jun-11	18:40:16	Exposure 4
097	40.892000	-1.924159	1096.02	09-Jun-11	18:41:49	Exposure 4
098	40.891977	-1.924152	1098.42	09-Jun-11	18:43:28	Exposure 4
099	40.891994	-1.924182	1098.42	09-Jun-11	18:49:38	Exposure 4
100	40.891424	-1.923538	1071.03	10-Jun-11	12:42:50	Unknown

101	40.891896	-1.923935	1081.36	10-Jun-11	17:55:36	Scour structure
102	40.891882	-1.924126	1079.68	10-Jun-11	18:05:56	Scour structure
103	40.891710	-1.924071	1079.68	10-Jun-11	18:21:11	Scour structure
104	40.891729	-1.924094	1081.60	10-Jun-11	18:42:05	Scour structure
105	40.890659	-1.923791	1067.90	10-Jun-11	19:15:25	Study area
106	40.890636	-1.923549	1061.41	10-Jun-11	19:22:03	Study area

N.B., Part of this data has not been used in this thesis.

Table A11. GPS Points Data Field Campaign 2012.

GPS Point	Latitude	Longitude	Altitude (m)	Date	Time	ID Code
001	40.892013	-1.924662	1135.91	05-May-12	12:06:46 PM	4
002	40.891815	-1.925297	1137.60	05-May-12	12:38:54 PM	4
003	40.893451	-1.927786	1169.08	05-May-12	2:07:15 PM	4
004	40.894582	-1.926177	1153.70	05-May-12	2:27:57 PM	4
005	40.892976	-1.924151	1143.61	05-May-12	2:41:15 PM	4
006	40.892598	-1.924128	1137.36	05-May-12	3:01:49 PM	4
007	40.890407	-1.923557	1112.36	06-May-12	12:04:46 PM	1
008	40.891217	-1.923878	1129.19	06-May-12	3:34:17 PM	1
009	40.891395	-1.923792	1131.35	06-May-12	3:35:18 PM	1
010	40.892041	-1.924730	1140.00	07-May-12	5:06:01 PM	2
011	40.892050	-1.924797	1141.20	07-May-12	6:35:26 PM	2
012	40.892139	-1.924824	1140.00	07-May-12	6:39:18 PM	2
013	40.89192	-1.925234	1130.87	07-May-12	7:10:14 PM	2
014	40.892361	-1.924395	1123.90	08-May-12	1:44:31 PM	2
015	40.892158	-1.924183	1139.28	08-May-12	2:15:42 PM	2
016	40.892071	-1.924176	1139.52	08-May-12	2:28:06 PM	2
017	40.892216	-1.924308	1143.61	08-May-12	3:44:40 PM	4
018	40.891936	-1.924063	1137.84	08-May-12	4:33:06 PM	2
019	40.891797	-1.924129	1135.43	08-May-12	6:21:56 PM	2
020	40.891790	-1.924036	1134.23	08-May-12	7:01:48 PM	2
021	40.891701	-1.924114	1125.10	10-May-12	11:07:52 AM	2
022	40.891705	-1.924100	1126.54	10-May-12	11:08:14 AM	2
023	40.891785	-1.924128	1125.10	10-May-12	11:42:20 AM	2
024	40.891723	-1.924144	1131.35	10-May-12	12:24:08 PM	2
025	40.891710	-1.924139	1127.98	10-May-12	12:29:36 PM	2
026	40.891709	-1.924069	1127.02	10-May-12	12:44:55 PM	2
027	40.891652	-1.924072	1133.51	10-May-12	1:22:01 PM	2
028	40.891683	-1.924147	1134.47	10-May-12	2:34:44 PM	2
029	40.891704	-1.924155	1128.71	10-May-12	2:42:11 PM	2
030	40.891702	-1.924135	1126.06	10-May-12	5:00:03 PM	2
031	40.891693	-1.924119	1129.43	10-May-12	5:11:14 PM	2
032	40.891651	-1.924121	1130.15	10-May-12	5:12:09 PM	2
033	40.891823	-1.924311	1125.10	10-May-12	7:51:40 PM	2
034	40.892713	-1.924492	1095.06	11-May-12	11:14:44 AM	3

035	40.892734	-1.923929	1105.63	11-May-12	11:29:48 AM	3
036	40.892304	-1.923555	1103.23	11-May-12	11:50:07 AM	3
037	40.892232	-1.923969	1104.43	11-May-12	12:05:36 PM	3
038	40.891925	-1.923975	1101.79	11-May-12	12:15:55 PM	3
039	40.891989	-1.924445	1119.81	11-May-12	12:33:22 PM	3
040	40.892174	-1.924840	1128.46	11-May-12	12:44:38 PM	3
041	40.892080	-1.925506	1134.71	11-May-12	1:01:59 PM	3
042	40.891736	-1.925878	1138.56	11-May-12	1:12:47 PM	3
043	40.891430	-1.924819	1124.62	11-May-12	1:47:41 PM	3
044	40.891194	-1.924194	1117.41	11-May-12	1:57:49 PM	3
045	40.891448	-1.923851	1122.70	11-May-12	2:05:34 PM	3
046	40.891411	-1.924023	1121.25	11-May-12	2:10:52 PM	3
047	40.891744	-1.924281	1129.91	11-May-12	2:55:13 PM	3
048	40.892202	-1.92438	1136.88	11-May-12	4:06:02 PM	3
049	40.891841	-1.924029	1136.40	11-May-12	4:11:29 PM	3
050	40.890921	-1.923994	1120.77	11-May-12	4:26:45 PM	3
051	40.891445	-1.923622	1119.57	11-May-12	4:49:09PM	3
052	40.891197	-1.923556	1115.73	11-May-12	4:56:10PM	3
053	40.890787	-1.923780	1113.32	11-May-12	5:16:57PM	3
054	40.890696	-1.923522	1109.72	11-May-12	5:26:11PM	3
055	40.890565	-1.923777	1113.08	11-May-12	5:34:40PM	3
056	40.890583	-1.923599	1109.72	11-May-12	5:37:29PM	3
057	40.890695	-1.923314	1104.43	11-May-12	5:42:21PM	3
058	40.890409	-1.923406	1102.51	11-May-12	5:46:35PM	3
059	40.890379	-1.923556	1102.27	11-May-12	5:59:48PM	3
060	40.891631	-1.923877	1089.77	12-May-12	9:16:10AM	2
061	40.891496	-1.924112	1120.53	12-May-12	9:52:23AM	2
062	40.891514	-1.924112	1126.30	12-May-12	10:16:11AM	2
063	40.891222	-1.924289	1120.53	12-May-12	11:09:31AM	2
064	40.891112	-1.924115	1117.65	12-May-12	11:44:44AM	2
065	40.890685	-1.923742	1109.72	12-May-12	12:28:51PM	2
066	40.890655	-1.923639	1114.53	12-May-12	1:07:00PM	2
067	40.890640	-1.923553	1114.29	12-May-12	1:38:06PM	2
068	40.890648	-1.923652	1113.80	12-May-12	1:42:27PM	4
069	40.890632	-1.923679	1113.08	12-May-12	1:44:15PM	4
070	40.890683	-1.923564	1112.36	12-May-12	2:00:11PM	2
071	40.890677	-1.923565	1109.48	12-May-12	2:13:17PM	2
072	40.890644	-1.923394	1109.00	12-May-12	2:28:47PM	2
073	40.890136	-1.922501	1099.87	12-May-12	4:17:24PM	5
074	40.890552	-1.922544	1098.66	12-May-12	4:19:59PM	5
075	40.891193	-1.922518	1115.25	12-May-12	4:32:33PM	5
076	40.891286	-1.922579	1116.45	12-May-12	4:44:44PM	4
077	40.891957	-1.923070	1120.29	12-May-12	4:49:18PM	4
078	40.893580	-1.923373	1108.76	13-May-12	8:05:45AM	5

079	40.892635	-1.924163	1094.58	13-May-12	8:11:24AM	5
080	40.892774	-1.925128	1121.98	13-May-12	8:15:28AM	5
081	40.892452	-1.924912	1115.97	13-May-12	8:16:49AM	5
082	40.892425	-1.925884	1127.98	13-May-12	8:21:12AM	5
083	40.893804	-1.925523	1124.14	13-May-12	8:30:14AM	5
084	40.892331	-1.926611	1144.33	13-May-12	8:39:32AM	5
085	40.891835	-1.925777	1137.60	13-May-12	8:49:21AM	5
086	40.891711	-1.925362	1133.75	13-May-12	9:06:03AM	6
087	40.891807	-1.925236	1136.40	13-May-12	9:10:37AM	6
088	40.891633	-1.925157	1137.36	13-May-12	9:35:37AM	6
089	40.891425	-1.924618	1131.35	13-May-12	9:50:46AM	6
090	40.891497	-1.924398	1131.11	13-May-12	9:56:53AM	6
091	40.891517	-1.924124	1123.42	13-May-12	10:13:18AM	6
092	40.891306	-1.923694	1128.22	13-May-12	10:34:17AM	6
093	40.890737	-1.923645	1110.44	13-May-12	10:58:05AM	6
094	40.890473	-1.922456	1100.83	13-May-12	11:25:25AM	6
095	40.890627	-1.923431	1111.88	13-May-12	11:40:50AM	6
096	40.890387	-1.923515	1057.33	23-May-12	6:32:33PM	7
097	40.890482	-1.923532	1103.47	23-May-12	6:36:17PM	7
098	40.890423	-1.923507	1102.03	23-May-12	6:38:37PM	7
099	40.890430	-1.923444	1102.51	23-May-12	6:44:14PM	7
100	40.890468	-1.923350	1101.55	23-May-12	6:46:22PM	7
101	40.890461	-1.923339	1101.55	23-May-12	6:50:59PM	7
102	40.890519	-1.923373	1103.95	23-May-12	6:54:13PM	7
103	40.890518	-1.923364	1103.71	23-May-12	6:56:14PM	7
104	40.890666	-1.923353	1107.32	23-May-12	6:58:44PM	7
106	40.890674	-1.923275	1094.82	23-May-12	7:03:03PM	7
107	40.890692	-1.923252	1106.84	23-May-12	7:06:47PM	7
108	40.890698	-1.923292	1108.04	23-May-12	7:08:55PM	7
109	40.890715	-1.923448	1108.76	23-May-12	7:12:49PM	7
110	40.890740	-1.923492	1109.48	23-May-12	7:17:01PM	7
111	40.890665	-1.923438	1109.00	23-May-12	7:20:42PM	7
112	40.890597	-1.923404	1109.48	23-May-12	7:22:01PM	7
113	40.890576	-1.923482	1109.24	23-May-12	7:26:20PM	7
114	40.890692	-1.923528	1110.44	23-May-12	7:29:43PM	7
115	40.890740	-1.923527	1111.64	23-May-12	7:31:50PM	7
116	40.890812	-1.923588	1112.60	23-May-12	7:34:26PM	7
117	40.890795	-1.923618	1112.84	23-May-12	7:37:07PM	7
118	40.890718	-1.923597	1110.44	23-May-12	7:44:34PM	7
119	40.890732	-1.923605	1113.08	23-May-12	7:49:33PM	7
121	40.890743	-1.923648	1112.36	23-May-12	7:53:25PM	7
122	40.890755	-1.923677	1112.12	23-May-12	7:59:22PM	7
123	40.890671	-1.923578	1112.60	23-May-12	8:01:48PM	7
124	40.890706	-1.923613	1112.12	23-May-12	8:04:03PM	7

125	40.890668	-1.923590	1112.84	23-May-12	8:05:48PM	7
126	40.890665	-1.923548	1112.12	23-May-12	8:08:31PM	7
127	40.890645	-1.923598	1112.60	23-May-12	8:10:21PM	7
128	40.890617	-1.923572	1101.55	23-May-12	8:13:22PM	7
129	40.890574	-1.923553	1109.48	23-May-12	8:22:50PM	7
130	40.890574	-1.923563	1106.84	23-May-12	8:26:59PM	7
131	40.890501	-1.923519	1108.28	23-May-12	8:31:29PM	7
132	40.890487	-1.923550	1104.43	23-May-12	8:37:32PM	7
133	40.890430	-1.923557	1107.32	23-May-12	8:43:43PM	7
134	40.890447	-1.923493	1109.48	23-May-12	8:48:35PM	7
135	40.890843	-1.923738	1112.12	23-May-12	8:55:55PM	7
136	40.890870	-1.923727	1110.44	23-May-12	8:57:21PM	7
137	40.890961	-1.923801	1111.16	23-May-12	9:02:40PM	7
138	40.890952	-1.923634	1110.68	23-May-12	9:05:13PM	7
139	40.890927	-1.923646	1099.39	23-May-12	9:07:02PM	7
140	40.890871	-1.923560	1112.60	23-May-12	9:09:36PM	7
141	40.890971	-1.923470	1100.35	24-May-12	10:54:30AM	7
142	40.890459	-1.923575	1110.92	24-May-12	11:00:21AM	7
143	40.890417	-1.923655	1110.92	24-May-12	11:04:57AM	7
146	40.890504	-1.923671	1111.64	24-May-12	11:07:36AM	7
147	40.89051	-1.923692	1113.56	24-May-12	11:12:43AM	7
148	40.890536	-1.923722	1114.77	24-May-12	11:14:57AM	7
149	40.890552	-1.923755	1114.53	24-May-12	11:19:00AM	7
150	40.890562	-1.923798	1114.77	24-May-12	11:22:34AM	7
151	40.890561	-1.923689	1114.77	24-May-12	11:26:52AM	7
152	40.890663	-1.923780	1114.05	24-May-12	11:31:14AM	7
153	40.890645	-1.923798	1115.73	24-May-12	11:34:23AM	7
154	40.890696	-1.923822	1117.17	24-May-12	11:44:32AM	7
155	40.890685	-1.923853	1117.89	24-May-12	11:52:26AM	7
156	40.890678	-1.923791	1116.45	24-May-12	11:54:58AM	7
157	40.890742	-1.923844	1116.69	24-May-12	11:56:31AM	7
158	40.890743	-1.923870	1118.13	24-May-12	11:59:33AM	7
159	40.890824	-1.923924	1118.85	24-May-12	12:02:38PM	7
160	40.890812	-1.923970	1118.85	24-May-12	12:04:53PM	7
161	40.890853	-1.924019	1121.25	24-May-12	12:06:31PM	7
162	40.890891	-1.923942	1118.37	24-May-12	12:10:29PM	7
163	40.890886	-1.923955	1119.33	24-May-12	12:13:44PM	7
164	40.890931	-1.923997	1118.61	24-May-12	12:15:39PM	7
165	40.890930	-1.924047	1119.81	24-May-12	12:18:43PM	7
166	40.890993	-1.924027	1120.29	24-May-12	12:21:43PM	7
167	40.891037	-1.924131	1121.01	24-May-12	12:28:56PM	7
168	40.891094	-1.924205	1122.22	24-May-12	12:32:57PM	7
169	40.891090	-1.924209	1121.98	24-May-12	12:38:20PM	7
170	40.891186	-1.924015	1122.22	24-May-12	12:40:35PM	7

171	40.891193	-1.924331	1124.38	24-May-12	12:46:59PM	7
172	40.891262	-1.924394	1124.14	24-May-12	12:49:12PM	7
173	40.891255	-1.924362	1126.30	24-May-12	12:51:30PM	7
174	40.891356	-1.924380	1127.26	24-May-12	12:53:49PM	7
175	40.891326	-1.924249	1126.06	24-May-12	12:56:43PM	7
176	40.891421	-1.924430	1128.22	24-May-12	12:59:36PM	7
177	40.891270	-1.924588	1128.46	24-May-12	1:02:10PM	7
178	40.891380	-1.924622	1129.67	24-May-12	1:04:07PM	7
179	40.891351	-1.924319	1127.50	24-May-12	1:08:40PM	7
180	40.891153	-1.923909	1122.94	24-May-12	1:16:39PM	7
181	40.891239	-1.923834	1124.38	24-May-12	1:21:36PM	7
182	40.891136	-1.923897	1124.14	24-May-12	1:24:26PM	7
183	40.891309	-1.923747	1126.54	24-May-12	1:27:16PM	7
184	40.891439	-1.923643	1128.71	24-May-12	1:31:44PM	7
185	40.891284	-1.92364	1126.54	24-May-12	1:34:06PM	7
186	40.891163	-1.923523	1126.06	24-May-12	1:38:38PM	7
187	40.891127	-1.923581	1125.82	24-May-12	1:42:04PM	7
188	40.891239	-1.923940	1127.74	24-May-12	1:47:39PM	7
189	40.891284	-1.923866	1128.46	24-May-12	1:50:38PM	7
190	40.891322	-1.923851	1129.43	24-May-12	1:53:00PM	7
191	40.891348	-1.924064	1128.71	24-May-12	1:55:10PM	7
192	40.891319	-1.924155	1128.71	24-May-12	1:57:13PM	7
193	40.891399	-1.924121	1129.91	24-May-12	1:59:19PM	7
194	40.891382	-1.923878	1130.15	24-May-12	2:03:06PM	7
195	40.891482	-1.924166	1130.63	24-May-12	2:05:30PM	7
196	40.891447	-1.924221	1129.67	24-May-12	2:07:49PM	7
197	40.891525	-1.924096	1131.59	24-May-12	2:10:11PM	7
198	40.891539	-1.924052	1129.19	24-May-12	3:30:59PM	7
199	40.891569	-1.923994	1130.39	24-May-12	3:33:15PM	7
200	40.891539	-1.924220	1128.95	24-May-12	3:40:22PM	7
201	40.891556	-1.924176	1130.39	24-May-12	3:42:42PM	7
202	40.891583	-1.924119	1130.87	24-May-12	3:45:31PM	7
203	40.891698	-1.924283	1132.07	24-May-12	3:49:42PM	7
204	40.891767	-1.924165	1132.07	24-May-12	3:52:57PM	7
205	40.891759	-1.923991	1134.71	24-May-12	3:55:00PM	7
206	40.891801	-1.923967	1131.11	24-May-12	3:57:07PM	7
207	40.891884	-1.923994	1134.95	24-May-12	4:00:15PM	7
208	40.892035	-1.923990	1135.67	24-May-12	4:02:08PM	7
209	40.891783	-1.924230	1133.99	24-May-12	4:08:40PM	7
210	40.89181	-1.924248	1135.43	24-May-12	4:10:41PM	7
211	40.891873	-1.924265	1135.91	24-May-12	4:12:56PM	7
212	40.892143	-1.92438	1139.28	24-May-12	4:20:50PM	7
213	40.892190	-1.924430	1137.84	24-May-12	4:22:12PM	7
214	40.892186	-1.924418	1140.72	24-May-12	4:23:55PM	7

215	40.892314	-1.924477	1142.88	24-May-12	4:26:08PM	7
216	40.892187	-1.924337	1132.79	24-May-12	4:33:19PM	7
217	40.892258	-1.924413	1139.28	24-May-12	4:37:23PM	7
218	40.892389	-1.924359	1140.48	24-May-12	4:39:45PM	7
219	40.892455	-1.924500	1142.40	24-May-12	4:41:17PM	7
220	40.892494	-1.924501	1141.68	24-May-12	4:42:53PM	7
221	40.892600	-1.924641	1146.25	24-May-12	4:44:56PM	7
222	40.892229	-1.924924	1133.99	24-May-12	4:51:31PM	7
223	40.892117	-1.924892	1141.92	24-May-12	4:53:45PM	7
224	40.892023	-1.924821	1137.84	24-May-12	4:55:36PM	7
225	40.891949	-1.924816	1140.24	24-May-12	4:57:33PM	7
226	40.891508	-1.924717	1133.51	24-May-12	5:02:30PM	7
227	40.891528	-1.924800	1136.16	24-May-12	5:04:32PM	7
228	40.891681	-1.925167	1129.19	24-May-12	5:07:05PM	7
229	40.89168	-1.925066	1138.08	24-May-12	5:09:20PM	7
230	40.891773	-1.925123	1132.79	24-May-12	5:10:54PM	7
231	40.891817	-1.925152	1139.28	24-May-12	5:12:36PM	7
232	40.891975	-1.925197	1140.24	24-May-12	5:14:38PM	7
233	40.891978	-1.925285	1144.57	24-May-12	5:16:42PM	7
234	40.891987	-1.925266	1144.33	24-May-12	5:18:13PM	7
235	40.892014	-1.925358	1143.85	24-May-12	5:19:46PM	7
236	40.892195	-1.925543	1144.09	24-May-12	5:23:17PM	7
237	40.891908	-1.925520	1145.29	24-May-12	5:25:45PM	7
238	40.891814	-1.925455	1143.37	24-May-12	5:27:14PM	7
239	40.892247	-1.923718	1139.76	24-May-12	5:41:21PM	7
240	40.892266	-1.923711	1138.32	24-May-12	5:45:03PM	7
241	40.892784	-1.923948	1141.68	24-May-12	5:52:27PM	7
242	40.891334	-1.923354	1129.19	24-May-12	6:02:59PM	7
243	40.891330	-1.923420	1127.98	24-May-12	6:04:58PM	7
244	40.894530	-1.929294	1142.64	25-May-12	9:41:18AM	7
245	40.894596	-1.929357	1148.89	25-May-12	9:47:59AM	7
246	40.895555	-1.930583	1159.71	25-May-12	10:04:26AM	7
247	40.897306	-1.931522	1166.20	25-May-12	10:21:03AM	7
248	40.897327	-1.931525	1166.92	25-May-12	10:26:56AM	7
249	40.899402	-1.930958	1179.90	25-May-12	10:55:34AM	7
250	40.899459	-1.930820	1179.41	25-May-12	11:07:13AM	7
251	40.899136	-1.931479	1180.38	25-May-12	11:19:59AM	7
252	40.899158	-1.931579	1181.34	25-May-12	11:21:23AM	7
253	40.899201	-1.93150	1181.10	25-May-12	11:23:17AM	7
254	40.900713	-1.934467	1168.36	25-May-12	12:28:46PM	7
255	40.900749	-1.934516	1170.28	25-May-12	12:30:49PM	7
256	40.889929	-1.923466	1120.29	25-May-12	1:12:25PM	7
257	40.894824	-1.919177	1138.80	25-May-12	2:55:54PM	7
258	40.89423	-1.919237	1129.67	25-May-12	3:03:32PM	7

259	40.89410	-1.919304	1127.26	25-May-12	3:07:08PM	7
260	40.893816	-1.919386	1127.74	25-May-12	3:17:16PM	7
261	40.892383	-1.919794	1118.85	25-May-12	3:46:33PM	7
262	40.891001	-1.922336	1111.40	25-May-12	3:57:04PM	7

N.B., ID Code where 1: exposure; 2: scour structure; 3: sample; 4: unknown; 5: perimeter study area; 6: lithological log and 7: palaeocurrent data.

Table A12. GPS Points Data Field Campaign 2013.

GPS Point	Latitude	Longitude	Altitude (m)	Date	ID Code
001	40.891250	1.924444	1127	01-June-2013	C1
002	40.880917	1.927306	1081	01-June-2013	C3
003	40.825111	2.002000	1017	28-May-2013	C4
004	40.874972	2.107861	1044	01-June-2013	C6
005	40.946694	2.258194	965	29-May-2013	C9
006	41.024889	2.297611	1176	29-May-2013	C10
007	40.891250	1.924444	1116	01-June-2013	C1
008	40.880917	1.927306	1033	29-May-2013	C3

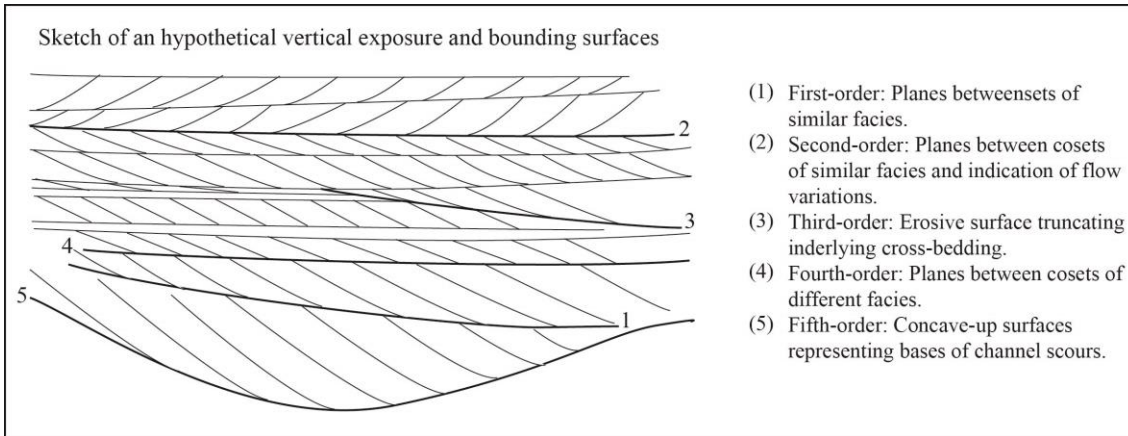


Figure A1. Boundary Surfaces classification

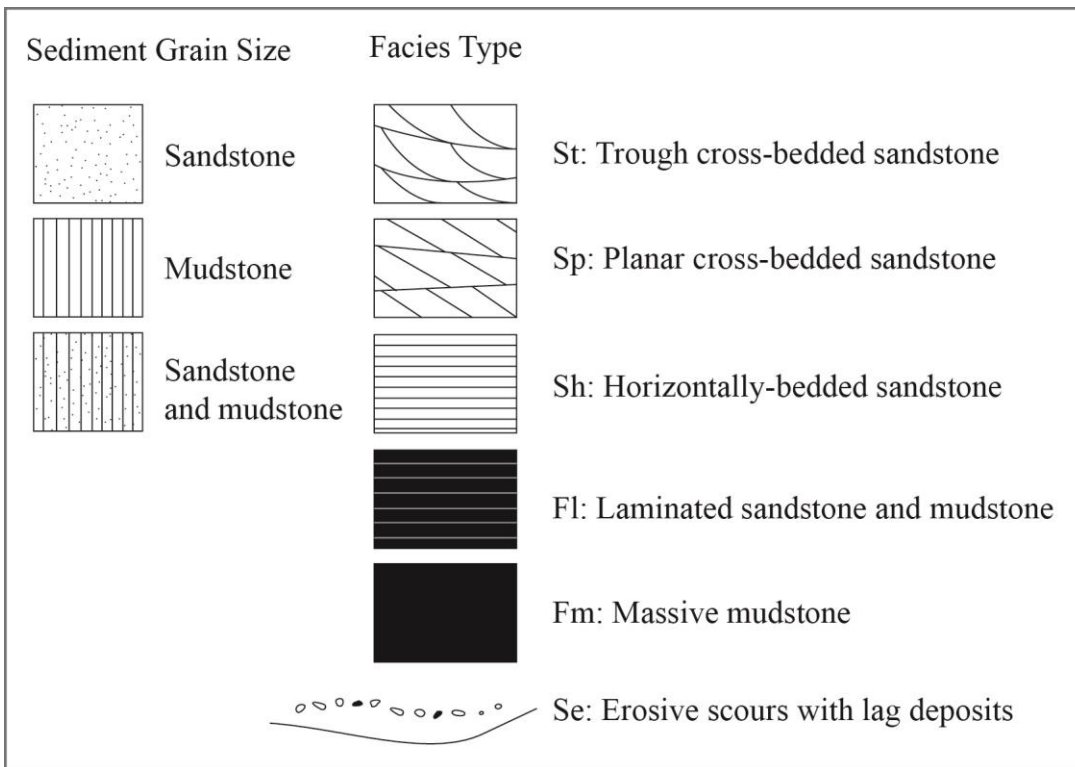


Figure A2. Key for lithological logs (valid for Chapters 2 and 3)

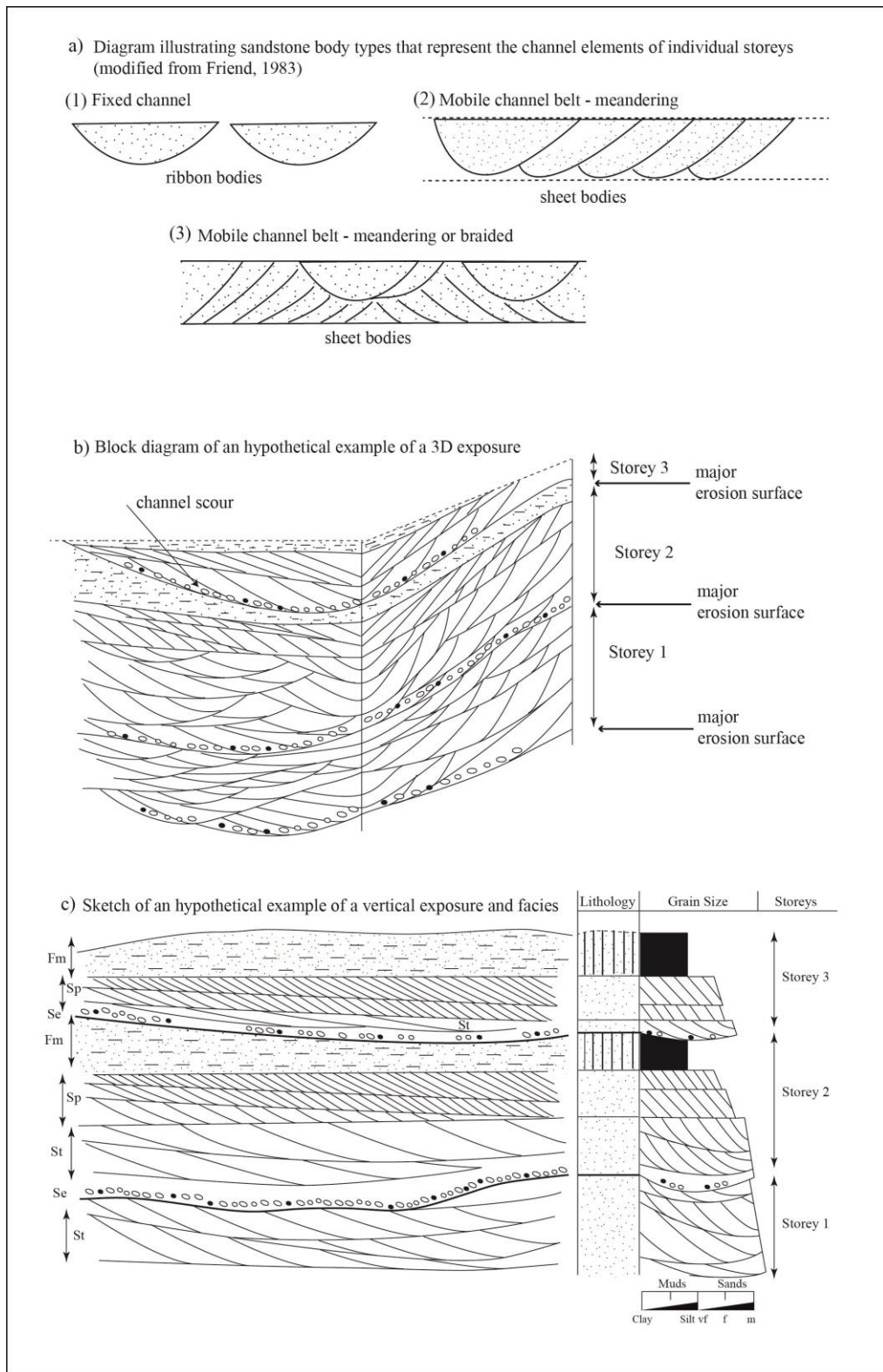

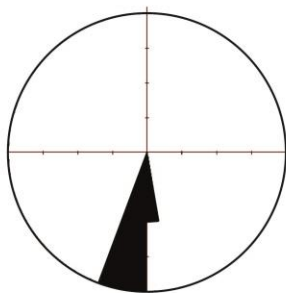

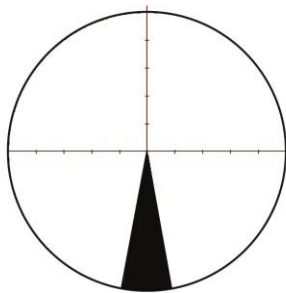


Figure A3. Illustration of field methodology used in this study for the identification of storeys, which led to interpretation and calculation of channel dimensions estimates: (a) Diagram illustrating types of sandstone bodies depending on type of channel (fixed or mobile); (b) Block diagram representing the deposits corresponding to three storeys generated by the evolution of a channel or multiple channels at different periods of time and (c) Sketch of an hypothetical example of a vertical exposure in which this criteria to identify storeys (Section 2.5.2) are used.

Plates illustrating and describing the characteristics of 42 scour structures identified in Rillo de Gallo study area:

SCOUR STRUCTURE 1.1	
<p>Description: Site: Rillo de Gallo Coordinates: N40°53'31.35" W001°55'29.03" Location: Towards top of Unit 7 (Fig. 2.7). General description of sand: fine red sands with laminae thickness from a few millimetres to 30 mm. Laminae thickness decreases upwards and laminae are inclined towards SW. Orientation: 182° Maximum width: 1.13 m Maximum length: 1.30 m Length to maximum width: 0.55 m (measurement taken from the upstream end)</p>	 <p style="text-align: right; font-size: small;">Photo scale: 1 m</p>
<div style="display: flex; align-items: center;">  <div style="margin-left: 20px;"> <p>Palaeocurrent data: Percentage frequency azimuthal plot of the palaeocurrent data measured (n = 5, scale tick 10%, sector angle 10°) Mean dip direction: 188°</p> </div> </div>	

SCOUR STRUCTURE 1.2	
<p>Description: Site: Rillo de Gallo Coordinates: N40°53'31.35" W001°55'29.03" Location: Towards top of Unit 7 (Fig. 2.7) General description of sand: Fine red sandstones. Laminae thickness increases upwards. Laminae are inclined towards the SSE to SSW. Orientation: 182° Maximum width: 0.88 m Maximum length: 1.51 m Length to maximum width: 0.47 m (measurement taken from the upstream end)</p>	 <p style="text-align: right; font-size: small;">Photo scale: 0.2 m</p>
<div style="display: flex; align-items: center;">  <div style="margin-left: 20px;"> <p>Palaeocurrent data: Percentage frequency azimuthal plot of the palaeocurrent data measured (n = 4, scale tick 10%, sector angle 10°) illustrating one primary mode towards the S. Mean dip direction: 181°</p> </div> </div>	

SCOUR STRUCTURE 1.3

Description:

Site: Rillo de Gallo

Coordinates: N40°53'31.35" W001°55'29.03"

Location: Towards top of Unit 7 (Fig. 2.7)

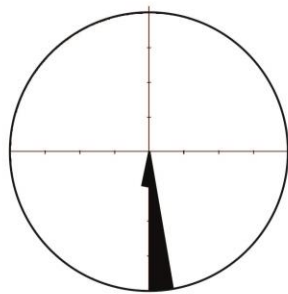
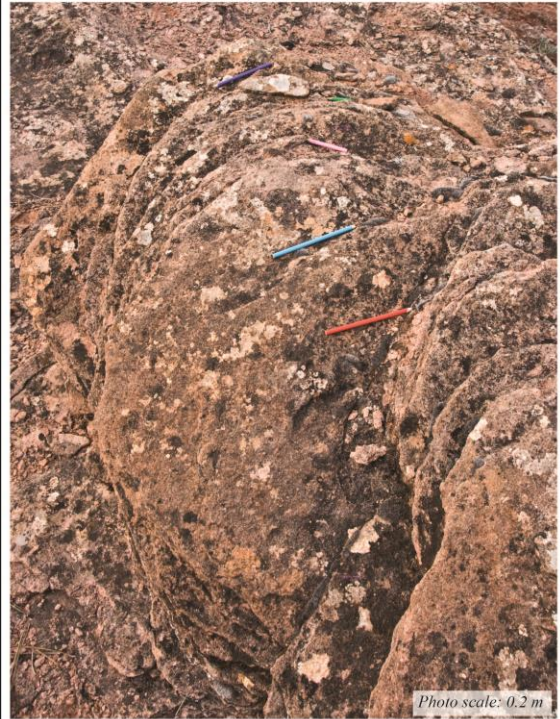
General description of sand: Fine red sandstones. Laminae thickness increases upwards. Laminae are inclined towards the SSE-SSW.

Orientation: 182°

Maximum width: 0.96 m

Maximum length: 1.35 m

Length to maximum width: 0.87 m (measurement taken from the upstream end)



Palaeocurrent data:

Percentage frequency azimuthal plot of the palaeocurrent data measured (n = 5, scale tick 20%, sector angle 10°) illustrating one primary mode towards the S. Mean dip direction: 178°

SCOUR STRUCTURE 02

Description:

Site: Rillo de Gallo

Coordinates: N40°53'31.38" W001°55'29.27"

Altitude: 1141.2 m

Location: Towards top of Unit 8 (Fig. 2.7).

General description of sand: White/pink sands with high content in micas. These sands have a crumble texture due weathering with micro-intraformational pink colour clasts. Laminae thickness is not well defined due to weathering, therefore the estimated thickness varies from a few millimetres to less than 20 mm. Laminae dip direction is towards SW.

Orientation: 180°

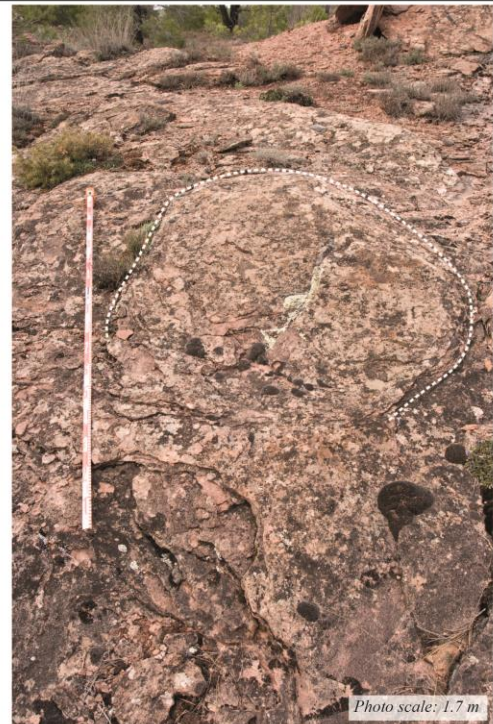
Maximum width: 1.20 m

Maximum length: 1.60 m

Length to maximum width: 0.60 m (measurement taken from the upstream end)

Palaeocurrent data:

Percentage frequency azimuthal plot: N/A due to the preservation of individual laminae. Palaeocurrent data measured (n = 1, Dip direction: 198°).



SCOUR STRUCTURE 03

Description:

Site: Rillo de Gallo

Coordinates: N40°53'31.70" W001°55'29.37"

Altitude: 1140.0 m

Location: Towards top of Unit 8 below structure 02 (Fig. 2.7).

General description of sand: White/pink sands with high content in micas. These sands have a crumble texture due weathering with micro-intraformational pink colour clasts. Laminae thickness is not well-defined due to weathering; the estimated thickness varies from a few millimetres to less than 20 mm. Dip direction of the laminae is towards SW.

Orientation: 182°

Maximum width: 0.97 m

Maximum length: 1.00 m

Length to maximum width: 0.50 m (measurement taken from the upstream end)

Palaeocurrent data:

Percentage frequency azimuthal plot: N/A due to the preservation of individual laminae. Palaeocurrent data measured (n = 1, Dip direction: 188°).



SCOUR STRUCTURE 04

Description:

Site: Rillo de Gallo

Coordinates: N40°53'31.35" W001°55'29.03"

Altitude: 1140.0 m

Location: Towards the base of Unit 8 above structure 01 (Fig. 2.7).

General description of sand: White/pink sands with high content in micas. These sands have a crumble texture due weathering with micro-intraformational pink colour clasts. Laminae thickness is well-defined due to weathering; the estimated thickness varies from a few millimetres to less than 20 mm. Dip direction of the laminae is towards SSE.

Orientation: 145°

Maximum width: 1.70 m

Maximum length: 2.00 m

Length to maximum width: 0.84 m (measurement taken from the upstream end)

Palaeocurrent data:

Percentage frequency azimuthal plot: N/A due to the preservation of individual laminae. Palaeocurrent data measured (n = 1, Dip direction: 175°).



SCOUR STRUCTURE 05

Description:

Site: Rillo de Gallo
Coordinates: N40°53.5152' W001°55.5140'
Altitude: 1130.9 m
Location: Middle section of Unit 7 below structure 01 (Fig. 2.7)

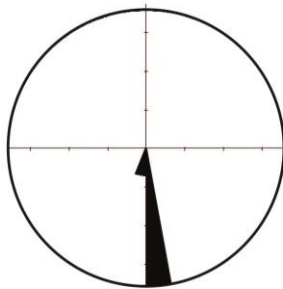
General description of sand: Fine grained reddish sands with high content in micas. Strata thickness decreases upwards in the sequence and laminae thickness decreases downstream. Laminae dip direction ranges from SSE to SSW.

Orientation: 185°

Maximum width: 3.70 m

Maximum length: 4.10 m

Length to maximum width: 2.40 m (measurement taken from the upstream end)



Palaeocurrent data:

Percentage frequency azimuthal plot of the palaeocurrent data measured (n = 7, scale tick 10%, sector angle 10°) illustrating one primary mode towards S. Mean Dip Direction: 180°

SCOUR STRUCTURE 06

Description:

Site: Rillo de Gallo
Coordinates: N40°53'32.50" W001°55'27.82"
Altitude: 1123.9 m
Location: Middle section of Unit (Fig. 2.7).

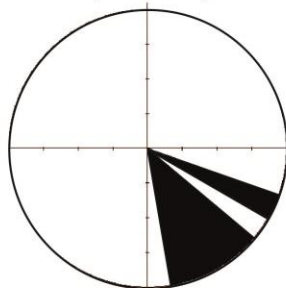
General description of sand: Very fine reddish sands with high content in micas and very fine laminae with a maximum thickness of approximately 15 mm. Laminae thickness fining-upwards pattern. Laminae inclined towards the SE.

Orientation: 014°

Maximum width: 1.77 m

Maximum length: From 2.6 m (unclear)

Length to maximum width: 1.33 m (measurement taken from the upstream end)



Palaeocurrent data:

Percentage frequency azimuthal plot of the palaeocurrent data measured (n = 5, scale tick 5%, sector angle 10°) illustrating one primary mode towards the SE. Mean Dip Direction: 142°

SCOUR STRUCTURE 07

Description:

Site: Rillo de Gallo

Coordinates: N40°53'31.77" W001°55'27.06"

Altitude: 1139.3 m

Location: Towards middle section of Unit 7 laterally equivalent to location of structure 01 (Fig. 2.7).

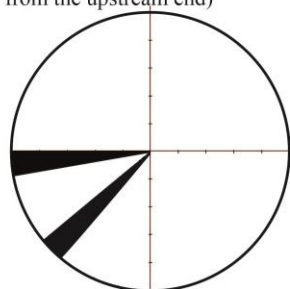
General description of sand: Fine reddish sands with high content in micas and very fine laminae with a maximum thickness of approximately 15 mm. Laminae thickness variation is not well-defined. Laminae dip direction towards SW.

Orientation: 141°

Maximum width: 0.70 m

Maximum length: 2.90 m

Length to maximum width: 2.25 m (measurement taken from the upstream end)



Palaeocurrent data:

Percentage frequency azimuthal plot of the palaeocurrent data measured (n = 2, scale tick 10%, sector angle 10°).
Mean Dip Direction: 247°



SCOUR STRUCTURE 08

Description:

Site: Rillo de Gallo

Coordinates: N40°53'31.46" W001°55'27.03"

Altitude: 1139.5 m

Location: Middle section of Unit 7 laterally equivalent to location of structure 01 (Fig. 2.7).

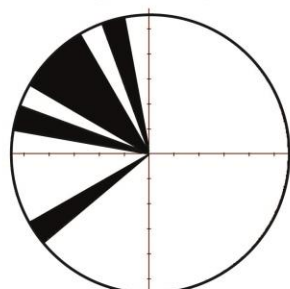
General description of sand: Fine reddish sands with high content in micas and very fine laminae (maximum thickness of 15 mm). Laminae thickness variation is unclear. Laminae dip direction varies from SW to NW.

Orientation: 038°

Maximum width: 2.80 m

Maximum length: 3.80 m

Length to maximum width: 2.50 m (measurement taken from the upstream end)



Palaeocurrent data:

Percentage frequency azimuthal plot of the palaeocurrent data measured (n = 6, scale tick 3%, sector angle 10°) illustrating two primary modes, one SW and the other NW.
Mean Dip Direction: 302°



SCOUR STRUCTURE 09

Description:

Site: Rillo de Gallo

Coordinates: N40°53'31.46" W001°55'27.03"

Altitude: 1139.5 m

Location: Towards middle section of Unit 7 laterally equivalent to location of structure 01 (Fig. 2.7).

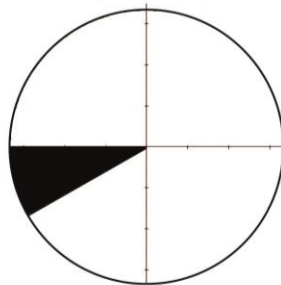
General description of sand: Fine reddish sands with high content in micas and very fine laminae with a maximum thickness of approximately 15 mm. Laminae thickness variation is unclear. Laminae are inclined towards the SW.

Orientation: 024°

Maximum width: 1.23 m

Maximum length: From 1.39 (unclear)

Length to maximum width: 0.84 m (measurement taken from the upstream end)



Palaeocurrent data:

Percentage frequency azimuthal plot of the palaeocurrent data measured (n = 3, scale tick 10%, sector angle 10°) illustrating one mode towards the WSW. Mean direction: 255°

SCOUR STRUCTURE 10

Description:

Site: Rillo de Gallo

Coordinates: N40°53'31.46" W001°55'27.03"

Altitude: 1139.5 m

Location: Towards middle section of Unit 7 laterally equivalent to location of structure 01 (Fig. 2.7).

General description of sand: Fine reddish sands with high content in micas. Laminae thickness is not well-defined due to preservation; from a few millimetres up to 20 mm. Laminae are inclined towards SW.

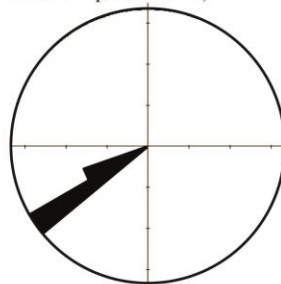
Sands characteristics are similar as structures 08 and 09.

Orientation: 165°

Maximum width: 2.80 m

Maximum length: 3.80 m

Length to maximum width: 2.50 m (measurement taken from the upstream end)



Palaeocurrent data:

Percentage frequency azimuthal plot of the palaeocurrent data measured (n = 3, scale tick 20%, sector angle 10°) illustrating one primary mode towards SW. Mean Dip Direction: 238°

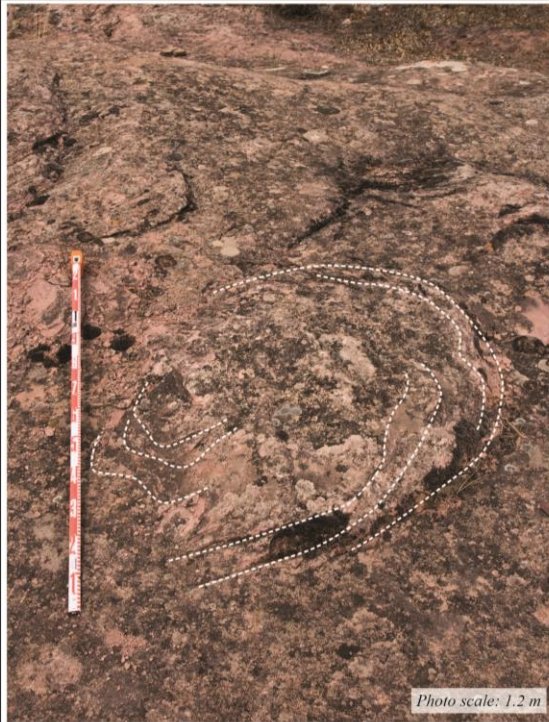
SCOUR STRUCTURE 11

Description:

Site: Rillo de Gallo
Coordinates: N40°53'31.46" W001°55'27.03"
Altitude: 1139.5 m
Location: Towards middle section of Unit 7 laterally equivalent to location of structure 01 (Fig. 2.7)
General description of sand: Fine reddish sands with high content in micas and very fine laminae. Laminae thickness is unclear. Laminae are inclined towards WSW.
Orientation: 155°
Maximum width: 1.10 m
Maximum length: 1.20 m
Length to maximum width: 0.64 m (measurement taken from the upstream end)

Palaeocurrent data:

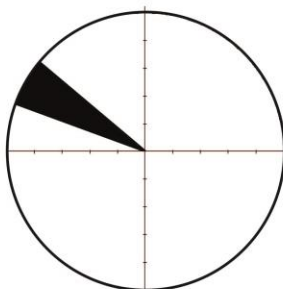
Percentage frequency azimuthal plot: N/A due to the preservation of individual laminae. Palaeocurrent data measured (n = 1, Dip direction: 269°).



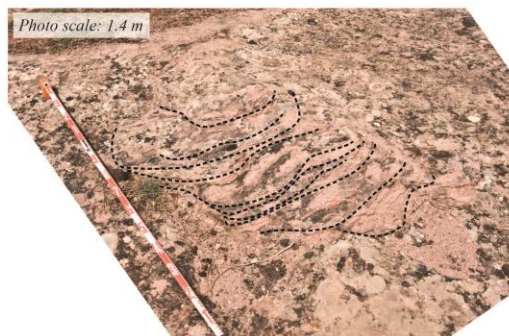
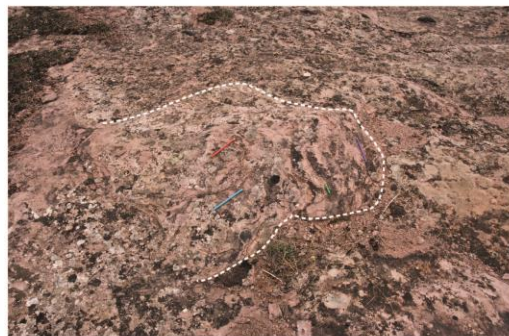
SCOUR STRUCTURE 12

Description:

Site: Rillo de Gallo
Coordinates: N40°53'30.97" W001°55'26.63"
Altitude: 1137.8 m
Location: Towards middle section of Unit 7 laterally equivalent to location of structure 01 (Fig. 2.7)
General description of sand: Fine reddish sands with high content in micas and very fine laminae. Laminae thickness is not well-defined due to preservation. Laminae are inclined towards NW.
Orientation: 180°
Maximum width: 1.23 m
Maximum length: 1.50 m
Length to maximum width: 0.72 m (measurement taken from the upstream end)



Palaeocurrent data:
 Percentage frequency azimuthal plot of the palaeocurrent data measured (n = 4, scale tick 10%, sector angle 10°) illustrating one primary mode towards NW.
 Mean Dip Direction: 300°



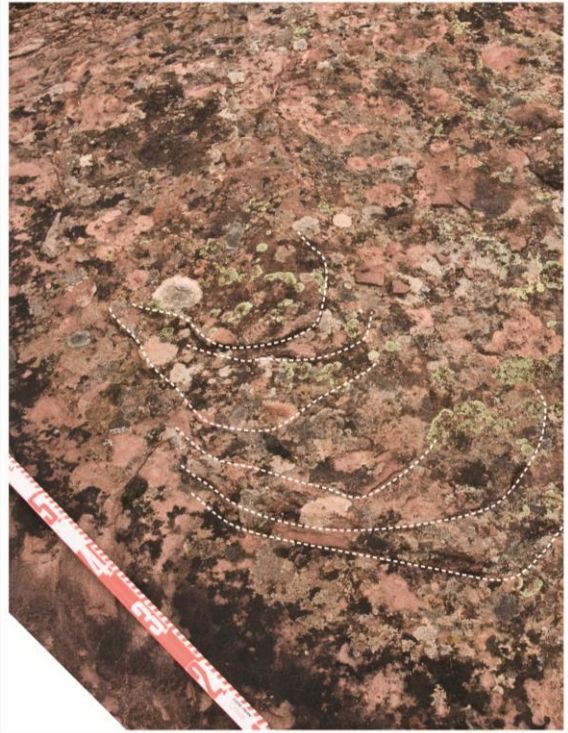
SCOUR STRUCTURE 13

Description:

Site: Rillo de Gallo
Coordinates: N40°53'30.97" W001°55'26.63"
Altitude: 1137.8 m
Location: Towards middle section of Unit 7 laterally equivalent to location of structure 01 (Fig. 2.7)
General description of sand: Fine reddish sands with high content in micas and very fine laminae. Laminae thickness is not well-defined due to preservation. Laminae are inclined towards NW.
Orientation: 044°
Maximum width: 1.43 m
Maximum length: 1.50 m
Length to maximum width: 0.70 m (measurement taken from the upstream end)

Palaeocurrent data:

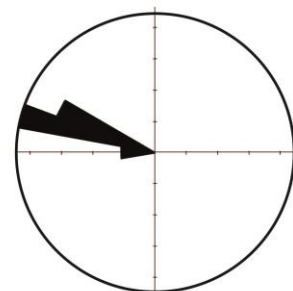
Percentage frequency azimuthal plot: N/A due to the preservation of individual laminae. Palaeocurrent data measured (n = 1, Dip direction: 285°).



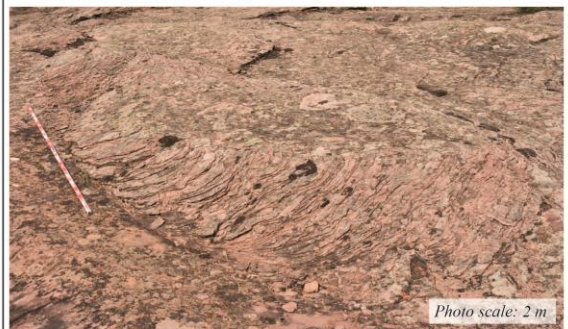
SCOUR STRUCTURE 14

Description:

Site: Rillo de Gallo
Coordinates: N40°53'30.97" W001°55'26.63"
Altitude: 1137.8 m
Location: Towards middle section of Unit 7 laterally equivalent to location of structure 01 (Fig. 2.7)
General description of sand: Fine reddish sands with high content in micas and very fine laminae. Laminae thickness is not well-defined due to preservation. Laminae are inclined towards NW and tend to decrease downstream.
Orientation: 035°
Maximum width: 4.05 m
Maximum length: 7.40 m
Length to maximum width: 2.73 m (measurement taken from the upstream end)



Palaeocurrent data:
 Percentage frequency azimuthal plot of the palaeocurrent data measured (n = 9, scale tick 10%, sector angle 10°) illustrating one primary mode towards WNW. Mean Dip Direction: 285°



SCOUR STRUCTURE 15

Description:

Site: Rillo de Gallo

Coordinates: N40°53'30.47" W001°55'26.86"

Altitude: 1135.4 m

Location: Towards middle section of Unit 7 laterally equivalent to location of structure 01 (Fig. 2.7)

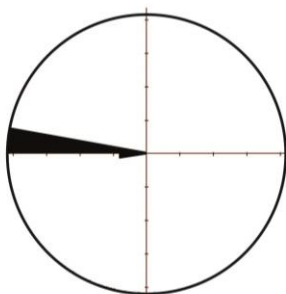
General description of sand: Fine reddish sands with high content in micas and very fine laminae. Laminae thickness is not well-defined due to preservation. Laminae dip towards the W.

Orientation: 165°

Maximum width: 1.10 m

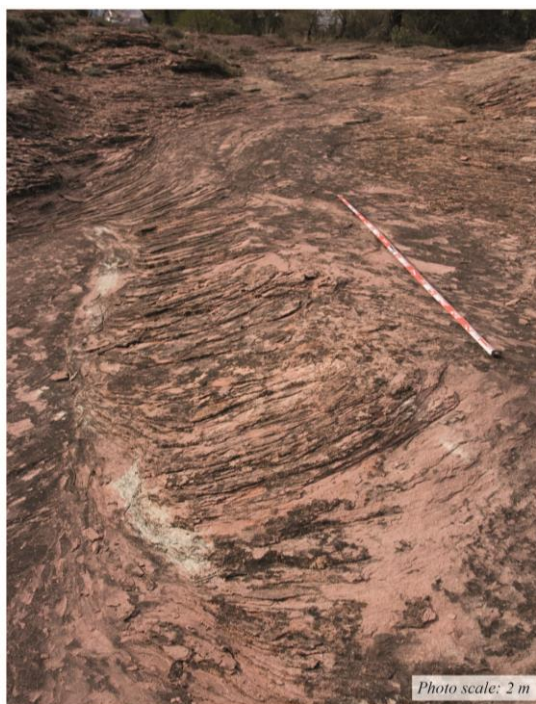
Maximum length: 4.10 m onwards

Length to maximum width: 2.25 m (measurement taken from the upstream end)



Palaeocurrent data:

Percentage frequency azimuthal plot of the palaeocurrent data measured (n = 6, scale tick 20%, sector angle 10°) illustrating one primary mode towards W.
Mean Direction: 274°



SCOUR STRUCTURE 16

Description:

Site: Rillo de Gallo

Coordinates: N40°53'30.44" W001°55'26.53"

Altitude: 1134.2 m

Location: Towards middle section of Unit 7 laterally equivalent to location of structure 01 (Fig. 2.7).

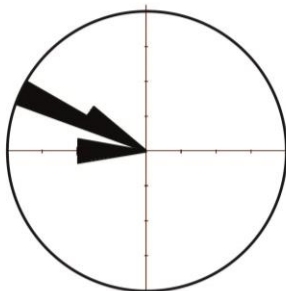
General description of sand: Fine reddish sands with high content in micas and very fine laminae. Laminae thickness is not well-defined due to preservation; it ranges from a few millimetres to a maximum of 20 mm. Laminae dip direction varies from WSW to WNW.

Orientation: 180°

Maximum width: 1.57 m

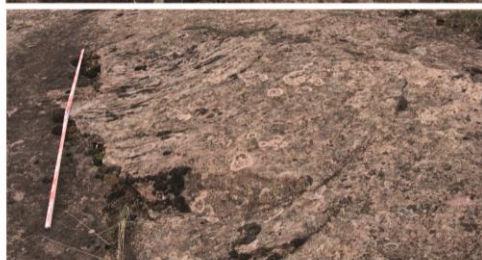
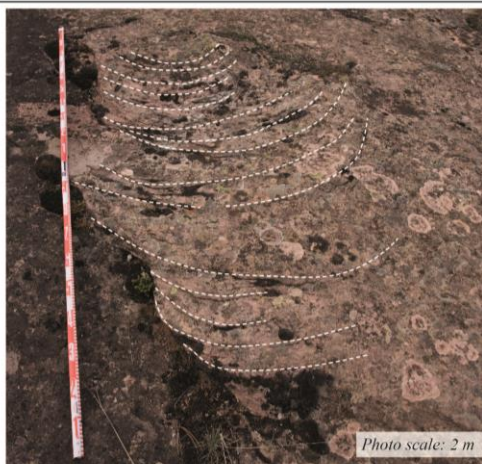
Maximum length: 3.10 m

Length to maximum width: 1.35 m (measurement taken from the upstream end)



Palaeocurrent data:

Percentage frequency azimuthal plot of the palaeocurrent data measured (n = 5, scale tick 10%, sector angle 10°) illustrating one primary mode towards WNW.
Mean Direction: 287°



SCOUR STRUCTURE 17

Description:

Site: Rillo de Gallo

Coordinates: N40°53'30.12" W001°55'26.81"

Altitude: 1125.1 m

Location: Towards middle section of Unit 7 laterally equivalent to location of structure 01 (Fig. 2.7).

General description of sand: Fine reddish sands with high content in micas. Laminae thickness increases upwards from a few millimetres to 15 mm. Individual laminae thickness appears to decrease downstream. Laminae are inclined towards WNW.

Orientation: 036°

Maximum width: 0.77 m

Maximum length: 1.33 m

Length to maximum width: 0.67 m (measurement taken from the upstream end)

Palaeocurrent data:

Percentage frequency azimuthal plot of the palaeocurrent data measured (n = 5, scale tick 10%, sector angle 10°) illustrating one primary mode towards WNW.
Mean Dip Direction: 288°

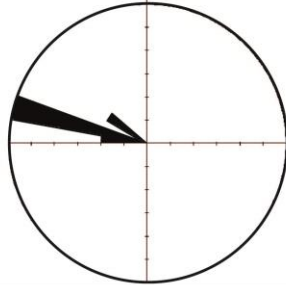


Photo scale: 1 m

SCOUR STRUCTURE 18

Description:

Site: Rillo de Gallo

Coordinates: N40°53'30.14" W001°55'26.76"

Altitude: 1126.5 m

Location: Towards middle section of Unit 7 laterally equivalent to location of structure 01 (Fig. 2.7).

General description of sand: Fine reddish sands with high content in micas. Very fine laminae; maximum laminae thickness 10 mm. Laminae are inclined towards WNW.

Orientation: 040°

Maximum width: 2.10 m

Maximum length: 2.80 m

Length to maximum width: 1.70 m (measurement taken from the upstream end)

Palaeocurrent data:

Percentage frequency azimuthal plot of the palaeocurrent data measured (n = 5, scale tick 10%, sector angle 10°) illustrating one primary mode towards WNW.
Mean Direction: 295°

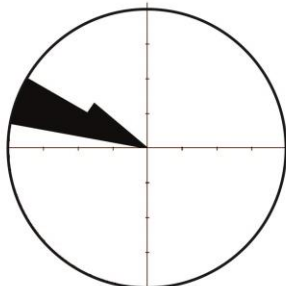


Photo scale: 0.2 m

SCOUR STRUCTURE 19

Description:

Site: Rillo de Gallo

Coordinates: N40°53'30.43" W001°55'26.86"

Altitude: 1125.1 m

Location: Towards middle section of Unit 7 laterally equivalent to location of structure 01 (Fig. 2.7).

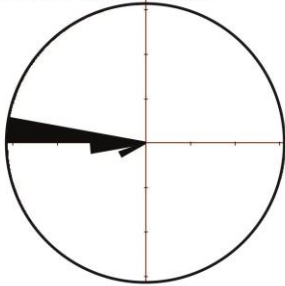
General description of sand: Fine reddish sands with high content in micas. Laminae thickness increases upwards from a few millimetres to 10 mm. Individual laminae thickness appears to decrease downstream. Laminae dip direction varies from WSW to WNW.

Orientation: 036°

Maximum width: 0.93 m

Maximum length: From 2.10 m (unclear)

Length to maximum width: 0.50 m (measurement taken from the upstream end)



Palaeocurrent data:

Percentage frequency azimuthal plot of the palaeocurrent data measured (n = 8, scale tick 20%, sector angle 10°) illustrating one primary mode towards WNW.

Mean Direction: 269°



SCOUR STRUCTURE 20

Description:

Site: Rillo de Gallo

Coordinates: N40°53'30.20" W001°55'26.92"

Altitude: 1131.3 m

Location: Towards middle section of Unit 7 laterally equivalent to location of structure 01 location (Fig. 2.7).

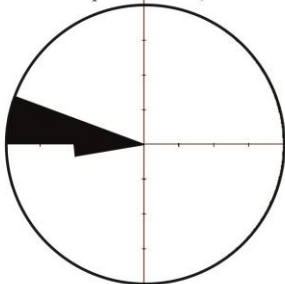
General description of sand: Fine reddish sands with high content in micas. Laminae thickness increases upwards from a few millimetres to 10 mm. Individual laminae thickness appears to decrease downstream. Lamina dip direction varies from WSW to WNW.

Orientation: 026°

Maximum width: 1.21 m

Maximum length: 2.46 m

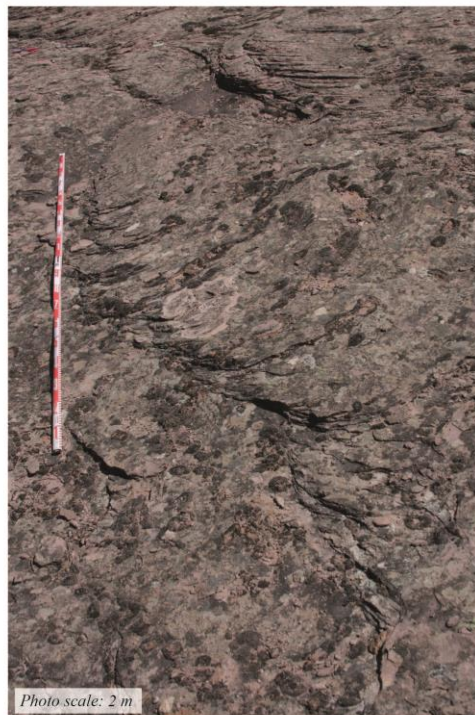
Length to maximum width: 0.93 m (measurement taken from the upstream end)



Palaeocurrent data:

Percentage frequency azimuthal plot of the palaeocurrent data measured (n = 5, scale tick 10%, sector angle 10°) illustrating one primary mode towards WNW.

Mean Direction: 278°



SCOUR STRUCTURE 21

Description:

Site: Rillo de Gallo

Coordinates: N40°53'30.16" W001°55'26.90"

Altitude: 1128.0 m

Location: Towards middle section of unit 7 laterally equivalent to location of structure 01 (Fig. 2.7).

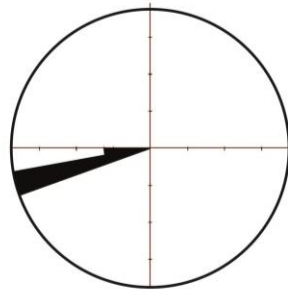
General description of sand: Fine reddish sands with high content in micas. Laminae thickness variation is unclear. Individual laminae thickness appears to decrease downstream. Laminae are inclined towards SW.

Orientation: 010°

Maximum width: 0.84 m

Maximum length: 1.20 m

Length to maximum width: 0.62 m (measurement taken from the upstream end)



Palaeocurrent data:

Percentage frequency azimuthal plot of the palaeocurrent data measured (n = 4, scale tick 20%, sector angle 10°) illustrating one primary mode towards WNW.

Mean Direction: 258°

SCOUR STRUCTURE 22

Description:

Site: Rillo de Gallo

Coordinates: N40°53'30.15" W001°55'26.65"

Altitude: 1127.0 m

Location: Towards middle section of Unit 7 laterally equivalent to location of structure 01 (Fig. 2.7).

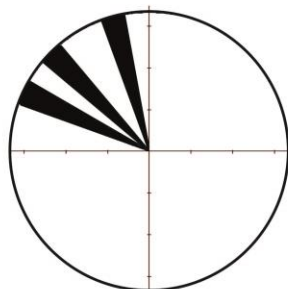
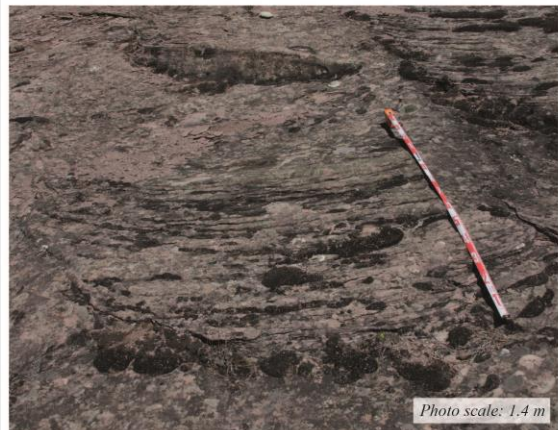
General description of sands: Fine reddish sands with high content in micas. Laminae thickness variation is unclear. Individual laminae appears to decrease downstream. Laminae are inclined towards NW.

Orientation: 018°

Maximum width: 1.95 m

Maximum length: From 2.10 m (unclear)

Length to maximum width: 1.05 m (measurement taken from the upstream end)



Palaeocurrent data:

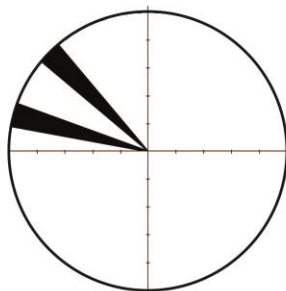
Percentage frequency azimuthal plot of the palaeocurrent data measured (n = 3, scale tick 10%, sector angle 10°) illustrating one primary mode towards NW.

Mean Direction: 318°

SCOUR STRUCTURE 23

Description:

Site: Rillo de Gallo
Coordinates: N40°53'29.95" W001°55'26.66"
Altitude: 1133.5 m
Location: Towards middle section of Unit 7 laterally equivalent to location of structure 01 (Fig. 2.7).
General description of sand: Fine reddish sands with high content in micas. Laminae thickness is up to 10 mm. Individual laminae appears to decrease downstream. Laminae are inclined towards WNW-NW.
Orientation: 170°
Maximum width: 1.20 m
Maximum length: 2.00 m
Length to maximum width: 0.96 m (measurement taken from the upstream end)



Palaeocurrent data:

Percentage frequency azimuthal plot of the palaeocurrent data measured (n = 4, scale tick 10%, sector angle 10°).
 Mean Direction: 299°



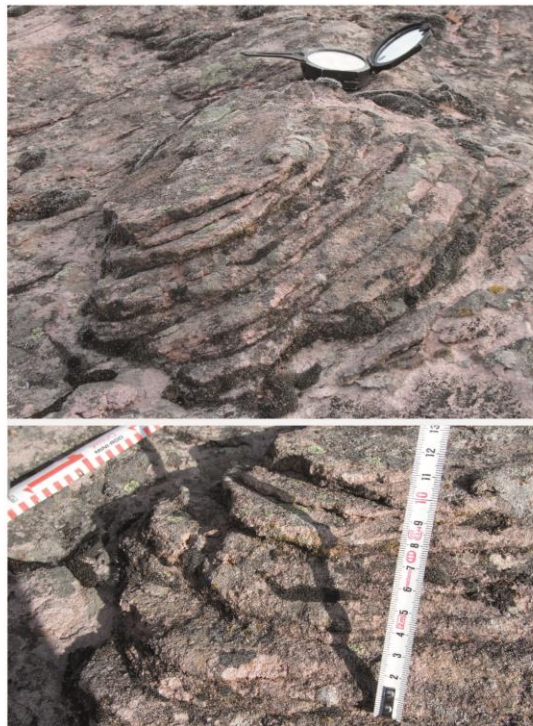
SCOUR STRUCTURE 24

Description:

Site: Rillo de Gallo
Coordinates: N40°53'30.06" W001°55'26.93"
Altitude: 1134.5 m
Location: Towards middle section of Unit 7 laterally equivalent to location of structure 01 (Fig. 2.7).
General description of sand: Fine reddish sands with high content in micas. Laminae thickness increases upwards (10 mm maximum). Individual laminae appears to decrease downstream. Laminae are inclined towards WNW.
Orientation: 018°
Maximum width: 0.43 m
Maximum length: 0.53 m
Length to maximum width: 0.30 m (measurement taken from the upstream end)

Palaeocurrent data:

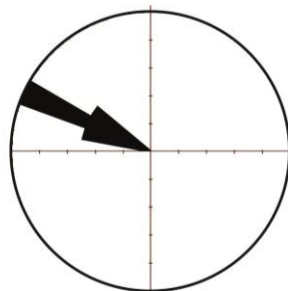
Percentage frequency azimuthal plot: N/A due to the preservation of individual laminae. Palaeocurrent data measured (n = 1, Dip direction: 282°).



SCOUR STRUCTURE 25

Description:

Site: Rillo de Gallo
Coordinates: N40°53'30.13" W001°55'26.96"
Altitude: 1128.7 m
Location: Towards middle section of Unit 7 laterally equivalent to location of structure 01 (Fig. 2.7).
General description of sand: Fine reddish sands with high content in micas. Laminae are very thin (a few millimetres). Individual laminae thickness appear to decrease downstream. Laminae are inclined towards WNW and NW.
Orientation: 027°
Maximum width: 1.22 m
Maximum length: From 1.70 m (unclear)
Length to maximum width: 1.10 m (measurement taken from the upstream end)



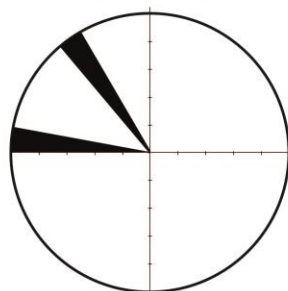
Palaeocurrent data:

Percentage frequency azimuthal plot of the palaeocurrent data measured (n = 4, scale tick 10%, sector angle 10°) illustrating one primary mode towards NW.
 Mean Direction: 297°

SCOUR STRUCTURE 26

Description:

Site: Rillo de Gallo
Coordinates: N40°53'30.13" W001°55'26.89"
Altitude: 1126.1 m
Location: Towards middle section of Unit 7 laterally equivalent to location of structure 01 (Fig. 2.7).
General description of sand: Fine reddish sands with high content in micas. Laminae thickness is up to 15 mm. Individual laminae appear to decrease downstream. Laminae are inclined towards NW and WNW.
Orientation: 022°
Maximum width: 0.52 m
Maximum length: From 1.40 m (unclear)
Length to maximum width: 0.32 m (measurement taken from the upstream end)



Palaeocurrent data:

Percentage frequency azimuthal plot of the palaeocurrent data measured (n = 2, scale tick 10%, sector angle 10°).
 Mean Direction: 301°

Photo scale: 1.1 m

SCOUR STRUCTURE 27

Description:

Site: Rillo de Gallo

Coordinates: N40°53'30.09" W001°55'26.83"

Altitude: 1129.4 m

Location: Towards middle section of Unit 7 laterally equivalent to location of structure 01 (Fig. 2.7).

General description of sands: Fine reddish sands with high content in micas. Laminae thickness variation is not well-defined. Laminae are inclined towards NW.

Orientation: 030°

Maximum width: 0.85 m

Maximum length: From 1.10 m (unclear)

Length to maximum width: 0.70 m (measurement taken from the upstream end)

**Palaeocurrent data:**

Percentage frequency azimuthal plot: N/A due to the preservation of individual laminae. Palaeocurrent data measured (n = 1, Dip direction: 345°).

SCOUR STRUCTURE 28

Description:

Site: Rillo de Gallo

Coordinates: N40°53'29.94" W001°55'26.84"

Altitude: 1130.2 m

Location: Towards middle section of Unit 7 laterally equivalent to location of structure 01 (Fig. 2.7).

General description of sand: Fine red sands turning into very fine white sands at the base with high content in micas. Laminae thickness variation is unclear. Laminae are inclined towards WNW.

Orientation: 045°

Maximum width: 0.95 m (unclear)

Maximum length: 1.50

Length to maximum width: 0.92 m (measurement taken from the upstream end)

**Palaeocurrent data:**

Percentage frequency azimuthal plot: N/A due to the preservation of individual laminae. Palaeocurrent data measured (n = 1, Dip direction: 286°).

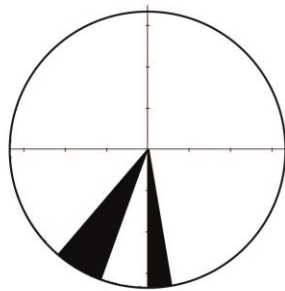
SCOUR STRUCTURE 29

Description:

Site: Rillo de Gallo
Coordinates: N40°53'30.56" W001°55'27.52"
Altitude: 1125.1 m
Location: Base of Unit 7 (Fig. 2.7).
General description of sand: Fine reddish sands with high content in micas. Laminae thickness is less than 10 mm. Laminae are inclined towards SSW.
Orientation: 035°
Maximum width: 4.20 m
Maximum length: From 9.80 m (unclear)
Length to maximum width: 5.80 m (measurement taken from the upstream end)



Photo scale: 1 m



Palaeocurrent data:

Percentage frequency azimuthal plot of the palaeocurrent data measured (n = 3, scale tick 10%, sector angle 10°).
 Mean direction: 200°

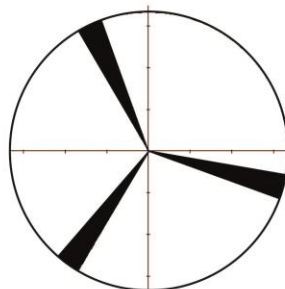
SCOUR STRUCTURE 30

Description:

Site: Rillo de Gallo
Coordinates: N40°53'29.87" W001°55'25.96"
Altitude: 1089.8 m
Location: Towards the top of Unit 5 (Fig. 2.7).
General description of sand: Fine-medium reddish sands with evidences of oxidation. Laminae thickness ranges from a few millimetres up to 15 mm. Laminae dip direction is unclear (see rose diagram; this might be due to measuring error).
Orientation: 020°
Maximum width: 0.53 m
Maximum length: From 2.00 m (unclear)
Length to maximum width: 0.72 m (measurement taken from the upstream end)



Photo scale: 2 m



Palaeocurrent data:

Percentage frequency azimuthal plot of the palaeocurrent data measured (n = 3, scale tick 10%, sector angle 10°)

SCOUR STRUCTURE 31

Description:

Site: Rillo de Gallo

Coordinates: N40°53'29.39" W001°55'26.80"

Altitude: 1120.5 m

Location: Towards the middle section of Unit 5 (Fig. 2.7).

General description of sand: Fine-medium reddish sands with evidences of oxidation. Laminae thickness ranges from a few millimetres up to 15 mm. Laminae dip direction is towards the NW.

Orientation: 015°

Maximum width: 0.90 m (unclear)

Maximum length: 2.00 m

Length to maximum width: 0.75 m (measurement taken from the upstream end)



Palaeocurrent data:

Percentage frequency azimuthal plot: N/A due to the preservation of individual laminae. Palaeocurrent data measured (n = 1, Dip direction: 330°).

SCOUR STRUCTURE 32

Description:

Site: Rillo de Gallo

Coordinates: N40°53'29.45" W001°55'26.80"

Altitude: 1126.3 m

Location: Towards the lower section of Unit 5 (Fig. 2.7).

General description of sand: Fine graded white sands with evidences of oxidation. Laminae thickness ranges from a few millimetres up to 10 mm.

Laminae dip direction N/A.

Orientation: 160°

Maximum width: 1.20 m

Maximum length: From 1.55 m (unclear)

Length to maximum width: 0.90 m (measurement taken from the upstream end)



Palaeocurrent data:

Percentage frequency azimuthal plot: N/A due to the preservation of individual laminae. Palaeocurrent data measured (n = 1, Dip direction unavailable due to measuring error).

SCOUR STRUCTURE 33

Description:

Site: Rillo de Gallo
Coordinates: N40°53'28.40" W001°55'27.44"
Altitude: 1120.5 m
Location: Towards the base of Unit 5 (Fig. 2.7).
General description of sand: Fine-medium reddish sands with high content in micas. Laminae thickness is not well-defined due to preservation. Laminae dip direction towards the SE.
Orientation: 012°
Maximum width: 1.55 m
Maximum length: 4.30 m
Length to maximum width: 2.60 m (measurement taken from the upstream end)

Palaeocurrent data:

Percentage frequency azimuthal plot of the palaeocurrent data measured (n = 2, scale tick 10%, sector angle 10°).
 Mean direction: 151°

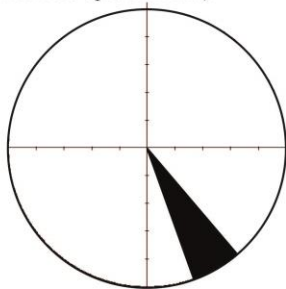


Photo scale: 2 m

SCOUR STRUCTURE 34

Description:

Site: Rillo de Gallo
Coordinates: N40°53'28.00" W001°55'26.81"
Altitude: 1117.7 m
Location: Towards the top of Unit 4 (Fig. 2.7).
General description of sand: Fine to medium white sands with evidences of oxidation. Laminae thickness is unclear. Laminae dip direction towards the NW-NNW.
Orientation: 070°
Maximum width: 4.30 m
Maximum length: From 3.20 m (unclear)
Length to maximum width: 1.50 m (measurement taken from the upstream end)

Palaeocurrent data:

Percentage frequency azimuthal plot of the palaeocurrent data measured (n = 3, scale tick 10%, sector angle 10°) illustrating one primary mode towards the NW.
 Mean direction: 338°

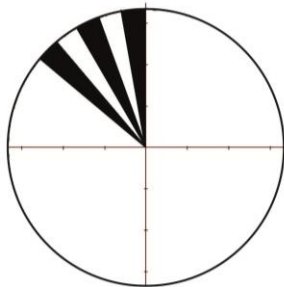
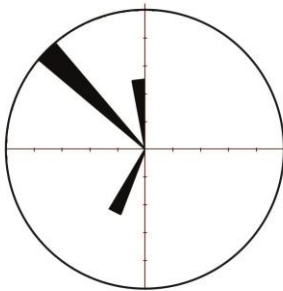


Photo scale: 2 m

SCOUR STRUCTURE 35

Description:

Site: Rillo de Gallo
Coordinates: N40°53'26.47" W001°55'25.47"
Altitude: 1109.7 m
Location: Towards the top of Unit 2 (Fig. 2.7).
General description of sand: Fine to medium white sands with evidences of oxidation. Laminae thickness is unclear. Laminae inclination ranges from SW to NW- NNW.
Orientation: 035°
Maximum width: 3.50 m (unclear)
Maximum length: 6.00 m
Length to maximum width: 3.90 m (measurement taken from the upstream end)

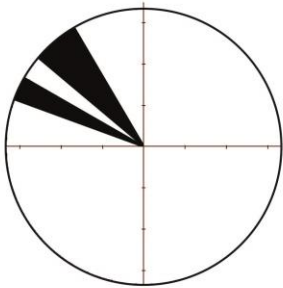


Palaeocurrent data:
 Percentage frequency azimuthal plot of the palaeocurrent data measured (n = 4, scale tick 10%, sector angle 10°).
 Mean direction: 298°

SCOUR STRUCTURE 36

Description:

Site: Rillo de Gallo
Coordinates: N40°53'26.36" W001°55'25.10"
Altitude: 1114.5 m
Location: Towards the top of Unit 2 (Fig. 2.7).
General description of sand: Fine to medium grade white-yellow sands with evidences of oxidation. Strata/laminae thickness appears to decrease downstream. Strata/laminae thickness varies from a few mm up to 120 mm. Laminae dip direction towards the NW.
Orientation: 165°
Maximum width: 2.00 m (unclear)
Maximum length: From 5.40 m (unclear)
Length to maximum width: 2.80 m (measurement taken from the upstream end)



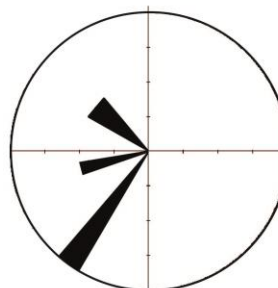
Palaeocurrent data:
 Percentage frequency azimuthal plot of the palaeocurrent data measured (n = 3, scale tick 10%, sector angle 10°).
 Mean direction: 314°

SCOUR STRUCTURE 37

Description:

Site: Rillo de Gallo
Coordinates: N40°53'26.30" W001°55'24.79"
Altitude: 1114.3 m
Location: Towards the top of the lower sandy package within Unit 2 (Fig. 2.7).
General description of sand: Fine reddish sands. Strata/laminae thickness appear to decrease downstream. Strata/laminae thickness ranges from a few millimetres up to a few centimetres (unclear due to weathering). Laminae dip direction ranges from the SW to NW.
Orientation: 176°
Maximum width: 12.80 m
Maximum length: From 12.5 m (unclear)
Length to maximum width: 2.30 m (measurement taken from the upstream end)

Palaeocurrent data:



Percentage frequency azimuthal plot of the palaeocurrent data measured (n = 5, scale tick 10%, sector angle 10°)
 Mean direction: 261°



(Photo scale: 0.5 m)

SCOUR STRUCTURE 38

Description:

Site: Rillo de Gallo
Coordinates: N40°53'26.46" W001°55'24.83"
Altitude: 1112.4 m
Location: Towards the top of the lower sandy package of Unit 2 (below structure 37), (Fig. 2.7).
General description of sand: Fine white sands with evidences of oxidation. Strata/laminae thickness varies from a few millimetres to a maximum of 20 mm. Laminae dip direction towards the SE.
Orientation: 170°
Maximum width: 1.50 m (unclear, structure overlapped by other spoon-shaped structure)
Maximum length: 2.10 m
Length to maximum width: 1.45 m (measurement taken from the upstream end)

Palaeocurrent data:

Percentage frequency azimuthal plot: N/A due to the preservation of individual laminae. Palaeocurrent data measured (n = 1, Dip direction: 156°).



Photo scale: 1.5 m

SCOUR STRUCTURE 39

Description:

Site: Rillo de Gallo

Coordinates: N40°53'26.44" W001°55'24.83"

Altitude: 1109.5 m

Location: Towards the middle part of the lower sandy package of Unit 2 (Fig. 2.7).

General description of sand: Fine reddish sands with evidences of oxidation. Laminae thickness is unclear. Laminae are inclined towards the SW.

Orientation: 125°

Maximum width: From 2.00 m (unclear)

Maximum length: Unclear

Length to maximum width: 1.50 m (measurement taken from the upstream end)



Palaeocurrent data:

Percentage frequency azimuthal plot: N/A due to the preservation of individual laminae. Palaeocurrent data measured (n = 1, Dip direction: 238°).

SCOUR STRUCTURE 40

Description:

Site: Rillo de Gallo

Coordinates: N40°53'26.32" W001°55'24.22"

Altitude: 1109.0 m

Location: Towards the middle part of the lower sandy package of Unit 2, below structure 39 (Fig. 2.7).

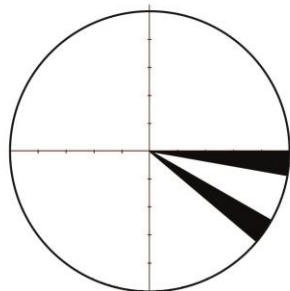
General description of sand: Fine reddish sands with high content in micas. Strata thickness decreases upwards and varies from 10 mm to 120 mm. Laminae are inclined towards ESE to SE.

Orientation: 036°

Maximum width: From 5.20 m (unclear)

Maximum length: From 4.20 m (unclear due to vegetation)

Length to maximum width: 2.50 m (measurement taken from the upstream end)



Palaeocurrent data:

Percentage frequency azimuthal plot of the palaeocurrent data measured (n = 2, scale tick 10%, sector angle 10°).

Mean direction: 114°



N.B., In some of the scour structures, laminae thickness appears to decrease downstream. This may be an apparent observation from the preserved exposures.

Appendix B

Table B1. Field Observations on scour structures of the Seaton Sluice Sandstone.

Seaton Sluice scour structures field observations									
ID	Max width (m)	Max Length (m)	W/L	Length to Max Width (m)	Average Dip Angle (degrees)	Lamina Thickness (m)	Trend of Scour (Respectively to the North)	Average dip direction (degrees)	Difference Trend – Dip (degrees)
ST01	2.7	4.5	0.60	1.60	19	< 0.01	275	207	68
ST02	2	n/a	-	1.60	25	n/a	300	310	10
ST03	n/a	3.7	-	N/A	24	n/a	275	301	26
ST04	3.4	n/a	-	1.60	23	< 0.01	310	325	15
ST05	3.2	4.4	0.73	2.00	18	n/a	290	253	37
ST06	4	6.6	0.61	5.10	21	n/a	125	286	19
ST07	1.5	n/a	-	0.72	25	n/a	n/a	n/a	n/a
ST08	0.55	0.58	0.95	0.29	18	n/a	275	270	5
ST09	1.3	1.5	0.87	0.80	11	n/a	280	265	15
ST10	1.2	1.6	0.75	0.82	18	n/a	310	270	40
ST11	1.3	1.6	0.81	0.92	25	n/a	290	298	8
ST12	1.02	2.2	0.46	1.43	26	n/a	290	290	0
ST13	1	1.5	0.67	0.80	20	n/a	300	315	15
ST14	1.2	1.6	0.75	0.90	19	n/a	270 (248 to 290)	320	50
ST15	2.7	n/a	-	1.20	26	n/a	275	219	56
ST16	1.9	3	0.63	1.90	20	< 0.015	290	279	11
ST17	0.83	1.3	0.64	0.70	25	< 0.01	270	288	18
ST18	0.55	1.2	0.46	0.50	20	< 0.015	300	258	42
ST19	115*	3	-	1.55	19	< 0.01	280	300	20

* Values of maximum length and width onwards the value in the table. N.B., Field Descriptive Notes and Data (data collected from upstream).

Table B2. Values of individual laminae dip and dip direction per scour structure.

Structure 01					
Direction	Dip Angle	Orientation	Sign	Palaeocurrent	Corrected Palaeocurrent
N175	21	WSW	90	270	270
N150	18	SW	90	272	272
N25	19	SE	90	315	315
Structure 02					
Direction	Dip Angle	Orientation	Sign	Palaeocurrent	Corrected Palaeocurrent
N40	25	NW	-90	310	310
Structure 03					
Direction	Dip Angle	Orientation	Sign	Palaeocurrent	Corrected Palaeocurrent
N45	31	NW	-90	315	315
N9	21	WNW	-90	279	279
N40	21	NW	-90	310	310

Structure 04					
Direction	Dip Angle	Orientation	Sign	Palaeocurrent	Corrected Palaeocurrent
N55	23	NW	-90	325	325
Structure 05					
Direction	Dip Angle	Orientation	Sign	Palaeocurrent	Corrected Palaeocurrent
N144	17	SW	90	234	234
N2	19	SW	-90	272	272
Structure 06					
Direction	Dip Angle	Orientation	Sign	Palaeocurrent	Corrected Palaeocurrent
N180	22	W	90	270	270
N182	26	W	90	272	272
N45	15	NW	-90	315	315
Structure 07					
Direction	Dip Angle	Orientation	Sign	Palaeocurrent	Corrected Palaeocurrent
N10	25	WNW	-90	280	280
Structure 08					
Direction	Dip Angle	Orientation	Sign	Palaeocurrent	Corrected Palaeocurrent
N180	18	W	90	270	270
Structure 09					
Direction	Dip Angle	Orientation	Sign	Palaeocurrent	Corrected Palaeocurrent
N130	13	SW	90	220	220
N40	9	NW	-90	310	310
Structure 10					
Direction	Dip Angle	Orientation	Sign	Palaeocurrent	Corrected Palaeocurrent
N180	18	W	90	270	270
Structure 11					
Direction	Dip Angle	Orientation	Sign	Palaeocurrent	Corrected Palaeocurrent
N180	27	W	90	270	270
N55	23	NW	-90	325	325
Structure 12					
Direction	Dip Angle	Orientation	Sign	Palaeocurrent	Corrected Palaeocurrent
N20	26	NW	-90	290	290
N20	25	NW	-90	290	290
Structure 13					
Direction	Dip Angle	Orientation	Sign	Palaeocurrent	Corrected Palaeocurrent
N50	19	NW	-90	320	320
N40	21	NW	-90	310	310
Structure 14					
Direction	Dip Angle	Orientation	Sign	Palaeocurrent	Corrected Palaeocurrent
N50	19	NW	-90	320	320
Structure 15					
Direction	Dip Angle	Orientation	Sign	Palaeocurrent	Corrected Palaeocurrent
N138	22	SW	90	228	228
N115	20	SWS	90	205	205

N135	35	SW	90	225	225
Structure 16					
Direction	Dip Angle	Orientation	Sign	Palaeocurrent	Corrected Palaeocurrent
N9	20	WSW	-90	279	279
Structure 17					
Direction	Dip Angle	Orientation	Sign	Palaeocurrent	Corrected Palaeocurrent
N18	25	NW	-90	288	288
Structure 18					
Direction	Dip Angle	Orientation	Sign	Palaeocurrent	Corrected Palaeocurrent
N168	20	SW	90	258	258
Structure 19					
Direction	Dip Angle	Orientation	Sign	Palaeocurrent	Corrected Palaeocurrent
N30	19	NW	-90	300	300

N.B., Units: degrees.

Table B3. Values of individual laminae dip and dip direction of Sections 1-3.

SECTION 1					
Direction	Dip Angle	Orientation	Sign	Palaeocurrent	Corrected Palaeocurrent
N155	22	SW	90	245	245
N10	16	WNW	-90	280	280
N50	8	NW	-90	320	320
N55	14	NW	-90	325	325
N20	5	NW	-90	290	290
N10	14	WNW	-90	280	280
N25	13	NW	-90	295	295
SECTION 2					
Direction	Dip Angle	Orientation	Sign	Palaeocurrent	Corrected Palaeocurrent
N35	14	NW	-90	305	305
N20	8	NW	-90	290	290
N55	14	NW	-90	325	325
N175	16	WSW	90	265	265
N35	26	NW	-90	305	305
N50	21	NW	-90	320	320
N25	28	NW	-90	295	295
N33	22	NW	-90	303	303
N51	7	NW	-90	321	321
N165	13	WSW	90	255	255
N26	26	WNW	-90	296	296
N55	19	NW	-90	325	325
N10	15	WNW	-90	280	280
N22	24	WNW	-90	292	292
SECTION 3					
Direction	Dip Angle	Orientation	Sign	Palaeocurrent	Corrected Palaeocurrent
N150	13	SW	90	240	240

N180	16	W	90	270	270
N20	20	NW	-90	290	290
N170	24	WSW	90	260	260
N185	30	W	90	275	275
N15	20	NW	-90	285	285
N180	19	W	90	270	270
N165	20	SW	90	255	255

N.B., Units: degrees.

Table B4. Palaeocurrent data of the Seaton Sluice Sandstone covering the study site (data from scour structures are not included in this table).

ID Number	GPS Location	Direction	Dip Angle	Orientation	Sign	Palaeocurrent	Corrected Palaeocurrent
1	044	N100	18	SW	90	190	190
2	045	N168	24	ENE	-90	78	78
3	046	N132	13	SW	90	222	222
4	047	N15	17	SE	90	465	105
5	n/a	N150	13	SW	90	240	240
6	n/a	N180	16	W	90	270	270
7	n/a	N20	20	NW	-90	290	290
8	n/a	N170	24	WSW	90	260	260
9	n/a	N185	30	W	90	275	275
10	n/a	N15	20	NW	-90	285	285
11	n/a	N180	19	W	90	270	270

N.B., Units: degrees.

Table B5. Bedding Plane data of the Seaton Sluice Sandstone covering the study site.

ID Number	GPS Location	Direction	Dip Angle	Orientation	Sign	Bedding Dip Direction	Corrected Palaeocurrent
1	15	N85	6	NNW	-90	355	355
2	16	N75	15	NNW	-90	345	345
3	34	N50	12	NW	-90	320	320
4	35	N75	13	NW	-90	345	345
5	36	N175	8	WSW	90	265	265
6	38	N142	2	SW	90	232	232
7	39	N85	9	NW	-90	355	355
8	41	N60	6	NW	-90	330	330
9	42	N25	7	NW	-90	295	295
10	55	N30	13	NW	-90	300	300
11	56	N55	1	NW	-90	325	325
12	57	N10	9	NW	-90	280	280
13	57	N60	6	SE*	-	-	-
14	58	N45	4	NW	-90	315	315
15	48	N165	12	WSW	90	255	255

16	59	N185	9	WNW	90	275	275
17	59	N90	7	W	-	-	-
18	59	N38	4	N	-90	308	308
19	59	N40	9	NW	-90	310	310
20	59	N180	11	W	90	270	270
21	59	N115	2	SW	90	205	205
22	59	N160	10	SW	90	250	250
23	61	N50	8	NW	-90	320	320
24	61	N55	14	NW	-90	325	325
25	61	N20	5	NW	-90	290	290
26	62	N10	14	WNW	-90	280	280
27	62	N25	13	NW	-90	295	295
28	68	N38	19	NW	-90	308	308
29	74	N43	4	NW	-90	313	313
30	74	N51	7	NW	-90	321	321
31	74	N85	4	WNW	-90	355	355
32	76	N28	8	WNW	-90	298	298
33	77	N45	3	NW	-90	315	315

*Only one data point orientated towards SE. This is possibly a field measuring error.


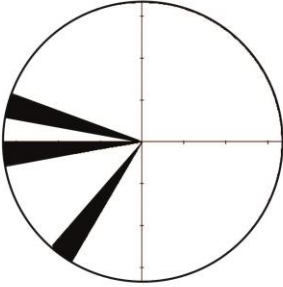
Table B6. GPS Points Data Field Campaign 2012.


GPS Point	Latitude	Longitude	Altitude (m)	Description
1	55.085645	-1.472588	55.085645	Scour structure
2	55.085546	-1.472622	55.085546	Scour structure
3	55.085528	-1.472581	55.085528	Scour structure
4	55.085472	-1.472426	55.085472	Scour structure
5	55.084784	-1.471212	55.084784	Unknown
6	55.084875	-1.470272	55.084875	Unknown
7	55.084780	-1.471147	55.084780	Unknown
8	55.085632	-1.473624	55.085632	Scour structure
9	55.085690	-1.473812	55.085690	Scour structure
10	55.085469	-1.473513	55.085469	Unknown
11	55.085644	-1.472884	55.085644	Scour structure
12	55.085735	-1.472624	55.085735	Scour structure
13	55.085733	-1.472547	55.085733	Scour structure
14	55.085706	-1.472160	55.085706	Scour structure
15	55.085641	-1.472119	55.085641	Scour structure and bedding plane
16	55.085555	-1.472076	55.085555	Bedding plane
17	55.085490	-1.472239	55.085490	Scour structure
18	55.085400	-1.473051	55.085400	Scour structure
19	55.084802	-1.471096	55.084802	Section 2
20	55.084824	-1.471038	55.084824	Section 2
21	55.084815	-1.470997	55.084815	Section 2

22	55.084806	-1.470936	55.084806	Section 2
23	55.084831	-1.470853	55.084831	Section 2
24	55.084827	-1.470789	55.084827	Section 2
25	55.084833	-1.470727	55.084833	Section 2
26	55.084845	-1.470647	55.084845	Section 2
27	55.084837	-1.470562	55.084837	Section 2
28	55.084814	-1.470505	55.084814	Section 2
29	55.084882	-1.470442	55.084882	Section 2
30	55.084867	-1.470341	55.084867	Section 2
31	55.084893	-1.470318	55.084893	Section 2
32	55.084857	-1.470674	55.084857	Scour structure
33	55.085671	-1.471534	55.085671	Scour structure
34	55.085635	-1.471548	55.085635	Bedding plane
35	55.085551	-1.471573	55.085551	Bedding plane
36	55.085273	-1.471106	55.085273	Bedding plane
37	55.085161	-1.471119	55.085161	Unknown
38	55.085111	-1.471128	55.085111	Bedding plane
39	55.085179	-1.471124	55.085179	Bedding plane
40	55.085408	-1.470114	55.085408	Unknown
41	55.085110	-1.470380	55.085110	Bedding plane
42	55.085057	-1.470307	55.085057	Bedding plane
43	55.083959	-1.469010	55.083959	Unknown
44	55.084486	-1.469679	55.084486	Palaeocurrent
45	55.084297	-1.469709	55.084297	Palaeocurrent
46	55.084310	-1.469683	55.084310	Palaeocurrent
47	55.084274	-1.469405	55.084274	Palaeocurrent
48	55.084489	-1.469857	55.084489	Bedding plane
49	55.085058	-1.470035	55.085058	Photograph
50	55.084944	-1.470186	55.084944	Photograph
51	55.084651	-1.469992	55.084651	Photograph
52	55.085637	-1.472118	55.085637	Scour structure
53	55.085574	-1.472293	55.085574	Sample (not used)
54	55.085631	-1.472516	55.085631	Scour structure
55	55.085399	-1.472881	55.085399	Bedding plane
56	55.085405	-1.472756	55.085405	Bedding plane
57	55.085452	-1.472166	55.085452	Bedding plane
58	55.085437	-1.472109	55.085437	Bedding plane
59	55.084417	-1.469893	55.084417	Bedding plane
60	55.085602	-1.473415	55.085602	Log (section 1)
61	55.085770	-1.473508	55.085770	Bedding plane and Log (section1)
62	55.085848	-1.473482	55.085848	Bedding plane and Log (section1)
63	55.085931	-1.473483	55.085931	Section 1
64	55.085803	-1.473497	55.085803	Section 1
65	55.085779	-1.473579	55.085779	Section 1

66	55.085659	-1.473542	55.085659	Section 1
67	55.085524	-1.473324	55.085524	Section 1
68	55.085432	-1.472779	55.085432	Photo Mosaic
69	55.085487	-1.472576	55.085487	Photo Mosaic
70	55.085506	-1.472277	55.085506	Photo Mosaic
71	55.084661	-1.470013	55.084661	Photo Mosaic
72	55.084895	-1.470226	55.084895	Photo Mosaic
73	55.085079	-1.470085	55.085079	Photo Mosaic
74	55.085240	-1.470765	55.085240	Photo Mosaic
75	55.085382	-1.471252	55.085382	Photo Mosaic
76	55.085443	-1.471642	55.085443	Photo Mosaic
77	55.085482	-1.472067	55.085482	Photo Mosaic

Plates illustrating and describing the characteristics of 19 scour structures identified in the Seaton Sluice study site:

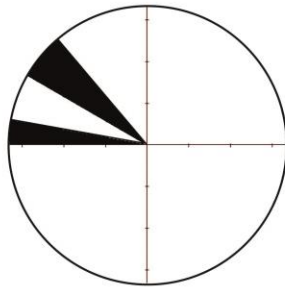
SCOUR STRUCTURE 01	
<p>Description: Site: Seaton Sluice Coordinates: N55°05.1331' W001°28.2601' Location: Upper layer, Section 1 (Fig. 3.10) General description of sand: medium grain size red sands with laminae thickness from a few millimetres to 100 mm. Laminae are inclined towards SW. Orientation: 95° Maximum width: 2.7 m Maximum length: 4.5 m Length to maximum width: 1.6 m (measurement taken from the upstream end)</p>	 <p style="text-align: right; font-size: small;"><i>Photo scale: 1.8 m</i></p>
<div style="display: flex; align-items: center;">  <div style="margin-left: 20px;"> <p>Palaeocurrent data: Percentage frequency azimuthal plot of the palaeocurrent data measured (n = 3, scale tick 10%, sector angle 10°) Mean dip direction: 257°</p> </div> </div>	

SCOUR STRUCTURE 02	
<p>Description: Site: Seaton Sluice Coordinates: N55°05.1271' W001°28.2621' Location: Upper layer, Section 1 (Fig. 3.10) General description of sand: medium grain size white sands. Laminae are inclined towards NW. Orientation: 120° Maximum width: 2 m Maximum length: n/a Length to maximum width: 1.6 m (measurement taken from the upstream end) Palaeocurrent data: Percentage frequency azimuthal plot: N/A due to the preservation of individual laminae. Palaeocurrent data measured (n = 1, Dip direction 310°).</p>	 <p style="text-align: right; font-size: small;"><i>Photo scale: 1 m</i></p>

SCOUR STRUCTURE 03

Description:

Site: Seaton Sluice
Coordinates: N55°05.1261' W001°28.2596'
Location: Upper layer, Section 1 (Fig. 3.10)
General description of sand: medium grain size white sands. Laminae are inclined towards NW.
Orientation: 95°
Maximum width: unclear
Maximum length: 3.7 m
Length to maximum width: n/a



Palaeocurrent data:

Percentage frequency azimuthal plot of the palaeocurrent data measured (n = 3, scale tick 10%, sector angle 10°)
 Mean dip direction: 301°



Photo scale: 1 m

SCOUR STRUCTURE 04

Description:

Site: Seaton Sluice
Coordinates: N55°05.1227' W001°28.2503'
Location: Upper layer, Section 1 (Fig. 3.10)
General description of sand: medium grain size, white sands. Laminae thickness < 100 mm. Laminae are inclined towards NW.
Orientation: 130°
Maximum width: 3.4 m
Maximum length: unclear
Length to maximum width: 1.6 m (measurement taken from the upstream end)

Palaeocurrent data:

Percentage frequency azimuthal plot: N/A due to the preservation of individual laminae. Palaeocurrent data measured (n = 1, Dip direction 325°).

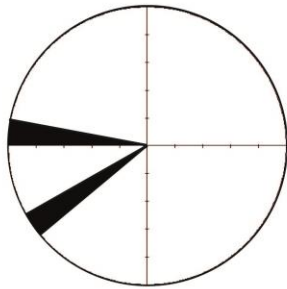
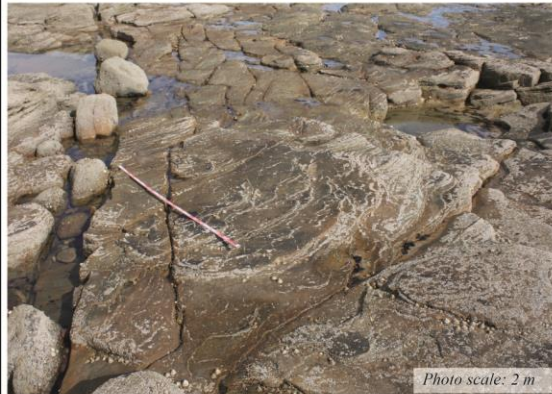


Photo scale: 1.5 m

SCOUR STRUCTURE 05

Description:

Site: Seaton Sluice
Coordinates: N55°05.1323' W001°28.3222'
Location: Upper layer, Section 1 (Fig. 3.10)
General description of sand: medium grain size, white/yellow sands and laminae are inclined towards WSW.
Orientation: 110°
Maximum width: 3.2 m
Maximum length: 4.4 m
Length to maximum width: 2 m



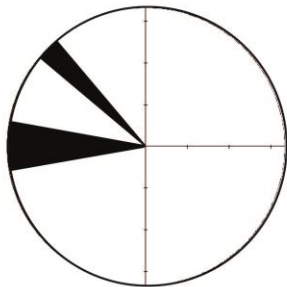
Palaeocurrent data:

Percentage frequency azimuthal plot of the palaeocurrent data measured
 (n = 2, scale tick 10%, sector angle 10°)
 Mean dip direction: 253°

SCOUR STRUCTURE 06

Description:

Site: Seaton Sluice
Coordinates: N55°05.1358' W001°28.3335'
Location: Upper layer, Section 1 (Fig. 3.10)
General description of sand: medium grain size yellow sands. Laminae are inclined towards NW.
Orientation: 125°
Maximum width: 4 m
Maximum length: 6.6 m
Length to maximum width: 5.1 m



Palaeocurrent data:

Percentage frequency azimuthal plot of the palaeocurrent data measured
 (n = 3, scale tick 10%, sector angle 10°)
 Mean dip direction: 286°



SCOUR STRUCTURE 07

Description:

Site: Seaton Sluice

Coordinates: N55°05.1330' W001°28.2778'

Location: Upper layer, Section 1 (Fig. 3.10)

General description of sand: medium grain size, white/yellow sands. Small clast of quartz visible. Laminae are inclined towards WNW.

Orientation: n/a

Maximum width: 1.5 m

Maximum length: unclear

Length to maximum width: 0.72 m (measurement taken from the upstream end)

Palaeocurrent data:

Percentage frequency azimuthal plot: N/A due to the preservation of individual laminae. Palaeocurrent data measured (n = 1, Dip direction 280°).



SCOUR STRUCTURE 08

Description:

Site: Seaton Sluice

Coordinates: N55°05.1385' W001°28.2622'

Location: Upper layer, Section 1 (Fig. 3.10)

General description of sand: fine/medium grain size, yellow sands with coarsel clasts of quartz. Laminae are inclined towards W.

Orientation: 95°

Maximum width: 0.55 m

Maximum length: 0.58 m

Length to maximum width: 0.29 m (measurement taken from the upstream end)

Palaeocurrent data:

Percentage frequency azimuthal plot: N/A due to the preservation of individual laminae. Palaeocurrent data measured (n = 1, Dip direction 270°).

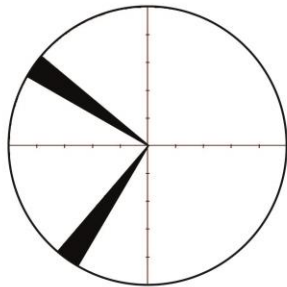


N.B., This structure may have been eroded significantly and its shape could be misleading.

SCOUR STRUCTURE 09

Description:

Site: Seaton Sluice
Coordinates: N55°05.1384' W001°28.2576'
Location: Upper layer, Section 1 (Fig. 3.10)
General description of sand: Unclear observations. Structure covered by barnacles.
Orientation: 100°
Maximum width: 1.3 m
Maximum length: 1.5 m
Length to maximum width: 0.8 m



Palaeocurrent data:

Percentage frequency azimuthal plot of the palaeocurrent data measured
 (n = 2, scale tick 10%, sector angle 10°)
 Mean dip direction: 265°

SCOUR STRUCTURE 10

Description:

Site: Seaton Sluice
Coordinates: N55°05.1384' W001°28.2576'
Location: Upper layer, Section 1 (Fig. 3.10)
General description of sand: medium grain size, white sands. Laminae are inclined towards W.
Orientation: 130°
Maximum width: 1.2 m
Maximum length: 1.6 m
Length to maximum width: 0.82 m (measurement taken from the upstream end)



Palaeocurrent data:

Percentage frequency azimuthal plot: N/A due to the preservation of individual laminae. Palaeocurrent data measured (n = 1, Dip direction 270°).

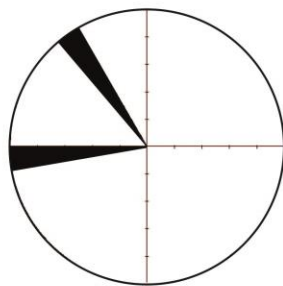
SCOUR STRUCTURE 11

Description:

Site: Seaton Sluice
Coordinates: N55°05.1367' W001°28.2344'
Location: Upper layer, Section 1 (Fig. 3.10)
General description of sand: medium grain size sands. Laminae are inclined towards NW.
Orientation: 110°
Maximum width: 1.3 m
Maximum length: 1.6 m
Length to maximum width: 0.92 m (measurement taken from the upstream end)



N.B., This structure may have been eroded significantly and its shape could be slightly misleading.



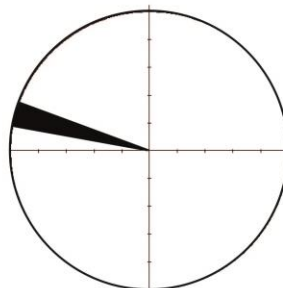
Palaeocurrent data:

Percentage frequency azimuthal plot of the palaeocurrent data measured (n = 2, scale tick 10%, sector angle 10°)
 Mean dip direction: 298°

SCOUR STRUCTURE 12

Description:

Site: Seaton Sluice
Coordinates: N55°05.1328' W001°28.2319'
Location: Upper layer, Section 1 (Fig. 3.10)
General description of sand: medium grain size, white sands. Laminae are inclined towards NW.
Orientation: 110°
Maximum width: 1.02 m
Maximum length: 2.2 m
Length to maximum width: 1.43 m (measurement taken from the upstream end)



Palaeocurrent data:

Percentage frequency azimuthal plot of the palaeocurrent data measured (n = 2, scale tick 10%, sector angle 10°)
 Mean dip direction: 290°

SCOUR STRUCTURE 13

Description:

Site: Seaton Sluice

Coordinates: N55°05.1238' W001°28.2391'

Location: Upper layer, Section 1 (Fig. 3.10)

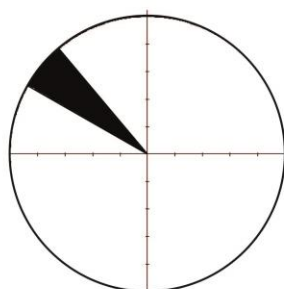
General description of sand: fine-medium grain size, white sands. Laminae are inclined towards NW.

Orientation: 120°

Maximum width: 1 m

Maximum length: 1.5 m

Length to maximum width: 0.8 m (measurement taken from the upstream end)



Palaeocurrent data:

Percentage frequency azimuthal plot of the palaeocurrent data measured (n = 2, scale tick 10%, sector angle 10°)
 Mean dip direction: 315°

SCOUR STRUCTURE 14

Description:

Site: Seaton Sluice

Coordinates: N55°05.1238' W001°28.2391'

Location: Upper layer, Section 1 (Fig. 3.10)

General description of sand: fine-medium grain size white sands. Laminae are inclined towards NW.

Orientation: 68° to 110°

Maximum width: 1.2 m

Maximum length: 1.6 m

Length to maximum width: 0.9 m (measurement taken from the upstream end)

Palaeocurrent data:

Percentage frequency azimuthal plot: N/A due to the preservation of individual laminae. Palaeocurrent data measured (n = 1, Dip direction 320°).



SCOUR STRUCTURE 15

Description:

Site: Seaton Sluice

Coordinates: N55°05.1184' W001°28.2878'

Location: Upper layer, Section 1 (Fig. 3.10)

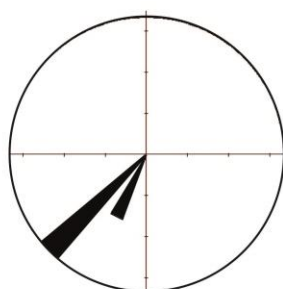
General description of sand: medium grain size, yellowish sands. Flakes of micas are observed. Laminae are inclined towards SW.

Orientation: 120°

Maximum width: 2.7 m

Maximum length: unclear

Length to maximum width: 1.2 m (measurement taken from the upstream end)



Palaeocurrent data:

Percentage frequency azimuthal plot of the palaeocurrent data measured (n = 3, scale tick 10%, sector angle 10°)
 Mean dip direction: 219°

SCOUR STRUCTURE 16

Description:

Site: Seaton Sluice

Coordinates: N55°05.0858' W001°28.1452'

Location: Upper layer, Section 1 (Fig. 3.10)

General description of sand: medium grain size white sands with very thin interbedded sandy laminae rich in micas. Laminae thickness ranges from a few mm to 15 mm. Laminae are inclined towards NW.

Orientation: 110°

Maximum width: from 1.9 m

Maximum length: 3 m

Length to maximum width: 1.9 m (measurement taken from the upstream end)



Palaeocurrent data:

Percentage frequency azimuthal plot: N/A due to the preservation of individual laminae. Palaeocurrent data measured (n = 1, Dip direction 279°).

SCOUR STRUCTURE 17

Description:

Site: Seaton Sluice

Coordinates: N55°05.1346' W001°28.1968'

Location: Upper layer, Section 1 (Fig. 3.10)

General description of sand: medium grain size white sands. Laminae thickness ranges from a few mm to 10 mm. Laminae are inclined towards NW.

Orientation: 90°

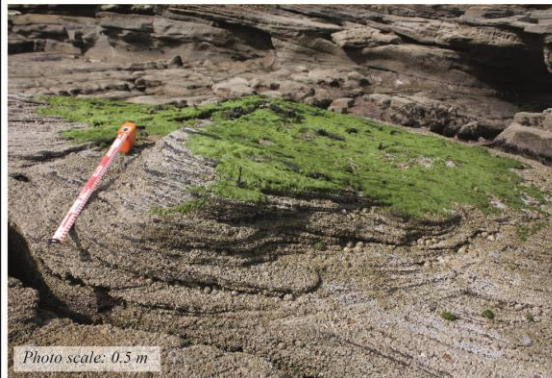
Maximum width: 0.83 m

Maximum length: 1.3 m

Length to maximum width: 0.7 m (measurement taken from the upstream end)

Palaeocurrent data:

Percentage frequency azimuthal plot: N/A due to the preservation of individual laminae. Palaeocurrent data measured (n = 1, Dip direction 288°).



SCOUR STRUCTURE 18

Description:

Site: Seaton Sluice

Coordinates: N55°05.1346' W001°28.1968'

Location: Upper layer, Section 1 (Fig. 3.10)

General description of sand: medium grain size white sands. Laminae thickness ranges from a few mm to 10 mm. Laminae are inclined towards SW.

Orientation: 120°

Maximum width: 0.55 m

Maximum length: from 1.2 m

Length to maximum width: 0.5 m (measurement taken from the upstream end)

Palaeocurrent data:

Percentage frequency azimuthal plot: N/A due to the preservation of individual laminae. Palaeocurrent data measured (n = 1, Dip direction 258°).



SCOUR STRUCTURE 19

Description:

Site: Seaton Sluice

Coordinates: N55°05.1326' W001°28.2319'

Location: Upper layer, Section 1 (Fig. 3.10)

General description of sand: medium grain size, white sands. Flakes of micas are observed.

Laminae thickness ranges from a few mm to 10 mm.

Laminae are inclined towards NW.

Orientation: 100°

Maximum width: from 1.15 m

Maximum length: 3 m

Length to maximum width: 1.55 m (measurement taken from the upstream end)

Palaeocurrent data:

Percentage frequency azimuthal plot: N/A due to the preservation of individual laminae. Palaeocurrent data measured (n = 1, Dip direction 300°).



Table C1. Observations on unit-bar geometry: Run 1, side wall 1 (right side).

RUN 1								
SIDE WALL 1 (RIGHT SIDE)								
Time Interval	Downstream Distance (m)	Bar Height, h (m)	Slip-face Length, Ls (m)	Lee-face Angle, α	Date	Real Time (hh:mm)	Cumulative Time (s)	Reset time (hh:mm)
Start Set-up	0.41	0.280	0.700	24	30/03/2012	16:15	-	-
1	1.18	0.100	0.190	32	30/03/2012	17:46	0	00:00
2	1.39	0.090	0.170	32	30/03/2012	18:33	2820	00:47
3	1.58	0.050	0.110	27	30/03/2012	19:41	6900	01:55
4	1.63	0.050	0.110	27	30/03/2012	20:38	10320	02:52
5	1.84	0.055	0.110	30	30/03/2012	21:39	13980	03:53
6	1.99	0.050	0.090	34	30/03/2012	22:37	17460	04:51
7	2.03	0.090	0.150	37	30/03/2012	23:34	20880	05:48
8	2.20	0.065	0.120	33	31/03/2012	00:38	24720	06:44
9	2.41	0.045	0.020	-	31/03/2012	01:40	28440	07:46
10	2.46	0.050	0.115	26	31/03/2012	02:39	31980	08:45
11	2.67	0.065	0.110	36	31/03/2012	03:49	36180	09:55
12	2.86	0.025	0.050	30	31/03/2012	04:39	39180	10:45
13	3.07	-	-	-	31/03/2012	05:57	43860	12:03
14	3.20	-	-	-	31/03/2012	06:42	46560	12:48

Table C2. Observations on unit-bar geometry: Run 1, side wall 2 (left side).

RUN 1								
SIDE WALL 2 (LEFT SIDE)								
Time Interval	Downstream Distance (m)	Bar Height, h (m)	Slip-face Length, Ls (m)	Lee- face Angle, α	Date	Real Time (hh:mm)	Cumulative Time (s)	Reset time (hh:mm)
Start Set-up	0.34	0.340	0.760	27	30/03/2012	16:30	-	00:00
1	0.88	0.220	0.890	14	30/03/2012	17:49	0	01:19
2	1.00	0.200	0.380	32	30/03/2012	18:35	2760	02:05
3	1.20	0.150	0.260	35	30/03/2012	19:47	7080	03:17
4	1.31	0.130	0.250	31	30/03/2012	20:43	10440	04:13
5	1.45	0.140	0.230	37	30/03/2012	21:44	14100	05:14
6	1.58	0.135	0.225	37	30/03/2012	22:44	17700	06:14
7	1.78	0.050	0.080	39	30/03/2012	23:38	20940	07:08
8	1.90	0.060	0.105	35	31/03/2012	00:40	24660	08:02
9	2.00	0.075	0.140	32	31/03/2012	01:42	28380	09:04
10	2.16	0.045	0.120	22	31/03/2012	02:41	31920	10:03
11	2.38	0.035	0.075	28	31/03/2012	03:53	32640	11:15
12	2.47	0.025	0.050	30	31/03/2012	04:42	39180	12:04
13	2.61	0.065	0.110	36	31/03/2012	05:41	42720	13:03
14	2.97	-	-	-	31/03/2012	06:45	46560	14:07

Table C3. Observations on unit-bar geometry: Run 2, side wall 1 (right side).

RUN 2								
SIDE WALL 1 (RIGHT SIDE)								
Time Interval	Downstream Distance (m)	Bar Height, h (m)	Slip-face Length, Ls (m)	Lee-face Angle, α	Date	Real Time (hh:mm)	Cumulative Time (s)	Reset time (hh:mm)
Start Set-up	0.10	0.480	0.910	32	10/04/2012	12:00	0	00:00
1	0.63	0.210	0.400	32	10/04/2012	13:00	3600	01:00
2	0.75	0.195	0.390	30	10/04/2012	14:00	7200	02:00
3	0.82	0.190	0.375	30	10/04/2012	15:00	10800	03:07
4	0.86	0.190	0.370	31	10/04/2012	16:07	14820	04:03
5	0.92	0.160	0.300	32	10/04/2012	17:03	18180	05:04
6	0.93	0.190	0.294	32	10/04/2012	18:04	21840	05:05
7	0.97	0.175	0.335	31	10/04/2012	19:02	25320	06:02
8	1.04	0.160	0.290	33	10/04/2012	19:58	28680	06:58
9	1.11	0.130	0.240	33	10/04/2012	21:05	32700	08:05
10	1.16	0.115	0.215	32	10/04/2012	22:01	36060	09:01
11	1.18	0.120	0.220	33	10/04/2012	23:04	39840	10:04
12	1.20	0.120	0.220	33	11/04/2012	00:04	43440	11:04
13	1.26	0.105	0.190	34	11/04/2012	01:04	47040	12:04
14	1.30	0.100	0.185	33	11/04/2012	02:03	50580	13:03
15	1.33	0.085	0.170	30	11/04/2012	03:03	54180	14:03
16	1.35	0.080	0.155	31	11/04/2012	04:03	57780	15:03
17	-	-	-	-	-	-	-	-
18	1.46	0.055	0.095	35	11/04/2012	06:05	65100	17:05
19	1.48	0.070	0.140	30	11/04/2012	07:06	68760	18:06
20	1.54	0.045	0.090	30	11/04/2012	08:00	72000	19:00
21	1.55	0.070	0.125	34	11/04/2012	09:03	75780	20:03
22	1.62	0.040	0.080	30	11/04/2012	10:03	79380	21:03
23	1.62	0.065	0.120	33	11/04/2012	11:03	82980	22:03

Table C4. Observations on unit-bar geometry: Run 2, side wall 2 (left side).

RUN 2								
SIDE WALL 2 (LEFT SIDE)		Bar Height, h (m)	Slip-face Length, L _s (m)	Lee-face Angle, α	Date	Real Time (hh:mm)	Cumulative Time (s)	Reset time (hh:mm)
Start Set-up	0.11	0.500	0.920	33	10/04/2012	12:00	0	00:00
1	0.61	0.225	0.390	35	10/04/2012	13:05	3900	01:05
2	0.68	0.225	0.430	32	10/04/2012	14:06	7560	02:06
3	0.86	0.160	0.300	32	10/04/2012	15:09	11340	03:09
4	0.92	0.145	0.280	31	10/04/2012	16:11	15060	04:11
5	0.95	0.155	0.295	32	10/04/2012	17:05	18300	05:05
6	1.03	0.130	0.245	32	10/04/2012	18:10	22200	06:10
7	1.12	0.095	0.165	35	10/04/2012	19:08	25680	07:08
8	1.07	0.150	0.275	33	10/04/2012	20:01	28860	08:01
9	1.13	0.100	0.180	34	10/04/2012	21:09	32940	09:09
10	1.15	0.125	0.220	35	10/04/2012	22:05	36300	10:05
11	1.25	0.090	0.165	33	10/04/2012	23:09	40140	11:09
12	1.27	0.090	0.170	32	11/04/2012	00:09	43740	12:09
13	1.35	0.085	0.130	41	11/04/2012	01:05	47100	13:05
14	1.39	0.075	0.135	34	11/04/2012	02:06	50760	14:06
15	1.42	0.070	0.125	34	11/04/2012	03:07	54420	15:07
16	1.53	0.060	0.110	33	11/04/2012	04:07	58020	16:07
17	-	-	-	-	-	-	-	-
18	1.62	0.030	0.065	27	11/04/2012	06:12	65520	18:12
19	1.66	0.030	0.050	37	11/04/2012	07:10	69000	19:10
20	1.675	0.030	0.050	37	11/04/2012	08:06	72360	20:06
21	1.675	0.030	0.095	18	11/04/2012	09:07	76020	21:07
22	1.75	0.020	0.045	26	11/04/2012	10:07	79620	22:07
23	1.78	0.030	0.055	33	11/04/2012	11:06	83160	23:06

Table C5. Observations on unit-bar geometry: Run 3, side wall 1 (right side).

RUN 3								
SIDE WALL 1 (RIGHT SIDE)								
Time Interval	Downstream Distance (m)	Bar Height, h (m)	Slip-face Length, Ls (m)	Lee-face Angle, α	Date	Real Time (hh:mm)	Cumulative Time (s)	Reset time (hh:mm)
Start Set-up	0	0.490	0.890	33	19/04/2012	11:00	0	00:00
1	0.51	0.240	0.440	33	19/04/2012	12:03	3780	01:03
2	0.66	0.205	0.400	31	19/04/2012	13:01	7260	02:01
3	0.77	0.170	0.330	31	19/04/2012	14:04	11040	03:04
4	0.77	0.185	0.365	30	19/04/2012	15:03	14580	04:03
5	0.86	0.165	0.300	33	19/04/2012	16:00	18000	05:00
6	0.91	0.150	0.288	31	19/04/2012	17:00	21600	06:00
7	1.00	0.120	0.225	32	19/04/2012	18:03	25380	07:03
8	0.96	0.155	0.300	31	19/04/2012	19:03	28980	08:03
9	1.05	0.135	0.255	32	19/04/2012	20:04	32640	09:04
10	1.11	0.105	0.185	35	19/04/2012	21:03	36180	10:03
11	1.13	0.105	0.200	32	19/04/2012	22:09	40140	11:09
12	1.15	0.110	0.200	33	19/04/2012	23:01	43260	12:01
13	1.21	0.090	0.165	33	20/04/2012	00:03	46980	13:03
14	1.25	0.090	0.160	34	20/04/2012	01:02	50520	14:02
15	1.20	0.120	0.220	33	20/04/2012	02:00	54000	15:00
16	1.35	0.060	0.110	33	20/04/2012	03:03	57780	16:03
17	1.31	0.075	0.150	30	20/04/2012	04:04	61440	17:04
18	1.41	0.050	0.085	36	20/04/2012	05:01	64860	18:01
19	1.35	0.085	0.155	33	20/04/2012	06:04	68640	19:04
20	1.39	0.055	0.155	21	20/04/2012	07:07	72420	20:07
21	1.48	0.045	0.075	37	20/04/2012	08:07	76020	21:07
22	1.48	0.045	0.085	32	20/04/2012	09:03	79380	22:03
23	1.52	0.045	0.080	34	20/04/2012	10:02	82920	23:02

Table C6. Observations on unit-bar geometry: Run 3, side wall 2 (left side).

RUN 3								
SIDE WALL 2 (LEFT SIDE)		Bar Height, h (m)	Slip-face Length, L _s (m)	Lee-face Angle, α	Date	Real Time (hh:mm)	Cumulative Time (s)	Reset time (hh:mm)
Time Interval	Downstream Distance (m)							
Start Set-up	0	0.510	0.940	33	19/04/2012	11:00	0	00:00
1	0.50	0.240	0.440	33	19/04/2012	12:08	4080	01:08
2	0.62	0.215	0.395	33	19/04/2012	13:05	7500	02:05
3	0.63	0.250	0.450	34	19/04/2012	14:08	11280	03:08
4	0.72	0.235	0.405	35	19/04/2012	15:07	14820	04:07
5	0.82	0.180	0.345	31	19/04/2012	16:04	18240	05:04
6	0.88	0.170	0.300	35	19/04/2012	17:03	21780	06:03
7	0.91	0.180	0.330	33	19/04/2012	18:07	25620	07:07
8	0.89	0.180	0.350	31	19/04/2012	19:08	29280	08:08
9	0.96	0.150	0.290	31	19/04/2012	20:07	32820	09:07
10	1.01	0.155	0.270	35	19/04/2012	21:06	36360	10:06
11	1.01	0.160	0.290	33	19/04/2012	22:12	40320	11:12
12	1.05	0.155	0.285	33	19/04/2012	23:04	43440	12:04
13	1.12	0.110	0.220	30	20/04/2012	00:06	47160	13:06
14	1.16	0.135	0.225	37	20/04/2012	01:05	50700	14:05
15	1.18	0.125	0.215	36	20/04/2012	02:03	54180	15:03
16	1.17	0.140	0.250	34	20/04/2012	03:06	57960	16:06
17	1.23	0.120	0.210	35	20/04/2012	04:07	61620	17:07
18	1.25	0.110	0.200	33	20/04/2012	05:04	65040	18:04
19	1.27	0.110	0.195	34	20/04/2012	06:07	68820	19:07
20	1.32	0.105	0.175	37	20/04/2012	07:10	72600	20:10
21	1.27	0.130	0.250	31	20/04/2012	08:14	76440	21:14
22	1.37	0.075	0.155	29	20/04/2012	09:06	79560	22:06
23	1.36	0.105	0.190	34	20/04/2012	10:06	83160	22:06

Table C7. Observations on unit-bar geometry: Run 4, side wall 1 (right side).

RUN 4						
SIDE WALL 1 (RIGHT SIDE)						
Downstream Distance (m)	Bar Height, h (m)	Slip-face Length, Ls (m)	Lee-face Angle, α	Date	Real Time (hh:mm)	Cumulative Time (s)
4.62	0.300	0	23	24/04/2013	10:13	00:00
4.56	0.160	0.250	40*	24/04/2013	10:24	00:11
-	0.126	0.250	30	24/04/2013	10:29	00:16
4.61	0.140	0.242	35*	24/04/2013	10:33	00:20
4.59	0.157	0.300	32	24/04/2013	10:39	00:26
4.59	0.150	0.275	33	24/04/2013	10:48	00:35
4.57	0.140	0.290	29	24/04/2013	10:53	00:40
4.59	0.178	0.278	40*	24/04/2013	11:11	00:58
4.64	0.146	0.278	32	24/04/2013	11:19	01:06
4.64	0.145	0.280	31	24/04/2013	11:28	01:15
4.65	0.145	0.230	39*	24/04/2013	11:45	01:32
4.69	0.107	0.230	28	24/04/2013	11:51	01:38
4.62	0.180	0.315	35*	24/04/2013	12:07	01:54
4.64	0.170	0.314	33	24/04/2013	12:17	02:04
4.66	0.163	0.285	35*	24/04/2013	12:34	02:21
4.69	0.143	0.255	34	24/04/2013	12:41	02:32
4.63	0.216	0.380	35*	24/04/2013	13:56	03:43
4.67	0.210	0.400	32	24/04/2013	13:59	03:46
4.70	0.172	0.360	29	24/04/2013	14:39	04:26
4.71	0.165	0.308	32	24/04/2013	14:42	04:29
4.72	0.180	0.330	33	24/04/2013	15:18	05:05
4.72	0.176	0.340	31	24/04/2013	15:23	05:10
4.72	0.258	0.320	54*	24/04/2013	15:41	05:28
4.72	0.155	0.320	29	24/04/2013	16:16	06:03

4.73	0.160	0.320	30	24/04/2013	16:41	06:28
4.69	0.210	0.390	33	24/04/2013	17:04	06:51
4.80	0.170	0.320	32	24/04/2013	17:48	07:35
4.75	0.210	0.382	33	25/04/2013	10:57	08:34
4.73	0.227	0.410	34	25/04/2013	11:32	09:09
4.76	0.225	0.422	32	25/04/2013	12:08	09:45
4.80	0.221	0.409	33	25/04/2013	13:39	11:16
4.78	0.256	0.472	33	25/04/2013	14:28	12:05
4.82	0.260	0.484	32	25/04/2013	17:04	14:41
4.85	0.258	0.476	33	26/04/2013	09:36	16:05
4.85	0.251	0.483	31	26/04/2013	10:36	17:05
4.88	0.237	0.444	32	26/04/2013	11:37	18:06
4.91	0.242	0.471	31	26/04/2013	12:26	18:47
4.82	0.289	0.573 (from here onwards $L_s = L_s$)	30	26/04/2013	14:16	20:37
4.86	0.279	0.530	32	26/04/2013	16:19	22:40
4.96	0.235	0.458	31	26/04/2013	16:58	23:19
4.91	0.271	0.523	31	27/04/2013	09:50	25:06
5.01	0.213	0.399	32	27/04/2013	10:49	26:05
4.99	0.244	0.457	32	27/04/2013	11:53	27:09
4.96	0.274	0.510	32	27/04/2013	12:47	28:03
5.00	0.244	0.409	37*	29/04/2013	07:58	28:29
5.05	0.244	0.470	31	29/04/2013	12:50	33:31
5.16	0.221	0.411	33	29/04/2013	19:40	40:21
5.13	0.249	0.461	33	30/04/2013	08:31	41:12
5.21	0.220	0.412	32	30/04/2013	14:35	47:08
5.26	0.209	0.388	33	30/04/2013	18:53	51:26
5.27	0.202	0.389	31	01/05/2013	07:41	51:45
5.39	0.157	0.306	31	01/05/2013	14:06	58:10

5.39	0.181	0.346	32	01/05/2013	18:15	62:19
5.41	0.185	0.339	33	02/05/2013	08:35	63:19
5.48	0.200	0.291	43*	02/05/2013	14:20	69:04
5.48	0.155	0.260	37*	02/05/2013	14:22	69:06
5.58	0.122	0.228	32	02/05/2013	18:05	72:49
5.57	0.121	0.236	31	03/05/2013	08:13	73:29
5.63	0.118	0.221	32	03/05/2013	12:21	77:37

N.B., Data in shaded boxes was only used to represent the variation of lee-face angle with time and downstream distance. These values were taken from photographs. *Values excluded in the representation of lee-face angle versus time and downstream distance due to their unrealistic nature.

Table C8. Observations on unit-bar geometry: Run 4, side wall 2 (left side).

RUN 4						
SIDE WALL 2 (LEFT SIDE)						
Downstream Distance (m)	Bar Height, h (m)	Slip-face Length, Ls (m)	Lee-face Angle, α	Date	Real Time (hh:mm)	Cumulative Time (s)
4.55	0.320	0.700	27	24/04/2013	10:14	00:00
4.57	0.295	-	-	24/04/2013	10:21	00:07
4.62	0.325	-	-	24/04/2013	10:30	00:16
4.59	0.300	-	-	24/04/2013	10:40	00:26
4.58		0.400	-	24/04/2013	10:52	00:38
4.85	0.350	0.380	67*	24/04/2013	11:08	00:54
4.60	0.350	-	-	24/04/2013	11:22	01:08
4.55	0.385	-	-	24/04/2013	11:40	01:26
4.62	0.305	0.355	59*	24/04/2013	11:55	01:41
4.65	0.285	0.325	61*	24/04/2013	12:23	02:09
4.57	0.357	0.410	61*	24/04/2013	12:51	02:37
4.63	0.326	0.360	65*	24/04/2013	13:11	02:57
4.66	0.330	-	-	24/04/2013	13:22	03:08
4.61	0.355	0.390	66*	24/04/2013	13:24	03:10
4.68	0.325	0.370	61*	24/04/2013	13:31	03:17
4.68	0.200	-	-	24/04/2013	13:44	03:30
4.67	0.240	0.430	34	24/04/2013	13:52	03:38
4.67	0.330	-	-	24/04/2013	14:03	03:49
4.68	0.320	-	-	24/04/2013	14:15	04:01
4.70	0.320	-	-	24/04/2013	14:26	04:12
4.67	0.290	-	-	24/04/2013	15:10	04:56
4.69	0.293	0.400	47*	24/04/2013	15:34	05:20
4.70	0.290	0.380	50*	24/04/2013	16:23	06:09
4.73	0.275	0.375	47*	24/04/2013	17:22	07:08

4.73	0.275	0.380	46*	24/04/2013	17:56	07:42
4.72	0.287	0.445	40*	25/04/2013	11:20	08:56
4.71	0.310	0.470	41*	25/04/2013	11:42	09:18
4.75	0.298	0.450	41*	25/04/2013	12:27	10:03
4.80	0.209	0.390	32	25/04/2013	14:02	11:38
4.80	0.225	0.410	33	25/04/2013	14:45	12:21
4.82	0.230	0.420	33	25/04/2013	17:27	15:03
4.81	0.237	0.472	30	26/04/2013	09:52	16:18
4.82	0.241	0.450	32	26/04/2013	11:02	17:28
4.87	0.221	0.410	33	26/04/2013	11:47	18:13
4.86	0.250	0.464	33	26/04/2013	12:34	19:00
4.86	0.247	0.460	32	26/04/2013	14:27	20:53
4.93	0.220	0.406	33	26/04/2013	16:23	22:49
4.95	0.234	0.432	33	26/04/2013	17:16	23:42
4.97	0.231	0.400	35*	27/04/2013	09:59	25:20
4.98	0.210	0.410	31	27/04/2013	10:58	26:25
4.96	0.224	0.432	31	27/04/2013	12:03	27:15
4.95	0.241	0.453	32	27/04/2013	12:53	28:05
5.00	0.212	0.410	31	29/04/2013	08:04	28:31
5.06	0.220	0.413	32	29/04/2013	12:55	33:22
5.73	0.213	0.398	32	29/04/2013	19:50	40:17
5.15	0.218	0.410	32	30/04/2013	08:38	41:05
5.21	0.207	0.399	31	30/04/2013	14:39	47:06
5.22	0.224	0.420	32	30/04/2013	18:57	51:24
5.19	0.247	0.478	31	01/05/2013	08:01	51:59
5.22	0.244	0.453	33	01/05/2013	14:11	58:09
5.32	0.210	0.393	32	01/05/2013	18:20	62:18
5.30	0.237	0.446	32	02/05/2013	08:40	63:18

5.36	0.225	0.428	32	02/05/2013	14:27	69:05
5.47	0.181	0.337	32	02/05/2013	18:10	72:48
5.47	0.176	0.335	32	03/05/2013	08:16	73:26
5.51	0.172	0.310	27	03/05/2013	12:26	77:36

N.B., *Unrealistic values of lee-face angle that have been excluded from any representation. This can be explained due to measurement error and distortion through the flume glass windows.

Table C9. Migration rates, Runs 1-4.

Run 1					
Time Interval	Downstream distance (m)	Bar height (m)	Cumulative time (s)	Migration rate (m s⁻¹)	
T0	0.41	0.280	0	0	
T1	1.10	0.100	3600	0.000191667	
T2	1.30	0.090	7200	5.55556E-05	
T3	1.58	0.050	10800	7.77778E-05	
T4	1.63	0.050	14400	1.38889E-05	
T5	1.84	0.055	18000	5.83333E-05	
Mean Migration rate: 7.94444E-05					
Run 2					
Time Interval	Downstream distance (m)	Bar height (m)	Cumulative time (s)	Migration rate (m s⁻¹)	
T0	0.00		0	0	
T1	0.62	0.210	3600	0.000170833	
T2	0.76	0.195	7200	4.02778E-05	
T3	0.78	0.200	10800	5.55556E-06	
T4	0.86	0.190	14400	2.08333E-05	
T5	0.91	0.160	18000	1.52778E-05	
T6	0.91	0.190	21600	0	
T7	0.96	0.183	25200	1.38889E-05	
T8	1.03	0.175	28800	1.94444E-05	
T9	1.09	0.160	32400	1.66667E-05	
T10	1.16	0.130	36000	1.80556E-05	
T11	1.18	0.115	39600	5.55556E-06	

T12	1.20	0.120	43200	5.55556E-06
T13	1.26	0.120	46800	1.66667E-05
T14	1.29	0.105	50400	8.33333E-06
T15	1.33	0.100	54000	1.19444E-05
T16	1.36	0.085	57600	7.5E-06
T17	1.46	0.080	61200	2.91667E-05
T19	1.50	0.055	68400	5.55556E-06
T20	1.53	0.070	72000	8.33333E-06
T21	1.54	0.045	75600	1.38889E-06
T22	1.59	0.070	79200	1.52778E-05
T23	1.60	0.040	82800	2.77778E-06
Mean Migration rate: 1.93237E-05				

Run 3				
Time Interval	Downstream distance (m)	Bar height (m)	Cumulative time (s)	Migration rate (m s ⁻¹)
T0	0.00	-	0	0
T1	0.52	0.240	3600	0.000144444
T2	0.63	0.205	7200	3.05556E-05
T3	0.76	0.170	10800	3.66667E-05
T4	0.82	0.185	14400	1.61111E-05
T5	0.84	0.165	18000	6.11111E-06
T6	0.89	0.150	21600	1.33333E-05
T7	1.00	0.120	25200	3.02778E-05
T8	1.06	0.155	28800	1.77778E-05
T9	1.03	0.135	32400	-1.02778E-05
T10	1.12	0.105	36000	2.47222E-05
T11	1.15	0.105	39600	9.72222E-06
T12	1.15	0.110	43200	5.55556E-07
T13	1.21	0.090	46800	1.47222E-05
T14	1.25	0.090	50400	1.11111E-05
T15	1.21	0.120	54000	-9.44444E-06
T16	1.34	0.060	57600	3.44444E-05
T17	1.35	0.075	61200	3.61111E-06
T18	1.41	0.050	64800	1.58333E-05
T19	1.43	0.085	68400	6.94444E-06

T20	1.46	0.055	72000	7.5E-06
T21	1.47	0.045	75600	3.61111E-06
T22	1.47	0.045	79200	5.55556E-07
T23	1.52	0.045	82800	1.38889E-05
Mean Migration rate: 1.83816E-05				
Run 4				
Time Interval (hh:mm)	Downstream distance (m)	Bar height (m)	Cumulative time (s)	Migration rate (m s⁻¹)
00:00	4.55	0.300	0	0
00:10	4.60	0.160	600	8.33333E-05
00:20	4.63	0.140	1800	2.5E-05
00:37	4.57	0.150	3420	-2.7027E-05
01:05	4.63	0.178	6120	1.58974E-05
01:35	4.70	0.145	9600	1.19298E-05
02:01	4.68	0.145	12960	-2.75482E-06
02:24	4.69	0.180	15900	1.15741E-06
03:42	4.64	0.163	21960	-4.12913E-06
04:26	4.71	0.216	29280	4.69925E-06
05:07	4.72	0.172	34380	5.42888E-07
05:09	4.74	0.180	36960	8.09061E-07
06:03	4.76	0.258	40320	9.64187E-07
06:29	4.76	0.155	45120	2.14225E-07
07:37	4.82	0.160	50760	1.96937E-06
08:38	4.79	0.210	58500	-9.65251E-07
09:08	4.75	0.170	63960	-1.00365E-06
09:50	4.77	0.210	68280	5.64972E-07
11:16	4.81	0.227	75960	9.36884E-07
12:05	4.78	0.225	84060	-7.35632E-07
14:40	4.82	0.221	96300	8.33333E-07
16:02	4.88	0.256	110520	1.00485E-06
16:04	4.89	0.260	115560	1.72891E-07
17:01	4.86	0.258	119100	-4.89716E-07
18:03	4.90	0.251	126240	6.15574E-07
18:51	4.90	0.237	132840	2.94724E-08
20:42	4.86	0.242	142380	-6.03865E-07

22:45	4.86	0.289	156420	8.54701E-08
23:24	4.96	0.279	166140	1.1396E-06
25:11	4.93	0.235	174900	-3.30907E-07
26:09	5.01	0.271	184800	8.81666E-07
27:13	4.99	0.213	192120	-2.34742E-07
28:34	5.01	0.244	200820	1.75029E-07
33:26	5.05	0.274	223200	3.48953E-07
40:16	5.16	0.244	265320	7.45033E-07
40:17	5.17	0.244	289980	6.8956E-08
40:58	5.14	0.221	292500	-2.23759E-07
47:01	5.19	0.249	316740	3.3676E-07
51:19	5.27	0.220	354000	3.9515E-07
51:38	5.27	0.209	370620	3.22789E-08
57:02	5.39	0.202	391200	5.94194E-07
61:11	5.39	0.157	425580	0
61:13	5.39	0.181	440640	-3.63009E-08
62:11	5.40	0.185	444240	5.36049E-08
67:59	5.49	0.200	468600	3.71823E-07
71:41	5.57	0.122	502800	3.25506E-07
72:21:00	5.54	0.121	518520	-1.1902E-07
76:29:00	5.61	0.118	535800	2.39704E-07
79:10:00	5.64	0.115	560340	1.22807E-07
Mean Migration rate: 1.94882E-06				

N.B., In Run 1, since the unit bar advanced over the trough in less than 5 hours, migration rates were calculated for the time interval $t = 0$ to $t = 5$.

Table C10. Calculated vales of non-static water surface elevation at individual time intervals.

Mean Water Surface Elevation at locations 1-5 for individual time intervals (m)						
TIME (hh:mm)	Downstream Locations					Slope
	1	2	3	4	5	
00:00	0.699	0.711	0.713	0.709	0.715	0.0013
01:00	0.698	0.705	0.708	0.711	0.715	0.0018
02:00	0.704	0.709	0.708	0.712	0.715	0.0011
03:00	0.705	0.720	0.709	0.711	0.714	0.0005
04:00	0.695	0.704	0.702	0.706	0.711	0.0015
05:00	0.693	0.702	0.700	0.702	0.706	0.0011
06:00	0.698	0.705	0.710	0.709	0.713	0.0015
07:00	0.699	0.704	0.706	0.710	0.711	0.0013
08:00	0.695	0.700	0.699	0.699	0.712	0.0014
09:00	0.701	0.609	0.699	0.702	0.712	-
10:00	0.695	0.697	0.697	0.702	0.705	0.0011
11:00	0.695	0.693	0.694	0.697	0.699	0.0005
12:00	0.694	0.700	0.699	0.698	0.698	0.0002
14:00	0.692	0.697	0.697	0.702	0.695	0.0004
15:00	0.693	0.696	0.696	0.699	0.700	0.0007
16:00	0.690	0.695	0.695	0.697	0.704	0.0013
17:00	0.688	0.701	0.701	0.704	0.704	0.0015
18:00	0.690	0.699	0.697	0.704	0.705	0.0015
21:00	0.689	0.693	0.686	0.688	0.700	0.0008
23:00	0.687	0.697	0.698	0.700	0.700	0.0012
24:00	0.678	0.682	0.686	0.689	0.689	0.0013
25:00	0.696	0.692	0.693	0.696	0.696	0.0002
27:00	0.695	0.692	0.693	0.698	0.695	0.0003
28:00	0.685	0.683	0.684	0.689	0.688	0.0005
33:00	0.672	0.672	0.673	0.677	0.678	0.0007
40:00	0.665	0.668	0.671	0.675	0.676	0.0013
46:00	0.663	0.666	0.668	0.672	0.673	0.0011
51:00	0.656	0.659	0.663	0.666	0.669	0.0014
57:00	0.657	0.656	0.661	0.665	0.668	0.0014
62:00	0.651	0.654	0.657	0.659	0.662	0.0012

68:00	0.645	0.652	0.654	0.657	0.660	0.0012
72:00	0.644	0.644	0.652	0.653	0.655	0.0013
73:00	0.645	0.646	0.649	0.651	0.654	0.0001
76:00	0.643	0.643	0.649	0.651	0.651	0.0011
79:00	0.649	0.647	0.653	0.655	0.655	0.0008

Table C11. Calculated values of static water surface elevation at individual time intervals.

Mean Static Water Surface Elevation at locations 1-5 for individual time intervals (m)						
TIME	1	2	3	4	5	Slope Value
00:00	0.708	0.712	0.718	0.716	0.713	0.0549
07:48	0.695	0.701	0.703	0.704	0.701	0.0634
15:42	0.694	0.695	0.694	0.695	0.697	0.0275
24:32	0.681	0.682	0.685	0.689	0.689	0.1050
28:32	0.678	0.677	0.679	0.685	0.684	0.0940
40:15	0.664	0.661	0.656	0.670	0.672	0.1182
51:25	0.659	0.658	0.662	0.666	0.665	0.0888
62:05	0.651	0.651	0.655	0.659	0.660	0.1128
72:35	0.645	0.641	0.647	0.651	0.651	0.0957

Table C12. Bed thickness data throughout Run 4 from both side walls.

Bed thickness (m)												
		Side Wall 1 (Right side)					Side Wall 2 (Left side)					
DATE	Cumulative Time	1	2	3	4	5	1	2	3	4	5	Mean Value (m)
24/04/13	00:00	0.167	0.232	0.322	0.161	0.183	0.115	0.250	0.370	0.190	0.205	0.219
	00:10	0.162	0.227	0.306	0.153	0.183	0.124	0.250	0.340	0.195	0.200	0.213
	00:16	0.162	0.222	0.322	0.155	0.183	0.117	0.250	0.363	0.197	0.200	0.216
	00:23	0.159	0.214	0.312	0.155	0.184	0.120	0.255	0.365	0.190	0.200	0.215
	00:30	0.162	0.214	0.318	0.153	0.181	0.120	0.230	0.363	0.190	0.202	0.213
	00:37	0.166	0.221	0.319	0.153	0.183	0.122	0.230	0.350	0.190	0.200	0.214
	00:44	0.164	0.231	0.236	0.153	0.186	0.122	0.235	0.361	0.193	0.203	0.208
	00:53	0.162	0.231	0.326	0.149	0.186	0.122	0.224	0.356	0.194	0.203	0.215
	01:05	0.163	0.216	0.337	0.160	0.185	0.120	0.220	0.360	0.197	0.203	0.216
	01:17	0.162	0.207	0.331	0.159	0.186	0.125	0.219	0.358	0.197	0.205	0.216
	01:29	0.168	0.206	0.332	0.159	0.185	0.125	0.220	0.345	0.185	0.203	0.211
	01:40	0.164	0.214	0.329	0.154	0.184	0.124	0.224	0.356	0.188	0.205	0.215
	01:51	0.169	0.225	0.313	0.164	0.182	0.127	0.227	0.340	0.195	0.200	0.215
	02:05	0.172	0.213	0.316	0.162	0.182	0.125	0.230	0.355	0.184	0.195	0.213
	02:16	0.172	0.205	0.338	0.159	0.181	0.130	0.250	0.346	0.183	0.203	0.215
	02:33	0.175	0.208	0.313	0.162	0.185	0.127	0.253	0.353	0.185	0.198	0.214
	02:44	0.174	0.215	0.337	0.164	0.187	0.127	0.255	0.338	0.182	0.197	0.215
	03:01	0.179	0.216	0.318	0.160	0.186	0.128	0.243	0.345	0.188	0.202	0.215
	03:15	0.180	0.222	0.327	0.151	0.188	0.136	0.242	0.334	0.187	0.202	0.215
	03:37	0.175	0.226	0.293	0.166	0.191	0.136	0.227	0.333	0.197	0.205	0.214
	03:49	0.177	0.219	0.300	0.170	0.192	0.135	0.230	0.338	0.195	0.206	0.217
	04:02	0.177	0.220	0.313	0.171	0.192	0.137	0.227	0.338	0.194	0.203	0.218
	04:12	0.178	0.217	0.308	0.172	0.191	0.135	0.226	0.338	0.195	0.210	0.215
	04:22	0.176	0.201	0.319	0.171	0.189	0.140	0.230	0.350	0.185	0.205	0.216
	04:31	0.175	0.200	0.316	0.168	0.188	0.135	0.225	0.320	0.185	0.212	0.210
	04:40	0.178	0.201	0.313	0.163	0.188	0.131	0.226	0.318	0.188	0.195	0.209
	04:49	0.180	0.198	0.301	0.159	0.183	0.131	0.224	0.322	0.187	0.198	0.209
	05:00	0.181	0.199	0.299	0.155	0.180	0.131	0.223	0.329	0.179	0.198	0.209
	05:10	0.183	0.204	0.314	0.155	0.176	0.131	0.217	0.347	0.170	0.193	0.211
	05:20	0.184	0.214	0.322	0.158	0.173	0.133	0.215	0.330	0.171	0.188	0.211

	05:30	0.183	0.212	0.339	0.153	0.176	0.137	0.216	0.342	0.180	0.192	0.215
	06:13	0.221	0.218	0.295	0.141	0.176	0.170	0.223	0.318	0.175	0.203	0.214
	06:32	0.242	0.202	0.307	0.145	0.178	0.180	0.223	0.343	0.173	0.203	0.219
	06:50	0.238	0.203	0.309	0.137	0.177	0.185	0.225	0.335	0.173	0.201	0.219
	07:11	0.258	0.207	0.308	0.149	0.177	0.201	0.230	0.338	0.173	0.203	0.222
	07:33	0.248	0.218	0.332	0.151	0.181	0.211	0.230	0.342	0.174	0.202	0.229
	07:45	0.240	0.207	0.312	0.162	0.176	0.220	0.230	0.334	0.173	0.215	0.225
25/04/13	07:48	0.237	0.218	0.317	0.162	0.180	0.252	0.230	0.328	0.168	0.182	0.229
	08:14	0.245	0.222	0.320	0.160	0.174	0.230	0.234	0.335	0.166	0.211	0.228
	09:18	0.230	0.206	0.307	0.148	0.166	0.226	0.228	0.326	0.182	0.206	0.221
	10:21	0.243	0.200	0.323	0.165	0.180	0.218	0.234	0.331	0.170	0.186	0.224
	11:30	0.252	0.214	0.338	0.163	0.183	0.202	0.221	0.321	0.180	0.183	0.226
	12:49	0.204	0.188	0.287	0.156	0.180	0.202	0.219	0.332	0.182	0.182	0.215
	14:08	0.213	0.220	0.319	0.158	0.178	0.207	0.206	0.333	0.162	0.175	0.219
	15:42	0.197	0.207	0.303	0.155	0.174	0.185	0.228	0.305	0.160	0.190	0.210
26/04/13	15:42	0.203	0.212	0.309	0.143	0.175	0.196	0.222	0.304	0.160	0.187	0.211
	16:39	0.199	0.213	0.280	0.147	0.173	0.185	0.235	0.295	0.158	0.191	0.209
	17:23	0.213	0.202	0.297	0.143	0.171	0.171	0.208	0.316	0.183	0.218	0.207
	18:33	0.206	0.199	0.298	0.139	0.189	0.202	0.209	0.297	0.184	0.210	0.215
	21:34	0.197	0.200	0.308	0.150	0.178	0.150	0.217	0.280	0.160	0.185	0.204
	23:36	0.171	0.213	0.302	0.156	0.176	0.137	0.221	0.293	0.164	0.200	0.204
27/04/13	24:32	0.189	0.223	0.319	0.156	0.172	0.134	0.214	0.285	0.154	0.183	0.204
	25:41	0.175	0.213	0.184	0.147	0.177	0.160	0.205	0.292	0.153	0.183	0.191
	27:14	0.186	0.206	0.296	0.147	0.179	0.133	0.197	0.297	0.175	0.207	0.202
	28:08	0.177	0.212	0.303	0.146	0.197	0.132	0.208	0.293	0.173	0.211	0.204
29/04/13	28:32	0.172	0.224	0.296	0.144	0.191	0.153	0.217	0.301	0.173	0.209	0.208
	28:36	0.170	0.229	0.321	0.146	0.192	0.147	0.214	0.315	0.164	0.209	0.211
	33:51	0.164	0.200	0.291	0.159	0.175	0.132	0.203	0.274	0.162	0.207	0.195
	40:38	0.141	0.212	0.301	0.142	0.178	0.103	0.194	0.292	0.163	0.200	0.191
30/04/13	40:15	0.140	0.206	0.289	0.142	0.171	0.098	0.199	0.296	0.160	0.201	0.189
	40:34	0.155	0.206	0.259	0.141	0.168	0.095	0.201	0.293	0.151	0.203	0.185
	46:31	0.142	0.225	0.267	0.140	0.187	0.078	0.213	0.273	0.165	0.182	0.187
	51:17	0.123	0.285	0.263	0.137	0.180	0.077	0.230	0.277	0.166	0.203	0.193
01/05/13	51:25	0.117	0.282	0.262	0.141	0.180	0.087	0.219	0.281	0.149	0.193	0.190
	51:32	0.117	0.296	0.233	0.151	0.182	0.077	0.221	0.273	0.152	0.199	0.188

	57:43	0.120	0.269	0.241	0.134	0.190	0.062	0.251	0.264	0.142	0.196	0.185
	62:04	0.118	0.261	0.255	0.152	0.183	0.042	0.265	0.250	0.155	0.188	0.186
02/05/13	62:05	0.118	0.253	0.256	0.153	0.183	0.053	0.264	0.243	0.157	0.175	0.186
	62:13	0.103	0.265	0.257	0.152	0.186	0.050	0.253	0.256	0.158	0.189	0.186
	68:42	0.106	0.252	0.236	0.151	0.197	0.045	0.252	0.284	0.141	0.196	0.184
	72:07	0.108	0.244	0.245	0.136	0.209	0.027	0.241	0.250	0.157	0.190	0.179
03/05/13	72:35	0.101	0.250	0.239	0.134	0.207	0.032	0.231	0.252	0.168	0.181	0.178
	73:11	0.095	0.266	0.233	0.126	0.203	0.032	0.249	0.272	0.166	0.190	0.182
	76:50	0.095	0.248	0.218	0.128	0.172	0.031	0.270	0.241	0.146	0.207	0.172
	79:52	0.083	0.253	0.257	0.134	0.203	0.008	0.245	0.235	0.137	0.166	0.171
Total Mean bed thickness: 0.21 m												

Table C13. Water surface elevation data throughout Run 4 from both side walls.

Water Surface Elevation (m)												
		Side Wall 1 (Right side)					Side Wall 2 (Left side)					
DATE	TIME	1	2	3	4	5	1	2	3	4	5	Mean Value (m)
24/04/13	0:10	0.693	0.703	0.698	0.696	0.709	0.714	0.705	0.710	0.720	0.720	0.707
	0:16	0.698	0.706	0.700	0.695	0.708	0.715	0.715	0.712	0.720	0.720	0.709
	0:23	0.702	0.690	0.707	0.701	0.711	0.713	0.713	0.712	0.717	0.722	0.709
	0:30	0.704	0.701	0.702	0.701	0.704	0.713	0.714	0.713	0.718	0.723	0.709
	0:37	0.698	0.708	0.696	0.698	0.707	0.712	0.715	0.711	0.716	0.728	0.709
	0:44	0.698	-	-	0.701	0.709	0.713	0.714	0.713	0.719	0.721	0.716
	0:53	0.695	0.707	0.708	0.693	0.709	0.716	0.713	0.712	0.718	0.723	0.709
	1:05	0.705	0.698	0.706	0.697	0.711	0.713	0.714	0.715	0.716	0.722	0.710
	1:17	0.690	0.699	0.694	0.701	0.709	0.712	0.720	0.718	0.718	0.720	0.708
	1:29	0.699	0.689	0.699	0.702	0.708	0.710	0.714	0.716	0.716	0.728	0.708
	1:40	0.692	0.695	0.700	0.704	0.705	0.712	0.714	0.714	0.717	0.722	0.708
	1:51	0.703	0.687	0.704	0.716	0.706	0.714	0.715	0.717	0.719	0.721	0.710
	2:05	0.703	0.700	0.699	0.705	0.703	0.713	0.715	0.714	0.718	0.723	0.709
	2:16	0.701	0.698	0.700	0.701	0.704	0.713	0.715	0.721	0.716	0.723	0.709
	2:33	0.709	0.708	0.703	0.707	0.715	0.712	0.712	0.715	0.717	0.722	0.712
	2:44	0.704	0.710	0.699	0.712	0.710	0.712	0.715	0.714	0.717	0.723	0.712
	3:01	0.712	-	0.700	0.713	0.705	0.708	0.712	0.712	0.713	0.724	0.714

	3:15	0.717	0.704	0.725	0.702	0.707	0.716	0.716	0.715	0.717	0.723	0.714
	3:37	0.693	0.698	0.696	0.709	0.703	0.714	0.715	0.714	0.720	0.726	0.709
	3:49	0.696	0.702	0.692	0.697	0.696	0.717	0.717	0.715	0.719	0.723	0.707
	4:02	0.694	0.701	0.694	0.692	0.706	0.716	0.717	0.715	0.718	0.723	0.708
	4:12	0.694	0.702	0.696	0.699	0.706	0.718	0.716	0.715	0.715	0.723	0.708
	4:22	0.693	0.693	0.695	0.703	0.703	0.711	0.710	0.712	0.720	0.715	0.705
	4:31	0.692	0.697	0.698	0.702	0.706	0.711	0.705	0.695	0.711	0.715	0.703
	4:40	0.699	0.701	0.698	0.699	0.708	0.708	0.706	0.709	0.704	0.712	0.704
	4:49	0.697	0.698	0.693	0.701	0.707	0.707	0.703	0.706	0.706	0.712	0.703
	5:00	0.698	0.699	0.694	0.700	0.702	0.701	0.703	0.705	0.705	0.714	0.702
	5:10	0.698	0.701	0.698	0.700	0.700	0.702	0.706	0.696	0.705	0.712	0.702
	5:20	0.696	0.705	0.702	0.700	0.704	0.707	0.701	0.702	0.705	0.712	0.703
	5:30	0.681	0.698	0.701	0.699	0.697	0.707	0.704	0.702	0.702	0.710	0.700
	6:13	0.701	0.702	0.703	0.703	0.704	0.713	0.713	0.715	0.717	0.723	0.709
	6:32	0.701	0.692	0.702	0.707	0.708	0.716	0.715	0.715	0.718	0.720	0.709
	6:50	0.692	0.689	0.708	0.695	0.700	0.715	0.720	0.716	0.716	0.723	0.707
	7:11	0.700	0.698	0.697	0.707	0.704	0.715	0.718	0.714	0.718	0.725	0.710
	7:33	0.708	0.694	0.708	0.710	0.712	0.715	0.716	0.715	0.718	0.723	0.712
	7:45	0.696	0.692	0.699	0.702	0.699	0.713	0.715	0.713	0.718	0.725	0.707
25/04/13	8:14	0.695	0.700	0.699	0.702	0.701	0.702	0.699	0.699	0.696	0.722	0.702
	9:18	0.701	0.695	0.697	0.701	0.701	0.703	0.702	0.701	0.702	0.723	0.703
	10:21	0.695	0.695	0.697	0.702	0.702	0.748	0.699	0.696	0.701	0.707	0.704
	11:30	0.695	0.695	0.694	0.702	0.698	0.697	0.690	0.694	0.692	0.699	0.696
	12:49	0.694	0.697	0.695	0.700	0.697	0.694	0.703	0.702	0.695	0.699	0.698
	14:08	0.692	0.693	0.696	0.702	0.699	0.695	0.700	0.698	0.701	0.690	0.697
	15:42	0.692	0.696	0.694	0.700	0.700	0.696	0.699	0.698	0.705	0.705	0.699
26/04/13	16:39	0.690	0.692	0.692	0.697	0.696	0.707	0.697	0.698	0.697	0.711	0.698
	17:23	0.688	0.693	0.693	0.697	0.693	0.706	0.708	0.708	0.710	0.715	0.701
	18:33	0.690	0.687	0.687	0.698	0.694	0.708	0.710	0.707	0.709	0.716	0.701
	21:34	0.689	0.688	0.688	0.683	0.693	0.703	0.697	0.683	0.692	0.707	0.692
	23:36	0.687	0.688	0.689	0.691	0.692	0.707	0.706	0.706	0.709	0.708	0.698
27/04/13	25:41	0.696	0.696	0.697	0.697	0.700	0.692	0.688	0.688	0.695	0.692	0.694
	27:14	0.695	0.696	0.696	0.700	0.699	0.687	0.687	0.690	0.695	0.691	0.694
	28:08	0.698	0.698	0.696	0.700	0.698	0.680	0.688	0.689	0.696	0.692	0.694
29/04/13	28:36	0.681	0.681	0.678	0.686	0.687	0.681	0.679	0.678	0.682	0.681	0.681

	33:51	0.672	0.668	0.673	0.676	0.675	0.678	0.675	0.673	0.677	0.680	0.675
	40:38	0.672	0.674	0.677	0.682	0.682	0.676	0.676	0.675	0.683	0.682	0.678
30/04/13	40:34	0.663	0.663	0.664	0.671	0.668	0.673	0.672	0.672	0.676	0.682	0.670
	46:31	0.663	0.661	0.664	0.671	0.667	0.673	0.670	0.671	0.672	0.679	0.669
	51:17	0.660	0.654	0.666	0.665	0.668	0.671	0.663	0.665	0.671	0.676	0.666
01/05/13	51:32	0.653	0.655	0.663	0.662	0.662	0.665	0.665	0.662	0.666	0.675	0.663
	57:43	0.657	0.651	0.661	0.663	0.660	0.657	0.661	0.661	0.667	0.676	0.661
	62:04	0.655	0.653	0.659	0.661	0.660	0.660	0.660	0.663	0.666	0.672	0.661
02/05/13	62:13	0.651	0.648	0.654	0.654	0.656	0.662	0.659	0.658	0.658	0.666	0.657
	68:42	0.645	0.646	0.652	0.653	0.653	0.661	0.657	0.656	0.660	0.666	0.655
	72:07	0.646	0.644	0.651	0.653	0.652	0.658	0.651	0.659	0.659	0.665	0.654
03/05/13	73:11	0.645	0.643	0.646	0.647	0.648	0.656	0.648	0.651	0.655	0.660	0.650
	76:50	0.643	0.639	0.646	0.647	0.646	0.655	0.646	0.651	0.655	0.656	0.648
	79:52	0.649	0.650	0.654	0.656	0.658	0.646	0.643	0.651	0.653	0.651	0.651
Total mean water surface elevation: 0.695 m												

N.B., Data in shaded boxes correspond to Static water elevation and data in white boxes correspond to Non-static water elevation.

Table C14. Cumulative percentage of average value of grain size class window, Run 3.

Sample Number	Grain Size Classes (μm)													
	83.26	99.34	118.53	141.42	168.74	201.33	240.22	286.63	342.00	408.06	486.88	580.93	693.14	827.04
	Average value of grain size class window (μm)													
	76.51605	91.29638	108.93177	129.97372	155.08028	185.03657	220.7794	263.4265	314.31172	375.02617	447.46861	533.90449	637.03688	760.09097
1	0.00	0.00	0.23	2.14	7.48	17.73	32.91	51.11	69.07	83.67	93.29	98.17	99.83	100.00
2	0.00	0.01	0.34	2.61	8.56	19.55	35.33	53.71	71.37	85.34	94.25	98.57	99.91	100.00
3	0.00	0.01	0.27	2.44	8.35	19.46	35.50	54.20	72.05	85.99	94.70	98.77	99.95	100.00

N.B., This table only presents grain size classes that apply to the sediments used in the experiments. (The sediment used in Run 3 has 0 % for grain size classes 0.1116 to 83.26 and 986.79 to 2000).

Table C15. Cumulative percentage of average value of grain size class window, Run 4.

Sample Number	Grain Size Classes (μm)																							
	82.25	91.818	102.49	114.42	127.73	142.58	159.17	177.69	198.36	221.43	247.19	275.94	308.04	343.87	383.87	428.52	478.37	534.02	596.14	665.48	742.89	829.30	925.77	1033.46
	Average value of grain size class window (μm)																							
	77.97	87.04	97.16	108.46	121.08	135.16	150.88	168.43	188.03	209.90	234.31	261.57	292.00	325.96	363.88	406.20	453.45	506.20	565.08	630.81	704.19	786.10	877.54	979.618
9	0	0	0.017	0.275	1.146	3.081	6.512	11.796	19.135	28.376	39.106	50.642	62.134	72.746	81.809	88.934	94.011	97.252	99.045	99.835	99.985	100	100	100
13	0	0.334	1.485	3.707	7.345	12.614	19.506	27.851	37.289	47.281	57.253	66.644	75.019	82.087	87.746	92.052	95.144	97.250	98.596	99.383	99.806	99.958	100	100
17	0	0	0.160	1.014	3.141	7.300	14.011	23.430	35.218	48.391	61.694	73.815	83.770	91.073	95.793	98.417	99.614	99.936	100	100	100	100	100	100
18	0	0	0.129	0.790	2.310	5.155	9.683	16.108	24.450	34.373	45.333	56.600	67.388	76.999	84.949	91.025	95.242	97.870	99.287	99.891	100	100	100	100
25	0	0.057	0.351	1.613	4.575	10.217	19.078	31.063	45.276	60.043	73.598	84.501	92.150	96.716	98.964	99.817	99.972	100	100	100	100	100	100	100
35	0	0.103	0.613	1.804	3.927	7.226	11.820	17.728	24.856	32.941	41.657	50.621	59.445	67.779	75.343	81.943	87.445	91.826	95.127	97.430	98.890	99.690	99.991	100
38	0	0.030	0.256	1.291	3.667	8.107	15.053	24.586	36.308	49.245	62.200	73.958	83.626	90.770	95.467	98.164	99.444	99.909	100	100	100	100	100	100
41	0	0.136	0.877	2.838	6.723	13.175	22.376	34.022	47.256	60.758	73.190	83.448	91.001	95.858	98.506	99.656	99.976	100	100	100	100	100	100	100
42	0	0	0.000	0.000	0.000	0.156	0.784	2.033	4.207	7.537	12.229	18.403	26.020	34.914	44.737	55.012	65.179	74.670	83.001	89.779	94.799	98.175	99.874	100
49	0	0	0.009	0.096	0.676	2.293	5.553	11.052	19.150	29.671	41.991	55.062	67.635	78.594	87.218	93.291	97.022	98.980	99.786	99.992	100	100	100	100

N.B., This table only presents grain size classes that apply to the sediments used in the experiments. (The sediment used in Run 4 has 0 % for grain size classes 0.1116 to 82.251 and 1033.46 to 2000).

Table C16. Cumulative percentage of average value of grain size class window, Run 4.

Sample Number	Grain Size Classes (µm)																		
	81.191	94.574	110.162	128.321	149.472	174.110	202.808	236.238	275.177	320.535	373.369	434.911	506.598	590.101	687.368	800.668	932.643	1086.372	1265.439
	Average value of grain size class window (µm)																		
	75.447	87.883	102.369	119.242	138.897	161.791	188.459	219.523	255.708	297.856	346.952	404.140	470.755	548.350	638.735	744.019	866.656	1009.508	1175.906
27	0	0	0.483	2.703	8.056	17.614	31.361	47.859	64.632	79.118	89.667	96.001	98.969	99.913	100	100	100	100	100
31	0	0.165	0.827	2.259	4.764	8.612	14.007	21.059	29.741	39.850	50.961	62.409	73.365	82.978	90.580	95.846	98.842	99.992	100
1	0	0	0.456	2.576	7.603	16.492	29.277	44.810	61.019	75.611	86.893	94.258	98.162	99.687	100	100	100	100	100
2	0	0	0.350	2.411	8.024	18.690	34.371	52.948	70.938	85.150	94.131	98.447	99.838	100	100	100	100	100	100
3	0	0	0.473	2.630	7.733	16.776	29.808	45.648	62.121	76.824	88.002	95.086	98.637	99.870	100	100	100	100	100
4	0	0	0.506	2.419	6.499	13.401	23.307	35.772	49.735	63.746	76.336	86.397	93.433	97.593	99.504	100	100	100	100
5	0	0.151	1.027	3.189	7.167	13.330	21.749	32.138	43.880	56.130	67.951	78.469	87.019	93.265	97.242	99.301	99.995	100	100
6	0	0.185	1.146	3.455	7.622	13.936	22.351	32.482	43.694	55.240	66.372	76.424	84.860	91.349	95.817	98.458	99.683	100	100
7	0	0.291	2.009	6.163	13.469	24.036	37.188	51.566	65.514	77.572	86.860	93.203	96.995	98.932	99.736	99.978	100	100	100
8	0	0.101	1.047	4.465	12.005	24.551	41.244	59.469	75.925	88.150	95.468	98.824	99.871	100	100	100	100	100	100
10	0	0	0.134	1.129	3.991	9.463	18.024	29.536	43.177	57.584	71.183	82.612	91.056	96.392	99.094	99.992	100	100	100
11	0	0	0.021	0.612	2.993	8.542	18.321	32.301	49.014	65.907	80.337	90.643	96.626	99.263	99.983	100	100	100	100
12	0	0	0.000	0.522	2.669	7.672	16.503	29.269	44.891	61.296	76.106	87.505	94.825	98.546	99.859	100	100	100	100
14	0	0	0.096	0.895	3.506	9.010	18.192	30.988	46.288	62.146	76.407	87.440	94.629	98.389	99.798	100	100	100	100
15	0	0	0	0.214	1.271	3.908	8.911	16.847	27.794	41.157	55.687	69.751	81.789	90.764	96.416	99.194	99.995	100	100
16	0	0	0.304	1.498	4.046	8.408	14.884	23.528	34.077	45.947	58.291	70.138	80.565	88.886	94.780	98.311	99.881	100	100
19	0	0	0.345	2.322	7.658	17.770	32.675	50.499	68.097	82.496	92.169	97.364	99.449	99.972	100	100	100	100	100
20	0	0	0.291	2.143	7.358	17.492	32.675	51.001	69.107	83.750	93.286	98.075	99.734	100	100	100	100	100	100
21	0	0	0.060	0.825	3.822	10.769	22.768	39.238	57.704	74.749	87.617	95.377	98.896	99.922	100	100	100	100	100
22	0	0	0.026	0.555	2.579	7.203	15.364	27.282	42.140	58.160	73.129	85.167	93.341	97.839	99.647	100	100	100	100
23	0	0	0.402	2.079	5.813	12.284	21.744	33.845	47.619	61.670	74.524	85.008	92.521	97.110	99.330	99.994	100	100	100
24	0	0	0	0.323	1.897	5.834	13.179	24.354	38.763	54.766	70.153	82.909	91.896	97.105	99.400	100	100	100	100
26	0	0.239	1.823	6.090	14.148	26.265	41.487	57.799	72.835	84.753	92.800	97.321	99.323	99.936	100	100	100	100	100
28	0	0	0.159	1.395	4.938	11.940	22.924	37.331	53.495	69.137	82.171	91.409	96.818	99.263	99.971	100	100	100	100
29	0	0	0.015	0.520	2.808	8.553	19.071	34.280	52.243	69.782	83.918	93.182	97.932	99.666	100	100	100	100	100

30	0	0	0.106	1.099	4.657	12.484	25.457	42.613	61.162	77.644	89.568	96.389	99.257	99.976	100	100	100	100	100
32	0	0	0.139	1.044	3.810	9.440	18.624	31.238	46.199	61.687	75.700	86.698	94.044	98.052	99.668	100	100	100	100
33	0	0	0	0.402	2.413	7.705	17.688	32.472	50.304	68.071	82.690	92.486	97.643	99.595	100	100	100	100	100
34	0	0	0.190	1.444	4.896	11.615	22.106	35.896	51.503	66.856	79.991	89.680	95.716	98.743	99.838	100	100	100	100
36	0	0	0.067	0.810	3.148	7.863	15.567	26.339	39.582	54.061	68.178	80.403	89.690	95.721	98.870	99.975	100	100	100
37	0	0	0.183	1.522	5.281	12.610	23.969	38.682	54.968	70.499	83.237	92.109	97.194	99.414	100	100	100	100	100
39	0	0	0.226	1.701	5.695	13.331	24.996	39.924	56.258	71.653	84.116	92.665	97.467	99.500	100	100	100	100	100
40	0	0.023	0.629	3.272	9.672	20.995	36.826	54.911	72.010	85.384	93.913	98.183	99.710	100	100	100	100	100	100
43	0	0	0.015	0.565	3.061	9.271	20.496	36.458	54.908	72.433	86.059	94.556	98.585	99.860	100	100	100	100	100
44	0	0.080	0.884	3.588	9.256	18.581	31.361	46.399	61.804	75.610	86.398	93.651	97.718	99.493	99.987	100	100	100	100
45	0	0.251	1.920	6.734	16.265	30.816	48.742	66.875	81.960	92.148	97.535	99.576	100	100	100	100	100	100	100
46	0	0.316	1.506	3.939	7.957	13.735	21.257	30.305	40.493	51.315	62.175	72.439	81.496	88.860	94.267	97.727	99.497	100	100
47	0	0	0.272	1.882	6.106	14.047	26.025	41.185	57.595	72.877	85.077	93.294	97.790	99.610	100	100	100	100	100
48	0	0.287	2.087	7.146	17.008	31.880	49.990	68.091	82.942	92.791	97.856	99.678	100	100	100	100	100	100	100
50	0	0.296	2.126	7.243	17.183	32.130	50.285	68.377	83.171	92.936	97.926	99.699	100	100	100	100	100	100	100

N.B., This table only presents grain size classes that apply to the sediments used in the experiments. (The sediment used in Run 4 has 0 % for grain size classes 0.011648 to 81.191 and 1265.439 to 2000). In addition, the grain size classes used for the grain size particle analysis of samples in Table C. 12 are slightly different than the ones used for samples in Table C. 13; this is explained but a slightly different set-up of the particle-sizer software.

